# Proceedings

## International Workshop

# *3D Remote Sensing in Forestry*

Vienna, 14th-15th Feb. 2006

organised by EARSeL SIG Forestry

co-sponsored by ISPRS WG VIII/11

*Tatjana Koukal, Werner Schneider (eds.)*

Sponsored by
Bank Austria Creditanstalt

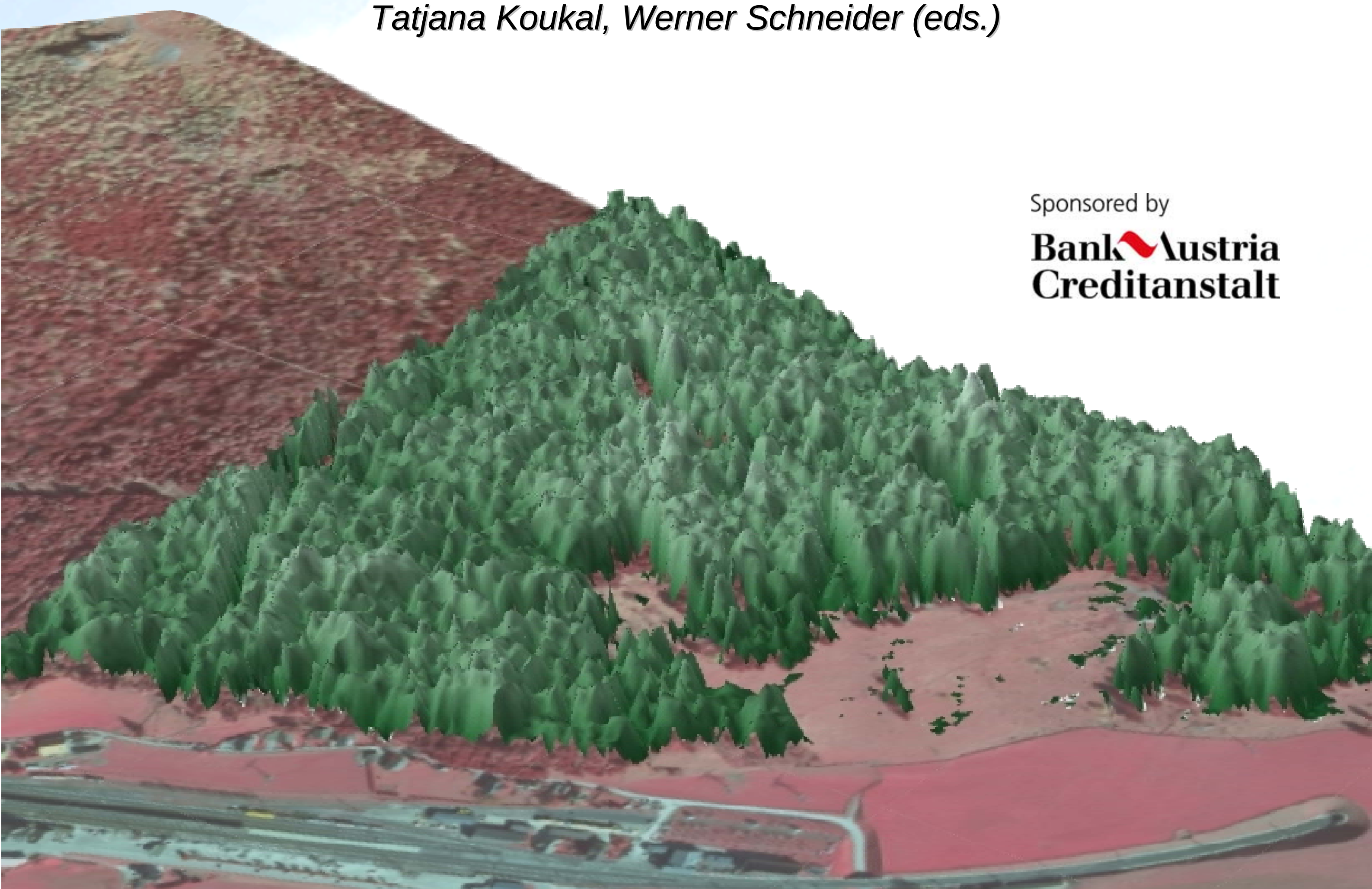

**University of Natural Resources and Applied Life Sciences, Vienna**
**Department of Spatial, Landscape and Infrastructure-Sciences**

Tatjana Koukal, Werner Schneider (Editors)

Institute of Surveying, Remote Sensing and Land Information
University of Natural Resources and Applied Life Sciences (BOKU)

Peter-Jordan-Straße 82
1190 Vienna, Austria
Phone: +43-1-47654/5100
e-mail: ivfl@boku.ac.at

May 2006 (Last update: January 2007)

The proceedings are available in digital form at http://www.rali.boku.ac.at/3drsforestry.html

# Table of Contents

## Session 4b - Forest Information Retrieval by Interferometric SAR



## Session 5 - Radiation Transfer Modelling



## Session 6a - Airborne Laser Scanning (2)



## Session 6b - Forest Parameters from Multi-angle and Hyperspectral Data

## Session 7 - Single Tree Detection from High Spatial Resolution Reflectance Data



## Session 8a - Full Waveform Laser Scanning



## Session 8b - Application-oriented Assessment of Forest Parameters



## Poster Session
(thematic order)

# 3D DATA FOR FOREST AND ENVIRONMENTAL PLANNING

*Barbara Koch, Ursula Heyder, Christoph Straub, Holger Weinacker*

University of Freiburg, Dept. Remote Sensing and Landscape Information Systems FeLis, Freiburg, Germany; barbara.koch@felis.uni-freiburg.de

## ABSTRACT

The assessment and visualisation of 3D information has increased its importance tremendously. This is due to the fact that the assessment of 3D information is with development of new measurement technologies of increasing quality and appropriate software makes the processing of 3D information more straightforward. These developments allow better applied research and successful practical applications. 3-D data are used in two aspects, to measure 3-D quantities and to provide 3-D visualization.

Forestry was one of the first disciplines which used 3-D information extracted from remote sensing data (aerial photographs). Already 1933 described Hugershoff stereo-photogrammetry as a suitable technology not only to assess large forest areas, map or open new forest land but especially to measure single trees and stands to derive quantitative measures needed for forest management, like tree height and crown diameter.

A literature review of new publications in the field of 3-D data for forest applications shows that application of airborne laser scanner data are in the focus of research today. Besides airborne laser scanner data for extraction of 3-D data also optical stereo data, and radar data, enabled to apply interferometric measurements, are used. This article will give a short overview on the status of the different remote sensing technologies for 3-D forest structure assessment. The evaluation shows that for large scale intensive forest structure as well as single tree assessment airborne laser scanner data provide most detailed information, while InSAR technology also has the potential to deliver spatially-explicit information but on a less detailed level. The automatic 3-D photogrammetric evaluation is not so much in focus of research today and published results are quite diverse.

Finally results on new processes for stand delineation and single tree extraction based on airborne laser scanner data will be presented. The results presented use laser scanning data acquired by the FALCON-System. For the single tree assessment an extraction algorithms will be presented which provides results with 87% correct delineated crowns for coniferous stands, while for dense multistorey broad leaf tree stands 61% of the crown were accessible in an automatic process. For the stand delineation different approaches have been tested. The solely full automatic process was not sufficient enough to achieve all requirements of a German stand delineation system. Nevertheless with a combined method of automatic stand delineation improved by minor manual interactions 85% of all forest stand boundaries as they are established by the State Forest management unit Baden-Württemberg were accessible. The algorithms developed for first and last pulse data are now adapted to full wave laser data.

**Keywords:** 3-D forest structure information, airborne laser scanner data, automatic single tree delineation, automatic stand delineation.

## 1 INTRODUCTION

The assessment and visualisation of 3D information has increased its importance tremendously. This is due to the fact that the assessment of 3D information is with development of new measurement technologies of increasing quality and appropriate software makes the processing of 3D information more straightforward. These developments allow better applied research and successful practical applications. 3-D data are used in two aspects, to measure 3-D quantities and to provide 3-D visualization.

While the 3-D visualization accommodates the human perception of environment it supports orientation and understanding and therefore better participation of people concerned as well as accessibility of target groups. How important the 3D visualization today is can be quantified by numerous 3D visualizations in the tourism marketing area. The other aspect of 3D visualisation is a better participation in planning processes. The often complex planning projects are better understood if a 3D presentation is provided. This is especially important for a better public participation in planning processes but also for decision makers who often overstrained by the complexity of the matter. Human being has better availability to interpret complex 3D visual information than abstract 2-D plans, therefore today in environmental planning the visualisation of 3 D models is becoming standard.

The measurement of 3-D quantities out of 3-D data is another use of 3-D data. For many years photogrammetric tools exist to provide 3-D measurements. Forestry was one of the first disciplines which used remote sensing (aerial photographs). The first documented aerial photograph for forest planning in Europe was in the year 1887 taken from a captive balloon to generate a forest map (Blachut 1988) (Fig. 1). Already 1933 described Hugershoff (Hildebrandt 1993) stereo photogrammetry as a suitable resource not only to assess large forest areas as well as to map and open them but also to measure single trees and stands to derive quantitative measures needed for forest management, like tree height and crown diameter as input for wood volume calculations.

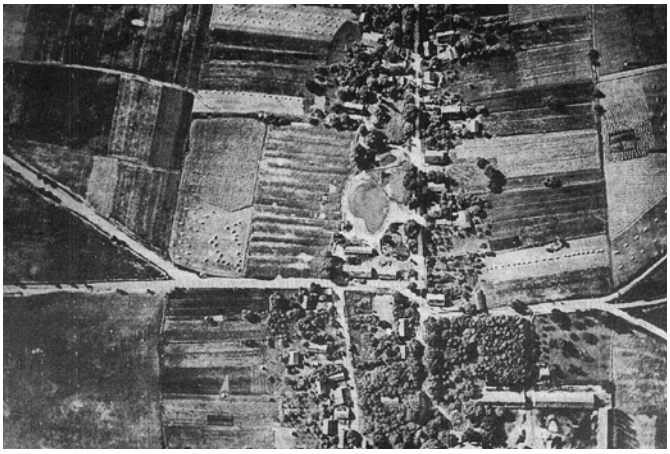

*Figure 1: First documented aerial photograph for forest planning in Europe 1887 (Blachut 1988)*

At the time first applications of aerial stereo photogrammetry for forest applications were developed it also was mentioned the use of terrestric photogrammetry to assess 3-D tree information to derive stem forms and volumes (Fig 2.). While the assessment of 3-D data from terrestrial photogrammetry developed intensively in non-forest areas like architectural photogrammetry in forest this field of research only gained importance again within the last 15 years (Pröbsting 1996).

*Figure 2: Terrestrial photogrammetry for single tree measures*

This tells us that forestry was always at the forefront to evaluate the potential of 3-D data. Having in mind that wood volume for decades was the key element in forestry and still is very important today it becomes evident that 3-D information provides key information for forest management. As described by Duvenhorst (1998) tree or stand height as well as crown diameter are together with a rough stratification of stand type the most important auxiliary variables to derive wood volume and increment from remotely sensed data. In his investigations he states, as many others, that a coefficient of determination between 0.7 and 0.9 can be achieved for wood volume if aforementioned information is correctly available. If natural age classes can be added as additional information the coefficient of determination is strictly above 0.8 for wood volume. Again for the assessment of natural age classes height and crown diameter are very important inputs together.

Besides wood volume today a number of other parameters are very necessary for a modern sustainable forest management. Today forest management needs parameters which describe the forest status and development in a holistic way. Besides wood production oriented parameters are parameters related to biodiversity, habitat structure and landscape are of interest. In respect to this tree and stand type compositions are important but also the 3-D forest structure and terrain is of highest relevance as well as infrastructure related information. To serve these information needs 3-D data are indispensable.

Finally, information is needed for utilization of wood resources. Most important are topography, forest roads as well as geometric and thematic single tree or stand information, always dependent on the utilization system applied.

The aforementioned indicates that the integration of 3-D data is a must in order to serve forest management needs in different working scales.

A literature review of new publications in the field of 3-D data for forest applications shows that application of airborne laser scanner data are in the focus of research today. Nevertheless for the extraction of 3-D data different remote sensing sources are possible and used. Data which are mostly used for 3-D information extraction are optical stereo data, radar data enabled to apply interferometric measurements and laser scanner data.

## 2 STATUS ON APPLICATION OF DIFFERENT 3-D MEASUREMENT TECHNOLOGIES IN FORESTRY

### 2.1 Status on photogrammetric forest applications

Photogrammetric measurements based on stereo data are a well known technology and still manually one of the most applied methods to assess 3-D information in practice. Nevertheless it has to be admitted that the manual applications are labour intensive and can only be realized for small areas or single trees. In respect of full automatic measurements there are a number of investigations in the area on automatic crown and stand delineation based on 2-D data. Besides that 2-D information is missing parameters on form and height, the results are quite diverse and therefore not reliable enough for practical applications. For solely automatic 3-D assessment of forest structure based on aerial photographs not many intensive investigations exist. Mallinger generated in 1997 a digital crown surface models but did not use this model for extraction of forest stand parameters because he found the surface model to imprecise for this purpose. Adler (2001) took up the research on automatic 3-D assessment on forest structures solely based on digital aerial photographs in scale 1:5000. She found that the height variations of full digital generated crown surface models are in the same range of those which are manually generated. This means for 65% of the measured heights the variance is within 5 m. Nevertheless the automatic delineation of crowns was not successful according to her investigations, especially due to strong reflectance differences between illuminated and shadowed part of the crown. Only 45% of the tree crowns in a coniferous stand were correctly delineated.

On the other hand it is stated (Svoboda 2000) that a precise crown delineation improves decisively the classification of tree species based on the reflectance values measured from digital IR aerial photographs. A few investigations are focused on the generation of digital surface models based on stereo data from very high resolution satellites. Poone et al. (2005) state a mean square error of 5 to 6 m for forest covers extracted from IKONOS stereo data, while the mean difference was only 0.7 meter.

Mosch (2006) investigated on the extraction of building heights from Quick Bird stereo data. Similar to other investigations he was able to extract buildings based on spectral and height information. The heights extracted from satellite based DOM for buildings had a mean difference from the manual measurements based on aerial photographs of around 1 m. This indicates good potential to extract 3-D information from very high resolution stereo satellite images.

## 2.2 Status interferometric radar forest applications

The application of radar interferometry for 3-D structural assessments becomes a more and more intensive investigation topic. A number of investigations are carried out in preparation of the TerraSAR TanDem-X mission. In 1999 FeLis was involved in ProSmart investigations in which the principle potential of SAR-Interferometry for forest applications was tested. Dees and Koch (1999b) demonstrated that the derived crown height model from data of the E-SAR system has a high correlation with terrestrial measured stand heights in flat areas. The DEM used was based on a digital elevation model from the state survey, while the crown height model was provided by DLR.

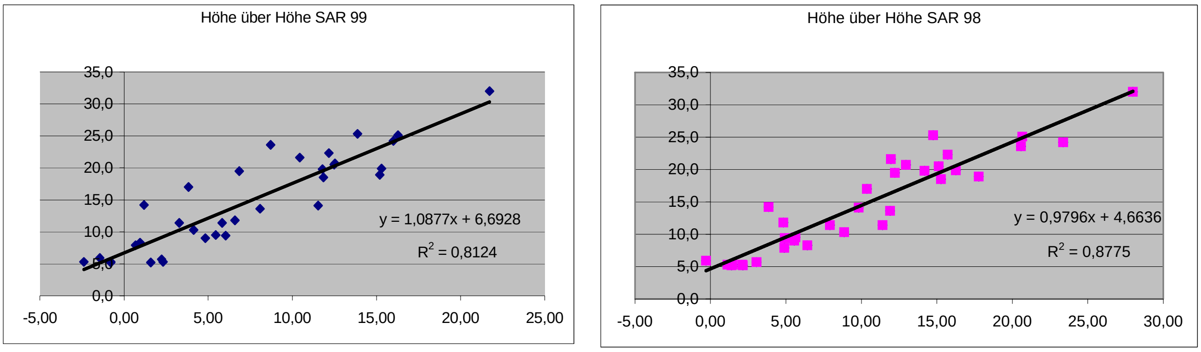


*Figure 3: Potential of SAR data derived crown height model for generation of stand heights*

As showed in Fig. 3 for 34 test stands more than 80% of the height variability can be explained. In this case it is of high relevance that the digital elevation model used is quite precise in order to achieve these results for the crown height measurements. Newer investigations on the estimation of forest height have been carried out mainly by Hajnsek and Papathanassiou (2003), Mette et al. (2004), Garestier et al. (2005), Hellwich et al. (2005), Hoekman & Varekamp (1998) and Breitenbach et al. (2006) in the frame of E-SAR flights. In all these investigations mainly the tree height accuracy was investigated. It is stated that tree height can be extracted with good accuracy of about 10% to 15% independent of the topography. Some of the publications refer to problems in correct establishment of ground elevation models, underestimation of tree heights due to over-lay effects or the influence of extinction coefficient on tree heights measurements. All together it can be stated that the application of interferometric radar data in X- and L-Band provide promising results for crown height measurements. Hoekmann (2005) even stated for tropical forests reliable measurements for ground and canopy heights based on Pol-InSAR E-SAR flights. The extraction of tree heights opens also a reasonable estimation of biomass.

## 2.3 Status Lidar forest applications

The end of 20 century and beginning of 21 century the research on airborne lidar data for forest applications was a central topic to assess 3-D forest structures. There exist a large number of publications which indicate the potential of airborne lidar data for exact height measurements as well as 3-D structural information (Hyyppä et al. 2001, 2003, Holmgren & Persson 2004, Naesset 2003, St. Onge & Achaichia 2001, Koch et al. 2006). The suitability of Lidar data for generation of detailed DTM and DSM is out of question. A investigation at the University of Washington (Anderson, H-E. et al. 2004) shows canopy-level models generated from high density laser scanner (3,5 pulses per m2) and X-band radar interferometry (post spacing 2.5 m). Both models have a relatively close qualitative agreement but the laser based model provides a more detailed representation of the forest canopy than the model produced by X-band radar interferometry. The results of the investigation also show that according to compared profiles LIDAR is more successful in detecting canopy gaps than photogrammetric measurements (RGB 1:3000) (Fig. 4). This is mainly due to the fact that in aerial photographs shadow limits the detailed assessment of canopy gaps.

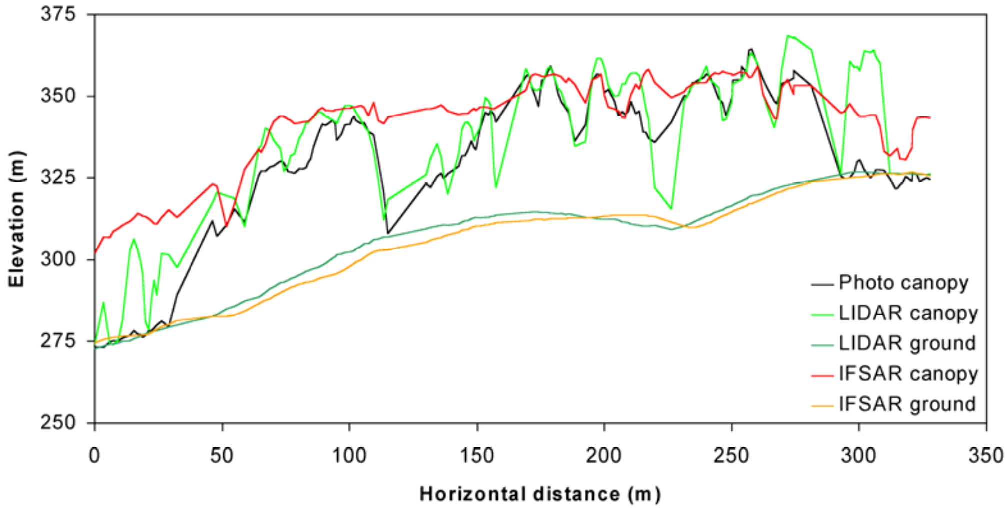


*Figure 4: Canopy models from measured LIDAR, IFSAR and aerial photographs. Source Anderson et al. 2004*

In general based on airborne laser scanner data there are two different main approaches. Several authors have shown mostly for coniferous forests that airborne LIDAR is a good means for estimating forest stand parameters (like volume or mean stand height) with an averaging, stand-wise approach (Naesset, 1997; Magnussen and Boudewyn, 1998; Lefsky et al., 1999). Nevertheless under typical conditions in temperate forests a stand-wise approach often is not considered sufficient enough. As several tree species with different growing behaviour can occur in one stand, a-priori knowledge of stem number, tree-species and diameter distribution is requested for calculating stand parameters. Additionally, in diverse forests a stand-wise result is usually not sufficient for harvest management purposes. Therefore, single tree delineation and tree species classification seem to be a prerequisite to use remote sensing technologies for operational large-scale forest management under in temperate forests especially for calculation of timber volume, but also for harvesting and silvicultural treatment schemes. First approaches of single tree delineation showed promising results for conifer forests (Gougeon, 1995; Pollock, 1996, Hyyppä and Hyyppä, 2001; Persson et al., 2002; Brandtberg et al. 2003) also by fusing LIDAR and RGB data (Popescu et.al. 2004; Popescu & Wynne 2004). For broadleaf stands not many investigations on single tree segmentation exist. Good potential was demonstrated by Heyder (2003). There have been some promising investigations on combination of information from laser scanner data and multispectral data as well as new investigation on the assessment of forest growth by airborne LIDAR scanning (Yu et al. 2003).

## 3 TREESVIS CROWN AND STAND DELINEATION METHODS

At the department FeLis within the last years a software for evaluation of airborne LIDAR data was developed. Main components of this software are the calculation of DTM and DSM, single tree and building extraction, tree and building modelling, stand delineation as well as the visualization. In addition most of the investigations up till now are concentrated on the northern type conifer forests while for broadleaf forest not very many investigations exist. This paper will present developed processing lines and results on single tree assessment and stand delineation based on airborne laser scanner data. The computer analyses are implemented in C++, with use of libraries from the image-processing system HALCON (MVTec, 2003).

### 3.1 Preprocessing for crown and stand delineation

As in most applications the first step for single tree delineation is the generation of a digital terrain and surface model. The digital crown height model (DCHM) is then derived by subtracting the height value of the DTM at each pixel from the height value of the DSM, that tree heights can be taken directly from the DCHM. Gaussian smoothing of the DCHM is applied, while the degree of smoothing is adapted to the stand height with a threshold operator for different height classes. Smaller holes within the area of one class are closed to decrease edge-effects. The classes are afterwards merged again. The optimal number of height-classes, the height-threshold and the smoothing intensity can be determined in pre-tests for the respective data

### 3.2 TreesVis single tree crown delineation

Based on the smoothed DCHM with a local maximum filter the tree tops are selected (Koch et al. 2006). Starting from those local maxima, with the pouring algorithm implemented in Halcon (Soille 1999) regions are extended, as long as neighbouring pixels with a lower or the same height value exist. Overlapping regions are finally distributed evenly to all involved trees (Fig 5).

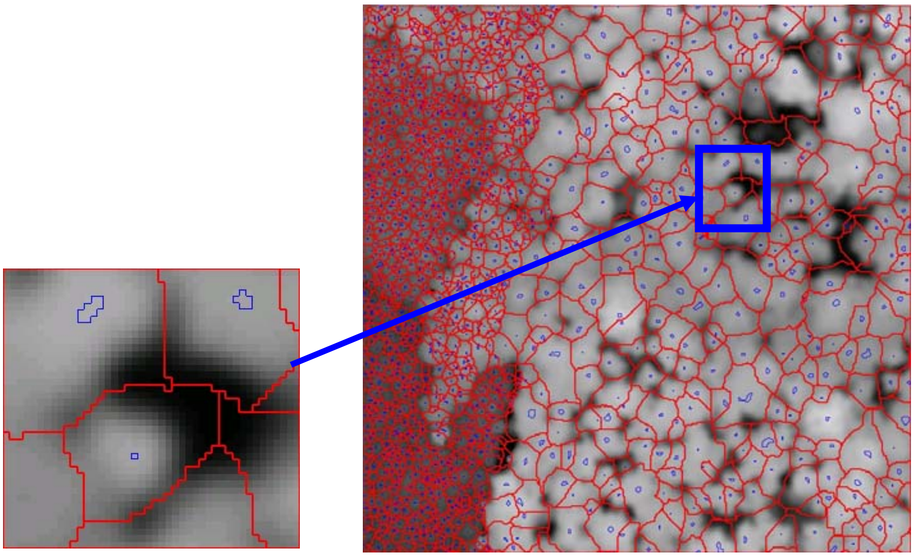

*Figure 5: Pouring algorithm for single crown delineation*

In order to remove remaining obviously wrong segments the crown regions are split into two height classes in order to adjust the threshold for the subsequent steps. Proceeding from the assumption (forest inventory directives) that a tree has a certain height and species dependent minimal area, for the tree in the higher class and for the trees in the lower class tree crown class the respective minimal areas can be determined. For all areas below the defined minimal areas the neighbour region with the longest common border is selected and is merged. The higher top of both trees becomes the top of the new tree. Additionally, a minimum distance in each height class is defined between tree tops. If two tree tops are within this distance, the corresponding crown-segments are merged.

After the previous delineation steps, there still exist groups of trees that could not be separated. If a region has got a length of at least 2.5 times its width and has got at least three times the respective minimal area for its height class, it is marked as a group. Those congregations are disjoined analogous to Straub and Heipke's (2001) approach, which has been developed for tree groups within settlements. For each tree group consecutively biggest inner circles are detected and subtracted from the region until the circle's area falls below the double minimal area for the height class.

The last part of the single-tree-detection-algorithm determines the actual crown edge to separate a tree from neighbouring canopy gaps or from adjacent understorey trees. It is based on the algorithm developed from the group at University of Freiburg within the HighScan project (Hyyppä et al. 2002, Friedländer 2002) and used to determine the final crown edge based on the previous segmentation results. Starting from the tree's top, a vector to each border point is calculated. Proceeding in one pixel wide steps on each vector, the slope of the tree crown at each of these points is measured as height-difference between two points. If this height difference exceeds 2.5m per 0.5m distance, the vector breaks and a new border point is generated. The crown edge is moved inside. Occasional occurring outliers are removed afterwards.

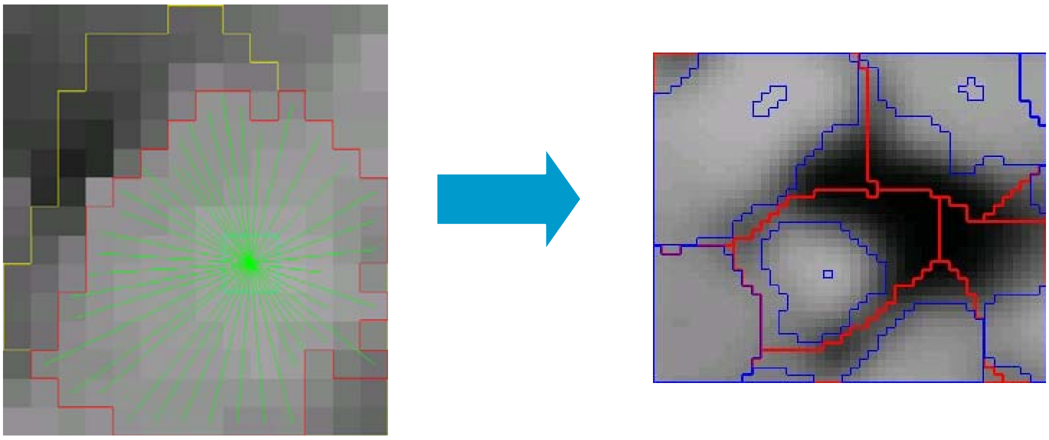

*Figure 6: Vector algorithm for sharp crown delineation*

### 3.2.1 TreesVis single tree classification

For the extraction of forest parameters not only structural information but also the tree type information is of high interest. This is the reason that a number of investigations try to combine LIDAR and RGB or multispectral information (Popescu and Wynne 2004). In this approach the classification of tree types was carried out based on LIDAR and RGB data. While for the LIDAR data form parameters were tested, for the RGB well known ratios were applied in order to classify single trees in different tree type classes. Form and spectral parameters are calculated for 16001 trees. 2122 (13,3%) are used to generate the stepwise linear discriminant function, another 5065 (31,7) trees are used to test the classification quality. For all trees the probability to belong to one of the defined classes

- Young broadleaf trees
- Old broadleaf trees
- Conifers

is calculated. In order to identify a training set with trees of known classes stands are selected based on the forest information age and type index which implies that more than 80% of trees belong to one of the defined classes. In addition a height criteria was included in the stand selection which groups trees below 20 m in the class young broadleaf trees while trees higher than 20 m are grouped in the class old broadleaf trees.

As criteria for the quality of the discriminant analysis the Wilks Lamda is used. The F probability for acceptance of a variable is 0.05 and for exclusion 0.10. The discriminant analysis is applied for the form parameters and subsequently for a combination of form and spectral parameters.

### 3.2.2 Form parameter

For the investigation on the usability of form parameters only trees are included higher than five meter. In a first step basic form parameters are calculated like, the crown area, the crown perimeter, the crown radius, tree height (difference between the highest point in the nDSM within a crown segment and DTM), the sun crown length (difference between the crown top and the average height of the delineated crown edge) as well as the sun crown volume. From these basic measures the following form parameters are calculated.

- Circularity
- Ratio sun crown to crown diameter

- Entropy
- Ratio of local maxima in the filtered image to local maxima in unfiltered image
- Crown percentage (ratio of sun crown length and tree height)
- Co-efficient of variance for grey values
- Ratio of sun crown and the volume of a cylinder derived form the crown projection area
- Distance of the geometric centre of the crown projection and the tree top divided by the crown radius.
- Roundness
- Ratio of sun crown volume and the volume of a fitted cone.
- Compactness
- Bulkiness
- Anisometry
- Ratio of sun crown volume and volume of a fitted ellipsoid

### 3.2.3 Spectral Parameters

In addition to the form parameters spectral measures are derived from the RGB images. Three often used spectral indices are calculated, the NDVI, the RVI, which is the ratio of NIR to red and the RVI green which is the ratio of NIR to green. These indices are calculated from ratio images and for each crown segment the average grey value is generated.

## 3.3 TreesVis Stand Delineation

The stand is the management unit. The characteristic of a stand is that it is a unit which allows common forest management measures. Often a stand has a similar tree age and a dominant tree type. Because the stand is the forest management unit, the assessment and delineation of such units is the basis for all operational management plannings. For operation tasks the information based on single tree assessment needs to be allocated to the management of stand unit.

A semi-automatic approach is developed combining different segmentation methods in a series of modules. The approach is based on generated nDTM and nDSM models from winter data. The first segmentation is the segmentation in planar and non planar areas, followed by an automatic segmentation of forest roads, watersheds and forest height classes. Finally based on training areas conifer and broadleaf stands are separated. After each segmentation step (module), the operator has the option to select suitable regions, which will be stored. After the last segmentation step additional regions can be digitized manually. This allows adding further regions which could not be detected with one of the automatic approaches. Finally all regions will be intersected with each other and the boundaries will be smoothed and adapted automatically. The resulting forest stands can be selected in the “Graphics window” and the following information can be displayed:

- Size of the forest stand
- Average stand height
- Developmental stage
- Total number of trees per stand / number of trees per hectare
- Crown closure
- Average slope value

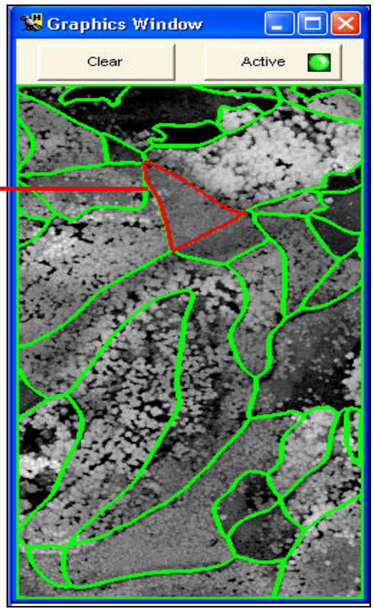


The contour of the forest stands will be exported in “Arc/Info generate format” (transformed to the world coordinate system) (Koch et al 2006).

# 4 RESULTS SINGLE TREE CROWN AND STAND DELINEATION

## 4.1 Results on single tree crown delineation

A comparison of the segmentation outcome with the reference trees gave the following results .

*Table 1: Results on the automatically detected tree crowns compared to measured reference trees*

| Plot | No of trees | No of seg. trees | No. of seg. trees | clear single tree assignment seg. trees | | merged seg. trees | | split seg. trees | | no assignment seg. trees | |
|---|---|---|---|---|---|---|---|---|---|---|---|
| | | | in % | | in % | | in % | | in % | | in % |
| Terrestrial measurements | | | | | | | | | | | |
| Douglas fir | 49 | 47 | 95,9 | 41 | 87,3 | 1 | 2.1 | 0 | 0 | 5 | 10.6 |
| Deciduous trees | 49 | 30 | 61,2 | 15 | 50 | 13 | 43.3 | 2 | 6.7 | 0 | 0 |
| Photogrammetric measurements | | | | | | | | | | | |
| Mixed forest | 535 | 457 | 85,4 | 282 | 61,7 | 117 | 25,6 | 19 | 4.2 | 39 | 8,5 |

For 49 terrestrial measured douglas firs (Pseudotsuga menziesii) 47 automatically detected trees are found. 87.3 % of them have a clear assignment to reference trees. The number of detected trees refers to over 94% of basal area which indicates that the interesting dominant trees for wood production are clearly segmented. The main mistake is the omission of some very small trees. Crown areas are overestimated: the mean crown area of the reference trees is 8.2m², compared to 11m² of the segmented trees. Corresponding to the 49 broad-leaved reference trees (Carpinus betulus, Acer pseudoplatanus and Fraxinus excelsior) 30 automatically delineated trees are found. Of those, 50% can be clearly assigned to reference trees, 43.3% include several merged reference trees. The merged trees combine mostly subdominant trees with an adjacent dominant tree. Partly dominant trees which build a dense, close, homogeneous canopy could not be separated. The 30 automatically segmented trees or tree groups again refer to over 70% of basal area which indicates as for the conifers that most of the dominant trees are segmented correctly.

Compared to the photogrammetrically measured reference crowns, 61.7% of the segmented trees have a clear assignment to reference trees, 25.6% merge two or more reference trees, and 4.2% are split. For 39 trees no reference trees (8.5%) could be assigned (Fig. 7).

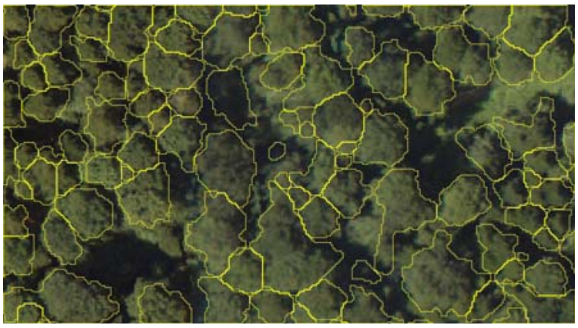

(a)

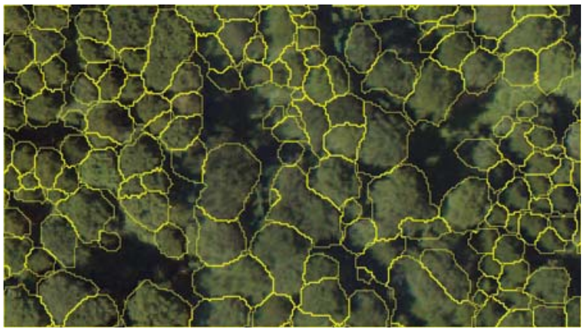

(b)

*Figure 7: Photogrammetric delineated tree crowns (a) compared with automatically segmented tree crown from LIDAR data (b).*

The segmentation results are very encouraging for coniferous species. Almost all dominant trees are found and the crown delineation is very close to terrestrially measured crown projections. Compared to the terrestrially measured crown polygon, the crown's edge is sometimes even more precise, although the crown area is overestimated, but it has to be taken into consideration, that also crown projections in the field have to deal with uncertainties, so the truth for crown area might be in between the two measurements. For deciduous species the automatic segmentation result underestimates the tree number. A number of trees are merged. This is partly due to not found subdominant trees (which are not very important from the forester's point of view), but also some dominant tree crowns are merged. Very densely growing dominant hornbeams with a homogeneous height-distribution could not be separated. However, if the crowns of dominant deciduous trees are not tightly interlocked but more isolated the segmentation outcome will be considerably improved.

## 4.2 Results of the single tree type classification

Besides circularity the three tree type classes differ in the mean values of all form variables with a significance level of 0.005. The discriminant function has an eigen value of 0.83 which means that 83% of the variance is explained through the function and the Wilks Lambda is 0.36. All together 74% of the trees are classified correctly. For the broadleaf trees nearly 80% are classified correctly and within the two broadleaf tree classes a correct assignment to the classes for more than 86% of the trees was possible. For the conifers 64% of the trees were classified correctly, but nearly 30% of the conifers have been classified into the class young broadleaf trees. The most important variables are circularity, crown ratio and entropy.

## 4.3 Results on stand border delineation

An interactive graphical processing chain is developed. All segmentation methods are combined in a sequence of modules. After each segmentation step (module), the user has the option to select regions manually. The tests carried out are in an area with pure conifer or broadleaf stands as well as in a mountainous area with diverse structured mixed stands. The automatic and semi-automatic generated stand borders based on LIDAR data are compared to the stand borders of the State Forest Information System FOGIS from Baden-Württemberg. The results presented are of different quality dependent on the degree of interaction by the user during the segmentation process. There are three options evaluated. The full automatic delineation, the automatic delineation combined with supervised classification and the automatic delineation combined with supervised classification as well as supplementary freehand delineation.

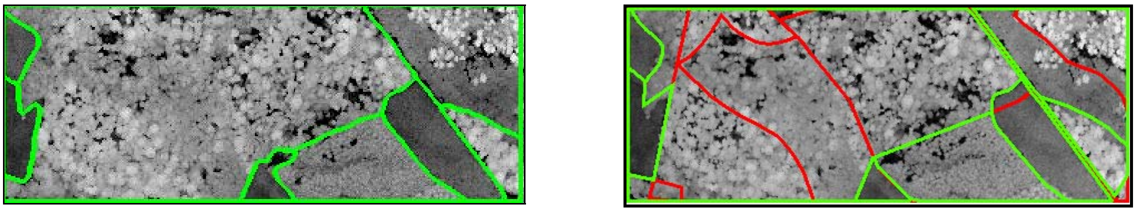

(a) (b)

*Figure 8: Green lines are detected by the full automatic segmentation process based on LIDAR data: (a) automatic LIDAR segmentation, (b) reference data set.*

The full automatic approach achieved dependent on the complexity of the stand structures a stand assessment between 50% and 53%. In the more simple structured stands all lines detected by the full automatic process are also displayed in the reference data set. In the area with complex structured stands more than 90% corresponded with the lines of the reference data set.

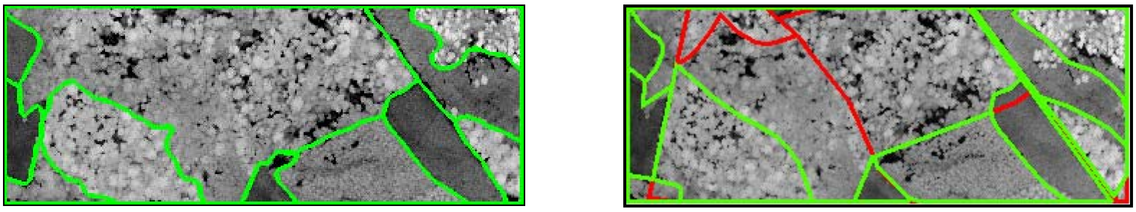

(a) (b)

*Figure 9: Green lines are detected by full automatic segmentation and classification process based on LIDAR: (a) automatic LIDAR segmentation, (b) reference data set.*

The approach with the combined method of full automatic delineation and supervised classification showed a successful delineation of stand borders between 67% and 73%. All delineation stand border in the simple and complex structured stand correspond to the border lines in the reference data set.

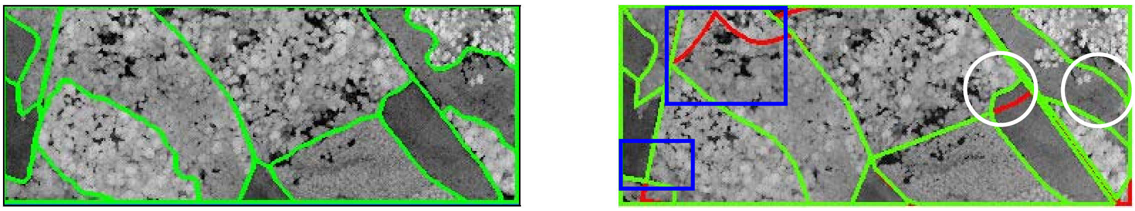

(a) (b)

*Figure 10: Green lines are detected by full automatic segmentation and classification process complemented by free hand delineation based on LIDAR: (a) automatic LIDAR segmentation, (b) reference data set.*

For the approach combining full automatic delineation with supervised classification and freehand delineation for both stand types more than 86% of the stand border have been delineated analogue to the reference data set. Some of the missed stand borders are obviously erroneous in the reference data set and for a few stand borders (far under 10%) it was not possible to assess them based on LIDAR data information only. For these borders displayed in the reference data set and not found in the LIDAR data it still needs to be clarified if they are based on physical differences or on other items like administrative ones.

All together it can be stated that more than 85% of the stand border lines can be generated from LIDAR data. All the generated border lines correspond with border lines in the reference data set when combining segmentation and supervised classification. Some of the missing lines in the laser data set which are displayed in the reference data set are due to obvious errors in the reference data set. This indicates that the missing of correct lines is far below 10%.

# 5 DISCUSSION AND CONCLUSIONS

The presented results show that LIDAR data have high potential to provide detailed forest structure information. Especially for automatic single crown derived information LIDAR is superior to other 3-D measurement technologies. Nevertheless it has to be taken into consideration that a single crown approach needs an assignment to management units. There are different approaches possible in this paper a LIDAR based approach showed to be quite successful. The investigations showed also that there are still limits with LIDAR single tree assessment therefore in future combinations of data from different systems have to be evaluated more intensively. Also new LIDAR systems like the full wave systems and imaging LIDAR will open new evaluation aspects. For practical applications it has to be taken into consideration that a single crown approach needs high resolution LIDAR data and only cost analysis will provide the efficiency aspect to use these data for operational forest management. In reference to the costs the new space-borne RADAR interferometry might provide good alternatives to assess 3-D information over forest areas. For fine operational management scales the resolution of space-borne radar might not be fine enough.

## REFERENCES


Adler, P. (2001). Einsatz digitaler Photogrammetrie zur Beschreibung von Waldbeständen. Am Beispiel der digitalen photogrammetrischen Erfassung der Level 2 Flächen Baden-Württemberg. Dissertation an der Albert-Ludwigs-Universität, Freiburg 2001 p. 148

Anderson, H-E., McGaughey, R. J., Carson, W. W., Reutbuch, ST. E., Mercer, B., Allan, J. (2004). A Comparison of Forest Canopy Models Derived from LIDAR and INSAR Data in a Pacific Northwest Confer Forest. International Archives of Photogrammetry and Remote Sensing. 34(Part 3/W13): 211-217.

Blachut, T. (1988). Die Frühzeit der Photogrammetrie bis zur Erfindung des Flugzeuges. Nachrichten aus dem Karten- und Vermessungswesen. Sonderheft Geschichte der Photogrammetrie. Verlag der Angewandten Geodäsie , Frankfurt a. Main, pp. 17-62

Brandtberg, T., Warner, T.A., Landenberger, R.E., and McGraw J.B. (2003). Detection and analysis of individual leaf-off tree crowns in small footprint, high sampling density lidar data from the eastern deciduous forest in North America. Remote Sensing of Environment, 85:290-303.

Breitenbach, J., Koch, B., Kändler, G., Kleusenberg, A. (2006). Comparison between the use of Lidar- and Radar data to calculate tree heights for forest inventories. Workshop on 3-D in Remote Sensing in Forestry. Vienna 14-15 February 2006.

Dees, M. & Koch, B. (1999). Prosmart Endbericht. Teilvorhaben -ZUFORST (Großräumige Waldinitialinventur - Holzvorrat). Schlussbericht. In: N.N./Dornier Satellitensysteme (Hrsg.). ProSmart. Endbericht. DLR Förderkennzeichen: 50 EE9816, S. 7.1-7.100.

Duvenhorst, J. (1998). Photogrammetrie und Luftbildinterpretationfür bestandes- und stichprobenweise Forstinventuren. Dissertation an der Albert-Ludwigs-Universität. 1998, p. 136

Friedlaender, H., 2002. Die Anwendung von flugzeuggetragenen Laserscannerdaten zur Ansprache dreidimensionaler Strukturelemente von Waldbeständen. Ph.D. dissertation, University of Freiburg, Freiburg, Germany, p. 64.

Garestier, F., Papathanassiou, K. P., Hajnsek, I., Dubois-Fernandez, P., Dupuis, X. (2005). Analysis of forest parameters and agricultural field structures from high resolution Pol-InSAR X-band data. Pol-InSAR 2005 workshop, Frascati, Italy, ESA publication ISBN 92-9092-897-2, 2005.

Gougeon, F. (1995). A Crown-Following Approach to the Automatic Delineation of Individual Tree Crowns in High Spatial Resolution Aerial Images, Canadian Journal of Remote Sensing, 21(3):274-284.

Hajnsek, I. and Papathanassiou, K. P. (2004). The Use of Synthetic Aperture Radar (SAR) Interferometry to Retrieve Bio- and Geo-physical Variables. Final Report. European Space Agency Contract No. 16366/02/NL/MM.

Hellwich, O., Reigber, A., Guillaso, ST., Jäger, M., Neuman, M., Bellmann, A. (2005). Current developments in Airborne SAR Remote Sensing. www.cv.tu-berlin.de/**publications**/

Heyder, U. (2003). Automatische Delinierung und Klassifizierung von Bäumen aus Laser- und Multispektraldaten. Diplom-Thesis, University of Freiburg, Freiburg, Germany, p. 87

Hildebrandt, G. (1993). Fernerkundung in der Forstwirtschaft. Zeitschrift für Photogrammetrie und Fernerkundung, No. 3, pp. 135-138.

Hoekman, D. and Varekamp, C. (1998) . High resolution single-pass interferometric radar observation of tropical rain forest trees. www.**estec**.**esa**.nl/**conference**s/98c07

Hoekmann, D. (2005). Experimental radar provides 3-D forest view. ESA News. The living planet programme. www.esa.int/esaLP/SEMJGLXEM4E_index_2.html

Holmgren, J., Persson, A. (2004) Identifying species of individual trees using airborne laser scanning. Remote Sensing of Environment 90, pp. 415-423.

Hyyppä, J., Schardt, M., Haggren H., Koch, B. (2001). HIGH-SCAN: The First European-Wide attempt to derive single tree information from Laserscanner Data. Photogrammetric Journal of Finland, Vol. 17, Nr. 2 2001:. 58-69.

Hyyppä, J., Yu, X., Rönnholm, P., Kaartinnen, H., Hyyppä, H. (2003b) Factors affecting object-oriented forest growth estimates obtained using laser scanning. The Photogrammetric Journal of Finland 18, pp. 16-31.

Koch B., Diederhagen O., Straub Ch., Weinacker, H. (2006). Standwise delineation based on 3-D information from LIDAR. Proceedings 3-D Remote Sensing in Forestry, 13. bis 14. Feb. 2006, Vienna.

Koch B., Svoboda J., Adler P. and Dees M. (2002): Automatische Baumartenerkennung auf der Grundlage digitalisierter CIR-Luftbilder, Allg. Forst- u. Jagd-Zeitung, 173. Jg., 7-8, 2002: 131-140.

Koch, B., Heyder U., Weinacker, H. (2006). Detection of individual tree crowns in airborne lidar data. An approach to delineate tree crowns in mixed and deciduous temperate forests. Photogrammetric Engineering and Remote Sensing. Accepted, issue scheduled March 2006.

Lefsky, M.A., Harding, D., Cohen, W.B., Parker, G., and Shugart, HH. (1999). Surface lidar remote sensing of basal area and biomass in deciduous forests of Eastern Maryland, USA. Remote Sensing of Environment, 67:83-98.

Magnussen, S., and Boudewyn P. (1998). Derivations of stand heights from airborne laser scanner data with canopy-based quantile estimators, Canadian Journal of Forest Research, 28:1016-1031.

Mallinger, A. (1997). Ermittlung forstlicher Bestandesparameter aus digitalen Oberflächenmodellen, Universität für Bodenkultur, Institut für Vermessung, Fernerkundung und Landinformation, Wien, p. 91.

Mette, T, Papathanassiou, K. P., Hajnsek, I., Pretzsch, H., Biber (2004). Applying a common allometric equation to convert forest height from Pol-InSAR data to forest biomass. IEEE Proceedings IGARSS 2004, Anchorage Alaska, 2004.

Mosch, M. (2006): 3-D Gebäudeextraktion aus Satellitenbilder suburbaner Regionen. Dissertation an der Albert-Ludwigs-Universität Freiburg. 2006, p. 211.

Naesset, E. (1997). Estimating timber volume of forest stands using airborne laser scanner data, Remote Sensing of Environment, 56:1-7.

Naesset, E. (2003). Laser Scanning of Forest Resources – the Norwegian Experience. Proceedings of the ScandLaser Scientific Workshop of Airborne Laser Scanning of Forests, September 3-4, Umea, Sweden, pp. 35-42.

Persson, Å, Holmgren, J., and Södermann U. (2002). Detecting and measuring individual trees using an airborne laser scanner. Photogrammetric Engineering and Remote Sensing, 68(9):925-932.

Pollock, R. (1996). The automatic recognition of individual trees in aerial images of forests based on a synthetic tree crown image model. Ph.D. dissertation, University of British Columbia, Vancouver, Canada.

Poon, J., Fraser, C. S., Chunsun, Z., Li, Z., Gruen, A. (2005). Quality assessment of digital surface models generated from IKONOS Imagery. The Prhotgrammetric Record 20 (110), 2005, pp. 162-171.

Popescu, S. and Wynne, R. (2004). Seeing the Trees in the forest: Using Lidar and Multispectral Data Fusion with Local Filtering and Variable Window Size for Estimating Tree Height. Photogrammetric Engineering and Remote Sensing, Vol. 70(5):589-604.

Popescu, S., Wynne, R., Scrivani, J. (2004). Fusion of Small-Footprint Lidar and Multispectral Data to Estimate Plot-Level Volume and Biomass in Deciduous and Pine Forests in Virgina, USA. Forest Science, 50(4):551-565

Pröbsting, T. (1996). Luftbildgestützte Verfahren für die Forstwirtschaft. Bedarf, Anwendungsbereiche, Auswertungssysteme. Cuvillier Verlag Göttingen, pp. 1-11. ISBN 3-89588-830-3.

Soille, P., 1999. Morphological Image Analysis, Springer, Berlin, 316 p.

St. Onge, B., Achaichia, N. (2001). Measuring forest canopiey height using a combination of lidar and aerial photography data. Proceedings of the workshop on land surface mapping and characterization using laser altimetry, Annapolis, Maryland, USA, 22-24 Oct, 2001.

Straub B.-M., Heipke C. (2001): Automatic extraction of trees for 3D city models from images and height data, in: Baltsavias E., Grün A., von Gool L. (Eds.), Automatic Extraction of Man-Made Objects from Aerial and Space Images (III), A. A: Balkema Publishers, Lisse, 267-277

TopoSys (2003). FALCON LIDAR Sensor System, URL: http://www.toposys.de/system/FALCON%20Outline%20-%20Jan%202003.pdf, (last date accessed: 1 February 2004).

Yu, X., Hyyppä J., Rönnholm, P., Kaartinen, H., Maltamo, M. and Hyyppä, H. (2003). Detection for harvested trees and estimation of forest growth using laser scanning. Hyyppä J., Naesset, E., Olsson, H., Granqvist Pahlen, T., and Reese, H (eds). Proceedings of Scandlaser Scientific Workshop on Airborne Laser Scanning of Forests. Septmeber 3-4, 2003 Umea, Sweden. Swedish University of Agricultural Sciences Department of Forest Resource Management and Geomatics:115-124

# EXTRACTION OF FOREST PARAMETERS IN A MIRE ENVIRONMENT USING AIRBORNE SPECTRAL DATA AND DIGITAL SURFACE MODELS

*Lars T. Waser, Klaus Ecker, Christian Ginzler, Meinrad Küchler, Markus Schwarz and Patrick Thee*

Swiss Federal Research Institute WSL, Department of Landscape Inventories, 8903 Birmensdorf, Switzerland; lars.waser@wsl.ch; klaus.ecker@wsl.ch, christian.ginzler@wsl.ch; meinrad.kuechler @wsl.ch; markus.schwarz@wsl.ch; patrick.thee@wsl.ch

## ABSTRACT

The present study was carried out in the framework of the Swiss Mire Conservation Program which aims at protecting 103 mire ecosystems of national importance and outstanding beauty in their present state. Shrub encroachment and increase of forest area are exerting vehement impact on the non-forest areas of the mire biotopes. The first objective of this study is to predict shrub and tree occurrence in open mire areas using generalized linear models and airborne remote sensing data (CIR-orthoimages, DSM, LIDAR). The second objective is to calculate the probability of each pixel belonging to one of the eight tree genera. This indicates which tree genera are most responsible for the shrub encroachment / increase of forest area. The study area is located in the Pre-alpine zone of Central Switzerland. 23 spectral and geometric explanatory variables are derived from the remote sensing data and step-wise reduced to the most contributing variables for both models. The prediction of shrub occurrence revealed good results with high accuracy. Prediction of tree genera was less satisfactory for all eight tree genera. Distinction was possible for Betula, Pinus and Picea. Further research and new spectral information (as provided by ADS40 data) would be appropriate for more precise prediction. This study also revealed that 3D information as obtained by means of digital photogrammetry is indispensable for modeling shrub / tree occurrence. DSMs may be used for retrospective analysis of shrub encroachment in a mire biotope since old aerial images are often available.

**Keywords:** Swiss Mire Conservation Program, General Linear Model, stand composition, LIDAR, CIR-orthoimage

## 1 INTRODUCTION

The aim of the Federal Mire Conservation Program is to conserve the 103 mire ecosystems of national importance and outstanding beauty in Switzerland in their present state. This implies no decrease of the mire area and no degradation of vegetation. To examine the effectiveness of the conservation status, a long-term monitoring program was set up in 1996. Within this program, the monitoring has to establish whether and how far this aim has been reached. Consequently, the mire areas and their vegetation must be described over time and space in sufficient detail (Grünig 1997; Grünig et al. 2004; Küchler et al. 2004). The monitoring also implies an assessment of shrub encroachment and increase of forest area exerting vehement impact on the non-forest areas of the mire biotopes. Shrub encroachment is a considerable danger for the biotope and accelerates a degradation of the mire area. To assess the magnitude of this impact the extraction of various forest related parameters (e.g. forest area, single tree occurrence, small shrubs, tree genera, canopy height etc.) is essential. However, such information is often difficult to acquire across mire ecosystems using traditional methods of field survey and aerial photograph interpretation. It is well known that obtaining different forest parameters, such as tree heights or stand composition through ground measurements or vegetation mapping is often not feasible in dense forest, too costly in terms of time and manpower, and also prone to errors (St-Onge and Achaichia 2001; Jan 2005, Wang et al. 2004). Costs of forest sampling can be reduced substantially by estimating forest and tree parameters directly from high-resolution remotely sensed data. Providing consistent and reproducible information on land cover at different scales proves to be the main advantage of remote sensing as a tool for both landscape monitoring and ecological analyses (Townshend 1991). Recent progress in three dimensional remote sensing mainly includes digital stereophotogrammetry, radar interferometry and LIDAR (Hyyppä et al. 2000;

Naesset 2002). E.g. by subtracting DTM from the DSM canopy height models can be calculated. DSM can be obtained by means of photogrammetric methods or by LIDAR. Using digital photogrammetry, DSMs are based on ATE algorithms with image correlation. This method is widely used and has proven to provide both, reliable and accurate results (Zhang and Miller 1997b). DTMs have been derived from manual photogrammetric or terrestrial measurements for a long time already (Gruen and Baltsavias 1987; Ackermann 1996b). Meanwhile several LIDAR systems are commercially available (e.g. Baltsavias 1999), enabling the derivation of DTMs from such data as well.

A number of studies reveal the successful application of these methods to assess tree (Persson 2002; Morsdorf et. al 2004) and stand attributes (stand composition, tree height, crown diameter, basal area, stem volume). Combining some of these attributes can be useful to evaluate growth estimations (including extent of forest area) and to detect changes in the forest stands (Lefsky et al. 2002; Schardt et al. 2002b; Naesset 2002; Yu et al. 2004). On the other side, a narrow tree apex is often missed by LIDAR hits or the top of a small tree is covered by branches of a tall tree. E.g. Naesset (1997), St-Onge (1999b), Heurich et al. (2003b) reveal in their studies that both DSMs of aerial images and LIDAR data systematically underestimate tree heights.

Spatially explicit predictive modeling of vegetation is often used to construct current vegetation maps using information on the relations between current vegetation structure and various environmental attributes (Davis and Goetz 1990 and Brown 1994). Guisan and Zimmermann 2000, Scott et al. 2002a point out that modern regression approaches have proven particularly useful for the modeling of the spatial distribution of tree species and communities. Thus, in combination with regression analyses airborne remote sensing data may considerably help to assess the increase of forest area in a mire ecosystem. Estimates of shrub encroachment of a region can then be used to focus on targets in inventories so that appropriate levels of sampling can be reached in these areas. To predict the magnitude of shrub encroachment might be helpful for conservation efforts in a mire, e.g. for an assessment of the mire itself and for future protection planning.

The present study was established in the framework of the Swiss Federal Mire Conservation Program which aims at conserving the mire biotopes in their entirety. The first objective of this study is to predict shrub and tree occurrence in open mire areas using generalized linear models and airborne remote sensing data. The second objective is to calculate the probability of each pixel belonging to one of the eight tree genera. This indicates which tree genera are most responsible for the shrub encroachment / increase of forest area.

# 2 MATERIAL AND METHODS

## 2.1 Study Area

Methods have been developed and tested for the mire “Eigenried” located in a north to south oriented plateau in the East of Lake of Zug, a sensitive environmental area in the Pre-alpine zone of Central Switzerland (approx. 47°07’ N and 8°32’ E). Parts of the region were drained in the last century. Most of the artificial ditches are still active – only a few are refilled. The mire is characterized by its rough micro relief with pastures that are crossed by shrubs and bright broad-leaved woodland (see figures 1 and 2). The altitudes inside the study perimeter vary from 850 m to 1000 m above sea level. The core area of the mire has an extent of 1.72 $km^2$. The dominant vegetation types are moist and wet meadows and pastures (Potentillo-Polygonetalia, Molinietalia caeruleae), low sedge poor fen (Caricetalia fuscae), bog forest (Sphagno-Betuletalia) and broad-leaved woodland and willow Carr. The bordering forested area, with an extent of approx. 2 $km^2$, is mostly characterized by opened mixed forest (40%) and coniferous forest (60%) with few storm losses and some new reforestations.

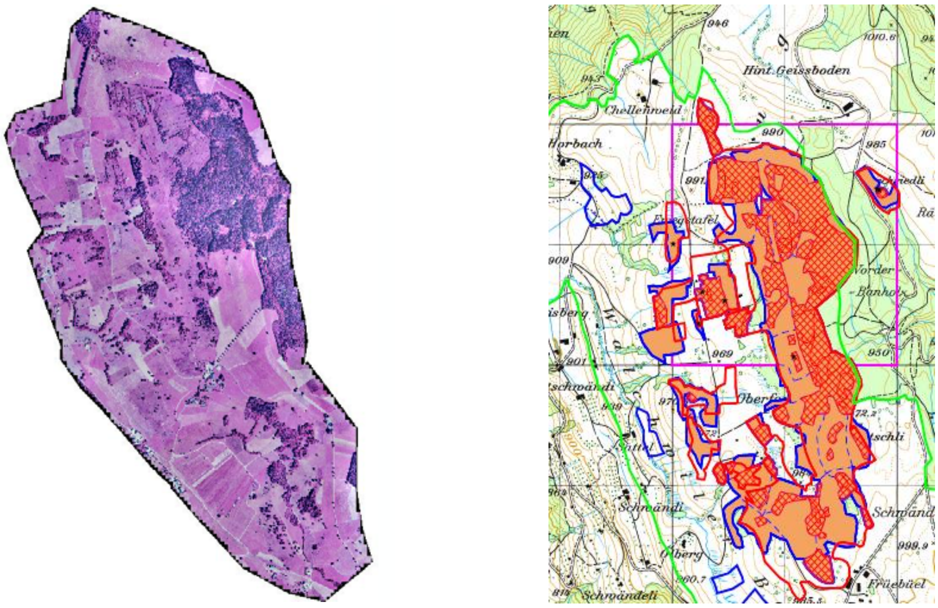


*Figure 1: Overview of the mire Eigenried (CIR-orthophoto © WSL 2003 and pixelmap © 2006 Swisstopo JD052552).*

*Figure 2: Bright broad-leaved woodland and mixed forest with meadows and pastures are typical for the site.*

## 2.2 Data

### 2.2.1 Remote sensing data

The fundamental datasets we used where the following: a digital CIR orthoimage of the year 2003, a corresponding digital surface model (DSM) using aerial images of 2003, and LIDAR terrain and surface models of 2002. The orthoimages provides a ground resolution of 0.3 m. Each image offers three color bands of numerical information with 256 intensity levels: visible green (500-600 nm), visible red (600-700 nm) and near infrared (750-1000 nm). From the set of stereo-pairs a DSM of 2003 with a spatial resolution of 0.5 m was created using the ATE facilities in SocetSet 5.1 from BEA Systems. The strategy for the DSM by means of digital photogrammetry applied to this study was specifically designed for mires at the Swiss Federal Research Institute (WSL) considering the specific conditions of open land in mire environments. The result is a less smoothed surface where terrain artefacts are skipped and single trees and bushes are clearly extracted. The DSM has a vertical accuracy of < 0.5 m. The LIDAR data were acquired in 2002 (leaf-on) with a mean density of one point per 2 $m^2$ depending on the terrain. Through several processing steps a DTM model was obtained from LIDAR last pulse information. The resulting DTM has a grain of 2.5 m and a vertical accuracy of 0.5 m to 1 m (Artuso et al. 2003b).

### 2.2.2 Field data

Field work was performed in 2003, estimating canopy closure and mapping dominant tree genera in 173 homogeneous areas in selected parts of the mire. These 173 records cover 10% of the entire mire area and serve as reference data for the tree cover and for model calibration data for the prediction of the tree genera. For the validation of tree genera we used the information on 130 tree individuals that was collected in a field survey in 2005.

## 2.3 Preliminary tree cover

The following example of a tree cover was developed at the Swiss Federal Research Institute WSL for the Federal Mire Conservation Program. This semi-automated extraction of trees was applied to all 103 mire biotopes and serves as basis for the extraction of small shrubs in this study. In a first step, a normalized DSM was generated by subtracting a resampled and smoothed LIDAR DTM from the fine DSM derived from the aerial images. Then a canopy cover was calculated by a multistage procedure using slope data of the DSM (see Fig. 3). This simple but robust algorithm mainly depends on a slope threshold determined by the grid spacing of the DSM and the surface height. Additionally, problematic features and errors are avoided by an object-oriented image analysis using spectral information of the CIR-orthoimages. This implies a two stage process with a multi-resolution segmentation and a fuzzy classification. Considering the fact that objects bulge the ground and produce shadow, respectively, enables us to identify and remove incorrect pyramids, when they do not border or cover a shadow object. The resulting tree layer is cleared from most of the previous errors and mirrors the real occurrence of trees with high accuracy. It serves as response variable in the model for the extraction of small shrubs / trees in this study.

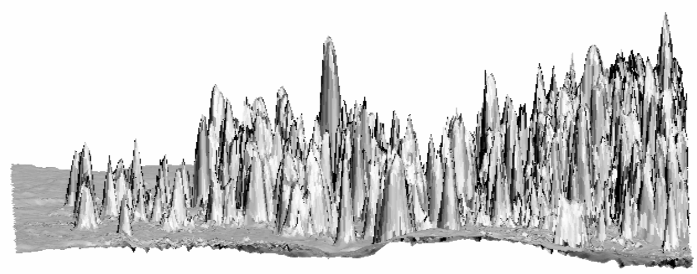

*Figure 3: Trees as detected in shaded normalized DSM 0.5 m (superelevation 5x)*

## 2.4 Extraction of small shrubs in open mire areas

To model pixel-wise shrub occurrence and tree genera probability our calculated tree cover has to be refined using additional variables. In this study, an attempt was made to develop a model that would be general, as well as applicable to other mire biotopes. Thus, only terrain and spectral variables that are available for all 103 mires of the Federal Mire Conservation Program are included as potential explanatory. Logistic regression is often used to predict probabilities for presence/absence of a specific vegetation type (or species) at each point (see e.g. Toner and Keddy 1997). A shrub occurrence map or a tree genera map can be constructed by analysis of these probabilities' actual occurrence. Models in this study were developed using a 2 m, 1 m and 0.5 m spatial resolution. The prediction of shrub occurrence is preliminary based on the previously developed tree cover. A logistic regression serves as our model, assuming a binomial distribution (see e.g. McCullagh and Nelder 1983a). In a first step, the total of 23 parameters was derived from the DTM, DSM and of the CIR-orthoimages. Altogether, seven spectral variables derived from the three color bands (three original and three ratio mean variables) and one variable containing an isocluster-classification of the CIR-orthoimage using 24 color classes were obtained. Additionally, 16 terrain variables (slope, aspect, and curvature) are derived from the DTM and DSM. In a second step, these 23 parameters have been tested for their model contribution and finally reduced to the most effective parameters. The 5 remaining parameters serve as explanatory variables for the final model and are solely derived from the DSM. Model accuracy was lower using also spectral variables. As response variable we used the previously extracted tree cover. The result (fitted values) is the probability for each pixel to represent a tree or a part of a tree.

### 2.5 Prediction of tree genera

The prediction of the tree genus is primarily based on the occurrence of shrubs - all pixels with a tree probability of less than 0.2 are skipped. As model we used a multinomial regression (multinomial due to the fact that we use different genera (eight categories): Acer, Betula, Frangula, Populus, Salix, Sorbus, Picea, Pinus. For an optimal distinction between the different genera we additionally used 6 spectral variables (original channels and ratio mean of channels) together with our 5 terrain parameters (all derived from curvature) as explanatory variables. The response variable is the dominant tree genus from each of the 173 field records. Subsequently, the predicted stand composition was extrapolated to the entire mire area. To validate the model we used over 130 tree individuals which were selected by an expert in the mire area representing the eight dominant tree genera.

## 3 RESULTS

### 3.1 Extraction of small shrubs / trees in open mire areas

Many small shrubs and trees are missed when modeling with 2 m spatial resolution. Small shrubs are significantly better detected using a spatial resolution of 1m. Best results are obtained with a spatial resolution of 0.5 m although incorrectly assigned pixels increase slightly (figure 4).

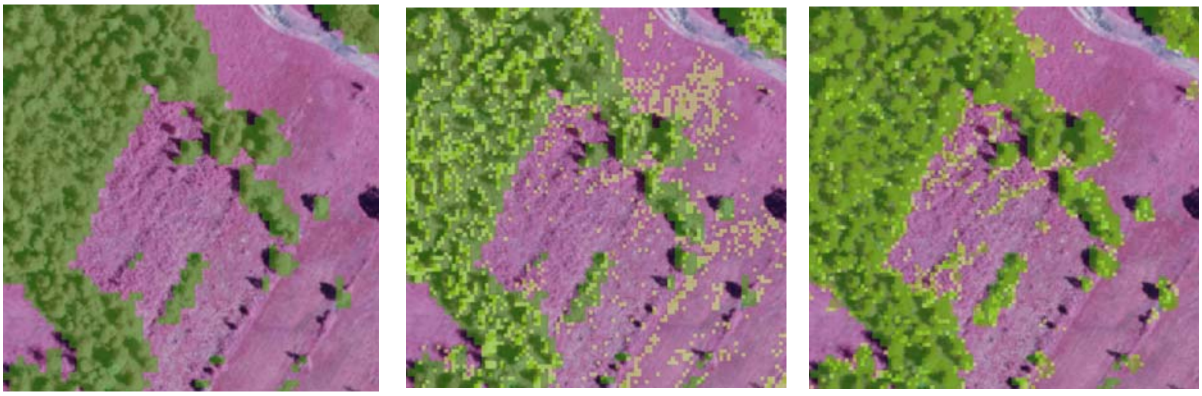

*Figures 4: a) Preliminary tree cover, b) tree cover using all spectral & DSM variables c) final tree cover allowing extraction of small shrubs / trees only using variables of the DSM*

Figure 4 illustrates the procedure from the tree cover to the extraction of small shrubs: the preliminary tree cover serves as basis for the logistic model (a). Using both spectral and terrain variables results in an over-detection of shrubs. Together with shrubs, pasture and herbage, ditches are also detected (b). The skipping of variables that are less contributively to the model reduces this over-detection significantly and therefore improves the extraction of real shrubs / small trees (c). This reduction is important for the further use of this more detailed tree cover. Visual tests using stereo-image interpretation revealed that pixels classified as shrubs with a probability less than 0.2 are still wrong and mostly belong to tall grasses. Correlating the detailed tree cover with the field mapping of the 173 homogeneous areas revealed a correlation coefficient of 0.87 using only pixels with a tree probability of > 0.2.

Figure 5 illustrates the fraction of forest for each pixel. A fraction of 80-100% represents the tree cover. Pixels less than 20% are ignored and not further used. Most shrubs and small trees have values between 60-80%.

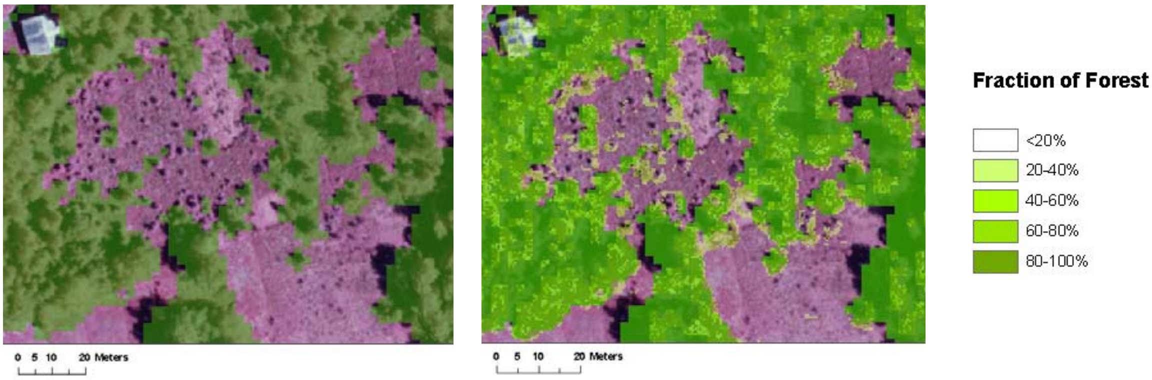


*Figures 5: a) Preliminary tree cover, b) fraction of forest as obtained by logistic regression*

## 3.2 Prediction of stand composition

The prediction of the stand composition is primarily based on the occurrence of shrubs – therefore a threshold of 0.2 was chosen that keeps all pixels belonging to real shrubs in open mire area and ignores incorrect shrub pixels. The prediction is validated with field samples of 130 tree individuals belonging to 4 groups: single trees, group of trees, trees at forest border, and trees within forest. A first test of predicting eight genera revealed no satisfactory results. E.g. it was not possible to predict Acer, Frangula, Populus although they are the dominant genera in several parts of the mire. Better prediction was obtained for Betula pubescens, Picea abies and Pinus silvestris. Prediction of these genera produced an overall accuracy of 0.83, a kappa coefficient of 0.73 and a gamma of 0.94. The latter is equivalent to the correlation coefficient. An independence test revealed that the classification of the tree individuals does not depend on their group affiliation. Table1 shows the detailed accuracies for each group of tree individuals.

*Table 1: Overview of accuracies for each group of tree individuals*

| Tree individuals belonging to | Overall accuracy | kappa | gamma |
|---|---|---|---|
| Single tree | 0.738 | 0.573 | 0.903 |
| Group | 0.833 | 0.706 | 0.963 |
| Forest border | 0.91 | 0.751 | 0.965 |
| forest | 0.833 | 0.739 | 0.894 |

Best accuracies are obtained for tree individuals that are located at the forest border. Highest gamma values are obtained for both trees in groups and at the forest border. Model prediction for an individual pixel/tree belonging to deciduous or coniferous forest rises to an overall accuracy of 0.98, a kappa coefficient of 0.961 and a gamma of 0.98. A more precisely look at the results reveals that prediction of coniferous trees (Picea versus Pinus) reveals less accurate results. Distinction between Pinus and Picea produced an overall accuracy of 0.72, a kappa coefficient of 0.39 and a gamma of 0.69. Table 2 shows highest overall accuracy for predicting Pinus and Picea within forest (0.85) and lowest for single tree individuals (0.56). Overall accuracy for trees belonging to the forest border is not possible since no Picea are represented. An independence test revealed that the distinction between Pinus and Picea depends on their group affiliation.

*Table 2: Distinction of Pinus and Picea: overall accuracies for each group of tree individuals*

| Tree individuals belonging to | Overall accuracy |
|---|---|
| Single tree | 0.56 |
| Group | 0.68 |
| Forest border | N.A. |
| forest | 0.85 |

## 4 DISCUSSION AND CONCLUSIONS

The preliminary tree cover served as starting point for the prediction of small shrubs in this study. It is a product of combining high-resolution DSM in a two stage process with a multi-resolution segmentation and fuzzy classification of the CIR orthoimages and was especially developed for mire environments. It was successfully applied to all 103 mire biotopes and serves as basis for vegetation modeling. This fuzzy classification enabled to identify and remove incorrect pyramids in the DSM, when they do not border or cover a shadow object, considering the fact that objects bulge the ground and produce shadow, respectively. Most of the previous errors have been eliminated from the resulting tree cover which therefore mirrors the real occurrence of trees with high accuracy.

The first objective, a prediction of shrub occurrence using a logistic model revealed satisfactory results. The step-wise selection of various variables derived from the DTM, DSM and of the CIR-orthoimages proved to be a good approach for the model. Shrub prediction was more accurate only using 5 terrain parameters. In this case tall grass (e.g. Molinia sp) was not predicted as shrub (due to its shape in the DSM) as it was using also spectral variables. Ignoring pixels with a probability < 0.2 helped us to extract real small shrubs and trees (<1.5 m) in the open mire area. Visual stereo image interpretation revealed that pixels with a probability of > 0.2 mostly belong to a shrub / tree. The detection of these shrubs is substantial for assessing shrub encroachment and extracting potential areas of encroachment over the entire area. Shrub encroachment often starts on small vegetation islands where a group of tree / shrubs are settled. This is high risk for the biotope and accelerates degradation of the mire area.

The second objective, a prediction of tree genera, was not satisfactory for all eight tree genera. Distinction was possible for Betula, Pinus and Picea. In general, Pinus are predicted more precisely than Picea. An analysis of the results reveals a certain trend: if the model predicts a Pinus it actually is a Pinus to 95%, if the model predicts a Picea it is actually only a Picea to 65%. The quality of the prediction of Picea and Pinus depends on the assignment to forest, forest border, and groups of trees or single tree. If the pixels belong to close forest and groups of trees the prediction is satisfactory. In contrary, a visual image interpretation allows to separate Pinus and Picea quite well. This is possible because Acer, Frangula, Sorbus are often partly covered by other tree genera. Test in other regions of Switzerland revealed that Leica ADS40 provides the spectral information as needed for detection of stand composition and tree species. In our case, to predict more tree genera the additional blue channel of ADS40 in combination with our DSM parameters would be most promising.

Furthermore, the study clearly showed that 3D information as obtained by the 0.5 m DSM is indispensable for prediction of shrub occurrence and tree genus. Preliminary tests showed that using the same terrain variables derived from the first pulse LIDAR data revealed less accurate results. This is due to its lower spatial resolution of 2.5 m. Small trees are often missed by LIDAR hits and the data were not consequently acquired during the vegetation period. An advantage of the LIDAR would be that first and last pulse is area-wide available for Switzerland in regions below 2000 m a.s.l. A disadvantage of this data is that it was only once acquired in 2002. According to Lillesand and Kiefer (1994a) aerial photographs have been archived in many countries for decades and therefore can be used for retrospective studies, even if the images are only in black and white. This also implies the generation of retrospective digital surface models. These are the two main advantages of aerial images also in Switzerland. To summarize:

- Generalized linear models are appropriate for the prediction of forest related parameters in a mire environment.
- Prediction of small shrubs and trees in open mire areas produced satisfactory results and therefore may be helpful for estimates on shrub encroachment in a mire biotope.
- Prediction of tree genus was not satisfactory or partly satisfactory respectively. Further research and new spectral information (as provided by ADS40 data) would be appropriate.
- 3D information as obtained by means of digital photogrammetry is indispensable for modeling shrub / tree occurrence. DSMs may be used for retrospective analysis of shrub encroachment in a mire biotope since old aerial images are often available.
- Possible sources of error should be discussed more in detail.

## ACKNOWLEDGEMENTS

The study was carried out in the frame of the Swiss mire monitoring program initiated in 1996 at the Swiss Federal Research Institute WSL and funded by the Swiss Agency for the Environment, Forest and Landscape and WSL. We are grateful to Ruedi Boesch and Ulrich Graf for fruitful comments and Heidi Paproth for linguistic improvements.

## REFERENCES

Ackermann, F. (1996a). Techniques and strategies for DEM generation, p.135-141, In: C. Greve, (ed.), Digital photogrammetry: An addendum to the manual of photogrammetry. ASPRS, Bethesa, Md.

Artuso, R., Bovet, St. and Streilein, A. (2003b). Practical methods for the verification of countrywide terrain and surface models. Proceedings of the ISPRS working group III/3 workshop XXXIV-3/W13. 3-D reconstruction from airborne laserscanner and InSAR data. Dresden, Germany, 8-10 October 2003.

Baltsavias, E. (1999). Airborne laser scanning: existing systems and firms and other resources. ISPRS Journal of Photogrammetry and Remote Sensing 54:164-198.

Brown, D. G. (1994). Predicting vegetation types at tree line using topography and biophysical disturbance variables. Journal of Vegetation Science 5:641-656.

Davis, F. W., and Goetz, S. (1990). Modeling vegetation pattern using digital terrain data. Landscape Ecology 4:69-80.

Gruen, A. and Baltsavias, E.P. (1987). High Precision Image Matching for Digital Terrain Model Generation. Photogrammetria 42:97-112.

Grünig, A., Steiner, G.M., Ginzler, C., Graf U. and Küchler, M. (2004). Approaches to Swiss mire monitoring. Int. Peat Journal 12:55-73.

Grünig, A. (1997). Surveying and Monitoring of mires in Switzerland. In: Parkyn L., Stoneman R.E., Ingram H.A.P. (eds): Conserving peatlands, Oxon, UK, CAB International: 217-227.

Guisan, A. and Zimmermann, N.E. (2000). Predictive habitat distribution models in ecology. Ecol. Model. 135: 147-186.

Heurich, M., Schneider, T., Kennel, E. (2003b). Laserscanning for identification of forest structure in the Bavarian forest national park. In: Hyppä J., Naesset H., Olssen H., Granqvist Pahlen T., Reese H. (editors). Proceedings of the ScandLaser Scientific Workshop on Airborne Laser Scanning of Forests, September 3-4, 2003, Umea, Sweden, Swedish University of Agricultural Sciences, Department of Forest Resource Management and geomatics, 2003, pp. 98-107.

Hyyppä, J., Hyyppä, H., Inkinen, M., Engdahl, M., Linko, S. and Yi-Hong, Z. (2000). Accuracy comparison of various remote sensing data sources in the retrieval of forest stand attributes. Forest Ecology and Management 128:109-120.

Jan, JF. (2005). Comparison of forest canopy height derived using LIDAR data and aerial photos. Taiwan Journal for Science 20:13-27.

Küchler, M., Ecker, K., Feldmeyer-Christe, E., Graf, U., Küchler, H. and Waser, L.T. (2004). Combining remotely sensed spectral data and digital surface models for fine-scale modelling of mire ecosystems. Community Ecology 5:55-68.

Lefsky, M.A., Cohen, W.B., Parker, G.G. and Harding, D.J. (2002). LIDAR remote sensing for ecosystem studies. BioScience 52:19-30.

Lillesand, T.M. and Kiefer, R.W. (1994a). Remote Sensing and Image Interpretation. John Wiley & Sons, New York Chichester Brisbane Toronto Singapore, pp. 750.

Morsdorf, F., Meier, E., Kötz, B., Itten, K.I., Dobbertin, M. and Allgöwer, B. (2004). LIDAR-based geometric reconstruction of boreal type forest stands at single tree level for forest and wild land fire management. Remote Sens. Environ. 92:353-362.

McCullagh, P. and Nelder, J.A. (1983a). Generalized linear models. Chapman and Hall, London, 261pp.

Naesset, E. (1997). Estimating Timber Volume of Forest Stands using Airborne Laser Scanning Data. Remote Sens. Environ. 61:246-253.

Naesset, E. (2002). Predicting forest stand characteristics with airborne scanning laser using a practical two-stage procedure and field data. Remote Sens. Environ. 80:88-99.

Persson, Å., Holmgren, J. and Söderman, U. (2002). Detecting and measuring individual trees using an airborne laser scanner. Photogrammetric Engineering and Remote Sensing 68:925-932.

Schardt, M., Ziegler, M., Wimmer, A., Wrack, R. and Hyyppä, J. (2002b). Assessment of forest parameters by means of laser scanning. In: Proceedings from the International Society for Photogrammetry and Remote Sensing (ISPRS). Commission III Symposium, Graz 2002, Austria, September 9-13, vol. XXXIV, Part 3A, pp. 302-309.

Scott, J.M., Heglund, P.J., Samson, F., Haufler, J., Morrison, M., Raphael, M. and Wall, B. (2002a). Predicted Species Occurrences: Issues of Accuracy and Scale. Island Press, Covelo, California.

St-Onge, B., (1999b). Estimating individual tree heights of the boreal forest using airborne laser altimetry and digital videography, ISPRS Workshop on "Mapping surface structure and topography by airborne and spaceborne lasers", Commission III, Working Group 3, La Jolla, Calif., 9-11 November 1999, pp. 179-184.

St-Onge, A. and Achaichia, N. (2001). Measuring forest canopy height using a combination of LIDAR and aerial photography data. International Archives of Photogrammetry and Remote Sensing, XXXIV-3/W4:131-137, 2001.

Toner, M. and Keddy, P. (1997). River hydrology and riparian wetlands: A predictive model for ecological assembly. Ecological Applications 7:236-246.

Townshend, J., Justice, C., Li, W., Gurney, C. and McManus, J. (1991). Global land cover classification by remote sensing - Present capabilities and future possibilities. Remote Sens. Environ. 35:253-255.

Wang, L., Gong, P. and Biging, G.S. (2004). Individual Tree-Crown Delineation and Treetop Detection in High-Spatial-Resolution Aerial Imagery. Photogrammetric Engineering & Remote Sensing 70:351-357.

Yu, X., Hyyppä, J., Kartinen, H. and Maltamo, M. (2004). Automatic detection of harvested trees and determination of forest growth using airborne LIDAR scanning. Remote Sens. Environ. 90:451-462.

Zhang, B. and Miller, S.B. (1997b). Adaptive automatic terrain extraction. McKeown, D.M., McGlone, J.C. and Jamet, O. (eds.), Integrating photogrammetric techniques with scene analysis and machine vision III, Proceedings of SPIE, Volume 3072, pp. 27-36.

# STAND HEIGHT ESTIMATIONS USING AERIAL IMAGES AND LASER DATASETS

*Josef Abraham[1], Radim Adolt[2]*

[1] University of Natural Resources and Applied Life Sciences (BOKU), Institute of Surveying, Remote Sensing and Land Information, Vienna, Austria; josef.abraham@boku.ac.at

[2] Mendel University of Agriculture and Forestry in Brno, Faculty of Forestry and Wood Technology, Brno, Czech Republic; adolt@mendelu.cz

## ABSTRACT

Effective and reliable biomass evaluation of forest stands is one of the most challenging issues in forestry today. Stand height is one of the most useful variables providing a link to biomass assessment. This article focuses on comparison of three types of data sources and combinations of these sources in the process of stand height assessment.

Our methods are based on creation of normalized DSM (nDSM) and comparison of several variables derived from nDSM to height values obtained from a field survey. The differences found are analyzed in detail. The spatial autocorrelation of differences is also explored. We used semivariogram models and a crossvalidation procedure to model spatial distribution of differences.

The study area is in the Drahanska vrchovina massif in the Czech Republic. The prevailing species are beech, larch and spruce, all of which are found in both pure and mixed stands. The spatial extent of the evaluated area is approximately 1 square kilometer. An analysis (namely height and stem diameter measurements, species identification and tree crown delineation on orthophoto printouts) of more than 2000 individual trees was carried out and mean plot variables were assessed (height, basal area and diameter). In order to evaluate the DGM's accuracy several vertical profiles were measured tacheometrically.

Our first approach uses stereophotogrammetric evaluation of DSM from aerial CIR images (summer aspect) and substracts DGM provided by the Czech cadastral service (CUZAK). The second approach employs a DGM derived from stereophotogrammetric measurements on winter images. Finally our third method builds on DGM as a result of a laser scanning mission. The results show that the combination of photogrammetrically obtained DSM and laser derived DGM can provide quality information about the height structure of a forest stand with a low frequency of outliers. The results achieved using photogrammetrically obtained DGM are also very promising but the accuracy of the DGM within densely vegetated areas remains insufficient. Therefore an approach using more overlapped (up to 90% ) stereo pairs from a high resolution digital camera is discussed.

**Keywords:** Tree height, Digital terrain model, Winter images, Laser scanning

## 1 INTRODUCTION

Determining forest inventory parameters is necessary for investigation of the state of a forest and detailed economic planning. In the Czech Republic forest inventory tasks have always been performed in a classical manner not developped further since 1950's. However, determination of forest parameters by terrestrial methods is becoming to be less economically acceptable. Our hope is that classical terrestrial inventory can be modified and its cost may be decreased by the use of remote sensing data. One of the main goals of our work was to evaluate the suitability of using various data sources to obtain tree stand height, as this is one of the most important stand characteristic in forest inventories and planning. Recently a huge attention has been paid primarily to laser based approaches and their applicatoin for the purposes of tree height estimation and forest inventories. This trend is understandable given the fact that one of the key data for obtaining tree height is terrain information, which can be reliably obtained using laser data. Photogrammetric procedures for digital terrain model (DTM) creation are difficult to use in forest areas because of "ground invisibility". A considerable part of European forests is comprised of broad-leaf trees, which lose their leaves in winter season. Our initial guess was if the leaf-off state of forest makes the measurements of ground points possible. Next we wanted to test whether it is possible to use winter images for DTM creation and if so, how accurate the resulting DTM is. We also focused on other sources of height information: specifically, on evaluating the suitability of commercially available DTM and on a combination of laser data and aerial images for tree height estimation. Our work was part of the BORKY project of a MZLU Brno grant project.

# 2 METHODS

## 2.1 Study area

The study area is located in the Czech Republic near Brno. The altitude varies from 380 to 520m above sea level. Prevailing tree species are beech, larch and spruce in unmixed as well as mixed stands. This test area of aproximately 6 km2 was chosen for its landscape variability and vegetation diversity. The investigations presented in this paper were applied over a 2km$^2$ site situated in the central part of the research area.

## 2.2 Input data

### 2.2.1 Aerial Images

In this project two different aerial images datasets were used: summer images and winter images. For DSM creation purposes and other applications, the area was photographed using infrared film at the end of September 2003 and six months later, in April 2004, winter images (also infrared film) were acquired as input for DTM creation. Aerial images were scanned to 1200 Dpi and 8bit per Band. After estimation of interior and exterior orientation parameters using ERDAS Orthobase, 12 stereopairs were created. The nominal scale of summer and winter images was 1:10 000.

### 2.2.2 Laser data

In order to obtain the most precise DTM possible, laser images were also taken in the leaf-off season. Helicopter-based laser scanning was performed by the TOPEYE company over an area that was identical to the 1x2km site where photogrammetric approaches for DTM creation were applied. The first and last pulses were recorded with an average density of 30 points per 1m$^2$ with a pulse rate of 50.000 Hz. Since the guaranteed accuracy lies in the centimeter range, the DTM derived from laser data was determined as a reference data source for photogrammetrically-obtained DTM.

### 2.2.3 DTM from the Cadastral Service (DTM CUZK)

One of the project goals was to verify whether it is possible to use a commercially available elevation data source for the purposes of determining tree heights. This source was provided by the Czech Cadastral Service with a 5m pixel resolution.

### 2.2.4 Reference Data

Data collection using ground methods was conducted in the area in order to evaluate the precision of the DTM and tree height. Using theodolites, about 500 terrain points were measured on the reference site with centimeter precision in ground distance and height. The DTM derived from this point field were used to check the photogrammetric and laser DTM.

For the purposes of determining stand parameters, specifically height for this project, about 2000 trees were examined in detail in the area. The location of each tree on the image was determined and the diameter and height of each tree was measured on the ground. However only 610 of these trees were situated in the area where laser scanning was performed and could be used for tree height evaluation.

## 2.3 Software

ERDAS and its Orthobase module were used to process the photo data from the summer and winter images for estimation of interior and exterior parameters and Stereoanalyst was used for photogrammetric evaluations. PHOTOPOL and ERDAS IMAGINE were used to create digital surface model (DSM). Laser data were processed using TERRASCAN and ARCGIS software. Geostatistical tool (GSTAT) and R (classical statistical analysis) were used for statistical analyssis and modellig of tree height information.

## 2.4 Methodological approach

### 2.4.1 DTM Creation Using the Photogrammetric Method

In order to prove the effectiveness of the photogrammetrical approach for creating terrain models in wooded areas, a site representing various terrain structures and vegetation coverage had to be chosen. Winter aerial images were amended to improve their visual interpretation. Tree shadows lying in one direction, almost perpendicular to the flight path, were sharpened using Fourier filtration.(Fig. 1) In regard to the fact that the vast majority of the shadows were lying on the ground, the ground surface was therefore sharpened. Using shadows for photogrammetric purposes understandably assumes that their position does not change as a result of tree movement due to wind. In our case this assumption was fulfilled.

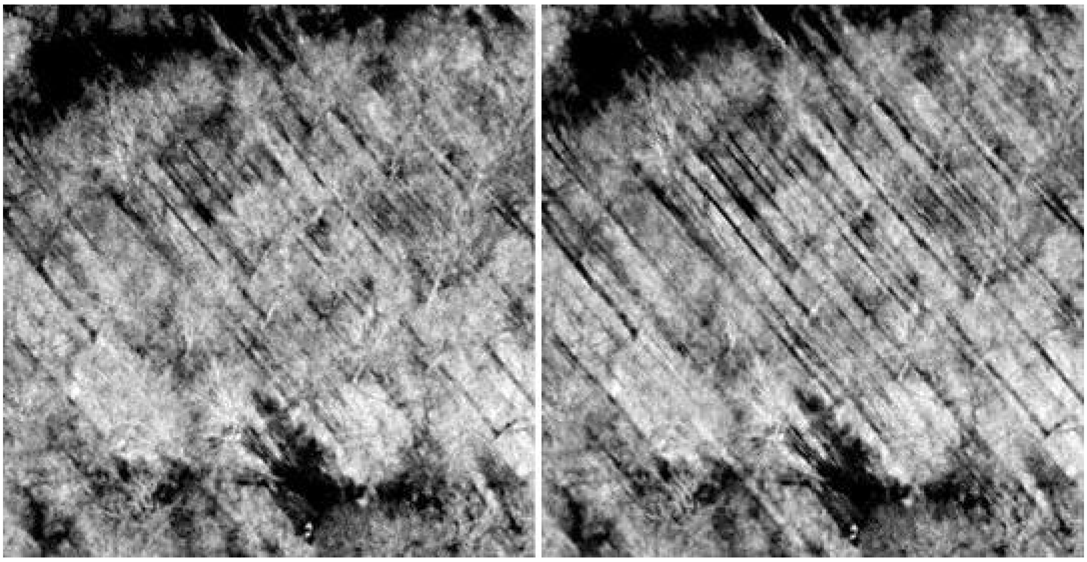

*Figure 1: Original winter image (left) sharpened by Fourier filtration (right)*

In terms of saving time, the ideal way to create DTM is application of automatic methods. However, this method was not used because it was impossible to filter the resultant point clouds. For this reason, the DTM from the winter images was created using data obtained manually. The density of the point field was optimized in regard to terrain variability. In areas with breaklines or terrain irregularities the density was greater and in areas with regular terrain fewer points were measured. Precision was emphasized to the greatest extent possible during measuring. The final average density of points was 25 points per hectare.

### 2.4.2 DSM Creation

Summer images were used to create the DSM. In order to improve the quality of the image information, the principal component was computed and images from the first component were used to create the DSM, while keeping 99% of the information from all three bands. This DSM was determined automatically using the image-matching capability of Leica and Photopol software. After comparing the results of the matching, we decided to utilize the results from the Photopol program in our subsequent work. The program uses feature based matching, the parameters of which can be optimized for specific data. In order to achieve the highest possible quality, we selected a point density network of 0.5m, which appears to be ideal in regard to the difficulty of the calculation and the number of points on one tree crown. The point cloud obtained through the image matching approach was filtered using outliers filtering applied to the normalized DSM.

### 2.4.3 Tree Height Estimation

The heights of 610 individual trees were evaluated using subsets of nDSM points defined by 2 meters radii around known tree top positions. The applied radius was chosen based on the semivariogram model for digital values of the red band layer (a spectrozonal image taken in summer season), (Fig. 2).

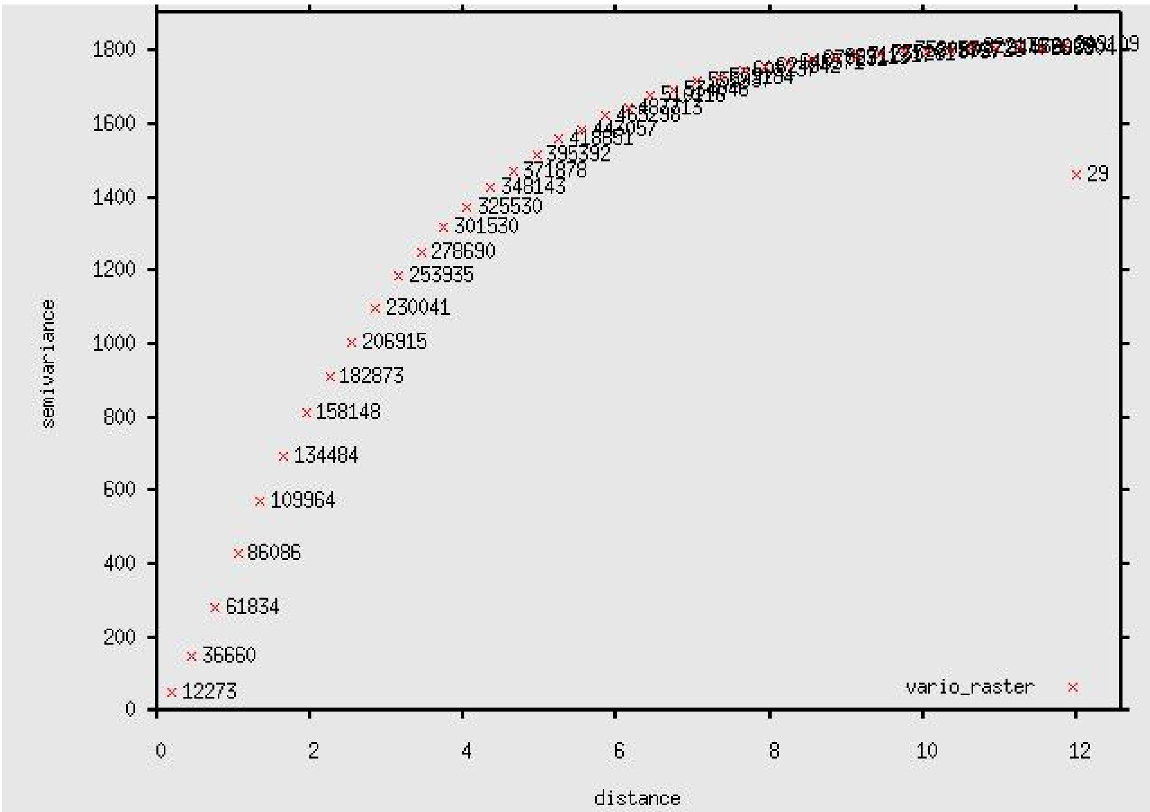


*Figure 2: Semivariogram model for digital values of the red band (summer images)*

The semivariogram clearly shows spatial dependency up to a distance of 6 meters. An ad-hoc assumption was taken, supposing that one third of the semivariogram range is a reasonable neighbourhood size that is generally suitable for small as well as larger tree crowns. Each subset contained approximately 25 – 50 nDSM points, from which distinct characteristics serving as height estimators for particular trees were calculated. The arithmetic mean, median, 75% percentile and 95% percentile were selected and evaluated in respect to variance of estimation error and robustness to outlier occurrence. For each tree the difference between the height as measured from the ground and the nDSM based height was evaluated. Means and variances of these differences were calculated for each species. In addition the correlation between the DBH (diameter at breast height) and observed height differences were studied using simple linear models. The significance of these models was tested using ANOVA. A null hypothesis supposes that the given linear model does not improve prediction when compared to a simple mean value model. Spatial autocorrelation of differences was explored using an empirical semivariogram.

For each species, a required number of height estimations was calculated. The criterion was a maximum 95% error of the arithmetic mean height, namely 1 m for all species. The calculation was based on the Lindeberg-Levy's theorem, which states that the sum of two random variables has a variance equal to the sum of their individual variances. One source of randomness was the height variability of trees within a stand and the second was the variance of nDSM height errors (both variances were evaluated per species).

# 3 RESULTS

## 3.1 DTM

Comparison of the DTM CUZK with the reference data shows that this source of height data is not suitable for our purposes. The error range was -28 to 19 meters and its dispersion was more or less random. Such data can be used solely for very rough analyses of the terrain or height or for simple visualizations.

The DTM created photogrammetrically is sufficiently precise, even in areas where we did not expect it to be so. Fig. 3 shows the difference between the DTM derived from laser points and the photogrammetrically measured DTM. More than 90% of the investigated area indicates a deviation up to 0.5m. The greatest deviation of the DTM appears in places with dense vegetation cover or terrain anomalies such as cliffs and dark valleys. In such places, terrain error is in the range of 3 to 4m.

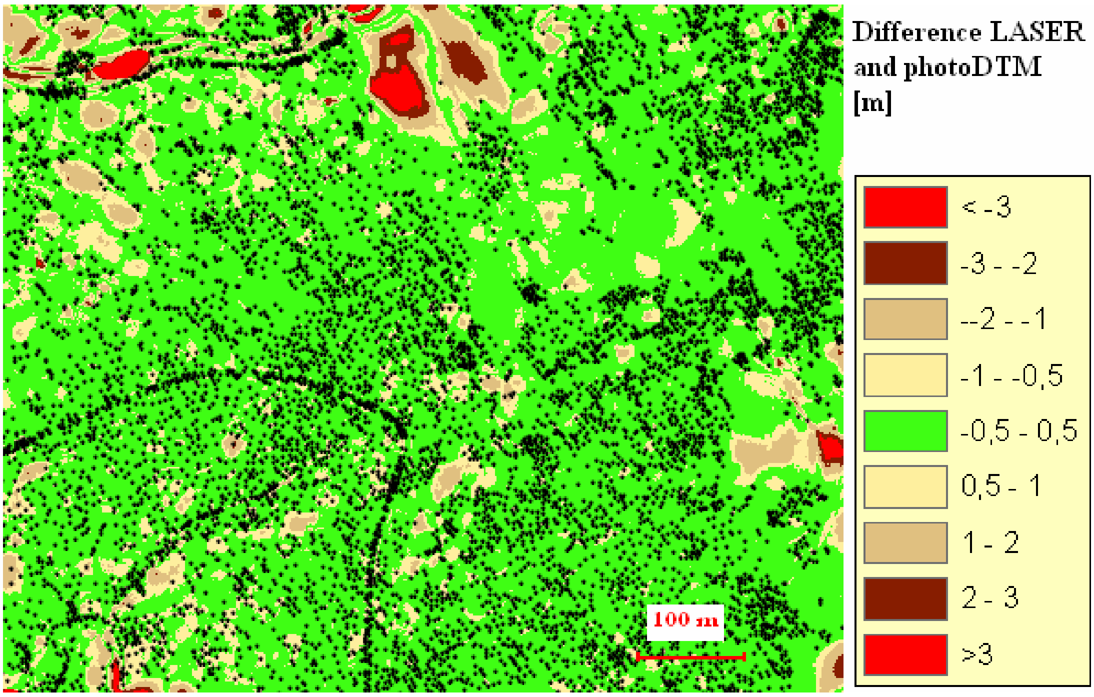


*Figure 3: Differences between laser DTM and photogrammetric measured DTM. Black dots represent manually measured points*

The quality of the DTM strongly depends on the type of vegetation cover. Particularly dense coniferous stands present the greatest problem in collection of terrain points, but even there it is possible to measure the terrain; in cases of thinner coniferous stands or mixed stands with a prevalence of older trees, the precision of the DTM remains in a 1m range. Imprecision of the DTM grows toward the edge of the image, where trees are shown in side view because of the central perspective and as a result the terrain on the edges is significantly more hidden by trees than in the middle of images. The worst combination is dense coniferous stands located on the image's range: a photogrammetric approach cannot deliver any satisfactory results here. When problematic areas (roughly 10%) are deleted, the quality of the photoDTM is entirely sufficient for the purposes of determining height.

The DTM derived from laser data is especially detailed and precise. The density of the point network allowed even individual stumps or tractor tracks to be captured and the resultant DTM can be used not only to determine heights but also for detailed surface analyses if needed.Fig. 4 shows an extent of an uphill covered by dense beech stands and the same extent modeled from laser ground poits.

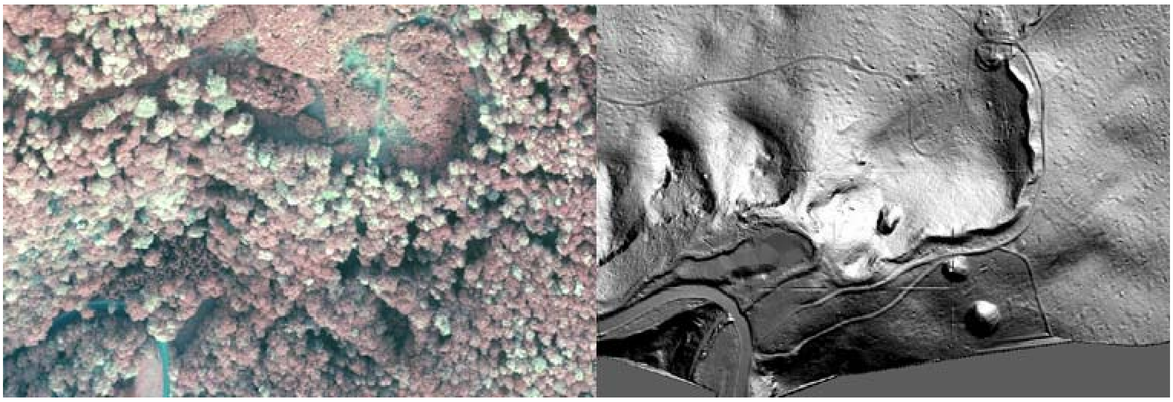

*Figure 4: Summer image (left) and shaded laser DTM over the same area (right)*

## 3.2 Tree heights

The evaluation of tree heights and their errors is based on the median. The 95% percentile showed the lowest biases for all species but the estimation variance was fairly large. Median was recognized as the best parameter in respect to its variance of estimation error and robustness to outliers. The arithmetic mean was too outlier sensitive. If it had to be used as a height estimator, a histogram based cut-out of outliers should be applied. All proposed parameters tend to underestimate tree height, regardless of species. The standard error of true height minus the modeled height differences is fairly low (1.6 to 2.5 m), thus modeled height could be used as a height estimator if the biases were smoothed out reliably (modeled). The linear models between height errors and the DBH as an explanatory variable were significant with 95% statistical certainty. The only exception was oak where the model was not significant for the chosen certainty level (p-value in ANOVA reached 0.08). All linear models were positively increasing models: as the value of the DBH increased, the bias in height estimation also increased (height is more underestimated). The coefficients of determination were fairly low (0.15 – 0.22). Height errors do not seem to be spatially dependent, which is a desirable feature as it makes modeling of biases easier and practically possible.

An overview of the main numerical results is provided in tab.1 The number of evaluated heights needed to comply with a maximum of 1-meter arithmetic mean height (95% security level) lies between 30 (spruce) and 60 trees (beech).

*Table 1: Tree heights estimation - overview of main results*

| Characteristic/species | Beech | Oak | Spruce | Larch |
|---|---|---|---|---|
| Mean value of differences between measured and modeled tree height (bias) | 1.3 | 1.43 | 3.8 | 4.08 |
| Standard error of differences | 2.52 | 1.77 | 1.6 | 1.84 |
| Minimum number of analyzed trees to comply with 1m mean height accuracy | 60 | 42 | 30 | 45 |
| Linear model DBH~ difference | Significant | Not significant | Significant | Significant |

# 4 DISCUSSION

Our experiments showed that DSM derived from frame camera images can be used for tree height evaluation. In our study we identified tree positions stereophotogrammetrically as well as through in-situ inspection, sketching the tree crown limits onto orthophoto outprints. Of course, for a practical application it would be desirable if tree tops were identified automatically. Based to our experience with data from a UltraCam digital camera, we feel confident in claiming that use of more overlapped images in combination with better radiometric resolution would yield significantly better results in DSM and DTM creation. The results which we achieved in DSM creation using digital camera data show that the more detailed character of these data enables creation of more detailed surface models upon which it would be possible to apply automatic tree top identification procedures.

The fact that nDSM tree heights underestimate true heights is easily explainable: subsets of nDSM contain many points situated next to the true tree top and computing median, arithmetic mean or percentiles is always influenced by lower nDSM points.To remove the bias its value could be easily added to the estimated heights. In that case we should assume possible positive/negative errors in the range of 3.2 (spruce) to 5 (beech) meters (95% errors) on individual tree bases.More precise results could be obtained using a particular linear model to remove the bias. This would lower the standard error by some 10% (a result that is not worth the extra effort in DBH incorporation and measurements).

All DBH~error models are positively increasing: the greater the DBH, the higher underestimation of tree height. With a fixed radius one would expect the opposite relationship: the larger the crown diameter (DBH also increases), the higher the relative share of points situated near the tree top and the lower underestimation of tree height. On the other hand, increasing the size of the tree crown also increases the uncertainty in tree top identification (in absolute measurements) by manual measurements. This would lead to a higher share of lower nDSM points.

Larger crowns often show a lack of contrast in the central part of the tree crown, as the digital numbers landscape is more flat around the central part of the crown. An automatic creation of nDSM points does not search for points in low contrast areas of the image, so the central crown pixels are generally missing. In our case this effect apparently prevailed which resulted in linear models with the above-described features.Oak was the only species for which the linear model was not significant on 95% statistical concordance. The p-value calculated by ANOVA testing was 0.08.

If we do not consider this model to be significant, a higher probability of type II error should be expected (unfortunately the exact value of the type II error probability is unknown for a general testing case). In reality it would be safer to assume the linear model is significant for oak as well (the probability that this result is not valid equals 0.08).

The relatively low number of evaluated trees needed for reliable arithmetic mean height estimation allows for manual stereophotogrammetric measurements of trees. If the measurements had to be taken fully automatically the tree tops would have to be identified and classified by species. This leads to a need for reliable species classification, possibly object-oriented to avoid undesirable dispersion of nDSM points belonging to one tree.

# 5 CONCLUSIONS

The quality of the DTM derived from winter images strongly depends on the type of vegetation cover. When problematic areas are avoided, the photogrametrically obtained DTM is sufficient for the purposes of tree height determination.Automatic methods for DTM creating are not able to give satisfactory results due to the lack of reliable filtering algorithm for separation of ground points from matching results. Presented methods used to tree height determination tend to underestimate the tree height, regardless of species. The standard error of true height minus the modeled height differences was fairly low (1.6 to 2.5 m), therefore modeled height could be used as a height estimator if the biases were smoothed out reliably. An approach using more overlapped stereo pairs from digital camera is proposed for our next investigations.

## ACKNOWLEDGEMENTS

We are much obliged to MZLU Brno for providing us with the aerial images and laser data and to IVFL BOKU Wien for technical support as well

## REFERENCES

Baltsavias, E.P., 1999. Airborne laser scanning: basic relations and formulas. ISPRS Journal of Photogrammetry & Remote Sensing, 54, pp. 199-214.

Gülch, E., 1994. Erzeugung digitaler Geländemodelle durch automatische Bildzuordnung. PhD thesis, Institute of Photogrammetry, University of Stuttgart. DGK-C 418.

Krzystek, P., 1991: Fully automatic measurement of digital terrain models. Proc. of the 43. Photogrammetric Week, Stuttgart, Germany, pp. 203-214

Kraus, K., Pfeifer, N., 1998. Determination of terrain models in wooded areas with aerial laser scanner data. ISPRS Journal of Photogrammetry &Remote Sensing 53, pp. 193-203.

Næsset, E., 1997. Determination of mean tree height of forest stands using airborne laser scanner data. ISPRS Journal of Photogrammetry & Remote Sensing, 52, pp. 49-56.

Nelson, R.F, Swift, R., and Krabill, W. 1988a. Using airborne lasers to estimate forest canopy and stand characteristics. Journal of Forestry, Vol. 86, pp. 31–38.

# AUTOMATED GENERATION OF THE 3D STRUCTURE OF FOREST CANOPY

*Armin Gruen, Li Zhang*

Institute of Geodesy and Photogrammetry, ETH Zurich, CH-8093 Zurich, Switzerland ;
{agruen,zhangl}@geod.baug.ethz.ch

## ABSTRACT

Image matching is a key procedure in the process of generation of Digital Surface Models (DMS). We have developed a new approach for image matching and the related software package. This technique has proved its good performance in many applications. Here we demonstrate its use in 3D forest canopy modelling. After a very brief description of our image matching technique we show results from high-resolution satellite images (IKONOS), analogue aerial and digital aerial images. The results indicate the very good performance of our matcher. Depending on the image scale not only closed forest areas can me modelled but also individual trees.

**Keywords:** Image matching, Digital satellite and aerial images, DSM generation, tree canopy

## 1 INTRODUCTION

Optical and image-based measurement methods are increasingly used in environmental modelling and monitoring. The recent development of sensor technology, e.g. very high-resolution satellite imagers, digital aerial cameras and laser-scanners open the path for new applications. This is supported by new advancements in algorithmic development, e.g. towards higher precision, reliability and automation. This paper reports about the use of satellite and aerial stereo images for the 3D modelling of forest canopy, using our recently developed image matching software.

The automatic Digital Terrain Model (DTM) or Digital Surface Model (DSM) generation through image matching has gained much attention in the past years, a wide variety of approaches have been developed, and automatic DTM generation packages are in the meanwhile commercially available on several digital photogrammetric workstations. Although these algorithms and the matching strategies used may differ from each other, the accuracy performance and the problems encountered are very similar in the major systems. The main problems in DTM/DSM generation are encountered with:

- Little or no texture
- Distinct object discontinuities
- Local object patch is no planar face
- Repetitive objects
- Occlusions
- Moving objects, incl. shadows
- Multi-layered and transparent objects
- Radiometric artifacts like specular reflections and others
- Reduction from DSM to DTM

The key to successful and reliable matching is the matching of a dense pattern of features with an appropriate matching strategy, making use of all available and explicit knowledge, concerning sensor model, network structure, image content and geometrical constraints such as the epipolar geometry constraint. For an appropriate matching strategy, we have to consider combining the area-based matching (ABM) and the feature-based matching (FBM), matching parameter self-tuning, generation of more redundant matches and a coarse-to-fine hierarchical matching strategy.

In this paper, we present an advanced image matching approach and report briefly about the key algorithms used, which has the ability to provide dense, precise, and reliable results. The proposed algorithms have been applied to different kinds of images from different sensors (including high-resolution satellite system, traditional aerial photographs and digital aerial images), over different areas with different distribution of trees and forest canopy structure. We will demonstrate here the capability of our software in several examples of Digital Surface Model (DSM) generation over forest canopies.

## 2 IMAGE MATCHING APPROACH

Our image matching approach uses a coarse-to-fine hierarchical solution with a combination of several image matching algorithms and automatic quality control. The approach was originally developed for multi-image processing of the very high-resolution Three-Line-Scanner (TLS and StarImager) aerial images (Gruen and Zhang 2003). Now it has been extended and has the ability to process other linear array images, e.g. satellite images of type SPOT-5, IKONOS, Quickbird, etc., as well as more traditional single frame images.

The approach essentially consists of 3 mutually connected components: the image pre-processing, the multiple primitive multi-image (MPM) matching and the refined matching procedure. The overall dataflow is shown schematically in Figure 1. The images and the given or previously estimated orientation elements are used as input. After pre-processing of the original images and production of the image pyramids, the matches of three feature types (feature points, grid points and edges) in the original resolution images are found progressively starting from the low-density features at the lowest resolution level of the image pyramid. A TIN form DSM is reconstructed from the matched features at each pyramid level by using the constrained Delauney triangulation method. This TIN in turn is used in the subsequent pyramid level for derivation of approximations and adaptive computation of some matching parameters. Finally and optionally, least squares matching methods are used to achieve more precise results for all matched features and for the identification of some false matches.

The matching approach is described very briefly in the next paragraphs. Details can be found in Zhang and Gruen (2004) and Zhang (2005).

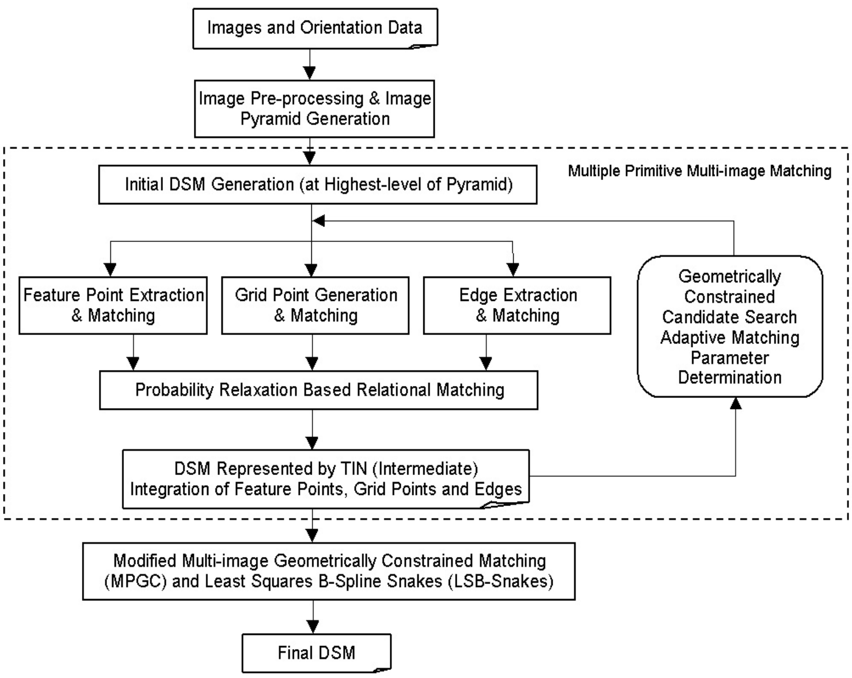


*Figure 1: Workflow of the automated DSM generation approach.*

## 2.1 Image Pre-processing

In order to reduce the effects of the radiometric problems such as strong bright and dark regions and to optimize the images for subsequent feature extraction and image matching, a pre-processing method (works on both 8 bit and more than 8 bit/pixel images), which combines an adaptive smoothing filter and the Wallis filter, was developed. Firstly, an adaptive smoothing filter is applied to reduce the noise level and to sharpen edges and preserve even fine detail such as corners and line endpoints. Next, the Wallis filter is applied to enhance and sharpen the already existing texture patterns.

After the image pre-processing, the image pyramid is generated starting from the original resolution images. Each pyramid level is generated by multiplying a generation kernel and reduces the resolution by factor 3. The pyramid level number is a pre-defined value that is either a user-input or can be determined according to the height range of the imaging area.

## 2.2 Multiple Primitive Multi-Image Matching

The Multiple Primitive Multi-Image (MPM) Matching procedure is the core of our developed approach for accurate and robust DSM reconstruction. Results from this approach can be used as approximations for the refined matching procedure with least squares matching methods. In the MPM approach, the matching is performed with the aid of multiple images (two or more), incorporating multiple matching primitives – feature points, grid points and edges, integrating local and global image information and utilizing a coarse-to-fine hierarchical matching strategy. The MPM approach consists mainly of 3 integrated subsystems: the feature point extraction and matching procedure, the edge extraction and matching procedure and the relaxation based relational matching procedure of grid points. Thus it combines all essential image primitives for matching. For details refer to Zhang and Gruen (2004), Zhang (2005).

## 2.3 Matching Through Image Pyramids

The MPM matching approach starts with an initial matching at the lowest resolution pyramid level. At each pyramid level, an intermediate terrain surface is reconstructed from the mass points and edges. It is modelled by the triangular irregular network (TIN) using a 2D constrained Delaunay triangulation method. This TIN-form intermediate surface model in turn is used in the subsequent pyramid levels for providing the approximations and adaptively computing the matching parameters. Thus, while the matching procedure is going through the image pyramids, the surface model computed from the higher level of the image pyramid is successively refined at the lower level and finally, the dense and accurate surface model is reconstructed.

At each pyramid level, an automatic blunder detection procedure is performed in order to delete some mismatches.

## 2.4 Least Squares Approach to Refined Matching

Least squares matching methods are used in our approach to achieve potentially sub-pixel accuracy results for all matched features and for the identification of some false matches. For this, a modified MultiPhoto Geometrically Constrained Matching (MPGC) algorithm is used. The MPGC combines grey level matching with geometrical constraints derived from multiple image ray intersection conditions and a priori knowledge about the image orientation elements (Gruen 1985, Baltsavias 1991). It permits a simultaneous determination of pixel and object coordinates and allows for simultaneous matching with any number of images.

In order to process linear array images, the standard MPGC algorithm is extended by integrating the geometric constraints derived from the linear array sensor models. In addition, we follow the algorithms proposed by Li (1997) and implement a simplified version of the Least Squares B-Spline Snakes (LSB-Snakes) to match the edges, which are represented by parametric linear B-spline functions in object space. LSB-Snakes can be seen as an extension of the standard MPGC algorithm. With this method, the parameters of linear B-spline functions of the edges in object space are directly estimated, together with the matching parameters in the image space of multiple images.

# 3 RESULTS

## 3.1 IKONOS images of Thun

The first dataset is an IKONOS stereo triplet, which was acquired in December of 2003 over a testfield in Thun, Switzerland. All IKONOS images are 1m panchromatic (PAN), Geo, 11-bit, with DRA (Dynamic Range Adjustment) off. The testfield consists of a steep mountainous region in the southwestern part and smooth hilly regions in the middle and northern parts. The town of Thun is located in the lower-middle part of the study area. The whole area is about 11 $\times$ 20 km$^2$ and 30% is covered by forests. The site has an elevation range of more than 1600 m and the land cover is very variable.

After the IKONOS image triplets were georeferenced by using 39 GCPs, which were collected with differential GPS in March 2004, our matching approach was applied. The three images were matched simultaneously in order to achieve more precise and reliable results. Some areas like lakes and rivers were manually defined as “dead areas” via a user-friendly interface and were excluded from matching. The matching approach resulted in about 11 million points and 800,000 edges, of which more than 80% were labeled as highly reliable. Finally, a 5 m regular grid DSM was interpolated from the raw matching results. Figure 2 shows the shaded terrain model for two sub-areas, together with corresponding sub-images. The resulted DSM reveal that our matching approach reproduces quite well not only the general features of the terrain relief but also small geomorphological and 3D forest canopy structures visible in the IKONOS images.

## 3.2 Analogue aerial images of Neuchatel

The second dataset contains two sets of Leica RC30 aerial photographs over a flat terrain along the lakeshore of Lake Neuchatel, a sensitive environmental area in the western part of Switzerland. The first set was acquired on 10th August 1998 and the second on 15th August 2003, respectively, providing a scale of 1:5 000, an overlap of 75% and a ground resolution of 7 cm. Each image offers three color bands: visible green (500-600 nm), visible red (600-700 nm) and near infrared (750-1000 nm). All images were oriented using SocetSet standard procedures with 12 GCPs. After all scanned aerial images (two groups, each contains 4 images) were pre-processed, our matching approach was applied. The four images of each group were matched simultaneously in order to achieve more reliable results. Some areas like lakes were manually defined as “dead areas” and were excluded from matching. Taking the results from the images of 2003 as an example, the matching resulted in ca. 14 million points and 538,000 edges, of which 7.1% were successfully matched in 4 four images, 61.7% were matched in 3 images and the others were matched in only 2 images.

Finally, two 50 cm regular grid DSMs were interpolated from the raw matching results of the two groups of images. Figure 3 shows the colour-coded point-clouds of two sub-areas of the 2003 DSM. The resulting DSMs reproduced quite well not only the general features of the terrain relief but also the detailed 3D structure of the forest canopy (Figure 4).

## 3.3 Digital aerial images

The last datasets relate to digital aerial imaging systems. One of these contains 32 digital images (belonging to 3 strips) of the new frame-based digital camera system - UltraCamD™ from Vexcel. The images cover an area of 4.2 km$^2$. The study area is covered partly by small patches of forest. The GSD (Ground Sample Distance) is 9 cm. One of the advantageous features of the UltraCamD™ system is that it can provide highly redundant image data sets (e.g. 80% forward overlap and 50% side overlap in our case), together with high radiometric quality. Therefore these images are well suited for automation and are a good data source for our matching approach. Figure 5 shows an example for the matching results achieved.

The other one is a test dataset which we obtained from Ordnance Survey®. It contains 68 digital images (belonging to 8 strips of 60% overlap in both directions, in which 4 strips are in East-West direction and another 4 strips are cross-strips) of the frame-based digital camera system DMC from Z/I Imaging. The images cover an area of 25 km$^2$ of an urban and suburban area of Bournemouth City.

The GSD is about 15 cm. Figure 6 shows a part of the whole DSM revealing clearly the 3D forest canopy structure and even single separated trees.

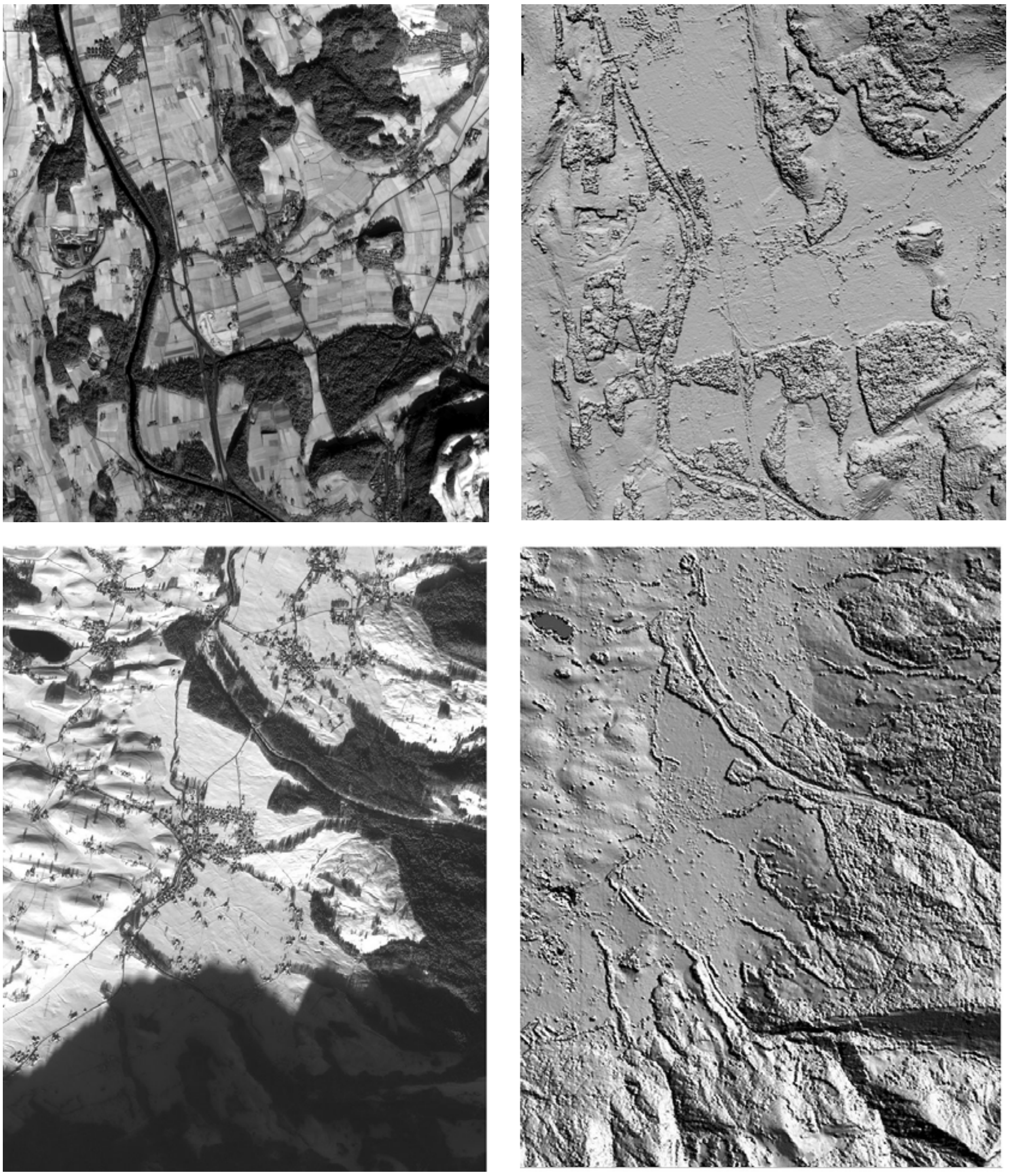

*Figure 2: DSM generated from IKONOS image triplets over our testfield Thun, Switzerland. Left: IKONOS subimages; right: 5 m DSM visualized in shading mode. The canopy structure is clearly visible, both in the images and in the 3D model.*

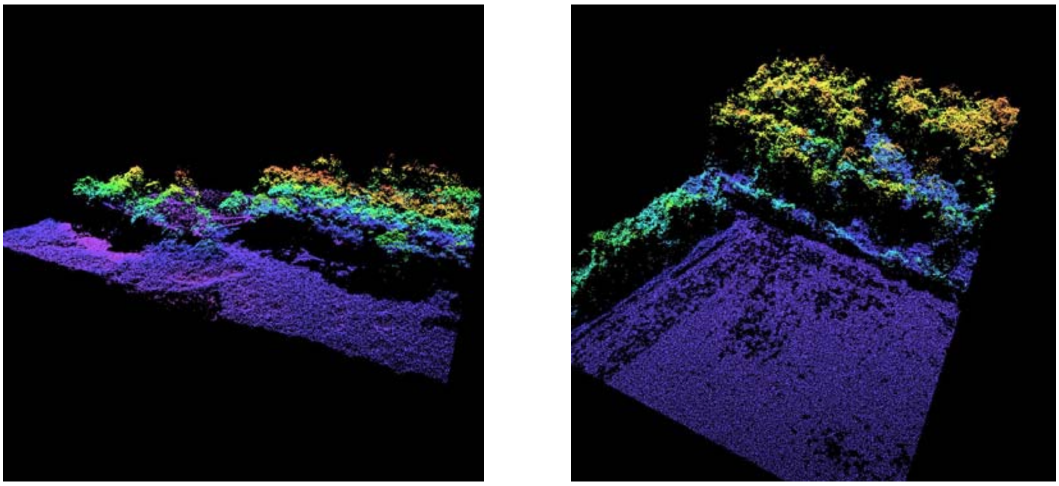

*Figure 3: 3D visualisation of the matched features for two sub-areas of the Neuchatel dataset. The heights are colour coded.*

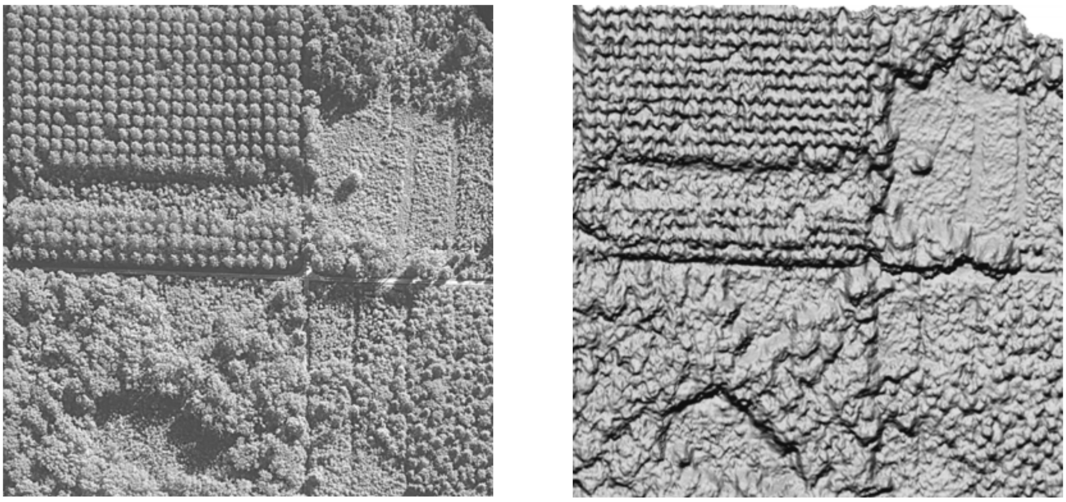

*Figure 4: Left: Part of an aerial image Neuchatel; right: Related 50cm DSM. Showing clearly the 3D forest canopy structure.*

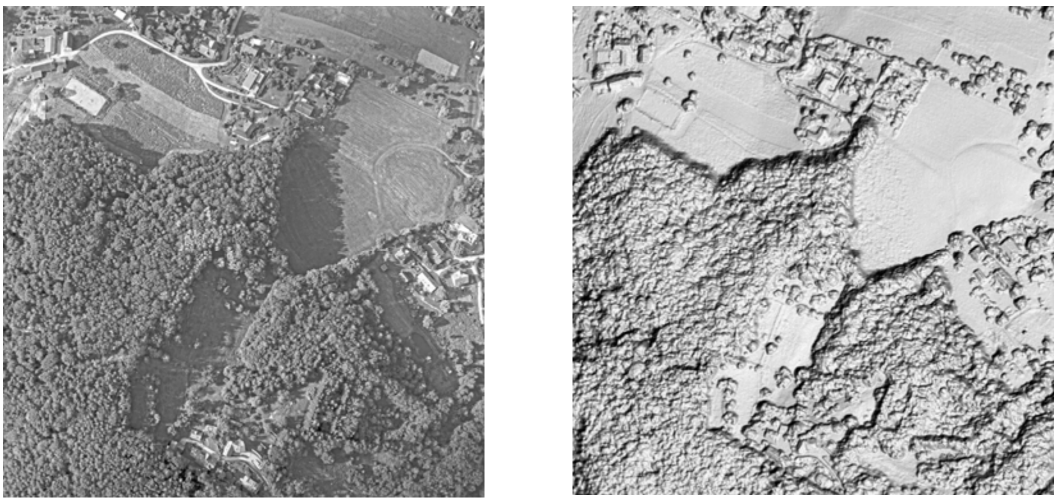

*Figure 5: Left: Part of a UltraCam-D$^{TM}$ aerial image; right: Related 50cm DSM, showing clearly the 3D forest canopy structure and even single separated trees.*

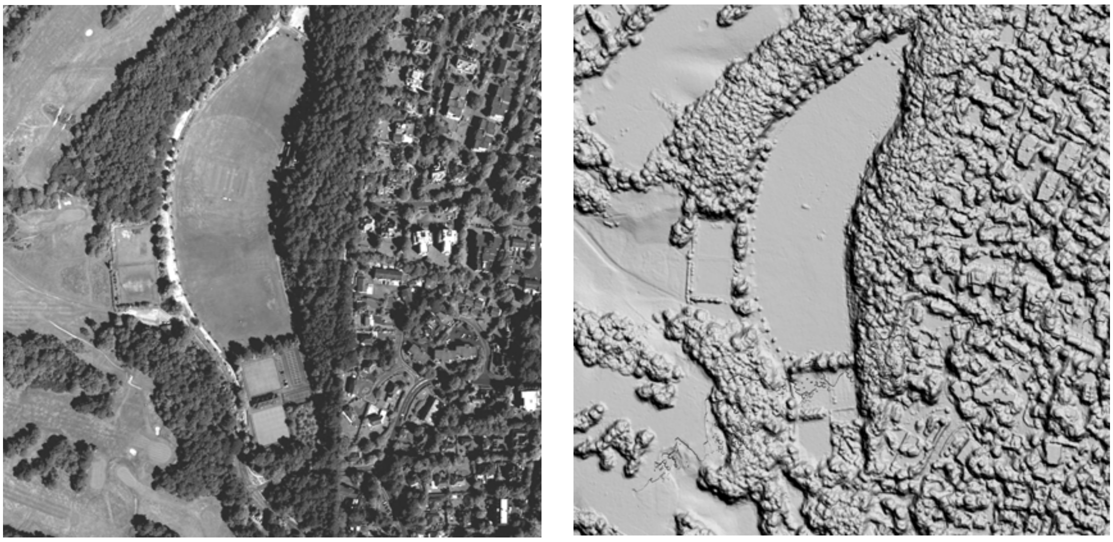

*Figure 6: Left: Part of a DMC™ aerial image; right: Related 60cm DSM, showing clearly the 3D forest canopy structure and even single separated trees.*

## 4 CONCLUSIONS

The recent development of a high-performance image matching technique allows the generation of high quality Digital Surface Models from images. We have shown with the help of practical data that 3D tree canopy information can be well and automatically extracted from satellite and aerial images in stereo and multi-image mode. The accuracy depends primarily on the image scale, image texture, imaging geometry and on the compactness of the tree canopy definition. Future investigations should focus on the accuracy verification, using reference data. Also, the usefulness for applications should be further studied.

## ACKNOWLEDGEMENTS

We acknowledge the support of Eidg. Forschungsanstalt für Wald, Schnee und Landschaft, Switzerland, which provided the aerial images of the Neuchatel study area. In particular, we would like to thank Lars Waser for providing the orientation parameters of these images. We also aknowledge provision of the Ikonos images by Space Imaging USA and of the DMC images by the Ordnance Survey, UK.

## REFERENCES

Baltsavias, E. P. (1991). Multiphoto Geometrically Constrained Matching. Ph.D. Dissertation, Report No. 49, Institute of Geodesy and Photogrammetry, ETH Zurich, Switzerland.

Gruen, A. (1985). Adaptive Least Squares Correlation: A Powerful Image Matching Technique. South Africa Journal of Photogrammetry, Remote Sensing and Cartography 14(3): 175-187.

Gruen, A., Zhang L. (2003). Automatic DTM Generation from TLS data. In: Gruen, A., Kahmen, H. (Eds.), Optical 3-D Measurement Techniques VI, Vol. I, ISBN: 3-906467-43-0, pp. 93-105.

Li, H. (1997). Semi-automatic Road Extraction from Satellite and Aerial Images. Ph. D. Dissertation, Report No. 61, Institute of Geodesy and Photogrammetry, ETH Zurich, Switzerland.

Zhang, L. (2005). Automatic Digital Surface Model (DSM) Generation from Linear Array Images. PhD Dissertation, Report No. 88, Institute of Geodesy and Photogrammetry, ETH Zurich, Switzerland. URL: http://e-collection.ethbib.ethz.ch/ecol-pool/diss/fulltext/eth16078.pdf

Zhang, L., Gruen, A. (2004). Automatic DSM Generation from Linear Array Imagery Data. The International Archives of the Photogrammetry, Remote Sensing and Spatial Information Sciences, Vol. 35, Part B3, pp. 128-133.

# A RETROSPECTIVE STUDY OF CANOPY GAP DYNAMICS OF A EUROPEAN BEECH STAND

*Robert Nuske*

University of Göttingen, Institute for Forest Biometrics and Applied Computer Science, Göttingen, Germany; rnuske@gwdg.de

## ABSTRACT

Canopy gaps have been widely neglected in current monitoring and forest management practices, which might be due to the fact that terrestrial and analogue photogrammetric measurements are labour-intensive, tedious, and error prone in dense broadleaved stands. In this study an automated approach to canopy gap mapping was used to study the gap dynamics of a European beech stand. The canopy gap mapping was accomplished by a filter based on local median and distribution of canopy heights. This filter provided better results for automated mapping of canopy gaps than conventional height thresholds. The automated processing of canopy height models derived from LiDAR data and a time series of aerial photographs enables the study of gap dynamics on a large scale. First results indicate that this method maybe a valuable tool to gain further understanding of natural canopy gap dynamics, which is valuable for forest conservation and semi-natural forest management.

**Keywords:** digital photogrammetry, digital surface model, canopy gap delineation, European beech, canopy gap dynamics

## 1 INTRODUCTION

Forest stands change their appearance and structure over the years, decades, or centuries. Dead or decaying trees or small groups of trees are replaced by the next generation of trees. This cycle of developmental phases (from regeneration to degradation phase) is the prevailing dynamic in unmanaged temperate deciduous forests. This concept is known as the forest cycle (Watt 1947). In semi-natural European beech forests canopy gaps are hotspots for tree regeneration because ecological conditions within gaps are usually very different from below-canopy conditions. Survival and species composition of the regenerating cohort are determined by the size and shape of the gap. Gap formation is thus a vital process in the continuous development of semi-natural forests.

Canopy gaps have been investigated in a number of studies, but predominantly mapped terrestrially. Only a few studies used remotely sensed data to map canopy gaps (cf. Brunig 1973; Tanaka and Nakashizuka 1997; Fox et al. 2000; Fujita et al. 2003; Nuske 2003). But, canopy gaps have been widely neglected in current monitoring and planning practices. This might be due to the fact that terrestrial and analogue photogrammetric measurements are particularly labour-intensive, tedious, and error prone in dense broadleaved stands.

High resolution Canopy Height Models (CHM) can be used to map canopy gaps. At the moment there are two main sources of high resolution CHMs of considerably large areas. On the one hand there is the airborne LIDAR system, which has a lot of potential, but is still far from being widely accepted, mainly because of its still high costs (Baltsavias 1999). On the other hand there is digital photogrammetry, a less expensive alternative that also offers other advantages. Since the use of aerial imagery is an old and widely used remote sensing technique, most of the German forests are flown as part of the standard forest inventory in a ten year cycle. Aerial imagery, thus, enables retrospective studies of the dynamics of forest canopies. But, in order to build a CHM from this type of data, a DTM from another source is needed.

Based on the CHM, not only stand heights (cf. Nuske and Nieschulze 2004), but also ecological parameters such as distribution and size of gaps can be obtained. Appropriate methods for a highly automated process based on remote sensing and GIS are to study the gap dynamics of a natural forest reserve.

## 2 MATERIAL

The study was carried out on two different sites. Both stands are forests reserves and unmanaged for about 30 years. They are both 150 years old pure European beech stands. The study area "Limker Strang" is part of the woodland Solling, which is situated in southern Lower Saxony 70 km south-west of Hanover. The other site, "Schäferheld", is part of the Nationalpark Eifel, which is located in North-Rhine Westphalia 60 km west of Bonn.

Color Infrared (CIR) aerial photographs from various dates were employed (cf. Table 1). The flights were done with sufficient overlap during the vegetation period to provide a stereoscopic view on the canopy surface. The chosen resolution of about 0.40 m corresponds to the accepted opinion that the spatial resolution for photogrammetric vegetation measurements should be 0.1 to 0.5 m. The DTM for the study site Limkerstrang was constructed by photogrammetric and terrestrial measurements, resulting in a rather coarse resolution of 12.5 m. A 1 m resolution DTM derived from LiDAR data was available for the Nationalpark Eifel. The LiDAR data were recorded between February and May 2004 before the trees were fully foliated.

*Table 1: Image and georectification details (* values in brackets show original resolution before resampling)*

| Area | Date of Flight | Nominal Scale | Spatial Resolution [m] | # GCPs | X-RMSE [m] | Y-RMSE [m] |
|---|---|---|---|---|---|---|
| Limkerstrang | Aug.1989 | 1:10400 | 0.36 | 16 | 0.87 | 0.74 |
| Limkerstrang | Sept.1992 | 1:6300 | 0.44 (0.22)* | 16 | 1.48 | 1.23 |
| Limkerstrang | Aug.1998 | 1:12800 | 0.45 | 12 | 1.69 | 1.56 |
| Limkerstrang | Sept.2000 | 1:5900 | 0.40 (0.20)* | 15 | 1.24 | 1.27 |
| Schäferheld | Aug.1989 | 1:3000 | 0.30 (0.06)* | 13 | 0.31 | 0.28 |
| Schäferheld | Jul.1995 | 1:4500 | 0.30 (0.10)* | 11 | 0.39 | 0.49 |
| Schäferheld | Aug.2001 | 1:4800 | 0.30 (0.10)* | 10 | 0.19 | 0.18 |

## 3 METHODS

The digitized and rectified stereopairs were used to automatically derive DSMs using digital photogrammetry methods. A postprocessing including noise removal and interpolation was carried out to enhance the quality of the DSM. The result is a digital image which represents a landscape and its components, such as trees and buildings, by height above sea level. To obtain the CHM the DTM was subtracted.

Our gap definition follows Runkle's definition (1992), which defines a canopy gap as an area within a forest where the canopy is noticeably lower than in adjacent areas. The minimum gap area in this study was set to 20 m², without an upper limit. Nuske (2003) tested a number of different methods to map canopy gaps and found the adaptive median threshold to be most suitable. This method classifies that area as a canopy gap, which is lower than a reference height minus a certain range given by variability of the neighbourhood. To create a reference height that is not influenced by the still to be detected gaps, the median of the height values of a moving window is used. The window has to be at least twice as large as the largest expected canopy gap to ensure that the median always represents a height value of the upper canopy. The interquartile distance serves as a fast and easy to calculate measure of dispersion. Hence, the classification threshold is calculated as the median minus the interquartile distance. The classification is based only on the distribution of the height values of the neighbourhood.

# 4 RESULTS

Two gap maps of one year for each study site are shown exemplary in figure 1. The canopy gap dynamics are displayed by means of cumulative distribution functions of the time series of the gap size distributions in figure 2.

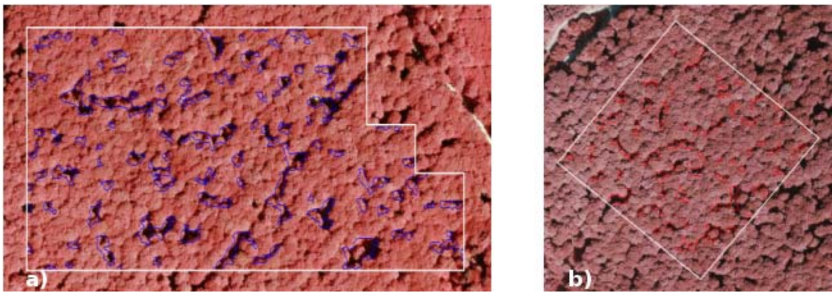


*Figure 1. Gap maps superimposed on CIR Orthophotos (a: Limkerstrang 1998, 10ha; b: Schäferheld 1989, 2ha)*

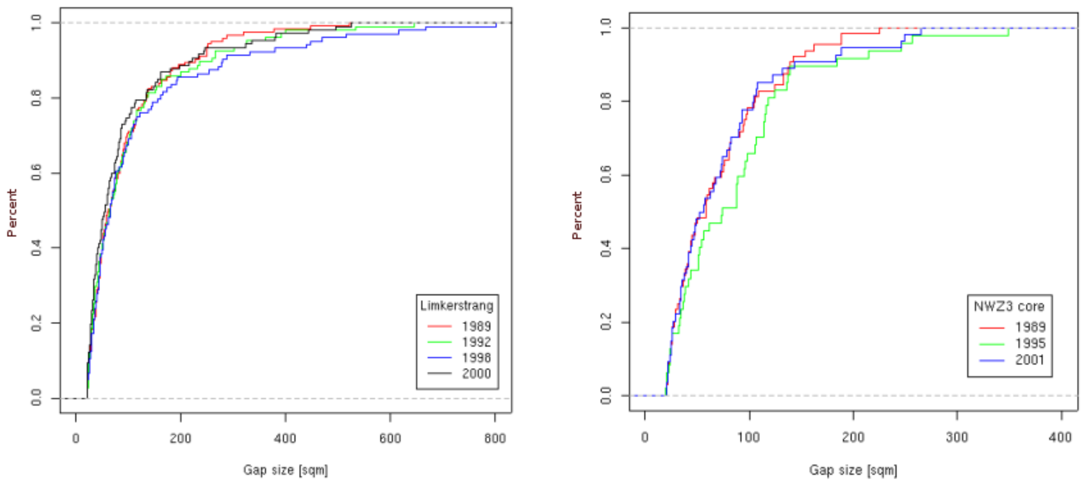


*Figure 2. Cumulative distribution functions of the time series of gap size distribution of both study sites.*

# 5 DISCUSSION

The Analysis of canopy surfaces can be automated using CHMs, digital photogrammetry, and a GIS. Because of the automation, this methodology can be applied on a large scale. It is a rather low-cost approach, using the software package OrthoEngine from PCI Geomatics (Brostuen et al. 2001), which runs on a standard PC. Although no high-tech equipment was chosen, the results produced were comparable to studies done on analytic stereoplotters.

The adaptive median approach canops gap mapping proved to represent the gap pattern best. In contrast to other approaches, it provided a consistent quality throughout the whole area. All larger gaps were found, but sometimes the shapes differed from the manuals delineated reference gap map. But, the method used detected most but not all of the small gaps.

The gap area found in the stand Limkerstrang was somewhat high compared to other studies carried out on the same site. This might be caused by the different methodologies or by different gap definitions. However, one can see that some of the smaller gaps vanish in the course of time and others appear. At a closer look, it is evident that more gaps vanish than arise. However, the larger gaps also tend to shrink, although this is harder to notice. The total gap area has a clear decreasing trend. These results agree with other studies in the same area (Spellmann 1991). These findings also agree with theoretical considerations that mature beech stands tend to close gaps via vertical growth of gap neighboring trees and height growth of understorey trees (Meyer et al. 2003).

The demonstrated technique ensures reproducible results for large areas and at different points in time. Aerial photographs, which are the basis of this method, are raw information, and therefore independent of different measurement schemes. Thus, this method can be regarded as a very robust monitoring scheme. Aerial photographs of the studied stand taken during the last decades do not only enable studies on canopy roughness and gap dynamics but also further ecological studies such as dynamic crown cover and dynamic stand structure, which have not been possible so far

## ACKNOWLEDGEMENTS

I would like to thank the Landesanstalt für Ökologie, Bodenordnung und Forsten Nordrhein-Westfalen and the Niedersächsischen Forstlichen Planungsamt for providing the aerial photographs and the Niedersächsischen Forstlichen Versuchsanstalt for the reference gap delineation done on an analytic stereoplotter. This work was supported by the Scholarship Programme of the German Federal Environmental Foundation.

## REFERENCES

Baltsavias, E.P. (1999). A comparison between photogrammetry and laser scanning. ISPRS Journal of Photogrammetry and Remote Sensing 54(2-3): 83-94.

Brostuen, D., S. Sutton and Y. Siddiqui (2001). OrthoEngine Software version 7.0. Photogrammetric Engineering and Remote Sensing 67(3): 245-247.

Brunig, E.F. (1973). Some Further Evidence on Amount of Damage Attributed to Lightning and Wind-Throw in Shorea-Albida Forest in Sarawak. Commonwealth Forestry Review 52(3): 260-265.

Fox, T. J., M. G. Knutson and R. K. Hines (2000). Mapping forest canopy gaps using air-photo interpretation and ground surveys. Wildlife Society Bulletin 28(4): 882-889.

Fujita, T., A. Itaya, M. Miura, T. Manabe and S. I. Yamamoto (2003). Long-term canopy dynamics analysed by aerial photographs in a temperate old-growth evergreen broad-leaved forest. Journal of Ecology 91(4): 686-693.

Meyer, P., V. Tabaku and B. von Lüpke (2003). Die Struktur albanischer Rotbuchen-Urwälder - Ableitungen für eine naturnahe Buchenwirtschaft. Forstwissenschaftliches Centralblatt 122(1): 47-58.

Nuske, R S. (2003). Digitale Höhenmodelle zur Beschreibung der Bestandesdynamik anhand von Lückenmuster und Oberflächenrauhigkeit am Beispiel des Naturwaldes Limker Strang. MSc thesis at Fakultät für Forstwissenschaften, Georg-August-Universität Göttingen.

Nuske, R.S. and J. Nieschulze (2004). Die Vegetationshöhe als Werkzeug zur Ermittlung von Bestandeshöhen: Eine Anwendung automatisierter digitaler Photogrammetrie in der Forstwissenschaft. Allgemeine Forst und Jagdzeitung 175(1/2): 13-21.

Runkle, J.R. (1992). Guidelines and sample protocol for sampling forest gaps, General Technical Report. Portland, OR, U.S. Department of Agriculture, Forest Service, Pacific Northwest Research Station**:** 44.

Spellmann, H. (1991). Beiträge der Forsteinrichtung und Ertragskunde für ein forstliches Informationssystem. Forst und Holz 46(3): 57-65.

Tanaka, H. and T. Nakashizuka (1997). Fifteen years of canopy dynamics analyzed by aerial photographs in a temperate deciduous forest, Japan. Ecology 78(2): 612-620.

Watt, A. S. (1947). Pattern and Process in the Plant Community. Journal of Ecology 35(1-2): 1-22.

# TREE HEIGHT MEASUREMENTS AND TREE GROWTH ESTIMATION IN A MIRE ENVIRONMENT USING DIGITAL SURFACE MODELS

*E. Baltsavias[1], A. Gruen[1], M. Küchler[2], P.Thee[2], L.T. Waser[2], L. Zhang[1]*

[1] Institute of Geodesy and Photogrammetry (IGP), ETH Zurich, Wolfgang-Pauli-Str. 15, 8093 Zurich, Switzerland; (manos, agruen, zhangl)@geod.baug.ethz.ch

[2] Swiss Federal Institute for Forest, Snow and Landscape Research (WSL), Department of Landscape Inventories, 8903 Birmensdorf, Switzerland; (lars.waser, meinrad.kuechler, patrick.thee)@wsl.ch

## ABSTRACT

This study is an interdisciplinary cooperation between Geomatics and Forestry and Landscape scientists with aim to examine the potential of automated image matching methods for DSM generation and the derivation of tree parameters, especially height and growth, in a mire environment. The matching DSMs were generated using the commercial SocetSet photogrammetric package and new high-quality methods developed at IGP. Furthermore, the matching DSMs are compared to an airborne lidar DSM and manual measurements in the images. The images used were scanned, 1 : 5.000 scale, CIR images of a mire in western Switzerland and were acquired in 1998 and 2003, while the laser DSM was acquired in 2002. A detailed analysis of the results is presented. As shown, the ETHZ matching DSM clearly outperforms the SocetSet DSM, while it is better even than the laser DSM, providing very dense results (here 0.5 m point density), a more accurate and detailed 3D canopy model, and more accurate estimation of tree height and growth.

**Keywords:** wetlands, tree height, tree growth, aerial images, image matching, airborne lidar, digital surface model, accuracy assessment.

## 1 INTRODUCTION

The aim of the Federal Mire Conservation Program, which is performed by WSL in partnership with the Swiss Federal Office for the Environment, Forest and Landscape, is to conserve the mire biotopes of national importance and outstanding beauty in Switzerland in their entire state. This implies no decrease of the mire area and no degradation of vegetation. Within this program, the monitoring has to establish whether and how far this aim has been reached. Consequently, the mire areas and their vegetation must be described over time and space in sufficient detail (Grünig 1994, Küchler et al. 2004).

The present study was established within the framework of the Swiss Federal Mire Conservation Program. The first objective is an evaluation of three different ways (two automated image matching methods and lidar data) to measure tree height for a range of common vegetation types within the forested area of a mire environment in western Switzerland. This assessment also implies a test of suitability of these measurement sets. The second objective is to determine (retrospectively) growth of deciduous and coniferous trees over a time period. A particular goal is to demonstrate the potential of high-quality matching algorithms and make a comparison to manual image measurements and lidar for derivation of vegetation parameters. The work is an interdisciplinary cooperation between the two sister institutions.

It is widely recognized that obtaining different forest parameters, such as tree height through ground measurements, is too costly in terms of time and manpower, and also prone to errors (St-Onge & Achaichia 2001). Obtaining tree height through ground measurements is often not feasible in dense and impenetrable forest stands and over large areas (St-Onge et al. 2004; Wang et al. 2004).

The main advantages of aerial photography over other remote sensing alternatives are the high geometric accuracy, large area coverage and a high spatial resolution of < 0.2 m (Gong et al. 2000). According to Wang et al. (2004), the cost of forest sampling can be reduced substantially by estimating forest and tree parameters directly from aerial photographs. Tree height measurement is one of the important tasks for an appropriate estimation of these parameters. Gougeon (1995) and Wulder et al. (2000) present a ‘tree top’ or ‘local maxima’ approach. It consists of detecting the most bright pixels (or local maxima) in an image. This approach uses a threshold to eliminate the majority of shaded pixels and also benefits from the presence of shade between tree crowns. Photogrammetric methods can be employed to measure tree heights in aerial photographs (St-Onge et al. 2004). Additional information, such as digital surface models (DSMs), can be also obtained. DSMs can be generated automatically by image matching methods, often using cross-correlation. To obtain tree height, canopy height models can be calculated by subtracting the digital terrain model (DTM) from the DSM (St-Onge & Achaichia 2001). Tree growth can be estimated using canopy height models of different dates. It is obvious, however, that not all important forest parameters can be derived from aerial photographs for all trees in a stand, e.g. due to the fact that parts of the tree crowns are occluded or shadowed – especially in dense forest stands and in mountainous regions - and the shape of a tree is varying according to its position in the stereo images.

Since several lidar systems are commercially available (e.g. Baltsavias 1999), DSMs and DTMs are also derived from such data. A number of studies reveal the successful use of lidar to assess tree (Persson et al. 2002; Morsdorf et al. 2004) and stand attributes (tree height, crown diameter, basal area, stem volume). Combining some of these attributes can be useful to evaluate forest stand growth estimations.

Repeated measurements of individual tree heights are traditionally used to measure tree growth (Hasenauer et al. 1998). On the other side, some studies also reveal an underestimation of tree and canopy height, a result common with many airborne lidar studies (e.g. Magnussen et al. 1999; Means et al. 2000; Gaveau & Hill 2003). Often, a narrow tree apex is missed by lidar hits or the top of a small tree is covered by branches of a tall tree. Other authors (e.g. Naesset 1997, St-Onge 1999, Heurich et al. 2003) report in their studies that DSMs of both aerial images and lidar data systematically underestimate tree heights.

# 2 MATERIAL AND METHODS

## 2.1 Study area, used images and reference data

Methods have been developed and tested for the mire “Le Fanel” located in a flat terrain along the shore of Lake Neuchatel, a sensitive environmental area in the western part of Switzerland (approx. 47°00’ N and 7°03’ E). Parts of the region were drained in the last century. Most of the artificial ditches are still active – only a few are filled up. The mire lies between the lakeshore itself and a small pasture line which is crossed by shrubs and bright broadleaved woodland (see Figs. 1 and 2). The terrain altitude inside the study perimeter varies from 428 m to 440 m.

The core area of the mire has an extent of 0.24 km$^2$. The dominant vegetation types are vegetation of open water (*Lemnetea minoris, Charetea fragilis, Potametea pectinati*), reed and tall sedge vegetation (*Phragmiti-Magnocaricetea*), meadow-sweet vegetation (*Filipendulo-Convolvuletea*), meadows and pastures, bog forest and bright broadleaved woodland (*Quercetea pubescentis*). The bordering forested area, with an extent of approx. 3 km$^2$, is mostly characterized by dense deciduous forest (80%) and coniferous forest (20%) with few storm losses and some new reforestations.

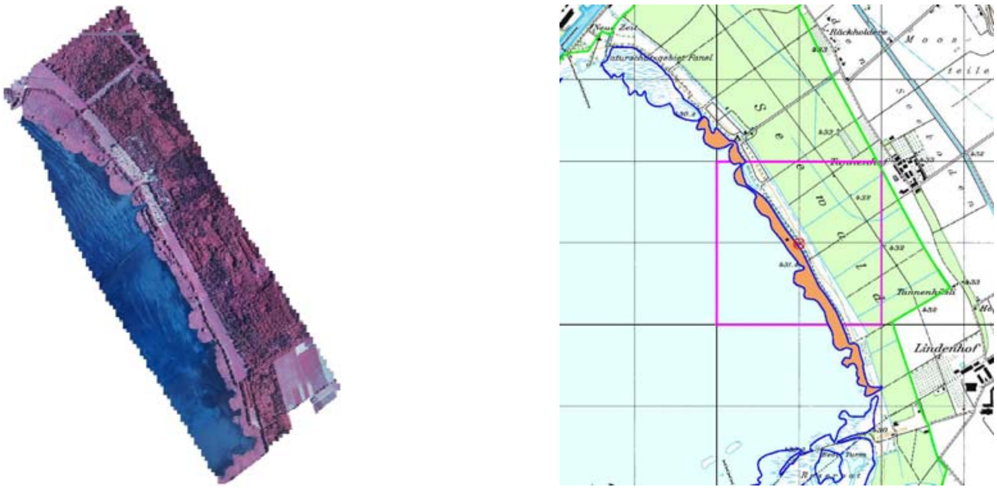


*Figure 1: Overview of the mire Le Fanel at the shore of lake Neuchatel. Left color infrared (CIR)orthophoto (© WSL 2003) and right digital rastermap, map sheet LK 1165 (© reproduced with permission of Swiss Federal Office of Topography (Swisstopo))*

*Figure 2: Bright broadleaved woodland with meadows and pastures are typical for the site*

The used images consisted of a multitemporal dataset. The first set was acquired on 10th August 1998 and the second on 15th August 2003. The image scale was 1:5 000 and the forward overlap 75%. The color channels of the images covered visible green (500-600 nm), visible red (600-700 nm) and near infrared (750-1000 nm). One strip with four images for the 1998 and 2003 datasets was scanned with 14 microns (7 cm ground pixel size). An example of the images is shown in Fig. 3. The images were oriented using SocetSet with 12 ground control points that were measured by differential GPS. Different orientation procedures were used for the 1998 and 2003 images (orientation of stereopairs vs. bundle block adjustment) and certain y-parallax was observed in some of the 2003 images. The interior and exterior orientation of SocetSet was used for DSM generation by matching and manual measurement of the reference data.

Reference data for tree heights were measured manually in the scanned stereopairs. The same points were measured in the 1998 and 2003 images, although the identification of the same point was difficult. This was made easier by using own software that allowed simultaneous stereoscopic viewing of both 1998 and 2003 images. When the planimetric difference of the tree tops between the two epochs was more than 2m, the points were discarded. The remaining points were 181 and had in most cases planimetric difference of less than 1m. Measured trees included both trees at the border and inside the forest, but not small trees among taller trees. The tree heights were 4-33 m and the estimated accuracy of the heights was 0.4-0.5 m. The average planimetric position of 1998 and 2003 measurements was used to interpolate the height in the DSMs from matching and airborne laser scanning (ALS) and the interpolated heights were compared to the manual measurements. The average planimetry was used to smooth the image orientation differences and reduce the uncertainty of tree top identification. The average tree growth was estimated by comparing the 1998 and 2003 manual measurements. A fifth (2003-1998) of this growth was added to the heights interpolated in the ALS DSM (acquired in 2002), in order to allow comparison with the 2003 manual measurements.

For computation of tree heights, both tree top elevation and the elevation of the ground point beneath are needed. The latter point however is almost always invisible in aerial images. One possibility is to measure in the images ground points nearby, but this can be used, only if the terrain is flat. Another alternative is to reduce the DSM to DTM using programs as for ALS, e.g. TerraScan, SCOP++ Lidar. However, this is more difficult for DSMs from matching, as they do not include measurements below the canopy, as is the case with ALS and its penetration capability. In this study, we used the ALS DTM as ground information with both 1998 and 2003 images. The ALS DTM may change height due to tree undergrowth, however here we assume that there is no ground deformation between the time epochs used.

## 2.2 DSM generation by matching

### 2.2.1 Image matching problems for DSM generation

Image matching is still a complicated and difficult problem. Difficulties when matching one image dataset include:

- occlusions
- repetitive patterns
- shadows
- perspective differences
- semi-transparent surfaces
- rough surfaces, surface discontuities, mixed surfaces

The above problems get worse when there are no leaves and when using feature-based image matching (points, edges). Possible improvements can be achieved by:

- use of more than two images (large forward and side image overlap)
- use of geometric constraints exploiting the known image orientation
- sophisticated matching methods
- automatic blunder detection
- dense matching
- use of small ground pixel size to reduce surface smoothing

When comparing multitemporal image datasets, additional difficulties may arise, such as:

- different image scales
- different image quality
- different growth state
- different illumination and atmospheric conditions
- different viewpoints
- different image orientation

Possible improvements can be achieved by:

- flying almost on the same date
- good and similar illumination and atmospheric conditions
- high sun elevation
- acquiring images with leaves on
- similar image acquisition parameters, using modern capabilities for precise navigation and pin-point photography

### 2.2.2 DSM generation using the commercial package SocetSet

From both sets of stereo-pairs, DSMs for the years 1998 and 2003 were generated using the widely used Automatic Terrain Extraction (ATE) approach (Zhang & Miller 1997) in SocetSet 5.1 from BAE Systems. The main advantage of SocetSet is the possibility of individually setting the matching parameters in ATE allowing the user to adapt the method to forest specific conditions and to possibly extract single trees and bushes (for further details see also SocetSet (2004)). The strategy applied in this study was specifically designed at WSL for mires, considering the specific conditions of open land in mire environments, aiming at preservation of surface details, reduction of artifacts and extraction of single trees and bushes. However, the meaning and exact effect of the matching parameters on the generated DSM is often not very clear and requests trial and error and fine tuning, while even with this the produced DSM contains often many errors and needs time-consuming manual editing. The resulting regular grid DSMs had a spacing of 0.5 m. An example of the DSMs for a representative part of the site is shown in Fig. 3.

### 2.2.3 DSM generation using refined methods developed at ETH Zurich

DSMs were derived automatically using the same scanned images and the same interior and exterior orientation using adaptive, high-quality matching algorithms developed at IGP. This method can simultaneously use any number of images (> 2), matches very densely various primitives (grid points, feature points with good texture and edges), uses geometrical constraints to restrict the search space, combines two matching algorithms (sum of modified cross-correlation, and least squares matching) to achieve speed but also higher accuracy if needed, combines the matching results of the three primitive types with another matching approach to ensure local consistency, and performs an automatic blunder detection. The resulting DSM is thus very dense, highly accurate and preserves very well surface details and discontinuities. Details about the method can be found in Zhang (2005) and Zhang & Gruen (2004). The matching method is implemented in the operational, quasi-complete photogrammetric processing package Sat-PP which supports satellite and aerial sensors with frame and linear array geometry. The result was a regular grid DSM with 0.5 m spacing which was interpolated from a matching point cloud of similar density (ca. 15 million match points per stereopair). The total processing time for the four images (without using least squares matching) was 5 h on a standard PC. An example of the DSMs is shown in Fig. 3.

### 2.3 Lidar DSM

The airborne lidar data were acquired for the Swisstopo in early October 2002 (leaves on) with a mean density of 1-2 points per $m^2$, depending on the terrain, and with first and last pulse recorded. The data have been controlled and edited by Swisstopo (Artuso et al. 2003). The accuracy (1 sigma) of derived DSMs and DTMs are 0.5 m and 1.5 m for vegetated areas. At WSL, these datasets were further processed and datasets with an average point distance of 1 m were generated. They were interpolated to a regular grid with 1 m spacing by IGP. An example of the ALS DSM is shown in Fig. 4 and it can be visually compared to the two matching DSMs.

## 3 RESULTS AND DISCUSSION

Fig. 4 shows a visual comparison of the two matching and the ALS DSMs. The SocetSet DSM compared to the ETHZ one is much smoother, can not model small features and small ground areas between trees and includes many blunders. Compared to the ETHZ DSM, the ALS one models worse the canopy (reduction of tree volume and smaller height), is noisy and models worse small features. This is partly due to the larger average point spacing of the ALS data. A quantitative evaluation of the ETHZ and ALS DSMs using the 181 reference points is shown in Table 1. The error statistics there are partly influenced by interpolating a regular grid and surface modelling errors. Again, the ALS DSM is worse and especially underestimates the canopy height, while it includes more blunders compared to the ETHZ DSMs. This is also clearly shown in the profiles of Fig. 5. The matching DSM will also always underestimate tree height, due to the surface smoothing that occurs with matching, but to a less extent than ALS. The 2003 matching DSM is better than the 1998 one, mainly due to the better image quality.

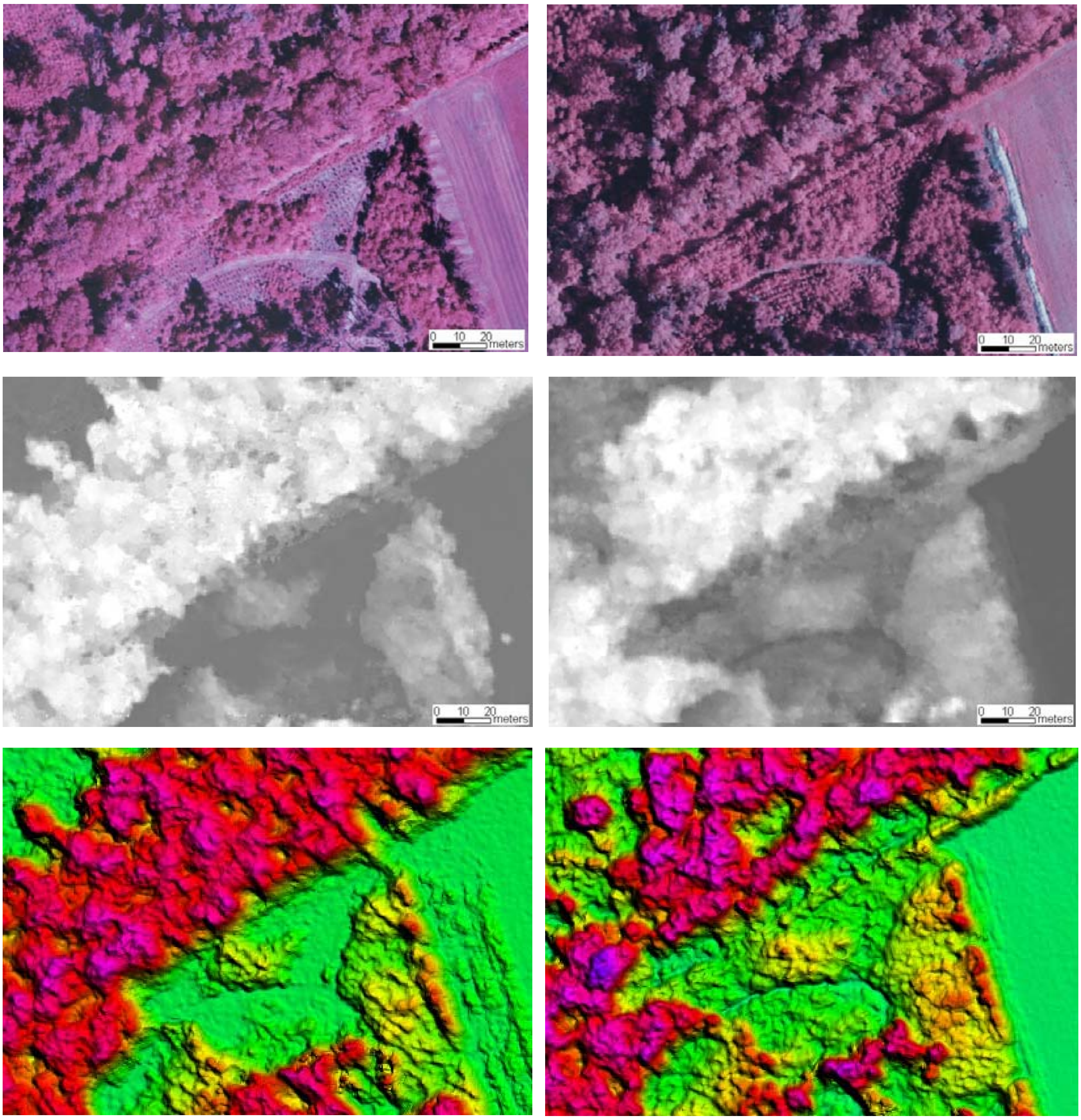


*Figure 3: Top: CIR-orthoimages 1998 and 2003. There are significant differences in color, texture, shadows etc. and slightly poorer image quality in the 1998 dataset. Middle: the corresponding DSMs generated by SocetSet coded with grey levels from lower (dark) to higher (bright) height values. Bottom: the DSMs generated by the ETHZ method, coded in color*

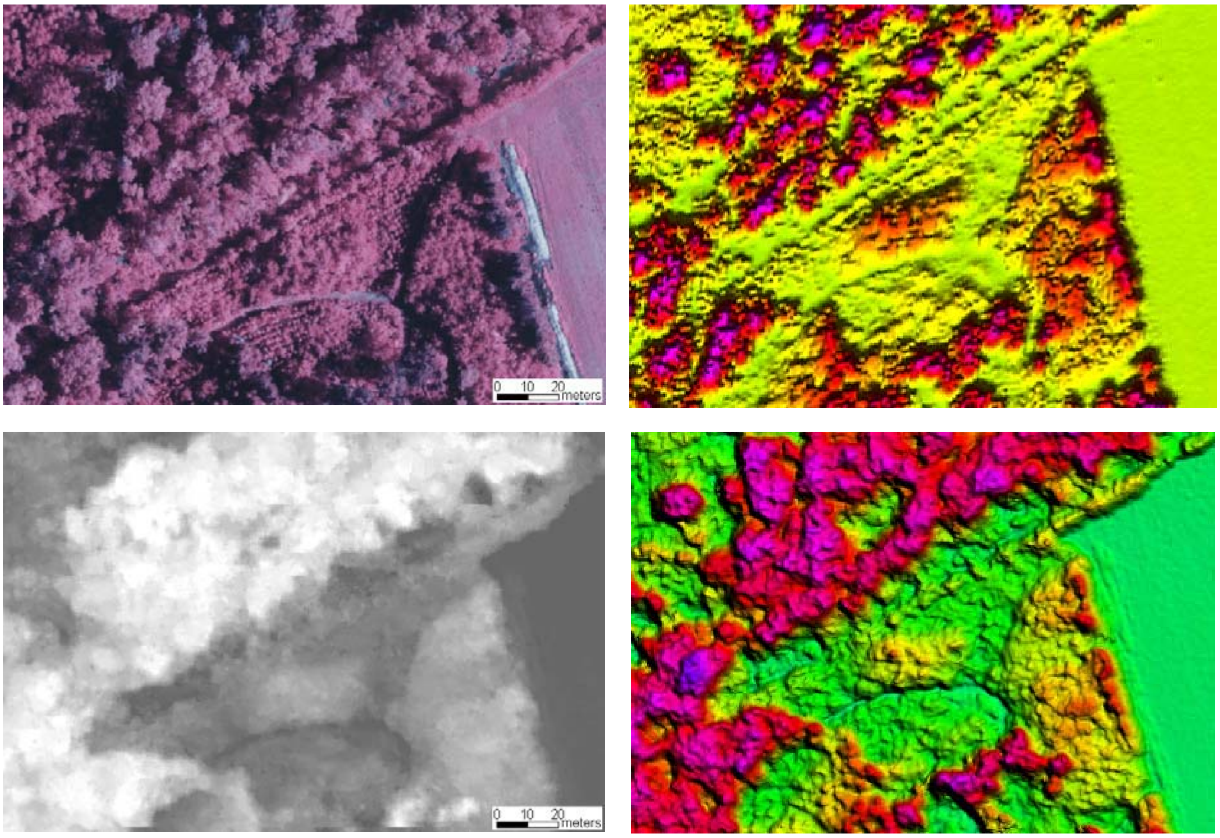


*Figure 4: From top left clockwise. A 2003 image and the corresponding DSMs from ALS (2002, 1 m spacing), ETHZ matching (0.5 m spacing) and ATE (0.5 m spacing)*

*Table 1: Statistics of differences (in m) between DSMs and 181 manually measured reference points (interpolated tree height in DSM – reference height)*

| | Average with sign | RMS | Max. / No. of absolute differences > 1.5 m & 5 m |
|---|---|---|---|
| ETHZ DSM, 1998 images | -1.36 | 2.35 | -16.92 / 44 & 6 |
| ETHZ DSM, 2003 images | -0.85 | 1.68 | -18.06 / 31 & 1 |
| ALS DSM, 2002 data, (corrected for 2002 to 2003 difference) | -6.44 | 7.83 | -21.77 / 168 & 100 |

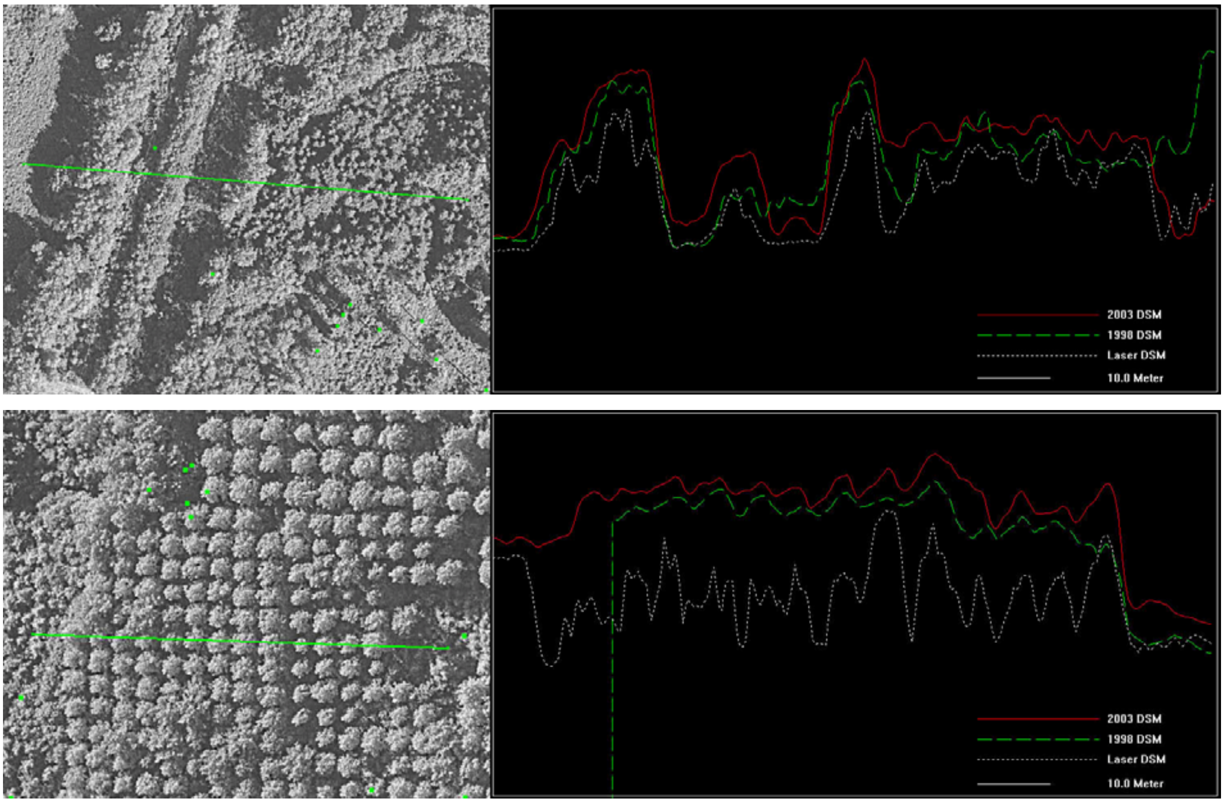


*Figure 5: Left: 2003 images and two profiles with different tree types and density. Right: the height values along the profiles from the 2003 (continuous lines) and 1998 (dashed lines) ETHZ DSMs and the ALS DSM (dotted lines)*

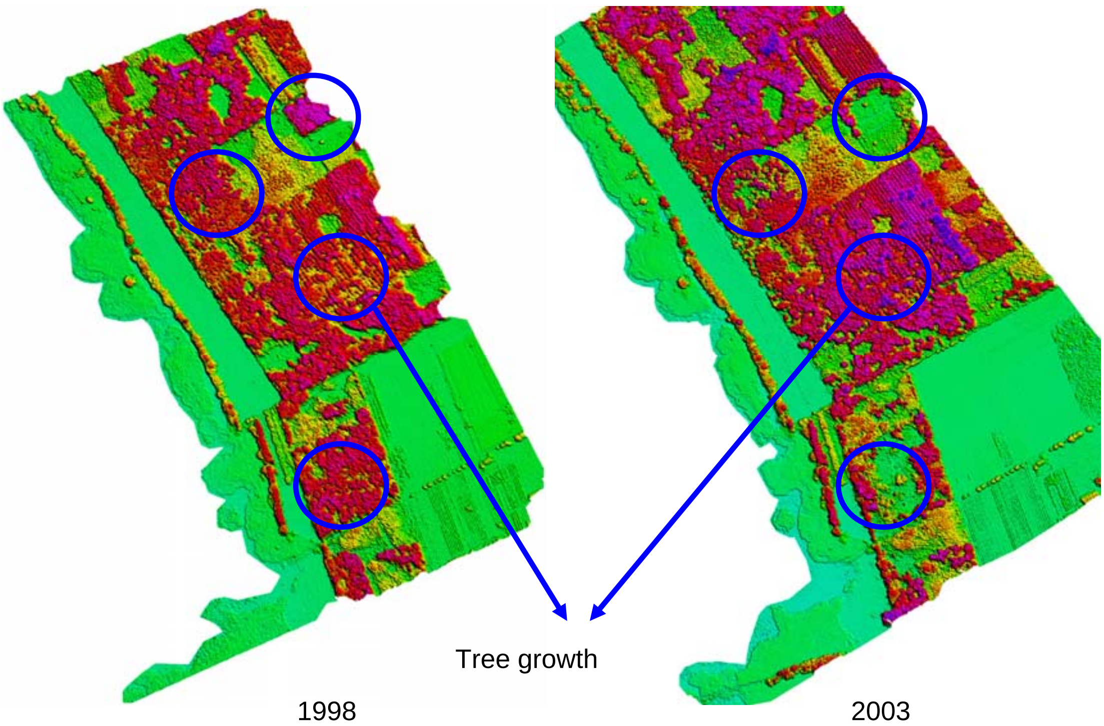


*Figure 6: Color coded ETHZ DSMs showing some areas of change. While one would expect a tree growth from 1998 to 2003, at some areas there is less or no vegetation in the 2003 DSM. This is due to destruction that occurred during the December 1999 hurricane Lothar*

*Table 2: Statistics of tree height differences (in m) between 2003 and 1998 at the position of the 181 reference points*

| | Manual measurements | ETHZ matching | Growth differences (ETHZ matching – manual) |
|---|---|---|---|
| Average with sign | 1.53 | 2.04 | 0.51 |
| RMS | 2.01 | 3.45 | 2.41 |

Regarding tree growth, the 1998 and 2003 ETHZ DSMs and occurred changes are shown in Fig. 6. A quantitative evaluation is shown in Table 2. The manually measured average tree growth of 1.5 m between 1998 and 2003 is very plausible. The difference between this growth and the one determined from the ETHZ DSM is 0.5 m, in spite of the uncertainty whether the same tree top was used in both methods. The good quality of the ETHZ DSMs show a high potential to derive accurate 3D canopy models and estimate growth using the whole tree volume.

## 4 FURTHER WORK AND CONCLUSIONS

There is a need for a more detailed analysis, e.g. finding the reasons for matching errors or an analysis of the relation of tree growth to tree type and height. More tests with better image data (better quality, digital sensors, at least 60 % sidelap and 6-wise image coverage of the scene, more similar imaging conditions and orientation) are planned to be performed. Of particular importance for WSL is the use of ADS40 data from Swisstopo, which are now regularly acquired over Switzerland. There is a need for more extensive and better reference data, including various tree types and sizes and small, possibly occluded, trees. For a more reliable growth analysis, the multitemporal DSMs should be first co-registered accurately before computing differences. This can be done by automated methods that coregister partially overlapping point clouds (see Akca 2005, Gruen & Akca 2005, Akca & Gruen 2005). Although such possible misregistration was not checked in this study, the profiles shown in Fig. 5 (especially at the top) do not show any major planimetric difference. Regarding ground information, a good quality existing DTM or DTM from manual measurements should be used. For growth analysis, only one DTM should be used, to avoid the influence of possible tree undergrowth. Instead of deriving tree height from a single point, maybe using a local average around the highest point should be preferred. The use of this local neighbourhood could also lead to detection of height blunders, while making easier a multitemporal comparison of the highest tree „point“. Tree area detection and tree height measurement can be further automated, especially through combination with information from digital image sensors (RGB, NIR, texture). A more practical alternative is to develop semi-automatic methods for the determination of tree area and height.

Newly developed, high-quality matching methods are by far better than existing commercial approaches and are a viable alternative to ALS. Such methods can generate DSMs that are at least as dense and of similar accuracy as DSMs generated by ALS. ALS DSMs also suffer more from canopy penetration and height underestimation, however, provide for estimation of the ground elevation which is more difficult using images. Dense automated measurements could lead in spite of few remaining errors to correct, more global estimates of: (a) tree height and other parameters, if the number of trees is high, and (b) tree growth by not taking outliers into account, e.g. for a certain tree type and size, the largest and lowest growth values could be left out. For frequent observation of small areas, there is the possibility to use other platforms, e.g. UAVs with medium format digital sensors. Summarising, the results of this study are very encouraging but there is need for further tests and increase of automation for tree height and growth estimation.

## ACKNOWLEDGEMENTS

The study was carried out in the frame of the Swiss mire monitoring program initiated in 1996 at WSL and funded by the Swiss Agency for the Environment, Forest and Landscape and WSL.

## REFERENCES


Akca, D. (2005). Registration of point clouds using range and intensity information. International Workshop on Recording, Modeling and Visualization of Cultural Heritage, Ascona, Switzerland, May 22-27, E. Baltsavias, A. Gruen, L. Van Gool, M. Pateraki (eds.), Taylor & Francis/Balkema, Leiden, pp. 115-126.

Akca, D., Gruen, A. (2005). Recent advances in least squares 3D surface matching. In: Gruen, A., Kahmen, H. (eds.), Optical 3-D Measurement Techniques VII, Vienna, Austria, October 3-5, Vol. II, pp. 197-206.

Artuso, R., Bovet, St., Streilein, A. (2003). Practical methods for the verification of countrywide terrain and surface models. Proceedings of the ISPRS working group III/3 workshop "3-D reconstruction from airborne laserscanner and InSAR data", Dresden, Germany, 8-10 October. In: International Archives for Photogrammetry, Remote Sensing and Spatial Information Sciences, Vol. 34, Part 3/W13, 6p. (on CD-ROM).

Baltsavias, E. (1999). Airborne laser scanning: existing systems and firms and other resources. ISPRS Journal of Photogrammetry and Remote Sensing, 54(2-3): 164-198.

Gaveau D., Hill R.A. (2003). Quantifying canopy height underestimation by laser pulse penetration in small footprint airborne laser scanning data. Canadian Journal of Remote Sensing, 29(5): 650-657.

Gong, P., Biging, G., Standiford, R. (2000). Use of digital surface model for hardwood rangeland monitoring. Journal of Range Management, 53(6): 622-626.

Gougeon, F.A. (1995). A crown following approach to the automatic delineation of individual tree crowns in high spatial resolution aerial images. Canadian Journal of Remote Sensing, 21: 274-284.

Gruen, A., Akca, D. (2005). Least squares 3D surface and curve matching. ISPRS Journal of Photogrammetry and Remote Sensing, 59(3): 151-174.

Grünig, A. (ed.) (1994). Mires and Man. Mire Conservation in a densely populated country – the Swiss experience. Excursion guide and symposium proceedings of the 5th field symposium of the international mire conservation group (IMCG) to Switzerland 1992. Birmensdorf, Swiss Federal Research Institute WSL, 415p.

Hasenauer, H., Monserud, R.A., Gregoir, T.G. (1998). Using simultaneous regression techniques with individual-tree growth models. Forest Science, 44(1): 87-95.

Heurich, M., Schneider, T., Kennel, E. (2003). Laser scanning for identification of forest structure in the Bavarian forest national park. In: Hyppä J., Naesset H., Olssen H., Granqvist Pahlen T., Reese H. (eds.), Proc. of the ScandLaser Scientific Workshop on Airborne Laser Scanning of Forests, September 3-4, Umea, Sweden, Swedish University of Agricultural Sciences, Department of Forest Resource Management and Geomatics, pp 98-107.

Küchler, M., Ecker, K., Feldmeyer-Christe, E., Graf, U., Küchler, H., Waser, L.T. (2004). Combining remotely sensed spectral data and digital surface models for fine-scale modelling of mire ecosystems. Community Ecology, 5(1): 55-68.

Magnussen, S., Eggermont, P., LaRiccia V.N. (1999). Recovering tree heights from airborne laser scanner data. Forest Science, 45(3): 407-422.

Means, J.E., Acker, S.A., Fitt, B.J., Renslow, M., Emerson, L., Hendix, C.J. (2000). Predicting forest stand characteristics with airborne scanning lidar. Photogrammetric Engineering and Remote Sensing, 66(11): 1367-1371.

Morsdorf, F., Meier, E., Kötz, B., Itten, K.I., Dobbertin, M., Allgöwer, B. (2004). LIDAR-based geometric reconstruction of boreal type forest stands at single tree level for forest and wildland fire management. Remote Sens. Environ., 92(3): 353-362.

Naesset, E. (1997). Determination of mean tree height of forest stands using airborne laser scanner data. ISPRS Journal of Photogrammetry and Remote Sensing, 52(2): 49-56.

Persson, Å., Holmgren, J., Söderman, U. (2002). Detecting and measuring individual trees using an airborne laser scanner. Photogrammetric Engineering and Remote Sensing, 68(9): 925-932.

SocetSet (2004). SocetSet User Manual 5.1. chapter 33, pp. 1-10. Copyright © 1998-2004, BAE Systems, 977 p.

St-Onge, B. (1999). Estimating individual tree heights of the boreal forest using airborne laser altimetry and digital videography, ISPRS Workshop on "Mapping surface structure and topography by airborne and spaceborne lasers", Commission III, Working Group 3, La Jolla,CA, USA, 9-11 November. In: International Archives of Photogrammetry, Remote Sensing and Spatial Information Sciences, Vol. 32, Part 3/W14, pp. 179-184.

St-Onge, B., Achaichia, N. (2001). Measuring forest canopy height using a combination of lidar and aerial photography data. International Archives of Photogrammetry, Remote Sensing and Spatial Information Sciences, Vol. 34, Part 3/W4, pp. 131-137.

St-Onge, B., Jumelet, J., Cobello, M., Vega, C. (2004). Measuring individual tree height using a combination of stereophotogrammetry and lidar. Canadian Journal of Forest Research, 34: 2122-2130.

Wang, L., Gong, P., Biging, G.S. (2004). Individual Tree-Crown Delineation and Treetop Detection in High-Spatial-Resolution Aerial Imagery. Photogrammetric Engineering & Remote Sensing, 70(3): 351-357.

Wulder, M., Niemann, K.O., Goodenough, D. (2000). Local Maximum Filtering for the Extraction of Tree Locations and Basal Area form High Spatial Resolution Imagery. Remote Sens. Environ., 73(1): 103-114.

Zhang, B., Miller, S.B. (1997). Adaptive automatic terrain extraction. In: McKeown, D.M., McGlone, J.C. and Jamet, O. (eds.), Integrating photogrammetric techniques with scene analysis and machine vision III, Proc. SPIE, Vol. 3072, pp: 27-36.

Zhang, L. (2005). Automatic Digital Surface Model (DSM) Generation from Linear Array Images. PhD Dissertation, Report No. 88, Institute of Geodesy and Photogrammetry, ETH Zurich, Switzerland. URL: http://e-collection.ethbib.ethz.ch/ecol-pool/diss/fulltext/eth16078.pdf.

Zhang, L., Gruen, A. (2004). Automatic DSM Generation from Linear Array Imagery Data. International Archives of Photogrammetry, Remote Sensing and Spatial Information Sciences, Vol. 35, Part B3, pp. 128-133.

# ANALYSIS OF THE INFORMATION CONTENT OF TERRESTRIAL LASERSCANNER POINT CLOUDS FOR THE AUTOMATIC DETERMINATION OF FOREST INVENTORY PARAMETERS

*Anne Bienert, Hans-Gerd Maas, Steffen Scheller*

Technische Universität Dresden, Chair of Photogrammetry, Dresden, Germany,
anne.bienert@tu-dresden.de

## ABSTRACT

Terrestrial laserscanners find rapidly growing interest in photogrammetry as efficient tools for fast and reliable 3D point cloud data acquisition. They have opened a wide range of application fields within a rather short period of time. Beyond interactive measurement in 3D point clouds, techniques for the automatic detection of objects and the determination of geometric parameters form a high priority research issue. The quality of 3D point clouds generated by laserscanners and the automation potential make terrestrial laserscanning also an interesting tool for forest inventory.

The paper will first review current laserscanner systems from a technological point of view and discuss different scanner technologies and system parameters regarding their suitability for forestry applications. In the second part of the paper, results of a pilot study on the applicability of terrestrial laserscanners in forest inventory tasks will be presented. The study concentrates on the automatic detection of trees and the subsequent determination of tree height and breast height diameter.

Reliability and precision of techniques for automatic point cloud processing were analysed based on scans of a test region in a Saxonian mixed forest. In the pilot study, which represents an early stage of software development, more than 95% of the trees in a test region could be detected correctly. Tree heights could be determined with a precision of 80 cm, and breast height diameters could be determined with a precision of less than 1.5 cm.

Keywords: Terrestrial laserscanning, forest inventory, automation

## 1 INTRODUCTION

Forest inventory and forest management and planning tasks require, beyond other parameters, the measurement of some parameters describing the geometry of trees. In the most simple case, these parameters are limited to the tree height and breast height diameter. In some tasks, many more geometry parameters, such as height-diameter profiles, ovality of the stem, open stem height, damages or branch diameters are required. As a full area coverage inventory is usually not possible, inventory schemes based on data acquisition in plots and statistical extrapolation schemes have been developed.

Terrestrial laserscanning, combined with automatic data processing tools, may depict a rather interesting tool to facilitate the data acquisition for tree geometry parameters in larger plots. Several studies on the applicability of terrestrial laserscanners in forest inventory tasks have been published: (Simonse et al., 2003) use a 2D Hough transform to detect trees in point clouds and to determine breast height diameters after height reduction to the digital terrain model. This approach is extended to the determination of diameters in different heights by (Aschoff/Spiecker, 2004). (Gorte/Winterhalder, 2004) and (Gorte/Pfeifer, 2004) generate tree topology skeletons by projecting point clouds into a voxel space, where stems and major branches are extracted by morphology operations using 3D structure elements and connectivity analysis. (Pfeifer/Winterhalder, 2004) model the stem and some major branches of a tree by a sequence of cylinders fitted into the point cloud. (Thies/Spiecker 2004) show the results of a pilot study based on the works mentioned above. They report a relatively low rate of only 22% of the trees detected in single scans and 52% detection rate in multiple scans. While the stem position could be determined at rather high precision, breast height diameters showed a standard deviation of 3.5 cm, obtained from a comparison of laserscanner data processing results with conventional calliper measurements. The standard deviation of tree height determination was 5.6 meters and thus not satisfactory.

The goal of the study presented here is to test the precision and reliability potential of terrestrial laserscanner data processing schemes, which were developed originally for building documentation and facility management tasks, in forest inventory applications. The paper will first give a short overview on the technology and performance parameters of different types of terrestrial laserscanners. Chapter 3 will discuss the techniques used for automatic geometry parameter extraction from laserscanner point clouds. The results of a pilot study in a Saxonian mixed forest will be presented and discussed in chapter 4.

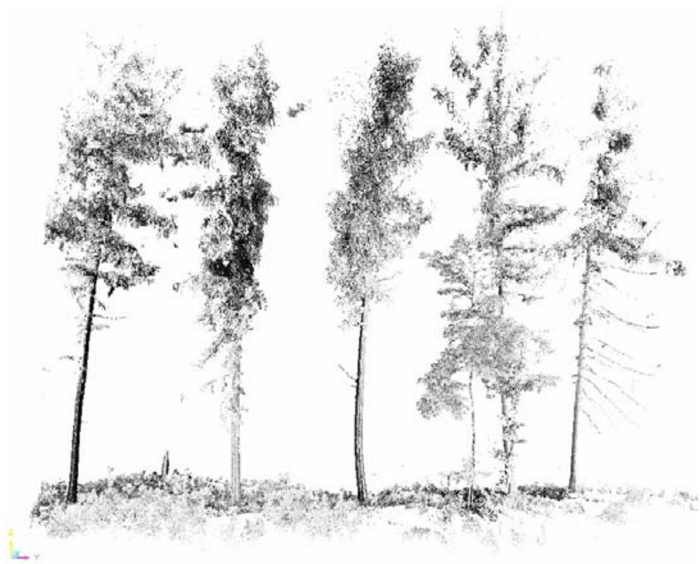

*Figure 1: Laserscanner data section with five trees (2D projection at reduced resolution)*

## 2 TERRESTRIAL LASERSCANNER INSTRUMENTS

Terrestrial laserscanners have become rather popular in geodesy and photogrammetry in the last five years. In fact, they can be considered a bridge between engineering geodesy and photogrammetry, combining tachymeter-like instrument design principles with data processing methods mostly derived from photogrammetric techniques. Laserscanners generate 3D point clouds representing an object surface. These 3D point clouds can be considered an end product or a basis for generating value added structured data products.

Laserscanner instruments, which are currently on the market, can be categorized after different criteria:

- Field of view: Many laserscanners offer a panoramic 360° horizontal field of view with a vertical opening angle between 80° and 135°. Fewer scanners offer a camera-like limited field of view.
- Range measurement principle: Most scanners use time-of flight measurement for range determination. The precision of time-of-flight measurement is usually limited to 5-10 mm. Some scanners use phase modulation techniques to achieve a higher range measurement precision of 1-3 mm. This principle comes with the disadvantage of a limited range due to wave number ambiguities. The highest precision, however at a rather limited range, can be achieved by scanners following the triangulation principle with a laser source and a receiver delivering an angular measurement arranged at a fixed base.
- Beam deflection principle: Laserscanners scan an object surface sequentially, with the beam deflected by galvanometric mirrors, polygon wheels, rotating elliptical mirrors, rotation of the instrument or combinations thereof.

Further differentiating factors may be the maximum range (between less than 20 meters for triangulation scanners and more than 1000 meters for some time-of-flight scanners) or the data rate (2'000 … 625'000 points per second with current instruments). Some instruments offer an integrated camera, allowing for the acquisition of high resolution surface texture and for the fusion of point cloud and image data processing.

A laserscanner to be used in forest inventory applications should have a maximum range of 20 … 100 meters and a data rate of at least 10'000 points per second. For flexibility in data acquisition, it should offer a panoramic field of view. The range measurement precision should be better than 10 mm. Special consideration has to be paid to problems caused by multiple echoes obtained from a single pulse, such as from twigs partially occluding each other: All range measurement principles may produce ghost points in these cases (Böhler/Marbs, 2004), which have to be considered in the development of data processing schemes.

# 3 DATA PROCESSING METHODS

Terrestrial laserscanners may be used as 3D point cloud generation tools with the goal of interactive measurement of relevant parameters in the point cloud, thus shifting the interpretation task from the field to the office. Much more interesting from an economic point of view, however, are techniques for automatic derivation of task-relevant parameters from point clouds. In the following, we will show a technique for point cloud segmentation with the goal of detecting and extracting stems, the determination of tree heights and the determination of breast height diameters and diameter-height profiles. The techniques presented here represent only an early stage of development, mainly documenting the applicability of techniques, which were originally developed for other purposes (Bienert, 2006; Scheller, 2006), to forest inventory tasks. Task-specific knowledge can be used in the parameterization of the methods in order to optimize the success rates.

## 3.1 Detection of trees

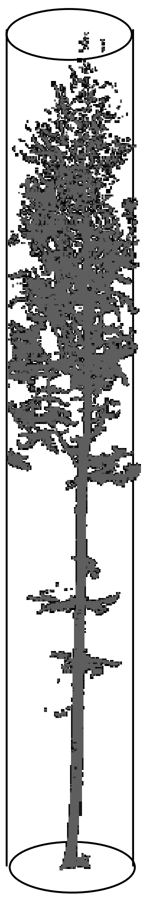

The tree detection process is based on the analysis of horizontal slices in the laserscanner data. A slice with a thickness d is cut out of the point cloud at a height of 1.30 meter above the ground. In rough terrain the digital terrain model can be obtained from percentile filtering of the point cloud. A structure element of a size *s* is moved over the X/Y-projection of the points in the slice in a morphology-like technique, defining clusters with more than a preset number of *n* points as an object and separating objects which are more than *s/2* cm apart.

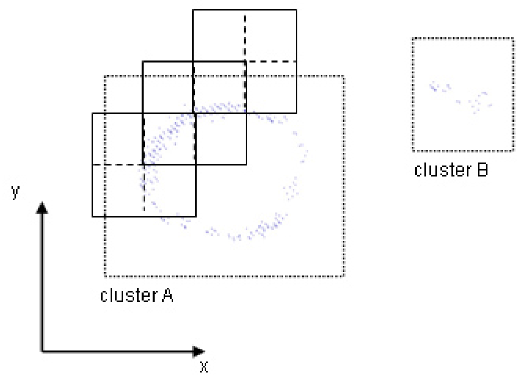


*Figure 2: Reduced 2D representation of a scanned tree and vertical cylinder, cluster search procedure*

In a next step, a circle is fit into the cluster. The cluster is accepted as a tree if the radius $r$ of the circle is above a threshold $r_{min}$ and if the standard deviation $\sigma$ of the cluster points to the circle is smaller than a preset maximum $\sigma_{max}$. The center of the circle defines the $(X,Y)$ coordinate of a detected tree. The technique can be applied to multiple scan data delivering full circles as well as to single scan data delivering ca. 160° sectors of tree cross sections.

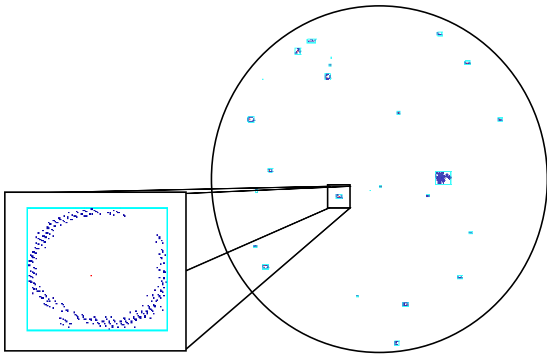

*Figure 3: Tree detection*

### 3.2 Tree height determination

The tree height is defined as the height difference between the highest point of the point cloud of a tree and the terrain model, accepting that the highest point of the cloud may not always represent the top of the tree and that a better definition of the representative terrain model point has to be used in rugged terrain. The point representing the terrain model is defined as the lowest point in a vertical cylinder of a radius $r_1$ around the tree center coordinates $(X,Y)$. The tree top is defined as the highest point in a vertical cylinder of a radius $r_2$ around the tree center coordinates (Figure 4), with $r_1 \leq r_2$.

### 3.3 Diameter determination

The breast height diameter is determined by cutting a slice of thickness $d$ in a height of 1.30 meter above the representative terrain model point. An adjusting circle is fit into the 2D projection of the points of the slice. As a result, we obtain the breast height diameter, the standard deviation of unit weight and the standard deviation of the diameter. Proceeding with the technique, stem diameters in arbitrary height and stem diameter height profiles can be determined straightforwardly.

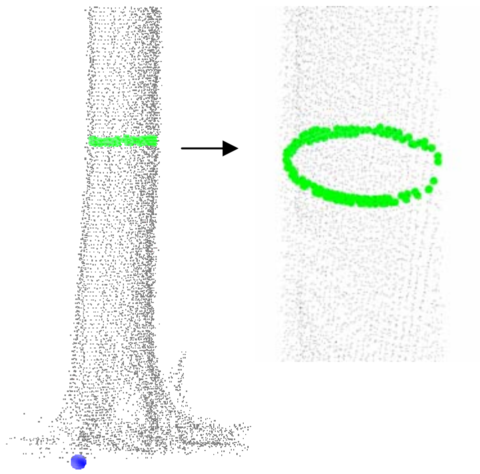

*Figure 4: Breast height circle*

## 4 PRACTICAL RESULTS

The practical data for the pilot study on the applicability, precision and reliability of the methods shown in chapter 3 were acquired with a terrestrial laserscanner Riegl LMS Z420i. The test site was a plot of mixed forest in Saxony. The plot contained a total of 14 trees and was recorded from two laserscanner positions.

All trees in the plot could be detected successfully (Figure 3). In a second test site, 32 out of 33 trees could be detected. The results of breast height diameter determination for the detected trees of the plot are listed in Table 1. The standard deviation of unit weight was 1.4 cm. The interior standard deviation of tree diameter determination, obtained from the circle fit procedure, was 0.5 cm. The RMS of the differences between tree parameters derived from laserscanner data and reference measurements with a tree calliper was 1.5 cm. On average, the diameter is determined slightly too high. This can be explained by the laserscanner spot diameter and could be compensated in the future by a distance and beam divergence dependent correction term, thus further improving the precision of tree diameter determination.

*Table 1: Differences between breast height diameter from laserscanner data and reference measurements*

| | Diameter [cm] |
|---|---|
| minimum deviation | -0.8 |
| maximum deviation | 3.3 |
| arithmetic mean | 0.9 |
| RMS | 1.5 |

Tree height reference measurements were available for only two trees of the plot. The height of the remaining trees was determined by an extrapolation technique based on the breast height diameter, as usual in today's forest inventory. The height differences of the two trees with reference measurements were 0.22m and 1.47m, respectively. Here it is doubtful if the conventional hand-held-tachymeter based measurement can be considered a reference. In a second test plot, reference heights of four trees were determined by a tachymeter. Here the comparison delivered an RMS tree height error of 80 cm.

In addition to the determination of breast height diameter, a height-diameter diagram was determined for one tree by repeating the diameter determination in regular height intervals (Table 2).

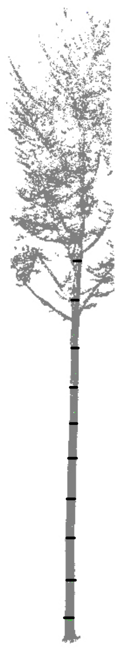

| Height [m] | Diameter [cm] |
|---|---|
| 1.30 | 19.5 |
| 3.30 | 18.6 |
| 5.30 | 17.9 |
| 7.30 | 17.2 |
| 9.30 | 16.5 |
| 11.30 | 16.0 |
| 13.30 | 15.4 |
| 15.30 | 14.7 |
| 17.30 | 12.9 |
| 19.30 | 10.6 |

*Figure 5 & Table 2: Beech tree with 10 diameters in 2m height intervals, height-diameter diagram*

## 5 DISCUSSION & CONCLUSION

Although the results presented here are only the outcome of a pilot study, which can be improved in many aspects, they show the application potential of terrestrial laserscanner in forest inventory and forest management tasks. Terrestrial laserscanning, combined with automatic data processing tools, may bridge the gap between conventional inventory techniques and airborne laserscanning. While conventional inventory techniques are based on small plots and have to rely on statistical extrapolation techniques, airborne laserscanning acquires full area data, but is limited to the determination of tree parameters, which can be derived from terrain and crown height model by applying suitable models. Terrestrial laserscanning has the potential of delivering reliable and precise information on geometric parameters of trees in larger plots.

The techniques shown in chapter 3 and 4 can be further improved by using multiple layer techniques to optimize the tree detection process and by slicing the cylinders used for tree height determination in order to avoid points of neighbouring trees affecting height determination. In addition to the parameters discussed in chapter 3, further parameters such as ovality of the stem, structure and damages of the bark, open stem height, tree topology, branch angles and diameters can be determined by an extension of the techniques. Using shape and texture information derived from laserscanner data in combination with classification techniques applied to images of an integrated camera, an automatic tree species recognition may be envisaged. Due to the character of an automated, objective measurement technique, the method is also well suited for change detection tasks in multi-temporal scans.

A very interesting option for the reduction of the effort of data acquisition is provided by novel range cameras, which will soon be commercially available. Range cameras (e.g. Oggier et al., 2003) are based on CMOS sensors, where each pixel can be considered an electro-optical distance meter. They deliver a greyscale image plus a range image with a distance measurement for each pixel. Range cameras are very compact, they can be used in a hand-held manner and their price will be much lower than the price of a terrestrial laserscanner system. Current cameras show several limitations such as a sensor format of only up to 176x144 pixels, a maximum range of 7.5 meters and a distance precision of about 1%. Once these limitations are overcome, range cameras could well be used for fast and flexible data acquisition in forestry tasks.

## ACKNOWLEDGEMENT

The authors would like to thank the Institute of Forest Economics and Forest Management Planning, TU Dresden, for their cooperation in the data acquisition for the pilot study.

## REFERENCES

Aschoff, T., Spiecker, H., 2004: Algorithms for the Automatic Detection of Trees in Laser-Scanner Data. International Archives of Photogrammetry, Remote Sensing and Spatial Information Sciences, Volume XXXVI, Part 8/W2

Bienert, A., 2006: Glättung von aus Laserscannerpunktwolken extrahierten Profilen. Photogrammetrie - Laserscanning - Optische 3D-Messtechnik (Beiträge Oldenburger 3D-Tage 2006, Hrsg. Th. Luhmann), Verlag Herbert Wichmann

Böhler, W., Marbs, A., 2004: Vergleichende Untersuchung zur Genauigkeit und Auflösung verschiedener Scanner. Luhmann, Th. (Ed.): Photogrammetrie, Laserscanning, Optische 3D-Messtechnik - Beiträge der Oldenburger 3D-Tage. Wichmann Verlag Heidelberg, pp. 82-89

Gorte, B., Pfeifer, N., 2004: Structuring laser-scanned trees using 3D mathematical morphology. International Archives of Photogrammetry and Remote Sensing, Vol. XXXV, B5, pp. 929-933

Gorte, B., Winterhalder, D., 2004: Reconstruction of Laser-Scanned Trees using Filter Operations in the 3D-Raster Domain. International Archives of Photogrammetry, Remote Sensing and Spatial Information Sciences, Volume XXXVI, Part 8/W2

Oggier, T., M. Lehmann, R. Kaufmann, M. Schweizer, M. Richter, P. Metzler, G. Lang, F. Lustenberger, N. Blanc, 2003: An all-solid-state optical range camera for 3D real-time imaging with sub-centimeter depth resolution (SwissRanger™). SPIE Proceedings Series Vol. 5249-65, pp. 534-545

Pfeifer, N., Winterhalder, D., 2004: Modelling of Tree Cross Sections from Terrestrial Laser-Scanning Data with Free-Form Curves. International Archives of Photogrammetry, Remote Sensing and Spatial Information Sciences, Volume XXXVI, Part 8/W2, pp. 76-81

Scheller, S., 2006: Extraktion von Primitiven aus Laserscannerpunktwolken zur Rekonstruktion von Tragwerken. Photogrammetrie - Laserscanning - Optische 3D-Messtechnik (Beiträge Oldenburger 3D-Tage 2006, Hrsg. Th. Luhmann), Verlag Herbert Wichmann

Simonse, M., Aschoff, T., Spiecker, H., Thies, M., 2003: Automatic Determination of Forest Inventory Parameters Using Terrestrial Laserscanning. Proceedings of the ScandLaser Scientific Workshop on Airborne Laser Scanning of Forests, Umeå/Sweden, pp. 251- 257

Thies, M., Spiecker, H., 2004: Evaluation and Future Prospects of Terrestrial Laser-Scanning for Standardized Forest Inventories. International Archives of Photogrammetry, Remote Sensing and Spatial Information Sciences, Volume XXXVI, Part 8/W2

# THREE-DIMENSIONAL FOREST CANOPY STRUCTURE FROM TERRESTRIAL LASER SCANNING

*F. Mark Danson[1], David Hetherington[1], Felix Morsdorf[2], Benjamin Koetz[2] & Britta Allgöwer[2]*

[1] Centre for Environmental Systems Research, University of Salford, Manchester M5 4WT, UK
f.m.danson@salford.ac.uk

[2] Department of Geography, University of Zurich, Zurich, Switzerland

## ABSTRACT

A terrestrial laser scanner was used to measure the three-dimensional structure of forest stands in the Swiss National Park, eastern Switzerland. Spatially coincident hemispherical photographs were taken at each sampling point and the position of each point was determined using differential GPS. A scanner model was derived in order to determine the expected number of laser shots in all directions, and these data were compared with the measured number of laser hits to determine directional gap fraction at nine sampling points. Directional gap fraction distributions were determined from the digital hemispherical photography and compared with distributions computed from the laser scanner data. The results showed that the measured directional gap fraction distributions were similar for both hemispherical photography and terrestrial laser scanner data with a high degree of precision in the area of overlap of orthogonal laser scans. Unlike hemispherical photography the laser scanner data offer semi-automatic measurement of gap fraction distributions, plus additional three-dimensional information about tree height, gap size distributions and foliage distributions.

**Keywords**: Terrestrial laser scanner, three-dimensional, forest structure

## 1 INTRODUCTION

The three-dimensional (3d) arrangement of forest canopy elements controls light interception, CO2 fluxes and canopy hydrometeorological characteristics. Conventional methods of measuring plant canopy structure are time-consuming, labour intensive and error-prone. Direct methods normally involve destructive sampling of canopy elements and in large complex forest or woodland canopies it may be impossible to collect sufficient samples to accurately characterize the structure (Jonckheere et al. 2004). Indirect methods of measuring canopy structure include both light interception instrumentation and hemispherical photography and there is an extensive literature showing how these methods may be used to measure forest leaf area index (LAI), canopy cover, gap size distributions and light climate (Weiss et al. 2004).

Terrestrial laser scanning (TLS) uses range-finding measurement technologies to derive the 3d position of objects within the scanner field of view. TLS are now capable of collecting 3d data clouds (x,y,z, intensity) of several million data points in less than five minutes. Their application in surveying and engineering is now well established and recent research has examined their application for 3d mapping in the environmental sciences (eg. Heritage and Hetherington 2005). Applications of terrestrial laser scanning in forestry have focussed on the rapid semi-automatic determination of stand characteristics like tree density, height and girth, and there now appears to be great potential for the application of TLS in forest inventory and monitoring (Thies et al. 2004, Hopkinson et al. 2004, Watt and Donoghue 2005). However this paper assesses the potential of TLS for measuring the 3d characteristics of forest canopies and specifically the extraction of canopy gap fraction measurements. Well established methods to measure plant canopy structure, based on the point-quadrat methods of Warren-Wilson (1963), have been adapted to use hemispherical photography below forest canopies in order to measure canopy structure. This paper compares hemispherical photography and TLS measurements to derive forest canopy gap fraction, and other stand attributes.

## 2 LASER SCANNER CHARACTERISTICS AND DATA PROCESSING

The laser scanner used in this research was a Riegl LMZ210i which uses a two-axis beam scanning mechanism and a pulsed time-of-flight laser rangefinder measure the 3d position of points within a range of about 350m. Line scan measurements are produced through the rotation of a rotating polygon-mirror and frame scan measurements through the rotation of the optical head of the scanner. The angular step width in both line and frame scan directions may be set by the user to determine the angular separation between laser shots. The line and frame scan angle ranges may also be determined by the user within the limits of the instrument (table 1).

*Table 1: Terrestrial laser scanner characteristics*

| | |
|---|---|
| Riegl LMZ 210i | |
| Two-axis beam scanning mechanism | |
| Single shot time of flight measurement | |
| Wavelength | 900nm |
| Range (typical) | 350m |
| Line scan angle range | 0 – 80o |
| Frame scan angle range | 0 – 333o |
| Laser beam divergence | 3 mrad |
| Angular step width | 0.072 - 0.36o |
| Measurement resolution (one shot) | 25mm |
| Pulse repetition rate (maximum) | 28,000 Hz |
| Measurement time (typical) | 3 mins for 1 million points |

Since the TLS used does not record laser ‘misses’, it was necessary to develop a laser scanner model to determine the total number of ‘shots’ per scan, which is dependent on resolution, and line and frame scan angle range. This involved five steps: Cartesian to cylindrical coordinate transform, cylindrical to spherical transform with fixed value of sphere radius (r), spherical to Cartesian transform, deletion of shots in segments at angles greater than or less than the specified line scan angle range. To test the scanner model a single scan was performed using the TLS indoors in an enclosed room with no windows with the scanner pointing towards the ceiling, a line scan angle range of 51.27 to 127.32 $^{o}$ and frame scan angle range of 0 to 180 $^{o}$, and a resolution in both directions of 0.18 $^{o}$. The frequency of laser shots in 5 $^{o}$ elevation bands from 0 to 90 $^{o}$ was calculated using both measured and modelled scanner data in spherical coordinates. The results showed very strong agreement between the measured and modelled frequencies giving high confidence in the validity of the scanner model.

## 3 METHODS

Spatially and temporally coincident TLS data digital hemispherical photographs were collected in a semi-natural forest area in the Swiss National Park, Switzerland, in August 2005. The forest is located in the Ofenpass valley at an altitude of approximately 1900m. The dominant tree species is mountain pine (Pinus mugo) and some stone pine (Pinus cembra). A 300m transect with nine sampling locations was employed. At each sampling point a surveying tripod was levelled and differential GPS data were collected to determine the geographic location of the sampling point. A single hemispherical photograph was taken using an upward looking Nikon Coolpix 4500 with a calibrated hemispherical lens. The hemispherical photographs were analyzed using the Gap Light Analyzer (GLA) software (Frazer et al. 1997). Gap fractions were computed for zenith angles from 0 to 90o with 5o spacing, and averaged over all azimuth angles. LAI was computed for each photograph using the GLA software.

The TLS was then mounted on the tripod at an inclination angle of 90° and a single scan recorded with a line scan angle of approximately 80° and a frame scan angle of 180° (figure 1). The TLS was then rotated through 90° and a second orthogonal scan recorded. The resolution of all scans was set at 0.108° in line and frame scan directions. A single scan recorded about one million points in around four minutes. The scanner data were converted to Cartesian coordinates using the RiScanPro™ software, which included a correction for an angle-dependent shift in the origin of the laser measurements.

*Figure 1. Terrestrial laser scanner deployed in Swiss National Park. Orientation of scanner to facilitate upward-looking scanning*

## 4 RESULTS

The laser scanner recorded the x,y,z position of all laser hits, plus the intensity of the return and colour information in an RGB file. Only the x,y,z position data are considered in this paper, although it is clear that the intensity data contained useful information on target reflectivity related to target type (figure 2a). Nine sampling locations were used but data for a sub-set of these is presented here. Overall the information content of the laser scans appeared to be similar to that of the hemispherical photographs (figure 2b) but additional range-related data could be easily extracted from the scans. For example the frequency of returns in the z-direction provided data on the vertical distribution of vegetation elements and height of the canopy and xy slices could be used to estimate canopy cover

After conversion to spherical coordinates (figure 2c), the measured scans were compared with the equivalent model scan in order to determine the angular gap fraction distribution. In contrast to the results of Lovell et al. (2003) who found that laser scanning overestimated gap fraction in a pine forest, the distributions derived from laser scanning in our work were very similar to those derived from the hemispherical photography and two contrasting examples are shown in figure 3. Canopy cover estimated from the hemispherical photograph, using only azimuth angles between 0 and 10°, for the site in figure 3a was 75.2% and using the ratio of laser shots to hits, over the same range of angles, cover was 75.6%. For the site in figure 3b the same figures were 10.8% and 14.3%.

The orthogonal laser scans sampled the same area of the canopy between zenith angles of 0 and 40° (since the line scan angle range was about 80°) and so provide an independent test of the precision of the laser scanner measurements. In all plots the difference between the gap fraction measurements for the two laser scans was generally small up to 40°. At zenith angles greater than 40° there was some divergence in the gap fraction measured reflecting azimuthal variation in canopy structure. Only a small segment of the hemisphere was not measured and averaging the two orthogonal scans would be a reasonable way to represent the complete gap fraction distribution.

Comparison between the gap fractions determined from the hemispherical photography and from the laser scanner showed general agreement. For the site shown in figure 3a there were some differences at zenith angles between 20-25°, with the hemispherical photography indicating a gap fraction of 40% and the laser scanner 20%. These differences may be due to the solar glare seen in the photograph, or errors related to the manual thresholding of the digital imagery. Alternatively there may be errors in the laser scanner data with underestimation of vegetation cover due to the fine structure of the tree needles and shoots in the canopy. However, the similarity of the data from the two orthogonal scans of the TLS does indicate consistency in the measurements and there is no general evidence of underestimation of vegetation cover with the TLS. In the example shown in figure 3b the fit between the photography and TLS data is closer but at zenith angles above 40$^o$ the laser data appear to show higher gap fraction than the photography which shows zero gap from 60$^o$ zenith and above. This is a feature of data from most of the nine plots sampled and suggests that the laser scanner is either measuring small gaps not detected by the photography, or that the laser shots are hitting low reflectance target at far range so that the return intensities are too low for detection.

(a) (b) (c)

*Figure 2. (a) Terrestrial laser scanner data of forest stand displaying intensity of returns in a cylindrical projection. Scan range 180x80 degrees (site 7). (b) Digital hemispherical photograph at same location as figure 5. Equiangular projection. (c) Processed x,y,z coordinate laser scanner data of location in figure 3 showing projection of laser hits onto a hemisphere of unit radius.*

(a)

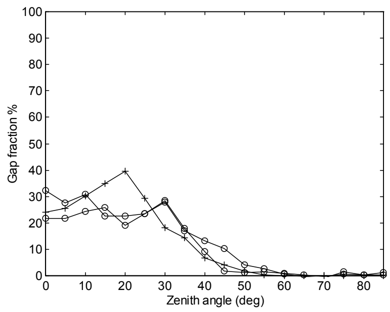


(b)

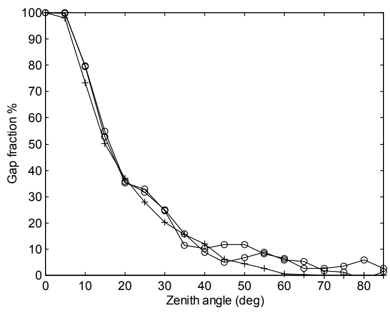


*Figure 3. Comparison of gap distribution derived from hemispherical photographs (solid line) and two orthogonal laser scan (broken line). The orthogonal scan sample the same part of the canopy up to a zenith angle of 40o.*

## 5 DISCUSSION

The results of this experiment confirm the potential of TLS for measuring the 3d structure of forest canopies. The fit of the hemispherical photography gap fraction data to the TLS gap fraction data was close for all the measured plots and we are now comparing LAI estimates form the two data sources. However, further work is required to understand the effects of beam divergence on gap detection. At a range of 10m the laser spot size is approximately 30mm in diameter and at 20m it is 60mm. The detectability of gaps with the TLS is therefore range dependent. Further experiments are also required to assess the effect of variation in angular sampling resolution since this is independent of beam divergence.

## 6 CONCLUSIONS

To date the only technique available for creating a permanent record of forest canopy structure is of hemispherical photography. There are a number of key advantages of hemispherical photography over light interception measurements (Jonckheere et al. 2004) but the weaknesses of the photographic approach are the requirement for manual intervention in post-processing the images, and the variability of the measurements with different sky conditions. In contrast, the TLS post-processing routines applied in this research could be automated, and sky conditions had little influence on the quality of the data collected. These factors, coupled with the additional 3d information that can be extracted from the data suggest that TLS will be central to future developments in the measurement of 3d vegetation canopy structure.

## ACKNOWLEDGEMENT

This research was partly funded by EU Spread Contract number EVG1-CT-2001-00043.

## REFERENCES

Heritage, G.L. and Hetherington, D. (2005) The use of high resolution field laser scanning for mapping surface topography in fluvial systems. Int. Assoc. of Hydrol. Sci., 291, 269-277.

Hopkinson, C., Chasmer, L., Young-Pow, C. and Treitz, P. (2004) Assessing forest metrics with a ground-based scanning lidar. Canadian Journal of Forest Research, 34, 573-583.

Jonckheere, I., Fleck, S., Nackaerts, K., Muys, B., Coppin, P., Weiss, M. and Baret, F. (2004) Review of methods for in situ leaf area index determination - Part I. Theories, sensors and hemispherical photography Agricultural And Forest Meteorology, 121, 19-35.

Lovell, J.L., Jupp, D.L.B., Culvenor, D.S., Coops, N.C. (2003) Using airborne and ground-based ranging lidar to measure canopy structure in Australian forests, Canadian Journal of Remote Sensing, 29, 607-622.

Thies, M., Pfeifer, N., Winterhalder, D., Gorte, B.G.H. (2004) Three-dimensional reconstruction of stems for assessment of taper, sweep and lean based on laser scanning of standing trees, Scandinavian Journal of Forest Research, 19, 571-581.

Watt, P.J., and Donoghue, D.N.M. (2005) Measuring forest structure with terrestrial laser scanning, International Journal of Remote Sensing, 26, 1437-12446.

Warren-Wilson, J. (1963) Estimation of foliage denseness and foliage angle by inclined point quadrats. Australian Journal of Botany, 11, 95–105.

Weiss, M., Baret, F., Smith, G.J., Jonckheere, I. and Coppin, P. (2004) Review of methods for in situ leaf area index (LAI) determination Part II. Estimation of LAI, errors and sampling. Agricultural and Forest Meteorology, 121, 37-53.

# MEASURING HYDRODYNAMIC VEGETATION DENSITY IN A FLOODPLAIN FOREST USING TERRESTRIAL LASER SCANNING

*Jord Warmink[1,a], Hans Middelkoop[1] and Menno Straatsma[1]*

[1] Utrecht University, Department of Physical Geography, Utrecht, The Netherlands

[a] Corresponding author, j.j.warmink@students.uu.nl

## ABSTRACT

In this paper a method is presented to extract the aggregated hydrodynamic vegetation density of a river floodplain forest using terrestrial laser scanning. Hydrodynamic vegetation density (*Dv*) is defined as the sum of the frontal areas of all vegetation elements divided by the ground surface occupied by the vegetation multiplied by the water depth. The laser-scan data and reference data were collected in a floodplain forest along the river Rhine. The laser scanning was carried out using a Leica HDS3000 laser scanner, a time of flight scanner. Field reference data consisted of (1) a stem map of 650 trees, describing the position and the diameter of these trees. Eleven plots were derived from the stem map. (2) 7 manually measured plots.

Data processing consisted of slicing the points around breast height. These points were selected to predict the vegetation density value. In a polar grid two models were used to predict the vegetation density: 1) the percentage value and 2) the vegetation area index. The percentage value was corrected for missing points which increased the $R^2$ value from 0.17 to 0.72. The vegetation area index ($R^2$ = 0.67) has to be corrected for missing points in future studies to increase the predictive quality. Furthermore a correction for distance is done by including the distance of the reference plots to the scan positions in the regression equation. This improved the predictive quality, but in later studies the correction for distance has to be improved. It has been concluded that both models are good predictors for the vegetation density values.

**Keywords:** Floodplain vegetation, hydrodynamic vegetation density, Terrestrial Laser Scanning

## 1 INTRODUCTION

Safety levels of rivers are computed using hydrodynamic models. Floodplain vegetation, which is inundated by water, causes a resistance to the water flow, thereby raising the water levels in the rivers. For forests, the vegetation density (*Dv*) is needed as an input variable, which is defined as the sum of the frontal areas of all vegetation elements divided by the ground surface occupied by the vegetation multiplied by the water depth when inundated (figure 1; equation 1; Petryk & Bosmajian, 1975).

$$Dv = \frac{\sum_{i=1}^{n} A_i}{V} \approx N \cdot d \qquad (1)$$

where $A_i$ is the sum of the frontal areas of the vegetation in the water flow, $V$ is the volume of water. Under the assumption of cylindrical vegetation, the vegetation density can be computed by the product of $N$, the number of stems per square meter and $d$ is the average diameter of the vegetation. Vegetation density is expressed as $m^2/m^3$.

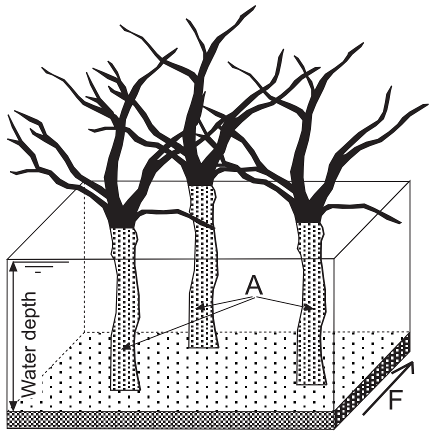


*Figure 1: Sketch of hydrodynamic vegetation density (Dv); the sum of the frontal areas of all vegetation elements divided by the ground surface occupied by the vegetation multiplied by the water depth when inundated*

To drive the hydrodynamic models, vegetation density needs to be mapped for all forested areas in the floodplain. Floodplain-wide mapping of vegetation characteristics is most appropriate using an remote sensing method, containing either spectral information from aerial photographs or satellites (Van der Sande et al., 2003), or height information from airborne laser scanning (Mason et al., 2003; Straatsma, 2005), or a combination thereof (Ehlers et al., 2003). Mertes (2002) gives an overview of remote sensing methods riverine landscapes. Independent of the remote sensing method however, accurate field reference data are needed for calibration or for a lookup table after classification of the vegetation types. The computation of the product of N times d does not generate reliable values in case the vegetation does not consist of cilindrical elements. Therefore, alternative methods have been proposed. Greame & Dunkerley (1993) determined the vegetation density using a photographic method. A white screen was used behind a vegetation plot and a photograph was made of the vegetation in front of the screen. The surface area of the frontal areas of the vegetation was determined by digitising the picture. The vegetation density was then acquired by dividing the percentage of coverage by the length of the plot. The number of stems per square meter ($N$) multiplied by the average diameter of the trees ($d$) at mid flow depth was used as reference data.

Other methods to measure the vegetation density in the field are compared by Dudley et al. (1998). The first method is the Cover Board method, where a person is walking backwards through the vegetation with a white board with a grid. An observer determines the distance where half of the board is covered and assuming a Poisson distribution the vegetation density can be calculated by the observed distance. A second method is the camera technique where the Leaf Area Index is measured by looking through a camera with a grid in the lens and measuring the distance for each grid point where the first vegetation element comes into focus. The digitisation process in the photographic method is done manually and introduces subjectivity. In the other methods the judgement of the observer is important on the measured values. Therefore the disadvantage of these methods is the high degree of subjectivity. Furthermore, the methods measure only a small plot and lack spatial variability.

In this pilot study, terrestrial laser scanning (TLS) is used for vegetation density measurements, which is a promising method for vegetation density mapping. TLS is currently used in vegetation research for recognition of individual trees. Gorte & Winterhalder (2004) used a voxel approach to reconstruct the branches of a single tree, which was scanned from multiple angles and Aschoff et al. (2004) used a tin triangulation for the digitisation of trees. Chasmer et al. (2004) characterized the three dimensional distribution of airborne and ground-based LiDAR data for conifer and mixed deciduous forest plots. For a plot containing large trees, object recognition techniques can be used for describing the vegetation, but when the vegetation consists of shrubs, with many small branches, object recognition is unlikely to give satisfactory results. The aim of this research is therefore to extract the aggregated hydrodynamic vegetation density of a river floodplain forest using terrestrial laser scanning. In this paper, we present two vegetation indices to extract vegetation density from TLS data: the Percentage and the Vegetation Area Index. This method was calibrated in a forest area with highly cylindrical stem shapes to enable the use of the Nd-method as a reference. The research was done in a test site along the lower river Rhine, where the TLS data and the reference data were collected.

# 2 METHODS

## 2.1 Study Area

The study was carried out in a forest patch in the “Gamerense Waard”, a floodplain area along the lower Rhine River in the Netherlands (figure 2). The forest is 60 meters wide and 120 meters long and consists of intermediate aged willow trees (Salix Alba). This forest was chosen, because little undergrowth was present and few side branches existed in the lower part which could limit the TLS measurements. These features made the vegetation close to cylindrical and therefore reference data could be collected using the Nd-method. The dense edges and the open middle part of the forest result in a wide range of *Dv* values in the forest. The dense parts have *Dv* values of 0.12 $m^{-1}$ and the open parts have *Dv* values of 0.01 $m^{-1}$. Furthermore the differences in surface elevation are small, with a maximum difference of 0.5 m.

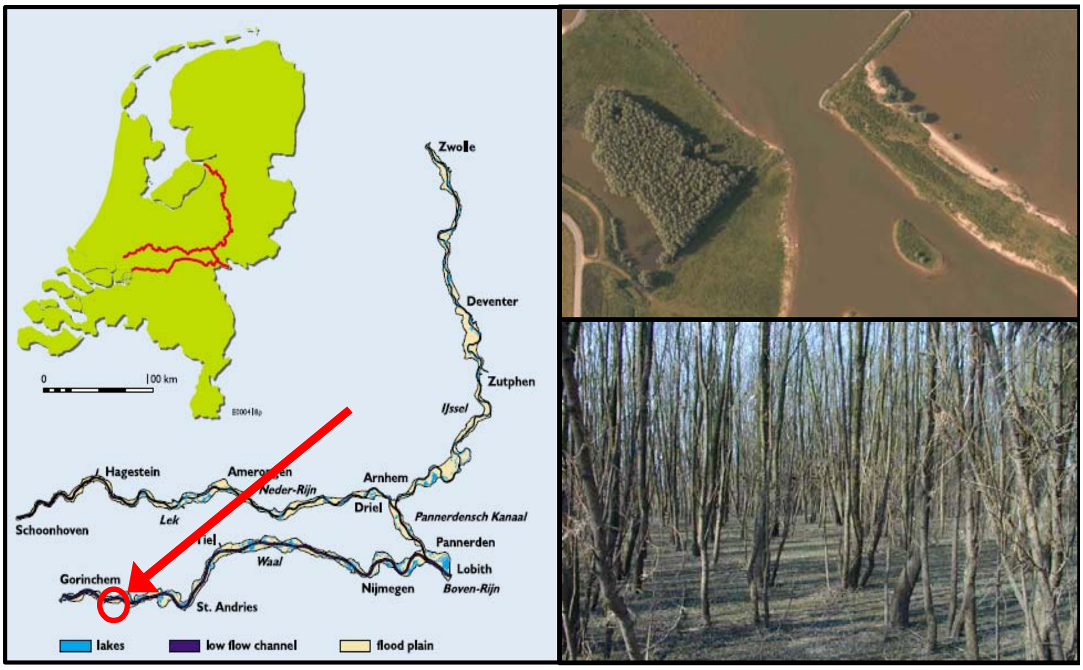


*Figure 2: a) Location of the ‘Gamerense Waard’ floodplain along the river Rhine (RIZA, 2001), b) aerial photograph of the studied forest and c) a side view of the forest*

## 2.2 Data Collection

### 2.2.1 Reference data

Firstly, to enable geo-referencing, 27 wooden poles were installed, distributed around the forest. The centres of these poles were marked and geo-referenced using differential GPS. Both TLS data as well as reference data were tied to these points. Secondly, two different types of field reference data were collected in the forest, simultaneously with the TLS data: (1) a stem map, and (2) plot level vegetation density measurements. The stem map contained 650 trees covering a quarter of the surface area of the forest (figure 3). A tacheometer was used to measure the coordinates of the centres of the trees, which was reconstructed by placing a reflector in front of the tree for the direction and beside the tree for the distance. The diameter was measured separately at breast height using a measuring tape. The accuracy of the stem map is 5 cm of which 2 cm of the uncertainty is caused by the inaccuracy of the tacheometer. Based on the stem map 11 plots were created of which the *Dv* value was computed using the Nd-method for comparison. Furthermore 7 plots were outlined in the field, and were measured manually for larger spatial variability and to obtain a larger range of *Dv* values. The corners of these plots were measured using a surveyor's level for geo-referencing. In total, 18 vegetation density values were available for comparison with the TLS data.

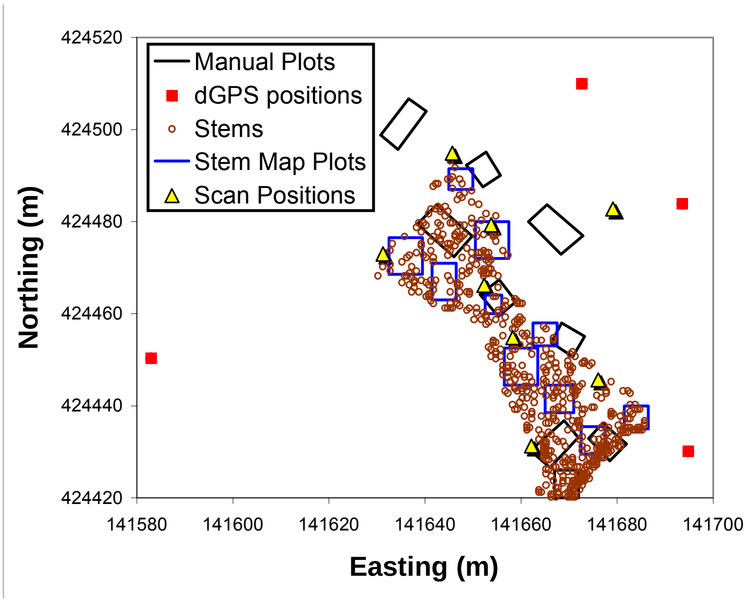


*Figure 3: Reference data collected in the study area.*

### 2.2.2 TLS data

The laser-scan data was collected in August 2005 using a Leica HDS3000 laser scanner. This scanner is a time-of-flight scanner, which was chosen because it has a large effective range (100 m). The disadvantage of this type of scanner is that it is slow compared to a phase based scanner. A scan with a horizontal angle of 360˚ takes approximately 1.5 hour per scan with the resolution set at 2 cm at 20 m distance. The specifications of the scanner are presented in table 1. The laser scanning was carried out by and geo-referenced by Delfttech and external company specialized in laser scanning projects.

*Table 1: Specifications of Leica HDS3000 (Leica Geosystems)*

| | |
|---|---|
| Field of View | 360˚ x 270˚ |
| Spot size | < 6mm @ 50m distance |
| Positional accuracy | 6mm @ 50m distance |
| Angle (horizontal & vertical) | 60 micro-radians |
| Optimal effective range | 1 - 100m |

In the forest, 8 different laser scans were made, with different resolutions set per scan (table 2). Because the resolution was kept constant per scan, the number of emitted points is known for each angle. After the first scan the decision was made for the next scan location and after 8 scans about half the forest was covered. The range of the scanner proved about 25 m effectively. For the scans the field of view was set at 360˚ horizontally and from 45˚ below horizontal to 35˚ above horizontal vertically. The scanner was positioned about 2 m above the forest floor. Detailed scans of the geo-referenced poles were made for initial geo-referencing, and subsequently the laser scans were tied together using the Iterative Closest Point algorithm.

*Table 2: Scan resolutions per scan position in cm @ 20m distance to the scanner*

| Scan | Horizontal Res. | Vertical Res. | Scan. | Horizontal Res. | Vertical Res. |
|---|---|---|---|---|---|
| 1 | 3.6 | 2.7 | 5 | 8.3 | 1.5 |
| 2 | 4.6 | 1.8 | 6 | 3.1 | 2.7 |
| 3 | 8.3 | 1.8 | 7 | 3.8 | 2.7 |
| 4 | 3.5 | 2.0 | 8 | 5.0 | 4.7 |

## 2.3 Data Analysis

The first step in the processing of the laser data was the selection of the points in a horizontal slice of 1m thick around breast height, thereby eliminating the ground points. The slice was corrected for ground level for each scan position. Subsequently a polar grid was created with cell sizes of 4 degrees and 0.5m length. At 25 m distance to the scanner a threshold was applied, because few points have penetrated the forest at larger distances. The points behind the threshold value are included in the calculation. For each cell in the polar grid, the number of hits in each cell is determined and the vegetation density was predicted using two models. The first model computes the percentage (P) of laser hits in each cell using the following equation:

$$P_{d1-d2} = \frac{1}{d2-d1} * \frac{N_{d1-d2}}{N_{tot}} \tag{2}$$

in which $N_{d1-d2}$ is the number of points between distance *d1* and *d2* to the scanner (*d*2 > *d1*) and $N_{tot}$ is the total number of emitted points in each horizontal angle increment. The first term of the equation is added to make the index independent of the cell length.

The second model was developed by MacArthur & Horn (1969) and verified by Aber (1979). This method is based on an extinction model in which a correction is included for the decreased probability of hitting a tree at larger distance to the scanner, caused by the occlusion effect. The occlusion or 'hiding' effect can be visualized by the decrease of the intensity of light with distance travelling through a forest. If we assume that the trees are randomly distributed a simple relation exists for this decrease of light intensity. Straatsma (2005) assumed that leafless trees show the same way of occlusion as trees in leaf on conditions and used the Vegetation Area Index as a predictor for vegetation density of airborne laser scanning data. This method was applied for predicting the *Dv* using terrestrial laser scanning, but has to be used horizontally resulting in the horizontal Vegetation Area Index:

$$VAI_{d1-d2} = \frac{1}{d2-d1} * \ln\left(\frac{N_{d1}}{N_{d2}}\right) \tag{3}$$

in which $N_{d1}$ and $N_{d2}$ are the number of points behind distances *d1* and *d2*. Three assumptions underlie this method: 1) the laser pulses travel parallel through the forest, 2) the trees are randomly distributed and 3) all emitted laser pulses have returned. Strictly speaking none of these assumptions hold.

For all plots, the P and VAI values were calculated by taking the average of all polar grid cells, which centres fall within the plot area. Because most plots are covered by more than one scan the P and VAI value resulting from the scan closest to the plot is taken as the representative value for the plot. For each plot, the P- and VAI-values are compared with the vegetation density values measured in the field. To assess the predictive quality of the models linear regression was used with the P- and VAI-values as independent variable and the observed values of vegetation density in the field as the dependent variable.

## 3 RESULTS & DISCUSSION

Figure 4 shows the results of the P and VAI calculation in the polar grid for a single scan position. The size of the circles represents the positive value of the P and VAI values. In this figure it can be seen that the values decrease with distance to the scanner. This is caused by the decreased probability of hitting a tree due to the radial emission of laser pulses. For the P value the occlusion effect enhances this. In the polar grid occlusion results in wedges where the values become zero, because all laser pulses were captured by trees close to the scanner. A smaller decrease of the VAI with distance can be seen compared to the P value. The correction for occlusion included in the VAI model can explain this effect.

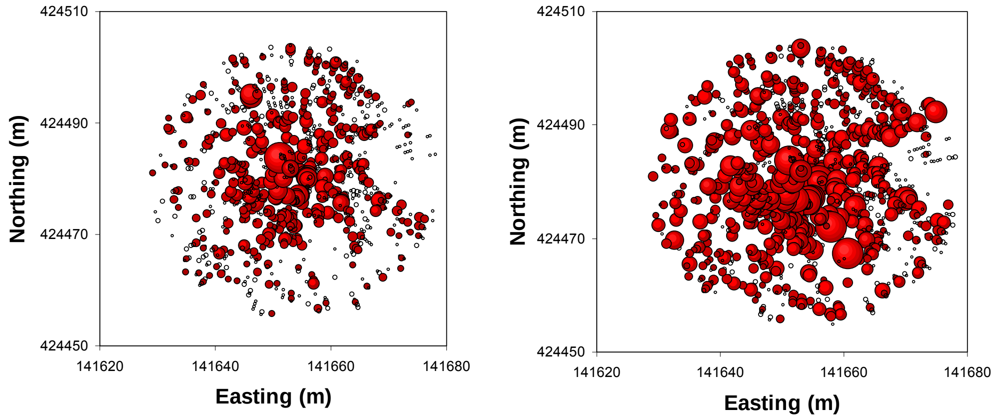


*Figure 4: The P (left) and VAI (right) values for the model values of a single scan in the polar grid. The size of the bubble is scaled to the P or VAI value in the cell*

The comparison between the reference data and the model values are presented in figure 5. Regression analysis shows that the P- values explains little variance ($R^2 = 0.13$). The VAI model explains more variance ($R^2 = 0.67$) because this model accounts for the occlusion effect. The regression equations are presented in table 2. Two complications however are not included in the calculation. Firstly, the assumption that all emitted pulses have returned does not hold in this case. About 5% of the emitted points have not returned and these points should be reconstructed. This can be done because the number of emitted points is known for each angle increment. The reconstruction is done for the P value to study the effect of this correction. The plot of the corrected P value ($R^2 = 0.72$) is presented in figure 5. The correction for missing points had a large effect on the predictive quality of the P-value. In future studies the VAI has to be corrected for missing points, which may improve the predictive quality.

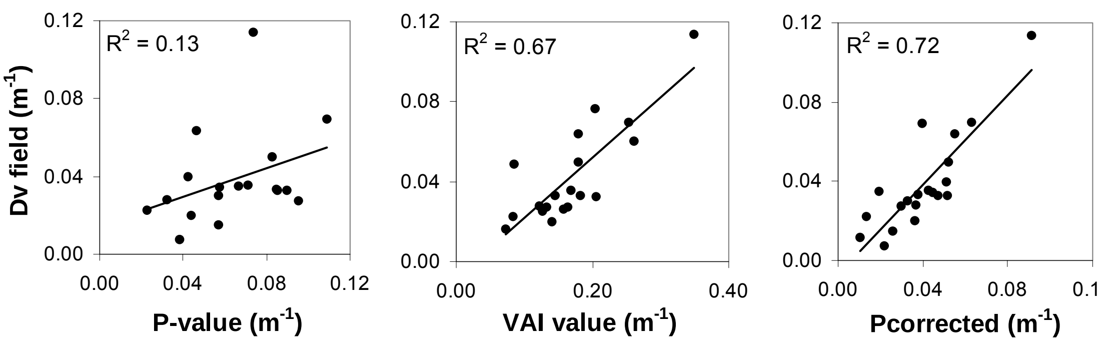


*Figure 5: Values of the vegetation density measured in the field of the plots versus 1) P-value not corrected 2) VAI-value and 3) Corrected P-value, with regression lines and explained variance.*

The second assumption that the laser pulses enter parallel into the forest is not valid. This results in an increasing deviance of the values of the predictors with larger distances to the scanner, because the pulses are emitted radially. This effect was corrected by including the distance in the regression equation. The regression results are presented in table 2. It can be seen that both predictors improve slightly when distance is included. The improvement is limited because the P and VAI values for the plots are calculated by the laser data of the scanner closest to the plot. This results in little variation of the distance for the different plots. This method for correcting for the radial emittence is not sufficient. It is expected that better correlation can be achieved when assigning a weight factor to the prediction values in the polar grid.

*Table 3: Regression analysis of different models*

| Method | Regression equation | R square | Standard Error |
|---|---|---|---|
| **P** value not corrected | Dv = 0.40*P + 0.014 | 0.17 | 0.023 |
| **VAI** not corrected | Dv = 0.31*VAI - 0.01 | 0.67 | 0.014 |
| **P** corrected | Dv = 1.13*Pcor -0.007 | 0.72 | 0.013 |
| **P** corrected distance included | Dv = 1.11*Pcor + 0.001*dist - 0.02 | 0.75 | 0.013 |
| **VAI** not corrected distance included | Dv = 0.27*VAI + 0.002*dist – 0.02 | 0.75 | 0.013 |

The presented single slice method can be further expanded to the creation of a 3-dimensional voxel space of the forest using multiple slices.

# 4 CONCLUSIONS

In this paper a method is presented to extract aggregated vegetation density parameters from terrestrial laser scanning data for application in hydraulic models. Two different models were tested to predict the vegetation density: (1) the percentage model and (2) the vegetation area index based on the extinction model of MacArthur & Horn (1969). It has been show that:

- Both models increase linearly with the vegetation density;
- Correction for missing point increases the predictive quality of the P-value
- Distance included in the regression equation improves the predictive quality of both models
- The presented method has a high degree of objectivity

For future studies a phase based scanner is more appropriate for forest scanning. It must be noted that it is essential to know the number of emitted points and the distribution of the laser points must be constant. The method will be improved by correcting the vegetation area index for missing points and applying a weight factor to correct for the distance to the scanner. Furthermore the presented method can be extended to a voxel space to create a 3 dimensional density map of a forest.

# REFERENCES

Aber, J.D. (1979). A method for estimating foliage-height profiles in broad-leaved forests. Journal of Ecology 67: pp 35-40

Aschoff, T., M. Thies, H. Spiecker (2004). Describing forest stands using terrestrial laser scanning. In the International Archives of the ISPRS, Istanbul, Turkey

Chasmer I., C. Hopkinson, P. Treitz (2004). Assessing the three-dimensional frequency distribution of airborne and ground-based LiDAR data for red pine and mixed deciduous forest plots. In the International Archives of the ISPRS, Freiburg, Germany

Dudley, S.J., C.D. Bonham, S.R. Abt, J.C. Fischenich (1998). Comparison of methods for measuring woody riparian vegetation density. Journal of arid environments 38: pp. 77-86

Ehlers, M., Gähler, M. & Janowsky, R. (2003). Automated analyses of ultra high resolution remote sensing data for biotope type mapping: new possibilities and challenges. ISPRS Journal of Photogrammetry & remote sensing, 57, 315-326.

Gorte B., D. Winterhalter (2004). Reconstruction of laser scanned trees using filter operations in 3D raster domain. In the International Archives of ISPRS, Freiburg, Germany

Graeme, D. & D.L. Dunkerley (1993). Hydraulic resistance by the river Red Gum, Eucalyptus Camaldulensis, in ephemeral desert streams. Australian Geographic Studies 31(2): pp. 141-154

Leica Geosystems: www.leica-geosystems.com (accessed on 31 Feb. 2006)

Mac Arthur, R.H. & H.S. Horn (1969). Foliage profile by vertical measurements. Ecology 50, issue 5: pp. 802-804

Mason, D.C., Cobby, D.M., Horrit, M.S. & Bates, P. (2003). Floodplain friction parameterization in two-dimensional river food models using vegetation heights derived from airborne scanning laser altimetry. Hydrological Processes, 17, 1711-1732.

Mertes, L.A.K. (2002). Remote sensing of riverine landscapes. Freshwater biology, 47 pp.799-816

Petryk, S. & Bosmajian, G. (1975). Analysis of flow through vegetation. Journal of Hydraulics Divisions 101: pp. 871-884

Silva, W., Klijn, F., Dijkman, J. (2001). Room for the Rhine Branches in The Neterhlands: what the research has taught us.

Straatsma, M.W. (2005). Quantitative mapping of hydrodynamic vegetation density of floodplain forests using airborne laser scanning. In the International Archives of the ISPRS, Enschede, The Netherlands

Van der Sande, C.J., De Jong, S.M. & De Roo, A.P.J. (2003). A segmentation and classification approach of IKONOS-2 imagery for land cover mapping to assist flood risk and flood damage assessment. International Journal of applied earth observation and geoinformation, 4, 217-229.

# METHODS OF AIRBORNE LASER SCANNING FOR FOREST INFORMATION EXTRACTION

*Juha Hyyppä[1], Xiaowei Yu[1], Hannu Hyyppä[2], and Matti Maltamo[3]*

[1] Finnish Geodetic Institute, Department of Remote Sensing and Photogrammetry, Masala, Finland, juha.hyyppa@fgi.fi, yu.xiaowei@fgi.fi

[2] Helsinki University of Technology, Espoo, Finland, hannu.hyyppa@hut.fi

[3] University of Joensuu, Faculty of Forestry, Joensuu, Finland, matti.maltamo@joensuu.fi

## ABSTRACT

Extracting forest information from airborne laser scanner has become an own discipline within its 10 years of history. This paper summarizes new findings in extracting forest attributes from laser scanner data, the use of multitemporal data sets for forest growth estimation and in quality of digital terrain models of forested areas based on experiments conducted in boreal forest zone in Finland.

**Keywords**: Digital terrain model, individual tree crown, segmentation, height growth, laser scanner

## 1 INTRODUCTION

Airborne laser scanners (ALS) providing small footprint diameters (10 – 30 cm) allow accurate height determination of the forest canopy (e.g. Næsset 1997a, Magnussen and Boudewyn 1998, Magnussen et al, 1999, Means et al. 2000). The two main approaches in deriving forest information from laser scanner data have been the laser canopy height distribution based and the individual tree detection based approaches. In the laser canopy height distribution based method, percentiles of the distribution of laser canopy heights are used as predictors to estimate forest characteristics. For example, Næsset (2002), Lim et al. (2003) and Holmgren and Jonsson (2004) have shown that this approach produces highly reliable estimates of stand variables. If the number of laser pulses is increased e.g. to more than about three measurements per square meter, individual trees can be recognized (Brandtberg 1999, Hyyppä and Inkinen 1999, Persson et al. 2002, Popescu et al. 2002, Leckie et al. 2003). From individual trees, height of the tree, crown diameter and tree species are then derived using laser and possibly aerial image data.

Timber volume is usually the most interesting stand characteristic to be considered. When using the laser canopy height distribution based approach, laser-derived height quantiles are related to the stem volume (e.g. Næsset 1997b, 2002, 2004, St-Onge and Renaud 2001, Lim et al. 2003, Holmgren 2004). In the individual tree based method, the volume of the individual tree stems is calculated using existing formulas from height, crown diameter and species information. Presently also formulas relating diameter breast height and crown diameter have been further developed for laser scanning purposes (e.g. Kalliovirta and Tokola, forthcoming). A Scandinavian summary of laser scanning including obtained accuracies in forestry can be read from Næsset et al. (2004).

ALS provides 3D characterization of forest canopy. From the original point cloud, digital terrain model (DTM) and digital surface model (DSM) corresponding to treetops can be calculated. Points forming the DTM are calculated using so-called filtering algorithms. Most usable technique to obtain DSM relevant to treetops is to calculate the TIN of the highest reflections and interpolate missing points e.g. by Delaunay triangulation. The canopy height model (CHM) is then obtained by subtracting the DTM of the corresponding DSM. The crown DSM is typically calculated by means of the first pulse echo and DTM with the last pulse echo. In order to guarantee, that there are no systematic errors between first and last pulse data, calibration using flat, non-vegetated areas, such as roads, roofs, and sports grounds are typically performed.

This paper summarizes recent advances in extracting forest information from airborne laser scanner data based on the Finnish experiments.

# 2 TEST SITE AND MATERIAL

## 2.1 Test Site and Applied Laser Scanner Data

The test site was located in a state owned forest area of approximately 50 hectares located in Kalkkinen, southern Finland, 130 km north of Helsinki. The 2-km-by-0.5-km intensive study area situated about 110 m above sea level, with slopes ranging between 0 and 66$^o$ and with 87 % of forest cover dominated by species such as spruce, pine and birch, was collected with Toposys I in 1998 and 2000, and with Toposys II in 2003. In all campaigns, the pulse repetition frequency (83 kHz), maximum scan angle (±7.1°), beam size (1 mrad) and wavelength of the system (wavelength of 1.5 µm) remained constant. The major difference between the Toposys I and II was the possibility to record first and last pulse simultaneously in the version II. Since the measurements were recorded at various times of the season, i.e. May 14th 2003 (leaf-off), June 14th 2000 (leaf-on, low development of undergrowth), and September 2nd 1998 (leaf-on, high undergrowth), it was possible to estimate the effect of leaves and undergrowth at boreal forest zone. That was performed using the high pulse density point cloud (8-10 pulses per $m^2$) obtained from 400 m flight altitude in each acquisition. The effect of the flight altitude was studied using the flight altitudes of 400, 800 and 1500 m above ground level collected in 2003 providing nominal pulse densities of 8-10, 4-5 and 2-3 pulses per $m^2$.

## 2.2 Field Reference for Volume Estimation Improvement

During the summer of 2001, 33 systematically located rectangular sample plots were established on the test site. The basic size of a sample plot was 30 m by 30 m, but to get around 100 trees per plot, plot sizes of 25 m by 25 m and 30 m by 40 m were also used. Most of the sample plots included dense understorey and were dominated by Norway spruce, although, each sample plot included more than one tree species. All trees having a diameter at breast height (DBH) of more than 5 cm were mapped using a measuring tape, and tree species, DBH, tree height, and height to the living crown were registered. All individual trees were classified as belonging to either the dominant or the suppressed tree layer. On the average there were 414 dominant and 435 suppressed trees per hectare in the data. 78 pine trees in 10 plots were selected to be used in this study in Section 3.

## 2.3 Reference for Growth Analysis

For individual tree height growth analysis (Section 4), 82 pines were selected and height, location and shoot elongation of these trees were measured in August 2002 and November 2004 using a tachometer. In addition to measuring the height of the trees, five to seven consecutive shoots below the top of the tree were also measured.

## 2.4 Digital Terrain Model Reference

Theodolite Wild T2002 with Distometer Di2002 was used to measure tree locations and terrain height points. Typically, coordinates for tree location in north and east direction were measured to the centre of the trunk and the height was measured next to the tree, thus making it possible to use the tree coordinates for DTM determination as well. In most cases, DTMs were measured as a grid of ground points. Measured points were distributed evenly inside the plots with a distance from each other of about 2 m. Altogether 2119 points were recorded (Section 5).

Test plot 5: Mainly tall spruces together with few tall birches, on one corner a more dense area of smaller spruces, no bushes. The plot is located on a gentle slope and terrain is very smooth.

Test plot 9: Tall birches and smaller spruces below them, practically no undergrowth. Terrain is fairly smooth and gentle slope.

Test plot 10: Mainly full-grown trees of various species, some bushes in the undergrowth. A small cliff and fairly large height differences in the plot.

Test plot 14: Mainly full-grown trees of various species together with smaller and denser undergrowth of trees. Middle part of the plot flat, steep slopes of few meters on two sides.

Test plot 22: Mainly tall pines, main part of the plot on top of a small hill, steep slope on one side.

Test plot 26: Mainly full-grown trees of various species. Some dense bushes in the undergrowth. Terrain is fairly flat.

Test plot 30: Mainly saplings of various species, partly very dense growth. Test plot is located on a hillside, so large height differences within the plot.

Test plot 34: Mainly tall birches together with some tall pines and spruces. Plot is located on a gentle slope, otherwise flat terrain.

# 3 TECHNIQUES FOR VOLUME ESTIMATION

## 3.1 Comparison of the Present Methods

As it was mentioned in the introduction, the two main approaches in deriving forest information from laser scanner data have been the statistical canopy height distribution based and the individual tree detection based approaches. There has not been careful comparison of these two techniques and the results obtained have been based on different type of reference data sets. Typically, distribution based techniques have been calibrated with a very large and accurate reference data and individual tree based approaches have not been properly calibrated at all. Thus, the obtainable results are not comparable. A short overview of the advantages and disadvantages of the techniques are given in Table 1.

*Table 1. Comparison of distribution and individual tree based methods.*

| | **Advantages** | **Disadvantages** |
|---|---|---|
| **Distribution based methods** | • Easy to integrate with present forest inventory practices due to common reference plots<br>• Strong statistical background<br>• Laser scanning data relatively inexpensive | • Requires large, accurate, representative, and expensive reference data<br>• Without large number of reference data, the possibility to have high errors in operative inventory is high |
| **Individual tree based methods** | • Good physical correspondence (existing models) with volume estimation<br>• Low amount of reference data needed for calibration<br>• Allows precision forestry and increased information amount of the forests | • More expensive laser data<br>• More complex system to be implemented |

In the following some other techniques are proposed and preliminary accuracy is either analyzed or discussed.

## 3.2 Tree Cluster Based Inventory

The typical hypothesis for individual tree based laser inventory (Hyyppä and Inkinen 1999) is that by measuring major individual tree characteristics, such as the height of the tree, tree species, and crown diameter, it is possible to derive other valuable tree characteristics, such as stem diameter, stem volume, and age for the same tree and to use these information to calculate standwise forest information (mean height, dominant height, stem volume, basal area, tree species proportions).

The accuracy obtained with the approach depends on the structure of the forest (number of tree layers, tree species, density), quality of images and density of laser point clouds and applied processing technique. It has been shown that trees can usually be recognized only in the dominant tree layer (Persson et al. 2002, Maltamo et al. 2004). Depending on the density of the forest and density of the point clouds, the discrimination of individual trees is a problem of varying complexity. In dense stands this leads to underestimation of the number of tree stems.

What about if the individual tree based technique is applied directly to tree clusters? A feasible algorithm could be

1. Moderate filtering to laser data in order to help in the finding of tree tops
2. Tree top finding of tree clusters
3. Rough segmentation using the top of the clusters
4. Analysis of large clusters

In the analysis part of the large clusters, there are several ways of performing the analysis. Analysis of tree species can be done either using digital aerial image or laser data (see e.g. Holmgren and Persson 2004) for each segment. Each segment is assumed to be homogeneous with respect to tree species. Based on the height of the tree and known tree species, an approximated crown diameter for one tree can be calculated. The relation between the size of the real segment and approximated crown area for one tree is used to estimate the number of trees. Alternatively, for smaller segments (1-4 trees in the segment), the existing volume formulas are used to directly estimate the volume corresponding to the trees in the segment.

In Hyyppä et al. (2005), the latter approach was tested for volume estimation of individual tree groups. The results indicate that individual trees volumes can be obtained, roughly speaking, with random error about 30 % and the volume related to small tree clusters or segments with random error of 37%. The $R^2$ values were almost identical. In conventional forest inventory, the random error of the volume estimation of individual trees using the diameter as predictor is 17.2 % for Scots Pine (Laasasenaho, 1982). These models are still used to calculate the volume of the individual tree from manual diameter measurements. From that point of view, the results are good. The splitting of the segments did not improve the results in Hyyppä et al. (2005), since the segments were already relatively small (1-3 trees) and most of the trees were optimally segmented.

In general the tree cluster technique is expected to work with lower density data (0.5-1 pulses per $m^2$) and it should be superior to distribution based techniques since it utilizes the homogeneity of laser hits in a cluster. However, the techniques how to derive volume from larger segments (clusters) should be further investigated.

## 3.3 Inventory Using Old Look-Up Tables

An old way of getting stem volume per hectare is the use of look-up-tables based on basal area per hectare and mean height, such as Nyyssönen 1954. The mean height is obtainable from height distribution or by calculating the average value of tree heights corresponding to each tree segment. The basal area needs to be modeled either from the number of canopy hits (e.g. Nelson et al. 1988) or from sum of areas of segments with proper calibration with the height. By this technique, only the basal area needs to properly calibrated with good reference data set and even heuristic and knowledge based rules can be defined to get good quality basal area statistics.

The technique should be more robust and not so dependant on high amount of good reference data as the direct distribution based method.

### 3.4 Extracting Height from Sparse Laser Data and Segments from Aerial Images

Individual tree crown based solutions have been first demonstrated with aerial images (e.g. Gougeon and Moore 1989, Gougeon 1997). In the case of aerial images and using individual tree based technique, the standard errors for volume estimation at stand level are usually considerably high being 35-60 % (Anttila and Lehikoinen 2002, Huitu 2005, Korpela et al. 2005). However, sparse laser scanning data are becoming increasing attractive due to state-wise laser scanning. It should be possible to improve the aerial image based estimates by giving the height for each crown (segment) using the sparse laser data.

In the test (Hyyppä et al. 2005), CIR derived segments were first used to calculate volume of the trees, Figure 1. The low coefficient of determination obtained using only aerial image segment for volume estimation ($R^2$=0.13-0.14) implies that at least in this test the obtained crown diameter did not correlate well with stem volume. The result was surprising, since proper segmentation for each tree was visually selected from seven possible choices and in typical ITC (individual tree crown) solution using aerial images, one stand is treated with same parameters in the segmentation. There was a large underestimation of stem volume, most probably due to the fact that the above-seen crown diameter was significantly smaller than that of the real one. Also, the trees are much taller and narrower (concerning crowns) in Kalkkinen than typical Finnish trees, in which Laasasenaho (1982) formulas are based on. It should be noticed that the test site has been difficult for remote sensing tests also previously, see Hyyppä et al. (2000a). Anyhow, the results show that aerial image based individual tree crown approach does not work in all forest conditions.

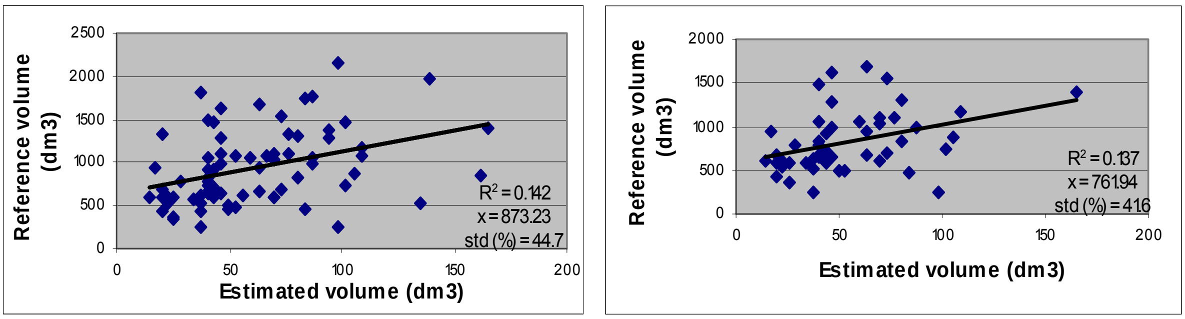


*Figure 1. Scattergram between estimated and reference volume when estimation was done using only diameters of segments from CIR. The reference consists of all trees (left) and individual trees (right) within the segment. Left: mean volume 934.4 dm3 and std 428.6 dm3 for the reference; right: mean volume 815.7 dm3 and std 349.3 dm3 for the reference.*

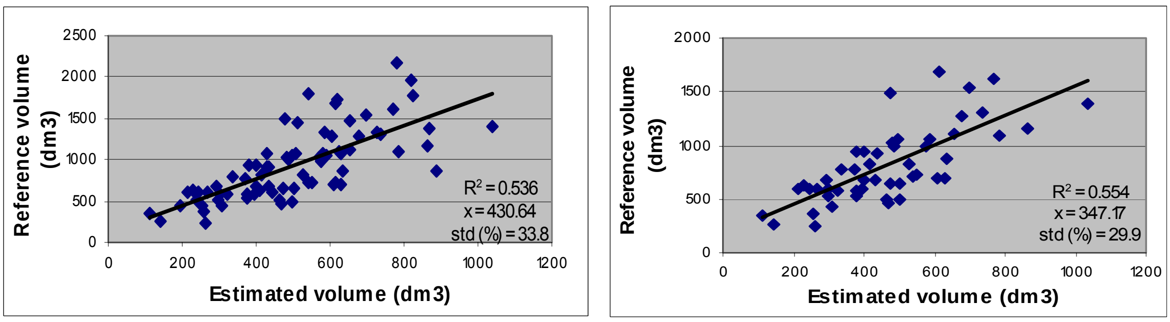


*Figure 2 Scattergram between estimated and reference volume when estimation was done using diameters of segments from CIR and height from laser data. The reference consists of all trees (left) and only individual trees (right) in the segment. Left: mean volume 934.4 $dm^3$ and std 428.6 $dm^3$ for the reference; right: mean volume 815.7 $dm^3$ and std 349.3 $dm^3$ for the reference.*

In the second phase (Hyyppä et al. 2005), each CIR segment was given the height from the laser derived canopy height model. Stem volume was calculated using Laasasenaho (1982) formulas for pine using both the height and diameter at breast height of the stem. From Kalliovirta and Tokola (forthcoming), the relation between stem diameter and height and crown diameter was obtained.

There is a significant improvement in performance when tree height information was added into the aerial image based ITC solution, Figure 2. In addition to the improvement in R2 values, the underestimation was significantly reduced. The results obtained with segments including only one tree showed slightly better results (0.55-0.56, 29.9 % error in segment wise volume estimation) compared to all segments (0.54, 33.8 % error in segment wise volume estimation), but the difference was not significant.

### 3.5 Use of Old Inventory Data to Improve Distribution Based Techniques

The major disadvantage of the distribution based technique or the technique depicted in 3.2 is that they require large, accurate, representative, and expensive reference data. However, from the most Scandinavian forests, there exists 10-20 years old inventory data. With change detection techniques, e.g. image differencing with two BRDF (Bidirectional Reflectance Distribution Function) corrected aerial image, it is possible to find areas that have not changed. Such areas can be updated with existing growth models with reasonably accuracy. These updated forest attribute information can then be used to calibrate any of the laser-based techniques applied. Volumes for all areas can then be estimated with laser data, but the overall calibration is based on the unchanged stands where old inventory data is updated with growth models.

As an alternative to BRDF correction, channel difference or ratio images or NDVI-compatible images can be used to substitute original images.

### 3.6 Conclusions

Four new inventory techniques for laser scanner data were proposed. These four techniques should be either more cost-effective or more robust than the pure distribution based or individual tree based techniques. They all work with sparser point clouds than original individual tree based methodology and they are more robust than the original distribution based technology. However, more detailed studies are needed to define the accuracy of the methods.

## 4 CHANGE DETECTION FOR CANOPY HEIGHT GROWTH MEASUREMENTS

### 4.1 Background for Change Detection

Change detection in forests using multitemporal airborne laser scanner point clouds has been demonstrated recently (Yu et al. 2003, Hyyppä et al. 2003, Yu et al. 2004, St-Onge and Vepakomma 2004, Gobakken and Næsset 2004). Yu et al. (2003, 2004) demonstrated the applicability of small footprint, high sampling density airborne laser scanners for estimating forest growth and the monitoring of harvested trees. Algorithms were developed for detecting harvested and fallen trees, and for measuring forest growth at plot and stand levels. An object-oriented tree-to-tree matching algorithm was presented to link the point clouds, one from each laser acquisition, of the same tree.

At the same time, the costs of laser scanning acquisition have decreased. Today, large areas (such as 500-10,000 $km^2$) can be collected with reasonably good density (1 point per $m^2$) at costs equivalent to 50-100 €/$km^2$. The increase in PRF will lead to a situation where dense point clouds, such as 10 points per $m^2$, can be collected for large forest areas at reasonable cost. This will allow commercially-oriented multi-temporal laser acquisitions in the near future.

The objective of this sub-study is to describe the potential for change detection using airborne laser scanners and the techniques and accuracies involved beyond those presented by Yu et al. (2004). In Yu et al. (2004), the accuracy of height growth was not examined in detail due to the lack of sufficient field data and some problems related to plotwise analysis. This paper not only describes individual tree height growth measurement, but also shows how it is derived using various techniques.

## 4.2 Methods

In this paper, three different change detection techniques are used to estimate growth

- Difference between DSMs (see Figure 3)
- Comparison between canopy profiles (i.e. cross-section of point clouds within a defined width), see Figure 4
- Analysis of difference between height histograms (see Figure 5)

The difference between DSMs is assumed to work in areas with wide crowns, but in coniferous forests with narrow crowns and tall trees (up to 35 m), the displacement between two acquisitions can be substantial. Height histograms can be applied to point clouds corresponding to individual trees or plots or stands, but the information contents of histograms is corrupted if thinning has occurred.

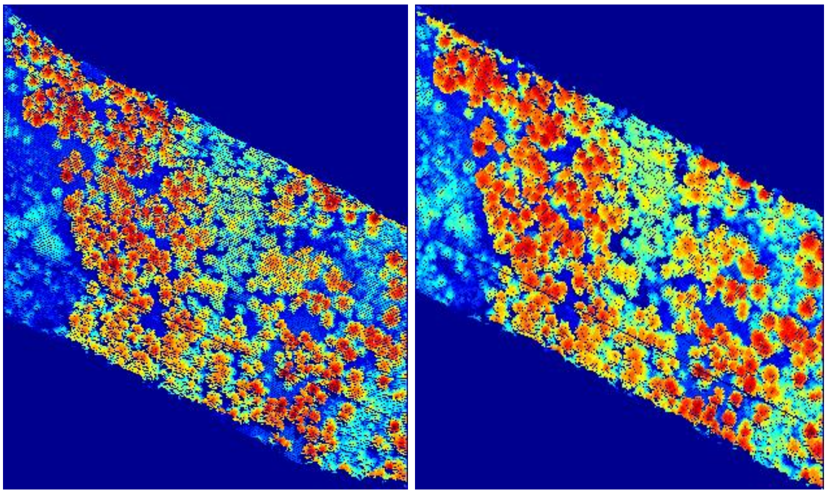

*Figure 3. DSMs from 1998 (left) and 2003 (right) data. The line in the image is the location of the profiles in Figure 4.*

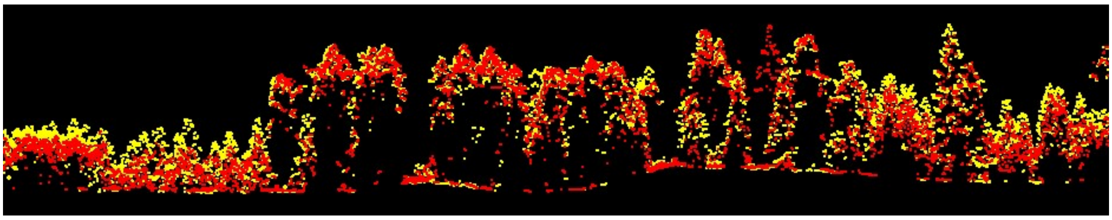

*Figure 4. 3-m wide canopy profile for a 150-m long cross-section. Yellow: 2003, Red-1998.*

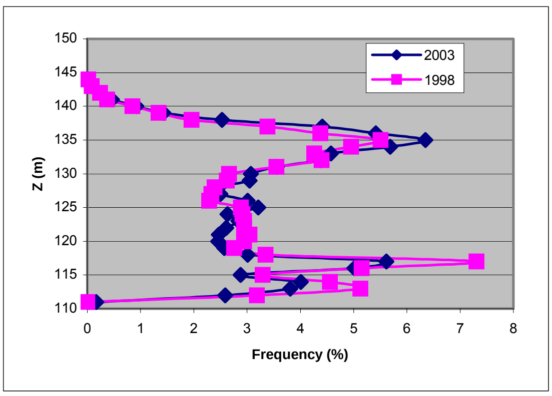


*Figure 5. Histograms of corresponding profiles in Figure 4.*

Eighty-two field-measured pine trees were used to demonstrate individual tree height growth. Since the location of the trees was known by reference measurements, treetop location on the laser acquisitions was searched in the close neighborhood of the field-measured location. The corresponding laser points falling within a cylinder around the found location of each trees were used to extract variables used for growth estimation. The radius of the cylinder, varied (between 0.76 to 3.58 m) according to the height of the tree. Three different types of variables were extracted from the point clouds using three techniques. First, the highest z value was taken among the points within the cylinder and the height growth was estimated as the difference between the highest z value in the 2003 and 1998 datasets (denoted by $MaxZ_1$-$MaxZ_2$). Secondly, the mean and median value of the difference between the DSMs (denoted by Mean($DSM_1$-$DSM_2$) and Median($DSM_1$-$DSM_2$)) and the difference between mean and median value of the DSM between the 2003 and 1998 datasets (denoted by Mean($DSM_1$)-Mean($DSM_2$) and Med($DSM_1$)-Med($DSM_2$)) were calculated. The DSMs were obtained by taking the highest point within each 50 cm grid. Thirdly, the height histograms of the point clouds for each tree were formed and the 85th, 90th and 95th percentiles were calculated. The height growth was assumed to be the difference between corresponding quantiles from the 2003 and 1998 datasets (denoted by $P85_1$-$P85_2$, $P90_1$-$P90_2$, $P95_1$-$P95_2$ respectively).

## 4.3 Results of Change Detection

Table 2 and Figure 6 show the results of individual tree height growth analyses. From all the techniques used, the difference between the treetops of each tree (in 1998 and 2003) resulted in the highest $R^2$ value (0.68). The underestimation was 7 cm and the RMSE was 43 cm. By using the quantiles of the height histograms, the $R^2$ values range between 0.51 and 0.6. The use of the mean or median of the difference between the DSMs or the difference between the mean/median of DSMs resulted in $R^2$ values between 0.33 and 0.53. The results indicate that it is possible to measure the growth of an individual tree, which has already been reported earlier by Yu et al. (2005a).

Since the tree crown is not a continuous surface, the laser pulses penetrated through gaps in the crown and were reflected from a lower layer or the ground. This has caused problems in growth estimation using DSM differencing. The effect is more significant in the crown boundary than in the very top of the crown. Therefore, the same analyses were carried out using the data extracted for each tree with the cylinder radius reduced by half to avoid the boundary effects (Table 3). The results show that histogram-based growth estimation was improved and was almost as good as with the maximum point method. The methods based on DSM differencing were not significantly improved.

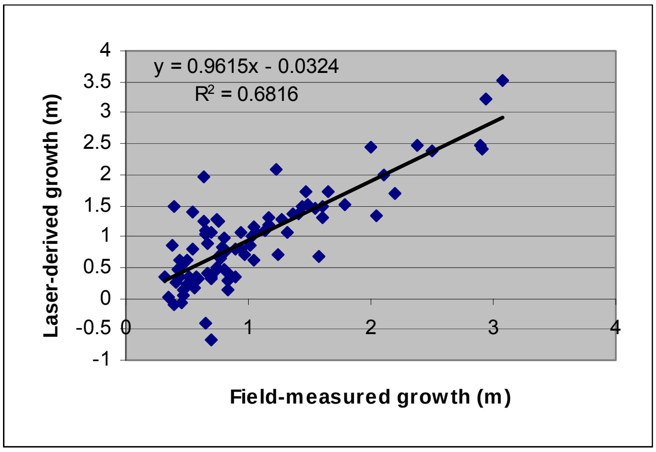


*Figure 6. Scatterplot and line of regression of tree height growth estimation versus field-measured growth. Tree height growth was estimated from the differences of maximum Z values of point clouds between 2003 and 1998.*

*Table 2. Statistics of individual tree growths: full radius*

| Method | $R^2$ | Bias (m) | Stdev (m) |
|---|---|---|---|
| $MaxZ_1$-$MaxZ_2$ | 0.68 | -0.07 | 0.43 |
| $P85_1$-$P85_2$ | 0.51 | 0.16 | 0.51 |
| $P90_1$-$P90_2$ | 0.55 | 0.10 | 0.48 |
| $P95_1$-$P90_2$ | 0.60 | 0.01 | 0.48 |
| Mean($DSM_1$-$DSM_2$) | 0.46 | 0.47 | 0.63 |
| Median($DSM_1$-$DSM_2$) | 0.53 | 0.36 | 0.60 |
| Mean($DSM_1$)-Mean($DSM_2$) | 0.53 | 0.11 | 0.47 |
| Med($DSM_1$)-Med($DSM_2$) | 0.33 | 0.15 | 0.63 |

*Table 3. Statistics of individual tree growths: half radius*

| Method | $R^2$ | Bias (m) | Stdev (m) |
|---|---|---|---|
| $P85_1$-$P85_2$ | 0.61 | 0.04 | 0.46 |
| $P90_1$-$P90_2$ | 0.66 | -0.04 | 0.43 |
| $P95_1$-$P90_2$ | 0.66 | -0.07 | 0.44 |
| Mean($DSM_1$-$DSM_2$) | 0.49 | 0.30 | 0.58 |
| Median($DSM_1$-$DSM_2$) | 0.53 | 0.24 | 0.53 |
| Mean($DSM_1$)-Mean($DSM_2$) | 0.44 | 0.24 | 0.57 |
| Med($DSM_1$)-Med($DSM_2$) | 0.38 | 0.32 | 0.62 |

## 4.4 Conclusions

This sub-study demonstrated the use of various techniques to measure individual tree height growth. Differences between DSMs, height histograms and the highest laser hits were used to derive growth-related statistics.

It was shown that it is possible to measure individual tree height growth. From all the techniques used, the difference between the treetops of each tree (in 1998 and 2003) resulted in the highest $R^2$ value (0.68). The underestimation was 7 cm and the RMSE was 43 cm. When the cylinder size was reduced to half, the results using histogram-based growth improved and were almost as good as the maximum point method. The error and bias obtained for individual tree height growth were lower than those reported in an earlier study concerning field measurements of height growth (Päivinen et al. 1992)

New growth models, monitoring climate change (and perhaps post-Kyoto protocols), and large area forest inventories as strip-based sampling can be seen as real-life applications.

# 5 DIGITAL TERRAIN MODELS FOR FOREST INFORMATION EXTRACTION

## 5.1 Background of DTM

Kraus and Pfeifer (1998) developed a DTM algorithm based on distinguishing laser points into terrain points and non-terrain points using an iterative prediction of the DTM and weights attached to each laser point depending on the vertical distance between the expected DTM level and the corresponding laser point. Pyysalo (2000) developed a modified recursive classification method for DTM extraction, where all points within 60 cm vertical distance from the lowest expected ground level were included equally in the next DTM model calculation. Axelsson (1999, 2000, 2001) developed a progressive TIN densification method. Elmqvist (2001) estimated the ground surface by employing active shape models by means of energy minimization. Sithole (2001) and Vosselman and Maas (2001) developed a slope-based filtering technique, which works by pushing up vertically a structuring element. In the method by Wack and Wimmer (2002) non-terrain raster elements are detected in a hierarchical approach that is loosely based on a block-minimum algorithm. An empirical comparison of the methods is depicted in detail in Sithole and Vosselman (2004).

Kraus and Pfeifer (1998) reported an RMSE of 57 cm in wooded areas using ALTM 1020 and average point spacing of 3.1 m. Hyyppä et al. (2000b) reported a random error of 22 cm for modulating forest terrain using Toposys-1 and nominal pulse density of 10 pulses per $m^2$ using the method of Pyysalo (2000). Ahokas et al. (2002) compared three algorithms (including Pyysalo and Axelsson) in forested hill in Finland and found random errors between 13 and 41 cm using Toposys-1. Reutebuch et al. (2003) reported random errors of 14 cm for clearcut, 14 cm for heavily thinned forest, 18 cm for lightly thinned forest and 29 cm for uncut forest using TopEye data with 4 pulses per $m^2$. However, in dense forests, errors up to 10 to 20 m can occur in the DTM estimation (Takeda, 2004).

The quality of DTM derived from laser scanning is influenced by a large number of other factors, the reader is referred to the introduction of Yu et al. (2005b). From the users point of view, the most relevant issues in the specifications of the data acquisition are date, point density, flight altitude and scan angle. According to Kraus (2004), point density is the most important parameter to explain the accuracy of the terrain model. In the assumption of Kraus (2004), the density was defined as the number of pulses on the ground, which is influenced by forest characteristics, beam size, and other parameters.

Therefore, this sub-study focused on factors affecting the DTM in boreal forest conditions, especially the effect of the date, flight altitude, pulse mode, forest cover and plot variation on the DTM accuracy. Details of the sub-study can be found in Hyyppä, H. et al. (2005).

## 5.2 Methods

The accuracy of the laser DTM was evaluated by comparing the DTM values with the corresponding reference points obtained by field measurements. Systematic elevation error was calculated as mean height differences between laser DTMs and field measurements, whereas the random error was obtained from standard deviation (STD) of the difference.

## 5.3 Results

### 5.3.1 Effect of the Date

The random errors varied from test site to test site. With the last pulse, the measurements conducted during leaf-off period resulted in the smallest random error, i.e. 7-17 cm, in most of the plots. The use of a non-optimal season resulted in increased random error by 3 to 9 cm (units). In general the differences were smaller than expected. Plot 14 has dense undergrowth and hence all date resulted in inferior performance. Plot 30 has dense high vegetation (mixed species), which was more difficult during leaf-on period.

Figures 7 and 8 show the random error of the DTM derivation using first and last pulse.

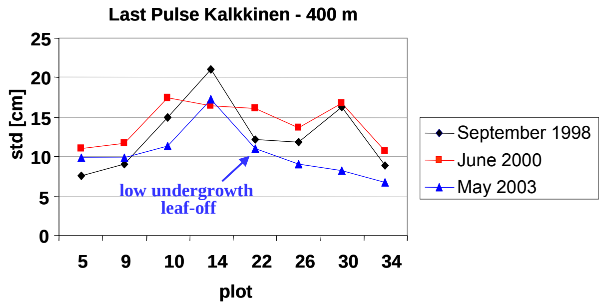


*Figure 7. The effect of the date on the DTM random error using last pulse.*

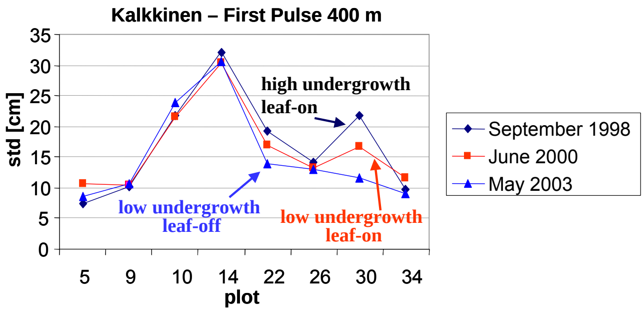


*Figure 8. The effect of the date on the DTM random error using first pulse.*

Even with the first pulse and with non-optimal season the obtained results were good.

### 5.3.2 Effect of Flight Height

By increasing the flight altitude, the density of the pulse decreases in the across-track direction. From the altitudes of 400, 800 and 1500 m, the across-track point spacings were 0.80, 1.6 and 3.0 m, respectively. The corresponding beam sizes on the ground were 0.4, 0.8 and 1.5 m. Therefore, the effect of the flight altitude is a combined effect of the across-track point spacing reduction and increase in the beam size. Figure 9 summarizes the results.

With Toposys II (i.e. acquisition done in 2003), the first and last pulse modes were acquired simultaneously. The systematic shifts with respect to ground references are shown in Figure 9. At 400 m, the first pulse overestimated DTM approximately 9 cm compared to the last pulse. In 800 m, the difference was 4 cm, and at 1500 m, the difference was –1 cm. This is most likely due to the effect of the beam size and sensitivity. At 400 m, the small beam more easily finds the undergrowth at first pulse. The small pits are also found if the system is sensitive enough. With a larger beam and from a higher altitude (lower return pulse level), the difference between the first and last pulse decreases.

The random errors obviously increase as flight altitude increases. This is mainly due to the decrease of the pulse density and increase in the planimetric error (for non-flat surface).

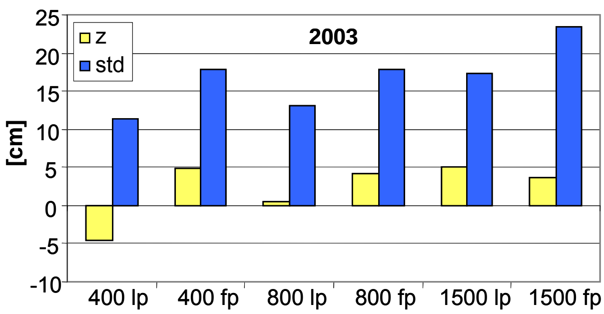


*Figure 9. The DTM systematic and random errors from different flight altitudes at first and last pulse modes.*

It can be concluded that the effect of the first versus last pulse on the errors is higher than doubling the flight altitude. The effect is approximately the same as making the flight altitude four times as high. An impressive random error of approximately 18 cm was obtained for hilly boreal forest area (relatively dense concerning forest cover) from the height of 1500 m with the last pulse.

### 5.3.3 Effect of Forest Cover

In order to evaluate the effect of forest cover on DTM derivation accuracy, tree-cover effects were examined. All plots were segmented into small regions corresponding to either open areas (no vegetation above) or under tree areas. Also the DTM beside the trunk was measured.

The effect of forest cover is higher when moving closer to the trunk. The maximum systematic difference due to the cover is 8 cm in the 400 m last pulse datasets. The random error increases 2 to 3 cm under the tree and it is 2-5 cm higher near the trunk with the last pulse, which indicates that the ground elevation can be reliably detected even under trees. With the first pulse, see the analysis in Yu et al. (2005b).

### 5.3.4 Within Plot Variation

Within plot variation is mainly caused by the variation in the terrain slope, undergrowth and vegetation cover. Figure 10 shows both systematic error and random error variation analyzed for example plots.

The results show that the systematic error variation is higher than the random error variation. The former is caused by changes in undergrowth, remaining errors in strip orientation and problems in the calibration of the elevation level. For example, for the test plot number 9, which is fairly smooth with gentle slope, the systematic error range between –18 to 11 cm, where-as the random error (with all flight altitudes and pulse modes and dates) ranges from 7 to 11 cm. Systematic error variation was higher than the random error variation except for the test site 14, which includes dense undergrowth and steep slopes.

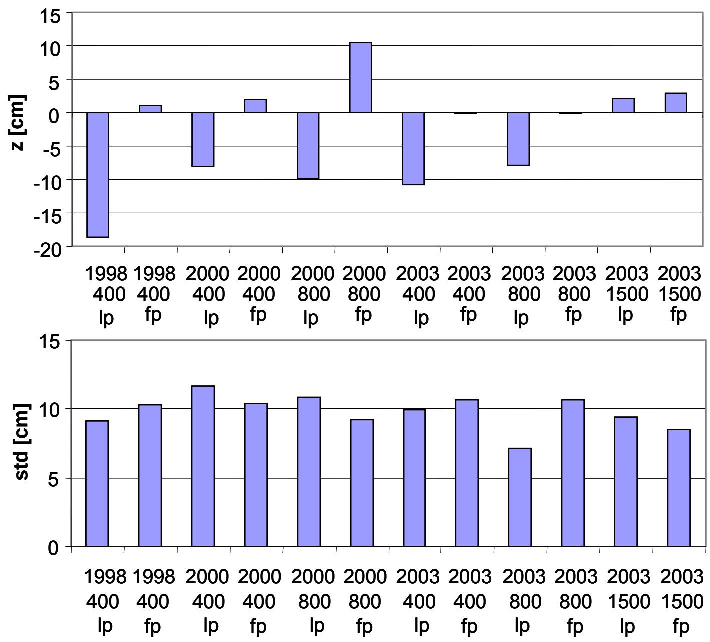


*Figure 10. Within systematic (top) and random (below) plot variation for plot 9.*

## 5.4 Conclusions

The following conclusions could be drawn from the high-density data:

- At boreal forest zone, random errors of less than 20 cm can be obtained in most conditions for non-steep terrain.

- The increase of flight altitude from 400 to 1500 m increased the random error of DTM derivation from 12 to 18 cm (i.e. 50%).
- The difference of using first or last pulse causes a corresponding random error difference, i.e. 5 cm.
- There are systematic shifts in the elevation models derived at various flight altitudes. It is expected that the beam size and sensitivity of the laser system cause this systematic behaviour. Additionally, the systematic shifts between last and first pulse are significant.
- The difference in DTMs derived at optimum and non-optimal season conditions is typically less than 5 cm –for high-density data (this is not relevant for most applications). In stand consisting of deciduous trees, the effects are the highest. Use of non-optimal flying season mainly causes that details of the terrain elevation can not been measured in the same accuracy.
- The effect of forest cover is higher when moving closer to the trunk. The random error is 2-5 cm higher.
- The results are site dependent, i.e. the accuracy varies as function of site conditions (slopes, undergrowth, forest cover).

## 6 CONCLUSIONS

For detailed conclusions see each sub-study and their conclusions in 3.5, 4.4 and 5.4. The major findings of the paper are summarized as follows

- Four improved inventory techniques, which are either more cost-effective or robust than pure distribution based or individual tree based techniques, were proposed.
- The use of various techniques to measure individual tree height growth was demonstrated. Differences between DSMs, height histograms and the highest laser hits were used to derive growth-related statistics. The error and bias obtained for individual tree height growth were lower than those reported in an earlier study concerning field measurements of height growth (Päivinen et al. 1992). New growth models, monitoring climate change (and perhaps post-Kyoto protocols), and large area forest inventories as strip-based sampling can be seen as real-life applications.
- From the practical inventory point of view the results on DTM accuracy imply that the flight parameters have a small effect on the precision of the DTM, but the systematic differences needs to be understood and taken into account. The most problematic areas are dense deciduous canopies or canopies with dense underground vegetation. In other areas, the applied algorithms have a negligible effect on DTM retrieval. Thus, also more automatic techniques may be used for terrain model calculation. In Yu et al. (2005b) it was also shown that in boreal forest zone the use of first pulse results in accuracy enough for forest studies due to the high amount of gaps for laser pulses in boreal forests.

## ACKNOWLEDGEMENTS

Academy of Finland is acknowledged for financial support (Measurement techniques for forest change detection).

## REFERENCES

Ahokas, E., Kaartinen, H., Matikainen, L., Hyyppä, J., Hyyppä, H. (2002). Accuracy of high-pulse-rate laser scanners for digital target models. In: Observing our environment from space. New solutions for a new millennium. Proceedings of the 21st EARSeL Symposium, Paris, 14-16 May, 2001. Balkema Publishers 2002, pp. 175-178.

Anttila, P. and Lehikoinen, M. (2002). Kuvioittaisten puustotunnusten estimointi ilmakuvilta puoliautomaattisella latvusten segmentoinnilla. Metsätieteen aikakauskirja 3/2002, pp. 381-389.

Axelsson, P. (1999). Prosessing of laser scanner data - algorithms and applications. ISPRS Journal of Photogrammetry and Remote Sensing 54, pp. 138-147.

Axelsson P. (2000). DEM Generation from Laser Scanner Data Using Adaptive TIN Models. International Archives of Photogrammetry and Remote Sensing. Vol. 33, Part B4., pp 110-117.

Axelsson, P. (2001). Ground estimation of laser data using adaptive TIN models. Proceedings of OEEPE workshop on airborne laserscanning and interferometric SAR for detailed digital elevation models, Royal Institute of Technology, Stockholm, Sweden. Publication No. 40. CD-ROM. pp. 185-208.

Brandtberg T. (1999). Automatic Individual tree-based analysis of high spatial resolution remotely sensed data. PhD thesis. Acta Universitatis Agriculutae Sueciae, Sivestria 118. Swedish University of agricultural Sciences, Uppsala. 47 p.

Elmqvist, M., Jungert, E., Lantz, F., Persson, Å., and Söderman, U. (2001). Terrain modelling and analysis using laser scanner data. estimation of laser radar data using active shape models. International Archives of Photogrammetry and Remote Sensing. Vol. 34-3/W4, pp. 219-227.

Gobakken, T. and E. Næsset (2004). Effects of forest growth on laser derived canopy metrics. International Archives of Photogrammetry, Remote Sensing and Spatial Information Sciences, 3-6 October 2004, Freiburg, Germany (Institute for forest growth, Dep. Of Remote Sensing and landscape Information Systems, University of Freiburg, Freiburg, Germany), Vol. XXXVI, Part 8/W2, pp. 224-227.

Gougeon, F. and Moore, T. (1989). Classification indiovidualle des arbres á partir d'images á haute resolution spatiale. Télédétection et gestion des resources Vol. VI, pp. 185-196.

Gougeon, F. (1997). Recognizing the Forest From the Trees: Individual Tree Crown Delineation, Classification and Regrouping for Inventory Purposes. Proceedings of Airborne Remote Sensing Conference and Exhibition, 7-10 July 1997 Copenhagen, Denmark, vol. 2, pp. 807-815.

Holmgren, J. (2004). Prediction of tree height, basal area and stem volume using airborne laser scanning. Scandinavian Journal of Forest Research 19: 543–553.

Holmgren, J. and Jonsson, T. (2004). Large scale airborne laser-scanning of forest resources in Sweden. In: Thies, M., Koch, B, Spiecker, H.and Weinacker, H.(eds.). Laser scanners for forest and landscape assessment. Proceedings of the ISPRS working group VIII/2. Freiburg, Germany, October, 3-6 2004. International Archives of Photogrammetry, Remote Sensing and Spatial Information Sciences. Volume XXXVI, Part 8/W2. pp. 157–160.

Holmgren, J. and Persson, Å. (2004). Identifying species of individual trees using airborne laser scanning. Remote Sensing of Environment 90, pp. 415-423.

Huitu, H. (2005). Tulkintavirheen muodostuminen yksittäisen puun ilmakuvamittaukseen perustuvassa metsänarvioinnissa -Sävyarvomaksimeihin ja Watershed-segementointiin perustuva kuvantulkintamenetelmä. M.Sc. Thesis. University of Helsinki. 45 p.

Hyyppä, H., Yu, X., Hyyppä, J., Kaartinen, H., Honkavaara, E. and P. Rönnholm (2005). Factors affecting the quality of DTM generation in forested areas. Proceedings of ISPRS Workshop Laser Scanning 2005, September 12-14, 2005, Enschede, The Netherlands, International Archives of Photogrammetry, Remote Sensing and Spatial Information Sciences, XXXVI(Part 3/W19) : 85-90, CD-ROM.

Hyyppä, J. and Inkinen, M. (1999). Detecting and estimating attributes for single trees using laser scanner. The Photogrammetric Journal of Finland 16: 27–42.

Hyyppä, J., Hyyppä, H., Inkinen, M, Engdahl, M., Linko, S., and Zhu, Y-H. (2000a). Accuracy comparison of various remote sensing data sources in the retrieval of forest stand attributes. Journal of Forest Ecology and Management 108, pp. 109-120.

Hyyppä J., Pyysalo U., Hyyppä H., Haggren H. and Ruppert G. (2000b). Accuracy of laser scanning for DTM generation in forested areas. Proceedings of SPIE. Vol. 4035, pp. 119-130.

Hyyppä, J., X. Yu, P. Rönnholm, H. Kaartinen and H. Hyyppä (2003). Factors affecting laser-derived object-oriented forest height growth estimation, The Photogrammetric Journal of Finland 18(2):16-31.

Hyyppä, J., Mielonen, T., Hyyppä, H., Maltamo, M., Yu, X., Honkavaara, E. and H. Kaartinen (2005). Using individual tree crown approach for forest volume extraction with aerial images and laser point clouds. Proceedings of ISPRS Workshop Laser Scanning 2005, September 12-14, 2005, Enschede, The Netherlands, International Archives of Photogrammetry, Remote Sensing and Spatial Information Sciences, XXXVI(Part 3/W19) : 144-149, CD-ROM.

Kalliovirta, J. and Tokola, T., forthcoming. Functions for estimating stem dimater and tree age using tree height, crown width and existing stand database information. Manuscript, version autumn 2004

Korpela, I., Anttila, P. and Pitkänen, J. (2005). A local maxima method for detecting individual tree tops in colour-infrared aerial photographs. Manuscript.

Kraus, K. and Pfeifer, N. (1998). Determination of terrain models in wooded areas with airborne laser scanner data. ISPRS Journal of Photogrammetry and Remote Sensing 53, pp.193-203.

Kraus, K., 2004. Lecture at Helsinki University of Technology, March 2004.

Laasasenaho, J. (1982). Taper curve and volume functions for pine, spruce and birch. Commun. Inst. For. Fenn. 108.

Leckie, D.L. Gougeon, F., Hill, D, Quinn, R., Armstrong, L. and Shreenan, R. (2003). Combined high-density lidar and multispectral imagery for individual tree crown analysis. Canadian Journal of Remote Sensing 29: 633–649.

Lim. K, Treitz, P., Baldwin, K., Morrison, I. and Green J. (2003). Lidar remote sensing of biophysical properties of tolerant northern hardwood forests. Canadian Journal of Remote Sensing 29: 648–678.

Magnussen, S. and Boudewyn, P. (1998). Derivations of stand heights from airborne laser scanner data with canopy-based quantile estimators. Canadian Journal of Forest Research, 28, 1016–1031.

Magnussen, S., Eggermont, P. and LaRiccia, V.N. (1999). Recovering tree heights from airborne laser scanner data. Forest Science 45: 407–422.

Maltamo, M., Eerikäinen, K., Pitkänen J., Hyyppä, J. and Vehmas, M. (2004). Estimation of timber volume and stem density based on scanning laser altimetry and expected tree size distribution functions. Remote Sensing of Environment, 90, 319–330.

Means, J.E., Acker, S.A., Brandon, J.F., Renslow, M., Emerson, L. and Hendrix, C.J. (2000). Predicting forest stand characteristics with airborne scanning lidar. Photogrammetric engineering & Remote Sensing 66: 1367–1371.

Næsset, E. (1997a). Determination of mean tree height of forest stands using an airborne lidar system. ISPRS Journal of Photogrammetry and Remote Sensing, 52, 49–56.

Næsset, E. (1997b). Estimating timber volume of forest stands using airborne laser scanner data. Remote Sensing of Environment 51: 246–253.

Næsset, E. (2002). Predicting forest stand characteristics with airborne scanning laser using a practical two-stage procedure and field data. Remote Sensing of Environment 80: 88–99.

Næsset, E., Gobakken, T., Holmgren, J., Hyyppä, H., Hyyppä, J., Maltamo, M., Nilsson, M., Olsson, H., Persson, Å. and U. Söderman (2004). Laser scanning of forest resources: the Nordic experience, Scandinavian Journal of Forest Research 19(6):482-499.

Nelson, R., Krabill, W. and Tonelli, J. (1988). Estimating forest biomass and volume using airborne laser data. Remote Sensing Enviroment, 24: 247-267.

Nyyssönen, A. (1954). Estimation of stand volume by means of the relascope. Communicationes Instituti Forestalis Fenniae, 44.6, Helsinki, 31 p.

Päivinen, R., M. Nousiainen and K. Korhonen (1992). Puutunnusten mittaamisen luotettavuus. English summary: Accuracy of certain tree measurements. Folia Forestalia 787. 18 p.

Persson, Å., Holmgren, J. and Söderman, U. (2002). Detecting and measuring individual trees using an airborne laser scanner. Photogrametric engineering & Remote Sensing 68: 925–932.

Popescu, S., Wynne, R.H. and Nelson, R.F. (2002). Estimating plot-level tree heights with lidar: local filtering with a canopy-height based variable window size. Computers and Electronics in Agriculture 37: 71–95.

Pyysalo, U. (2000). Generation of elevation models in wooded areas from a three dimensional point cloud measured by laser scanning. MSc Thesis, Helsinki University of Technology, Espoo, Finland, 68 p.

Reutebuch, S., McGaughey, R., Andersen, H., Carson, W. (2003). Accuracy of a high-resolution lidar terrain model under a conifer forest canopy. Canadian Journal of Remote Sensing, 29, pp. 527-535.

Sithole, G. (2001). Filtering of laser altimetry data using a slope adaptive filter. International Archives of Photogrammetry and Remote Sensing. Vol. 34-3/W4, pp. 203-210.

Sithole, G. and Vosselman, G. (2004). Experimental comparison of filter algorithms for bare-Earth extraction from airborne laser scanning point clouds. ISPRS Journal of Photogrammetry and Remote Sensing 59, pp. 85-101.

St-Onge, B.A. and Renaud, A. (2001). Estimating merchantable timber volume of aspen and spruce stands of the boreal forest using airborne scanning laser altimetry. in: Proceedings of the 23rd Canadian Symposium on Remote Sensing, 21-24 August, Quebéc, Que. CASI, Ottawa, Ont. pp. 259–264.

St-Onge, B. and U. Vepakomma (2004). Assessing forest gap dynamics and growth using multi-temporal laser-scanner data. International Archives of Photogrammetry, Remote Sensing and Spatial Information Sciences, 3-6 October 2004, Freiburg, Germany (Institute for forest growth, Dep. Of Remote Sensing and landscape Information Systems, University of Freiburg, Freiburg, Germany), Vol. XXXVI, Part 8/W2, pp. 173-178.

Takeda, H. (2004). Ground surface estimation in dense forest. The International Archives of Photogrammetry, Remote Sensing and Spatial Information Sciences, Vol. 35, part B3, pp. 1016-1023.

Vosselman, G. and Maas, H-G. (2001). Adjustment and filtering of raw laser altimetry data. Proceedings of OEEPE workshop on airborne laserscanning and interferometric SAR for detailed digital elevation models, Royal Institute of Technology, Stockholm, Sweden. paper 5, 11 p.

Wack, R. and Wimmer, A. (2002). Digital terrain models from airborne laser scanner data – a grid based approach. . International Archives of Photogrammetry and Remote Sensing. Vol. 35, Part 3B, pp. 293-296.

Yu , X., J. Hyyppä, P. Rönnholm, H. Kaartinen, M. Maltamo and H. Hyyppä (2003). Detection of harvested trees and estimation of forest growth using laser scanning, Proceedings of the Scandlaser Scientific Workshop on Airborne Laser Scanning of Forests, 3-4 September 2003, Umeå, Sweden, (Swedish University of Agricultural Sciences), pp. 115-124.

Yu, X., J. Hyyppä, H. Kaartinen and M. Maltamo (2004). Automatic detection of harvested trees and determination of forest growth using airborne laser scanning, Remote Sensing of Environment, 90:451-462.

Yu, X., Hyyppä, J., Kaartinen, H., Hyyppä, H., Maltamo, M. and Rönnholm, P. (2005a). Measuring the growth of individual trees using multitemporal airborne laser scanning point clouds. Proceedings of ISPRS Workshop Laser Scanning 2005, 2005, September12-14, 2005, Enschede, The Netherlands, International Archives of Photogrammetry, Remote Sensing and Spatial Information Sciences, XXXVI(Part 3/W19) : 204-208, CD-ROM.

Yu, X., Hyyppä, H., Kaartinen, H., Hyyppä, J., Ahokas, E. and Kaasalainen S. (2005b). Applicability of first pulse derived digital terrain models for boreal forest studies. Proceedings of ISPRS Workshop Laser Scanning 2005, September12-14, 2005, Enschede, The Netherlands, International Archives of Photogrammetry, Remote Sensing and Spatial Information Sciences, XXXVI(Part 3/W19) : 97-102, CD-ROM.

# ESTIMATING FOREST STAND PARAMETERS APPLYING AIRBORNE LASER SCANNING AND QUICKBIRD IMAGES

*Géza Király[1] and Gábor Brolly[2]*

[1] University of West-Hungary, Department of Surveying and Remote Sensing, Sopron, Hungary; kiraly.geza@emk.nyme.hu

[2] University of West-Hungary, Department of Surveying and Remote Sensing, Sopron, Hungary; gbrolly@emk.nyme.hu

## ABSTRACT

The main purpose of this study is analysing the ability of stand height evaluation based on ALS datasources captured in leaves-off state of deciduous stands. Capturing in leaves-off state is favourable to calculate DTM, but the less for analysing vegetation canopy. Although significant underestimation is expected in stand heights, it is necessary considering the opportunity to use the same dataset for extracting DTM and stand properties due to financial reasons. Hierarchic Ro-bust Filtering was used to obtain DTM, sampling of raw data was used to assess tree tops. Data fusion of ALS and a QuickBird image from the vegetation season makes crown-parameters estimation possible. The segmentation of the very high-resolution satellite image and a geometric evaluation of the segments combined with the ALS data were performed. The photogrammetric assessment of a bundle block adjusted scanned aerial photographs are also performed for automatic digital canopy model extraction. The traditional digital photogrammetric evaluation, and national forest inventory data are used for accuracy assessments.

**Keywords:** Forestry, Laser scanning, Quickbird, parameters estimation

## 1 INTRODUCTION

The airborne laser-scanning (ALS) is as rare as the white crown in Hungary. The first one was in August, 2004, on a small, biotope reconstruction area, by the side of Lake-Fertő (Márkus - Király 2005). Unfortunately there were no forested areas on this dataset.

The ALS processed in this paper was made in the frame of a SISTEMaPARC project. This project made us possible to get the ALS and as well as the QuickBird data. The SISTEMaPARC project, which is the abbreviation of ***S***patial ***I***nformation ***S***ystems for ***T***ransnational ***E***nvironmental ***Ma***nagement of ***P***rotected ***A***reas and ***R***egions in ***C***ADSES, is an EU INTERREG III B CADSES Programme, leaded by Prof. Csaplovics, at the Institute of Photogrammetry and Remote Sensing, Dresden University of Technology (SISTEMaPARC website).

There are experiences on stand parameters estimation in leaf-off crown conditions in mixed stands. Although with density of 0.8 – 1.0 pts/m$^2$ in leaf-off conditions the laser height metrics showed reduced value, after multiplicative regression analysis there was no significant difference between predicted and ground-truth stand height. (Naesset 2005)

## 2 INVESTIGATED AREA

The test area is located in the region Hanság on the border of Austria and Hungary, which is a flatland, with 450 km$^2$ area, and 114-120 m above sea level (Figure 1). Due to its relief, it had an importance as a natural catchment area of the Danube, and so a wetland with mosaic patterned soiltypes and sparsely, opened alder groves (*Carici elongatae-Alnetum*) evaluated. The artificial water management of the last centuries made possible the existence of extended forest vegetation here. The climate is dry, the annual amount of rain is around 600 mm, which in itself is hardly enough for woodlands. From hydrological point of view the area has changed in the last decades; the groundwater decreased dramatically, and therefore the conditions of stands have turned worse. Mainly low-grade poplar plantations are found here, with 150 $m^3$/ha stem volume in average at present. The primary function of this stand will be changed gradually from commercial to protection expectedly, but a detailed forest inventory and monitoring is required for this.

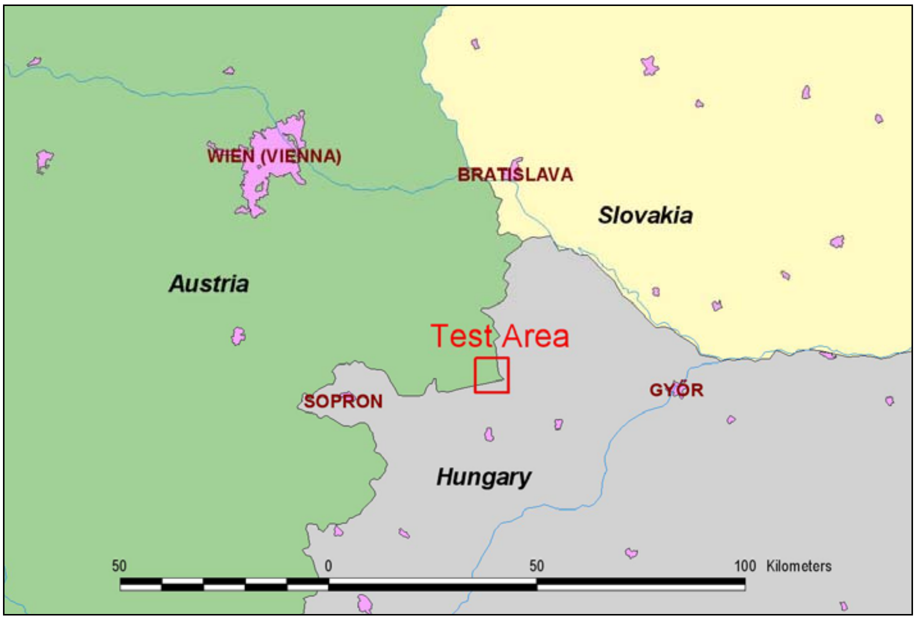


*Figure 1: The situation of the test area*

## 3 APPLIED DATA

We applied two different kinds of data in our investigation. One is the source data, and the other is the reference data for forest stand parameters.

### 3.1 Source Data

The two main data sources of our investigation were the aerial laser-scanning (ALS), and the QuickBird very high resolution (VHR) imagery.

#### 3.1.1 The airborne laser-scanning

The ALS flight was performed within the frameworks of an EU INTERREG IIIB SISTEMaPARC project. The customer of the ALS was the Government of Burgerland (Amt der Burgenländischen Landesregierung). The data cover all together 250 $km^2$ in the transborder area of Austria and Hungary, 24 $km^2$ on the Hungarian side (see Figure 1). The flight mission was made by TopScan Ltd. on 24-25th of November, 2004 with an average density of 1.5 points/$m^2$. The georeferencing was made by the Institute of Photogrammetry and Remote Sensing, Vienna University of Technology (IPF, TU WIEN). The data acquisition covers 35.5 $km^2$ forested area in 70 forest compartments in the Hungarian part. This is the first time in Hungary that woodlands involved in ALS data capture. The most important parameters of the campaign can be found in Table 1.

The RAW data were supplied to IPF, who made the stripe-adjustment, and the geocorrections to the ETRS 89 based UTM Zone 33 Projection.

The Digital Terrain Model (DTM) was derived by IPF as well, with 'Hierarchic Robust Interpolation' method in the software package SCOP++ from last echo data. The Digital Surface Model (DSM) was interpolated using 'Moving Planes' algorithm on first echo data. Then the normalised DSM (nDSM) was calculated by subtracting the DTM from the DSM on a 1 m cell-size basis (see Figure 2) (Attwenger and Chlaupek, 2006).

*Table 1: The parameters of the Airborne Laser-Scanning*

| | |
|---|---|
| Date | 24-25/11/2004 |
| Area | 220 km2 |
| Stripes | 57 |
| Density | 1.5 point / m2 |
| Firm | TopScan |
| Scanner | ALTM250 |
| Projection | UTM Z33 / ETRS 89 |

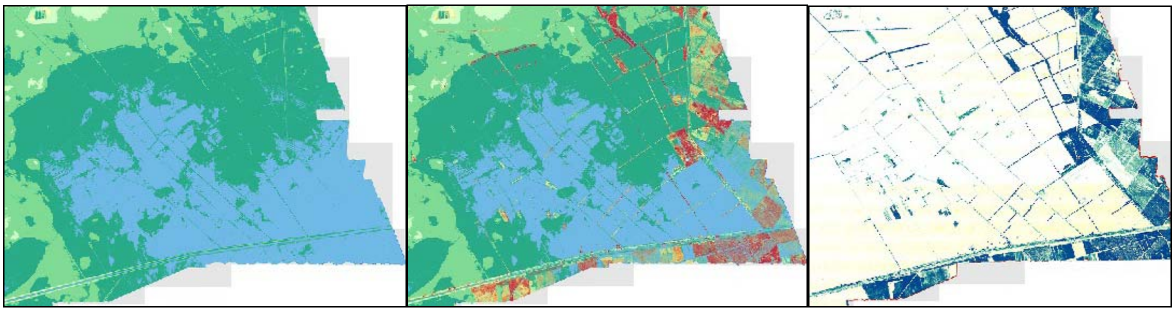

*Figure 2: The 3 different model, DTM, DSM and nDSM (from left to right). Subsets*

### 3.1.2 The QuickBird Imagery

The applied imagery was a QuickBird standard imagery with four multispectral and one panchromatic band (bundle). The image parameters can be found in Table 2.

*Table 2: The parameters of the QuickBird Imagery*

| | |
|---|---|
| Date | 30/07/2005 |
| Area | 64 $km^2$ |
| Type | Standard Imagery |
| Spectral Bands | 4 MS+ 1 P (Bundle) |
| Ground resolution | MS: 2.4 m; P: 0.6 m |
| Projection | UTM Z33 / WGS-84 |

## 3.2 Reference data

The test area was planned for forest management in 2005. An aerial photograph series were taken according to this planning. A detailed forest inventory was also surveyed. We utilised these data as reference.

### 3.2.1 Aerial photographs

The most important parameters of the aerial photography are shown on Table 3.

*Table 3: The parameters of the aerial photographs*

| | |
|---|---|
| Date | 17/08/2004 |
| Nominal scale | 1 : 30 000 |
| Camera | Wild RC20 |
| Cone type and serial | 15/4 UAG-II; 3029 |
| Film type | True-colour negative, KODAC CN 2444 |
| Scan resolution | 21 µ |
| Ground resolution | 0.64 m |

Two important parameters of the photos were worth than usual unfortunately: the scale, which used to be 1 : 20 000; and the film-type, which used to be CIR. The first one reduced the geometric accuracy of the data; the second one reduced the thematic information.

### 3.2.2 National Forest Inventory Data

The National Forest Inventory of the area was updated in year 2005. The boundaries of the compartments were corrected based upon the orthophotos. All the compartments were surveyed by sampling plots, with different methods. The overview of the methods on the selected compartments can be seen in Table 4.

*Table 4: The sampling methods of the selected compartments*

| **Method** | **No** | **Area (ha)** |
|---|---:|---:|
| Yield table estimation | 24 | 147.0 |
| Single basal area meas. | 11 | 84.3 |
| Common tree estimation | 1 | 18.7 |
| **SUM** | **36** | **250.0** |

We utilised the following data-field from the approx. 65 fields/compartments: *area, age, crown closure, timber volume, basal area and height*. The height was calculated for each compartment with the average weighted by the basal area function (Lorey's height).

## 4 METHODS

We applied different kind of methods at different scale. From large to small scale we delineated three different levels, as the followings:

- Single-tree level
- Groups of tree
- Sub-compartments

We developed different algorithms at each different scale on both source data.

### 4.1 ALS

In the case of the ALS data we applied methods on two different kinds of data. One was the nDSM model was created by the IPF, TU Wien, and another was the first pulse RAW data.

The nDSM model was a 1 m cell-size raster data. We didn't apply this source data at single-tree level, because the resolution of this raster was a little bit course for it.

The first-pulse RAW data were adopted on all the three levels. We applied a tree-tip allocation for single-tree detection. At the 2nd and 3rd level we computed a raster-based height estimation. At the sub-compartment level we calculated linear regressions of stand heights as well.

### 4.1.1 Tree Tip Allocation

We utilised a local maximum searching algorithms on the first echo raw data for looking up tree tips. All points at the lowest 5 m height range were eliminated to get rid of points scattered from bushes and the ground in the first step. We assumed that beside a critical area of circle only one tree top should exist. The highest point was accepted as treetop inside the circle. To assess the critical area of circle it was supposed that it can be approximated from other stand parameters, e.g. age, number of trees, and so on. This approximation can be derived from the QuickBird data also (see later). In the case of more points in the highest 10 cm range within the circle, the average of those points were calculated.

### 4.1.2 Raster-based height estimation

In our investigations generally we used 5 m cell size for raster-based calculations. We had tried several different methods for calculating the height value of a cell. The most important were:

- Most frequent value
- max (n) – min (n)
- weighted by number of points (Naesset, 1997)

Average stand heights were assessed from ALS raw data point clouds. It was assumed that first echoes returns from both tree tops and – due to the leafless state – the ground. We used a grid approach to sample first echo points with varying radius of searching circle. Finally we found the following method the most reliable: Using 5×5 meters grid size collecting the 25 closest points to the grid centre, than calculating the average of the 3 highest and the 3 lowest points representing the canopy top and the ground respectively. The local vegetation height was calculated as the difference of the canopy top and the ground. The distribution of local vegetation heights for each stand represents the stand vertical structure. After smoothing the vertical profiles with moving averages the mode of the upper part of the distribution function was determined as average stand height.

In the second method the same grid was used with another sampling. The average laser height of a stand was computed as the weighted mean value of the laser observations within the cells. The number of laser measurements within each cell was used as weights, such that the significance of each of the selected laser heights was proportional to the number of observations they represented (Naesset 1997).

### 4.1.3 Linear regression of stand heights

The different percentiles of height-distribution were applied. Then the function between vegetation and inventory heights was formed, and a linear regression was calculated.

So far only the first echo raw data was used to predict stand height. To calculate the vegetation height a 5 m grid approach was used, where each cell gets value according to its nearest 25 points: the mean difference of the 3 highest and the 3 lowest points. The canopy height profiles were appropriate to get information about vertical stand structure and so the stand condition. For further stand height analysis 31 stands with single storey were chosen. We found high correlation between mean stand height and canopy height percentiles as expected based on previous studies (Holmgren J., Jonsson T. 2004). We used the 90th and 95th percentile of canopy height for each stand as independent variable for linear regression.

## 4.2 QuickBird

There were several steps in the processing of the QuickBird image, but most of these steps can be categorised as:

1. Image pre-processing

2. Image segmentation and classification
3. Post-processing

### 4.2.1 Image Pre-Processing

The GCPs surveyed for the orientation of the aerial photographs were utilised for evaluating the geometric accuracy of the image. It is found that the average accuracy of the image was better than 0.4 m. The geometric re-correction of the image was not necessary then. We should note, that the test area is very flat with less then few meters height difference.

The Pan-sharpened images were calculated for better visual interpretation. However the original bands were applied for the image segmentation and classification.

### 4.2.2 Image Segmentation and Classification

The segmentation of the image was done by the commercial software, eCognition, at the different levels mentioned above.

The segmentation at single-tree level was applied on the panchromatic band only. Then a rule-base classifier was applied. The rules for the single tree light-crown detection are shown on Figure 3.

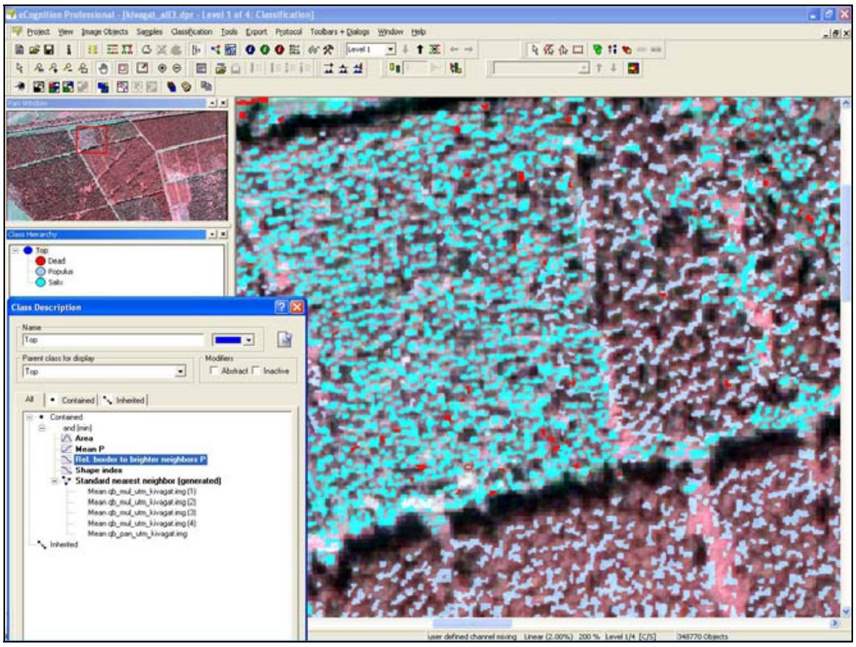

*Figure 3: The scheme of the rule-based classifier for segment-based light-crown classification*

The single-tree detection is very useful for determining single crowns, their geometry, and stem number. The mixture rate estimation is also obtainable with the classification of the crown segments. The two most important species in the test-area, the poplars and the willows, are distinct in spectral space.

At the 'groups of tree' level, the segmentation was done by the 4 multispectral and the panchromatic bands. Then the segments were classified based on both spectral characteristics, and sub-object information. The categorised 'light-crown' segments and some further information derived from those, were applied as sub-object input.

At the highest, sub-compartment level, the segmentation was performed by all five bands. At this level, the classification was done by spectral characteristics.

The compartment level on the top was created because of statistical purposes. The different evaluation and statistics of the sub-objects are available for the vector-based compartments-segments in eCognition.

The overview of the segmentation and classification hierarchy is shown in Table 5.

*Table 5: The segmentation and classification hierarchy*

| Level | Scale parameter | Segmentation | Classification |
|---|---|---|---|
| Compartments | vector | Map | Sub-object |
| Sub compartments | 300 | P+MS | Spectral |
| Groups of tree | 50 | P+MS | Spectral and sub-object |
| Single-tree | 5 | P | Rule-based |

## 4.3 Data Fusion

The data fusion of ALS and QuickBird give much more possibilities, then the two dataset separately. The most important advantages are follows:

1. Visual interpretation
2. Segmentation based on ALS and QuickBird
3. Classification based on ALS and QuickBird

The search radius of the treetop allocation was defined based upon the visual interpretation of the QuickBird image (See Ch. 4.1.1.).

We found the data fusion of the QuickBird imagery and the ALS profiles are very informative for visual interpretations (Figure 4).

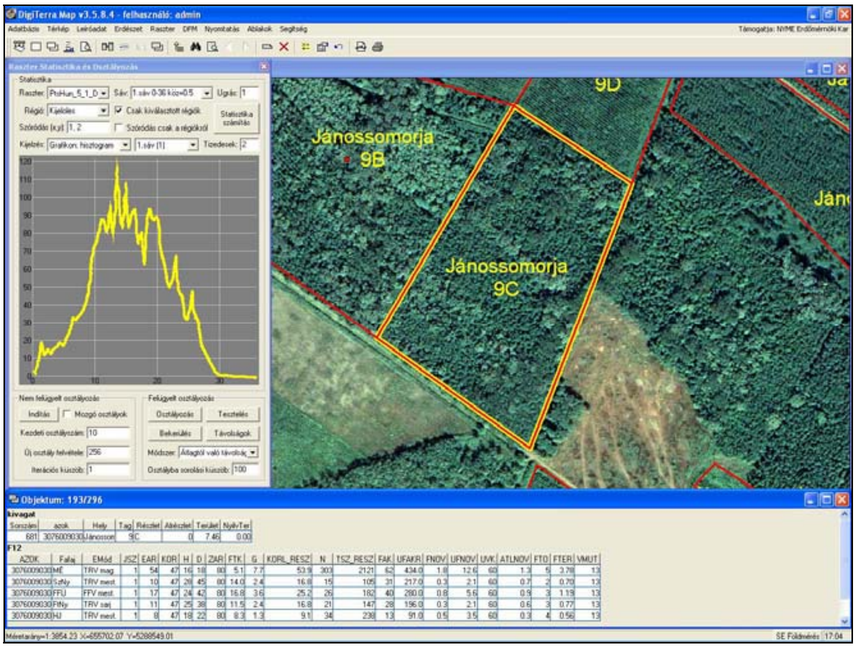


*Figure 4: Data fusion for visual interpretation*

The segmentation based not only on the imagery, but also on the ALS is much better in some cases. The segmentation of the border area with shrubs and bushes is a typical case. The sub-compartment segmentation for stand height estimation is more accurate with nDSM as well (See Ch. 5.2)

The classification is easier, when the ALS data (the nDSM) are involved in the process. The separation of some vivid vegetation and vivid plantations are difficult sometimes. The separation is much easier and accurate applying the ALS data, too.

## 4.4 Aerial Photographs

The aerial photographs were oriented applying the bundle block adjustment methods (Kraus, 1994). The ground control points (GCPs) were surveyed with Trimble 4000 SSTs, two-frequencies geodetic GPS receivers. The average orientation accuracy of the block is 0.239 m. The height accuracy of the model – which is the achievable height accuracy of a (manually or automated) measured point – is about 1.5 times of the orientation accuracy in this case.

The orthophoto-mosaic and the automatic digital surface model (DSM) were calculated after the orientation (Figure 5)

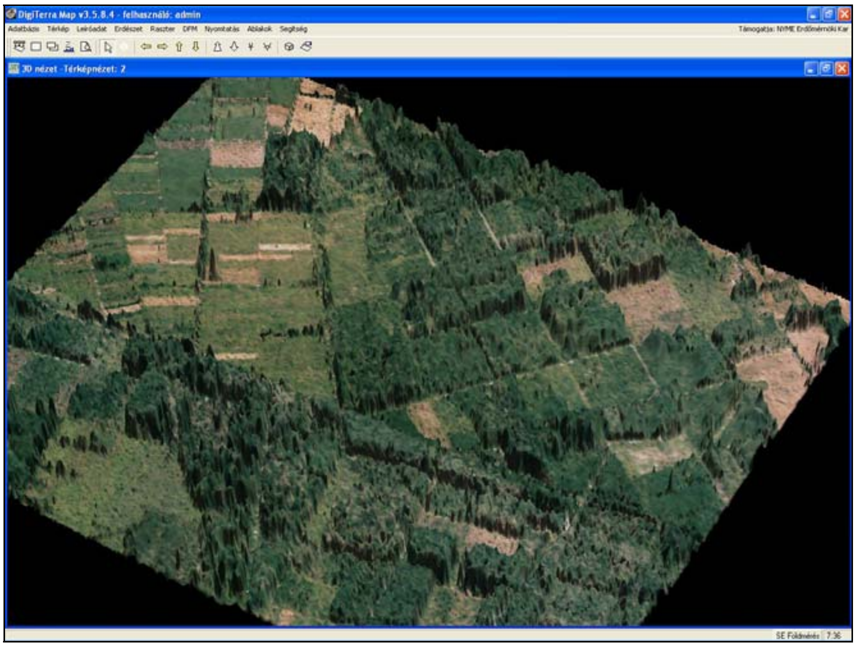


*Figure 5: The orthophoto mosaic draped on the DSM derived from the aerial photographs*

Detailed 3D measurements were done on a photogrammetric workstation. 20 points of stand top and 10 terrain points were measured in every compartments as an average. The statistics of these measures were calculated then for stand heights.

# 5 RESULTS

We grouped our results to 3 different scale-groups: stand, subcompartment and crown. The stand, and especially the height of it was the most important parameter in our investigation.

## 5.1 Stand parameters

We calculated the following parameters at stand level:

- Heights
- Mixture rate
- Stem number

The heights were calculated for all the 36 test compartments with all the methods described above. The overview of the height-estimation can be seen on Table 6.

*Table 6: The residuals of the height-estimation*

| Forest inventory | Residuals | | | |
|---|---|---|---|---|
| | min | max | mean | RMSE |
| **Stereo** | -2.47 | 8.90 | 0.63 | 2.88 |
| **profile** | -3.75 | 3.44 | 0.36 | 2.17 |
| **No. weighted** | 0.19 | 3.90 | 1.80 | 2.15 |
| **percentile 90** | -2.94 | 2.92 | -0.05 | 1.68 |
| **percentile 95** | -3.18 | 3.13 | 0.00 | 1.63 |

The linear regression of the stand heights gives a very precise estimation. The graphic representation of the regression, as well as the coefficients of the regression, can be seen on Figure 6.

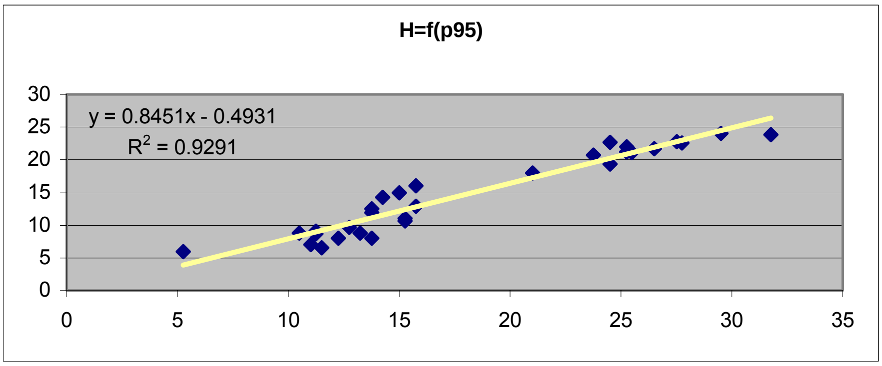


*Figure 6: Linear regression for stands heights*

The mixture rate of the compartment is a very rough estimation in the frame of the National Forest Inventory. The mixture rate was estimated based on the QuickBird image segmentation as stem number proportion and as 'light crown' area proportion.

The stem number estimations were done based upon the ALS and the QuickBird imagery. The results for selected poplar plantations are shown on Table 7.

*Table 7: The stem number estimations on selected compartments*

| **Compartment** | **Area** | **Stem number (No/ha)** | | |
|---|---|---|---|---|
| | ha | Inventory | P Segm. | ALS |
| Csorna 1A | 18.72 | 708 | 412 | 683 |
| Kapuvár 58A | 3.73 | 802 | 487 | 620 |

## 5.2 Sub-compartment delineation

The test area is very variable from forest site point of view. The stand height is also variable in some plantations reflecting this. This was the main reason why we calculated the stand heights for the sub-compartments segments. The variations in a young plantation can be seen on Figure 7.

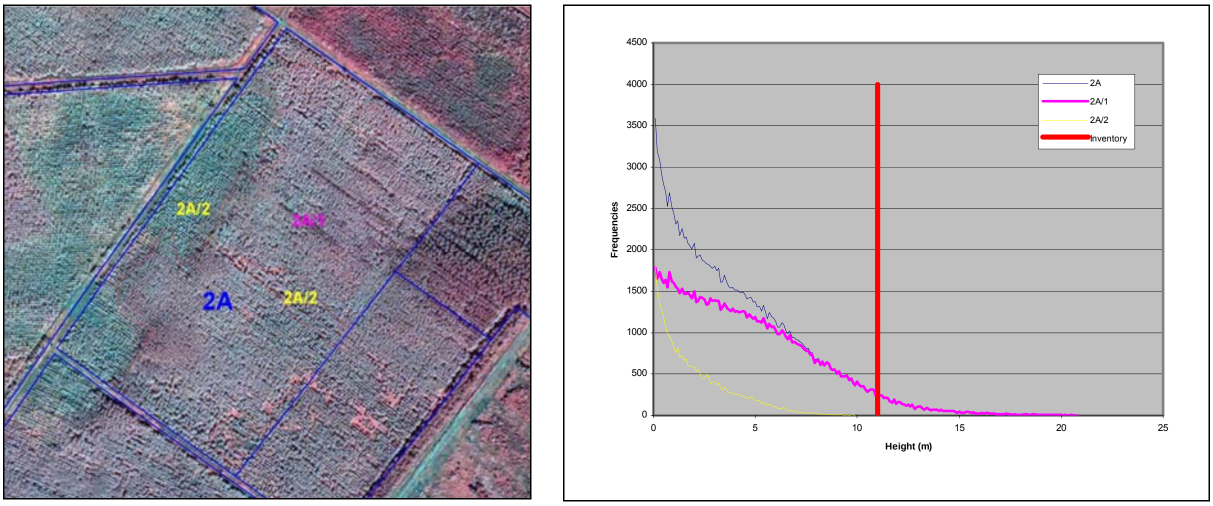


*Figure 7: Forest site variations and height distribution of a young poplar-plantation*

## 5.3 Crown parameter

The panchromatic band of the QuickBird imagery was suitable for crown delineation at single-tree level in most cases. The segmentation gives very nice result in the occurrence of poplar plantations, and gives still adequate results in multi-age stands (See Figure 8.)

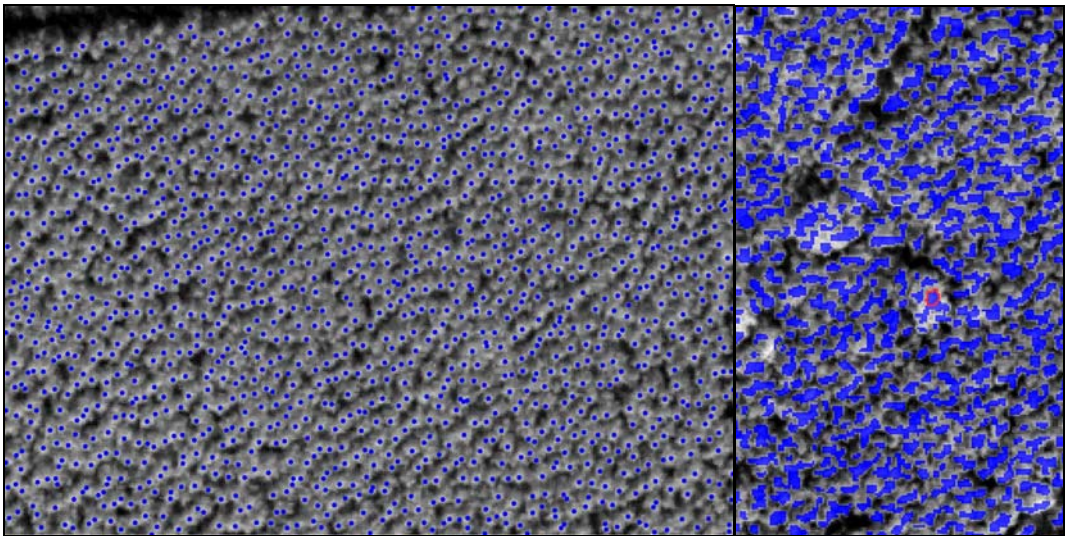

*Figure 8: Single crown delineation in poplar-plantations and multi-age stands based upon the QuickBird P band.*

The size and shape of the light-crown is more important in the case of 'natural' stands, but the segmentation is sometimes deceived. The results of this process also helped the determination of the searching radius of the tree tips routine (Ch. 4.1.1.).

# 6 DISCUSSION

Our investigation has shown the ALS data is very practicable for forest stand parameter estimations. The utilisation of the VHR imagery data raised the obtainable accuracy. The reference data was not precise enough in our investigation unfortunately. The Forest Inventory data were updated, but much coarser then the data can be derived from the source data. The aerial photography was coarser a bit than usual. These showed us clearly the necessity of the field reference data.

The average stand height is insufficient in some forest stands affected by the different forest site. The estimation of the timber volume would be much informative in these cases. On the basis of the results of the stem number estimation can be presumed the inaccurate reference data also. The crown parameter estimation showed the limitation of our source data, because of the unsatisfactory resolution.

## 7 CONCLUSIONS

The very general conclusions of our research are:

- ALS for stand heights within the tolerance
- QuickBird radiometric resolution is far better than analogue aerial film/scanning
- The P band is suitable for single tree detection
- The fusion of ALS and QuickBird give a lot of possibilities

Besides these advantages, there are also disadvantages of estimating the forest stand parameters from ALS and VHR image data:

- Date of ALS
- Resolution of ALS
- Price of ALS
- Co-registration for single trees

The leaves-off state of the trees are not ideal for tree height estimation, especially when the resolution is not so high. The average 1.5 hits/$m^2$ resolution of the ALS dataset we used also limited the single tree detection.

We have no possibilities to get ALS and VHR imagery data from other forested area at the moment, so we will continue this research with detailed field survey, development of new methods and putting more stress to the fusion of data sources.


## ACKNOWLEDGEMENTS

This research is not the part of the SISTEMaPARC project, however we would not have been able to acquire these data without this project.

We say thanks to the Hungarian National Forest Service (ÁESZ) for the inventory data as well as for the aerial photographs.

The Institute of Photogrammetry and Remote Sensing, Vienna University of Technology (TU Wien, IPF) was very helpful providing the ALS data, as well as further technical assistance. Special thanks to Ms. Maria Attwenger for the quick responses and data shipments.

The Varinex Ltd., the Hungarian distributor of PCI Geomatics and eCognition was very helpful with technical assistance.

Dr. István Márkus, the project manager of the SISTEMaPARC project at our department…

## REFERENCES


Attwenger, M. and Chlaupek, A. (2006): Erstellung eines grenzüberschreitenden digitalen Geländemodells im Nationalpark Neusiedler See-Seewinkel/Fertö Hanság aus Laserscanner-Daten. Submitted to AGIT2006.

Holmgren, J. and Jonsson, T. (2004). Large scale airborne laser scanning of forest resources in Sweden. International archives of Photogrammetry, Remote Sensing and Spatial Information Sciences. Vol. XXXVI, Part 8/W2 pp.157-160

Krauss, K.(1994): Photogrammetrie. Ferd. Dümler Verlag, Bonn, Germany, p.378.

Márkus, I. and Király, G. (2005): Production of Digital Terrain Model (DTM) from airborne laser-scanning data for researches on landscape-ecology and nature conservation. In Geomatikai Közlemények Vol VIII. MTA GGKI, Sopron, 2005. pp. 247-256.

Naesset, E. (1997). Determination of mean tree height of forest stands using airborne laser scanner data. SPRS Journal of Photogrammetry & Remote Sensing Vol. 52, pp. 49-56.

Naesset, E. (2005). Assessing sensor effects and effects of leaf-off and leaf-on canopy conditions on biophysical stand properties derived from small-footprint airborne laser data. Remote Sensing of Environment Vol. 98, pp. 356 – 370

SISTEMaPARC website (2006): http://www.tu-dresden.de/sistemaparc/

TOPSCAN (2005): Projektbericht, Laserscannermessung mit zeitgleicher digitaler Bilddaten-erfassung Neusiedler See, März 2005.

Wagner, W., Eberhöfer, C., Hollaus, M., and Summer, G. (2004). Robust Filtering of Airborne Laser Scanner Data for Vegetation Analysis. In The International Archives of Photogrammetry, Remote Sensing and Spatial Information Sciences, Freiburg, Germany, Vol. XXXVI, Part 8/W2, pp. 56.

# IDENTIFICATION OF TREE SPECIES OF INDIVIDUAL TREES BY COMBINING VERY HIGH RESOLUTION LASER DATA WITH MULTI-SPECTRAL IMAGES

*Åsa Persson[1], Johan Holmgren[2] and Ulf Söderman[1]*

[1] Swedish Defence Research Agency, Department of Laser Systems, Linköping, Sweden; Asa.Persson@foi.se, Ulf.Soderman@foi.se

[2] Swedish University of Agricultural Sciences, Department of Forest Resource Management and Geomatics, Umeå, Sweden; Johan.Holmgren@resgeom.slu.se

## ABSTRACT

The purpose of this work is to identify tree species of individual trees through combining features of high resolution laser data with high resolution multi-spectral images. Tree species identification is the last step in a method with the following steps: (1) delineation of individual tree crowns using laser data, (2) estimation of tree height and crown area using laser data, and finally (3) identification of species of the delineated tree crowns by combining features extracted from laser data with data from multi-spectral digital images. Features derived from laser data could be grouped into the categories: (1) height distribution, (2) proportion of pulse types, (3) canopy shape, (4) intensity of returns, and finally (5) clustering of returns, describing branch pattern. Laser generated tree crown segments were mapped to the corresponding pixels in the multi-spectral image and then spectral data within a crown segment could be extracted. An experiment has been performed at a test site in southern Sweden (lat. 58°30'N, long. 13°40'E) with forest dominated by Norway spruce (*Picea abies*), Scots pine (*Pinus sylvestris*), and deciduous trees, mainly birch (*Betula* spp.); classification of trees into these three tree species groups was validated. The laser data, acquired by the TopEye system, had a density of about 50 laser measurements per square meter. Multi-spectral images were recorded using the Z/I Digital Mapping Camera (DMC). For all detected trees (1721 trees) within 14 plots (sizes of 50x20 $m^2$ or 80x80 $m^2$), the position were measured in field and tree species recorded. The results imply that by combining features from laser data together with information from multi-spectral images, the classification can be improved (95 % accuracy).

**Keywords:** Tree species identification, crown delineation, crown segmentation, laser scanning

## 1 INTRODUCTION

Airborne laser scanning offers the possibility to efficiently obtain high precision measurements of individual trees. The position and size of trees can be measured with sub-meter accuracy (e.g. Hyyppä & Inkinen, 1999; Hyyppä et al., 2001; Persson et al., 2002; Schardt et al., 2002). This possibility could benefit both commercial forestry and natural conservation. For planning commercial forestry in Sweden, it is very interesting to know tree position and tree size as well as tree species. The Swedish forest is dominated by Norway spruce (*Picea abies*), Scots pine (*Pinus sylvestris*), and a smaller portion of deciduous trees. It is therefore important to be able to classify trees into these groups. Since the Swedish National Land Survey recently bought a Z/I DMC camera, digital images will soon be available for most of the Swedish forest. Thus, at most places where high resolution laser data are available so are also multi-spectral images. Laser data has previously shown to be useful for tree species classification (e.g. Brandtberg et al., 2003; Holmgren & Persson, 2004; Moffiet et al., 2005). Also, digital near-infrared images have been useful for tree species classification of laser segmented tree crowns (Persson, et al., 2004). The purpose of this study is to identify tree species of individual trees through combining features of high resolution laser data with high resolution multi-spectral images, and to validate the classification accuracy.

## 2 MATERIAL

The experiment was performed at a test site situated in southern Sweden (lat. 58°30'N, long. 13°40'E). The forest is dominated by Norway spruce (*Picea abies*), Scots pine (*Pinus sylvestris*), and deciduous trees, mainly birch (*Betula* spp.). For all detected trees (1721 trees) within 14 plots (50x20 or 80x80 $m^2$), the position were measured in field and tree species recorded. Six plots each were dominated by Scots pine or Norway spruce, respectively, and two plots were dominated by deciduous trees. For the classification, there were 550 pine trees, 708 spruce trees, and 463 deciduous trees.

The laser data, consisting of first and last return, was acquired in August 2004 using the airborne laser scanning TopEye MkII system (www.topeye.com). The system uses a pulse rate of 50 kHz, a wavelength of 1064 nm and a pulse length of 5 ns. An elliptic scanning pattern is used. The flight height was 130 meters and the point density was about 50 laser measurements per square meter.

Multi-spectral images were recorded using the Z/I Digital Mapping Camera (DMC) (www.intergraph.com/dmc/). In this study, three of the four spectral bands were used (B1 (500-650 nm), B2 (590-675 nm) and B3 (675-850 nm)). The images used were compositions of a high resolution panchromatic image (ground resolution of 0.1 m) and the multi-spectral image (ground resolution of 0.6 m). Exterior orientation parameters were calculated by performing block triangulation using ground control points. Two sets of multi-spectral images at different times of the year were used in this study; one set collected in October 2003 (autumn images) and one in June 2005 (summer images), both from an altitude of 1200 m above ground level. The images are stored as 16 bit images and include 12 bits (4096 digital levels).

## 3 METHODS

Tree species identification is the last step in a method that has the following steps: (1) delineation of individual tree crowns using laser data, (2) estimation of tree height and crown area using laser data, and finally (3) identification of species of the delineated tree crowns by combining features extracted from laser data with data from multi-spectral digital images. A previously developed method was used for delineation of individual tree crowns (Persson et al., 2002). Features were derived from laser data using all laser measurements within a delineated crown segment. For the multi-spectral images, the camera position and orientation of each image was used to map laser generated tree crown segments to the corresponding pixels in the multi-spectral image and then spectral data from a crown segment could be extracted.

### 3.1 Features from laser data

For tree species identification, it is necessary to not only separate trees from each other in two dimensions but also to separate a tree crown from small trees and bushes below. Thus, the crown base height was first estimated by defining an approximate shape of the crown using alpha shapes (Edelsbrunner and Mücke, 1994). An alpha shape is derived from the Delaunay triangulation of the point cloud and can be seen as having a sphere with a certain radius, α, that carves out all places where the sphere does not enclose any point. The size of the sphere, α, determines the level of detail of the resulting alpha shape. For $\alpha=\infty$ the alpha shape is the convex hull of the point cloud and as alpha decreases cavities and finer details such as branches will appear, and finally for $\alpha=0$ the result is equal to the point cloud.

In Figure 1a, the point cloud of a pine tree is shown. By using an alpha of 1.5 meters, an approximate shape of the tree was obtained (Figure 1b). All tetrahedrons that belonged to the shape were inserted into a 3D volume (voxel size: 0.15x0.15x0.15$m^3$). For each voxel height, the area was calculated (the area was normalized by the maximum area) (Figure 1c). Values that were smaller than 0.1 were considered to be zero (dashed horizontal line). The height corresponding to the smallest area below the maximum area in the top half of the tree was used as the crown base height (vertical dark grey line). A minimum height (12% of the tree height above ground) was defined when searching for the smallest area to avoid values below this height from being chosen (dashed vertical line). In cases when more than one value equalled the minimum area (e.g., several values below 0.1), the highest height was used.

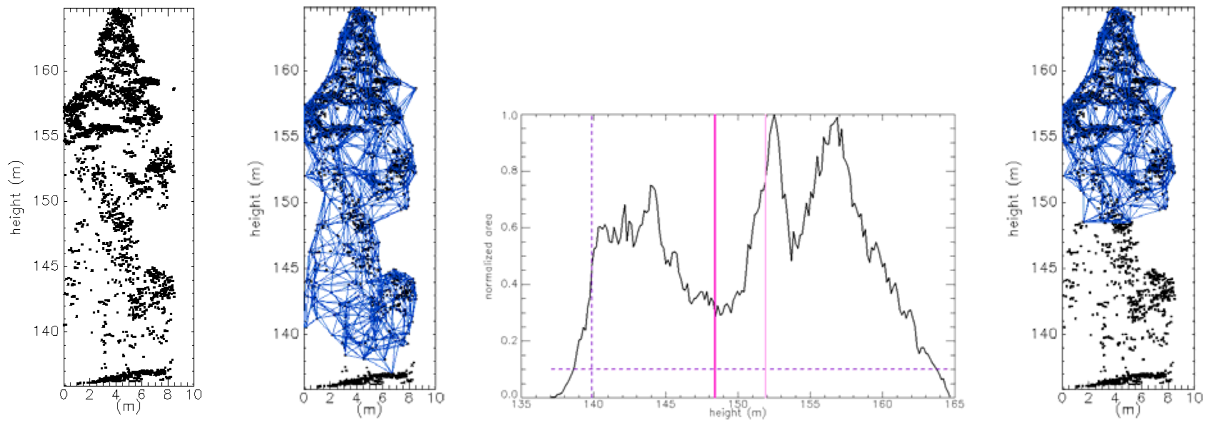


(a) (b) (c) (d)

*Figure 1: Estimation of crown base height. From left to right: (a) Point cloud of a pine tree. (b) Alpha shape (α=1.5). (c) Area of shape along height. Estimated (dark grey line) and field measured (grey line) crown base height. (d) Alpha shape (α=1.5) using points above estimated crown base height.*

When the border of the crown was defined, all points below the crown base height were excluded using only points belonging to the defined tree crown to derive features from the point clouds. Figure 1d shows the alpha shape (α=1.5) of the points above the estimated crown base height. The features derived from laser data could be grouped into the categories (1) height distribution, (2) proportion of pulse types, (3) canopy shape, (4) intensity of returns, and finally (5) clustering of returns, describing branch pattern.

*Height distribution*: The relative crown base height ($C_b$) was derived as the ratio between estimated crown base height and estimated tree height.

*Proportion of pulse types*: As a measure of crown density, the proportion of single returns in the crown ($P_s$) and the proportion of returns in the crown ($P_c$) were derived as the number of single returns and the number of total returns in the crown divided by the number of emitted pulses that had hit the crown, respectively. All returns that originated from pulses that had a first return in the crown were used to calculate these two measures. Thus, some returns could be positioned outside the crown segment. Since only the first and the last return were available, $P_c$ represents in this test the proportion of second returns in the crown.

*Canopy shape*: A parabolic surface, $z=a(x-x_0)^2 + b(y-y_0)^2 + c$, was fitted to the returns on the canopy surface. The mean of the two parameters $a$ and $b$ ($S_m$), the ratio between the minimum and maximum of the two parameters ($S_r$) and the rmse ($S_f$) were derived.

*Intensity of returns*: The mean value ($I_m$) of the intensity of all returns from the crown was derived.

*Clustering of returns*: In order to describe clustering of the returns, the K-function (Bailey & Gatrell, 1995) was used. The estimated K-function, $K(r)$, was compared with $4\pi r^3/3$ to detect if clustering was present; the radius, $r$, at the maximum derivate of the function $((3*K(r)/(4\pi))^{1/3}-r)$ was used as a feature ($K_r$).

## 3.2 Spectral values from aerial images

For the multi-spectral images, spectral data within each extracted laser crown segment were used for the classification. By using the camera position ($X_0, Y_0, Z_0$) and orientation ($\Omega, \varphi, \kappa$) of each image, the laser generated tree crown segments were mapped to the corresponding pixels in the multi-spectral image (Figure 2). Each coordinate within an extracted crown segment in the laser data ($X_p, Y_p, Z_p$) was projected to the corresponding pixel in the image ($x_p, y_p$)

$$x_p - x_0 = -f\left[\frac{m_{11}(X_p - X_0) + m_{12}(Y_p - Y_0) + m_{13}(Z_p - Z_0)}{m_{31}(X_p - X_0) + m_{32}(Y_p - Y_0) + m_{33}(Z_p - Z_0)}\right] \quad (1)$$

$$y_p - y_0 = -f\left[\frac{m_{21}(X_p - X_0) + m_{22}(Y_p - Y_0) + m_{23}(Z_p - Z_0)}{m_{31}(X_p - X_0) + m_{32}(Y_p - Y_0) + m_{33}(Z_p - Z_0)}\right] \quad (2)$$

where **M** = 3x3 rotation matrix containing trigonometric expressions of the orientation angles, $f$ = focal length and ($x_0$, $y_0$) = principal point. For each crown segment in the image, the mean value of the three bands (*B1*, *B2*, *B3*) was used as features.

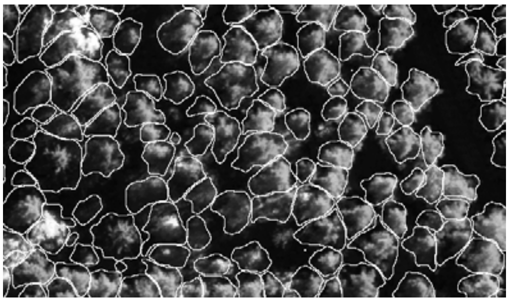

*Figure 2: Extracted crown segments from laser data projected on aerial image (field plot 13).*

### 3.3 Classification

The extracted trees in laser data were linked to the field measured trees using the laser estimated and the field measure tree positions. For each laser generated crown segment, the closest field measured tree (x, y-distance) within the segment was linked to the tree. To reduce linking errors, trees were not linked if the height of the field tree was more than 1.5 times smaller than the laser estimated tree height (a simple function relating tree height to stem diameter was used to estimate the height of non-sampled field trees). Having linked laser detected trees with field measured trees, tree species identification on an individual tree basis was performed. A maximum likelihood classification was used with relevant features, derived from both laser data and DMC images, as input. A cross validation procedure was applied, i.e., the tree that was to be classified was excluded from the training dataset.

## 4 RESULTS AND DISCUSSION

All of the presented classification variables were useful for discrimination of at least one tree species group (Table 1). The feature describing height distribution ($C_b$) was useful for separation between the pine group and the other two groups. The shape variable ($S_m$) was useful to distinguish between all three tree species groups. Spruce trees usually had the sharpest treetops and deciduous trees the least sharp treetops. The spruce trees usually had the most symmetrical tree crowns ($S_r$) and the best fit to the parabolic surface ($S_f$).

Since the tree canopy is not compact, trees will give rise to varying amounts of vertical distributed returns depending on the density and crown length of trees. The proportion of single returns ($P_s$) could be used to separate between deciduous trees and the other two tree species groups. The variable ($P_s$) was in general higher for the coniferous trees which indicated that pine and spruce were denser than the deciduous trees. Extraction of additional returns from waveform data, in addition to first and last return, has also indicated that deciduous trees give rise to more returns within the canopy (Persson et al., 2005). The proportion of returns from the crown ($P_c$) was useful in distinguishing between pine trees and the other two tree species groups. However, if more than first and last return could be extracted, the proportion of returns in the crown might be a more useful feature for separating deciduous trees from coniferous trees. Extraction of additional returns in the middle layers of crowns may also improve the vertical description of tree crowns and features such as crown base height. The deciduous tree also had, in general, a lower intensity than the denser coniferous trees. The spruce trees usually had the highest intensity values. The clustering variable ($K_r$) was useful for separation of deciduous trees, for which the maximum derivative occurred, in general, at a larger radius. The mean value of the near-infrared band (*B3*) was usually larger for the deciduous trees compared to the coniferous trees for the $DMC_{summer}$ images but not for the $DMC_{autumn}$ images.

*Table 1: The t-statistic for different classification variables and tree species pairs; a high absolute value indicates that the variable is efficient for discrimination between a tree species pair*

| Type | Variable | Pine-spruce | Spruce-deciduous | Pine-deciduous |
|---|---|---|---|---|
| Height distribution | Cb | 23 | -3 | 16 |
| Canopy shape | Sm | 24 | -52 | -29 |
| | Sr | -7 | 12 | 7 |
| | Sf | 7 | -20 | -13 |
| Proportion of pulse types | Ps | -3 | 19 | 16 |
| | Pc | -36 | -2 | -15 |
| Intensity of returns | Im | -10 | 34 | 21 |
| Clustering | Kr | -1 | -12 | -13 |
| $DMC_{autumn}$ | B1 | 28 | -21 | -2 |
| | B2 | 27 | -32 | -18 |
| | B3 | 13 | 4 | 16 |
| $DMC_{summer}$ | B1 | 7 | -27 | -24 |
| | B2 | 13 | -28 | -21 |
| | B3 | 8 | -37 | -33 |

*Table 2: Proportion correctly classified trees on 14 field plots, 1721 trees*

| Data source | Pine | Spruce | Deciduous | All trees |
|---|---|---|---|---|
| Laser | 87.6% | 88.7% | 84.7% | 87.3% |
| $DMC_{autumn}$ | 87.3% | 92.1% | 93.3% | 90.9% |
| $DMC_{summer}$ | 83.3% | 79.5% | 88.8% | 83.2% |
| Laser, $DMC_{autumn}$ | 94.5% | 94.9% | 96.1% | 95.1% |
| Laser, $DMC_{summer}$ | 91.3% | 93.9% | 93.3% | 92.9% |

Classification with variables from each data source alone resulted in an accuracy of 87% for the laser variables and 91% for the $DMC_{autumn}$ images. The $DMC_{summer}$ images resulted in lower classification accuracy (83%). By combining the two data sources, laser data and $DMC_{autumn}$, the classification accuracy could be improved to 95%. Almost the same classification accuracy (93%) was achieved by combining laser data and the $DMC_{summer}$ images (Table 2).

One reason for the divergent results of the classification with the different DMC images could be that spectral values vary between different times of the years; also the quality of the images could vary depending on different circumstances at the time of acquisition. Somewhat higher classification accuracy was achieved for the $DMC_{autumn}$ images but lower accuracy was achieved for the $DMC_{summer}$ images compared to the laser variables. However, combining laser data and DMC images always yielded better classification accuracy than either of the data sources alone. The results indicated that the derived laser variables were most efficient for separation between pine trees and spruce trees, and the DMC images were most efficient for separation between coniferous and deciduous trees.

## ACKNOWLEDGEMENTS

This work was financed by Carl Tryggers Foundation. The field data and remote sensing data were financed by and Hildur and Sven Wingquist Foundation. We would also like to thank TopEye for delivering the laser data and the Swedish National Land Survey for delivering the DMC images. Heather Reese helped us to improve the language.

# REFERENCES


Bailey, T.C., and Gatrell, A.C. 1995. Interactive spatial data analysis. Addison Wesley Longman Ltd., Edinburgh. pp. 90-96.

Brandtberg, T, Warner, T.A., Landenberger, R.E. and McGraw, J.B. 2003. Detection and analysis of individual leaf-off tree crowns in small footprint, high sampling density lidar data from eastern deciduous forest in North America. Remote Sensing of Environment, 85, pp.290-303.

Edelsbrunner, H. and Mücke, E. P. 1994. Three-Dimensional Alpha Shapes. ACM Transactions on Graphics, Vol. 13, No. 1, January 1994, pp. 43-72.

Holmgren, J. and Persson, Å. 2004. Identifying species of individual trees using airborne laser scanner. Remote Sensing of Environment, 90(4), pp. 415-550.

http://www.intergraph.com/dmc/

http://www.topeye.com

Hyyppä, J. & Inkinen, M. 1999. Detection and estimating attributes for single trees using laser scanner. The Photogrammetric Journal of Finland, 16, pp. 27-42.

Hyyppä, J., Kelle, O., Lehikoinen, M. & Inkinen, M. 2001. A segmentation-based method to retrieve stem volume estimates from 3-D tree height models produced by laser scanners. IEEE Transactions on Geoscience and Remote Sensing, 39, pp. 969-975.

Moffiet, T, Mengersen, K, Witte, C, King, R. and Denham, R. 2005. Airborne laser scanning: Exploratory data analysis indicates potential variables for classification of individual trees or forest stands according to species. ISPRS Journal of Photogrammetry & Remote Sensing, 59, pp. 289-309.

Persson, Å., Holmgren, J. and Söderman, U. 2002. Detecting and measuring individual trees using an airborne laser scanner. Photogrammetric Engineering and Remote Sensing, 68, pp. 925-932.

Persson, Å., Holmgren, J., Söderman, U., and Olsson, H. 2004. Tree species classification of individual trees in Sweden by combining high resolution laser data with high resolution near-infrared digital images. International Society of Photogrammetry and Remote Sensing, Proceedings of the ISPRS working group VIII/2, Laser-Scanners for Forest and Landscape Assessments, Freiburg, Germany, 2004-10-03 to 2004-10-06.

Persson, Å., Söderman, U., Töpel, J., Ahlberg, S. 2005. Visualization and analysis of full-waveform airborne laser scanner data. In proceedings of the ISPRS Workshop Laser scanning. vol. 36 (Part 3/W19), pp. 103-108.

Schardt, M., Ziegler, M., Wimmer, A., Wack, R. & Hyyppä, J. 2002. Assessment of forest parameters by means of laser scanning. In: (eds.). Photogrammetric computer vision, ISPRS Commission III Symposium. Graz, Austria. September 9-13. pp. 302-309.

# RECONSTRUCTING FOREST CANOPY HEIGHT USING STEREO-IKONOS PANCHROMATIC IMAGES AND A LIDAR DTM

*Benoît St-Onge, Yong Hu and Cédric Véga*

University of Quebec at Montreal, Department of Geography, Montreal (Quebec), Canada;
st-onge.benoit@uqam.ca

## ABSTRACT

The objective of this study was to assess the accuracy of 1) individual tree height measurements and 2) automated mapping of canopy height based on a combination of an Ikonos stereo-model and a lidar DTM. The Ikonos stereo-model was registered to the lidar DTM with sub-meter accuracy. The height of 99 trees was measured manually by subtracting the lidar DTM elevation from the tree top elevation measured by spatial intersection of Ikonos conjugate points. An $R^2$ of 0.87 between Ikonos-lidar estimates and field measurements was achieved. A DSM was computed using stereo-matching applied to the Ikonos stereo pair and an Ikonos-lidar CHM was obtained by subtracting the lidar DTM elevations from this DSM. The average co-dominant height of 43 field plots was predicted based on the Ikonos-lidar CHM percentiles. The best $R^2$ was of 0.53, but increased to 0.91 when five outliers caused by mismatches were removed (compared to 0.95 for the lidar-only CHM). In addition, the Ikonos-lidar plot heights were regressed against the corresponding lidar-only CHM heights for 4800 plots (without field check). The highest $R^2$ between both CHM statistics was of 0.87. This study shows that the photogrammetric quality of the Ikonos stereo pair is sufficient to measure the height of individual trees with good accuracy. Apart from local mismatches, the Ikonos-lidar CHM is very similar to the lidar-only equivalent and would allow updating forest height information at a lower cost than re-surveying a region with lidar.

**Keywords:** Lidar, Ikonos, forest, height, stereo-matching

## 1 INTRODUCTION

It has now been demonstrated numerous times that laser scanning altimetry data can be used to accurately measure, on the one hand, ground topography, and on the other hand, the height of individual trees or the average tree height within plots or stands (Lim et al. 2003). The acquisition of laser altimetry data however remains onerous, and large area surveys conducted for forestry purposes are still rare. It appears unlikely that forest companies would be willing to pay for large area lidar surveys on a regular basis to monitor change for updating their inventory. Another option is to survey a region once using laser altimetry, and update forest information using a combination of digital stereo-photogrammetry techniques applied to aerial photos and a lidar digital terrain model (DTM). We have recently shown that the height of individual trees can be very accurately measured manually (St-Onge et al. 2004), and that the height of forest canopies can be automatically mapped with an acceptable level of error using stereo-matching (St-Onge and Véga 2003). Over large areas however, numerous aerial photos would be needed to implement that approach, creating the need for assembling and processing large blocks of photos.

Satellite based photogrammetry could provide a solution to this problem. Recent studies concerning the geometric accuracy of Ikonos images suggest that high precision 3D measurements of the forest could be performed on Ikonos stereo pairs. Researchers have shown that the planimetric error of ortho-rectified Ikonos images can be at the sub-meter level (Hu et al. 2004). Moreover, it was demonstrated that digital surface models (DSMs) generated by applying automated stereo matching to an Ikonos stereo pair are very accurate (Poon et al. 2005). In forested environments, subtracting lidar DTM elevations from a stereo-Ikonos DSM would theoretically yield a canopy height model (CHM). Because the usable stereo area of an Ikonos stereo-pair is slightly larger than 100 $km^2$, large areas can be rapidly assessed. Once a lidar DTM exists, the cost per unit area for acquiring and processing an Ikonos stereo pair for updating forest information is advantageous compared to a full fledged lidar survey, especially considering the fact the that high resolution images themselves are also a valuable product for forest management. This approach would also enable the use of the wide area lidar DTMs to create CHMs over extensive parts of the United States and of some European countries such as Switzerland, the Netherlands, Germany, and Austria.

The objective of this study is to assess the accuracy of 1) individual tree height measurements and 2) automated mapping of canopy height derived from a combination of an Ikonos stereo-model and a lidar DTM. For this purpose, the Ikonos-lidar heights are compared to field heights and also to that a concomitant high-resolution lidar CHM.

# 2 METHODS

## 2.1 Study area

The study site consists of an 80 km$^2$ area falling within the Training and Research Forest of Lake Duparquet (TRFLD), located in Quebec, Canada (79°22' W, 48°30' N). The area comprises small hills with elevations between 227 m and 335 m. Forest vegetation is typical of the southeast boreal forest, characterised by an abundance of stands of mixed composition with hardwoods and conifers. Balsam fir (*Abies balsamea L.* [Mill.]) is the co-dominant species in mature forests and is associated with white spruce (*Picea glauca* [Moench] Voss), black spruce (*Picea mariana* [Mill] B.S.P.), white birch (*Betula paprifera* [Marsh.]), trembling aspen (*Populus tremuloides* [Michx]), and jack pine (*Pinus banksiana*). The age structure found at this site results from a fire driven disturbance regime. Most sample stands originate after a fire that occurred in 1923, while some are populated by trees regenerating after recent clearcuts.

## 2.2 Data

The lidar survey was conducted on August 14-16, 2003 using Optech's ALTM2050 lidar flown at 1 000 m AGL with 50% overlap between adjacent swaths, recording the first and last returns for each pulse with a maximum scan angle of 15 degrees. The pulse frequency was 50,000 Hz. Average densities of first and last returns were 3 and 0.19 hit(s)/m$^2$, respectively. The data was registered to ground profiles and the inter-swath geometrical fit was improved using the TerraMatch algorithm by Terrasolid Ltd. (Helsinki). The last returns were classified by the provider as ground and non-ground returns using Terrasolid's Terrascan, followed by manual verification and editing.

One epipolar-resampled Ikonos reference level stereo pair (Figure 1) was acquired on 11 September 2003 (four weeks after the lidar dataset), consisting of two 1-m resolution panchromatic 11-bit images. The RPCs supplied with the images represent the imaging geometry to a planimetric accuracy of 25 m CE90 and a vertical accuracy of 22 m LE90. The base to height ratio of the stereo pair was 0.8. The altitude and azimuth angles of both sun and sensor at the time of image acquisition are given in Table 1.

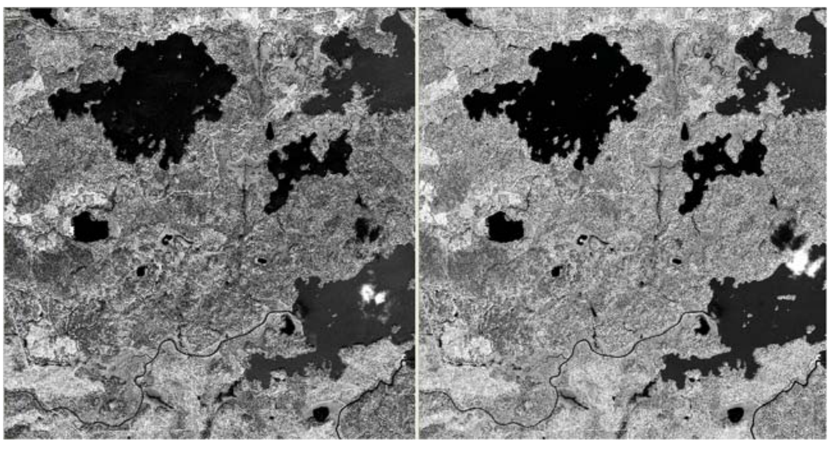

*Figure 1: The Ikonos stereo-pair (images shown are 10.7 km x 10.3 km).*

*Table 1: Altitude and azimuth angles.*

| | Sun | | Sensor | |
|---|---|---|---|---|
| | Elevation | Azimuth | Elevation | Azimuth |
| **Left image** | 47.27518 | 162.4977 | 67.47898 | 27.8251 |
| **Right image** | 47.33482 | 162.9307 | 67.42718 | 180.5202 |

The height of 211 individual trees was measured in the field in summer of 2003. In addition, a total of 43 plots each having a size of 20 x 20 m were inventoried for mean stand height assessment in 2003 and 2005. For each plot, the average height of the co-dominant trees was assessed by calculating the mean of 3 to 16 co-dominant trees. The height measurements were carried out using a Vertex III clinometer's (Haglöf, Sweden). Printouts of aerial photos acquired in 2003 were carried in the field to mark the position of all the measured individual trees. Plot positioning was done using a Panasonic SXBlue differential GPS allowing an accuracy of 2-3 m under canopy.

## 2.3 Data pre-processing

The lidar point clouds were interpolated using the IDW (Inverse Distance Weighted) method to create a grid image. To remove low canopy hits within crowns in the lidar DSM, a modified median filter was applied to the interpolated grid image. If the height value of the centre cell in a 3 by 3 window was at least 0.25 meters lower than the median value in that window, the centre cell was replaced by the median value. The filtered lidar DSM and corresponding CHM were used in all analyses.

Since the RPCs provided with the reference stereo images may be biased, we acquired control points by visually comparing features appearing on the lidar DSM and the Ikonos images. Various visualisation techniques were used to precisely identify control points (small building corners, etc.). Based on these, the shifts in line and sample directions detected in these features were used to update the *LineOffset* and *SampOffset* parameters of the Ikonos RPCs. This step removes the most significant biases of the RPCs and creates refined RPCs. To check the registration results, we used 25 independent features and compared their RPC-predicted coordinate to the corresponding lidar points.

## 2.4 Photogrammetric measurement of tree and canopy height

To assess the feasibility of measuring tree heights using the Ikonos stereo images, we measured the image coordinates of the conjugate points corresponding to 112 individual tree tops ranging from about 10 m to 30 m, both hardwoods and softwoods, chosen from the 211 tree heights that were measured on the ground. Only those trees that could be unambiguously identified on both Ikonos images and linked to reference measurements were kept. The interpreter was trained at identifying tree top conjugate points by trying to perform measurements that agreed with the field data using 13 training trees. Afterward, 99 trees were measured without knowledge of the field height. The elevations of these tree tops were then computed using the RPC-based 3D intersection method, briefly described in Hu et al. (2004). The heights of these tree tops were obtained by subtracting their underlying ground heights read from the lidar DTM. The heights of the corresponding tree tops are also read from the lidar CHM for comparison purposes.

With PCI's OrthoEngine, we generated 20 DSMs using different combination of some parameters, such as the window size, resolution and hole-filling, from the Ikonos stereo pair with refined RPCs. It was found that the 2-meter resolution with hole-filling produced the best overall results. The DSM was re-sampled to 1 m resolution to match that of the lidar DSM. Since feature-lacking areas, such as lakes, rivers, clouds and shadows, do not have image details that can be used for matching during the DSM extraction, we created a mask using a vector map of the water bodies with an added 20 meters buffer. We manually generated a second mask for the clouds and the cloud-shadowed areas. To evaluate the general quality of the DSM generated from the Ikonos stereo pair, we compared the lidar and Ikonos DSMs. Using thresholds on the lidar CHM, the DSM differences were assessed under three masks that separate the bare (< 0.5 m), regeneration (0.5 – 5 m) and forested areas (> 5 m).

The mean height and the height at percentiles 0%, 50%, 75%, 90%, 95%, 99% and 100% for both the Ikonos and lidar CHMs over 20 m x 20 m windows corresponding to field plots was computed. The Ikonos-lidar percentiles were regressed against the average co-dominant height measured in the field for the 43 plots. In addition, both the lidar and Ikonos lidar CHMs were sampled every 100 m in both X and Y direction to generate 4803 virtual 20 m x 20 m plots. In each of these plots, the above statistics were computed for both CHMs and compared by calculating the coefficient of determination (R2) between the lidar-only and the corresponding Ikonos-lidar values.

## 3 RESULTS AND DISCUSSION

Table 2 shows the mean and RMS error of the positions calculated based on the original (uncorrected) and the refined RPCs. The bias (mean) of the latter is almost null and the RMSE well below one meter. This shows that the control points considerably improved the co-registration between the Ikonos stereo-model and the lidar DTM by bringing down the error to a sub-meter level.

*Table 2: Positioning accuracies of the original and refined RPCs (meters).*

| | Original RPCs | | | Refined RPCs | | |
|---|---|---|---|---|---|---|
| | *X* | *Y* | *Z* | *X* | *Y* | *Z* |
| **Mean** | -11.79 | 10.39 | -1.26 | 0.02 | -0.05 | 0.07 |
| **RMSE** | 11.81 | 10.43 | 1.30 | 0.57 | 0.60 | 0.36 |

Figure 2 shows the lidar and Ikonos CHMs, and the corresponding height difference image. The height patterns are very similar but the lidar CHM is however crisper than the Ikonos-lidar CHM.

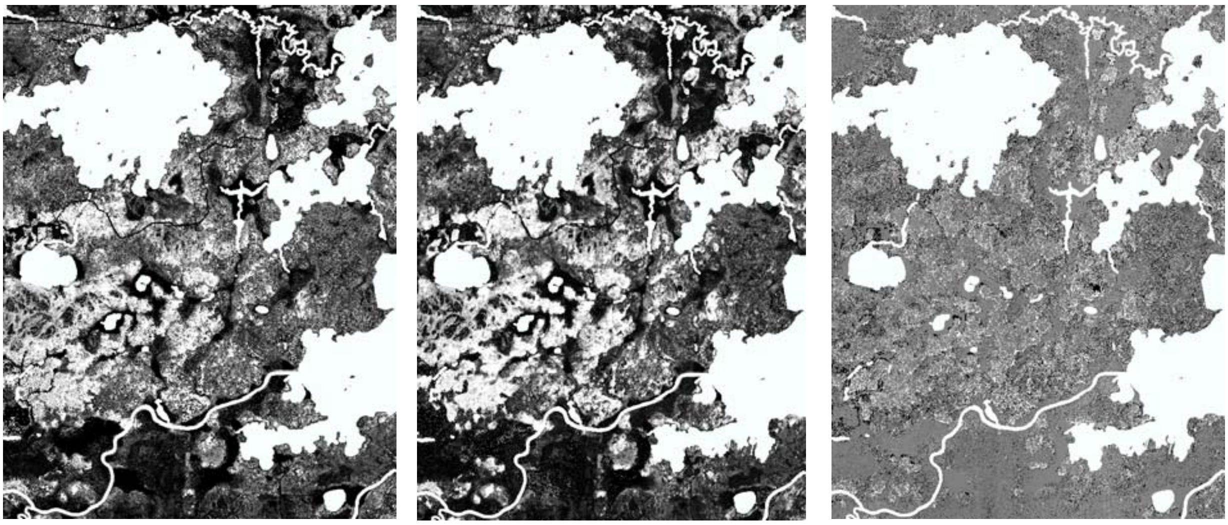

*Figure 2: Left: the lidar-only CHM, middle: the Ikonos-lidar CHM, right: the difference image. The displayed sector is 7.8 km x 10.3 km.*

The differences between the lidar and Ikonos DSMs appear in Table 3. As expected, the Ikonos surface is very close to the lidar one in bare areas, but greater differences exist for vegetated areas, especially for forests. The overall bias of the Ikonos DSM is in all cases below 1 m, and surprisingly, very low for forested areas (-0.38 m). The results quite clearly show that the stereo-matching performs better in open areas than in mature forests. The lower bias in forested areas is likely due to a chance cancellation of under- and over-estimations.

The mean error (bias) of the individual tree height measurements based on the Ikonos-lidar combination was -2.58 meters, revealing a significant downward bias (Table 4). This downward bias is consistent with that observed on medium scale air photos. Lack of resolution explains why the interpreter cannot precisely locate the tree apex, and hence, why a bias appears. Regressing Ikonos-lidar heights against field heights yielded an $R^2$ of 0.87 with a standard error of estimate of 1.72 m. It should be noted that using the lidar CHM only, the bias was also non-negligible at -2.03 m. Because lidar statistics were affected by one sharp outlier (height error of 18 m), statistics for the lidar were recomputed without it. Bias and RMSE then dropped respectively to -1.84 m and 2.77 m. Note that part of the error is due to the field measurements themselves. From these results we can conclude that the photogrammetric accuracy of the Ikonos stereo-model and its registration to the lidar DTM is excellent, and that the images are sharp enough to measure individual tree heights to within 2 m when trees are at least 10 m tall.

*Table 3: Statistics of the difference image (unit: meters)*

| | **Bare** | **Regeneration** | **Forested** |
|---|---|---|---|
| **Mean (bias)** | 0.74 | 0.93 | -0.38 |
| **Mean absolute** | 0.87 | 1.78 | 3.06 |
| **RMSE** | 1.23 | 2.62 | 4.24 |

*Table 4: Individual tree height measurement error (unit: meters)*

| | **Ikonos vs. Field** | **Lidar vs. Field** | **Lidar vs. field (outlier removed)** |
|---|---|---|---|
| **Mean** | -2.58 | -2.03 | -1.84 |
| **RMSE** | 3.10 | 3.31 | 2.77 |
| **$R^2$** | 0.87 | 0.75 | 0.84 |

The mean and height at percentiles 0, 50, 75, 90, 95, 99, and 100 were computed for the 43 field plots for both the Ikonos-lidar and the lidar-only CHMs. Table 5 shows the coefficient of determination ($R^2$) computed between the average per-plot field heights and CHM corresponding mean and percentile heights obtained through regression. Graphing the data revealed that most Ikonos-lidar height estimates where close to the regression line, with the notable exception of five clear outliers, obviously the results of mismatches. When these outliers were removed (leaving 38 plots), the maximum Ikonos-lidar $R^2$ increased from 0.53 to 0.91, approaching the lidar maximum of 0.95. This demonstrate that except for localized blunders resulting from stereo matching problems, the height of the canopy surface is well estimated from the Ikonos DSM – lidar DTM combination. In the case of the highest $R^2$ (Ikonos-lidar height at 100th percentile), the standard error of estimate was of 2.08 m (without outliers). These results demonstrate that it is possible to map average co-dominant tree height per plot based on an Ikonos-lidar DTM with an average error of approximately 2 m if matching blunders are ignored.

*Table 5: Coefficient of determination between field reference average plot heights and Ikonos-lidar statistics*

| | **mean** | **0th** | **50th** | **75th** | **90th** | **95th** | **99th** | **100th** |
|---|---|---|---|---|---|---|---|---|
| **Ikonos-lidar** | 0.42 | 0.29 | 0.39 | 0.48 | 0.50 | 0.52 | 0.52 | 0.53 |
| **Ikonos-lidar minus 5 outliers** | 0.72 | 0.45 | 0.68 | 0.82 | 0.85 | 0.88 | 0.90 | 0.91 |
| **Lidar only minus 5 outliers** | 0.86 | 0.21 | 0.89 | 0.93 | 0.94 | 0.94 | 0.95 | 0.93 |

Statistics for 4803 plots of 20 m x 20 m were extracted from both the lidar-only CHM and the Ikonos-lidar CHM. $R^2$ were calculated between these and are reported in Table 6 only for corresponding variables (e.g. lidar 90th with Ikonos-lidar 90th). The highest $R^2$ are obtained for mean, and height at the 50th and 75th percentiles. The standard error of estimate for the regression of lidar and Ikonos-lidar mean heights was of 1.90 m. This reflects the combination of the high photogrammetric accuracy of the Ikonos stereo-model and the overall effect of matching blunders. The low value of the standard error of estimate indicates that the latter effect is relatively minor.

*Table 6: Coefficient of determination between field reference average plot heights and Ikonos-lidar statistics*

| mean | 0th | 50th | 75th | 90th | 95th | 99th | 100th |
|---|---|---|---|---|---|---|---|
| 0.87 | 0.38 | 0.85 | 0.85 | 0.83 | 0.79 | 0.72 | 0.66 |

# 4 CONCLUSIONS

The height of individual trees and the mean height of co-dominant trees within plots was measured on an Ikonos-lidar CHM and compared to corresponding field measurements. The results lead us to the following conclusions:

- An Ikonos stereo-model can be registered to a lidar DTM with a sub-meter accuracy.
- The height of well defined individual trees can be manually estimated from the Ikonos stereo-model and the lidar DTM with an RMSE of approximately 1.7 m once the 2.6 m downward bias is corrected.
- The average co-dominant plot height can be estimated with a standard error of estimate of approximately 2 m where no matching blunder occurred.
- The effect of localized matching blunders is minor as reflected by the fact that the mean lidar height within 4803 plots could be predicted based on the Ikonos-lidar CHM with a standard error of estimate of 1.9 m.

As a general conclusion, we state that an Ikonos-lidar DTM can be used as a lidar substitute for updating information on canopy height over large areas at a cost that is at least four times lesser than a full lidar CHM. It should be noted that these results were obtained using a commercial software application with a standard product purchased from Space Imaging. There is therefore a very great potential for using this technique operationally over the vast areas in the United States and Europe for which state wide lidar DTMs already exist. Another advantage is that an Ikonos-lidar CHM not only brings 3D information, but also image data that is useful to understand changes. Future work will consist of extending the prediction of forest attributes to volume and biomass and improving on the stereo matching results.


# ACKNOWLEDGEMENTS

The authors wish to acknowledge the financial help of the Biocap Foundation of Canada, of the Canadian Foundation for Innovation, and of the Natural Sciences and Engineering Council of Canada. We also thank LaserMap Image Plus for their collaboration in acquiring and processing lidar data and PCI Geomatics for an advantageous pricing on the software applications.


# REFERENCES


Hu, Y., Croitoru, A. and Tao, V. (2004). Understanding the rational function model: methods and applications. International Archives of Photogrammetry and Remote Sensing, 12-23 July, Istanbul, vol. XX, pp. 119-124.

Lim, K., P. Treitz, M. Wulder, B. St-Onge, and Flood, M. (2003). LiDAR remote sensing of forest structure. Progress in Physical Geography, 27(1): 88-106.

Poon, J., Fraser, C., Zhang, C., Zhang L. and Gruen, A. (2005). Quality assessment of digital surface models generated from Ikonos imagery. Photogrammetric Record, 20(110): 162-171.

St-Onge, B., Jumelet J., Cobello M., and Véga, C. (2004). Measuring individual tree height using a combination of stereophotogrammetry and lidar. Canadian Journal of Forest Research, 34:2122-2130.

St-Onge, B. and Véga, C. (2003). Combining stereophotogrammetry and lidar to map forest canopy height. Proceedings of the workshop “3-D reconstruction from airborne laserscanner and InSAR data”, ISPRS commission III working group 3, 8-10 October, Dresden, Germany, pp. 205-210.

# VIEWING FOREST IN POL-INSAR

*Tobias Mette, Florian Kugler, Konstantinos Papathanassiou, Irena Hajnsek*

German Aerospace Center (DLR e.V.), Microwaves and Radar Institute, 82230 Wessling, Germany
Email: tobias.mette@dlr.de, Tel.: +49-8153-283507

## ABSTRACT

Forest height and biomass are economically and ecologically important forest parameters. Since inventories from the ground are very elaborate, the use of remote sensing in forestry is continuously investigated and improved. Radar waves, in contrast to conventional optical remote sensing, penetrate the forest canopy and are backscattered from crown structures, stem and ground. Therefore, in radar, forests are termed volume scatterers. Polarimetric interferometric SAR (Pol-InSAR), is a radar technique that allows to determine the height of a volume scatterer, i.e. forest height. Forest biomass, in a 2nd step, is derived from forest height with allometry. This paper explains the theory of volume scattering in forests and reviews experimental results of the L-band radar of DLR's E-SAR sensor.

**Keywords:** Radar, SAR Interferometry, SAR Polarimetry, Forest height, Forest biomass

## 1 INTRODUCTION

Forests are an important natural resource, and regular inventories aim at assuring the sustainable management of this resource. With respect to the large and often remote extension of forests, forestry institutions and science community rely upon remote sensing data and techniques (FAO 2001a/b).

For radar remote sensing of forest, an important feature is the capability to penetrate the canopy and the sensitivity to underlying tree structures and the ground. Larger wavelengths like L- and P-band ($\lambda$ ~0.15-1m) are mainly backscattered from branches and trunks and, hence, sensitive to biomass. Backscatter saturation occurs at 40 t/ha in L-band and 120 t/ha in P-band (LeToan 1992, Imhoff 1995).

SAR interferometry refers usually to the acquisition of a scene under two slightly different viewing angles. Like in photogrammetry these different angles enable the extraction of the 3rd (height) dimension, and the generation of digital elevation models, DEMs (Bamler and Hartl 1998). Over forests, the height information depends on the penetration depth of the radar wave, which is a function of the wavelength and medium density. It is therefore possible to obtain a first order forest height estimate as the difference of X-band and P-band DEM (Moreira et al. 2001) where the X-band DEM represents the canopy and the P-band DEM the ground. Another parameter from interferometry is the coherence $\gamma$, the cross-correlation of the images. For volume scatterers like forests, the coherence decreases with increasing height, a phenomenon termed volume decorrelation.

In this article, volume decorrelation is the basis for the forest height inversion from InSAR data (Fig. 1). In the simplest form it is a sinc-function between height and coherence, scaled by the imaging geometry, i.e. the interferometric baseline (Hagberg et al. 1995, Askne et al. 1997, Bamler et al. 1998). It needs no calibration from ground data if coherence is only affected by volume decorrelation and not by temporal and/ or system/ processing effects. The Random Volume over Ground-model (RVoG) extends the sinc-function by respecting also attenuation and ground effects (Treuhaft 1996). To match this increase in variables, the number of observables is increased by using polarimetric interferometric SAR data (PolInSAR). Height results for L-band data from the E-SAR system of DLR were already shown in Papathanassiou, Cloude (2001).

In a second step, the extracted heights can be converted to biomass by means of allometry, i.e. biological size relations (Fig. 1). In Mette et al. (2004a), a reference height-biomass allometry was derived from standard yield tables for Germany (Schober 1985, Assmann 1967):

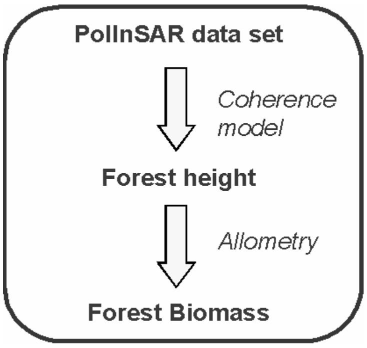


Figure 1: From Pol-InSAR data to forest biomass: (1) height estimation from radar data with a coherence model, and (2) the subsequent conversion of the forest heights to forest biomass with allometry.

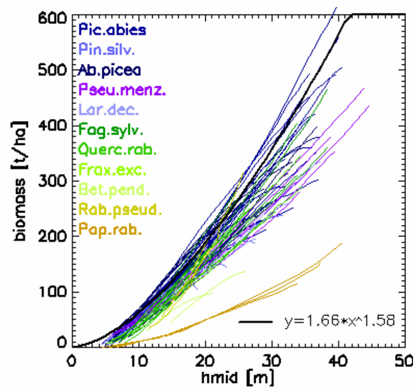


Figure 2: Height-biomass allometry for 11 different species from standard yield tables in Germany.

$$biomass_{usable} = 1.66 \cdot height_{canopy}{}^{1.58} \quad (1)$$

In Fig. 2, the height-biomass data are plotted for 11 different species, some of them differentiating up to six yield classes. Obviously, the reference equation lies close to the upper biomass end. Yet, except for poplar and birch, species usually do not fall more than 20% below the reference function.

The forest structure beyond the yield table is simple; it refers to single species, even-aged forests with a narrow height distribution. Of course, allometric predictions from yield table forest types cannot represent the wide spectrum of forest types, but are well suited as a first order reference for a height-biomass conversion. Problems arise for deviating densities and heterogeneous canopy structures. A certain adaption is possible with a linear density factor, but for strong height variations of the canopy even the definition of a reference height can become a problem.

This paper provides an overview over the relation between coherence and forest height. The performance of the forest height inversion from L-band coherence at different polarizations (Pol-InSAR) is validated for a data set of the test site 'Traunstein'. Then, the retrieved forest heights are converted to forest biomass by means of forest allometry, i.e. biological size relations. Finally, the conclusion summarizes the results and points out future steps in research and system design.

## 2 METHODS

**Test site and data:** The test-site Traunstein is located in the pre-alpine moraine landscape of south-east Bavaria near the city of Traunstein. It forms a mosaic of agricultural fields, and forests. The topography varies from 600-650 m a.s.l., with only few steep slopes. The climatic condition of 7.8°C mean annual temperature and precipitation of 1600 mm/ a favour mixed mountainous forests, dominated by spruce (Picea abies), beech (Fagus sylvatica) and fir (Abies alba). The test-site forest includes the two forest districts "Bürgerwald" and "Heilig-Geist" and covers a total area of 218 ha.

Based on aerial photography, forest inventory, and the forest management plan, 21 homogeneous stands between 1 ha and 23 ha size were selected for the validation. Most of the stands were dominated by spruce, only few by beech or maple. Heights reach up to 40 m and biomass levels up to 450 t/ha. The height and biomass data were estimated from forest inventory data (1 plot/ ha). Height was defined as upper canopy height and calculated as the mid height of the highest inventory layer(s). The usable wood biomass was derived from wood volume multiplied by the raw wood density. Since the attribute 'usable' only includes stem and branches where exceeding 7 cm diameter, trees below 10 m height are not well represent by this biomass definition.

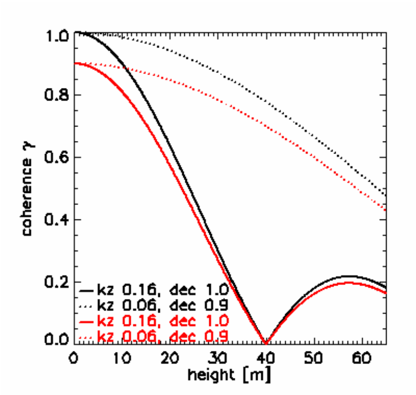


*Figure 3: idealized coherence height relation, the sinc-function. Different combinations of Δkz and decorrelation (denoted 'dec') lead to different relations.*

| *System observables:* | | *RVoG unknowns:* |
| --- | --- | --- |
| *HH coherence + phase* | | *height h* |
| *VV coherence + phase* | $\Leftrightarrow$ | *extinction* $\alpha$ |
| *HV coherence + phase* | | *gr.contrib.* $HH \neq VV \neq HV$ |
| | | *ground phase* $\phi_0$ |

*Figure 4: PolInSAR system observables vs. RVoG inversion parameters.*

The radar data were acquired on the morning of Oct. 11, 2003 with the E-SAR system of DLR. The validation has focused upon an interferometric fully polarized L-band data set with a spatial baseline of 5m (horizontal) at a flight altitude of 3000 m above ground, the temporal baseline 20 min. The data were processed for 1.5 m range resolution (100 MHz bandwidth) and 3 m resolution in azimuth single look. The incidence angle ranges from 25° in near range to 60° in for range.

**Interpretation of the radar data:** The interpretation of the interferometric data follows an understanding of interferometric coherence according to the interferometric system model described in Hagberg et al. 1995, Askne et al. 1997, Bamler and Hartl 1998. Here, only the most basic relations will be summarized. The interferometric coherence is calculated as the cross-correlation coefficient between the interferometric images i1 and i2 for a certain window size N. It scales between 0 and 1:

$$\gamma = \frac{\sum_{n=1}^{N} i_1 \cdot i_2^*}{\sqrt{\sum_{n=1}^{N} |i_1|^2 \cdot \sum_{n=1}^{N} |i_2|^2}} \quad (2)$$

In forests, coherence is a function of the vertical distribution of the scatterers and decreases with increasing height, a process termed volume decorrelation. For a random volume with no extinction and ground, the coherence height relation is a sinc-function scaled by Δkz, an equivalent of the baseline ($\gamma_V$=volume coherence, h=height, λ=wavelength, $B_{eff}$=effective baseline, R=distance, θ=look angle):

$$|\gamma_V| = \frac{\sin(\frac{1}{2} \cdot \Delta kz \cdot h)}{\frac{1}{2} \cdot \Delta kz \cdot h} \qquad where \qquad \Delta kz = \frac{4\pi}{\lambda} \cdot \frac{B_{eff}}{R \cdot \sin\theta} \quad (3)$$

Since Δkz is known from the flight geometry, it is possible to invert the coherence to volume height, i.e. to forest height. A refinement of eq. 3 is the Random-Volume-over-Ground model (RVoG) which accounts also for extinction effects and ground contribution. The model was described by Treuhaft (1996), and applied to invert polarimetric interferometric SAR data by Cloude, Papathanassiou (1998/ 2003), and Papathanassiou, Cloude (2001). These articles also treat the mathematical formulation and inversion procedure of the RVoG. Here, it is sufficient to note that the increase in model parameters requires an increase in observation parameters which are given by the polarizations (HH, VV, HV/VH). For a Pol-InSAR acquisition the system in Fig. 4 holds.

Unfortunately, the coherence is not only influenced by volume decorrelation. Other decorrelation processes, such as: range decorrelation (due to finite resolution), system and processing decorrelation (due to system noise and processing inaccuracies), and temporal decorrelation (due to changes in the scattering elements) also affect coherence and introduce errors in the height inversion:

$$\gamma = \gamma_{Volume} \cdot \gamma_{range} \cdot \gamma_{temp} \cdot \gamma_{system} \quad (5)$$

Typically, the contribution of non-volume decorrelation leads to a height overestimation, especially for lower heights. In practise, it is helpful to assume a constant non-volume decorrelation, and respect it in the coherence-height relation. For the height inversion of the Traunstein data, a decorrelation factor of 0.9 can be explained from the non-volume contributions. Fig. 3 highlights two aspects about the flight geometry: (1) for high Δkz values, the sinc-function becomes ambiguous for high heights, (2) for low Δkz-values, the height inversion becomes very sensitive to non-volume decorrelation.

# 3 RESULTS

Fig. 6 shows the Traunstein-radar images for L-band HH-polarization. It can be seen that the volume scattering over forests is higher than the surface scattering of the surrounding fields (Fig. 6A). Differences within the forest are small. The interferometric phase (after flat earth removal) for forests is much noisier compared to fields (Fig. 6B), which leads to a lower coherence of forest in the coherence image (Fig. 6C). Differences in the forest structure can be observed.

The heights that were extracted from the coherence are displayed in Fig. 6D for the sinc-inversion and for the RVoG-inversion in Fig. 6E. For both images, forest heights between 0-60m are extracted in near range (left), but the averaging over the selected sites does not exceed 45m in the sinc-inversion and 40m in the RVoG inversion (Fig. 5A/B). Lower heights occur where the average decorrelation factor of 0.9 assumes a too high decorrelation; higher heights vice versa. For the RVoG inversion a simple backscatter ground mask was applied (white areas), because the model does not work on surfaces. Towards far range, the height variations increase and frequently 60m are reached or even exceeded. This phenomenon results from a loss of sensitivity to volume decorrelation due to a the low Δkz in far range than in near range (see the end of Ch. 2.2).

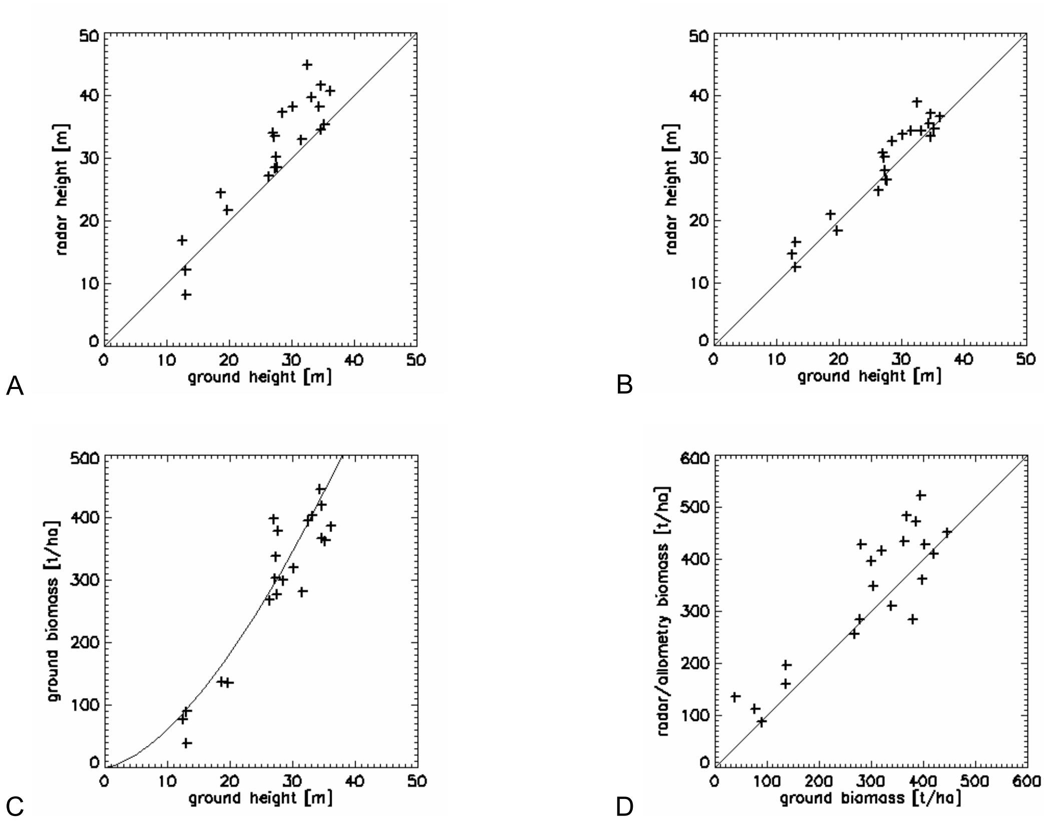


*Figure 5: Height and biomass validation based on the 21 selected validation sites. (A) ground height vs. sinc-inverted height. (B) ground height vs. RVoG-inverted height. (C) height biomass allometry from the ground data. (D) ground forest biomass vs. biomass from the RVoG-height inversion and allometric biomass conversion*

Comparing the sinc- and the RVoG inversion in Fig. 5A/B, it can be noted that (1) the sinc-inversion (shown for HH, but similar for VV and HV/VH) already yields good results, and (2) the RVoG inversion avoids the overestimation of tall heights.

The height-biomass allometry in Fig. 5C corresponds well to the proposed reference height-biomass allometry in eq. 1. This indicates that most of the selected sites are probably homogeneous forest areas not too different from the forest structure in the yield tables. The good applicability of the height-biomass allometry is responsible for the reasonable performance of the biomass estimation. Note that the height biomass allometry refers to 'usable' biomass which leads to low biomasses for low tree heights. This results in the biomass overestimation for low heights in Fig. 5C/D.

# 4 CONCLUSIONS AND OUTLOOK

The presented results were based on a physical interpretation of the forest coherence as volume decorrelation. The sinc inversion for a random volume was introduced and refined in the Random Volume over Ground model (RVoG) which also takes extinction and ground into account. While the sinc can be inverted from a single coherence, the RVoG needs a larger observation space and can be inverted from interferometric coherences at different polarizations (PolInSAR). The height inversion showed a good performance, and improved from the sinc to the RVoG. For the biomass inversion, the reference height biomass allometry from the yield tables applied well to the selected validation sites, and made a reasonable biomass estimation from the PolInSAR heights possible.

The coherence inversion showed no saturation effects up to 40m and 450t/ha. As to my knowledge it is currently the only method with space-borne potential for forest biomass estimations of this magnitude. For the inversion algorithm, a height inversion is feasible even for larger heights, because it is just a question of adjusting the $\Delta kz$ sensitivity. Yet, with increasing extinction, lower parts of the volume and ground can be hidden which leads to an underestimation of the forest height. This problem was recently addressed by the INDREX campaign of the European Space Agency, ESA. This radar experiment over tropical forest in Indonesia indicated that even dense dipterocarp forest was penetrated to the ground by L-band (see proceedings Kugler et al. 2006).

The interpretation of forest structure from PolInSAR is ongoing. Currently under investigation are the error sources in the data, model and the inversion procedure, and their quantification under controlled conditions. The potential of space-borne systems like the Japanese ALOS–satelllite (launch 23.1.2006, Hamazaki 1999) or Terra-SAR-X (June 2006, Wernighaus et al. 2004)/ TanDEM-X (proposed, Krieger et al. 2005) are evaluated, and recommendations for system configurations are made.

*Figure 6: Radar images of the Traunstein test sites with 21 selected validation sites, E-SAR L-band HH-polarization, repeat pass interferometry with 5m baseline at 3000m flight height, looking angle from 25-60°. (A) backscatter amplitude, (B) interferometric phase, (C) interferometric coherence, (D): height extraction with the sinc-inversion from InSAR data (E-SAR L-band HH), (E): height extraction with the Random-volume over ground model from PolInSAR data (E-SAR, L-band, HH, VV, VH/HV)*

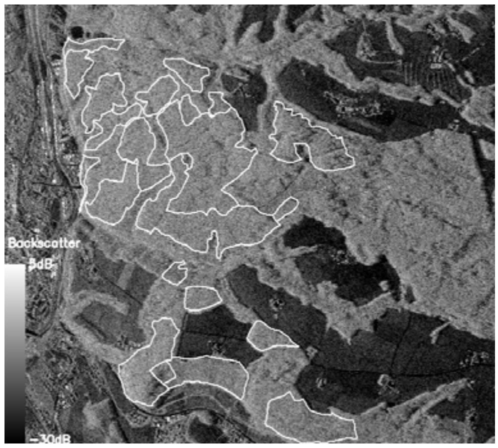


*A*

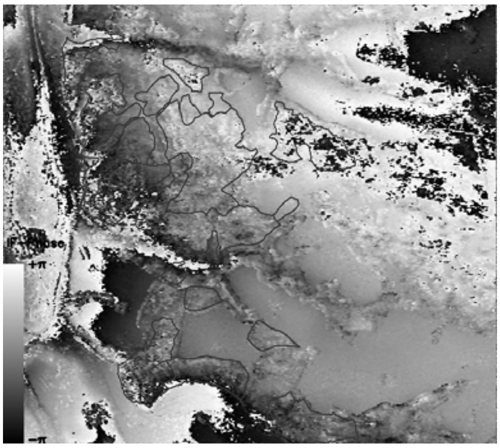


*B*

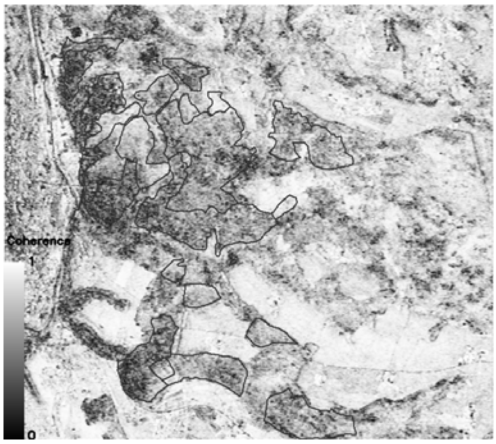


*C*

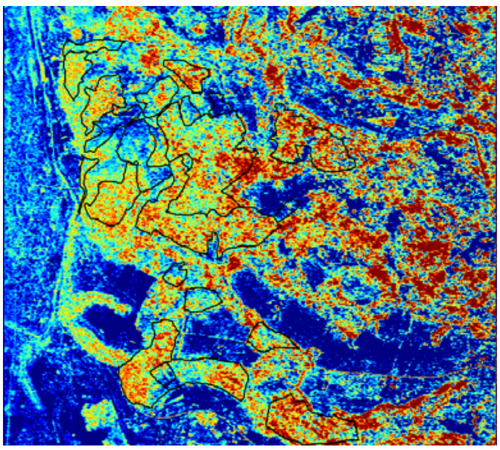

D

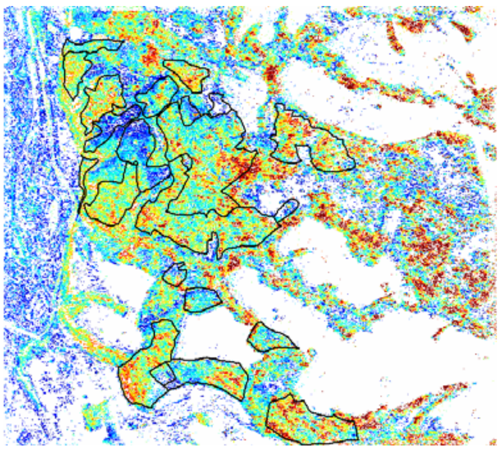

E

## REFERENCES


Askne et al. (1997). C-Band Repeat-Pass Interferometric SAR Observations of the Forest. IEEE TGRS, 35(1)

Assmann & Franz (1963). Vorläufige Fichtenertragstafel für Bayern. Forstl. Versuchsanstalt München.

Aulinger et al. (2005). Heights from IF-SAR and Lidar in NP Bayerischer Wald. PolInSAR, Frascati, 24.-28.Jan.

Bamler & Hartl (1998). Synthetic aperture radar interferometry. Inverse Problems, 14(4), R1-54.

Cloude & Papathanassiou (1998). Polarimetric SAR interferometry. IEEE TGRS, 36(5), 1551-1565.

Cloude & Papathanassiou (2003). 3-stage inversion process for PolInSAR. Radar Sonar Navig., 150(3), 125-134.

FAO (2001a). Forest Resource Assessment 2000. Rome, www.fao.org

FAO (2001b). State of World's forest 2000. Rome, www.fao.org

Hamazaki (1999). ALOS: Requirements, Sensors, Satellite System. ISPRS, Hanover, Germany, Sept, 27-30.

Imhoff (1995). Radar backscatter and biomass saturation. IEEE TGRS, 33/3: 511–518

Krieger et al. (2005): TanDEM-X: Concept and Performance Analysis. Proc. IGARSS, Seoul, Korea, Jul. 25-29

Le Toan et al. (1992). Relating forest biomass to SAR data. IEEE TGRS, 30(3): 403–411

Mette et al. (2004a). Forest height from PolINSAR to estimate forest biomass. EUSAR, Ulm, May, 16.-18.

Mette et al. (2004b). Estimating Forest Biomass from Pol-InSAR Data and Forest Allometry. Results from the Temperate Spruce Forest Test Site Traunstein. BioGeoSAR 4, 16.-19.Nov.2004, Innsbruck/ Austria

Moreira et al. (2001). Surface and ground topography determination in tropical rain forest areas using airborne interferometric SAR. Photogrammetric Week, 24.-28.Sept.2001, Stuttgart

Papathanassiou & Cloude (2001). Single baseline polarimetric SAR interferometry. IEEE TGRS 39(11)

Schober, R (1985). Ertragstafeln wichtiger Baumarten. Sauerländer's J.D. Verlag.

Treuhaft et al. (1996). Vegetation and topography from interferometric radar. Radio Science, 31(6), 1449-1485.

Werninghaus et al. (2004). The TerraSAR-X Mission. Proc. EUSAR 2004, Ulm, Germany, May 25-27

# ASSESSING THE INFLUENCE OF FLIGHT PARAMETERS AND INTERFEROMETRIC PROCESSING ON THE ACCURACY OF X-BAND IFSAR-DERIVED FOREST CANOPY HEIGHT MODELS

*Hans-Erik Andersen[1], Robert J. McGaughey[2] and Stephen E. Reutebuch[2]*

[1] University of Washington, College of Forest Resources, Seattle, Washington, USA; hanserik@u.washington.edu

[2] USDA Forest Service, Pacific Northwest Research Station, Seattle, Washington, USA; (bmcgaughey@fs.fed.us, sreutebuch@fs.fed.us)

## ABSTRACT

High resolution, active remote sensing technologies, such as interferometric synthetic aperture radar (IFSAR) and airborne laser scanning (lidar), have the capability to provide forest managers with direct measurements of 3-D forest canopy surface structure. While lidar systems can provide highly accurate measurements of canopy and terrain surfaces, high resolution (X-band) IFSAR systems provide slightly less accurate measurements of canopy surface elevation over very large areas with a much higher data collection rate, leading to a lower cost per unit area. In addition, canopy height can be measured by taking the difference between the IFSAR-derived canopy surface elevation and a lidar-derived terrain surface elevation. Therefore, in areas where high-accuracy terrain models are available, IFSAR may be used to economically monitor changes in forest structure and height over large areas on a relatively frequent basis. However, IFSAR flight parameters and processing techniques are not currently optimized for the forest canopy mapping application. In order to determine optimal flight parameters for IFSAR forest canopy measurement, we evaluated the accuracy of high resolution, X-band canopy surface models obtained over a mountainous forested area in central Washington state (USA) from two different flying heights (6,000 and 4,500 meters), from different look directions, and with different interferometric processing. High-accuracy lidar-derived canopy height models were used as a basis of comparison.

**Keywords:** Forest, canopy, height, cover, radar, interferometry, IFSAR, INSAR, lidar

## 1 INTRODUCTION

Accurate, reliable, and spatially-explicit (i.e. mapped) information relating to three-dimensional (3-D) forest canopy structure is required to support a wide variety of resource management applications, including timber inventory, habitat monitoring, and fire management. It has been well established that the two most important metrics in describing 3-D forest canopy structure are canopy cover (horizontal extent of canopy), and canopy height (vertical extent of the canopy). Foresters have long used measurements of canopy cover and canopy height to obtain estimates of stand volume from aerial photo volume tables (Paine and Kiser 2003). Estimates of canopy height and canopy cover are also needed as inputs to fire behaviour models such as FARSITE (Finney 1998). In addition, when combined with stand age information, spatially-explicit maps of maximum canopy height can provide information relating to the growth potential for a given forest area (site index).

Active remote sensing provides an efficient means of obtaining spatially-explicit information related to canopy height and cover over large areas. Lidar remote sensing provides highly-accurate, high-resolution measurements of canopy surface morphology and the underlying terrain (Andersen et al. 2001; Reutebuch et al. 2003). X-band interferometric synthetic aperture radar (IFSAR) can also provide high resolution measurements of the forest canopy surface (not the underlying terrain), but with a lower accuracy than lidar (Andersen et al. 2003). However, X-band IFSAR is typically acquired from a much higher altitude and at a higher speed than lidar, leading to significantly lower costs per unit area ($10-50/km$^2$ for IFSAR vs. $250/km$^2$ for lidar). Therefore, if accurate terrain data have been previously acquired for a given area (e.g. from lidar) then IFSAR may provide an economical means of monitoring forest structure change at more frequent intervals than would be possible with lidar. However, the accuracy of IFSAR canopy measurements is dependent upon a number of different factors, including flying height, sensing geometry, and interferometric processing. The dominant source of error in X-band IFSAR elevation measurement is “phase noise,” therefore height error is largely a function of the signal-to-noise ratio (SNR) (Mercer 2004). The SNR for IFSAR measurements can be increased by acquiring the data from a lower flying height (increasing signal power) or filtering the interferogram (decreasing noise power) (Mercer 2004; Rodriguez and Martin 1992). Because radar data are acquired at very shallow look angles, the accuracy of IFSAR measurements in forested areas is also significantly affected by sensing geometry and terrain relief (shadowing). In order to assess the influence of these various parameters on the quality of the canopy measurements (height, cover) obtained from IFSAR, we compared canopy height measurements obtained from high density lidar to those obtained from IFSAR data collected at two different flying heights, from three different look directions, and with four different levels of interferogram filtering.

# 2 DATA AND METHODS

## 2.1 Study Area

The study area for this project was a 5 square kilometre area within Wenatchee National Forest, located in the Mission Creek drainage, just west of the city of Wenatchee in Washington State (USA). This is a mixed-conifer forest, composed primarily of mature Douglas-fir (*Pseudotsuga menziesii*), ponderosa pine (*Pinus ponderosa*), and various shrub species. Since the focus of this study was on the accuracy of IFSAR canopy measurements, and not terrain measurements, a GIS polygon layer of vegetation cover type was used to isolate and restrict the analysis to the forested regions within the study area. An orthophotograph of the study area is shown in Figure 1.

*Figure 1: Orthophotograph of Mission Creek study area, Washington State, USA.*

## 2.2 Lidar data

The lidar data used in this study were acquired in the summer of 2004 with an Optech ALTM 3070 system mounted on a fixed-wing aircraft. This system acquires data with a pulse rate of 70 KHz, and provided data at a nominal density of 4 points/$m^2$.

The lidar vendor provided all-return lidar data in UTM, zone 10, NAD 83 coordinates. Ground returns were filtered by the vendor and were gridded into a digital terrain model with 1 meter resolution. Lidar returns from the canopy surface were identified by filtering out the highest return within a 1 m x 1 m grid cell. These filtered, canopy-level returns were then gridded into a 1.25 m canopy surface model. The lidar-derived terrain model for this area is shown in Figure 2.

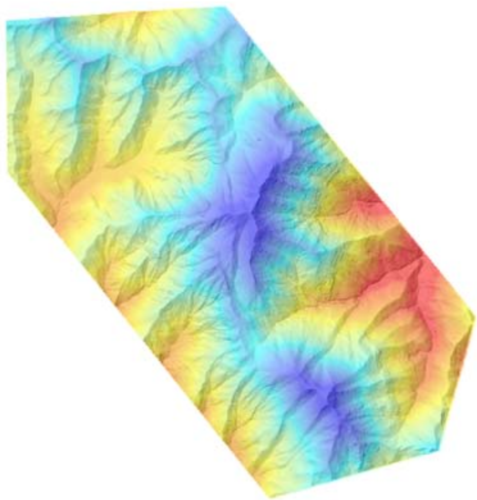

*Figure 2: Lidar-derived terrain model for Mission Creek study area.*

## 2.3 IFSAR data

IFSAR data were acquired in the summer of 2005 with the Intermap Star 3i X-band system, operating from a Lear jet aircraft platform. The wavelength for this system was 3.1 cm, and the flying speed was 720 km/h.

In order to assess the effect of flying height on the accuracy of IFSAR canopy measurements, data were collected from both 15,000 ft (appox. 4500 m) and 20,000 ft. (approx. 6000 m). Additionally, the IFSAR data were processed by the vendor using four different levels of interferogram filtering (or levels of oversampling (OSF)). The highest level of filtering (OSF factor of 8) represents the standard (default) processing parameter for the 5-meter digital surface models, and has a filtering window of slightly greater than 5 meters. An OSF factor of 1 corresponds to no filtering, so the fundamental pixel size is 1.25 meters, and OSF factors of 2 and 4 correspond to intermediate filter widths (Mercer 2005). Three flight lines, from one look direction, were acquired from 6000 meters, and 13 flight lines, from three orthogonal look directions, were acquired from 4500 meters.

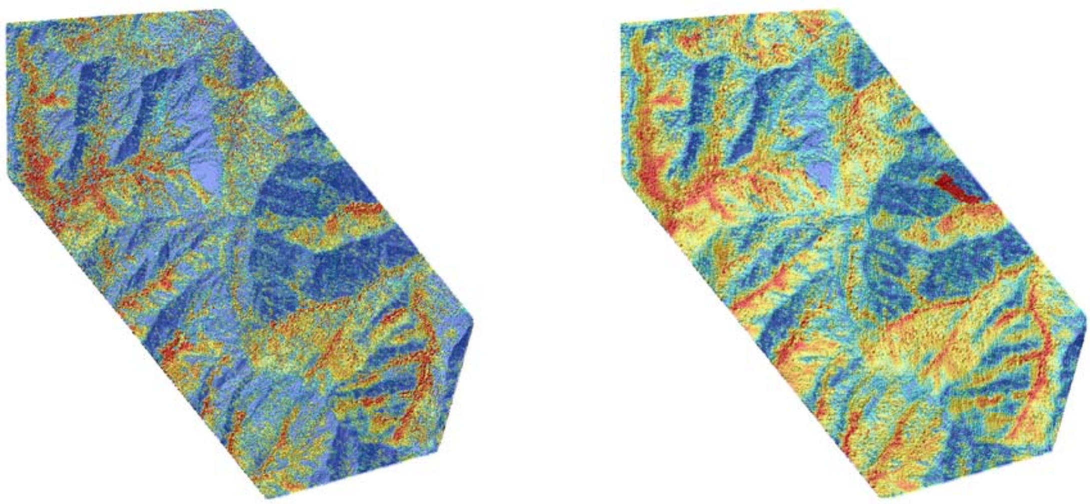

*a) Lidar canopy height model* *b) IFSAR canopy height model*

*Figure 3: Lidar and IFSAR canopy models for Mission Creek study area. Color-coded by height (blue is low; red is high canopy).*

### 2.4 Estimation of canopy height, maximum height, and canopy cover

Lidar- and IFSAR-derived canopy height models were generated by subtracting the lidar digital terrain model from the lidar and IFSAR canopy surface models, respectively (see Figure 3). Estimates of canopy height and maximum height were generated at each 30 × 30-m grid cell over the entire study area. Use of an aggregated canopy height measurement at a 30-m resolution provides GIS-ready coverages and also minimizes the effect of any spatial offset between IFSAR and lidar measurements at the individual tree level. In this study, the 90th percentile surface height within a grid cell area (30 m × 30 m) was used as a surface-based estimate of canopy height, in order to exclude measurements of the ground, understory vegetation, and the sides of overstory trees. The maximum height was simply estimated by the height of the highest surface point within the grid cell. The 90th percentile height therefore represents a generalized (i.e. smoothed) description of canopy height, while the maximum height will capture the direct measurement of emergent canopy features. In this study, only measured elevations were included in the calculation of canopy heights – void (shadow) areas were excluded from the analysis. The difference between the IFSAR- and lidar-derived estimates of canopy height (90th percentile and maximum heights) at each 30 meter grid cell was calculated over only the forested areas of the scene, and is assumed to represent the error in the IFSAR canopy height measurement. The distribution of IFSAR error was then described via several summary statistics (mean, standard deviation, median, and quartile deviation). Quartile deviation was computed as one half of the difference between the 75th percentile height and the 25th percentile height. Canopy cover was estimated as the percentage of surface heights within the 30 meter grid cell exceeding 5 meters.

## 3 RESULTS

### 3.1 Influence of flying height

The summary statistics of the IFSAR error (IFSAR height – LIDAR height) associated with single passes at the 6000 and 4500 meter flying heights are shown in Tables 1. The study area was located close to the center of the swath for both flight lines, and only the elevations obtained via the standard interferometric processing settings (OSF of 8) were used in the comparison.

*Table 1: Differences between IFSAR- and lidar-derived height estimates for 4500 m and 6000 m flying heights.*

| | Canopy Height | | | | Maximum Height | | | |
|---|---|---|---|---|---|---|---|---|
| | Mean | SD | Median | QD | Mean | SD | Median | QD |
| 6000 m AGL | -7.5 | 4.9 | -7.2 | 2.9 | -10.7 | 6.9 | -10.3 | 2.9 |
| 4500 m AGL | -7.0 | 4.9 | -6.7 | 2.8 | -10.2 | 6.3 | -9.9 | 3.6 |

### 3.2 Influence of filtering parameters

The summary statistics for IFSAR elevations generated using the four different levels of interferogram filtering for a single flight line are shown in Table 2. Only the elevations obtained from the lower flying height (4500 m) were used in this comparison.

*Table 2: Differences between IFSAR- and lidar-derived height estimates using different levels of interferogram filtering.*

| | Canopy Height | | | | Maximum Height | | | |
|---|---|---|---|---|---|---|---|---|
| | Mean | SD | Median | QD | Mean | SD | Median | QD |
| OSF 1 | -6.5 | 4.4 | -6.1 | 2.2 | -1.6 | 9.6 | -2.5 | 4.4 |
| OSF 2 | -6.5 | 4.5 | -6.0 | 2.3 | -2.7 | 9.5 | -3.3 | 4.3 |
| OSF 4 | -6.5 | 4.6 | -6.1 | 2.5 | -4.1 | 8.6 | -4.6 | 4.3 |
| OSF 8 | -7.0 | 4.9 | -6.7 | 2.8 | -10.2 | 6.3 | -9.9 | 3.6 |

### 3.3 Influence of sensing geometry

Previous studies have indicated that using a combination of IFSAR elevations obtained from different look directions can improve canopy height models (Andersen et al. 2003). In order to reduce the underestimation of canopy height due to shadowing effects, the IFSAR elevations obtained from overlapping flight lines were merged by extracting the maximum elevation within each grid cell. The error associated with the merged surfaces obtained from overlapping flight lines with the same look directions, opposite look directions, orthogonal look directions, and all look directions are compared in Table 3.

*Table 3: Differences between IFSAR- and lidar-derived height estimates. IFSAR collected at a multiple passes at 4500 m flying height (two side looks from same direction, two orthogonal looks, opposite look directions, and combination of all looks). Oversampling factor of 8.*

| | Canopy Height | | | | Maximum Height | | | |
|---|---|---|---|---|---|---|---|---|
| | Mean | SD | Median | QD | Mean | SD | Median | QD |
| Side looks | -3.2 | 4.9 | -3.2 | 2.9 | -5.4 | 7.5 | -5.8 | 3.6 |
| Opposite looks | -2.2 | 3.5 | -2.5 | 2.0 | -4.4 | 5.5 | -5.0 | 2.6 |
| Orthogonal looks | -1.6 | 4.1 | -1.6 | 2.1 | -3.4 | 7.1 | -4.2 | 2.8 |
| All looks | -0.6 | 3.9 | -0.8 | 2.0 | -2.1 | 7.1 | -3.2 | 2.9 |

### 3.4 Estimation of canopy cover

A scatterplot showing the correspondence between lidar- and IFSAR-derived estimates of fractional canopy cover for the merged surface generated from all four look directions (flying height of 4500 m; standard filtering level of 8) is shown in Figure 4.

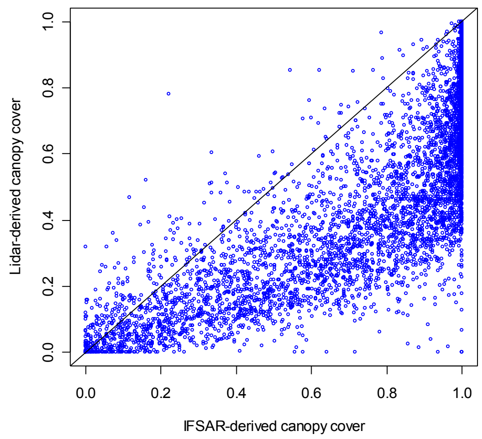


*Figure 4: Scatterplot showing relationship between Lidar- and IFSAR-derived fractional canopy cover estimates at 30 m grid cells. Line indicates 1:1 relationship.*

## 4 DISCUSSION

The results shown in Table 1 indicate that the difference in flying heights studied here has little effect on the accuracy of canopy height measurements. For both of the single flight lines used in this comparison of flying heights, the median error for 90th percentile canopy height measurements was approximately -7 meters, with a QD of approximately 3 meters. The maximum height measurements were also not significantly different at the two different flying heights. This indicates that there would be a minimal gain by acquiring IFSAR at 4500 meters vs. 6000 meters for forestry purposes.

Varying the filtering parameters does not appear to have a significant effect on the accuracy of 90th percentile canopy height measurements. The median error is approximately -6 meters, with a QD of approximately 2.5 meters at all filtering levels. The level of filtering does have a significant effect on the measurement of maximum height, with higher levels of filtering leading to greater underestimation of maximum canopy height. The magnitude of the median error ranges from -2.5 meters (QD of 4.4 m) for the filtering level of 1 (no filtering) to -9.9 meters (QD of 3.6 m) for the highest filtering level.

As expected, using a combination of several overlapping looks can significantly improve the accuracy of canopy measurements. Due to the shallow look angles characteristic of IFSAR sensing, measurements of forest canopy surface acquired from a single flight line will have many void (shadow) areas which are occluded by the topography and localized canopy relief. Acquiring data from several different directions can help to fill in void areas and improve overall characterization of forest canopy surface structure. The results of this study indicate that using a combination of two different looks will generally provide a significant increase in accuracy over a single look, as the errors of the merged surfaces for all combinations of looks (median errors of -1 to -3 meters, from Table 3) are lower than that for that for a single look (median error of -7 meters, from Table 1). Not surprisingly, the highest quality surface is the result of merging the data from all four looks, with a median error of -0.8 meters and a QD of 2.0 meters. The results indicate that acquiring IFSAR data from multiple look directions is critically important in forestry applications, especially in mountainous areas.

Estimating canopy cover using only IFSAR elevation data is a difficult proposition. In general, the sensing geometry of IFSAR does not allow for accurate measurement of high frequency details in the morphology of the canopy surface, including canopy gaps and smaller individual tree crowns. In the IFSAR canopy height model, individual tree crowns tend to be smoothed, and canopy gaps are “filled in.” Therefore, in forested areas with relatively low canopy density or many small canopy gaps, a canopy cover estimate derived from the IFSAR canopy height model will tend to overestimate the lidar-based canopy cover estimate, as Figure 4 indicates.

## 5 CONCLUSION

This study confirms that X-band IFSAR can be an economical source of data in the measurement and monitoring of canopy height over large areas. The results presented here do not indicate a significant improvement in the accuracy of canopy height measurements by acquiring the data at a lower flying height, and suggest that the typical mission parameters used for high accuracy (Type II) IFSAR topographic survey may be also be adequate for forest monitoring applications (Mercer 2004). The results also indicate that the accuracy of general canopy height measurements is not greatly influenced by the level of interferogram filtering, but can be highly influenced by sensing geometry. These findings support the conclusion that acquiring data from multiple look directions may be the most important consideration in the planning of IFSAR flights for forest monitoring applications.

## ACKNOWLEDGEMENTS

The authors would like to thank the University of Washington Precision Forestry Cooperative, the Joint Fire Science Program, the USDA Forest Service Pacific Northwest Research Station, and the Wenatchee National Forest for supporting this research.

## REFERENCES

Andersen, H.-E., S.E. Reutebuch, and G.F. Schreuder (2001). Automated individual tree measurement through morphological analysis of a LIDAR-based canopy surface model. In Proceedings of the 1st International Precision Forestry Symposium. University of Washington College of Forest Resources, Seattle, WA. pp. 11-22.

Andersen, H.-E., R.J. McGaughey, W. Carson, S.E. Reutebuch, B. Mercer, and J. Allan (2003). A comparison of forest canopy models derived from lidar and InSAR data in a Pacific Northwest conifer forest. In Proceedings of the ISPRS WG III/3 Workshop on 3-D Reconstruction from airborne laserscanner and InSAR data, Dresden, Germany.

Finney, M.A.(1998). FARSITE: Fire Area Simulator-model development and evaluation. Research Paper RMRS-RP-4. USDA Forest Service, Rocky Mountain Research Station, Ogden, UT.

Mercer, B. (2004). DEMs created from airborne IFSAR – an update. In International Archives of the Photogrammetry, Remote Sensing and Spatial Information Sciences, Istanbul, Turkey, Vol. XXXV, Part B. CD-ROM.

Mercer, B. (2005). Personal communication.

Paine, D. and J. Kiser (2003). Aerial photography and image interpretation. Wiley, Hoboken.

Reutebuch, S.E., R.J. McGaughey, and H.-E. Andersen, and W.W. Carson (2003). Accuracy of a high-resolution lidar terrain model under a conifer forest canopy. Canadian Journal of Remote Sensing 29(5):527-535.

Rodriguez, E., and J.M Martin (1992). Theory and design of interferometric synthetic aperture radars. IEE Proceedings-F, Vol. 139, No. 2, pp. 147-159.

# RETRIEVAL OF FOREST PARAMETERS FROM MULTI-POLARIMETRIC, MULTI-FREQUENCY INTERFEROMETRIC SAR DATA

*Karlheinz Gutjahr*[1] *and Mathias Schardt*[1,2]

[1] Joanneum Research, Institute of Digital Image Processing, Graz, Austria; karlheinz.gutjahr@joanneum.at

[2] University of Technology, Institute of Remote Sensing and Photogrammetry, Graz, Austria; mathias.schardt@tugraz.at

## ABSTRACT

Different methods for the retrieval of relevant forest parameters, especially canopy heights, from fully polarimetric and interferometric SAR data at different frequency bands are presented. The obtained results are compared to each other and to simultaneously acquired laser scanner data.

**Keywords:** SAR, interferometry, polarimetry, canopy height

## 1 INTRODUCTION

Experimental and theoretical investigations have shown that SAR backscattering from land surfaces is sensitive to vegetation features. The SAR signal is indeed strongly influenced by the dielectric characteristics of vegetation material and moisture content. In addition geometrical features of plant constituents affects scattering in a different fashion according to frequency and polarization, so that a properly designed sensor can give significant information on the whole canopy cover.

The sensitivity of the interferometric phase and coherence to spatial variability of vegetation height and density make the estimation of vegetation parameters from interferometric measurements at low frequencies a challenge. On the other hand, scattering polarimetry is sensitive to the shape, orientation and dielectric properties of the scatterers. This allows the identification and separation of scattering mechanisms of natural media employing differences in the polarisation signature for purposes of classification and parameters estimation. Thus the combination of the qualitative information provided from the two approaches is very promising concerning the extraction of forest structure parameters.

The inversion of a recent established scattering model which relates the physical forest parameters to the interferometric observations at different polarisations allows estimating forest height, average forest extinction and underlying topography.

The potential and challenges of this new technique in comparison to conventional interferometry and SAR signal analysis is demonstrated using a fully polarimetric, interferometric and multi-frequency (X-, L- and P-bands) dataset. For an alpine test site the data was acquired by the airborne SAR system E-SAR which is developed by DLR. In addition the SAR related results are compared to results of a simultaneous laser scanner acquisition.

## 2 TEST SITE AND DATA

The area of "Kobernausser Wald" in the Austrian province of Upper Austria was selected as the test site for the forest investigation. The terrain of the area is not highly rugged and the topography is relatively low, averaging about 700 m a.s.l.. This guarantees successful data acquisition by reducing layover, foreshortening and shadow effects.

Due to the high cost of the E-SAR data and the limited budget available for the project, the number of acquired E-SAR products was restricted to the wavelength of X-, L- and P-band. Moreover the actual area to be covered was limited to 3 km x 9 km (red box in Figure 1). The E-SAR flight campaign took place on the 11th May 2004. Details about the acquired E-SAR products are listed in Table 1. RGB composites of the E-SAR intensity products are shown in Figure 2.

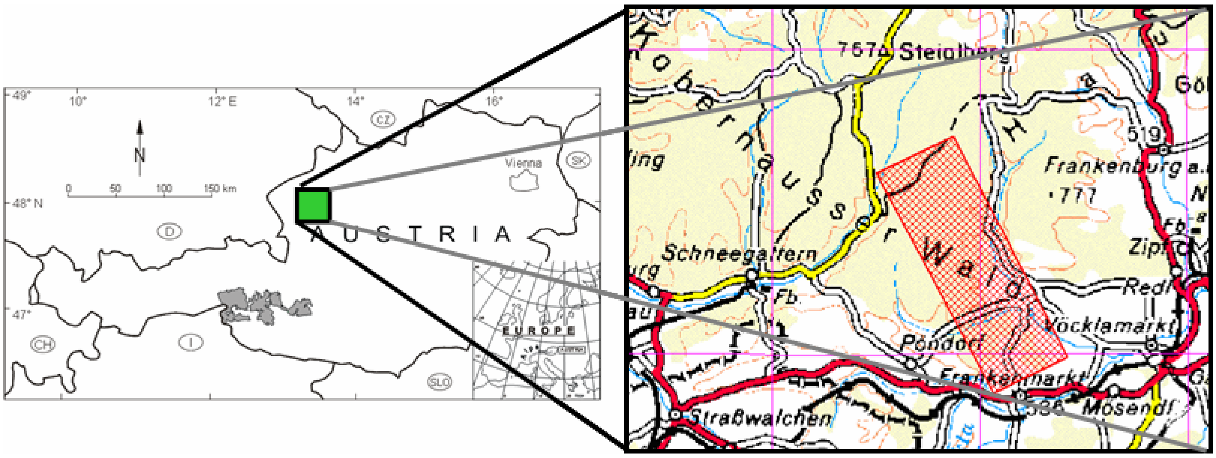


*Figure 1: Location of the test site "Kobernausser Wald" in the province of Upper Austria. The test area is marked with the red box in the topographic map (left).*

*Table 1: Details about the acquired and processed E-SAR data of the test site "Kobernausser Wald".*

| Frequency | Polarisation | Baseline |
|---|---|---|
| X-band | HH and VV | Approx. 1 m |
| L-band | HH / HV / VV / VH | Approx. 10 m |
| P-band | HH / HV / VV / VH | Approx. 20 m |

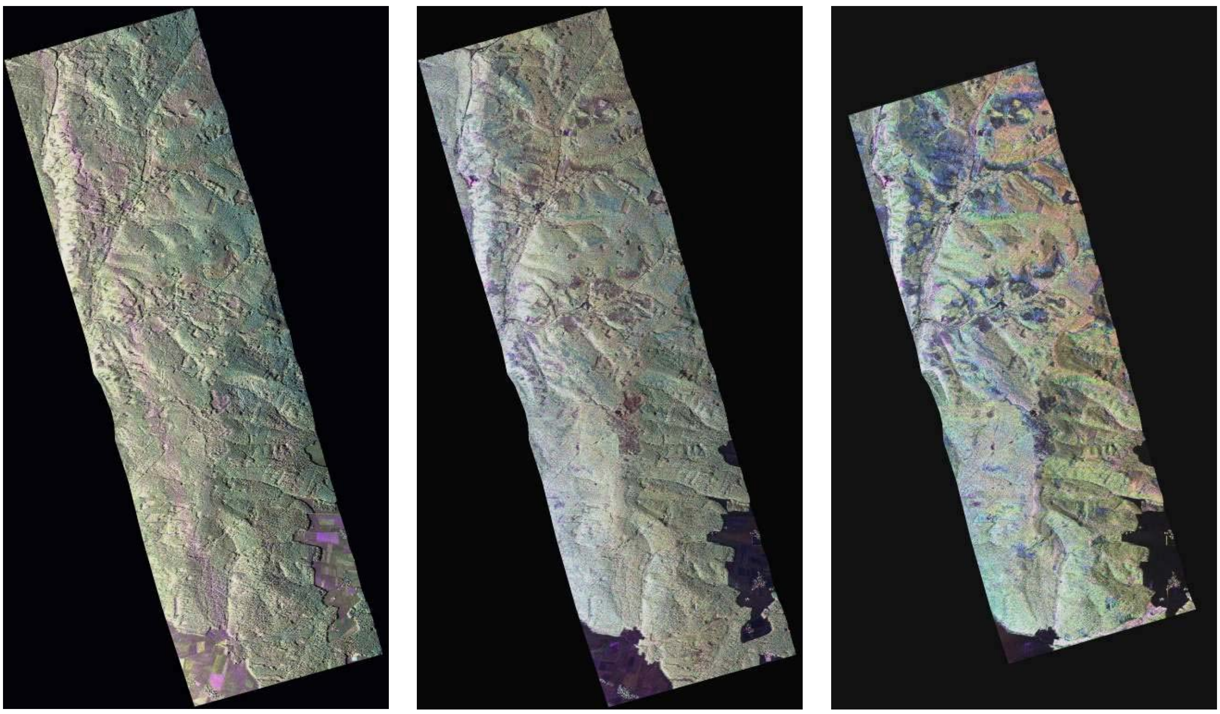

X-band HH, VV, HH/VV L-band HH, HV, VV P-band HH, HV, VV

*Figure 2: RGB composites of the acquired E-SAR data of the test site "Kobernausser Wald".*

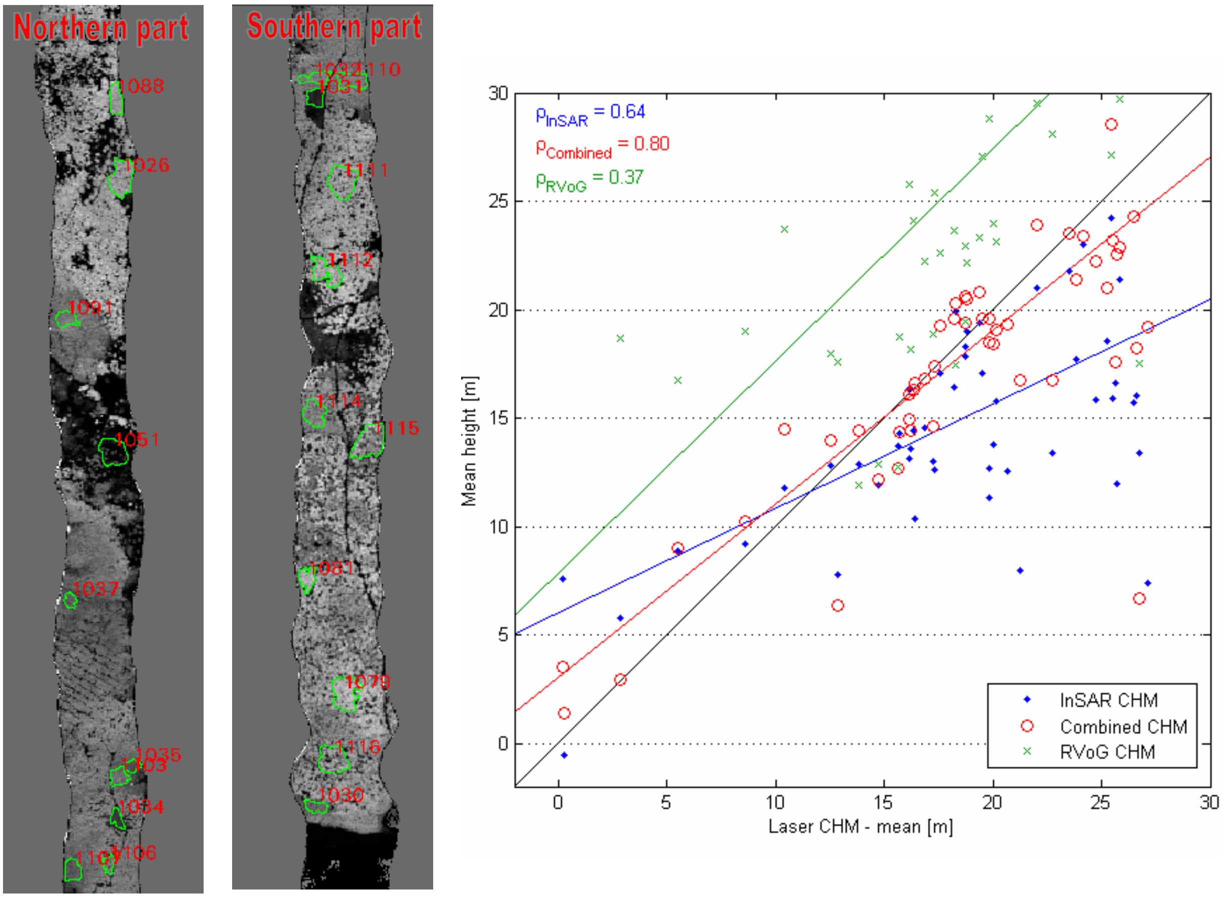


*Figure 3: Reference laser scanner canopy height model (CHM)(left) and regression of statistical values of manually defined segments (right).*

As reference canopy height data, laser scanner data consisting of surface height model (first returns) and a digital terrain model (last returns) were acquired on 28th August 2004 by the LIDAR system of the company TopoSys. The area covered by the LIDAR sensor was a strip of ~200 m wide along the 9 km of the test site. The horizontal resolution of the LIDAR is about 50 cm and the height accuracy is 15 cm. The laser scanner canopy height model (CHM) is shown in Figure 3.

## 3 METHODS

Basically the information content of the available E-SAR data could be analysed by three different approaches:

1. Polarimetry: Only the intensity of the backscattered SAR signal at different polarizations and wavelengths is analysed.
2. Interferometry: Only the phase of the interferometric SAR signals at different wavelengths is analysed.
3. Polarimetric SAR Interferometry: The complex coherence of the interferometric SAR signals at different polarizations is analysed.

A short introduction to the different methods is given in the next sub-sections. To compare the results of the different approaches we concentrate on the derivation of canopy height models (CHM).

### 3.1 Polarimetry

Experimental and theoretical investigations have shown that SAR backscattering from land surfaces is sensitive to vegetation features. The SAR signal is indeed strongly influenced by the dielectric characteristics of vegetation material and moisture content. In addition geometrical features of plant constituents affects scattering in a different fashion according to frequency and polarization, so that a properly designed sensor can give significant information on the whole canopy cover.

In order to exclude radar and site specific influences while analyzing the relation of polarized features and forest parameters, a sensitivity analysis should be carried out investigating the influence of local incidence angle, range position and tree species on radar backscatter.

### 3.2 Interferometry

SAR interferometry (InSAR) is a well established technique to derive digital height models from interferometric SAR data. According to Gabriel and Goldstein (1988) the interferometric phase $\varphi$ is related to range difference between the two sensor positions $\Delta r$ :

$$\varphi = \frac{2k\pi}{\lambda} \Delta r \tag{1}$$

where $\lambda$ is the wavelength of the SAR system and $k = 1, 2$ depending on single or dual pass acquisition. More details about this technique can be found in e.g. Gutjahr (2002).

To avoid the crucial phase unwrapping step we applied a modified differential InSAR approach. The simulation of the topographic phase term was based on the method of Eineder (2003) and an available coarse reference digital terrain model (DTM).

At X-band the height model is supposed to represent more or less the top of the vegetation layer. Thus the interferometric result can be assigned as digital surface model (DSM). In case of longer wavelengths (L- or P-band) the SAR signal is assumed to penetrate the vegetation layer and height model is close to a DTM. Thus the difference between an X-band DSM and P-band DTM leads to an interferometric canopy height model (InSAR CHM). In absence of a DTM of longer wavelengths a reference DTM can be subtracted. Here we call this difference “combined CHM”.

### 3.3 Polarimetric SAR interferometry

One of the most promising scattering models for polarimetric and interferometric SAR (Pol-InSAR) data is the Random Volume over Ground (RVoG) model introduced by Papathanassiou and Cloude (2001). The complex interferometric coherence $\tilde{\gamma}(\vec{w})$ may be written as:

$$\tilde{\gamma}(\vec{w}) = \tilde{\gamma}\left[h_V, \exp(\Im\varphi), \sigma, m(\vec{w})\right] \tag{2}$$

where $\tilde{\gamma}$ depends on the extinction coefficient $\sigma$ for the random volume, and it's thickness $h_V$ . $\varphi_0$ is the phase related to the ground topography and $m(\vec{w})$ the effective ground-to-volume amplitude ratio accounting for the attenuation through the volume.

The inversion of the Random Volume over Ground Scattering model as described in (2) involves taking the observations of the complex coherence at a number of different polarisations and/or polarimetric bases and then minimising the discrepancies between the model predictions and observations in a least squares sense.

In Papathanassiou and Cloude (2001) this has been implemented as a multidimensional optimization problem which could be solved by e.g. the function minimization algorithm proposed by Nelder and Mead (1965). Due to the highly non-linear nature of the optimization problem, the obtained solution depends strongly on the choice of the starting values. Thus Cloude and Papathanassiou (2003) showed how to break down the inversion process into three separate stages:

1. Least squares line fit,
2. Vegetation bias removal, and
3. Height and extinction estimation.

The vegetation height of the RVoG model is assumed to overestimate the canopy height in comparison to a mean value of the respective area.

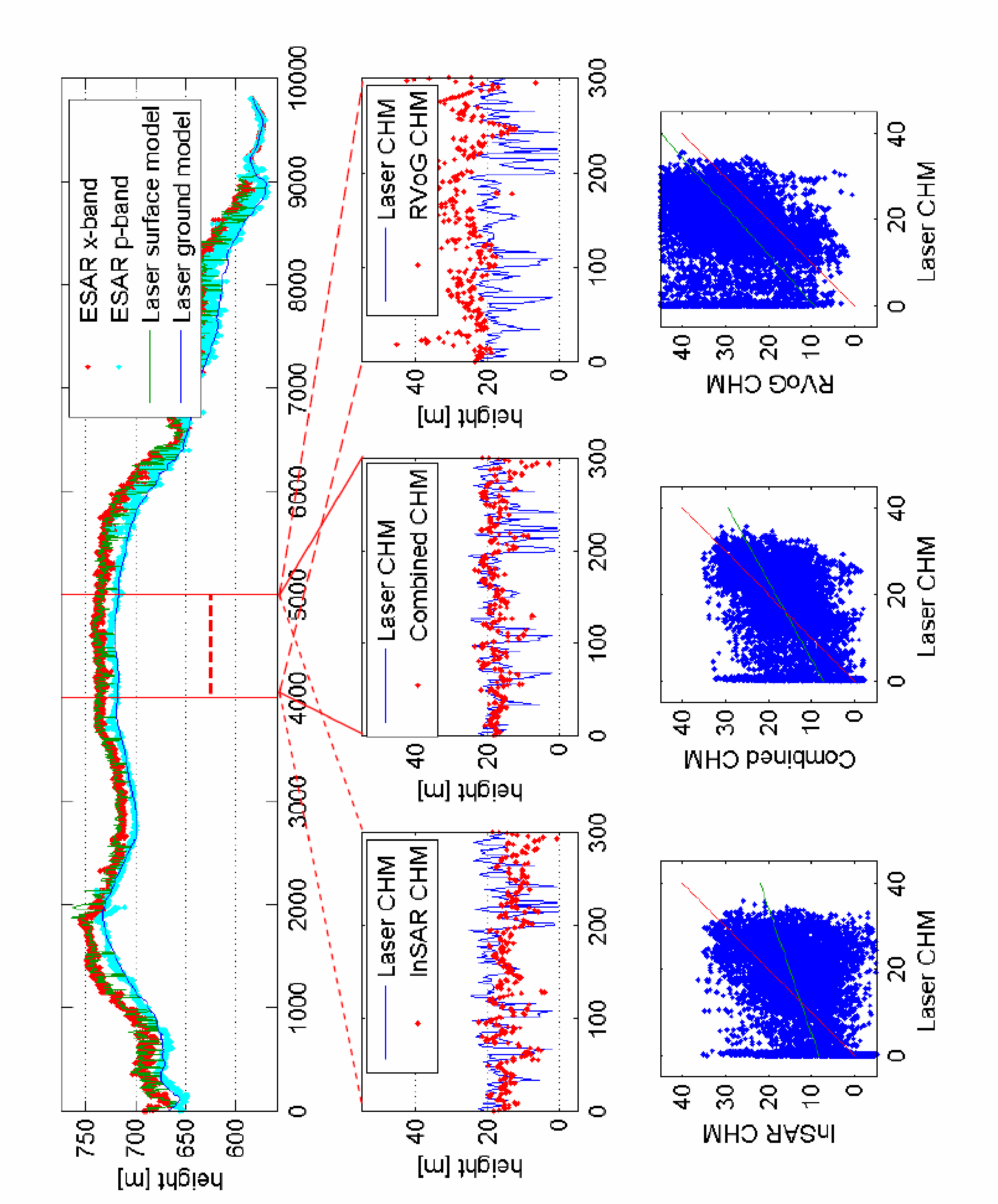


*Figure 4: Comparison of InSAR CHM, combined CHM and Pol-InSAR CHM with laser scanner reference data along a profile going from North to South in the mid of the laser scanner strip.*

# 4 RESULTS

Due to the fact that the field survey of forest parameters is very time consuming and topical forest inventory data was not available, about 110 segments of homogeneous forest stands were manually identified in the laser scanner CHM (green plots on the left side of Figure 3). For each of these segments forest parameters like canopy closure and statistical values like mean value or standard deviation of the laser scanner CHM could be derived automatically.

On the other hand the same statistical values of the InSAR CHM, combined CHM and Pol-InSAR CHM in the same segments were computed. The comparison of the mean values of the InSAR CHM, the combined CHM and the Pol-InSAR CHM with respect to the laser scanner CHM mean is shown on the right side of Figure 3. Each dot represents one identified segment whereas the solid lines are robust estimates of the actual regression.

Additionally the height values of a profile from North to South in the mid of the laser scanner strip were used for evaluation. The upper graph of Figure 4 plots all the DTM and DSM height values along this profile. In order to analyse the profile in more detail a zoom-in of the whole profile as indicated by the red lines is enlarged below. The InSAR CHM (left), the combined CHM (mid) and the Pol-InSAR CHM (right) are drawn with respect to the laser scanner CHM. The graphs below show the scattergramm and the regression of the height values again with respect to the laser scanner height. The red line indicates the 1:1 regression whereas the green line is a robust estimate of the actual regression.

# 5 DISCUSSION AND CONCLUSIONS

Because of the economical value of this forest, regular comprehensive forest inventory data are collected. The last ground truth campaign was conducted during the year 2003. However, due to some reasons the collected data was not available to this study. Thus a sound statement is not possible for the polarimetric analysis of the E-SAR data of the test site ”Kobernausser Wald”.

On the contrary the interferometric derived surface model at X-band gives a promising approximation to the “real” surface. The difference between X-band surface model and P-band terrain model shows a small bias of about 1.5 m to the laser scanner CHM. This is mainly due to a shifted P-band DTM (median approximately 2 m). Thus a reference DTM can release this problem as was shown by combining X-band DSM and laser scanner DTM.

By analysing larger image samples or forest stands the Pol-InSAR CHM systematically overestimates the mean canopy height in comparison to the laser scanner CHM showing a large standard deviation. A pixel wise comparison of height values turned out to be very difficult.

## ACKNOWLEDGEMENTS

The research was part of the Austrian Space Applications Programme contract No. ASAP-CO-006/03 “Management of Natural Resources in Alpine Regions by Advanced Remote sensing Techniques”. Vicarious for the people at the Microwaves and Radar Institute of German Aerospace Centre (DLR) the authors would like to thank Mr. K.P. Papathanassiou for his many advices.

## REFERENCES

Cloude S.R. and K.P. Papathanassiou (2003). A 3-Stage Inversion Process for Polarimetric SAR Interferometry. IEE Proceedings Radar Sonar and Navigation, Vol. 150, No. 3, June 2003, pp. 125-134.

Eineder M. (2003). Efficient Simulation of SAR Interferograms of Large Areas and of Rugged Terrain, IEEE Transactions on Geoscience and Remote Sensing, Vol. 41, No. 6, June 2001, pp. 1415-1427.

Gabriel A. and R. Goldstein (1988). Crossed Orbits Interferometry: Theory and Experimental Results from SIR-B, Int. Journal of Remote Sensing, Vol. 9, pp. 857 – 872.

Gutjahr KH. (2002). INSAR Blockausgleich, Ph. D. Thesis, Techn. Univ. Graz, Graz, Austria.

Papathanassiou K.P. and S.R. Cloude (2001). Single-baseline polarimetric SAR interferometry, IEEE Transactions on Geoscience and Remote Sensing, Vol. 39, No. 6, November 2001, pp. 2352-2363.

# COMPARISON OF LIDAR AND INSAR DATA TO ESTIMATE TREE HEIGHT IN FOREST INVENTORIES

*Johannes Breidenbach[1], Barbara Koch[2], Gerald Kändler[1], Alfred Kleusberg[3]*

[1] Forest Research Institute (FVA) Baden-Württemberg, Department of Biometry and Information Sciences, Freiburg, Germany; Johannes.Breidenbach@forst.bwl.de

[2] University of Freiburg, Department of Remote Sensing and Landscape Information Systems (FELIS), Freiburg, Germany; ferninfo@felis.uni-freiburg.de

[3] University of Stuttgart, Institute for Navigation (INS), Stuttgart, Germany; ins@nav.uni-stuttgart.de

## ABSTRACT

The study presented in this paper compares the use of X-Band InSAR data and lidar data for estimating the mean tree height within inventory plots. The average tree height at a given inventory point can be estimated with an RMSE of 2.69 m or 9.5% using radar data; or 1.85 m or 6.6% using lidar data. The most effective estimator for both radar and lidar is the third quartile of the vegetation height at the plot. This variable, however, systematically underestimates the average tree height. Estimation results can be improved considerably by incorporating slope into the model. A reduction in the underestimation of the average tree height using the third quartile of the vegetation height is observed with increasing slope. Additionally, an interdependency between slope and aspect was recognised for radar data. It was also noted that the usual reduction in tree height underestimation with increasing slope is not observed in radar data for western aspects (i.e. for slopes directly facing the radar sensor). Tree height estimations derived from lidar data are observed to be influenced by the proportion of conifer trees within the plot. A higher proportion of conifer trees within a plot results in a higher underestimation of the average tree height using the third quartile of vegetation height.

**Keywords:** Tree Height, Forest Inventory, InSAR, Lidar, Laserscanning

## 1 INTRODUCTION

Tree height is an important forest characteristic that can be used to estimate further parameters relevant to forestry. Moreover, tree height is a parameter that can be measured directly by height measuring systems such as SAR and laserscanner systems. As a result, the measurement of tree height has often been the focus of scientific research. Previous research undertaken into estimating tree height using laserscanner data has either involved single tree measurements (Hyyppä et al. 2001, Persson et al. 2002, Leckie et al. 2003, Breidenbach 2003, Gaveau and Hill 2003, among others) or the use of quartile estimators to derive the vegetation height within a plot (Naesset 1997, Magnussen and Boudewyn 1998, Means et al. 2000, Wulder et al. 2001, Naesset and Okland 2002, Naesset 2004, among others).

Tree height can be estimated using two different SAR systems: SAR sensors that operate across several frequency bands in order to simultaneously measure the terrain height (P-Band) and the surface height (L or X-Band) (Andersen et al. 2004, Moreira et al. 2001, among others); and full polarimetric SAR instruments that enable polarimetric SAR interferometry (Cloude and Corr 2003, Woodhouse et al. 2003, among others). Surface models are calculated from radar data using interferometric methods involving the use of two scene images with slightly different positions. These images should be acquired simultaneously for forestry purposes, as decorrelation in phase due to the interaction of tree crowns with wind, for example, compromises the accuracy of the resulting surface model. Studies comparing InSAR and lidar data can be found in Mercer 2001, Andersen et al. 2003 or Wallington and Suárez 2005, among others.

The study presented in this paper has been undertaken within the “MatchWood” research project, which aims to practically optimise processes in the forest-timber supply chain. The subproject “Precise Forest Stand Surveying” involves the regionalisation of sample-based forest inventories, and aims to develop methods for extrapolating terrestrial information obtained from point-like sample plots onto complete forest areas with the assistance of remote sensing data acquired under Western European conditions. Such methods are currently operational in Scandinavia (Naesset 2004). The project should lead to the development of forest management practices that are more goal-orientated and easier to plan. The ability to accurately estimate tree height across a large area is therefore of great importance.

The current need to increase work efficiency makes the use of data for multiple purposes essential in today’s workplace. As a result, this investigation should also determine how accurate tree height can be estimated using SAR data and laserscanner data that was originally commissioned for non-forestry purposes. Furthermore, the applicability of currently available inventory sample data (over 30,000 sample inventory points have been surveyed in the last ten years in the state of Baden-Württemberg alone) as validation material for scientific studies involving remote sensing is also evaluated.

# 2 METHODS

## 2.1 Materials

### 2.1.1 Study Area

The 16 km² study area (upper left corner coordinate: 9.50° East / 48.79° North) is located approximately 25 km east of Stuttgart (see Figure 1). The test area is traversed by several valleys and lies between 300 m and 500 m above sea level. The average gradient across the site is approximately 12°, however, some extreme slopes of up to 35° are also found. The most common tree species within the test area include beech (Fagus sylvatica, 42 %), Norway spruce (Picea abies, 20 %) and oak (Quercus robur and Q. petrea, 10 %). A total of 30 different tree species are found within the test site. The average forest stand is approximately 1.2 ha in size. Tree heights within the study area range from between 10 m and 44 m, with an average height of 33 m.

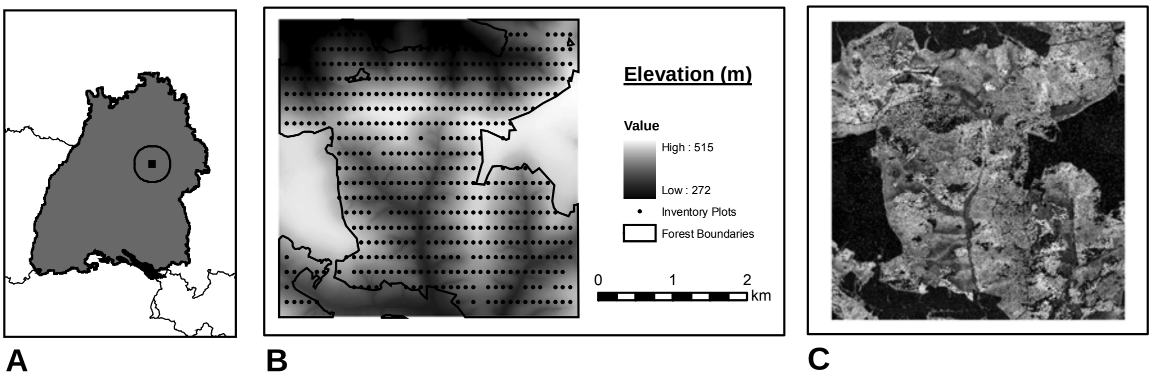


*Figure 1: A) Location of study area; B) Terrain model with forest layer and inventory points; C) Vegetation height model*

### 2.1.2 Remote Sensing Data

Lidar were acquired in spring 2002 using the Optec ALTM 1225 airborne laser scanner from a flight height of approximately 900 m above the test site. The average interval between laser points is 1.5 m. First and last pulse data have been automatically classified into ground and vegetation hits by the Baden-Württemberg State Surveying Office during geometric transformation from UTM to the Gauß-Krüger coordinate system (Schleyer 2001).

The radar data used in this study was acquired by Intermap Technologies in July 1998 using the Star3i X-band radar unit with HH polarisation from a flight height of approximately 6,500 m and an east-southeast (110°) look direction. The resulting radar DSM was produced with a pixel size of 5 m. According to the producers, the DSM has a maximum RMSE of 1 m in the vertical plane. It should be noted that the accuracy of a radar DSM is reduced by increasing slope within the area of acquisition (Intermap 2004).

#### 2.1.3 Ground truth data

A regular forest enterprise inventory was conducted in the second half of 2001 across more than 1,100 ha of state and community forest within the study area, using plots positioned on a standard 100 x 200 m grid. The positional accuracy of the inventory points is estimated to be better than 10 m. Forest characteristics were recorded within concentric circle plots with radii of 3 m, 6 m and 12 m. Trees with a DBH greater than 10 cm, 15 cm and 30 cm, respectively, were recorded within the three circle plots. The heights of four to five trees were measured in each plot using a Vertex ® angle measurement instrument. The heights of the remaining trees within a plot were estimated using forest stand height curves and the trees' DBH (Kon-Allan 2004).

A total of 250 inventory plots, covering a area of 11.4 ha, were used as terrestrial reference data for the remotely sensed data.

### 2.2 Methods

#### 2.2.1 Data Preparation

DTMs with a resolution of 1 m and 5 m were generated from the lidar last pulse ground data using the TreesVis programme (Weinacker et al. 2004).

The height of vegetation within the test area was determined from the laserscanner data by calculating the difference between the first pulse data (raw data) and the 1 m lidar DTM data. The corresponding vegetation height for radar data was calculated by subtracting the radar DSM from the 5 m lidar DTM.

Several points were observed in the first pulse laser scanner data with heights of between 50 m and 100 m above the ground. As the maximum tree height recorded during the inventory was 44 m, laser points higher than 50 m were assumed to be errors and were subsequently deleted.

#### 2.2.2 Calculation of Independent Variables

Quadratic subsets measuring 30 x 30 m were created from the remote sensing data and extracted to the inventory points. Vegetation height quartiles were calculated for each subset (minimum, first quartile, mean, median, third quartile, maximum).

The average slope and the dominant aspect at each inventory point were calculated using a terrain model with a resolution of 1 m. Areas with a height of less than 3 m were classified as crown gaps using a canopy model based on a normalised DSM (DSM minus DTM). The degree of canopy closure can be calculated from the remaining proportion of a plot.

The proportion of conifer trees within a plot was also calculated using the inventory data.

#### 2.2.3 Modelling

Independent variables were incorporated as additive components of linear regression models. The influence of these variables on the model was examined using a t-test; with only those variables exceeding the level of significant by 5% being incorporated. Further criteria for selecting independent variables included plausible model behaviour and improvements in RSME, as well as the coefficient of determination.

# 3 RESULTS

## 3.1 Tree Height Estimation with SAR

As opposed to models containing other quartiles (for example the mean or max), the model containing the third quartile of the vegetation height as an independent variable explains the majority of variance. The relationship between radar height and average tree height proceeds linearly until a tree height of 25 m. The terrestrially-measured average tree height is clearly underestimated at this point. This underestimation reduces after a height of 25 m and the curve flattens. This relationship can be modelled using a second order polynom as displayed in Figure 2 left.

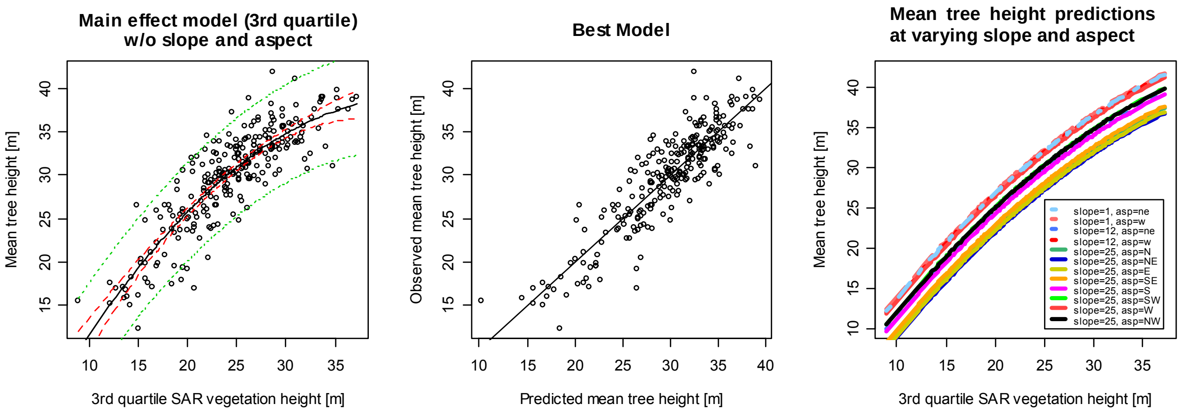


*Figure 2: Models for estimating the average tree height in plots using SAR data. Left-hand diagram: average tree height derived from the most influential independent variable. Middle: Observed vs. predicted mean tree height. Right-hand diagram: the influence of slope and aspect on the estimation of average tree height.*

The model containing the third quartile of the vegetation height as the only independent variable permits the estimation of the average tree height with an RMSE of 2.8 m. No indication of heteroscedasticity can be found in the distribution of residuals. As a result, it was not necessary to apply a transformation to the data. The residual plots for slope and aspect indicate that the error is not evenly distributed. A bias is to be expected on aspects southwest, west and northwest especially with higher slopes (see Figure 3, upper row). The inclusion of the independent variables slope and aspect in the model results in an even distribution of the residuals (see Figure 3, lower row). The aspect variable is incorporated with a dependency on slope, as the influence of aspect increases with increasing slope. The RMSE is reduced, albeit minimally, to 2.7 m; which corresponds to a relative error of approximately 9.5%.

The right-hand diagram in Figure 2 clearly displays the influence of aspect in relation to slope. Western and northeastern aspects exhibit the greatest difference. Southern, southwestern and northwestern aspects take an intermediate position; while northern, eastern and southeastern tend to be similar to northeastern aspects. The difference becomes greater as the slope increases. Sites with a western aspect, however, are the only areas that remain uninfluenced by increasing slope. On other sites, the estimation of average tree height is underestimated to a lesser extent (the curves are lower than for western aspects) with increasing slope. Sites with a slope of 25° and a northeastern aspect produce an almost bisecting line in the lineal area of the curve, which indicates that the average tree height is barely underestimated. The corresponding underestimation for western aspects, however, is 4.6 m.

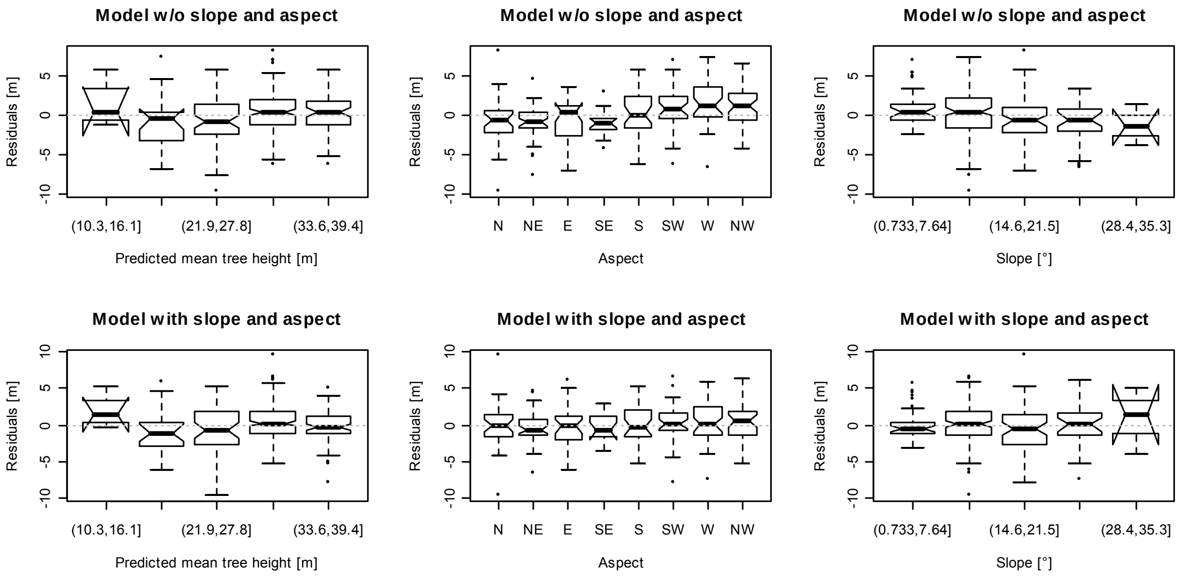


*Figure 3: Residual plots of the model for estimating average tree height derived from the third quartile of vegetation height obtained from radar data without (upper row) and with (lower row) slope and aspect as independent variables.*

## 3.2 Tree Height Estimation with Lidar

As opposed to the other quartiles, the third quartile of the vegetation height of the first pulse vegetation hits displays the highest correlation with the average tree height. An RMSE of 1.9 m indicates that the model incorporating the third quartile as the only explanatory variable explains the majority of variance (see the left-hand diagram in Figure 4). The proportion of conifer trees within a plot, as well as the slope, have an influence on average tree height estimations. Accuracy can be improved significantly by including these variables in the model. The RMSE is 1.8 m or 6.6%. The slope has a stronger influence on tree height estimations than the proportion of conifer trees within a plot. While an increasing proportion of conifer trees leads to an increasing underestimation of average tree height using the third quartile model, tree height underestimation reduces greatly with increasing slope (see middle and right-hand diagrams in Figure 4).

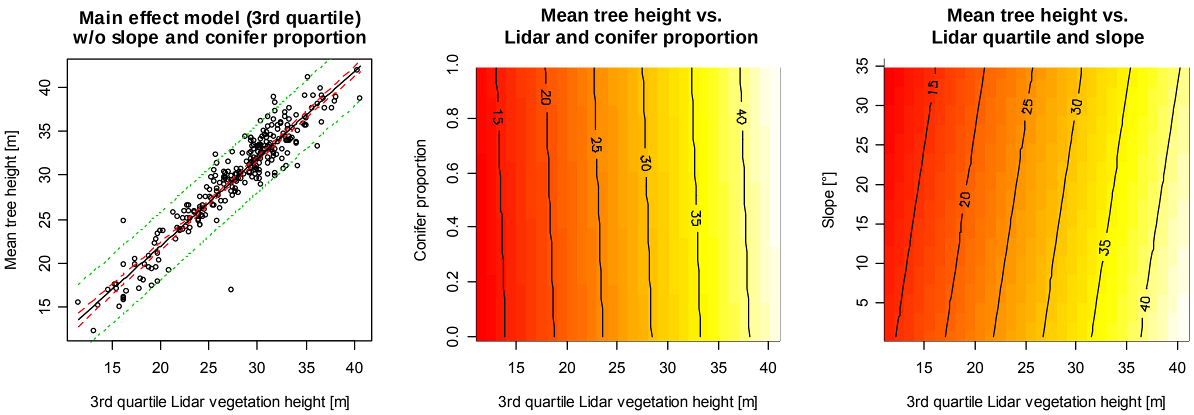


*Figure 4: Model with the most influent independent variable (left); The influence of conifer proportion on tree height estimations (middle) and the influence of slope on tree height estimations (right)*

## 3.3 Comparison of Tree Height Estimations Derived from SAR Data and Lidar Data

Evaluations of Lidar-DTM and InSAR-DSM on a 7.2 ha agricultural area showed that the radar DSM lies an average of 1 m above the Lidar-DTM (+2.75 to -1.5 m). This is also visible in Figure 5, left-hand graphic. Differences vary heavily from pixel to pixel and no obvious explanation (such as changes in land use) could be found in aerial photographs.

Severe edge effects occur in the InSAR DSM at forest boundaries. The InSAR DSM at first underestimates and than overestimates the canopy surface (Figure 5, left-hand graphic). The forest fringe is 1 to 2 Pixels (5-10 m) displaced in a westerly direction. The forest glade (Figure 5, left hand graphic, G-K easting 3537915 to 3537935), which is apparent in the Lidar-DSM, is not visible in the InSAR DSM. The crown surface of the forest stand east of the meadow is also underestimated and may be due to an edge effect.

The surface of the InSAR DSM is not as variable as the Lidar-DSM due to the lower spatial resolution. At the western aspect transect (Figure 5, right-hand graphic), the InSAR DSM seems to be located slightly lower than the Lidar DSM when compared to the eastern aspect transect (Figure 5, left-hand graphic). This observation becomes more noticeable east of the Gauß-Kruger coordinate 3539250. At this coordinate, a forest road that separates a dense forest stand from a sparse stand (to the east of the road) appears as a cut in the Lidar-DSM.

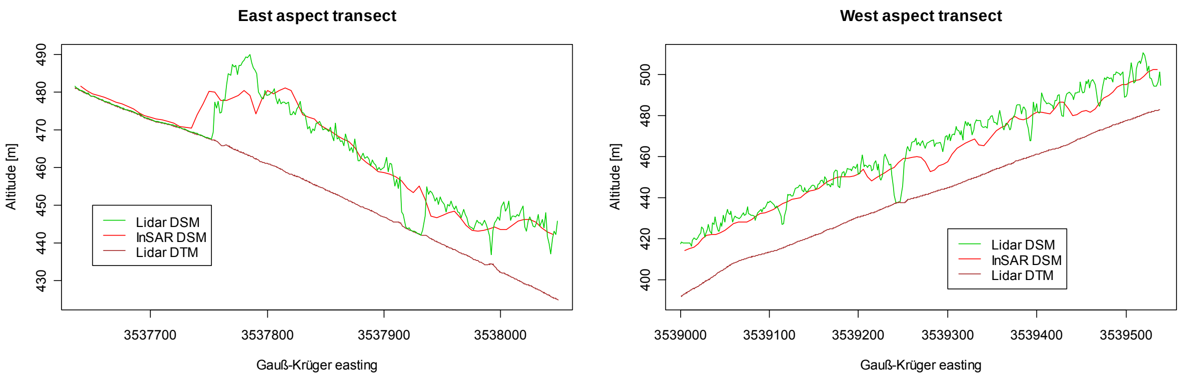


*Figure 5: Comparison of InSAR DSM, Lidar DSM und Lidar DTM along an easterly (left hand graphic) and a westerly (right hand graphic) exposed transect.*

The third quartile of vegetation height is the most influential variable for tree height estimation for both SAR and Lidar data. As opposed to Lidar data, the correlation between mean tree height and SAR vegetation height is not linear. Both radar and Lidar third quartile of vegetation heights underestimate the mean tree height to a lesser degree with increasing slope. Canopy closure does not significantly influence any of the models, despite the fact that the InSAR DSM lies slightly further below the canopy surface in sparse stands than for dense stands (Figure 5, right-hand graphic). Table 1 provides an overview of both models.

*Table 1: Comparison of the models to derive mean tree height from SAR and Lidar data.*

| Regression Equation | RMSE | RMSE |
|---|---|---|
| $H_{Mean}$ = -2.35 + 1.79*3rdQu_Radar – 0.02*3rdQu_Radar² - 0.17*slope –<br>0.03*slope:NE – 0.02*slope:E + 0.01*slope:SE + 0.06*slope:S +<br>0.10*slope:SW + 0.15*slope:W + 0.09*slope:NW | 2.7 m | 9.5% |
| $H_{Mean}$ = 2.06 + 1.04*3rdQu_Lidar – 1.12*slope + 0.94*conifer_proportion | 1.8 m | 6.6% |

# 4 DISCUSSION

The results clearly show that vegetation height derived from both SAR surface models and from raw laserscanner data are suitable as independent variables for estimating average tree height. The relationship between the vegetation height derived from laserscanner data and average tree height is closer than the corresponding relationship for vegetation height derived from SAR data. As a result, a lower degree of error can be expected from the use of laserscanner data. This may be due to the reduced geometrical resolution of SAR data (5 m) compared to Lidar data (approximately 1.5 m). Another reason for the higher variance in the radar data may be the temporal difference between the acquisition dates of the SAR data and the terrestrial data. As the radar data was acquired three years before the terrestrial data, forestry activities or other events may have lead to changes in the crown cover within the test area. Nevertheless, both sources of data permit the estimation of average tree height with an error of less than 10%.

It should be noted that approximately 1.7% of the raw laserscanner points had to be removed before calculating the quartiles, as these were clearly over the highest possible tree height (50m). Possible causes for this may be internal instrument errors or bird strikes.

Figure 4 (left) clearly displays two outliers. The average tree height is clearly overestimated by the laserscanner at one point and is possibly due to a positional error at the inventory point, which is located directly on the border of an old stand. The second outlier may also be the result of positional errors or may have been caused by timber harvesting activities or natural mortality at the point.

The inclusion of slope as a predictor variable significantly improves the estimation of average tree height for both models. As the reduction in estimation error is similar for both radar and laser data, it can be assumed that this improvement method functions independently from the means of data acquisition. One possible explanation for the reduced underestimation of average tree height with increasing slope may be due to the fact that tree crowns are often orientated towards the valley. In these cases, the bulk of the crown is often projected onto the ground at a point lower than the base of the trunk. As vegetation height is measured vertically by remote sensing equipment, without considering the slope angle, vegetation height is often estimated somewhat higher on a slope than in more level areas. As a result, the underestimation of vegetation height that is prevalent in the data is not as noticeable in areas with a higher slope (see Figure 6 A, the red lined surface model).

As expected, an interdependency between aspect and slope is observed when using radar data to estimate average tree height. While very little influence on the estimation of average tree height is observed for sites orientated towards the west (i.e. facing the radar sensor), it is clearly observed in the remaining aspects that the underestimation of the average tree height using the third quartile reduces with increasing slope. When the influence of tree crown orientation on the estimation of average tree height is taken into consideration, one would assume that surface models generated from slopes with a westerly aspect would be somewhat lower than for other aspects (see Figure 6 A, blue dotted surface model). This assumption can be confirmed by subtracting the third quartile of the vegetation height derived from lidar data from the third quartile of the vegetation height derived from the radar data. This calculation clearly shows that vegetation heights measured on western slopes using radar data are noticeably further below lidar vegetation heights than vegetation heights measured on other aspects.

The interdependency between slope and aspect possibly results from the construction of the radar sensor, which, as opposed to a nadir-oriented laserscanner, has a sensor offset by 30-60°. As this leads to distorted results in rough terrain (Intermap 2004), it would therefore be prudent to consider the aspect in relation to the flight direction, rather than the absolute aspect. Radar waves will obviously have a lower incidence angle when the sensor directly faces an inclination (in this case, western aspects) than for other aspects or level ground. Consequently, radar waves seem to penetrate the crown canopy more easily on western aspects; which results in a surface model that is somewhat further below the actual crown surface than surface models derived from other aspects (see Figure 7 A). This effect seems to be more pronounced in sparse canopies (see Figure 5). The reason why canopy closure does not have a significant influence on the model may be due to the limited number of observations for sparse forest stands.

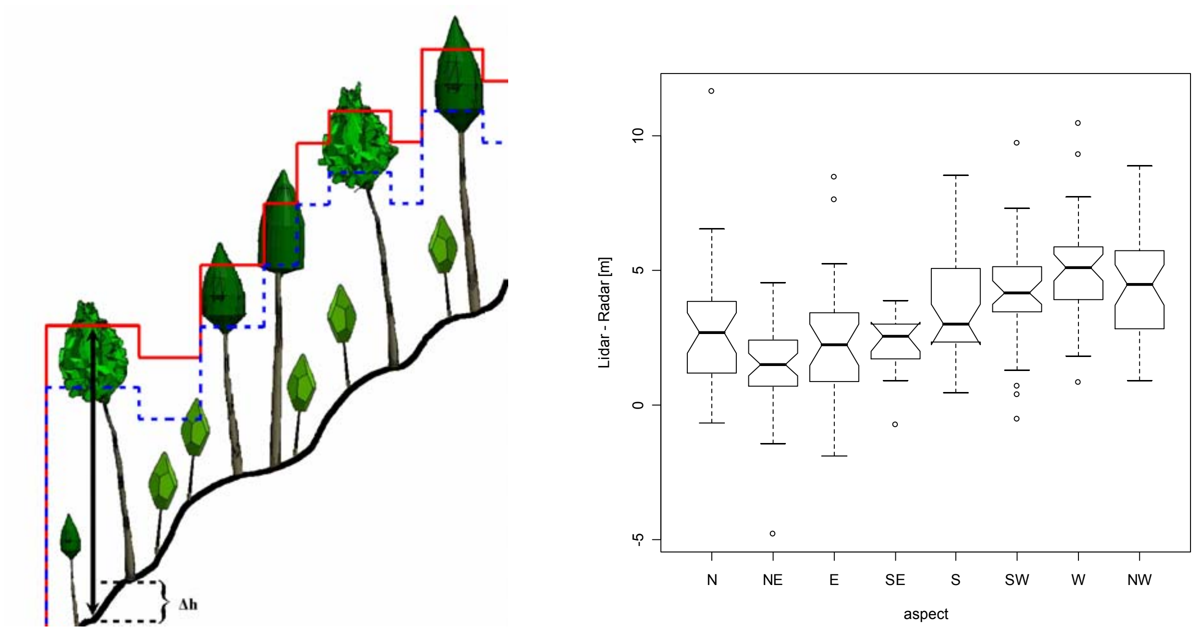


A) B)

*Figure 6: A) Differences of SAR DSMs on slopes according to aspect. Blue dotted line: western aspect, the surface is even more underestimated than at other aspects. Red solid line: other aspects. B) The SAR DSM is located more deeply below the Lidar DSM on western aspects.*

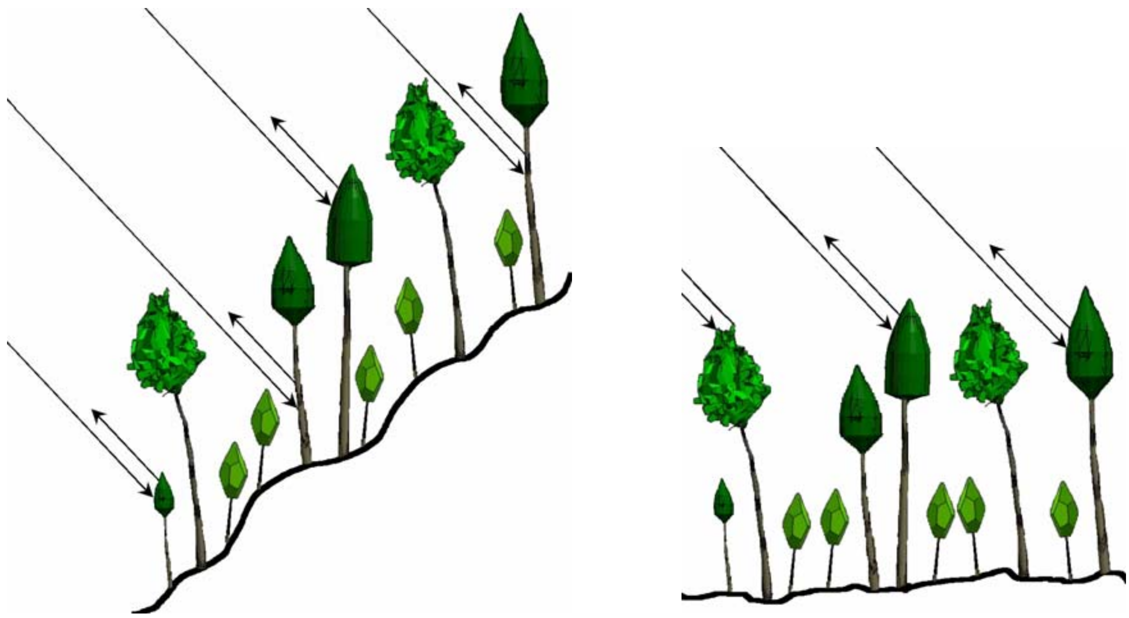

A) B)

*Figure 7: Penetration of radar waves into the crown canopy A) sensor directly facing an inclination B) flat terrain.*

As opposed to estimations using laserscanner data, the relationship between the third quartile of the vegetation height measured by radar data and the average tree height is not linear. As a result, the third quartile is incorporated into the model as a second order polynom. The explanation as to why the height of higher forest stands are underestimated to a lesser extent than lower stands may be found in the composition of tree crowns in older stands or in the different interactions between radar waves and larger tree crowns.

The somewhat higher underestimation of average tree height by the third quartile of Lidar vegetation heights with increasing conifer proportion might be explained by the different crown forms of deciduous and conifer trees. As the top of a conifer crown is much smaller in area than the crown of a deciduous tree, a laser beam will penetrate deeper into the conifer crown and result in a greater underestimation of the tree height.

As the InSAR DSM was acquired during the vegetation period, it is not surprising that the DSM appears to be approximately 1 m higher than the Lidar DSM, which was derived from data acquired in winter. The difference, however, is rather minimal and could have also been introduced during image processing (reference ellipsoid etc.).

The underestimation of the crown surface at forest edges is assumed to be caused by the 30-60° look angle of the radar antennae: the radar waves reach not only the crown surface, but also the trunks of trees located at the forest edge. As a result, mixed pixel are produced, which lead to an underestimation of the crown surface. Interactions between radar waves and forest edges, however, are not fully understood and require further investigation. Forest clearings and other features such as paths or forest glades are often lost in InSAR DSMs due to shadowing effects resulting from the sensor angle.

A proportion of the variance in the estimation of tree height may also result from the fact that the ground truth data used in this study was acquired during a regular forest inventory rather than a specific scientific study. As a result, positional errors in the inventory sample points, tree height measurements and height estimations for trees not measured are possible sources of variance in the regression introduced by terrestrial data acquisition.

# 5 CONCLUSIONS

The SAR and lidar data tested in this study have been shown to provide very good results for the estimation of average tree height across large areas, despite not having been acquired specifically for this purpose. The 6% error for average tree height estimations using laserscanner data corresponds roughly to the results achieved in other studies; such as those undertaken by Naesset 1997, Magnussen and Boudewyn 1998 or Means et al. 2000. Theses authors also report a systematic underestimation of tree height by laserscanners. The results from tree height estimations derived from radar data also correspond to previous studies, such as those conducted by Andersen et al. 2004 or Fransson et al. 2000. While no reference to the influence of aspect on the estimation of tree height using SAR-DSMs could be found in the literature, the influence of slope on estimation accuracy has been described previously (Fransson et al. 2000 or Wallington and Suárez 2005). Heurich et al. 2005 and Breidenbach 2003 proved during investigations into single tree height estimation using laserscanner data that tree height is underestimated to a lesser extent in steep areas than in level areas. Overestimations on steep slopes were also observed during these studies.

As to which of the two sensors would be best for subsequent data acquisitions depends on the accuracy required and the availability of data. In cases where a terrain model with an appropriate resolution is not available, laserscanner data can be used to generate a new terrain model. In this case, information on vegetation height is collected simultaneously. A radar sensor operating in the P and X bandwidths can also be used to simultaneously generate surface and terrain models. The use of laserscanner data is more appropriate when a high level of accuracy for the estimation of tree height or vegetation height structure is required. This applies especially to fragmented forests where edge effects in the InSAR data will have a stronger influence. However, due to the lower maximum flight speed and height required during laserscanner data acquisition, costs can be higher than for radar data.

While the results generally show that the currently available inventory data is appropriate for use in scientific studies, an improvement in positional accuracy could lead to an expected reduction in variance. Furthermore, future studies should ensure that less time elapses between the acquisition of remote sensing and terrestrial data. The models presented in this paper will be tested in other sites within the project area in subsequent phases of the project. Model behaviour will be tested especially in areas where tree heights exceed 38 m, as these areas were rare in the present study. The interaction of radar waves with large tree crowns and forest boundaries will also be studied within the scope of further investigations.

## ACKNOWLEDGEMENTS

The research project MatchWood is financed by the Bundesministerium für Bildung und Forschung (German Ministry of Education and Research).

I would like to thank Scott Hemphill for translation of the text and creating various graphics, as well as Matthias Schmidt, Edgar Kublin, Holger Weinacker and Manfred Reich for the many supportive discussions and suggestions.

## REFERENCES

Andersen, H.-E., McGaughey, R., Carson, W., Reutebuch, S., Mercer, B., Allan, J. (2003): A Comparison of Forest Canopy Models Derived From Lidar And InSAR Data In A Pacific Northwest Conifer Forest. Proceedings of the ISPRS working group III/3 workshop '3-D reconstruction from airborne laserscanner and InSAR data' Dresden, Germany 8-10 October 2003. VOLUME XXXIV, PART 3/W13. Commission III, WG II/3.

Andersen, H.-E., McGaughey, R., Reutebuch, S., Schreuder, G., Agee, J., Mercer, B. (2004): Estimating Canopy Fuel Parameters In a Pacific Northwest Conifer Forest Using Multifrequency Polarimetric IFSAR. XXth ISPRS Congress, Istanbul, Turkey. http://www.isprs.org/istanbul2004/comm3/papers/419.pdf (accessed 1 May 2005).

Breidenbach, J. (2003): Verwendung von Laserscannerdaten in Forstinventuren. Diplom Thesis, Department of Remote Sensing and Landscape Information Systems, University Freiburg. http://omnibus.uni-freiburg.de/~breidenb/diplomarbeit/diplomarbeit.pdf (accessed 5 Dez. 2004)

Cloude, S. and Corr, D. (2003): Tree-height retrieval using Single Baseline Polarimetric Interferometry. Proceedings of the POL-INSAR Workshop, Frascati, Italy, from 14 to 16 January 2003. http://earth.esa.int/cgi-bin/polinsar_query.pl?abstract=17 (accessed 7 May 2004).

Fransson, J.E.S., Walter, F. and Ulander, L.M.H. (2000): Estimation of Forest Parameters Using CARABAS-II VHF SAR Data, IEEE Transactions on Geoscience and Remote Sensing 38(2): 720-727.

Gaveau, D.L.A. and Hill, R.A. (2003): Quantifying canopy height underestimation by laser pulse penetration in small-footprint airborne laser scanning data. Can. J. Remote Sensing, Vol 29, No. 5: 650-657.

Heurich, M., Günther, S., Schröder, S., Kennel, E. (2004): Baumhöhenmessung mit flugzeuggetragenen Laserscannern. AFZ Der Wald, 17/04.

Hyyppä, J., Schardt, M., Haggren, H., Koch, B., Lohr, U., Scherrer, H.U., Paananen, R., Luukkonen, H., Pyysalo, U., Friedläder, H. Uttera, J., Wagner, S., Inkinen, M., Wimmer, A., Kukko, A., Ahokas, E., Karjalainen, M. (2001): High-Scan: The first European-wide Attempt, to derive Single-Tree Information from Laserscanner Data. The Photogrammetric Journal of Finland, Vol. 17, No. 2: 58-68.

Intermap (2004): Product Handbook and Quick Start Guide. Version 3.3. http://www.intermap.com/images/handbook/producthandbook.pdf (accessed 23 Oct. 2005).

Kon-Allan, E., v.d. Goltz, H., Blust, M., Nothdurft, A. (2004): Verfahrenshandbuch Betriebsinventur. Version 1.1. Verlag Landesforstverwaltung.

Leckie, D., Gougeon, D.H., Quinn, R., Armstrong, L., Shreenan, R. (2003): Combined high-density lidar and multispectral imagery for individual tree crown analysis. Canadian Journal on Remote Sensing, Vol 29, No. 5: 633-649.

Magnussen, S. and P. Boudewyn (1998): Derivations of stand heights from airborne laser scanner data with canopy-based quantile estimators. Can. J. of For. Res. 28: 1016-1031.

Means, J.E., Acker, S.A., Fitt, B.J., Renslow, M., Emerson, L., Hendrix, C.J. (2000): Predicting Forest Stand Characteristics with Airborne Scanning Lidar. Photogrammetric Engineering & Remote Sensing Vol. 66, No. 11: 1367-1371.

Mercer, B. (2001): Combining LIDAR and IfSAR: what can you expect?. In: GeoBit, 6,12: 12-19.

Moreira, J., Schwäbisch, M., Wimmer, C., Rombach, M., Mura, J. (2001): Surface and Ground Topography Determination in Tropical Rain Forest Areas Using Airborne Interferometric SAR. Proceedings of the Photogrammetric Week 2001, Stuttgart, Germany.

http://www.ifp.uni-stuttgart.de/publications/phowo01/Moreira.pdf (accessed 11 June 2004)

Naesset, E. (2004): Accuracy of Forest Inventory Using Airborne Laser scanning: Evaluating the First Full-scale Operational Project. Scand. J. For. Res. 19: 554.557.

Naesset, E. and Okland, T. (2002): Estimating tree height and tree crown properties using airborne scanning laser in a boreal nature reserve. Remote Sensing of Environment 79: 105-115.

Naesset, E. (1997): Determination of mean tree height of forest stands using airborne laser scanner data. ISPRS Journal of Photogrammetry & Remote Sensing 52: 49-56.

Persson, A., Holmgren, J., Söderman, U. (2002): Detecting and Measuring Individual Trees Using an Airborne Laser Scanner. Photogrammetric Engineering & Remote Sensing Vol. 68, No. 9: 925-932.

Schleyer, A (2001): Das Laserscan-DGM von Baden-Württemberg. Reports on the Photogrammetric Week 2001, Stuttgart, Germany. http://www.ifp.uni-stuttgart.de/publications/phowo01/Schleyer.pdf (accessed 1 Sep. 2003).

Wallington, E.D. and Suárez, J.C. (2005): Evaluation of commercial airborne LiDAR and SAR products to estimate top height in production forests in Britain. In Proceedings of IUFRO Conference, Edinburgh, UK, 5th-8th April 2005.

Weinacker, H., Koch, B., Weinacker, R. (2004): TreesVis a Software System for Simultaneous 3D-Real-Time Visualisation of DTM, DSM, Laser Raw Data, Multispectral Data, Simple Tree and Building Models. Proceedings of the ISPRS working group VIII/2 'Laser-Scanners for Forest and Landscape Assessment' Freiburg, Germany 03-06 October 2004.

www.isprs.org/commission8/workshop_laser_forest/WEINACKER2.pdf (accessed 12 April 2005).

Woodhouse, I., Cloude, S., Hutchinson, C, Papathanassiou, K. (2003): Evaluating PolInSAR Tree Height and Topography Retrievals in Glen Affric. Proceedings of the POL-INSAR Workshop, Frascati, Italy, from 14 to 16 January 2003. http://earth.esa.int/cgi-bin/polinsar_query.pl?abstract=27 (accessed 7 May 2004).

Wulder, M., Seemann, D., Bouchard, A. (2001): Within polygon grid based sampling for height estimation with LIDAR data. In: 23rd Symposium of the Canadian Remote Sensing Society and the 10th Congres de l'AQT, Laval University August 20-24.

# PREDICTING FOREST GROWTH PROCESSES BY USING LASERSCANNER DERIVED STAND MODELS AND SIMULATING SUN ECLIPTIC

*Michael Thies[1], Holger Weinacker[2], Rudi Weinacker[3] and Norbert Pfeifer[4]*

[1] RP Tuebingen, Department of Forestry, Tuebingen, Germany; Michael.Thies@rpt.bwl.de

[2] University of Freiburg, Department of Remote Sensing and Landscape Information Systems, Freiburg, Germany; Holger.Weinacker@felis.uni-freiburg.de

[3] Rudi Weinacker Software Development, Ludwigshafen, Germany

[4] Delft University of Technology, Section of Photogrammetry and Remote Sensing, Delft, The Netherlands; N.Pfeifer@LR.TUDelft.NL

## ABSTRACT

Competition for light is the most driving factor for differentiation processes in forest stands. With increasing portion of the sun exposed surface of a single tree's crown photosynthetic activity will increase correspondingly. Thus, trees receiving a high amount of solar radiation will grow faster than more shaded trees. Based on this simple assumption a methodological approach for the prediction of undisturbed future development of forest stands on a regional scale is presented.

Spatial explicit forest stand models with individually delineated single trees derived from airborne laser scanning were used to describe the forest scenery of a mixed stand. Sun position was modelled and combined with ray tracing to decide whether a simulated sun beam of a defined patch size hits the crown surface of a certain tree or not. This decision is carried out for each single tree inside a predefined stand polygon. As a first approximation in this approach simply the number of hits per tree were counted, summed up and taken as surrogate for the individual tree's radiation consumption.

In 2002 airborne laserscanner (ALS) data of the above mentioned stand were collected. One year later terrestrial measurements of forest inventory data took place. These terrestrial measurements were repeated in 2005 at the end of the vegetation period. Diameter at breast height (DBH) was used as indicator for single tree's growth. After identifying congruent trees from both data sets (ALS and terrestrial data), DBH of the trees in 2003 was compared to DBH in 2005 and finally correlated with the individual tree's number of sun hits. From a methodological point of view DBH comparisons from only three vegetation periods are critical, however the results encourage to intensify this approach in the near future.

## 1 INTRODUCTION

Light is one of the most important site factors affecting tree growth (1, 2). Thus, in closed forests stand development is closely connected to light regime. For this reason several scientific investigations have been carried out to measure or estimate radiation in forest stands. Three main topics in this context are of special interest; (i) silvicultural questions on (natural) regeneration (i.e. 3, 4), (ii) tree growth, differentiation processes in forest stands and their simulation (i.e. 5, 6, 7) and (iii) issues related to forest ecology (i.e. 8, 9).

Generally solar radiation or photosynthetic active radiation (PAR) can be measured directly by the use of self-integrating light sensors or can be estimated by analysing hemispherical photography (10). The last-mentioned method is highly developed and often used for investigations on light climate in closed forests (11, 12, 13). Both methods are suitable for data acquisition on a local stand level. A description of light climate for larger forested areas or landscapes is not possible. In addition, data acquisition is carried out from the ground, consequently radiation in most cases is not directly measured nearby the assimilating crown surfaces.

These disadvantages can be solved by using 3-dimensional models derived from airborne laser-scanner data. The current state of large wooded areas is documented very detailed and can be used for various ecological investigations (14). In this study a method to calculate light reception of single trees in user-defined landscape regions is presented. Abiotic factors (as slope or exposition) as well as biotic factors (as crown competition of neighbouring trees) are taken into account. Sun ecliptic is simulated and combined with ray-tracing to decide whether a tree crown is exposed to sunlight or not. As a first validation the hypothesis is proved that trees receiving a high amount of sun beams will grow faster than more shaded trees. The overall aim is to predict undisturbed future development and differentiation processes of forest stands on a regional scale.

## 2 METHODS

The approach for determining light reception of single trees consists of two components; the determination of the sun's position and the ray tracing algorithm. These are applied to 3D stand models were single trees are separated. All calculation modules are embedded in the TREESVIS-Software (15).

### 2.1 3D forest stand models

The derivation of 3D stand models has been done according to the method described by (16). Both, digital surface (DSM) and digital terrain model (DTM) are created by assigning the lowest (DTM) and highest (DSM) 3D coordinate to certain raster areas followed by an active contour filtering. Single trees are delineated by applying a local maximum filter to find tree tops. These are used as starting points for a pouring algorithm to detect the outer tree borders. Additional algorithms separate merged trees and reduce number of edges of the polygons representing the outer border line of the single tree crowns.

### 2.2 Calculating sun position

In this simplified model only direct sunlight is considered. The rays coming from the sun are considered to be parallel, thus a set of parallel sun rays is generated with a predefined orthogonal distance between them, e.g. 1m by 1m. This ray bundle is intersected with the crown surfaces. The first crown surface along each ray absorbed the light, casting shadows on the crown surfaces behind. The spatial discretization of the crown surfaces is in the same order of magnitude as the distance between the rays.

The position of the sun is calculated following the 'Astronomy Answers' from the Astronomical Institute at Utrecht University, the Netherlands (17). Input values are the time (i.e., date, time zone and time) and the geographical position. With the time the position of the sun is computed in a coordinate system that is independent of the observer position (i.e., the equatorial coordinates expressing ascention and declination). Then the sun's position is transformed into a local coordinate system of the observer and the resulting values are the altitude and azimuth of the sun. The altitude is the angle enclosed by horizon-observer-sun, and the azimuth is the angle enclosed by north-observer-'projection of the sun to the horizon'.1

While it is also possible to calculate the time and azimuth of sunrise and -set, we suggest to use a simpler approach and to compute the position of the sun for fixed intervals. The interval length can be chosen arbitrarily. Times without sunshine are those where the altitude of the sun is negative, i.e., the sun is below the horizon. For calculating the exposure of (a part of) the crown to the sun the exposition and slope have to be known. The angle between the vector to the sun and the local normal finally determine how much energy is incident to the sun.

The above calculations do not consider refraction and other phenomena. Also the amount of energy, which depends on the sun earth distance and the path length through the atmosphere, is not considered. Likewise, only direct and no diffuse radiation is considered here.

---

[1] An alternative resource for computing the sun position using the Matlab script sun_position.m can be found at the Matlab Central file exchange (under MATLAB Central > File Exchange > Earth Sciences > General > sun_position.m).

## 2.3 Ray tracing

Ray tracing algorithms can be used to analyse the path taken by light by following rays of light as they interact with optical surfaces (18. For applying the algorithm presented in this study DTM, DSM, and polygons of separated single trees are necessary. In addition a region of interest (ROI) has to be defined to indicate the trees for which exposure to the sun should be calculated (see fig. 1).

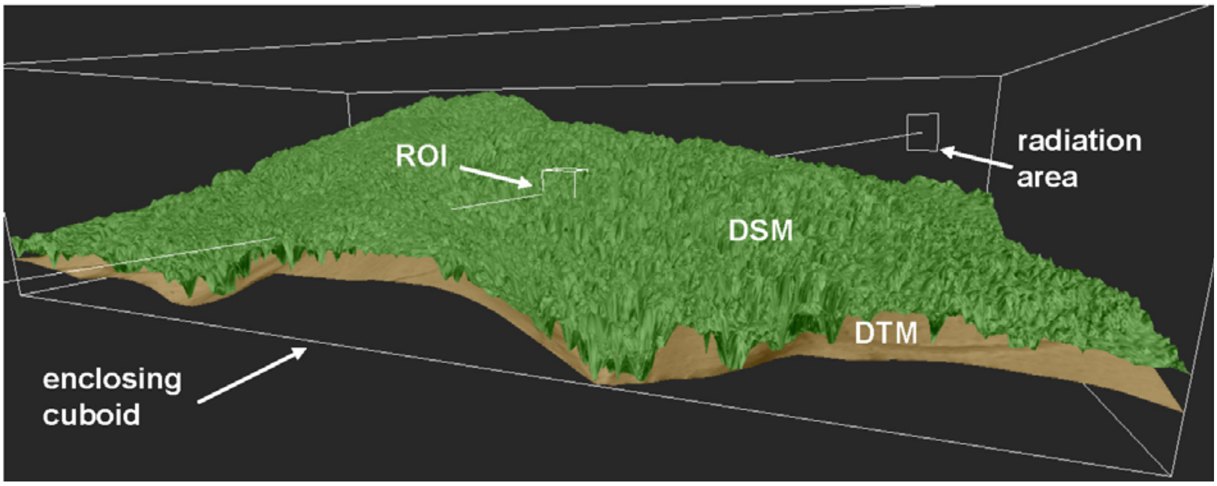


*Figure 1: Setup for using the ray tracing algorithm to calculate the intersection of tree crowns with sun rays.*

Before the algorithm is started an enclosing cuboid is calculated which contains all surfaces and models. This is necessary to guarantee that the ray source is behind all geometry and to consider possible shading effects caused by terrain morphology. To improve the performance of the algorithm the region of interest is represented by a second cuboid. This makes it easy to decide whether a beam is able to intersect the ROI or not. Depending on the chosen time interval from the beginning to the end of day sun position is calculated. For each sun position (represented by its vector) a radiation area is acquired which is perpendicular to the sun vector and covers the whole region of interest. Moreover the radiation area has to be outside the cuboid which encloses the whole scenery. From the radiation area in pre-selected density sun rays are sent following the direction of the sun vector. As far as a ray intersects a tree crown the number of sun hits of this tree is incremented by one. In each case only the shortest distance between the radiation area and the point of intersection with the tree crown is considered.

The result of the procedures described here is the number of sun hits per tree crown for each tree inside the region of interest. It is possible to choose the calendar date of the beginning and the end of the calculations.

## 2.4 Study area and sample data set

The method was applied to a study area in the Southern Black Forest foothill range in southwest Germany close to the city of Freiburg. Height above sea level differs from 500 to 800m. In summer 2002 LIDAR data of an area of 70 hectares has been acquired by using the TopoSys FALCON system. Inside the study area a sample plot of 40 x 40m size has been selected as the region of interest (see above) for this study. It is located on an intensively mixed and unevenly-aged stand which is mainly (95%) composed of the deciduous tree-species beech (Fagus sylvatica L.) and a 5% portion of oak (Quercus spec.) in the dominant crown layer. The medium and lower crown layers consists of silver-fir (Abies alba Mill.) and beech trees. The vertical and the horizontal structure of the stand are very high. Age of the dominant trees ranges from 68 to 223 years. In spring 2003 diameter at breast height (DBH) was measured by circumference tapes and the height of 1.3m above ground was permanently marked (19). After the end of vegetation period in 2005 DBH of the trees were measured again. The DBH-increment of the trees given by the DBH-difference between 2005 and 2003 has been used to prove the hypothesis that trees with sun exposed crowns grow faster than others.

# 3 RESULTS

In the region of interest a number of 55 trees could be delineated from airborne laserscanner data. The sun hits per m² crown surface were calculated for each tree separated for the whole year and the vegetation period (see fig. 2, on the left). Vegetation period was defined forestry specific according to (20) from 1st of May to 30th of September. For both calculations high resolution data sets were created with 30 rays per m² radiation area and starting the ray tracing with a new sun position each 10 minutes. It is obvious that for all trees the number of sun hits during vegetation period is 50% or more of the total number. Calculation time for the whole year was 21 hours and 52 minutes and for vegetation period 8 hours and 34 minutes. For investigations with deciduous tree-species focusing on vegetation period will be sufficient.

Two parameters which can be modified by the user were varied to verify their influence on runtime performance (see fig. 2, on the right). With increasing rays per m² of radiation area calculation time is increasing linearly. In contrast the time interval of starting the ray tracing algorithm affects calculation time exponentially. Whereas time intervals between 20 and 60 minutes cause calculation times between 20 and 260 minutes, calculation time for a 10 minute interval is disproportionately high.

The plot in fig. 3 shows the tree positions and diameters as a result of the terrestrial measurements. The crosses indicate the position of the tree tops derived from single tree delineation of airborne laserscanner data. The total number of trees from both methods is nearly identical, although tree positions differ remarkable. The most important reason for this is the inhomogeneous mixed structure of the study site. Therefore the identification of congruent trees in both datasets has been done manually and the number was reduced to the individuals which could be identified without any doubt (trees marked by the rectangles in fig. 3, on the left). For this subset of only seven trees the diameter increment from 2003 to 2005 (three vegetation periods) was calculated and related to the number of sun hits per m² crown surface during vegetation period. The ray tracing algorithm was carried out with 30 rays per m² radiation area and executed for sun position intervals of ten minutes. Although the number of trees is far from statistical standards, a trend of increasing diameter increment with higher numbers of sun hits can be observed (fig. 3 on the right).

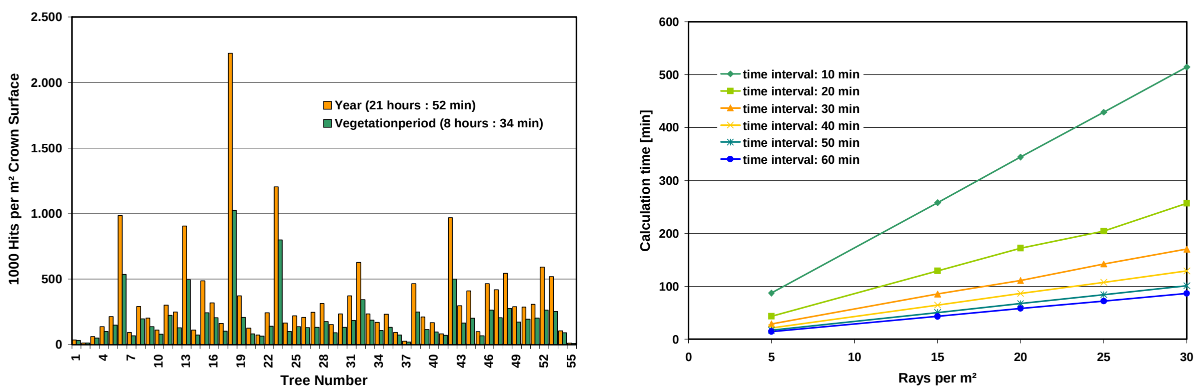


*Figure 2: Runtime performance of the algorithm. Depending on the rays per m² and time interval of the calculation (right) and differentiated between the whole year and the vegetation period (left).*

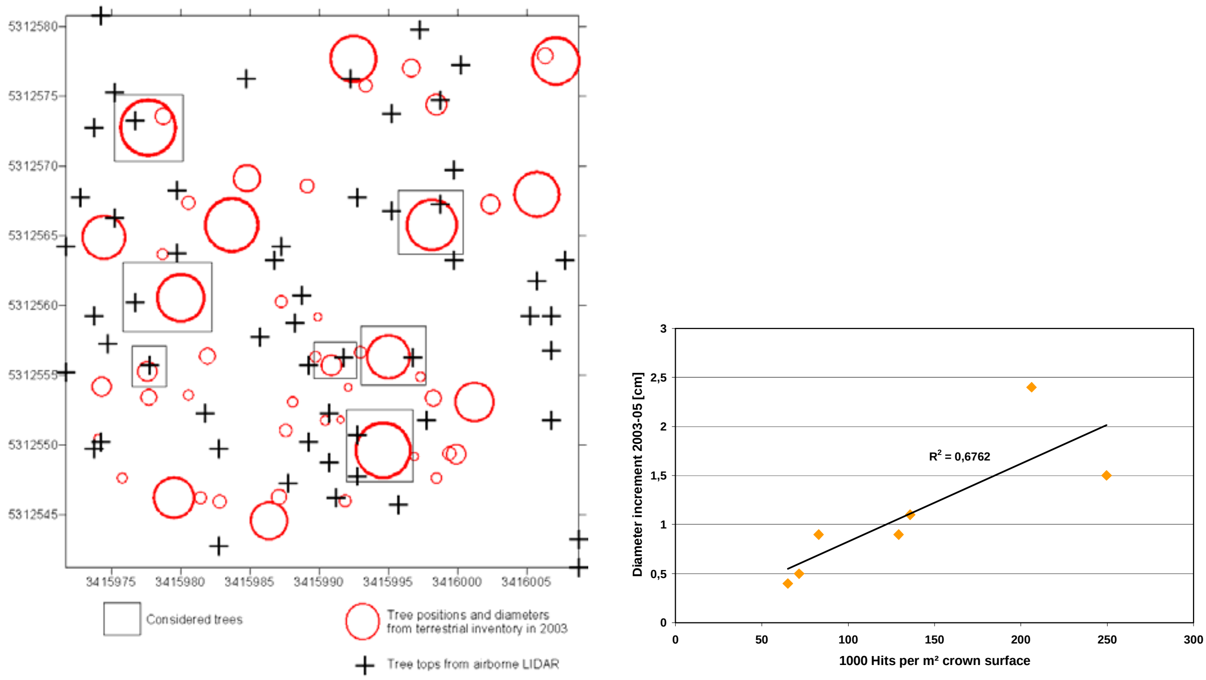


*Figure 3: Selection of sample trees (left) and relation between diameter increment and number of sun hits (right).*

## 4 CONCLUSIONS AND OUTLOOK

A simple model to calculate the number of sun hits for tree crowns in forest stands is presented by taking into account terrain morphology. Because of the integration in a software package which allows to visualise and analyse 3D data, radiation analysis is a by-product from the analysis of airborne laser scanner data. As far as the requirements (DTM, DSM, single tree polygons) are complied, the algorithms can be executed. Although the results indicate a relation between diameter increment of trees and theirs crown exposure to sunlight, because of the reduced sample size additional studies are necessary to prove this hypothesis in more detail. Afterwards the next step will be to quantify radiation energy a tree crown receives instead of only counting sun hits. The model up to now only considers direct radiation, which for dominant trees is sufficient but unsatisfactory for trees in the understorey. For these trees diffuse radiation is of higher importance (21). Developments in full waveform digitization (i.e. 22) raise the expectation of improved possibilities to detect understorey trees. Thus, the better understorey trees can be detected the higher is the need to integrate a model for diffuse radiation. This will help to improve a prediction of future development of forest stands on a regional scale.

## ACKNOWLEDGEMENTS

This study was funded by the German Federal Ministry of Education and Research (natscan-project FKZ: 13N8102) and the Society for the Promotion of Forest and Wood Science Research at the University of Freiburg, Germany (GFH Freiburg e.V.).

## REFERENCES

1 Kramer, P.J.; Kozlowski, T.T., 1960. Physiology of trees. (McGraw-Hill) 642 pp.

2 Horn, H.S., 1971. The adaptive geometry of trees. (Princeton University Press) 144 pp.

3 Holbo, H.R.; Childs, S.W.; McNabb, D.H., 1985. Solar radiation at seedling sites below partial canopies. Forest Ecology and Management, 10: 115-124.

4 Phares, R.E., 1971. Growth of red oak (Quercus rubra L.) seedlings in relatin to light and nutrients. Ecology, 52: 669- 672.

5 Sterck, F.J., 1997. Tree development and morphology in relation to light availability in a tropical rain forest in French Guiana. Wageningen, Landbouwuniv., Diss.

6 Küppers, M.; Timm, H.; Orth, F.; Stegemann, J.; Stöber, R.; Schneider, H. Paliwal, K. Karunaichamy, K.S.T.K.; Ortiz, R., 1996. Effects of light environment and successional status on lightfleck use by understory trees of temperate and tropical forests. Tree Physiology, 16: 69-80.

7 Takenaka, A., 1997. A simulation model of tree architecture development based on growth response to local light environment. Journal of Plant Research, 107: 321-330.

8 Bouget, C.; Duelli, P., 2004. The effects of windthrow on forest insect communities: a literature review. Biological Conservation, 118: 281-299.

9 Faccio, S.D., 2003. Effects of ice-storm-created gaps on forest breeding bird communities in central Vermont. Forest Ecology and Management, 186: 133-145.

10 Rich, P.M.; Clark, D.B.; Clark, D.A.; Oberbauer, S.F., 1993. Long-term study of solar radiation regimes in a tropical wet forest using quantum snesors and hemispherical photography. Agricultural and Forest Meteorology, 65: 107-127.

11 Anderson, M.C., 1964. Studies of the woodland light climate: I. The photographic computation of light conditions. Journal of Ecology, 52: 27-41.

12 Brunner, A., 1998. A light model for spatially explicit forest stand models. Forest Ecology and Management, 107: 19-46.

13 Wagner, S., 1998. Calibration of grey values of hemispherical photographs for image analysis. Agricultural and Forest Meteorology, 90: 103-117.

14 Lefsky, M.A.; Cohen, W.B.; Parker, G.G.; Harding, D.J., 2002. Lidar remote sensing for ecosystem studies. BioScience, 52: 19-30.

15 Weinacker, H.; Koch, B.; Heyder, U.; Weinacker, R., 2004. TREESVIS-A Software System for Simultaneous 3D-Real-Time Visualisation of DTM, DSM, Laser Raw Data, Multispectral Data, Simple Tree and Building Models. International Archives of Photogrammetry, Remote Sensing and Spatial Information Sciences, 36: 90-95.

16 Weinacker, H.; Koch, B.; Heyder, U.; Weinacker, R., 2004. Development of Filtering, Segmentation and Modelling Modules for LIDAR and Multispectral Data as a Fundament of an Automatic Forest Inventory System. International Archives of Photogrammetry, Remote Sensing and Spatial Information Sciences, 36: 50- 55.

17 http://www.astro.uu.nl/~strous/AA/en//reken/zonpositie.html. last accessed: 2006-02-06.

18 Wilt, N., 1994. Object-oriented ray tracing in C++. (Wiley). 441 pp.

19 Thies, M.; Spiecker, H., (2004). Evaluation and future prospects of terrestrial laser scanning for standardized forest inventories. International Archives of Photogrammetry, Remote Sensing and Spatial Information Sciences, 36: 192-197.

20 Otto, H.-J., 1994. Waldökologie. (Ulmer). 391 pp.

21 Chazdon, R.L.; Field, C.B., 1987. Photographic estimation of photosynthetically active radiation: evaluation of a computerized technique. Oecologia, 73: 525-532.

22 Hug, C.; Ullrich, A. Grimm, A., 2004. Litemapper-5600 – a waveform-digitizing lidar terrain and vegetation mapping system. International Archives of Photogrammetry, Remote Sensing and Spatial Information Sciences, 36: 24-29.

# PHYSICALLY-BASED PARAMETERIZATION OF THE REFLECTANCE OF CONIFEROUS STANDS

*Miina Rautiainen, Matti Mõttus and Pauline Stenberg*

University of Helsinki, Department of Forest Ecology, Helsinki, Finland;
miina.rautiainen@helsinki.fi, matti.mottus@helsinki.fi, pauline.stenberg@helsinki.fi

## ABSTRACT

We discuss the reasons for the distinct spectral behaviour of boreal coniferous forests. As a tool for assessing the questions, we use a parameterization model, the PARAS forest reflectance model. The model incorporates a simple parameterization based on a canopy specific relationship between the so-called 'photon recollision probability' ($p$) and leaf area index (LAI). The recollision probability is a spectrally invariant (i.e. wavelength independent) canopy structural parameter, which can be interpreted as the probability by which a photon scattered (reflected or transmitted) from a leaf or needle in the canopy will interact within the canopy again. It increases as a result of within-shoot scattering in coniferous canopies. In a coniferous canopy a photon may interact several times within the same shoot. This could be one of the explanations for the typically observed lower reflectance (higher absorption) of coniferous forests.

**Keywords:** leaf area index, clumping, boreal forest, recollision probability, PARAS model

## 1 INTRODUCTION

The boreal forests of the northern hemisphere, dominated by coniferous tree species, form the largest unbroken, circumpolar forest zone in the world. Ecologically, the zone has a considerable influence on global carbon, water and energy cycles. From the perspective of optical remote sensing, a widely acknowledged, but poorly explained phenomenon is the generally observed lower reflectances of coniferous forests, when compared to broadleaved forests, and the inability of spectral vegetation indices to describe the basic biophysical variables. In the recent years, modeling the radiation regime of coniferous forests has begun to attract more attention as the specific problems of the boreal zone have become known to the remote sensing community.

Several explanations for the low reflectances of boreal coniferous forests have been put forward. The crown structure of the forests is unique: the canopy is formed of dense, narrow and deep tree crowns, which have a highly hierarchic inner structure. In addition, since the forests are often rather open, the crowns are separated from each other and an abundant green understory (or moss or lichen layer) is visible to the satellite instruments. The distinct geometrical structure affects considerably the bidirectional reflectance factor (BRF) of conifer stands, making it more difficult to compare measurements made at different illumination conditions or from different view nadir angles. The documented complex structure of the forests is further complicated by the fact that acquiring ground observations from many parts of the boreal zone is especially difficult due to the remoteness and climate of the region.

Analyzing all the characteristics specific to boreal forests is challenging as the structural features are interconnected with each other in a complicated manner. Our recent interest has been in understanding how various levels of clumping (e.g. shoots (Rautiainen & Stenberg, 2005, Smolander & Stenberg, 2005) or crowns (Rautiainen et al., 2004)) influence the spectral signature of coniferous forests. Our current understanding is that the conic shape of the coniferous tree species, clumping of needles into shoots, and the relatively high absorption rate of needles result in the complicated reflectance patterns of coniferous forests, but that interpreting the effect of each of these factors is difficult due to the presence of the abundant understory layer.

## 2 METHODS

In the current study, the approach used to address the problem involves the application of the so-called 'photon recollision probability' ($p$). The recollision probability is a spectrally invariant (i.e. wavelength independent) canopy structural parameter, which can be interpreted as the probability by which a photon scattered (reflected or transmitted) from a leaf or needle in the canopy will interact within the canopy again. The theoretical background for the concept of the spectral invariants has been described in the so-called eigenvalue theory (Knyazikhin et al., 1998a). The theory states that the radiation budget of a vegetation canopy can be parameterized using only two parameters: the amount of radiation absorbed by a canopy should depend only on the wavelength and a canopy structural parameter (recollision probability, $p$) and the amount of radiation transmitted should depend on the wavelength and another spectrally invariant canopy structural parameter ($p_t$). These parameters depend on canopy structure in a rather complex manner (Panferov et al., 2001; Wang et al., 2003; Shabanov et al., 2003). The spectrally invariant parameters can also be used in solving the inverse problem of vegetation remote sensing (Knyazikhin et al., 1998a and b).

Two modelling exercises were carried out to evaluate the applicability of photon recollision probability in coniferous canopy reflectance calculations. We developed a demonstration tool, the PARAS model (Rautiainen & Stenberg, 2005) to quantify the effect that clumping of needles into shoots has on coniferous stand reflectance. The PARAS model is a simple parameterization model prototype which can incorporate clumping at multiple scales, but is currently parameterized to account for the clumping at the shoot scale only. The parameterization builds upon the basic principle that the recollision probability increases as a result of within-shoot scattering in coniferous canopies (Smolander & Stenberg, 2005): unlike the case in broadleaved forest where a photon scattered from a leaf will not interact with the same leaf again, in a coniferous canopy a photon may interact several times within the same shoot. In the PARAS model, forest BRF is calculated as a sum of the ground and canopy components:

$$BRF = cgf(\theta_1)cgf(\theta_2)\rho_{ground} + f(\theta_1,\theta_2)i_0(\theta_2)\frac{\omega_L - p\omega_L}{1 - p\omega_L}$$

where $\theta_1$ and $\theta_2$ are the viewing and illumination zenith angles, *cgf* denotes the canopy gap fraction in the directions of view and illumination (Sun), $\rho_{ground}$ is the BRF of the ground (which may also be expressed as a function of $\theta_1$ and $\theta_2$, depending on the data available), $f$ is the canopy scattering phase function, and $i_0(\theta_2)$ is canopy interceptance or the fraction of the incoming radiation interacting with the canopy, $\omega_L$ *is* needle (or leaf) albedo. The model and its background have been published in Rautiainen & Stenberg (2005).

The second exercise consisted of testing the compatibility of a hybrid geometric-optical reflectance model with the concept of photon recollision probability (Mõttus et al., 2006). The Kuusk-Nilson forest reflectance and transmittance (FRT) model (Kuusk and Nilson, 2000) is a radiative transfer model that calculates reflectance and transmittance factors for canopies consisting of geometrical crown envelopes with uniform distribution of foliage density and orientation. First-order scattering is calculated by numerical integration over the envelopes using canopy bidirectional gap probabilities and the average leaf scattering phase function. Diffuse fluxes are calculated using the analytical solution of a two-stream radiative transfer model. Tree characteristics were generated using allometric data for Scots pine trees of different ages growing in Southern Finland. To evaluate specifically the applicability of the p-theory to non-homogeneous canopies composed of separate tree crowns, clumping inside the crowns was ignored in this test. Other input parameters were chosen to ease the interpretation of modelling results: ellipsoidal crown shape was assumed, the tree pattern was Poisson, diffuse sky radiation was ignored, and soil was considered black. As a reference, reflectance and transmittance predictions of a simple two-stream model were used.

## 3 RESULTS AND DISCUSSION

Simulation runs using the PARAS model showed that a major improvement in simulating canopy reflectance in near-infrared (NIR) was achieved by accounting for the within-shoot scattering. This suggests that the low NIR reflectance observed in coniferous areas could be due to within-shoot scattering. On the other hand, there are still several conifer-specific characteristics which were not studied: clumping at other scales, other phenomena related to crown geometry and roughness of the canopy surface, and the interconnected effect of canopy cover and green understory. Currently, our efforts are directed at developing allometric models for crown shape and canopy cover, and using these models for simplified parameterizations of crown geometry in forest reflectance models.

If used for predicting canopy absorption, the Kuusk-Nilson model was shown to be compatible with the *p*-theory. This result is not surprising as both approaches (hybrid geometric-optical models and photon recollision probability theory) are based on the physical theory of photon transport. However, to allow for the calculation of photon recollision probability from modelling results, the model had to be renormalized to achieve energy conservation. Comparisons with the simple two-stream approximation that contains no data on canopy structure show that higher-order canopy clumping, or clumping of elementary scatterers into crown envelopes, increases recollision probability thus enhancing canopy absorption. This effect is more evident in young and sparse stands; in stands where leaf area index approaches 5, the differences are negligible.

An obvious shortcoming of the *p*-theory is its inability to describe the angular distribution of scattered radiation. To overcome this problem it may be combined with other (physically-based) reflectance modelling concepts. Although this was proven possible, a considerable amount of crucial information and numerical models is still missing. For example, the actual BRF of a conifer shoot needs to be determined and efficiently parameterized to accurately predict the angular reflectance characteristics of boreal forests.

From these tests it is clear that, for application of any forest reflectance models in the boreal zone, high priority should be given to modeling the hierarchic canopy structure. The concept of photon recollision probability may be a useful tool for parameterizing these structural effects describing canopy clumping at various hierarchical levels.

Canopy clumping affects strongly both the direct visibility of background (ground surface of undergrowth) and its contribution to the diffuse fluxes as registered by a satellite or an air-borne sensor. As geometric-optical models can be used efficiently to improve the estimates canopy transmittance at different viewing angles, combining them with an efficient parameterization of higher-order canopy clumping can yield a powerful and computer-efficient tool for interpreting remotely sensed data obtained over the boreal zone.

## REFERENCES

Knyazikhin, Y., Kranigk, J., Myneni, R., Panferov, O. and Gravenhorst, G. (1998a). Influence of small-scale structure on radiative transfer and photosynthesis in vegetation cover. Journal of Geophysical Research, D103, 6133-6144.

Knyazikhin, Y., Martonchik, J., Myneni, R., Diner, D. and Running, S. (1998b). Synergistic algorithm for estimating vegetation canopy leaf area index and fraction of absorbed photosynthetically active radiation from MODIS and MISR data. Journal of Geophysical Research, D103, 32 257 – 32 276.

Kuusk, A., and Nilson, T. (2000). A directional multispectral forest reflectance model. Remote Sensing of Environment, 72, 244 – 252.

Mõttus, M., Stenberg, P., Rautiainen, M. (2006). Photon recollision probability in heterogeneous forest canopies. Submitted manuscript.

Panferov, O., Knyazikhin, Y., Myneni, R., Szarzynski, J., Engwald, S., Schnitzler, K. and Gravenhorst, G. (2001). The role of canopy structure in the spectral variation of transmission and absorption of solar radiation in vegetation canopies. IEEE Transactions on Geoscience and Remote Sensing, 39, 241-253.

Rautiainen, M. and Stenberg, P. (2005). Application of photon recollision probability in coniferous canopy reflectance simulations. Remote Sensing of Environment, 96, 98-107.

Rautiainen, M., Stenberg, P., Nilson, T. and Kuusk, A. (2004). The effect of crown shape on the reflectance of coniferous stands. Remote Sensing of Environment, 89: 41-52.

Rautiainen, M. and Stenberg, P. (2005). Application of photon recollision probability in coniferous canopy reflectance simulations. Remote Sensing of Environment, 96: 98-107.

Shabanov, N., Wang, Y., Buermann, W., Dong, J., Hoffman, S., Smith, G., Tian, Y., Knyazikhin, Y. & Myneni, R. (2003). Effect of foliage spatial heterogeneity in the MODIS LAI and FPAR algorithm over broadleaf forests. Remote Sensing of Environment, 85(4), 410-423.

Smolander, S. and Stenberg, P. (2005). Simple parameterizations for the radiation budget of uniform broadleaved and coniferous canopies. Remote Sensing of Environment, 94, 355-363.

Wang, Y., Buermann, W., Stenberg, P., Smolander, H., Häme, T., Tian, Y., Hu, J., Knyazikhin, Y., and Myneni, R. (2003). A new parameterization of canopy spectral response to incident solar radiation: case study with hyperspectral data from pine dominant forest. Remote Sensing of Environment, 85, 304-315.

# ASSESSMENT ON THE INFLUENCE OF FLYING HEIGHT AND SCAN ANGLE ON BIOPHYSICAL VEGETATION PRODUCTS DERIVED FROM AIRBORNE LASER SCANNING

*Felix Morsdorf[1], Othmar Frey[1], Erich Meier[1], Klaus I. Itten[1], Britta Allgöwer[2]*

[1] University of Zürich, Remote Sensing Laboratories, Department of Geography, Zürich, Switzerland; morsdorf@geo.unizh.ch

[2] University of Zürich, Geographic Information Sciences, Department of Geography, Zürich, Switzerland.

## ABSTRACT

Airborne Laser Scanning (ALS) has been established as a valuable tool for the estimation of biophysical vegetation properties such as tree height, crown width, fractional cover and leaf area index (LAI). It is expected that the conditions of data acquisition, such as viewing geometry and sensor configuration influence the value of these parameters. In order to gain knowledge about these different conditions, we test for the sensitivity of vegetation products for viewing geometry, namely flying altitude and scanning (incidence) angle. Based on two methodologies for single tree extraction and derivation of fractional cover and LAI previously developed and published by our group, we evaluate how these variables change with either flying altitude and scanning angle. These are the two parameters which often need to be optimised towards the best compromise between point density and area covered with a single flight line. Our testsite in the Swiss National Park was overflown with two nominal flying altitudes, 500 and 900 m above ground. Incidence angle and local incidence angle were computed based on the digital terrain model using a simple backward geocoding procedure. We divided the raw laser returns into several different incident angle classes based on the flight path data; the TopoSys Falcon II system used in this study has a maximum scan angle of ±7.15º. We compare the derived biophysical properties from each of these classes with field measurements based on tachymeter measurements and hemispherical photographs, which were geolocated using differential GPS. It was found that with increasing flying height the well-known underestimation of tree height increases. A similar behavior can be observed for fractional cover; its respective values decrease with higher flying height. The behavior for incidence angles is not so evident, probably due to the small scanning angle of the system used. LAI seems to be most affected by incidence angles, with higher values for locations further away from nadir. Incidence angle seems to be of higher importance for vegetation density parameters than local incidence angle. We conclude that a more detailed knowlegde of beam-canopy interaction is needed, be it through empirical test such as ours or through using numerical models such as ray tracers.

**Keywords:** incidence angle, flight altitude, LAI, tree height, fractional cover

## 1 INTRODUCTION

In recent years, Airborne Laser Scanning (ALS) was established as a valuable tool for the horizontal and vertical characterization of the canopy. A number of studies prove ALS to be capable of deriving canopy height, be it for stands or single trees. Furthermore, ALS was used to derive measures of vegetation density such as fractional cover (fCover) or leaf area index (LAI). Tree height and crown width are mostly directly computed from either a gridded canopy height model (CHM) or the point cloud itself, whereas approaches deriving fCover and LAI most often use regression models to link ground measurements with laser predictor variables. These products comprise site and instrument specific properties, such as different sensor types, vegetation types and viewing geometry. This makes the comparison of results from different sites and sensor configurations hard, if not impossible. For instance, it is expected that scan angle and flying height have an influence on the magnitude of these parameters. Some research has already been pointing in this direction. A study of Yu et. al. (2004) showed that tree height underestimation was larger for higher flying heights, as well as that fewer trees were detected the higher the flying altitude was. Ahokas (2005) showed that tree height estimations would vary to some extent with scan angle. It is expected that especially estimations of vegetation density will be influenced by variations of incidence angle, since the distance the laser pulse travels through the canopy will increase with scanning angle. One has to discriminate between the local incidence angle and the incidence angle. **Loca**l incidence angle is the angle between the slope of a surface (e.g. of a gridded height model) and the laser beam, while the incidence angle is the angle between the horizontal plane going through a point of a gridded height model and the laser beam. We expect the latter to have a larger influence on vegetation density estimations by ALS, while the local incidence angle will most likely have a larger influence on the accuracy of terrain height estimation, and thus on tree height estimation. Our objective is to study this effect empirically by computing incidence and local incidence angles for each flight strip and to assign differences between ALS estimates and field measurements for fCover, LAI and tree height to different angle classes of both incidence and local incidence angles.

## 2 LASER DATA

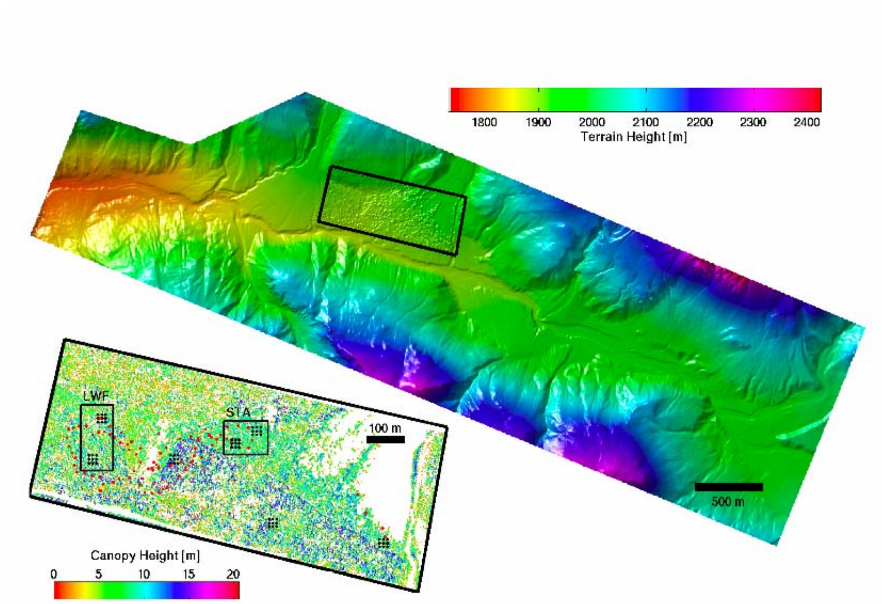


*Figure 1: The Digital Terrain Model (DTM) of the Ofenpass area in the Swiss National Park. The smaller area marked by the black box was sampled with higher point density due to the lower flying height of 500 m above ground. A canopy height map of that area is displayed in the lower left. Black dots mark positions of hemispherical photographs that were taken in 2002 using a handheld GPS for georeferencing. Red dots indicate positions were hemispherical photographs were taken using differential GPS for georeferencing (2005).*

In October 2002, a helicopter based ALS flight was carried out over the test area, covering a total area of about 14 km$^2$. The ALS system used was the Falcon II Sensor developed and maintained by TopoSys.The system is a fibre-array laser altimeter recording both first and last intensity peaks from the laser return signal (first/last echo **FE**/**LE**) with a fixed scan angle of ±7.15 degrees.

A flight of higher altitude was conducted with a nominal height over ground of 900 m, leading to an average point density of more than 5 points per square meter. A smaller subset of the area (0.6 km$^2$) was overflown with a height of 500 m above ground, resulting in a point density of about 10 point per square meter in each flight strip. The footprint sizes were about 0.9 m in diameter for 900 m flight altitude and about 0.5 m in diameter for 500 m altitude. The raw data delivered by the sensor (x,y,z - triples) was processed into gridded elevation models by TopoSys using the company's own processing software TopPIT. The Digital Surface Model (DSM) was processed using the first pulse reflections, the Digital Terrain Model (DTM) was constructed using the last returns and filtering algorithms. The grid spacing was 1 m for the large area and 0.5 m for the smaller one, with a height resolution of 0.1 m in both cases. A quality analysis of the raw data was done using six artificial reference targets and is described in detail in Morsdorf et al. (2004). The standard deviations of height estimates based on raw echos on these targets were as low as 6 cm, with the internal accuracy of the ALS data being well below the pixel size, which is 0.5 m.

# 3 METHODS

## 3.1 Field measurements

We took hemispherical photographs as field samples using a Nikon Coolpix 4500 with a fish-eye lens. The small plot in Figure 1 shows a canopy height model (CHM) of the area over flown with the lower altitude. Black dots indicate positions where hemispherical photographs were taken in 2002. In 2005, another data collection was carried out at locations marked by red dots. In 2005, a total of 83 hemispherical photographs were taken, and the location of each image was estimated by differential GPS measurements. We used three Trimble GPS receivers (one 5700 receiver and two 4700 receiver types) stations for GPS measurements. The GPS was utilized using varying occupation times according to satellite availability. GPS RMS achieved was in the range of 0.5 to 5.4 centimeters with a mean of 1.84 centimeters. For tree heights, a dataset of about 2000 dominant and subdominant tree locations was provided by the Swiss Institut for Snow and Landscape Research (WSL). The dataset included tree height and crown diameter for each tree. We only used the dominant trees for our statistics, since tree clumping is a major issue in the study area and we were only interested in tree height understimation and not in the number of correctly identified trees. Dominant trees were selected from groups of trees in a radius of 1.5 meter as the tallest tree of that group. Out of originally 1984 trees, 1138 were selected as being dominant.

## 3.2 Derivation of geophysical properties

We derived tree height, fractional cover (fCover) and leaf area index (LAI) for each of the flight tracks separately. For the estimation of the tree heights, we used the single tree extraction algorithm presented in Morsdorf et al. (2004). This approach uses local maxima extracted from a Digital Surface Model (DSM) as seedpoints for a clustering algorithm being applied to the raw data. Thus, for each flight strip we computed a DSM using only returns from the respective flight track. The raw laser echo heights were transformed into vegetation height by subtracting interpolated terrain heights from the DTM Toposys provided for the lower overflight. fCover and LAI were computed directly from the laser returns, without the need of utilizing a DSM, as presented in Morsdorf et al. (2005). The algorithms include the computation of echo ratios (e.g. number of vegetation echos divided by number of total echos for fCover) for defined areas containing the raw data. We set up a grid of two meter resolution for both fCover and LAI computation. Again, for each flight track a single grid of these two parameters was computed. For both LAI and fCover, we used regression models derived from all data from the lower overflight. The regression models were used as they are presented in Morsdorf et al. (2005).

## 3.3 Computation of the incidence angle

Toposys provided us with the original flight path data, including sensor location and sensor attitude at a sampling rate of about 200 Hz. We used this information together with the DTM of the lower flight to reconstruct the viewing geometry for each of the selected flight tracks. A simple backward geocoding algorithm was implemented for the computation of the incidence angle and the local incidence angle for each pixel of the DTM. For the lower overflight, a total number of five flight tracks were used to compute the incidence angle of the laser beam for every pixel of a ALS-derived DTM, while for the higher overflight only three flight strips were necessary to cover the area of the DTM. These angles were then used to classify differences between ALS estimates of fCover, LAI and tree height into different angle classes. For each of these angle bins being one degree wide, mean and standard deviation of the differences were computed.

# 4 RESULTS

Figure 2 shows the differences of fCover and LAI estimations for different angular classes of incidence angles from flight tracks being 500 m above ground level (AGL). Figure 2 a shows the difference of fCover (upper panel) and LAI (lower panel) between ALS based estimations and field measurements. One can note that there is no significant increase of differences for both fCover and LAI towards smaller incidence angles (meaning larger scan angles). The standard deviations are much larger than the differences itself, being between 30 and 50 % for fCover and between 0.2 and 0.6 for LAI, while the differences are in the range of -10 to 20 % for fCover and -0.3 and 0.2 for LAI. Values at the smallest incidence angles (80-82 degrees) should be taken with caution, since only few samples contribute to the estimates. Figure 2 b shows the relative difference of the fCover and LAI estimations from all the data compared with the largest incidence angle (smallest scan angle). This comparison is based on the assumption that the values of fCover and LAI are distributed in each class in the same way. One can note that there is no increase of fCover towards smaller incidence angles, but a slight increase of LAI of about 30 % towards incidence of about 80 degrees. The standard deviations are again large, thus this increase of LAI might only be a hint, but not a proof of an angular influence on the computation of LAI. Tree height did not show any angular behavior in the small range of incidence angles we computed, and thus, we do not show it here. It is expected that the accuracy of ALS based tree height derivation might be influenced by terrain slope, but since we did not compute a DTM for each flight strip, we could not single out this effect.

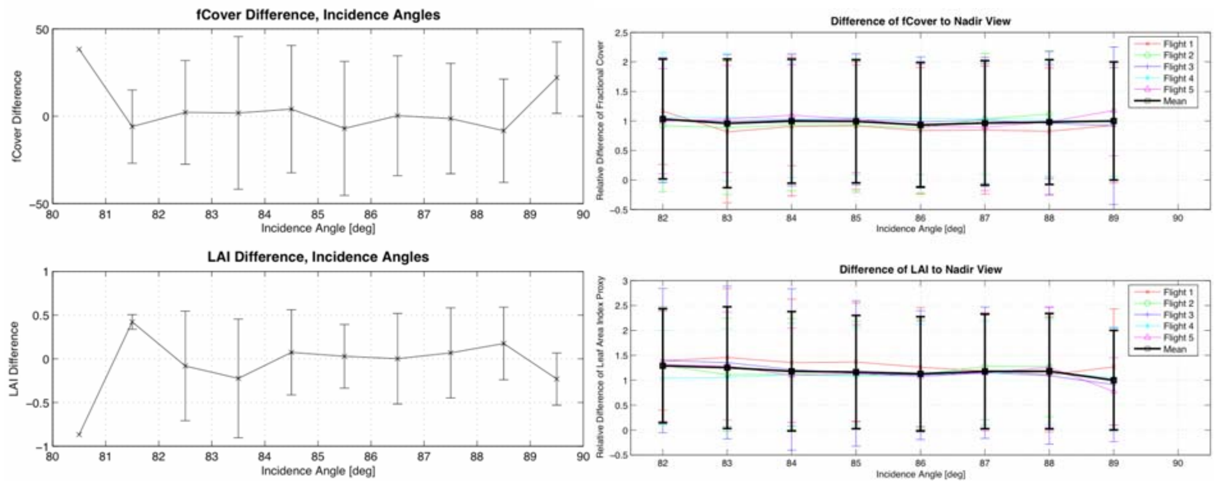


*Figure 2 a and b: Difference of fCover and LAI for each incidence angle class at 500 m above ground level (AGL). Vertical bars indicate the standard deviation for each class, while the star marks the mean value. Left figure displays differences with field measurements, right figure displays differences solely based on ALS data, assuming spatial homogeneity of both fCover and LAI in each angle class.*

Table 1 contains the differences between fCover LAI and tree height due to change of flight altitude. For each flight altitude, we computed the difference of field estimates and ALS based estimates using data from all angle classes. fCover is overestimated by ALS at 500 m AGL, while values derived from data acquired with 900 m AGL underestimates absolute fCover values by about 10 %. Thus, one can state that ALS based estimates of fCover will decrease with flying height. LAI shows a different behavior, with a small underestimation by ALS at 500 m AGL (-0.06 and -0.18 for mean and median), but a larger overestimation for 900 m AGL with a mean of 0.29 and a median of 0.18. The standard deviation is large for both fCover (33.7 / 30.7) and LAI (0.56 / 0.63) and is not much influenced by flying altitude. For tree height, we find a small underestimation of field values by ALS for 500 m AGL (-0.38 m mean and -0.05 m median), which is getting larger for 900 m AGL with a mean underestimation of 0.69 m, while the median difference is at -0.29. The standard deviation is only a little larger for 900 m AGL, being 1.49 m, while the standard deviation at 500 m is 1.39 m.

*Table 1: Differences between ALS estimates and field measurements for fCover, LAI and tree height. The mean, median, standard deviation and number of samples are given for each property and flying altitude. Negative values denote underestimation by ALS.*

| Absolute difference: ALS estimates - field measurements | Mean | Median | Std. Deviation | Samples |
|---|---|---|---|---|
| fCover 500 m AGL [%] | 1.21 | 10.7 | 33.7 | 139 |
| fCover 900 m AGL [%] | -10.2 | -8.3 | 30.7 | 166 |
| LAI 500 m AGL | -0.06 | -0.18 | 0.56 | 156 |
| LAI 900 m AGL | 0.29 | 0.18 | 0.63 | 177 |
| Tree Height 500 m AGL [m] | -0.38 | -0.05 | 1.39 | 658 |
| Tree Height 900 m AGL [m] | -0.69 | -0.29 | 1.49 | 485 |

## 5 DISCUSSION AND CONCLUSIONS

Using flight path data and sensor attitude together with field measurements of biophysical properties, we studied the influence of incidence angle and flying height on fCover, LAI and tree height. Probably due to the small scan angle (±7.15 degrees) of the system used, we could not find significant differences of ALS based estimates of fCover and tree height for different incidence angle classes. This is backed by the results from Ahokas et al. (2005), who found significant differences only for scan angles larger than 15 degrees. LAI estimates showed a small increase of values for larger incidence angles, but further studies are needed to test whether this finding is robust. Flight altitude dependencies were much more evident in our data. Tree height underestimation by ALS increased from 500 to 900 m flying altitude by about 30 cm, which is in good agreement with previous findings. ALS based LAI estimates were overestimating true LAI for the higher overflight by about 0.2, opposed to underestimation at 500 m AGL. ALS based fCover estimates decreasd with flying altitude by about 10 %. It should be noted that the errors of the biophysical parameters are still in a tolerable range at 900 m AGL, and that flying at 500 m does not improve that much on the differences. Yu et.al. (2004) made similar observations in a study using three flight altitudes (500,900 and 1500 m AGL), the quality of the ALS based data dropped only significantly when changing from 900 m AGL to 1500 m AGL. In order to study further the effect of scan angle on vegetation density products, we propose using ALS data acquired using larger scan angles. This is especially necessary, as for smaller scanning angles errors induced by field measurements are probably in the same order of magnitude as the variations induced by scan angle changes. Furthermore, it might be helpful to utilize radiative transfer models such as the ones which are commonly used in the passive optical remote sensing community. These should enable one to simulate individually the effects of acquisition properties such as incidence angle, point density, terrain slope, laser footprint size, laser wavelength and canopy reflectance on the accuracy of biophysical vegetation data products opposed to real-world scenarios, where all these effects contribute indifferently to differences between ground truth and ALS based estimations of biophysical parameters.

## REFERENCES

Naesset, E., Effects of different flying altitudes on biophysical stand properties estimated from canopy height and density measured with a small-footprint airborne scanning laser. Remote Sensing of Environment, 2004 , 91 , 243-255

Ahokas, E.; Yu, X.; Oksanen, J.; Hyyppae, J.; Kaartinen, H. & Hyyppae, H., Optimization of the scanning angle for countrywide laser scanning, International Archives of Photogrammetry, Remote Sensing and Spatial Information Sciences, 2005 , VOLUME XXXVI, PART 3/W19

Gaveau, D. & Hill, R., Quantifying canopy height underestimation by laser pulse penetration in small-footprint airborne laser scanning data. Canadian Journal of Remote Sensing, 2003 , 29 , 650-657

Morsdorf, F.; Koetz, B.; Meier, E.; Itten, K. & Allgöwer, B., The potential of discrete return, small footprint airborne laser scanning data for vegetation density estimation, International Archives of Photogrammetry, Remote Sensing and Spatial Information Sciences, 2005 , VOLUME XXXVI, PART 3/W19

Morsdorf, F.; Meier, E.; Kötz, B.; Itten, K.I.; Dobbertin, M. & Allgöwer, B., LIDAR-based geometric reconstruction of boreal type forest stands at single tree level for forest and wildland fire management, Remote Sensing of Environment, 2004 , 3 , 353-362

Yu, X.; Hyyppae, J.; Hyyppae, H. & Maltamo, M., Effects of flight altitude on tree height estimation using airborne laser scanning International Archives of Photogrammetry, Remote Sensing and Spatial Information Sciences, 2004 , VOLUME XXXVI, PART 8/W2 , 96-101

# PROCESS ORIENTED OBJECT-BASED ALGORITHMS FOR SINGLE TREE DETECTION USING LASER SCANNING

*Dirk Tiede[1], Christian Hoffmann[2]*

[1] University of Salzburg, Centre for Geoinformatics (Z_GIS), Salzburg, Austria; dirk.tiede@sbg.ac.at

[2] Definiens AG, Munich, Germany; choffmann@definiens.com

## ABSTRACT

This research details the development and testing of new object-based algorithms for individual tree crown delineation using the commercial object-based image intelligence software Definiens eCognition™ (Definiens AG, Munich; http://www.definiens.com). A two-stage algorithm is developed, where single tree crowns are identified by a local maximum detection and consecutively, each tree crown is grown with a region growing algorithm. This was possible due to the new capabilities of eCognition, where single objects created from a multi-resolution segmentation can be broken down to pixel-sized objects and rebuilt to meaningful objects based on local object parameters. The results are promising, especially concerning the problems which occurred in earlier studies on object-based delineation of single trees. However, new possibilities are extending the software package to a sort of modular, process oriented programming language. Consequently the research taken herein can only illuminate a small aspect of the new and complex opportunities in the case of single tree detection.

**Keywords:** LiDAR, object based, Laser scanning, crown delineation, region growing algorithm, tree identification

## 1 INTRODUCTION

Earlier studies on object-based tree detection and accordingly tree crown delineation concluded that one of the biggest problems was the difference between a segmentation algorithm based on homogeneity and the complex, inhomogeneous canopy representations in VHSR (Very high spatial resolution) data (Tiede et al. 2004, Burnett et al. 2003). They assumed that a centre-weighted segmentation algorithm might be better suited to forest applications. The most recent version of Definiens eCognition™ allows to develop scalable algorithms including the use of different segmentation techniques (e.g. chessboard segmentation) is enabled. This provides the chance to overcome the limitations regarding single tree delineation in the object-based image analysis domain.

In this study we used the same datasets as Tiede et al. (2004) to ensure the comparability of the different approaches. The calculations were conducted on six plots in the Bavarian Forest National Park, which represent the three major forest types that are present in the park. In the plots every tree position was measured with an accuracy of centimetres. The TopoSys airborne LiDAR system ("Falcon") was used to survey the test areas.

## 2 MATERIAL AND METHODS

### 2.1 Test Site

The test sites used in this study are located in the Bavarian Forest national park which is located in south eastern Germany along the border with the Czech Republic. There are three major forest types present in the park: mountain spruce forest with *Picea abies* and some *Sorbus aucuparia* above 1100 m, submontane mixed forest with *Picea abies*, *Abies alba*, *Fagus sylvatica* and *Acer pseudoplatanus* on the slopes between 600 and 1100 m and spruce forest in moist depressions in the valleys where cold air may collect. Much of the mountain spruce stands were severely attacked by the spruce bark beetle (*Ips typographus*) in the 1990s.

## 2.2 Data

To capture some of the different canopy characteristics, six plots were chosen from a set of 44 reference sites. For a more detailed overview about the study area and the datasets used herein see Heurich et al. (2003) and Tiede et al. (2005).The size of the test plots varied from 20 by 50 to 20 by 100 meters. Field measurements for each plot were available including tree positions at the ground with an accuracy of several centimetres.

Laser scanning data for each plot were recorded by the airborne LiDAR system ”Falcon” from TopoSys GmbH on three dates: leaf-off (March and May, 2002) and leaf-on (September 2002). For further details about the TopoSys System see Wehr and Lohr (1999) and Schnadt and Katzenbeisser (2004). The average point density for these flights was 10pts/m², collecting first and last pulse data. The datasets were processed and classified using TopPit (TopoSys Processing and Imaging Tool) software to interpolate a Digital Surface Model (DSM) and a Digital Terrain Model (DTM). The work in this study was done using a Digital Crown Model (DCM) - derived by a subtraction of DSM and DTM - with a ground resolution of 0.5 m.

The visual accuracy assessment of the tree crown delineation was carried out by using additional image data. The image data was recorded with the line scanner camera of TopoSys simultaneous to the LiDAR range measurements. The camera provides 4 bands: B (440-490 nm), G (500-580 nm), R (580-660 nm) and NIR (770-890 nm). Ground resolution was also 0.5 meters.

## 2.3 Algorithms

Figure 1 gives an overview about the workflow and the algorithms used in this study. The individual algorithms were programmed in Definiens’ Cognition Network Language (CNL) where single algorithms form a complete ruleware, which is available for automated information extraction in a high –throughput environment.

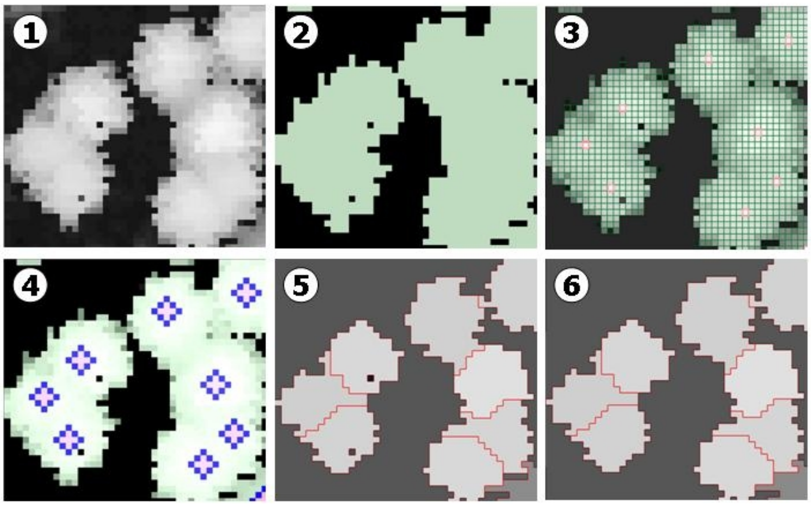

*Figure 1: Workflow for single tree crown delineation: (1) Digital Crown Model (DCM); (2) Segmentation and pre-classification of tree / non-tree objects (3) Break down of pre-classified tree objects to small objects and extraction of local maxima (4) Rebuilding of meaningful objects by using a region growing algorithm (local maxima acting as “seed” points) (5) Extracted single tree crowns - holes are caused by the laser scanning data basis (cf. picture 1) (6) ”Cleaning” of the single tree crown objects using neighbourship information.*

### 2.3.1 Pre-classification

For a coarse pre-classification a multiresolution segmentation was applied and the objects were classified in two classes to differentiate between ground and tree area (non-tree / tree areas - here defined as below / above 5 metres in height). The concept of using an image object domain allows focusing in the following steps on the pre-classified tree crowns. This leads to a performance gain, because more complex algorithms can be limited to sub areas of the dataset.

### 2.3.2 Local maxima detection

Single objects created from the multi-resolution segmentation can be broken down to small objects and rebuild to meaningful objects based on local object parameters. This is done here by segmenting only objects which were classified as potential tree crowns in the pre-classification step. The objects are broken down to pixel-sized objects, by using a so called chessboard segmentation with a minimal object size (= 1 pixel). This has to be done to find local maxima – assumed tree tops – in a subsequent step. At the moment, the search radius for the local maxima extraction has to be adapted manually for different forest stand types. In this case a smaller search radius was used for coniferous forests whereas in deciduous dominated forest types, a bigger search radius seemed to be better suited.

### 2.3.3 Object-growing

The local maxima are used as “seed” points to build up new meaningful objects, representing single tree crowns. eCognition provides the possibility to construct looping process structures similar to a modular programming language. Variables can be used to implement stopping criteria and to coordinate object growth.

An approach of simultaneous object-growing was used, providing a more accurate separation of the extracted crowns instead of treating the objects sequentially. For the growing tree crowns only candidate neighbouring objects are taken into account, if the difference in height between the regarded objects does not exceed a certain limit.

An additional stopping criterion for the region growing algorithm is a maximal crown width parameter. This should avoid uncontrolled growing of tree crown objects into other tree crowns, which might happen, if a local maximum was not recognized correctly: this was mainly the case in dense deciduous stand types due to very planar tree surface or missing tree top representations in the laser scanning data. The growing limit resulted in a more accurate delineation of the tree crowns, but accepted the fact, that some trees were not taken into account. Because of the small amount of affected cases this was acceptable.

### 2.3.4 Object “cleaning”

Due to limitations of the laser scanning datasets the resulting tree crown objects partly contain holes or empty spaces, which are not intended. A subsequent “cleaning” process was applied to classify these holes according to the surrounding objects. Because the objects have specific attributes and mutual relations, an algorithm (“find enclosed by”) can be used to find all holes which are surrounded by a tree crown image object. These holes can than be classified and fused with the target object.

## 3 RESULTS

The accuracy assessment for the delineation of the tree crowns was carried out only visually, due to the fact that reference data of measured tree crowns was not available as well as the lack of object-based accuracy assessment techniques (cf. chapter 5). A first qualitative visual accuracy assessment with image data of the TopoSys line scanner camera shows promising results. Figure 2 shows the results for a well spaced matured spruce forest; Figures 3 is an example of a deciduous forest type.

An accuracy assessment for the local maxima method is shown in Table 1. Obviously a local maxima method is best suited to find dominant trees (cf. Maltamo et al., 2004 and Pitkänen, 2001), hence the accuracy assessment is conducted only for this type. A conservative calibrated search radius was utilised to find the local maxima, which normally leads to a rather underestimation of trees but also to a smaller amount of false positives. Best results were reached in well spaced conditions with a detection rate of more than 91% for dominant trees. In less spaced forest stands (22, 57 and 60) the identification rates are dropping noticeably (75%, 70.5% and 66.7%). The average detection rate of dominant trees for all plots is almost 81% with a quite low error of commission (false positives) of approx. 3%.

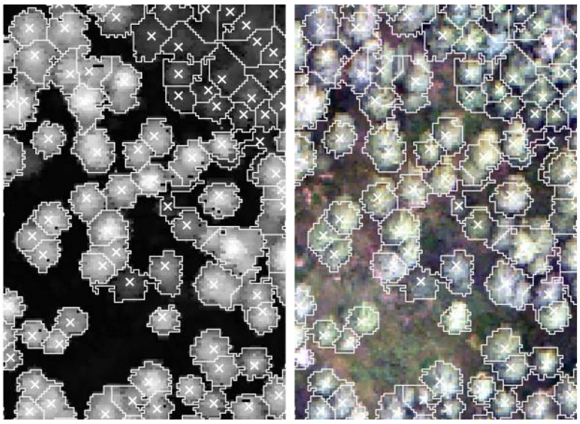

*Figure 2: Tree crown delineation for a well spaced mature spruce forest type with underlying LiDAR data (left) and image data (right). Local maxima are marked by white crosses.*

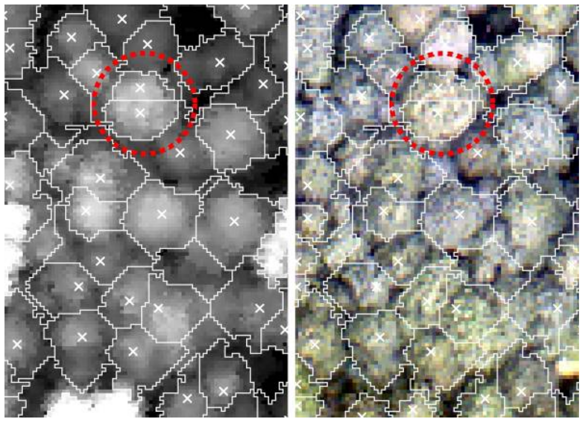

*Figure 3: Tree crown delineation for a mature deciduous forest type with underlying LiDAR data (left) and image data (right). Dashed line indicates wrongly delineated double tree crown. Local maxima are marked by white crosses.*

*Table 1: Accuracy assessment of the local maximum calculation for the six test plots (only dominant trees are taken into account). The numbering of the plots is an internal code used by the Bavarian Forest national park.*

| Sample plot | Field measurements | Local maximum calculation | | % of found dominant trees |
|---|---|---|---|---|
| | Dominant trees | Dominant trees | False positives | |
| **Plot 22:** mature mixed forest | 32 | 24 | 0 | 75.0 |
| **Plot 50:** sub-alpine well spaced mature spruce | 43 | 35 | 1 | 81.4 |
| **Plot 57:** mature spruce | 44 | 31 | 0 | 70.5 |
| **Plot 59:** juvenile spruce | 79 | 72 | 4 | 91.1 |
| **Plot 60:** mature beech | 30 | 20 | 1 | 66.7 |
| **Plot 64:** mature beech | 38 | 33 | 3 | 86.8 |
| **Sum of all plots** | 266 | 215 | 9 | 80.8 |

## 4 DISCUSSION

The results for single tree crown delineation are strongly linked to the results of the local maxima extraction. They vary between the different forest types and are also depending on the selected search radius; whereby a smaller radius is increasing the hit rate but also the false positives. Problems occurred mainly in dense deciduous forest stands. The local maxima method used to find "seed" points partially failed when the shape of the tree crowns tended to be rather flat than conical. This sometimes lead to non-recognised tree crowns or doubles. Another problem encountered, is that the delineated objects are sometimes not compact enough or grow to next located areas. The use of a growing limit (crown width limit) could not solve the problem completely. Therefore the use of an object shape parameter is considered. For example the use of a feature reflecting the shape of the object ("shape index") could contribute to control the object growing to get even more compact tree crown objects.

## 5 CONCLUSIONS

The results are promising, especially concerning the problems which occurred in earlier studies on object-based delineation of single trees. The disadvantages of a segmentation algorithm based on homogeneity concerning the detection of non-homogeneous objects have been overcome by the new user selectable and customizable processes. But the delineation of tree crowns should not be an end in itself. It should be a starting point for subsequent work concerning:

- Single tree classification on a species level, using additional information (e.g. image data or raw LiDAR point data)
- Deriving a type of 3D metrics from raw LiDAR point data using the delineated tree crowns to provide a 3D forest structure on a single tree level (cf. Blaschke 2004 and Tiede 2005)

One problem still remains: “Classic” accuracy assessment techniques from pixel-based remote sensing are not fully satisfying for quantifying the accuracy of delineated tree crowns (cf. Blaschke, 2005). Currently, additional studies are being conducted to include an object-based accuracy assessment to compare automatically delineated crowns and manually delineated crowns by an interpreter with the help of a new tool called LIST (Lang et al., in press).

Another future goal is to build an automated system, where in a first step - on a higher level – forest stand types will be delineated and separate modules for each stand type will be implemented. This should solve the problem that the ruleware has to be manually adapted for different stand types.

New possibilities are extending the eCognition software package to a modular, process oriented programming language. Consequently the research taken herein can only illuminate a small aspect of the new and complex opportunities for the case of single tree detection.

## ACKNOWLEDGEMENTS

We would like to thank the administration of the Bavarian Forest national park for the provision of the data used in this study.

## REFERENCES

Blaschke, T., 2005. A framework for change detection based on image objects. In: Erasmi, S., Cyffka, B., Kappas, M. (Eds.) Göttinger Geographische Abhandlungen, Vol. 113, Göttingen, pp. 1-9.

Blaschke T., Tiede, D. and Heurich, M. (2004). 3D landscape metrics to modelling forest structure and diversity based on laser scanning data. The International Archives of Photogrammetry, Remote Sensing and Spatial Information Sciences, vol. XXXVI-8/W2, Freiburg, Germany, pp. 129-132.

Burnett, C., Heurich, M. and Tiede, D. (2003). Exploring Segmentation-based Mapping of Tree Crowns: Experiences with the Bavarian Forest NP Lidar/Digital Image Dataset. Poster presented at ScandLaser 2003 International Conference and Workshop, Umeå , Sweden, September 2-4, 2003.

Heurich, M., Schneider T., Kennel E. (2003). Laser Scanning for Identification of Forest Structures in the Bavarian Forest National Park. In: Hyyppä, Naesset, Olsson, Pahlen, Reese (eds.) Proceedings Scandlaser Scientific Workshop on Airborne Laser Scanning of Forests. pp. 97-106.

Lang, S., Schöpfer, E., Langanke T. (in press). Combined object-based classification and manual interpretation – Synergies for a quantitative assessment of parcels and biotopes. Geocarto International.

Maltamo, M., Mustonen, K., Hyyppä, J., Pitkänen, J., Yu, X. (2004). The accuracy of estimating individual tree variables with airborne laser scanning in boreal nature reserve. Canadian Journal of Forest Research, 34, pp.1791-1801

Pitkänen, J., (2001). Individual tree detection in digital aerial images by combining locally adaptive binarization and local maximal methods. Canadian Journal of Forest Research, 31, pp. 832-844.

Schnadt, K., Katzenbeisser, R. (2004). Unique airborne fiber scanner technique for application-oriented LiDAR products. International Archives of Photogrammetry, Remote Sensing and Spatial Information Sciences, vol. XXXVI-8W2, Freiburg, Germany, pp. 19-24

Tiede, D., Burnett, C. and Heurich, M. (2004). Objekt-basierte Analyse von Laserscanner- und Multispektraldaten zur Einzelbaumdelinierung im Nationalpark Bayerischer Wald. In: S. Strobl, T. Blaschke, G. Griesebner (Hrsg.), Angewandte Geoinformatik 2004, Wichmann Verlag, Heidelberg, Germany, pp. 690–695.

Tiede, D., Hochleitner, G. and Blaschke, T. (2005). A full GIS-based workflow for tree identification and delineation using laser scanning. The International Archives of Photogrammetry, Remote Sensing and Spatial Information Sciences. Vol. XXXVI, Part 3/W24, Vienna, Austria, pp. 9 - 14

Wehr, A., Lohr, U. (1999). Airborne Laser scanning - an introduction and overview. ISPRS Journal of Photogrammtry & Remote Sensing, 54, pp. 68-82

# ESTIMATION OF TREE SIZE DISTRIBUTIONS BY COMBINING VERTICAL AND HORIZONTAL DISTRIBUTION OF LASER MEASUREMENTS WITH EXTRACTION OF INDIVIDUAL TREES

*Johan Holmgren and Jörgen Wallerman*

Swedish University of Agricultural Sciences, Department of Forest Resource Management and Geomatics, Umeå, Sweden; Johan.Holmgren@resgeom.slu.se, Jorgen.Wallerman@resgeom.slu.se

## ABSTRACT

Information about diameter distributions is important for estimation of the harvest outcome of timber and pulpwood from final felling areas. Several algorithms for tree detection using LIDAR data are available to find local maxima of a digital surface model (DSM) or a canopy height model. In this study, we applied a different approach by using a segmentation algorithm based on template matching. A correlation surface was first created by setting the value of the best template fit at a pixel location. Seeds were then placed at each pixel with DSM values above a threshold and they climbed on the correlation surface to the neighbour pixel with largest slope until a local maximum was reached. Pixels that climbed to the same maximum formed a tree crown segment. The performance of the tree detection is dependent on forest structure, thus statistical analysis is needed to relate tree detection results to true tree size distributions. Here, a new laser measure, the semivariogram, is applied with the aim to summarize the spatial as well as the non-spatial variation of the forest. Results from the tree detection, the semivariogram, and measures of the distribution of laser canopy heights were used as input for modelling stem diameter distribution and tree height distribution. The stem diameter and tree height distributions were estimated using the Seemingly Unrelated REgression (SURE) framework. Also, regression modelling of Weibull distribution parameters was evaluated.

**Keywords:** template matching, crown segmentation, stem diameter, tree height

## 1 INTRODUCTION

Several important forest management planning applications are dependent on information about the stem diameter distribution of forest stands. Accurate information on stem diameter distribution is useful to predict harvest outcome in terms of pulpwood and saw timber proportions, to optimize the selection of forest stands for harvesting given the market demands, and to forecast growth and evaluate alternative treatments using single-tree based models in the next generation of forest management planning systems (e.g., the Heureka project; http://heureka.slu.se).

Within several studies, stem diameter distributions have been estimated for forest stands using various statistical methods as well as various sources of explanatory data. Kangas and Maltamo (2000) used stand registry data to estimate diameter distribution, and compared two different methods: regression of Weibull parameters, and the percentile method presented by Borders et al. (1987). Application of Weibull parameter regression is based on the assumption that a general shape of the diameter distribution approximately follows a Weibull distribution function. The shape and location parameter of the Weibull distribution function are modelled by regression using independent data. Alternatively, the percentile method of Borders et al. (1987) is applied where no assumption of a specific shape of the distribution function is needed. Instead, each percentile is modelled using a separate regression model. That is, a system of regression models is fitted to the data, using the Seemingly Unrelated REgression framework (SURE). This framework provides optimal and simultaneous parameter estimation and significance tests, and also takes dependency in residuals between models into consideration. Kangas and Maltamo (2000) conclude that the percentile method is preferred, since it can easily model multimodal distributions which occur in forest data.

LIDAR data having both low (one meter or more between measurements) and high resolution (several measurements per square meter) have been used for estimation of stem diameter distributions. Gobakken and Næsset (2004) used low resolution LIDAR data (one measurement per square meter) to derive several variables, and then used these as independent variables for regression models. Maltamo et al. (2004) used high resolution LIDAR data (10 measurements per square meter) for tree detection and then used the results of the tree detection as input to statistical models. In this study, we used data with approximately seven laser measurements per square meter, and combined several measures derived from LIDAR height data with the result from tree detection in order to model stem diameter distribution. Automatic tree detection provides high accuracy estimates of single tree heights, crown diameters, and spatial patterns of tree positions information that is potentially valuable for modelling stem diameter distribution. In this study, we test a new segmentation method, based on template matching, for tree detection. The accuracy of the height measurements for detected trees is high (e.g., Hyyppä and Inkinen, 1999; Hyyppä et al., 2001), but the proportion detected trees is dependent on forest structure (e.g., Persson et al., 2002). Therefore, the results from the single tree detection should be combined with other measures related to forest structure. Usually, measures applied do not utilize the spatial properties of LIDAR data; information such as strength and structures of spatial dependence are ignored. One alternative to incorporate such information may be provided by the spatial statistic semivariogram (Cressie, 1993; Goovaerts, 1997).

The aim of this work is to evaluate the information content in a new tree detection algorithm and the semivariogram measure for estimation of stem diameter distributions. Furthermore, identification of additional variables that are efficient for the estimations is also addressed. These information sources are utilized in the percentile method (Borders et al., 1987) as well as in regression modelling of Weibull parameters.

## 2 MATERIAL AND METHODS

### 2.1 Data

Data utilized in this study were collected at the Remningstorp research site (lat. 58°30’N, long. 13°40’E) in the south of Sweden. The estate is privately owned and dominated by Scots pine (*Pinus sylvestris*), Norway spruce (*Picea abies*), and birch (*Betula* spp.).

Field data were collected in 2004 using a systematic grid (40 m spacing) of 10 m radius plots using the methods of the Forest Management Planning Package (FMPP) (Jonsson et al., 1993). This approach includes callipering of all trees on each plot with diameter in breast-height greater than 0.05 m and sub-sampling of trees where tree height is also measured. Height of each callipered tree was estimated using diameter and height relations developed using the sub-sample of trees and the methods of the FMPP. Plots were located on forest land only, based on existing map data, and a total of 849 plots were measured. The geographic position of each plot centre was measured using differentially corrected GPS. Stand boundaries were delineated using manual interpretation of digital aerial photographs viewed in a stereo instrument. Forest stands containing more than 5 field plots, altogether 45 forest stands, were selected for the analysis. For these stands, the average tree density was 867 stems $ha^{-1}$ (286-2475 stems $ha^{-1}$), average stem diameter was 0.20 m (0.10-0.34 m), and average tree height was 16.9 m (8.3-26.5 m).

The laser data were acquired by a laser scanner from TopEye (www.topeye.com), a laser scanning system operated from a helicopter, the 19th of August 2004. The flight altitude was 130 m above ground level, flight speed 16 $ms^{-1}$, scan angle ±20 degrees, and pulsing frequency 7000 Hz. The swath overlap resulted in an average measurement density of 7 measurements per square meter (3 to 16 measurements per square meter). The laser returns were classified as ground or vegetation points by using the TerraScan software (www.terrasolid.fi). Based on the points classified as ground, a Digital Elevation Model (DEM) with 0.25 m resolution was created.

### 2.2 Tree detection

The tree detection method included the following steps: (1) derive a digital surface model, (2) calculate a correlation surface, (3) segmentation based on the correlation surface, and (4) derive tree attributes.

1. A Digital Surface Model (DSM) with 0.25 m raster cells was created by setting each raster cell value to the maximum height of the laser points within the raster cell. Then a normalized DSM (nDSM) was derived as the difference between the DSM and the DEM. A binary image was created with value one where the nDSM had a height value above a threshold (here set to 2 m), otherwise zero. Closing was performed on this image by using a 3x3 structure element; the output image of the closing is referred to as crown area image. A Crown Surface Model (CSM) was created: first, each raster cell value of the CSM was set to the corresponding value of the nDSM if the value was above the threshold, otherwise zero; second, for each raster cell value of the CSM with a zero value but value one for the crown area image, a height value was calculated. This height value was calculated by taking the average of the nDSM values, greater than the threshold, that were within the smallest window needed in order to have at least one value for the average.

2. For each raster cell, different templates were tested and the raster cell value was set to the highest found correlation. The template was a generalized ellipsoid of revolution (Pollock, 1996). Templates were tested for each raster cell if the CSM had a height value greater than zero. The height of the template was set to the value of the corresponding CSM raster cell. Templates with the set height but with different radii were tested. Here, the radius was $R_i$ = 0.5, 0.7, …4.0 m, restricted by the radius- height ratio of the templates (here set to 0.1), i.e., no templates were tested with a corresponding smaller radius. Correlation values were not calculated using less than nine laser points. Both vegetation laser and ground laser points were used for calculation of the correlation between laser data and the template. The resulting Correlation Surface (CS) was then smoothed by using the quartic kernel (Trevor and Anthony, 1995), with a small band width (here set to one meter).

3. Segmentation was performed based on the smoothed CS. One starting point was placed at each raster cell if the raster cell had a correlation value greater than a threshold (here set to zero) and a height value of the CSM greater than a threshold (here set to 2 m). From each starting point, climbing was done to the neighbour pixel with the greatest correlation value until a local maximum was found. The raster cells with starting points climbing to the same maximum defined a segment if the correlation value of this local maximum was greater than a threshold (here set to 0.2).

4. For the segments, tree attributes were derived. The tree height of a segment was set to the maximum value of the CSM within the segment, and tree position was set to the raster cell location of this maximum value. Crown diameter was derived from the segment area assuming that a tree crown is circular.

## 2.3 Semivariogram

The semivariogram originates from the field of spatial statistics (Cressie, 1993; Goovaerts, 1997) and is used to model spatial dependence of a spatial stochastic process. It is a function, $\gamma(\mathbf{h}) = ½\mathrm{Var}\{Y(\mathbf{x}) - Y(\mathbf{x}+\mathbf{h})\}$ (Cressie, 1993), describing the spatial variation of the random variable $Y(.)$ in any two spatial observation locations, $\mathbf{x}_i$ and $\mathbf{x}_j$, as a function of the separation distance $h = |\mathbf{x}_i - \mathbf{x}_j|$. The semivariogram is modelled using point-estimates made by the semivariance estimator (Cressie, 1993),

$$\hat{\gamma}(h_i) = \frac{1}{2N_{h_i}} \sum \left[Y(\mathbf{x}) - Y(\mathbf{x}+\mathbf{h}_i)\right]^2, \; h_i = \left|\mathbf{h}_i\right|, \tag{1}$$

where $N_{hi}$ is the number of pairs of observations on which the estimate for a specific distance $h_i$ is based. Semivariograms were calculated for LIDAR measurements directly as well as the height of detected trees. Here, the exponential semivariogram model $\gamma(h) = \theta_n + \theta_s(1-\exp(-h/\theta_r))$ (Cressie, 1993) was used and fitted to the point estimates. The first parameter, $\theta_n$, the *nugget*, measures the micro-scale variation, the spatial variation occurring at a smaller scale than observed. The sum of $\theta_n$ and $\theta_s$, the *sill*, measures the limit to which the semivariogram increases asymptotically, i.e., the variance, and, $\theta_r$, the *range*, measures the spatial distance at which observations of $Y(.)$ are independent (approximately $3\theta_r$). The spatial ratio ($S_r$) was derived as $S_r = \theta_s / (\theta_n + \theta_s)$, and evaluated as a measure of the spatially dependent fraction of the total variance.

## 2.4 Diameter distribution models

Two methods for modelling and estimation of diameter distributions were investigated. First, Seemingly Unrelated REgression (SURE) (Borders et al., 1987; Kangas and Maltamo, 2000) models were applied. Secondly, an approach based on regression modelling of Weibull distribution parameters (i.e., Maltamo et al., 2000) was used. The SURE approach models selected diameter percentiles by a system of models, allowing residual dependency between the models. The model is

$$y_{ti} = \sum_{j=1}^{Ki} x_{tij}\beta_{ij} + \varepsilon_{ti} \quad (2)$$

where $y_{ti}$ is the $t$'th observation on the $i$'th dependent variable; $x_{tij}$ is the $t$'th observation on the $j$'th independent variable appearing in the $i$'th equation; $\beta_{ij}$ is the coefficient associated with the $x_{tij}$ at each observation; $\varepsilon_{ti}$ is the $t$'th value of the random error associated with the $i$'th equation of the model (Srivastava and Giles, 1987).

The parameters of the two parameter truncated Weibull distribution were estimated based on the field measured stem diameter distributions, resulting in a scale parameter ($b$), and a shape parameter ($c$), and a truncation limit (set to 5 cm). The parameters $b$ and $c$ were estimated separately using linear regression models with various laser derived variables as independent variables.

## 2.5 Evaluation

Several measures derived from LIDAR data were evaluated as independent variables in models for estimating diameter distributions and tree height distributions: the percentiles ($H_{10...100}$), mean ($M_H$), and variance ($S_H$) of LIDAR canopy heights; the percentiles ($T_{10...100}$), mean $M_T$, and variance $S_T$ of detected tree heights. Estimations using field measured mean diameter, $D$, was also validated. Additional independent variables were also derived and were specifically used for regression of Weibull parameters namely, the shape and scale parameter which were calculated based on the distribution of laser canopy heights; tree heights of detected trees; and the crown size of detected trees.

Regression models were developed by selection of significant ($p$<0.05) variables and evaluation of model fit ($R^2$). For selection of models with SURE, all variables to be tested were first included into the model; then the least significant variable was removed and the model refitted, and repeated until all variables were significant. For estimation using the regression of Weibull parameters, the data were modified to only include the top tree layer if a stand had two distinct tree layers. Seven stands were subjectively judged to be two layered by inspection of the stem diameter histograms. For calculation of the error index, cross validation was performed, with the forest stand for which the distribution was to be predicted excluded from the training dataset. The error index was defined as the sum of absolute differences between number of estimated and observed trees for diameter classes divided by the total number of trees.

# 3 RESULTS AND DISCUSSION

There was a higher correlation between percentiles of stem diameter and percentiles of attributes of the detected trees compared with percentiles of canopy heights. This is something that could also be observed for the field measured tree height distribution (Table 1). The correlation with attributes of detected trees would probably increase if higher laser measuring density were used. One reason for the observed low correlation between stem diameter and the lower percentiles of canopy heights could be a large amount of low vegetation in some forest stands. For estimation of stem diameter distributions using SURE, percentiles from the tree detection yielded higher $R^2$ values compared with using percentiles of the laser canopy heights. The percentiles of the product of laser measured tree height and laser measured crown diameter were most efficient. This may be explained by the high correlation between this product and the stem diameter on an individual tree level (Persson et al., 2002). The $R^2$ could be improved, with and without tree detection, by adding additional variables such as the variance of canopy heights and the spatial ratio. However, the same results were not obtained for the error index (Table 2).

*Table 1: Correlation between percentiles of field measured stem diameter, field measured tree height, laser canopy height (CH), tree heights of detected trees (LH), and the crown size (CS), i.e., product of tree height and crown width of the detected trees*

| *Percentiles* | | *10* | *20* | *30* | *40* | *50* | *60* | *70* | *80* | *90* | *95* | *100* |
|---|---|---|---|---|---|---|---|---|---|---|---|---|
| Stem diameter | CH | 0.12 | 0.47 | 0.46 | 0.59 | 0.75 | 0.87 | 0.90 | 0.90 | 0.92 | 0.91 | 0.46 |
| | LT | 0.72 | 0.68 | 0.80 | 0.82 | 0.86 | 0.93 | 0.93 | 0.92 | 0.92 | 0.92 | 0.46 |
| | CS | 0.76 | 0.77 | 0.82 | 0.81 | 0.84 | 0.91 | 0.92 | 0.92 | 0.93 | 0.92 | 0.48 |
| Tree height | CH | 0.15 | 0.52 | 0.57 | 0.62 | 0.80 | 0.93 | 0.96 | 0.96 | 0.96 | 0.96 | 0.54 |
| | LT | 0.70 | 0.68 | 0.79 | 0.84 | 0.89 | 0.97 | 0.98 | 0.98 | 0.97 | 0.96 | 0.55 |

*Table 2: Independent variables for estimation of stem diameter percentiles with the SURE model, R2 values, and error index, using measures from laser canopy heights (H) or from tree detection (T), or a combination*

| *Independent variables* | *$R^2$* | *Error index* |
|---|---|---|
| Percentiles (H) | 0.45 | 76 |
| Percentiles (H), mean (H), variance (H) | 0.65 | 168 |
| Percentiles (H), variance (H), spatial ratio (H) | 0.63 | 104 |
| Percentiles (T) | 0.50 | 63 |
| Percentiles (T), variance (H) | 0.60 | 88 |
| Percentiles (T), spatial ratio (T) | 0.55 | 131 |
| Percentiles crown size (T) | 0.54 | 59 |
| Percentiles crown size (T), variance (H) | 0.69 | 66 |
| Percentiles crown size (T), variance (H), spatial ratio (H) | 0.71 | 107 |

*Table 3: Independent variables for estimation of the shape and scale parameter of the Weibull distribution for describing the stem diameter distribution, $R^2$ values, using measures from canopy heights (H) or from tree detection (T), or a combination*

| *Independent variables* | *Shape* | *Scale* |
|---|---|---|
| Mean (H), Variance (H) | - | 0.87 |
| Variance (H) | 0.30 | - |
| Shape (T), Scale (T) | - | 0.86 |
| Shape (T), Variance (H) | 0.39 | - |
| Shape Crown size (T), Variance (H) | 0.47 | - |

The Weibull method resulted in lower error index (39) compared with the SURE method when applied on the modified dataset (subjectively removed low tree layer). The best $R^2$ value for estimation of the scale parameter was obtained by using the mean and variance of laser canopy heights. The best $R^2$ value for estimation of the shape parameter was obtained by using shape parameter from the crown size distribution together with the variance of the laser canopy heights (Table 3).

The error index (cross validation) was high for some of the SURE models, despite high R2 values; indicating that too less data were used given the number of independent variables. The results also indicate that the forest is intensively managed because the scale explained very much of the stem diameter distribution, something that also was confirmed when the field measured mean diameter was tested alone as independent variable and $R^2$ values above 0.99 were obtained.

Future research will be performed in order to improve the implementation of both the SURE and Weibull approach. Also, additional variables will be included, for instance tree species information from remote sensing. Predictions based on grid cells instead of forest stands will be validated.

## ACKNOWLEDGEMENTS

This work was financed by the HEUREKA research program at SLU (http://heureka.slu.se) and Carl Tryggers Foundation. The Remningstorp field data surveys and the LIDAR data were exclusively financed by the Hildur and Sven Winquist Foundation. Special gratitude is directed to Associate Professor Sören Holm who provided essential statistical consultation. We thank Associate Professor Johan Fransson and Mattias Magnusson for creating the field database. We also thank Heather Reese for improving the language.

## REFERENCES

Borders, B. E., Souter, R. A., Bailey, R. L., and Ware, K. D. 1987. Percentile-based distributions characterize forest stand tables. Forest Science, 33:570-576.

Cressie, N.A.C. 1993. Statistics for spatial data (Revised ed.). New York: John Wiley & Sons Inc., pp 1-900.

Gobakken, T. and Næsset, E. 2004. Estimation of diameter and basal area distributions in coniferous forest by means of airborne laser scanner data. Scandinavian Journal of Forest Research, 19: 1-14.

Goovaerts, P. 1997. Geostatistics for natural resources evaluation. New York: Oxford University Press Inc. pp 1-483.

http://www.terrasolid.fi

http://www.topeye.com

Hyyppä, J. and Inkinen, M. 1999. Detecting and estimating attributes for single trees using laser scanner. The Photogrammetric Journal of Finland, 16, pp. 27-42.

Hyyppä, J., Kelle, O., Lehikoinen, M., and Inkinen, M. 2001. A segmentation-based method to retrieve stem volume estimates from 3-D tree height models produced by laser scanners. IEEE Transactions on Geoscience and Remote Sensing 39, 969-975.

Jonsson, B., Jacobsson, J. and Kallur, H. 1993. The forest management planning package. Theory and application. Studia Forestalia Suecica 189:1-56.

Kangas, A., and Maltamo, M. 2000. Percentile based basal area diameter distribution models for Scots pine, Norway spruce and Birch species. Silva Fennica, 34:371-380.

Maltamo, M., Kangas, A., Uuttera, J., Torniainen, T., and Saramäki, J. 2000. Comparison of percentile based prediction methods and the Weibull distribution in describing the diameter distribution of heterogeneous Scots pine stands. Forest Ecology and Management, 133:263-274.

Maltamo, M., Eerikäinen, K., Pitkänen, J., Hyyppä, J., and Vehmas, M. 2004. Estimation of timber volume and stem density based on scanning laser altimetry and expected tree size distribution functions. Remote Sensing of Environment, 90: 319-330.

Persson, Å., Holmgren, J., and Söderman, U. 2002. Detecting and measuring individual trees using an airborne laser scanner. Photogrammetric Engineering & Remote Sensing, 68(9): 925-932.

Pollock, R. 1996. The automatic recognition of individual trees in aerial images of forests based on a synthetic tree crown image model. Ph.D. thesis, University of British Columbia, Vancouver, B.C., Canada.

Srivastava, V.K., and Giles, D.E.A. 1987. Seemingly unrelated regression equations models, estimation and inference. Marcel Dekker, Inc., New York, pp. 4.

Trevor, C.B., and C.G. Anthony. 1995. Interactive spatial data analysis. Addison Wesley Longman Ltd., Edinburgh, pp. 266-269.

# FOREST STRUCTURE CLASSIFICATION EXPLORING THE ANISOTROPY INFORMATION FROM MOMS-2P THREE LINE STEREO SCANNER DATA

*Malte Sohlbach[1], Thomas Schneider[2]*

[1] Technical University of Munich, Department for Eco-System and Landscape Management, Chair of Forest Yield Science, Freising, Germany; malte.sohlbach@lrz.tu-muenchen.de

[2] Technical University of Munich, Department for Eco-System and Landscape Management, Institute of Forest Management, Freising, Germany; tomi.schneider@lrz.tu-muenchen.de

## ABSTRACT

The synergy of spectral and anisotropy information from remotely sensed data for forest classification is investigated. Mode D of the Modular Optoelectronic Multispectral Scanner 02 (MOMS-2P) combined "on track" stereo data registration in bands 6 and 7 (panchromatic, 520-760 nm, +/-21.4°) with narrow band spectral data registration in bands 1 (blue, 450-520 nm) and 4 (NIR, 770-810 nm). The reflectance difference between forward and backward looking stereo bands is related to the anisotropy of backscattering of the surface, which is considered to be a function of the surface structure. The work was guided by the options offered by the object oriented image analysis software eCognition. In a three level hierarchical "top down" evaluation chain first forest and non forest are discriminated on base of band 1 (Blue) (level 3), followed by a kind of unsupervised classification which subdivides the forest segment on base of band 4 (NIR) into three classes and on base of band 1 (blue) each of the three classes into two new, equally large classes (level 2). Finally on level 1 the "anisotropy ratio" (band 6/band7) is used to split the six classes from level 2 into two again equally large groups, arriving at twelve end classes. The significance of class separation is calculated by a SPSS based comparison of inventory point information and class statistics. The results demonstrate the potential of the anisotropy approach to complement the spectral information by information, which is mainly related to surface structure elements, especially the leaf area distribution (LAD).

**Keywords**: Anisotropy, on track stereo, MOMS-2P, angular signature, forest inventory

## 1 INTRODUCTION

Continuously increasing requests on accurate 3D representations of the Earth´ surfaces on different scales since the late 80th of the last century initiated the development of optical instruments for the digital stereo data registration. Systems with pointing capability like Spot 1, 2, 4, Ikonos, QuickBird, are able to provide data needed for digital terrain modelling (DTM) but the unforeseeable time period and registration geometry between the two data takes is limiting the practical application. The "on track" stereo data registration technique is imaging the same surface from at least two distinct view directions at quasi the same time. Restricting the enumeration on Germany, at least four digital airborne systems, DPA, WAOS/WAAC, HRSC-A, ADS as well as the spaceborne MOMS-02 system have been developed during the last decades. At the present the operational optical systems Spot 5, IRS-P, ALOS/PRISM, but experimental systems like Chris on Proba, etc. assure the continuous provision with on track stereo data from space.

At present the operational usage of stereo data sets is restricted on DEM/DHM generation and topographic mapping. In latest research the registration geometry of "on track" the stereo data sets is seen as a key to get access to a second basic property of Earth surfaces, the anisotropy of backscattering. The "anisotropy approach" on which this paper focus, starts from the consideration, that the time period from forward to backward looking observation is negligible. Under this assumption the differences in signal intensity between forward and backward looking stereo band allows an estimate of the anisotropic behaviour of surface backscattering. Gerstl & Simmer (1986) concluded that "instant crop identification may be possible only by combining different signature types where angular signatures may contribute the greatest identification value" (cited in Gerstl, 1990).

The mono-temporal MOMS-02 mode D data base evaluated in this paper, allows investigating three of the five signature types: spatial, spectral and angular signatures. The thematic evaluation of these signatures is possible in a “multispectral”, an “anisotropy” and a “combined approach” (Schneider et al., 1999). The **"multispectral approach"** is based on the different reflectance behaviour of surfaces with and without vegetation cover (Gates, 1970). The **“anisotropy approach”** evaluates information from angular signatures which superimpose the "basic" spectral information. The approach explore the fact that soils and vegetation surfaces show in general a strong backward orientated backscatter characteristic (Irons et al., 1990), while vegetation show a weaker one (Deering et al., 1989) (see figure 2). For vegetated surfaces the property of anisotropic backscattering is considered to be a function of plant architecture and stand structure. The expectancies on the approach are in the derivation of structure parameters, especially of the leaf angle distribution (LAD). LAD is a very sensitive parameter describing phenological /physiological differences inside a unit and one of the most important parameter in physical backscatter models. LAD can not be derived from mono directional spectral data sets.

Previous investigations with MOMS-02/D2 and MOMS-2P data sets (Schneider et al., 1999 a, b, c) confirmed the prediction of Gerstl (1990) and moreover, led to the conclusion that a further substantial increase can be expected using adopted classification routines. The presented paper reports about a study in a managed, Mid-European forest of a flat to hilly landscape in Bavaria. The question to be answered was **which is the potential for forest applications?**

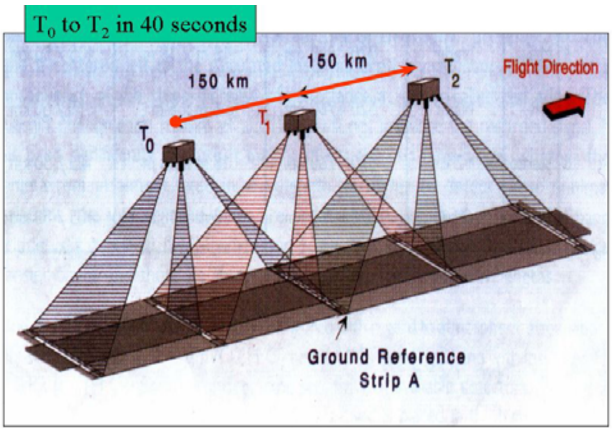


*Figure 1: MOMS-2P stereo data registration principle*

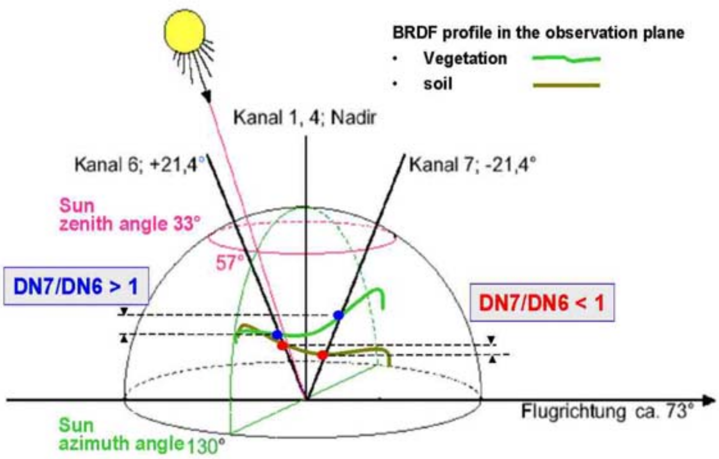


*Figure 2: Principle of anisotropy ratio calculation from on track stereo data drawn into the scheme of illumination to observation geometry during MOMS-2P mode 3 data take 08FE from 25th of June 1998, 9.30h MET*

# 2 MATERIALS AND METHODS

## 2.1 Materials

The test site Kranzberger Forest is located about 40 km North of Munich, between 11°38'09'' and 11°45'05'' longitude and 48°23'11'' and 48°26'04'' latitude (see Figure 3). The dominating stand types in the Kranzberger Forest are pure coniferous, pure broadleaved and mixed forests. Main tree types are spruce (Picea abies), pine (Pinus silvestris), beach (Fagus silvatica), larch (Larix decidua) and oak (Quercus robur). The management goal is toward a mixed, uneven aged forest.

The MOMS-2P mode D data investigated in this study was registered on an ascending track during data take 08FE on 25th of June 1998. Scene 22 (id: To8FeMDC01SO22L0) was recorded at 9.30h MET with a path azimuth of around 73°, from a orbit height of 376,7 km, at a sun azimuth of 131° and a sun elevation of 57° (see figure 2). The atmosphere was cloudless. “mode D” combines stereo data of bands 6 and 7 (panchromatic 520-760 nm, 21,4° off nadir ) with multispectral data of bands 1 (blue 450-520 nm) and 4 (NIR 770-810 nm).

Pre-processing steps of geometric rectification have been done by use of the image processing software ENVI 3.0 of RSI. The image analysis is performed with the software package eCognition 3.0 of DEFINIENS AG. The tests of the statistical significance of the classification results to forest inventory information was performed with the statistic software package SPSS.

For verification resp. analysis of classification results forest inventory information was used. The inventory point sample grid concept is one of the basic columns of the Bavarian forest management information system. Inventory points are distributes with a grid of 140 m to 140 m. Each inventory point represents three concentric circles with a diameter of 6.3 m, 12.6 m and 25 m. While the inner circle is used to register all trees within this circle, the mid zone represents all trees with a breast height diameter (bhd) > 12 cm. In the last circle, the outer circle, all trees with a bhd > 30 cm are measured. For each zone the found tree types are described by their tree type ratio, mean age, mean diameter, tree number and mean height. For the investigated forest area (Kranzberger Forst) 629 inventory points registered in 2001 were provided by the Bavarian State Forest Administration.

## 2.2 Methods

### 2.2.1 Data Analysis

The data analysis with eCognition is an iterative sequence of segmentation and classification procedures. Thus segmentation is followed by a classification that again could be followed by a segmentation using the previous classification as additional information for segmentation. The approach described in this paper is following a computation efficient top down concept where segmentation alternates with classification routines three times. Except the band weights which are different for each run the segmentation parameters are the same for all object levels whereas the main focus is on the intensity information of the bands (“Colour” in eCognition nomenclature)(see Table 1). The results are three image object levels with four hierarchical structured classification layers. After each classification all objects of the same class are merged not to impact the following steps of information extraction.

At object level 3 forested and non forested areas are separated. The segmentation is considering all available bands. Because of the very good representation of forested areas the blue band is weighted three times a high as the other bands (see Table 1). The classification resulting in the forest mask is based on the mean values of objects (band 1, 6 and 7), the difference of the mean values of the objects to the whole scene (band 6 and 7) and finally a combination of band 6 and 7: (band 6 + band 7) / 2. The not forested areas are simply defined as the opposite of the forest mask.

At object level 2 the spectral information is explored (multispectral approach). Consequently only the multispectral bands 1 (blue) and 4 (NIR) are used for segmentation (see Table 1). For classification in a first step the object values of band 4 (NIR) were subdivided in three visually distinguished intensity ranges: low, mid and high intensity. In the next step the intensity information of band 1 (blue) is used to subdivide the previously created classes in two new classes each. Due to the poor radiometric performance in band 1a visually control of the separation of the classes as described for the first step failed. Thus the area was split according to the condition to create two equally sized parts. The resulting six classes represent the discrimination potential of the multispectral approach.

The final level, level 1, is used to investigate the anisotropy approach. Thus the focus is on evaluation of the stereo bands 6 and 7. Both in the segmentation and in the following classification only these bands are used (see Table 1), solely influenced by the object levels created before.

*Table 1: Segmentation parameters and level preparation*

| Level | Theme/ approach | Layer Weight | | | | Scale Para-meter | Colour | Shape | Smooth-ness | Compact-ness |
|---|---|---|---|---|---|---|---|---|---|---|
| | | blue | NIR | St 6 | St 7 | | | | | |
| Object-level 3 | forest mask | 3 | 1 | 1 | 1 | 10 | 0.9 | 0.1 | 0.6 | 0.4 |
| | **fusion of objects assigned to the same class** | | | | | | | | | |
| Object-level 2 | multispectral | 1 | 1 | 0 | 0 | 10 | 0.9 | 0.1 | 0.6 | 0.4 |
| | **fusion of objects assigned to the same class** | | | | | | | | | |
| Object-level 1 | anisotropy | 0 | 0 | 1 | 1 | 10 | 0.9 | 0.1 | 0.6 | 0.4 |

The classification of level 1 again subdivides the object classes separated in level 2 (six classes) in two new classes each, resulting in twelve final classes. The anisotropy phenomenon explored for the differentiation was assessed on behalf of the Anisotropy Ratio (Band 6 / Band 7 described by Schneider et al. 1999). Since differences of this Anisotropy Ratio were not obvious again thresholds were used splitting the area of each class in two parts with approximately the same size. The mapping result of the classification procedure is shown in figure 3.

This process of information extraction can be described as a user defined unsupervised classification. Indeed the thresholds for separation of the classification are defined by the user but not with the intention to differentiate to known features. Rather the resulting classes have to be analysed after the classification process to show if useful information is integrated in the investigated remote sensing information (blue band, NIR band, Anisotropy Ratio).

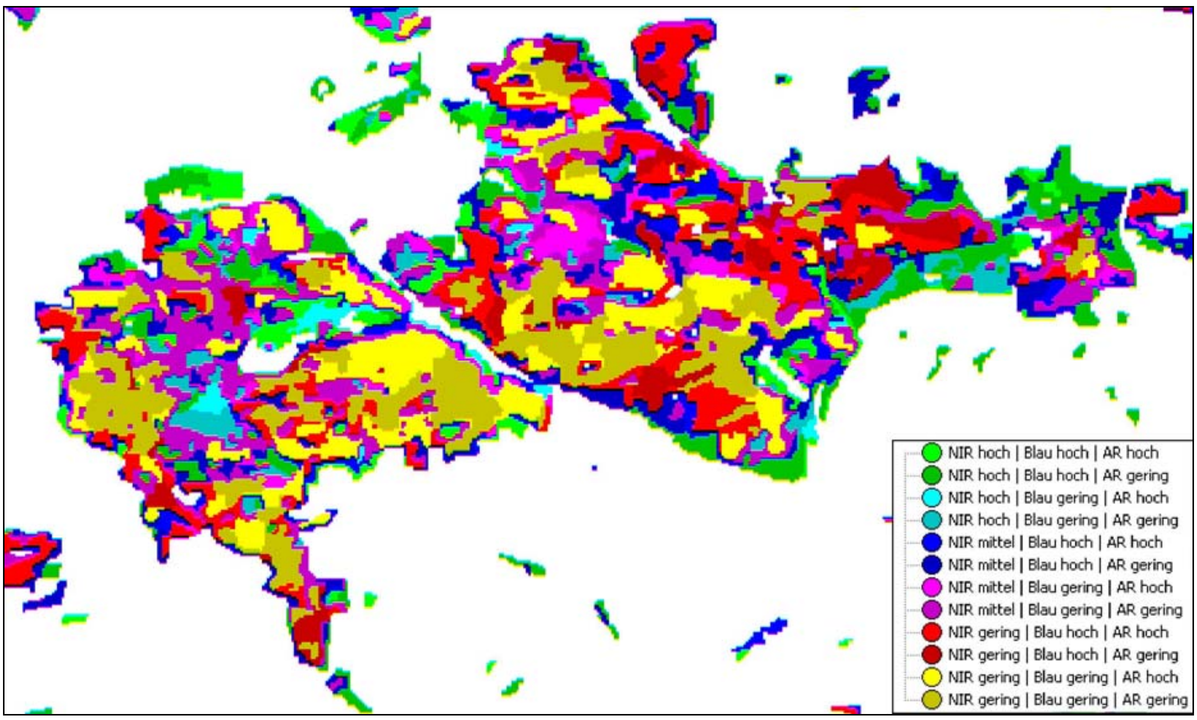


*Figure 3: Mapping result of the classification*

## 2.3 Analysis of Results

For analysis of the classification results the above described forest inventory information was used. The main advantage compared to stand based forest management information is the fact, that not a whole stand represented by some numbers is used for verification but only a single inventory point. Thus the fitting of the borders of the classification results and the forest sub compartments is not mandatory. Due to the fact, that remote sensing data represents the current state concerning tree types and forest structures more accurate than stand based management data, this becomes an important criterion for selection of the suited data for evaluation. A higher correlation between the extracted classes and the point based inventory information can be expected.

To reduce spatially related inaccuracies of remote sensing data, the corresponding classification results and forest management data and therefore to improve the analysis of classification, all inventory points with a distance smaller than 20 m to an object border as result of the segmentation were removed. Therewith the spatial impreciseness could be reduced as far as possible. However 432 of primarily 629 were lost caused by the heterogeneity of the research area.

After combination of the classification results and the inventory data, the classification results were analysed by means of statistical methods in reference to silvicultural relevant parameters like tree type mixture ratios, tree numbers, average age, mean stem diameter and mean tree height. It has to be mentioned, that not single tree types were compared but tree type groups like coniferous trees, deciduous trees and larch.

Due to the low number of ground control points and the bad representation of some of the extracted classes with the corresponding number of inventory points the statistical analysis of the classification results required the application of a special strategy using different statistical methods. Thus it became important to analyse the classes of each classification step separately and to follow the tree structure of the classification: One class (Forest) is divided in three (blue band) resp. two (NIR band, Anisotropy Ratio) new classes and solely this three resp. two classes are compared with each other.

The three classes as result of the first classification step (NIR band) were compared to the inventory information with an Analysis Of Variance (ANOVA) combined with an Analysis Of Homogeneity and a Post Hoc Multiple Comparison. If there is no homogeneity as precondition for using ANOVA the Post Hoc Multiple Comparison can be used to say which of the classes are significantly different.

The classes of the second and third classification step (blue band, Anisotropy Ratio) were compared concerning possibly included forest inventory information solely with the so called T-Test. Here only two classes as result of the splitting of one of the previously derived classes are compared.

# 3 RESULTS

The analysis of the NIR band based classification results revealed a significant relation between the intensity of the NIR and tree type groups resp. the mixture ratio of different tree type groups. Even in case the significance is not approved by ANOVA due to missing homogeneity, the multiple comparison show significant relations. Only exception is the larch that seams to be clearly separated by the mean ratio, but this difference is not statistically significant. Nevertheless three stand types can be determined: “coniferous dominated” represented by low intensity values in the near infrared (95% coniferous trees, <3% deciduous trees, <3% larch), “deciduous dominated” represented by high intensity values (69% deciduous trees, 26% coniferous trees, 5% larch) and “mixed” with a high fraction of coniferous trees and larch represented by mid intensity values of the near infrared (60% coniferous trees, 26% deciduous trees, 14% larch).

The three previously described classes are separated in two new classes each based on the blue band. The two new classes resulting from splitting of the class describing high intensity values of the NIR are represented by only a few intensity points. Thus a statistical analysis cannot provide plausible results and it will not further be discussed. The other four classes indicate a similar behaviour of the blue band compared to the NIR band. According to the T-Test all four classes show significant differences concerning the portion of the tree type groups. Lower intensity values point to suggest higher ratios of coniferous trees. But this is not the only relation resulting from the statistical analysis. As described above the class described by low intensity values in the NIR is dominated by coniferous trees (95%). A further separation evaluating the response in the blue band leads to ratios of coniferous trees of 89% and 97%. Based on these small differences the detected significance of differentiation concerning age, diameter and height of the stands becomes very interesting.

Due to the number of inventory points representing the extracted classes further statistical analyses were restricted to the classes with low intensity values in the near infrared and with high respective low intensity values in the blue band. All four classes splitting the two previously mentioned classes (low NIR/low blue, low NIR/high blue) in two new classes each show significant differences concerning the portion of the tree type groups as result of the T-Test. Lower values of the Anisotropy Ratio suggest higher portions of coniferous trees. But again this is not the only correlation resulting from the statistical analysis. As described above the class representing low intensity values in the NIR and blue band is clearly dominated by coniferous trees (97%). Further splitting of the class leads to significantly different ratios of coniferous trees of 93% and 99%. Nevertheless this significant difference could be neglected due to its low value. Based on these minor differences the significant difference concerning mean age, mean diameter and mean height of the stands become an obvious very promising result. Nevertheless the differences of the stand parameters between the two classes are very low. Further research will be necessary to show the full potential of the Anisotropy Ratio.

# 4 DISCUSSION

The research on the implementation of the anisotropy information in a thematic evaluation of Earth observation data revealed a couple of open questions starting from the specific MOMS-registration constellation up to fundamental once like the need of a BRDF for status assessment after illumination to registration geometries adjustment. The MOMS-02 system being history, the discussion is restricted on fundamental questions like the implication of the pixel size (i), stereo segment registration geometry (ii), pre-processing requirements (iii), evaluation strategy (iv), verification related issues (v), etc., but the anisotropy ratio as a new analytical feature as well (vi).

i) The spatial resolution of about 18 m of the MOMS-2P system is delivering a mixed signal, integrating over a group of trees. Especially in uneven aged, well structured stands the roots of the anisotropic behaviour are not traceable. Additionally, sub-segmenting well structured patches results in an insufficient representation by inventory points. Consequently the analysis of the anisotropy effects must be restricted on the more or less pure coniferous object class in this case.

ii) The imaging geometry is influencing the data evaluation by at least two basic components: First, the illumination to observation geometry, which is changing between two observations and is controlled by the phase angle between illumination and observation directions. The information content may be described by a function. Whether this function is more a linear or a sinusoidal one is subject of ongoing investigations. Second, the atmospheric attenuation of the two stereo bands, whereby especially the Raleigh scattering phenomenon witch is anisotropic as well, may alter the two observation directions different.

iii) Pre-processing of the data should assure a comparable data quality (radiometric correction) and the fit of the resulting output in the geographic reference system of the project (geo-coding, geo-rectification). Looking forward to the inversion of physical models for getting information on the status of vegetation canopies, a very precise radiometric calibration of the data set is requested. This concerns sensor, path radiance, topography as well as illumination to observation effects (BRF effects). Path radiance differences between the three view directions of the MOMS-2P mode D data set may influence the results in case of a quantitative radiometry based study and have to be considered in future studies. Within the MOMS-02 processing chain a sensor calibration for the stereo bands was not foreseen. On the other hand, the mono-temporal, experimental character of the presented demonstration does not necessarily require an atmospheric correction. The results should simply to be treated as a qualitative assessment of the approach.

iv) The evaluation takes advantage from the eCognition method. Performing the evaluation on base of objects instead of pixels and working with the mean value of these objects the striping problem of MOMS-2P band 1 (blue) is reduced to a minimum. The following analysis steps are performed by evaluating features of the attribute table. Starting the image analysis process on forest solely with the brightness information of the NIR band broad leaf and coniferous dominated objects are already separated with a statistical accuracy of 97%. The subsequent evaluations have been restricted on selected classes. The previous fusion of objects of the same class allowed segmentation on base of completely different features, such supporting the creation of a knowledge based evaluation hierarchy, assuming the spectral information to be more stable and the anisotropy information to serve solely as additional decision criteria in this kind of unsupervised classification. The question, weather the top down approach is superior a bottom up approach, is not answered.

v) Verification, but labelling the forest segments created at the different steps of the procedures is done on behalf of the inventory point data base. The usage of the stand wise inspection data proved to be inadequate for our purposes. In general forest management information is related to forest stand units. Usually the whole stand is represented by one number for each feature. A very common experience in forest related RS data evaluations is that classification results and forest stand borders as delineated by the forest management maps do not necessarily match together. The distribution of forest tree types and structure elements within a forest is imaged more precise by remote sensing data. The decision to verify the classification results on base of the eCognition object borders and the regular inventory point grid data was guided by such thoughts. Weather the inventory point information used, which was updated in summer 2000, two years after the MOMS-2P data take, still correctly represent all inventory points used, could not be verified and may be an error source.

vi) The anisotropy information is assumed not to be correlated with the spectral information and thus can be considered as an independent information source. The access to a quantification of the anisotropy information is tried via the angular signature as calculated from the on track registered panchromatic stereo bands of the MOMS-2P system. The usage of such an “anisotropy ratio” requires a stable and symmetric geometry of the two stereo bands. Nevertheless, to relate such information to bio-geo-physical properties a physical model is required, describing the backscatter behaviour of the surfaces. The presented results are solely to be considered as a first test checking the information potential of the approach for forest applications.

## 5 CONCLUSION

The quasi-simultaneous stereo data sets from the MOMS-02 system allowed the analysis of angular signatures, giving access to an additional physical parameter of Earth’s surfaces, the anisotropy of backscattering. The study demonstrated the value adding effect for forest classification by combining the well-known multispectral information with the information on surface anisotropic effects in a hierarchical approach, guided by the logics of the object oriented image analysis software eCognition.

The MOMS-2P system was destroyed on 23rd of March 2001 as the Russian space platform MIR was conducted into a controlled deorbit/reentry manoeuvre which ends with the final crash in the Pacific Ocean. After more than seven years the Japanese ALOS/Prism system again offers the opportunity to investigate the anisotropy phenomenon with a stable geometry and in combination with simultaneously acquired multispectral data. The increased spatial resolution of Prism is connected to new challenges but new prospects concerning the location accuracy and assignments to objects of interest as well.

## REFERENCES

Gates, D.M., 1970: Physical and physiological properties of plants; Remote Sens. With special ref. to agriculture and forestry; Nat. Academy of Sciences, Washington D.C.

Gerstl, S.A.W., Simmer, C. & B.J. Powers, 1986.:The canopy hot spot as crop identifier. Symposium on Remote Sensing of Resources Development and Environment Management, Enschede, F.R.G., August, 261-263.

Deering, D.W., 1989. Field measurements of bidirectional reflectance. Theory and Applications of Optical Remote Sensing (ed. G. Asrar), John Wiley, New York, 14-65.

Irons, J.R. & J.A. Smith, 1990: Soil surface roughness characterization from light scattering observations. 10th Annual International Geosciences and Remote Sensing Symposium, II, 1007-1010.

Schneider, Th, Buhk, R., Ammer, U., (1999): Investigations on synergy and complementa¬rity of multispectral and anisotropy information from MOMS-02/D2-Mode 3-data for land use classification in the Sinaloa district of Mexico;: Int. Journal of Remote Sensing, Vol. 20, No. 8, pp1499-1526.

Schneider, Th., Manakos, I., 2003: BRDF Approximation of maize and canopy parameter retrieval by ProSail inversion; Procc. EARSeL Workshop Imaging Spectroscopy, Herrsching, May 13-16 ; ISBN 2-908885-56-5

Schneider, Th, Manakos, I., Reinartz, P., Müller, R., 1999: The evaluation of spectral and angular signatures from MOMS-2/P mode D data sets - an application case study for land use purposes: Joint WSf ISPRS WG I/1, I/3 and IV/4: SENSORS AND MAPPINHG FROM SPACE 1999; Hannover, September 27-30, 1999

Schneider, T., Manakos, I., 2000. Anisotropie der Rueckstrahlung - Stoerfaktor oder Informationsquelle? Eroerterung anhand des Beispiels "precision farming". Referate der 21 GIL - Jahrestagung in Freising-Weihenstephan, Berichte der GIL, Band 13, S. 187-190, Berlin.

Sohlbach, M., 2002: Der Anisotropie-Effekt in Fernerkundungsdaten operationeller Along-Track-Stereosysteme – Informationsgewinn für forstliche Anwendungen ?; Diploma thesis, Chair for Forest Yield Science, TUM

# THE USE OF AIRBORNE HYPERSPECTRAL REFLECTANCE DATA TO CHARACTERIZE FOREST SPECIES DISTRIBUTION PATTERNS

*Philipp Weihs[1], Franz Suppan[2], Werner Schneider[2], Hubert Hasenauer[3] and Katja Huber[1]*

[1] University of Natural Resources and Applied Life Sciences (BOKU), Department of Water, Atmosphere and Environment, Institute of Meteorology, Vienna, Austria; weihs@mail.boku.ac.at

[2] University of Natural Resources and Applied Life Sciences, Department of Landscape, Spatial and Infrastructure Sciences, Institute of Surveying, Remote Sensing and Land Information, Vienna, Austria; werner.schneider@boku.ac.at

[3] University of Natural Resources and Applied Life Sciences, Department of Forest and Soil Sciences, Institute for Forest Growth and Yield Research, Vienna, Austria; hubert.hasenauer@boku.ac.at

## ABSTRACT

The aim of this study was to test the potential of Remote Sensing technologies for retrieving information on forest growth and forest status using airborne hyperspectral data from the experimental forest of BOKU. First it is shown that it is easy to distinguish beech from spruce using the spectral reflectance. The large fluctuation in reflectance between more than 150 pixels of the same “homogeneous” stands (pure beech or pure spruce) indicates that even in these uniform conditions large inhomogeneities exist (i.e. due to texture and density). In a second step the hyperspectral reflectance (measured with airborne imaging spectrometer HyMap) was compared with simulated reflectance using forest reflectance models. For spruce no match between measured and modelled data was obtained. However, it was possible to get an agreement for beech taking into account the uncertainties in model input parameters. In a third step model inversion was performed to estimate leaf area index (LAI) on the Hymap reflectance spectra. We also analysed geographical influences (i.e. elevation) using a vegetation index, the red edge index, yellowness index and the PRI index, applied for reflectance of 7 pure beech plots and 7 pure spruce plots. The results suggest that there is a reduction in LAI and vegetation density and an enhancement in stress of the vegetation with increasing elevation.

**Keywords:** hyperspectral data, forest reflectance models

## 1 INTRODUCTION

Within the scope of this study we present first results of investigations performed to test the potential of airborne hyperspectral data to retrieve information on forest growth and on forest status. These investigations were performed using hyperspectral data of the experimental forest of BOKU, which is situated in the Rosalian Mountains 70 km south to Vienna. The forest covers 1000 ha, with elevations between 400 and 900 m. The dominating tree species are Norway Spruce, Common Beech, but also Silver Firs and a few Scots Pines. At Rosalia a typical forest inventory is routinely performed, in addition more extensive measurements were carried out at several research plots. On June 21, 2005, 10:53 UTC, HyMap measurements of the Rosalian area were performed. HyMap is an airborne imaging system onboard a Do 228 aircraft belonging to Deutsche Gesellschaft für Luft- u. Raumfahrt (DLR). The HyMap sensor has 4 spectrometers with 128 spectral bands which cover the wavelength range from 400 to 2500 nm. The bandwidth of the spectrometers is approximately 15 nm. The flight altitude of the aircraft was 1910 m above ground level, which results in a 4 m pixel resolution. The flight direction was with 343 degrees almost northern direction. The sun position was 24 degrees zenith angle and 178 degrees azimuthal angle. Therefore we did not expect any hot spot effects.

## 2 METHODS

In order to determine the reflectance a Pre processing of the data had to be performed. An atmospheric correction was applied to the HyMap data using the 6S code. A recalibration function was applied to the data in order to remove spectral artefacts, by using ground based spectrometer reflectance measurements following the procedure of Guanter et al. (2004). For taking into account the influence of inclination and obstruction of the horizon a topographic correction was carried out using a digital elevation map with 25 m resolution.

In this study two forest reflectance models, the ACRM (Kuusk, 2001) and the FRT (Kuusk and Nilson, 2002), were used. The model ACRM is a directional multispectral homogeneous two layer canopy reflectance model. The input parameters include the leaf area index (LAI), leaf angle inclination, leaf size, biochemical parameters of the leaves and the soil reflectance. The FRT model is also a homogeneous two layer canopy reflectance model, but additionally includes the exact dimension of the trees (height, crown radius, trunk radius) as well as trunk and branch reflectance.

Both models simulate reflectance spectra in the wavelength range from 400 to 2400 nm (1 nm resolution), taking into account bidirectional effects. Model inversion is performed using iterative optimisation technique.

## 3 RESULTS

### 3.1 First analysis of data

Fig 1 a and b show the comparison of spectral reflectance of beech with spruce. Spectral reflectance of beech is much higher than that of spruce. Fig. 1 b also shows that the spectral features may be easily used to distinguish between both tree species. Reflectance of beech in the near IR is much higher whereas the reflectance in the visible is almost in the same order of magnitude.

The reflectance spectra of 191 pixels of one homogeneous pure spruce stand are shown in Fig. 2, demonstrating large fluctuations between the individual spectra. The maximal deviations reach an order of magnitude of ± 50%, indicating that even in “homogeneous” stands large inhomogeneities exist.

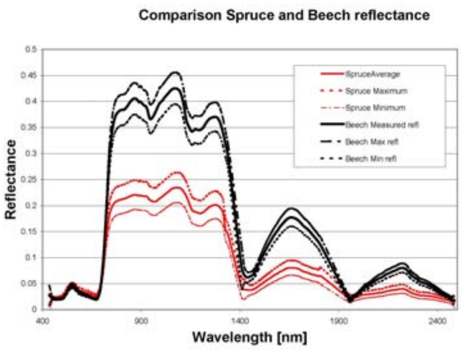


a)

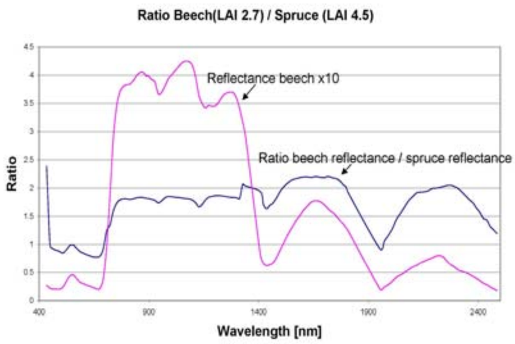


b)

*Figure 1 a and b: a) Average reflectance of pure beech (black) and spruce (red) stands (approximately 200 pixels) with their respective standard deviations (dotted lines) b) Ratio of beech reflectance to spruce reflectance compared with beech reflectance multiplied by a factor of 10.The average LAI of the spruce stand is around 2.7 and the average LAI of the spruce stand is 4.5.*

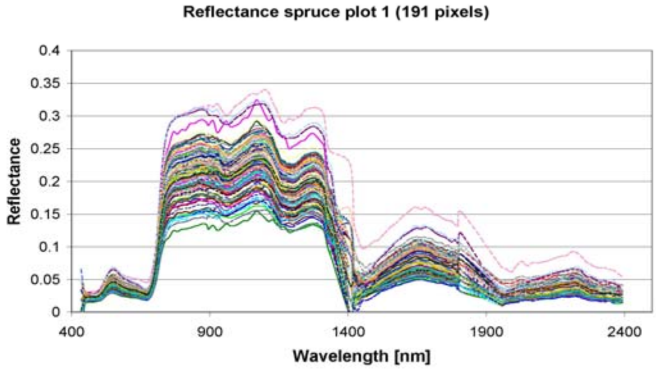


*Figure 2: Reflectance of 191 pixels (covers appr. an area of 3000 m²) of one homogeneous pure spruce stand*

*Table 1: Overview of the known model input parameters for the reflectance calculations.*

| Selected reference forest plots | Beech 480m /E 20° incl. | Spruce 1 610m/W 18° incl | Spruce 2 670m/SW 16° incl |
|---|---|---|---|
| Age [years] | 65 | 120 | 130 |
| LAI | 2.7 ± 0.5 | 4.9± 0.5 | 4.6± 0.5 |
| Height [m]/ Crown dim.[m] | 25 / -- | 25/ (2.7-5.9) | 30/ (4.5-7.2) |
| Canop. Closure [%] Stand density /m² | 100 / 0.054 | 60 / 0.037 | 90 / 0.062 |
| Ground vegetation | none | none | none |

## 3.2 Comparison of measured and modelled reflectance

HyMap reflectance measurements were compared with simulated spectra by means of the two forest reflectance models ACRM and FRT. Reflectance of two pure spruce stands and one pure beech stand were compared with the model simulations. The model input parameters known for these three stands are shown in Table 1. LAI was estimated using direct measurements combined with forest growth models. Most of the information is known from more extensive measurements performed at the research plots. Some of the information was obtained using airborne low resolution data. Some of the model input parameters such as soil reflectance, leaf inclination/eccentricity, bark and trunk reflection, total dry leaf weight, leaf weight per area, BAI/LAI ratio, shoot shading coefficient, markov parameter, percentage of constituents in leaves (dry matter, water content, chlorophyll, pigments) were however taken from literature. The results of these comparisons are shown in Fig. 3. For beech, agreement between model and HyMap measurements was achieved only when the uncertainty in measurements (LAI) and in the assumptions of some model input parameters was taken into account. The large fluctuations of the model simulations due to these uncertainties may be seen in Fig. 3. For spruce no agreement between measured reflectance and simulated reflectance was achieved. Fit between models and measurements was only obtained using a LAI around 1.57 which is however a unrealistic value. This overestimation of reflectivity by models is a well known problem in literature (e.g. Rautiainen, 2005).

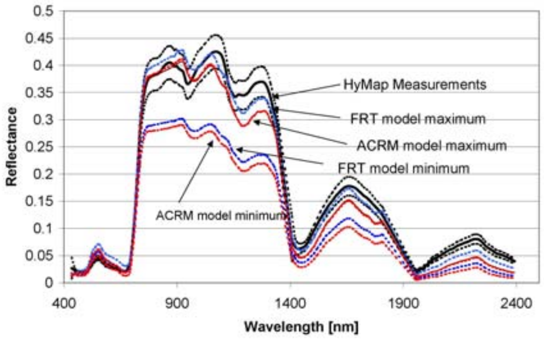


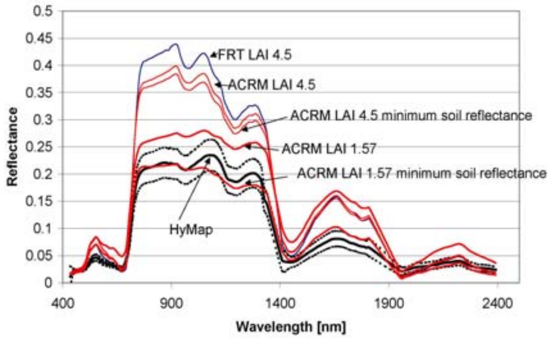


a) b)

*Fig 3 a and b: Comparison of HyMap reflectance measurements with model simulations for beech (a) and spruce (b). The black lines show the HyMap measurements with their respective standard deviations. These measurements are compared with minimum and maximum of model simulations (due to uncertainty in input parameters). No agreement between model and measurements is achieved for spruce.*

*Table 2: Overview of the method or equations used to determine the different indices. First preliminary results regarding an eventual dependence on altitude are shown. These results were obtained using 7 pure beech and 7 pure spruce stands. LAI inversion was not performed for spruce since no agreement was obtained for the forward modelling (section 3.2). Some of the results (yellowness and red edge index for spruce) were not available at the time when this paper was prepared.*

| Index name | Method / Equation | Correlation coefficient with elevation for beech (First results !!!) | Correlation coefficient with elevation for spruce (First results !!!) |
|---|---|---|---|
| LAI | Inverted with ACRM model | -0.59 | ---- |
| Vegetation index | (R(767to 894 ) – (R (646 to 707 )) /(R (767 to 894 ) + (R (646 to 707 )) | -0.43 | -0.71 |
| Red edge index | R 740 / R 720 | -0.56 | -0.68 |
| Red edge LANDSAT | R( 730 to 950) / R (580 to 740) | -0.6 | ---- |
| Yellowness index | R580 – 2* R624 + R668 | -0.08 | ---- |
| PRI index | (R 531 – R570)/(R531 + R570) | -0.21 | ---- |

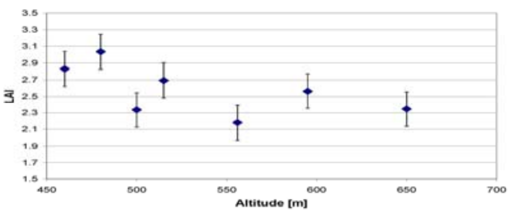


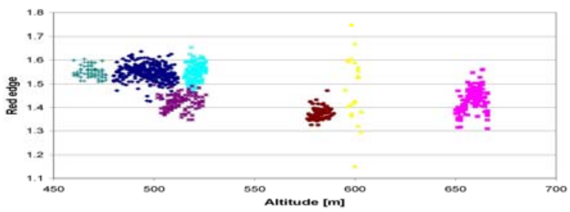


a) b)

*Fig. 4 a and b: Two examples of altitude dependence. a) With ACRM model inverted LAI of 7 pure beech plots as a function of elevation. The standard deviation was roughly estimated. b)Red edge index for 7 pure beech plots as a function of elevation (857 pixels were used, each colour represents one stand).*

### 3.3 Investigation of regional influences by using forest reflectance model inversion and well known indices.

Forest growth is driven by climate, water, energy and nutrition. These factors influence the carbon cycle and forest growth. The limiting factors are very often the key driver e.g. drought stress may be the limiting factor for vegetation growth. Regional influences were investigated using 7 pure beech plots and 7 pure spruce plots. Beside the inversion mode of the forest reflectance models to derive the LAI, other vegetation indices were used. A vegetation index, the red edge index which is an indicator of vegetation stress (Vogelmann, 1993; Zarco Tejada, 1999), the yellowness index (indicator of chlorosis in stressed leaves) (Richardson et al., 2003; Adams et al., 1999) and the PRI index (photosynthetic radiation use efficiency)(Richardson et al., 2003; Gamon et al., 1997; Penuelas et al., 1995; Fillela et al., 1996). The definitions of the different indices as well as first results are shown in table 2. First preliminary results suggest that there is a dependence of the red edge index, of the vegetation index on altitude for beech and for spruce (table 2; fig. 4). The dependence on elevation of the yellowness index and of PRI seemed to be less pronounced.

## 4 DISCUSSION AND CONCLUSIONS

Study results show that even in homogeneous stands large inhomogeneities can be found. This is one of the reasons for the large effort of the scientific community to develop and improve 3-D forest reflectance models. Beech and spruce may be easily distinguished from each other by comparing their spectral reflectance. The much larger reflectance of beech in the IR is a well known fact (Rautiainen, 2005). The comparison of modelled and measured reflectance shows that agreement is reached for beech if uncertainty of the LAI measurements and of the model input parameters are taken into account. Future effort will concentrate on the determination of exact information for more plots and on the determination of more model input parameters such as ground reflectance or bark and trunk reflectance. No agreement between measurements and model was obtained for spruce even if all uncertainties were taken into account. This well known problem is attributed to the shape and to the clumpiness of coniferous trees which make an approximate modelling very difficult. The studies of regional influences suggest that there is a decrease of LAI with altitude, a decrease of the vegetation index with altitude (which would indicate a loss of density of the vegetation with increasing elevation) and an increase of the red edge index with increasing altitude (increase of vegetation stress with elevation).

## ACKNOWLEDGEMENTS

These investigations were performed within the scope of the project “Crop Drought Stress Monitoring by Remote Sensing (DROSMON)” supported by the Austrian Science foundation (FWF)

## REFERENCES

Adams, M.L., Philpot, W.D. and Norvell, W.A. (1999). Yellowness index: an application of spectral second derivatives to estimate chlorosis of leaves in stressed vegetation. Int. J. Remote Sens. 20 : 3663-3675.

Fillela, I., Amaro, T., Araus, J.L. and Penuelas, J. (1996) Relationship between photosynthetic radiation-use efficiency of barley canopies and the photochemical reflectance index (PRI). Physiol. Plant. 96: 211-216.

Gamon, J.A., Serrano, L. and Surfus, J.S. (1997). The photochemical reflectance index: an optical indicator of photosynthetic radiation use efficiency across species, functional types, and nutrient levels. Oecologia 112: 492-501.

Guanter, L., Alonso, L. and Moreno, J. (2004). Atmospheric correction of CHRIS/Proba data acquired in the SPARC campaign. Proc. of the 2nd CHRIS/Proba Workshop, ESA/ESRIN, Frascati, Italy 28-30 April (ESA-SP-578, July 2004).

Kuusk, A. (2001). A two-layer canopy reflectance model. J. Quant. Spectroscopy & Radiative Transfer 71: 1-9.

Kuusk, A., and Nilson, T. (2002). Forest reflectance and transmittance FRT user guide. Tartu Observatory 2002.

Penuelas, J., Filella, I. And Gamon, J.A., (1995). Assessment of photosynthetic radiation-use efficiency with spectral reflectance. New Phytol. 131: 291-296.

Rautiainen, M. (2005). The spectral signature of coniferous forests: the role of stand structure and leaf area index. Academic dissertation. The Finnish Society of Forest Science. ISBN 1795-7389.

Vogelmann, J.E., Rock, B.N., and Moss, D.M., (1993). Red edge spectral measurements from sugar maple leaves, Int. J. Remote Sens. 14: 1563-1575.

Zarco-Tejada, P.J., Miller, J.R., Mohammed, G.H., Noland, T.L., Sampson, P.H., (1999). Optical Indices as Bioindicators of Forest Condition from Hyperspectral CASI data. Proc. 19th Symposium of the European Association of Remote Sensing Laboratories (EARSeL), Valladolid, Spain, 31st May – 2nd June, 1999.

# USING HYPERSPECTRAL DATA AND BAYESIAN CALIBRATION FOR PREDICTING FOREST GROWTH USING THE 3-PG MODEL

*Genevieve Patenaude[1], Ronald Milne[2] and Marcel Van Oijen [2]*

[1] The University of Edinburgh, Geosciences, Edinburgh, UK: genevieve.patenaude@ed.ac.uk

[2] Centre for Ecology and Hydrology, Penicuik, Midlothian, UK; rmilne@ceh.ac.uk & mvano@ceh.ac.uk

## ABSTRACT

Process-based models (PBM) have been used to simulate 3 dimensional complexities of forest ecosystems and their temporal changes but their extensive data requirement and complex parameterisation has often limited their use for practical management applications. Increasingly, information retrieved with remote sensing techniques can help in data collection and model parameterisation by providing spatially and temporally resolved forest information. In this paper, we illustrate the potential of Bayesian calibration as a framework for integrating various data sources, including remote sensing, to simulate forest production. As an example, we use the 3-PG model combined with field based and hyperspectral data to simulate the growth of Corsican pine stands in Thetford forest, UK. Hyperspectral data are used to estimate LAI dynamics, while a Bayesian calibration is applied to provide estimates of uncertainties to model parameters and outputs. In the past, goodness-of-fit approaches have been used to optimise parameter values given available data. However, such techniques do not provide uncertainties to parameters and model outputs. With Bayesian calibration, the parameters and the data used in the calibration process are presented in the form of probability distributions, reflecting our degree of certainty about them. A Markov Chain Monte Carlo (MCMC) sampling method is used to approximate the full posterior probability distribution. The results show the ability to use a Bayesian framework to conduct truly integrative work for forest analyses, both in the consideration of field-based and remotely sensed datasets available and in estimating data, parameter and model output uncertainties.

**Keywords:** Hyperspectral data, Bayesian calibration, Forest production, 3-PG.

## 1 INTRODUCTION

Process-based models have been widely used in the fields of forest physiology and forest ecology as they enable deeper insights into the drivers of forest production and growth and offer higher flexibility than conventional production tables (Landsberg & Waring 1997). This flexibility enables the quantification and prediction of forest 2 and 3-D structural variables owing to deterministic, mechanistic and/or stochastic algorithms simulating the processes affecting growth. However, their practical value has been limited owing to their complexity, their extensive data requirement, and the difficulty in quantifying parameters and model output uncertainty (e.g. Gertner et al. 1999). In this paper, a Bayesian approach is used to calibrate the 3-PG model (Physiological Processes Predicting Growth, Landsberg & Waring 1997, Sands & Landsberg 2002) for the production of a typical UK Corsican pine (CP) plantation (*Pinus nigra* car. *maritima* (AIT.) Melv.). Hyperspectral data are used to provide information on LAI growth dynamics, which are integrated into the calibration process. In this context, the aim of this paper is twofold: (i) to describe a Bayesian calibration to 3-PG for future applications of the approach (ii) to illustrate the potential of Bayesian calibration as a means to integrate multi-source datasets (including remote sensing) for reducing model parameters and output uncertainty.

### 1.1 Bayesian Calibration of 3-PG

3-PG is built on a combination of process-based calculations, several key simplifying assumptions and few empirical relationships. The model predicts gross and net primary production and has monthly or annual time steps. It has five state variables – foliage, stem and root biomass, stocking density and available soil water – in conjunction with five submodels – biomass production, biomass allocation, soil water availability and evapotranspiration, mortality, and inventory variables. It has been widely and successfully applied worldwide and increasingly to new species (Waring 2000, Sands & Landsberg 2002). However, "in only a few cases have parameters characterising a species been rigorously determined, and even then this has been largely by a process of trial and error (2002)" (Sands 2004, p.3). By providing parameter estimates, along with measures of uncertainties, Bayesian calibration offers a solution (Gertner et al. 1999, Van Oijen et al. 2005). The chief characteristic of the approach is that the parameters and the data used in the calibration process are presented in the form of probability distributions, reflecting our degree of certainty about them (Jansen 1999). As further information is gained, the distributions are updated. By doing so, Bayesian calibration targets the much-needed platform for expressing parameter and output uncertainty in forest-growth modelling (Van Oijen et al. 2005).

## 2 METHODS

### 2.1 3-PG calibration, study site and input variables

Three of the five 3-PG submodels were implemented here: biomass production, biomass allocation and soil water balance. No stand inventory variables were estimated and mortality was prescribed in a 5-year thinning regime. The model was initialised for a stand aged 15 years and the required climatic data were derived from the Climate Research Unit datasets and the Cambridge botanical garden meteorological station (New et al. 2000, http://badc.nerc.ac.uk/home/index.html). Other input variables include site latitude, an estimate of soil fertility, maximum available soil water (mm per depth of rooting zone, in meters) and a general description of soil texture. 3-PG outputs considered in this study were stem, foliage, root and above ground biomass along with leaf area index (LAI, projected). For a comprehensive description of the model, see Landsberg and Waring (1997) and Sands and Landsberg (2002).

The calibration of the 3-PG model was conducted for CP stands of yield class 14 using data from a 100 ha forest plantation, located in East Anglia, UK (52°30´ N, 0°30´ E). The following datasets were used: (i) The Maestro-1 1989 campaign and the 2000 SHAC campaign datasets (Baker *et al*. 1994, Skinner and Luckman, 2000) which consist of ground data collected on stand level information such as management practices, species composition, tree age, DBH, top height, stemwood volume and basal area. Each sampled stand was allocated a Forestry Commission code, enabling its location on a GIS database. (ii) The Forestry Commission GIS database is a spatially exhaustive catalogue comprising stand level information on species, yield class, planting year, planting density and stemwood volume. (iii) Hyperspectral data acquired using the SHAC airborne hyperspectral imaging spectrometer in June 2000 (126 contiguous bands 436-2486 nm at 15 nm spectral resolution, 4m spatial resolution). Atmospheric correction was applied by DLR and georectification by CEH Monks Wood, UK. The overlapping scenes were mosaicked and normalised to minimise the effect of sensor look angle. A total of 9 noisy bands, corresponding mainly with atmospheric water absorption bands, were removed. CP stands on the GIS database were then located on the image for chronosequencing.

### 2.2 Bayesian Calibration

In Bayesian statistics, probability reflects the degree of certainty for some quantity, conditional to available data and knowledge. As many parameters are not precisely known, this uncertainty is represented as a probability distribution over the parameters. Thus, if we define $\theta$ as a parameter vector for 3-PG, then $P(\theta)$ represents its probability distribution and $P(f(\theta))$ the uncertainty in model outputs, $f(\theta)$, generated by the uncertainty in the parameters. In this context, Bayesian calibration is a method enabling $P(\theta)$ to be updated as new data come in. Given a dataset $D$, we can derive $P(\theta|D)$ from $P(\theta)$ by applying Bayes Theorem: $P(\theta|D) = P(\theta)\ P(D|\theta) / P(D)$. In Bayesian terminology, $P(\theta|D)$ is the updated or posterior parameter distribution; $P(\theta)$ is the original distribution, referred to as the prior; $P(D|\theta)$ is the conditional probability of the data for a given parameterisation, called the likelihood; and $P(D)$ is a normalization constant that may be referred to as the evidence.

#### 2.2.1 Prior and likelihood

The prior distribution is built from distributions for individual parameters that best describe available information about them (e.g. normal, beta, *t*, or uniform). Here, the calibration was applied to 22 3-PG parameters which are listed in Figure 3 (acronyms defined in Sands 2004). As this is our first attempt at quantifying parameters for CP, for each parameter the distributions were set uniform bounded by a biophysically or biologically reasonable maximum and minimum values. These boundaries were derived from ground observations, literature and educated guess and were set to be as inclusive as possible. A remaining 14 parameters were prescribed constant values because the parameter had no influence on the dynamics of the stand (as initialised at 15 years), is a model specific parameter whose value was considered as non sensitive by Esprey *et al.* (2004).

To calculate the likelihood $P(D|\theta)$, i.e. the probability of the data given a specific model parameterisation, information about measurement error must be available. Here we assumed that the errors were independent and Gaussian. $P(D|\theta)$ then follows from the comparison of each datum point $D_i$ with the corresponding model output $f_i(\theta)$ as:

$$P(D|\theta) = \prod_{i}^{n} \varphi(D_i - \mathrm{f_i}(\theta); 0, SD_i) \qquad \textbf{Equation 1}$$

where, $\varphi$ symbolises a Gaussian function with 0 and $SD_i$ as mean and standard deviation, and *n=30*, the number of points in the data sample (detailed below).

The application of Bayes Theorem to process-based models has traditionally been hampered by two problems. Firstly, the models cannot be solved analytically, so a sampling method to explore the parameter space is required. Secondly, the models need to be run at every sampled point in parameter space (to calculate the likelihood), a highly time consuming and computer-intensive process. In recent years, Markov Chain Monte Carlo (MCMC) methods have been found useful to resolve this type of problem (Van Oijen et al. 2005). Here, we used the MCMC Metropolis Hastings Random Walk, which has the two following steps: 1. After randomly choosing a first parameter vector, propose a new candidate for the next parameter vector in the chain from the parameter space as $\theta' = \theta t + \varepsilon$ Where $\theta'$ is the proposed candidate, $\theta t$ is the current parameter vector and $\varepsilon$ is a random vector enabling the exploration of the parameter space. $\varepsilon$ is selected from a Gaussian distribution with mean 0. Its standard deviation should be chosen to enable a wide exploration of the parameter space and to yield acceptance rates (of the rule described below) between 20 and 50%. We found that a standard deviation of 0.05 times the parameter range gave good results. 2. Run the model with the proposed candidate. The rule for accepting or rejecting the candidate has two components, namely (i) Calculate the ratio of probabilities $\beta$ (Eq. 2), which cancels out the need for estimating $p(D)$ and (ii). Generate a uniform random variable *u* ($0 \le u \le 1$). The new candidate $\theta'$ is accepted and becomes $\theta t+1$ *if* $u \le \beta$. If $\beta \ge 1$, the proposal is always accepted. $\beta$ is calculated as:

$$\beta = \frac{p(\theta' | D)}{p(\theta_t | D)} = \frac{p(D | \theta') p(\theta')}{p(D | \theta_t) p(\theta_t)} \qquad \textbf{Equation 2}$$

The acceptance criterion, based on the selection of a random variable, thus may sometimes accept a parameter vector $\theta i$ with lower probability than its predecessor in the chain. This procedure contrasts with many optimisation approaches by allowing downhill steps.

30 data points were used in the calibration exercise derived from the datasets described in section 2.1. These included total above-ground biomass (11), stem biomass including branches (3), foliage biomass (3), root biomass (5) and LAI (8). Although no detailed information on measurement errors was available, we assumed that errors were equal to 5 t $ha^{-1}$ for root, stem and ABG biomass and 1 for LAI. This assumption can be justified by the fact that the emphasis of this paper is to illustrate the applicability of Bayesian calibration for system uncertainty quantification, rather than for gaining explicit knowledge of Corsican pine growth in Thetford.

Above-ground biomass data were derived from the Maestro dataset and the forestry yield tables for Corsican stands of yield class 14, under an intermediate thinning strategy and planted at 2 meters spacing. A biomass expansion factor, converting stemwood biomass to total above-ground biomass was derived from the Maestro dataset, in which both stemwood biomass and total above-ground biomass data are available. The average ratio across ages was used (i.e. 1.2). Stem and foliage biomass data points were derived from Baker et al. (1994). For root biomass, a ratio above to below-ground biomass data was derived from other pine biomass data available from Thetford (Ovington

1957). LAI data points were derived from hyperspectral and ground-based measurement (Ovington, 1957). Leaf area index for pine plantations generally exhibit the growth pattern expressed mathematically as follow (e.g. Mencuccini and Grace 1996):

$$LAI = ae^{-0.5\left(\frac{\ln(x/x_0)}{b}\right)^2}$$ **Equation 3**

Where $a$ represents the maximum LAI value reached by a stand, $x_0$ the age at which this maximum is reached and $b$, a parameter controlling the tailing off of the LAI curve. Equation 3 was solved in a two way procedure: (i) Based on the results by Lee et al. (2004) and Pu and Gong (2004) where close proportionality was found between LAI and the primary axis of a principal component analysis (PCA) for the different wavelengths, PCA was used to estimate LAI growth patterns in Thetford CP stands. Averaged values per stand were plotted against stand age using the GIS attribute database. The parameters $x_0$ and $b$ of Equation 3 were then derived from the remote sensing data points by minimising the distance between the points and the model (Figure 1, right). These parameters pertain to the shape of the curve only, not the magnitude of LAI. (ii) To convert PCA values to LAI, the available projected LAI datum was used. In using Bayesian calibration, the limited information available on LAI does not preclude the use of this data source. Instead, large uncertainties to this dataset are given (Figure 3).

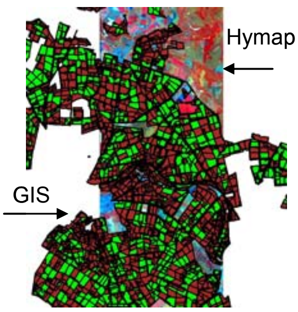


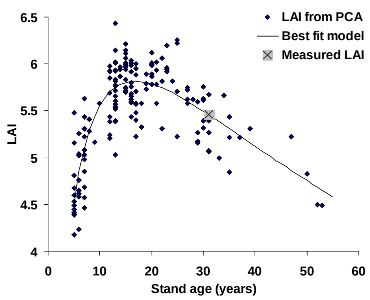


*Figure 1: (Left) False color hymap image with GIS overlay displaying in green areas CP stands of yield class 14. (Right) growth dynamic of leaf area index derived from remote sensing PCA..*

## 3 RESULT

It would be impractical to present the full posterior distribution over the 22-D parameter space. Instead, marginal posterior distributions for each calibrated parameter generated from the MCMC sampling are presented (e.g. Figure 2, left). As an example, the updated distribution for the light extinction coefficient ($k$), a parameter expressing light transmission through canopies, is provided in Figure 2. In Figure 3, the four graphs present the model simulations for stem, foliage and root biomass along with LAI. Three datasets per graph are shown. Firstly, the measured data or the data used in the calibration are shown in red. Standard deviations are also provided. Secondly, the average model outputs from the marginal posterior distributions are shown as black rectangles. Finally, the 3-PG outputs from the parameter vector considered as the single "best" set are shown as the light grey line. In Bayesian terms, best-fit should be understood as the model output generated from the parameter vector with highest a posteriori probability given the available data.

The graph at the right of Figure 3 shows partial correlations between parameters and outputs. Dark blue squares indicate high negative correlations and the dark red, high positive correlations. This fingerprint graph allows insights into how parameters and outputs co-vary. For instance, SLA1, the specific leaf area for mature aged stands, is highly and positively correlated with LAI. Additionally, this correlation is strongest towards the end of the rotation.

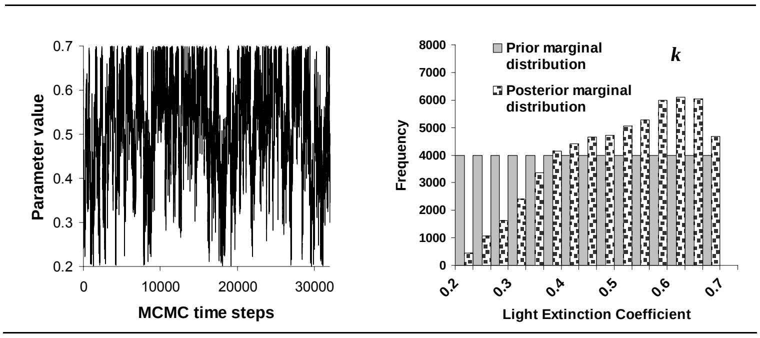


*Figure 2: (Left) part of the MCMC trace plot for the light extinction coefficient (k) (~60 000 steps were executed). (Right) marginal prior (grey) and posterior distributions (dotted).*

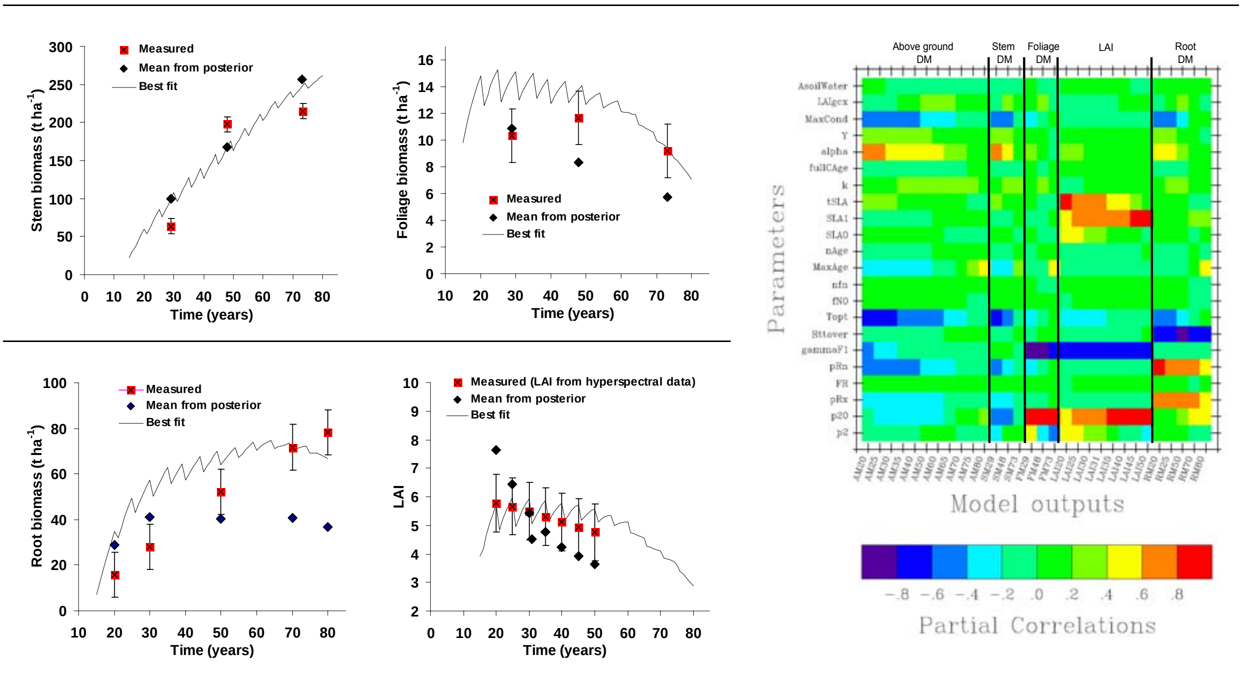


*Figure 3: (Left) the 4 graphics summarise the results from the MCMC sampling (average model outputs from the marginal posterior, black rectangles, and best fit, grey line) in comparison with available data. The grey line and the dark rectangle points were calibrated using the red data points. (Right) partial correlations between parameters and model outputs (see Sands 2004 for parameter notation and description). High positive and negative correlations are indicated as dark red and blue respectively. Model outputs are sorted according to age.*

## 4 DISCUSSION AND CONCLUSION

The results shown in Figures 2 and 3 demonstrate the ability of the calibration to achieve the following aims: (i) Update parameter distributions, given existing knowledge and available data. In this study, a posterior marginal distribution has been generated for each parameter. Knowledge has been gained and this updated distribution can further serve as prior into subsequent calibrations. (ii) Generate marginal posterior distributions for model outputs, thereby providing output uncertainties. The four graphs in Figure 3 suggest that while the stem biomass is well captured by the average model output, the small uncertainty in the stem data, relative to that of foliage biomass, root biomass and LAI, dominates the calibration. Improved datasets on these latter 3 variables may be necessary to fully capture growth dynamics with 3-PG of CP stands in Thetford. (iii) Characterise the joint probability distribution and provide a window into the multivariate interactions embedded in the model by (a.) providing a "best set" parameter vector and (b.) conducting partial correlation analysis between parameters and outputs. While marginal distributions are informative of individual parameters and model outputs, the "best set" vector and the fingerprint figure provide further insights into the model structure. Furthermore, the partial correlation analysis may help in identifying critical model outputs to target in order to reduce the uncertainty of a given parameter and vice versa.

Model parameterisation has too often been achieved by adjusting the value of scalar parameters for the model output to fit data time series, without any indication of parameter and output uncertainty (Sands 2004). This has had two important implications. Firstly, by ignoring uncertainty, such error minimisation approaches have hampered the management of natural resources. Secondly, useful but uncertain data have been ignored in the analyses, thereby excluding important sources of information such as that retrieved from remotely sensed data. The use of RS data in ecological modelling has too often been hampered by the belief that ground surveys provide superior information about forest parameters. By doing so, ecological modellers may have disregarded important data sources providing unique means for temporal and spatial scaling. By advocating the quantification of uncertainties of parameters, thereby yielding uncertainties in model outputs, rather than the derivation of a single, optimised set of parameters based on a goodness-of-fit approach (e.g. the maximum-likelihood approach), Bayesian calibration provides a framework by which information of all sources can be integrated for ecological studies. The use of Bayesian calibration is therefore particularly relevant in conducting truly integrative work, by uniting methods, expertise, data, and systems.

## ACKNOWLEDGEMENTS

The authors would like to thank Richard Waring (Oregon State University), Maurizio Mencuccini (University of Edinburgh) and Peter Savill (University of Oxford) for sharing data and advice. Thanks are due to the BADC for providing access to the Met Office Land Surface Observation Stations Data. This research was supported by the BNSC-Link Carbon Offset Verification project, the Biffaward initiative and the Fonds Québécois de la Recherche sur la Nature et les Technologies (FCAR).

## REFERENCES

Baker, J. R., P. L. Mitchell, Cordney, R.A., Groom, G. B., Settle, J. J. and Stileman, M. R. (1994). Relationships between physical characteristics and polarimetric radar backscatter for corsican pine stands in Thetford forest, Uk. International Journal of Remote Sensing, 15(14): 2827-2849.

Esprey, L.J., Sands, P.J., Smith,C.W. (2004). Understanding 3-PG using a sensitivity analysis. Forest Ecology and Management, 193:235-250.

Gertner, G.Z., Fang, S.F., Skovsgaard, J.P. (1999). A Bayesian approach for estimating the parameters of a forest process model based on long-term growth data. Ecological Modelling, 119:249-265.

Jansen, M.J.W. (1999). Data use and Bayesian statistics for model calibration. In: Stein A., Penning de Vries F.W.T. (eds). Data and models in action. Kluwer, Dordrecht, p 69-80.

Landsberg, J.J., Waring, R.H. (1997). A generalised model of forest productivity using simplified concepts of radiation-use efficiency, carbon balance and partitioning. Forest Ecology and Management, 95:209-228.

Lee, K. S., Cohen, W. B., Kennedy, R. E., Maiersperger, T. K., Gower, S. T. (2004). Hyperspectral versus multispectral data for estimating leaf area index in four different biomes. Remote Sensing of Environment, 91(3-4): 508-520.

Mencuccini, M., Grace, J. (1996). Hydraulic conductance, light interception and needle nutrient concentration in Scots pine stands and their relations with net primary productivity. Tree Physiology, 16:459-468.

New, M., Hulme, M. and Jones, P. (2000). Representing twentieth-centurey space-time climate variability. Part II: Development of 1901-96 monthly grids of terrestrial surface climate. Journal of Climate, 13(13):2217-2238.

Ovington, J.D. (1957). Dry-matter production by Pinus sylvestris L. Annals of Botany, XXI:288-314.

Pu, R.L. and Gong, P. (2004). Wavelet transform applied to EO-1 hyperspectral data for forest LAI and crown closure mapping. Remote Sensing of Environment, 91(2): 212-224.

Sands, P.J. (2004). Adaptation of 3-PG to novel species : guidelines for data collection and parameter assignment. Technical Report. No. 141, CSIRO, CRC Sustainable Production Forestry, Hobart.

Sands, P.J., Landsberg, J.J. (2002). Parameterisation of 3-PG for plantation grown Eucalyptus globulus. Forest Ecology and Management, 163:273-292.

Skinner, L., Luckman, A. (2000). Thetford forest ground data collection campaign in support of the SHAC SAR aquisition, June 2000, University of Wales Swansea, Swansea, Unpublished report. 34p.

Van Oijen M., Rougier J., Smith R. (2005) Bayesian calibration of process-based forest models: bridging the gap between models and data. Tree Physiology 25 (7): 915-927

Waring, R.H. (2000). A process model analysis of environmental limitations on the growth of Sitka spruce plantations in Great Britain. Forestry, 73:65-79.

# FOREST RECONSTRUCTION FROM LIDAR AND CASI DATA: A CASE STUDY FROM AUSTRALIA

*Richard Lucas[1], Alex Lee[2], Peter Bunting[1] and Mark Williams[3]*

[1] Institute of Geography and Earth Sciences, the University of Wales Aberystwyth, Aberystwyth, Ceredigion, UK, SY23 3DB; e-mail rml@aber.ac.uk

[2] School of Resources, Science and Society, the Australian National University, Canberra, ACT 0200, Australia; email alex.lee@anu.edu.au

[3] Defence Science and Technology Organisation, Adelaide, Australia.

## ABSTRACT

Using Light Detection and Ranging (LiDAR) and Compact Airborne Spectrographic Imager (CASI) data (nominal 1 m spatial resolution) acquired over mixed species forests in Queensland, Australia, algorithms for automatically registering the two datasets, delineating tree crowns, discriminating tree species, locating tree trunks, quantifying forest structural attributes (tree height, diameter, crown cover) and estimating total and component (leaf, branch and trunk) biomass are presented. The integration of these products to provide a three-dimensional reconstruction of the forest volume is outlined. Current and potential uses of these datasets for applications ranging from forest inventory and carbon cycle science to assessment of biodiversity are indicated.

**Keywords:** LiDAR, CASI, forests, Australia

## 1 INTRODUCTION

Conveying remote sensing data as a complement or even supplement to ground-based inventory of forests has presented a significant challenge to the scientific community, particularly as many of the basic attributes (e.g., tree diameter, density and species type) that are commonly required (e.g., by forest managers) have proved difficult to retrieve. However, the research outlined in this paper demonstrates that by combining small footprint Light Detection and Ranging (LiDAR) and Compact Airborne Spectrographic Imager (CASI) data (nominally 1 m spatial resolution) acquired over open forests and woodlands in Australia, detailed characterisation can be undertaken to a level considered appropriate for assisting forest inventory and management and informing both science and policy.

An overview of the LiDAR and CASI processing algorithms developed and the integration of forest-related products from both datasets is presented in Figure 1. In addition to the height and reflectance data from the LiDAR and CASI instruments respectively, the suite of algorithms requires prior calculation of derived data, including a LiDAR canopy height model (CHM) and Height Scaled Crown Openness Index (HSCOI) plus simple ratios of CASI reflectance bands. Registration of the CASI and LiDAR data and delineation of tree crowns is a pre-requisite and both procedures are now automated. The LiDAR data are then used primarily to retrieve structural attributes (e.g., diameter, crown height and cover, and tree density) whilst the CASI data are used for differentiating and classifying common tree species. The integration of these derived products (i.e., height and species maps) with species-specific allometric equations allows estimation of total and component (leaf, branch and trunk) biomass for delineated crowns. The three-dimensional distribution of these components can also be reconstructed to provide a quantitative and visual representation of the forest volume. Such information can be used subsequently to support biodiversity assessment, carbon cycle science, forest management and the interpretation of other remotely sensed data (e.g. radar).

The following sections provide more detail on these algorithms, most of which are fully automated and can be applied across large areas where appropriate datasets are available. However, as many are quite complex, these are described only briefly and the interested reader is directed to the cited papers for more information.

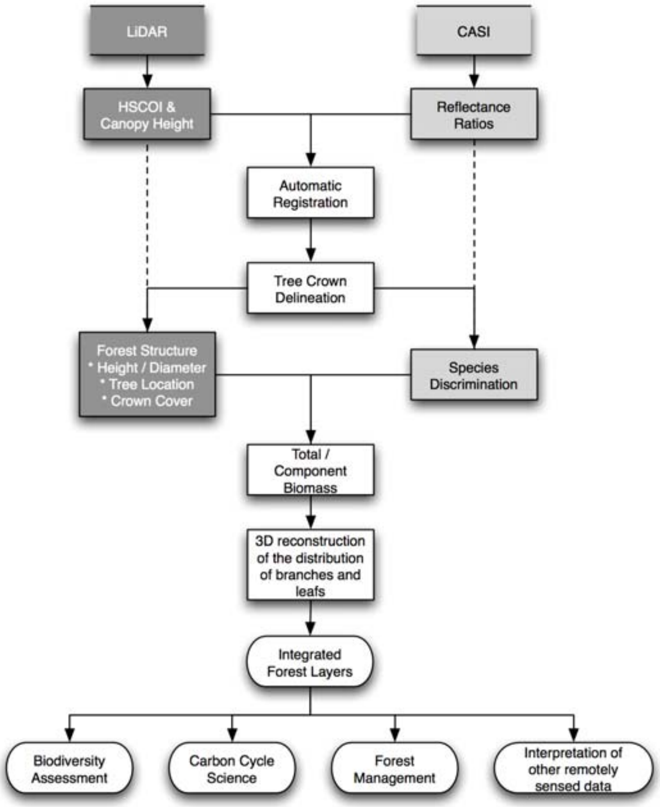


*Figure 1. An overview of algorithms developed for quantitative reconstruction of the forest volume and to support forest-related applications.*

## 2 DERIVED DATASETS

Several surfaces derived from the LiDAR data are necessary for delineating crowns and retrieving forest attributes (e.g., crown cover, height). From the LiDAR data, the highest returns within the vertical profile (nominally 1 m grid cells) are used to produce the CHM, whilst the relative penetration of near infrared pulses into the forest volume, with respect to the highest return in the stand, is described using the HSCOI. HSCOI raster values range from 0 and 100 %, with these values associated with no and complete penetration to the ground surface respectively. Simple ratios of the CASI reflectance bands (typically the red, red edge and near infrared) are also calculated for use in automated registration and crown delineation procedures.

## 3 AUTOMATED REGISTRATION

As is common in many studies, the CASI and LiDAR sensors were mounted on different aircraft, although the data were acquired over a similar time period. Both datasets were acquired with full Differential Global Positioning Systems (dGPS) and Inertial Navigation Systems (INS), but differences between data types, flying conditions and flight paths led to inconsistencies in registration between images. Whilst interactive procedures based on ground control point selection provided reasonable registration between the LiDAR and CASI data, these were time-consuming and automated registration procedures were therefore considered necessary. Appearance-based methods were therefore applied to the CASI ratio bands and the LiDAR CHM and resulted in better registrations compared to the more traditional method. For the registration, histogram (e.g., Mutual Information; Varshney and Arora, 2004) and vector-based (e.g., Euclidean distance, Manhattan distance) measures provided similar successes in registration.

## 4 DELINEATION OF TREE CROWNS

The delineation of tree crowns is needed to define the extent of forest cover but also to map individuals or clusters of crowns (herein referred to as crowns only) and attribute these subsequently with information relating to their structure, biomass and species type. Procedures for delineating crowns were developed independently for the LiDAR and CASI data, although these produced similar results in terms of the location, number and areas of crowns delineated.

To delineate crowns within the CASI data, an algorithm was developed within eCognition Expert (Bunting and Lucas, 2006) that first divided the scene into forest and non-forest objects (groups of pixels) using a combination of the $\rho_{446}$ (red) $\rho_{714}$ (red edge) and $\rho_{838}$ (near infrared) reflectance bands. Processes were then implemented that successively split and merged forest objects to delineate crowns, with rules for identifying and classifying objects as crowns based on a combination of the reflectance ($\rho$) ratios $\rho_{741}/\rho_{680}$ and $\rho_{741}/\rho_{714}$. The delineation was assisted by the prior division of objects into different spectral types that could be associated with common species groups. Comparisons with ground data indicated accuracies ranging from 48 % to 80 %, with these decreasing as tree density and the degree of canopy layering increased.

To delineate crowns within the LiDAR data, a threshold of the HSCOI surface that encompassed ~ 90–95 % of the original LiDAR point height data was first used to map forest extent. Spatial smoothing of the HSCOI surface undertaken at multiple scales allowed crown of varying size within the forest area to be identified. These were then delineated by applying hydrological basin delineation routines. LiDAR apparent vertical profiles for each crown object facilitated their division into decurrent (wide-spreading crowns typical to *Eucalyptus* species) or excurrent (small, compact crowns typical to *Pinus* species) forms and appropriate refinement of the delineation based on form-specific empirical relationships between the tree height and crown area. A close correspondence with crowns delineated within the CASI data and observed in the field was obtained.

## 5 TREE SPECIES DISCRIMINATION

Several studies have established that the classification of delineated crowns to species from optical remote sensing is best achieved by extracting spectra from the sunlit (meanlit) portions of crowns. The meanlit area is determined by first taking the average values of each delineated crown object in a particular band (or a derived product such as a vegetation index) and identifying all pixels in the crown object with values above this threshold. Spectra from all bands are then extracted from these pixels only and averaged such that a single spectrum is associated with the crown.

Using 343 crowns of known species to train and test a multiple (stepwise) discriminant analysis, the meanlit spectra extracted using the $\rho_{742}/\rho_{714}$ ratio image provided better accuracies (typically exceeding 80 %) in the classification of species compared to when reflectance bands or other derived measures were used. The levels of accuracy assumed some *a priori* knowledge of the species composition of the forests and reduced where rare or particular combinations (with similar spectral characteristics) of species occurred within the same area of forest.

## 6 FOREST STRUCTURAL MAPPING

Forest structure at the plot level is typically described in terms of tree stem density, height and diameter distributions (including basal area), and canopy cover. However, LiDAR offers opportunities also for quantitatively describing the vertical distribution of canopy elements (foliage and wood), either through summary statistics of LiDAR returns within the vertical profile or through three dimensional visualisation and characterisation.

An approach considered for estimating stem density was to simply count the centroids of the crown polygons delineated using the CASI and/or LiDAR. However, many trees occurring beneath the sub-canopy or as individuals within a cluster were often excluded. Comparisons with the locations of field stems indicated that the minima within a LiDAR-derived HSCOI surface smoothed using a 5 m square kernel corresponded to the locations of larger individuals within both the overstorey and crown clusters. Smaller trees (typically with $D_{130} \leq 10$ cm), including those in the sub-canopy, were also encompassed using the local minima of the HSCOI smoothed with a circular kernel of 1 m radius. Therefore, by combining these two surfaces, trees occurring within different canopy layers (i.e., overstorey, sub-canopy) could be located and their position in the vertical strata noted, and stem density could be estimated.

For overstorey trees, the LiDAR measure of tree height corresponded well with that measured in the field and the diameter (@ 130 cm; $D_{130}$) could be estimated using empirical relationships established between field measurements of height and $D_{130}$. For trees in the sub-canopy, a close relationship between height and the HSCOI value was also observed. Therefore, when the LiDAR CHM was deemed inappropriate, heights were retrieved from the HSCOI instead. By integrating the relationships with the LiDAR height and HSCOI surfaces, a greater number of trees could be attributed with both height and $D_{130}$, to reasonable levels of accuracy. In complex forest situations with multiple stems in close proximity to larger overstorey crowns, the overall retrieval of height and $D_{130}$ was less successful, as indicated by the reduced correspondence with field measurements. Once retrieved, both attributes were scaled up to the stand level to generate estimates of basal area and predominant height. A summary of correspondence between these field and remotely sensed measures is presented in Table 1 (Tickle *et al*., 2006; Lee & Lucas, 2006).

Several approaches were successful in obtaining stand-level estimates of canopy cover including a) establishing empirical relationships between LiDAR data and field measures (Tickle *et al*., 2006) and b) summing the area of crowns delineated within the LiDAR data to obtain an estimate of cover. In the latter case, a closer correspondence with the summed crown area at the plot level was observed when crown cover was estimated using the LiDAR HSCOI surface rather than the LiDAR CHM as a better representation of the amount and distribution of foliage and branch elements in the vertical profile was obtained. The vertical distribution of foliage and wood distributions at both the crown/cluster and plot level could also be represented using apparent vertical profiles to give an insight into layering within the forest.

*Table 1. Comparisons between LiDAR and field-derived measures of tree and stand attributes*

| Tree Level Attribute | $r^2$ | RMSE | N | Plot Level Attribute[4] | $r^2$ | RMSE | N |
|---|---|---|---|---|---|---|---|
| Height (m) [1] | 0.91 | 1.34 | 100 | Basal area ($m^2\ m^{-2}$) | 0.61 | 2.69 | 30 |
| Height (m) [2] | 0.81 | 1.85 | 115 [3] | Predominant Height (m) | 0.91 | 0.77 | 30 |
| $D_{130}$ (cm) [2] | 0.65 | 6.89 | 119 | Crown Cover (%) | 0.78 | 9.24 | 30 |
| | | | | FBPC (%) | 0.89 | 5.49 | 30 |

[1]LiDAR CHM, single isolated overstorey trees only (Tickle *et al*., 2006); [2]LiDAR canopy height and HSCOI, for random selection of trees $D_{130} \geq 5$cm; [3] four outliers removed; [4]HSCOI-derived (Lee & Lucas, 2006).

## 7 FOREST BIOMASS (TOTAL AND COMPONENT) DISTRIBUTIONS

Following the retrieval of structure and species information from the LiDAR and CASI data respectively, the total above ground and component (leaf, branch and trunk) biomass of delineated crowns could be quantified by applying species-specific biomass equations (e.g., Burrows *et al*., 2002). This process was optimized by the automated registration procedures as crowns delineated and discriminated to species using the CASI data could be better associated with the LiDAR measurements of height, which was used as the primary independent variable in the equations. Estimates of biomass were then scaled-up to the stand level. An alternative approach that produced satisfactory results was to apply step-wise linear regressions established using six different heights from both sub-canopy and overstorey layers, and crown cover (Lucas *et al*., 2006a).

The three-dimensional distribution and amount of biomass held within tree components was also approximated by modelling leaf and branch locations and linking these to tree stems mapped using the HSCOI. The modelling first involved creating a 1 $m^3$ voxel grid based on the horizontal and vertcal distribution of LiDAR returns. Foliage and small branches were then distributed in equal proportions to voxels associated with individual stems of known species (Lucas *et al*., 2006b). Large branch distributions were determined by identifying local clusters of voxels and modelling a branch emanating towards the trunk at an angle approximating the mean angle, as determined for different species and growth forms from field data. Secondary branches were modelled by assuming these emanate from the base of voxels and join onto the primary branch at a position proportional to their distance away from the main trunk. On this basis, the distribution of all components (leaves, branches of varying order and trunks) within the forest volume was determined. Subsequent conversion of these components to biomass utilised rules associated with their sizes (e.g., volume) and wood densities (in the case of woody material; Lucas *et al*., 2006b). Using visualisation software, the forest was also reconstructed to produce a visual representation of the distribution of tree components within the forest volume, with these comparing well to field-based photographs.

## 8 WIDER APPLICATION

The algorithms developed for the characterisation and reconstruction of the selected forests are considered to be robust for wider implementation and have direct application to forest assessment in other regions of Australia, and also overseas. The data and products have already been used to support the development of forest mapping using other remote sensing datasets including a) 3D forest quantitative reconstruction for coherent SAR simulation (Lucas *et al*., 2006b, Williams *et al*., 2006), b) better understanding of microwave interaction with different components of the forest and the importance of sensor parameters (frequency, polarisation and incidence angle) for biomass retrieval (Lucas *et al*., 2004; 2006a), c) improved techniques for mapping woody regrowth using a combination of lower frequency radar and Landsat-derived FPC data (Lucas *et al*., 2006c), and d) interpretation of coarser spatial resolution hyperspectral (e.g., HyMap) data for forest classification and assessment of tree species diversity. In future work, the algorithms will be implemented across the Injune study area to provide baseline datasets of forest biomass, structure and species to support regional mapping using spaceborne remotely sensed data including that provided by Japan's Advanced Land Observing Satellite (ALOS), which was launched successfully in 2006.

## ACKNOWLEDGEMENTS

The authors thank the Australian Research Council, the Queensland Department of Natural Resources and Mines, the Bureau of Rural Sciences, the Australian National University, the Australian Defence Science and Technology Organisation, the Cooperative Research Centre for Carbon Accounting, Definiens Imaging and the EU AMPER Network, UWA IGES and Ball Aims.

## REFERENCES

Bunting, P. and Lucas, R.M. (2006). The delineation of tree crowns within CASI data of Australian mixed species woodlands (*Remote Sensing of Environment, in press)*

Burrows, W.H., Hoffman, M.B., Compton J.F., Back, P.V., & Tait, L.J. Allometric relationships and community biomass estimates for some dominant eucalyptus in central Queensland woodlands. *Australian Journal of Botany*, 48, 707-714, 2000.

Varshney, P.K. and Arora, M.K. (2004). Hyperspectral Sensors: Past, Present and Future: In P. K. Varshney and M. K. Arora (Eds.) *Advanced Image Processing Techniques for Remotely Sensed Hyperspectral Data*, John Wiley.

Leckie, D.G., Gougeon, F.A., Tinis, S., Nelson, T., Burnett, C.N., & Paradine, D. (2005). Automated tree recognition in old growth conifer stands with high resolution digital imagery. *Remote Sensing of Environment*, 94, 311-326.

Lee, A. and Lucas, R.M. (2006). A LiDAR-derived canopy density model for tree stem and crown mapping in Australian forests. Forest Ecology and Management (in preparation).

Lucas, R.M., Moghaddam, M. and Cronin, N (2004a). Microwave scattering from mixed species woodlands, central Queensland, Australia. *IEEE Transactions on Geoscience and Remote Sensing*, 2142-2159, October, 2004.

Lucas, R.M., Cronin, N., Lee, A., Witte, C. and Moghaddam, M. (2006a). Empirical relationships between AIRSAR backscatter and forest biomass, Queensland, Australia, *Remote Sensing of Environment*, 100 (2), 407–425.

Lucas, R.M., Lee, A. and Williams, M. (2006b). The role of LiDAR data in understanding the relationship between forest structure and SAR imagery. *IEEE Transactions in Geoscience and Remote Sensing* (submitted).

Lucas, R.M., Cronin, N., Moghaddam, M., Lee, A., Armston, J., Bunting, P. and Witte, C. (2006c). Integration of Radar and Landsat-derived Foliage Projected Cover for Woody Regrowth Mapping, Queensland, Australia. *Remote Sensing of Environment*, 100 (3), 388 – 406.

Tickle, P.K., Lee, A., Lucas, R.M., Austin, J. and Witte, C. (2006). Quantifying Australian forest and woodland structure and biomass using large scale photography and small footprint Lidar. *Forest Ecology and Management*, 223 (1-3), 379-394.

Williams, M.L., Lucas, R. M., Lee, A. C. and Cloude, S. R., (2006) *Potential of Proposed Sensors for PolInSAR with Mixed-Species Forest in Australia*, Proc. EUSAR 2006, Dresden, Germany (in preparation).

# PROSPECT OF AUTOMATED CLASSIFICATION OF TREE SPECIES COMPOSITION FROM IKONOS SATELLITE IMAGERY

*Filip Hájek*

University of Agriculture Prague, Department of Forestry Management, Prague, Czech Republic; hajek@fle.czu.cz

## ABSTRACT

Forest inventories conducted on large areas with laboured manual RS data interpretation increasingly call for a development of knowledge-based classification methods. Considering multitemporal image analysis, VHR satellite data have many advantages over traditional aerial photos for such purposes. This study explores and demonstrates technique of automated identification of tree species composition from Ikonos imagery using object-oriented classification approach. Methodology developed to process 4m/pan data incorporates two major steps. In order to enlarge class signature space, additional channels were calculated and their contribution to class separation assessed by discriminant analysis. Besides, the height information from 2-m resolution DEM was also employed. The image segmentation and classification were conducted on several levels to create hierarchical image object network, where the higher level aimed to separate image into smaller parts regarding stand maturity and canopy structure and the lower (detailed) level assigned individual tree clusters into classes for the main forest species. The developed rule-base was applied on datasets of different resolution and the results were compared by means of classification accuracy (KIA). Further, the utilization of 4-m and 1-m images in different forestry management tasks is discussed.

**Keywords:** OO image analysis, Ikonos VHR, tree species composition, forest management

## 1 INTRODUCTION

Lately, the methods of tree species identification from satellite imagery have been widely explored. Some studies (Bucha 1998) aimed to estimate forest species composition using moderate resolution data such as Landsat TM, Spot HRV, while the relevant studies on VHR satellite imagery (Ikonos, QuickBird) seem promising for the species identification at the individual tree level. As demonstrated by several authors (Hill and Leckie, 1999) (Gougeon, 1997b), working at a tree scale has a potential to extend digital remote sensing into many new areas such as forest stand extraction, forest regeneration, logging practices, etc. In the same time, however, many studies proved the RS methods based solely on spectral classification insufficient for detailed forest mapping (Wack and Stelcl, 2005). The enhanced height information from LiDAR and its integration with the tree species estimates from optical data are nowadays in the main focus for purpose of detailed 3D stand modelling.

In the environment of Czech forest sector, the estimation of species distribution is traditionally based on the area coverage acquired by terrestrial methods. Even manual interpretation of aerial photos never quite met the needs of forest inventories, as reported by the official authorities. Nevertheless, the increasing demands on the level of inventory precision, information resolution and repeatability call for the development of practical application based on automated image analysis to be utilised in forest management. This study deals with the automated method of tree species composition estimation from Ikonos imagery using object-oriented approach. The presented methodology was tested on both 4-meter and pan-sharpened Ikonos images with the aim to compare and describe the two datasets to meet the forestry needs. Besides, the prospect of the knowledge-based classification using VHR data in operational forestry was suggested.

# 2 METHODS

## 2.1 VHR imagery and additional input data

### 2.1.1 Image data

The image from sensor IKONOS-2 acquired on 7th June 2003 with spatial resolution of 4m in MS and 1m in pan mode were processed. The nominal Collection azimuth and elevation were 105.4862° and 76.79404°, the Sun angle azimuth and elevation were 155.8632°and 61.15952°.

The subset of 4x4km representing an industrial forest area close to town Žlutice (50°05'N, 13°12'E), CZ was selected. The predominantly flat site comprised of large patches of old Spruce (Picea Abies L.) often mixed with Pine (Pinus Silvestris L.), extensive mature Oak (Quercus Robur L.) forests and also Birch (Betula pendula L.), Larch (Larix deciduas Mill.) and young plantations of Pine and Oak. Besides, smaller proportions of Maple (Acer pseudoplatanus L.) could be found inside forest stands and along the margins. In both areas, planted mature stands were mostly of the same age, but very heterogeneous in species composition, stocking density and canopy structure. The natural regeneration in addition to the planted trees sometimes occurred.

### 2.1.2 DTM

The digital contour map from ZABAGED® GIS database produced by Czech Office for Surveying, Mapping and Cadastre (COSMC) in scale of 1: 10 000 were used as a source of height information. Then the DEM was created with resolution 2m/pixel. Lambertian Reflection Model was initially tested in order to reduce topographic effects. However, the transformed image was unsuitable to use due rapid radiometric shift and so the shade layer was instead calculated to normalise the image for varying illumination. Besides, the height information was used as an additional input during the classification phase.

### 2.1.3 Field GIS

Based on the previous information from LHPO forest inventory database, twenty 400m$^2$ plots covering areas with 100% species composition were located as a reference data. Sample plot selection put emphasis on size and class purity to provide representative basis for accuracy assessment. The boundaries of each plot were determined with differential GPS SX Blue™ and PDA with ESRI ArcPad™ mobile GIS.

## 2.2 Image analysis

Object-oriented classification in software eCognition (Definiens Imaging, Germany) was the main image analysis method. This approach features an enhanced technique of multi-resolution image segmentation, complex capability in object description (spectral, geometric, textural and contextual), hierarchical image object network and fuzzy rule base classification.

### 2.2.1 Segmentation

Segmentation was conducted stepwise on three levels using different scales to construct the hierarchical image object network. The primary level was created using large Scale parameter and after preliminary classification was done for basic landuse classes. Other two sublevels were segmented only within the forested area using smaller Scale parameter and using classification-based segmentation (Table 1.)

*Table 1. Segmentation parameters for analysis of Ikonos 4-m and Ikonos pan-sharpened images*

| Segmentation level | Scale 4m/pan | Homogeneity criterion | | | |
|---|---|---|---|---|---|
| | | Color | Shape | Shape settings (Compact/Smooth) | |
| Level I – Landuse | 25 / 60 | 0.8 | 0.2 | 0.5 | 0.5 |
| Level II – Forest | 18 / 45SB | 0.7 | 0.3 | 0.5 | 0.5 |
| Level III - Stand | 5 / 12 SB | 0.7 | 0.3 | 0.7 | 0.3 |

### 2.2.2 Signature space enlargement and feature selection

In order to enhance class separability, the signature space was enlarged by the calculation of additional channels in pre-processing phase in Erdas Imagine 8.7. Various spectral features based on original channels and also derived band rationing were calculated as “Customised features” in eCognition 4.06. Considering all relevant features (color, texture, and context), the dimensionality of dataset increased and therefore methods of feature selection were needed. Layers tested for the significant contribution included: spectral ratios and vegetation indices (NDVI), Tasseled cap and IHS transformation, low-pass filters, Sobel edge detection and GLCM texture measures.

In each class, 30 sample objects were manually classified based and the reference field data and then the visual and statistical techniques of feature contribution were tested. Discriminant analysis was used to find optimal variables for distinction of different stand structures. The contribution of 15 selected features was assessed using F-test and the best feature combination was found using Wilks Lambda statistics in stepwise procedure. Further, the result of the statistical analysis was reviewed using the visual assessment of the feature distribution comparing histograms of two selected classes at the time. The significant contribution to class separation was found for these features:

- Mean spectral values of visible Green and NIR Ikonos bands together with the Customized features such as NIR/Red, Green/NIR, NDVI ratios and their derivatives normalized by Shade layer were predominantly used for the classification of tree species based on spectral information
- Sobel Edge layer calculated for IR Ikonos band, 2nd (saturation) channel of IHS transformation and GLCM texture feature Variance of window size 3 x 3 were applied to separate agriculture and vegetation areas of different textures and to differentiate forested areas, regenerating areas and clearcuts
- DEM values served to separate forest/agriculture bare soil areas

Besides the classification stage, channel of Median filter with kernel 3 x 3 was tested and used during initial segmentation of highly textured pan sharpened data.

### 2.2.3 Fuzzy rule-based classification

The classification process was controlled by a rule base describing characteristics of individual classes by means of fuzzy membership functions. Each class description consisted of a set of fuzzy expressions allowing the evaluation of specific features and their logical operation.

The three levels of hierarchical image object network were used to delimit classes. Level 3 comprised basic “Landuse” types - Urban, Fields and Forest. This served to mask all non-forest areas. The lower level 2 “Forest” aimed to separate forest regions into areas of bare ground, mature stands and young stands, where classes “plantation (transition)” and young stages of conifers, broadleaves and other were further distinguished. “Other” young forests were mostly consisted of Larch and Birch trees. The detailed level 1 “Stand” was set to distinguish four main forest species in the area - Quercus, Acer Picea, Larix and Betula. Further, structures of shadows and bare ground were classified on this level. All classes of “Forest” level were also recognised at the lower “Stand” level for purpose of post classification improvement.

## 3 RESULTS

The knowledge base initially created for 4m image was also applied with minor threshold modifications to the pan-sharpened data, so the comparative results were achieved. Then 20 samples for each class of the “Forest” and “Stand” classification levels were selected in accordance with the GIS field reference data and the common accuracy statistics were calculated from the assembled error matrix.

The overall classification result at the lowest “Stand” level was very similar for both tested datasets. As deduced from the accuracy assessment (Table 2), there is no crucial difference between 4-meter and pan-sharpened Ikonos imagery in ability of identifying tree species composition in terms of area coverage. The very good result of more than 90% was obtained for classes Acer and Picea, and class ground with approx. 80 %. The lower agreement (around 75%) was achieved for Betula and Larix and for the class transition (60%). Besides, some differences linked the image resolution occurred. This was most evident for shadows, where pan Ikonos gained nearly 30% in accuracy for over 4-m image.

*Table 2. Selected accuracy measures for "Stand" level of Ikonos 4m / pan classification. The statistics were derived for each class, Overall Accuracy and the Kappa index of agreement represent aggregated results*

| Cover type / Stats | shadows | ground | transition | Acer | Querc | Picea | Betula | Larix |
|---|---|---|---|---|---|---|---|---|
| KIA per class (4m) | 0.68 | 0.85 | 0.63 | 0.92 | 0.92 | 0.92 | 0.70 | 0.77 |
| KIA per class (pan) | 0.94 | 0.78 | 0.58 | 1.00 | 0.77 | 0.94 | 0.82 | 0.61 |
| Overall acc (4m/pan) | 0.83 / 0.83 | | | | | | | |
| KIA (4m/pan) | 0.80 / 0.81 | | | | | | | |

*Table 3. Selected accuracy measures for "Forest" level of Ikonos 4m / pan classification. The statistics were derived for each class, Overall Accuracy and the Kappa index of agreement represent aggregated results*

| Cover type / Statistics | ground | plantat | mature | Y conifer | Y broadl | Y other |
|---|---|---|---|---|---|---|
| KIA per class (4m) | 0.63 | 0.64 | 0.74 | 0.36 | 0.30 | 0.76 |
| KIA per class (pan) | 0.48 | 0.36 | 0.87 | 0.61 | 0.88 | 0.82 |
| Overall accuracy (4m/pan) | 0.63 / 0.71 | | | | | |
| KIA (4m/pan) | 0.57 / 0.66 | | | | | |

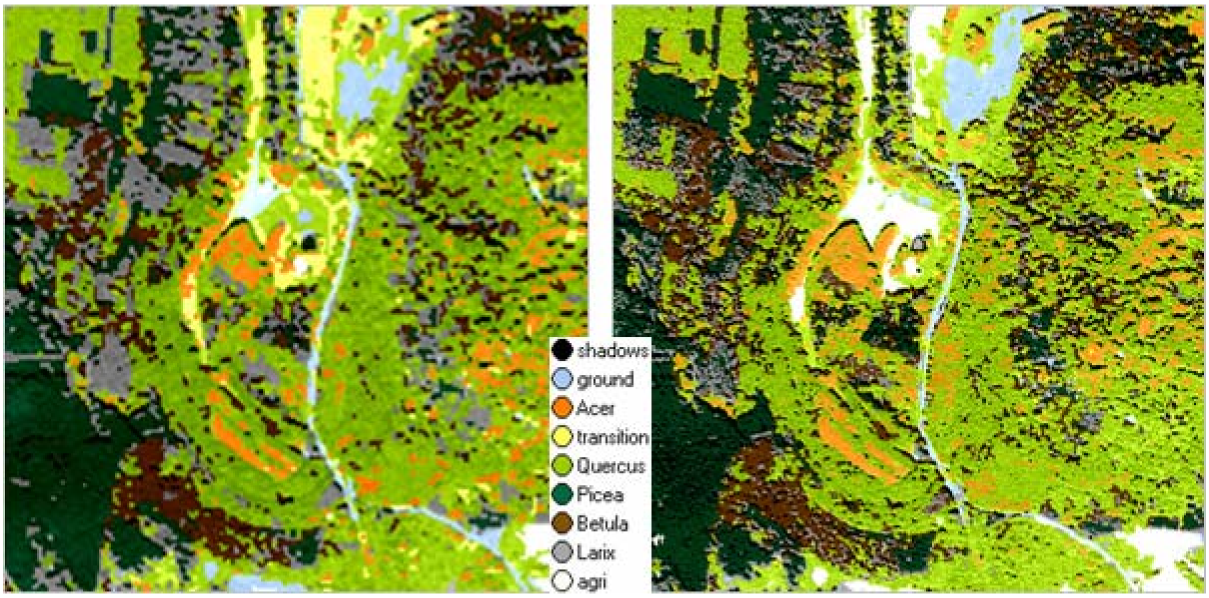


*Figure 1: Forest species classification from Ikonos 4m vs. pan-sharpened imagery*

The result of classification at the "Forest" level was also evaluated and the datasets of 4m/1m spatial resolution compared. The statistical measures (Table 3) indicate the overall accuracy improvement of nearly 10% when analysing pan sharpened Ikonos data. This was especially evident for delineation of the stand boundaries of young forest stages (conifers, broadleaves, other). Classes ground and plantation (transition), on the other hand, were better identified in 4-meter data. The fact is possibly connected to the different influence of textural information, as it was substantial for classification at this level.

## 4 DISCUSSION

As shoved in several previous studies, the standalone optical RS methods are insufficient for classification of complex forest structures. This is particularly true for young succession stages and heterogeneous mature stands. For purpose of tree species identification, however, very good results can be achieved by the combination of object-oriented approach and the topo-corrected VHR (both 4m and pan) Ikonos data with derived image transforms. The OO classification rules based on fuzzy membership functions are highly convertible and the knowledge-base can be transferred and applied to other data by means of recorded protocols. Among the calculated layers contributing to the classification, ratios of Green and NIR bands, Sobel edge and GLCM Variance are the most significant. The spectral signatures normalised with the high resolution DEM can further enhance the classification. Besides, the segmentation of pan-sharpened images can benefit from use of median filtering. The ability of delineation of young stands is dependent the amount of texture information, thus the analysis of 1-m spatial resolution imagery is suggested. Such data require careful determination of object scale with the perspective of broader context. However, the higher amount of detail brings the new opportunities in object description, where the multilevel mutual relations are of special advantage.

## 5 CONCLUSIONS

This study aimed to compare classification results of 4-m and 1-m resolution Ikonos imagery. Both data types have their benefits and should be utilised in different forest management tasks with respect to the price. While 4-m Ikonos allows to estimate percentage distribution of the tree species at sufficient scale, the pan-sharpened data has potential to expose detailed structures within forest stands but also canopies of individual trees. Classification of tree species composition with such high level of detail and accuracy would be suitable to combine with LiDAR data for advanced 3D stand modelling. Still, the prospect of the method utilisation is dependant on the existence of capable knowledge-based system, sufficiently robust for high level of automation. The further research will focus on object analysis of IR aerial photos.

## ACKNOWLEDGEMENTS

This study was supported by Grant Project No. QG50097/2004 funded by the National Agency for Agricultural Research (NAZV) under the research program MZe 2005-2009.

## REFERENCES

Baatz, M. and Schäpe A., 1999. Object –oriented and multi-scale image analysis in semantic network Proc. Of the 2nd International symposium on operationalization of remote sensing, Enschede ITC.

Brandtberg, T. 1999. Automatic individual tree-based analysis of high spatial resolution remotely sensed data. Acta universitatis agriculturae Sueciae, Silvestria 118,

Bucha, T. (2004). Classification of health condition of forests from Ikonos satellite scenes by the methods of spectral and object-oriented analysis. Lesnicky Casopis. 2004; 50(1): 63-83.

Halounová, L. 2003. Textural classification of B&W aerial photos for the forest classification. EARSeL conference, Gent, Belgium

Leckie, D.G., Gougeon, F.A., Walsworth, N., Paradine, D. 2003. Stand delineation and composition estimation using semi-automated individual tree crown analysis. Remote Sensing of Environment 85, 355–369

Rencher, Alvin C. (2002). Methods of Multivariate Analysis, 2nd Edition. © 2002 John Wiley & Sons, Inc. pp 270-298

# SINGLE TREE DETECTION IN HIGH RESOLUTION SATELLITE IMAGES AND DIGITAL AERIAL IMAGES USING ARTIFICIAL NEURAL NETWORKS AND A GEOMETRIC-OPTICAL FOREST MODEL

*Kenneth Olofsson and Olle Hagner*

Swedish University of Agricultural Sciences, Remote Sensing Laboratory, Umeå, Sweden;
kenneth.olofsson@resgeom.slu.se, olle.hagner@resgeom.slu.se

## ABSTRACT

The presentation reports on the work and preliminary results of an on-going 3-year project aimed at the development of advanced methods for detection and measurement of single trees in high-resolution satellite imagery e.g. IKONOS, Quick Bird and airborne optical sensors. The apparent radiance pattern of single tree canopies and corresponding cast shadows depends on the viewing and illumination directions, tree species, topography and atmospheric conditions. There is also a large variation among trees of the same species, due to age, size, branch structure etc. The patterns are also affected by the spatial arrangement of neighbouring trees due to cast shadows and occlusion effects. If the forest is dense and regularly spaced the contrast between the sunlit part of tree crowns and shaded background allows for the use of simple “blob segmentation” algorithms or template matching techniques. However, sparse or open forest conditions motivate more advanced methods that explicitly accounts for the spatial arrangement of neighbouring trees. The detection algorithms developed in this project are based on a learning system approach using artificial neural networks. The networks are trained on datasets generated by a new geometric-optical model developed specifically for this application. Early results show single tree detection, by artificial neural networks, in high resolution remote sensing images using the geometric-optical model.

**Keywords:** Single tree detection, geometric-optical model, high-resolution satellite images, neural networks, National forest inventory

## 1 INTRODUCTION

The spectral signature alone for groups of trees (many trees per pixel, as obtained with for example Landsat TM or SPOT HRV) does not contain sufficient information to effectively resolve tree size and structural parameters. The reason for this ambiguity is that canopy closure; leaf area index, species composition and the ground cover type are the main driving factors for the spectral reflectance (Syrén, 1990, Hagner, 1997, Nilsson et al., 2003). The specific effects of tree size and vertical canopy structure are quite marginal. It has however been shown that the structural properties of the forest canopy has a significant influence on bi-directional reflectance (Li and Strahler, 1986) thus indicating that repeated imaging from multiple viewing angles might resolve some of the ambiguity. As a consequence, the spectral response to increased stem volume saturates as the forest canopy approaches full closure. Another problem is that the response from the forest canopy cannot easily be separated from that of the ground vegetation. The inability to separate density from size and ground vegetation severely limits the utility of medium resolution satellite imagery for operational forestry management at the stand level (Holmgren and Thuresson, 1998).

The new generation of high-resolution satellite imagery with a resolution of 2 meters or better allows for individual tree canopies to be resolved and separated from the background which provides the means for truly effective characterisation of tree size, stand structure, and ground vegetation.

Single tree detection in high-resolution optical imagery has been demonstrated in several studies. It has been shown that relatively simple algorithms are quite sufficient in the case of well-stocked homogenous coniferous stands viewed in nadir (Pinz, 1989, Dralle and Rudemo, 1996). Broadleaf trees with irregular crown shapes can be delineated with contour-following methods (Gougeon, 1995, Brantberg, 1999). Medium-stocked or open uneven-aged forests are much more challenging, since the pattern and contrast of cast shadows tend to dominate over the tree crown pattern. These cases require more advanced methods based on a geometric-optical model of tree canopies that accounts for the specific illumination- and viewing geometry (Pollock, 1996, Korpela 2004). One of the more problematic forest types are dense stands of broadleaf trees with irregular shaped crowns that blend into each other and form a more or less continuous forest canopy. Although it is almost impossible to identify individual trees in this case, the pattern still contains valuable information on species, age- and size distribution etc. that can be extracted with texture-based methods (Pollock, 1996, Hagner, 1997, Franklin, 2001). If the spatial resolution is sufficient to derive textural characteristics from within individual tree crowns the classification of species can be improved (Pollock, 1996, Brandtberg, 1999).

A common feature of the detection algorithms mentioned above is that they do require some form of parameter tuning in order to produce useful results. Unless there is reliable ground truth available, the tuning has to be done subjectively with ad-hoc methods, which is not satisfactory if the method is required to produce consistent or repeatable results. To address these problems an improved detection algorithm should also utilise the cast shadow from the tree itself and account for the occlusion and shadowing effects from adjacent trees. It should also be more flexible in terms of crown shapes and branch structure in order to account for the natural variability.

Due to the very complex nature of the underlying model, the inversions problem cannot be solved with analytical methods without too much simplification. Hence empirical methods have to be used instead. Neural networks have been shown to be an excellent tool for model inversion (Pinz et al 1993, Pierce et al 1994, Hagner, 1997, Kimes et al 1998, Jensen et al 1999, Atzberger, 2001, Udelhoven et al 2001). The problem is that the higher degree of model complexity, the larger training set is required. This means that in practice huge training sets (in the order of hundreds of thousands sample plots) are needed to derive the kind of inversion model mentioned above. For obvious reasons the effort and costs required to derive such a dataset by field measurements is prohibitive.

Fortunately there is a solution to the problem. By development of a geometric-optical model capable of realistically simulating the response of high-resolution optical sensors for groups of trees in representative viewing and illumination conditions, such datasets could be derived. By integrating the model with the National Forest Inventory (NFI) database for individual tree positions on permanent plots, training sets can be derived by simulation techniques that represent the full spectrum of forest types.

As part of an ongoing three year project financed by the Swedish National Space Board, such a geometric-optical model is being implemented at the Remote Sensing Laboratory, SLU, Sweden. The current implementation has a branching structure in the tree canopy in order to make all trees have individual appearances.

As an early test of this geometric-optical model a back propagation neural network was set to learn single tree detection on a virtual aerial image. The trained configuration was then tested on a real aerial image to show the feasibility of the technique.

## 2 METHODS

### 2.1 Test site

The forest area in the experiment is a Scots pine *(Pinus Sylvestris)* dominated plot, located at the Remningstorp estate in the south west of Sweden (lat. 58° 30' N, long. 13° 40' E). The plot has 280 stems/hectare and an average stem diameter of 383.6 mm.

### 2.2 Aerial image

The digital aerial imagery consists of a Z/I DMC image (www.ziimaging.com) that were captured June 28, 2005, 07:42 GMT. The flying height over mean sea level was 4800 m and the average ground height was approximately 100 m which gave a ground resolution of approximately 0.47 m/pixel. The pan sharpened composite Colour Infrared (CIR) virtual image from the sensor was used. The resolution is 13824 x 7680 pixels, with 12 bit /channel, from the bands green, 500 – 650 nm, red, 590 – 675 nm, NearIR, 675 – 850 nm and panchromatic. The image was rotated with 4x4 cubic spline interpolation resampling, to make the cast shades point down in the image.

### 2.3 Geometric-optical model

A geometric-optical forest model, Hagner and Olofsson 2005, was used to create a high resolution remote sensing image to be used as training data for the neural network, figure 1 and 3. The number of stems/hectare and the illumination angles corresponded to the test site and the aerial image.

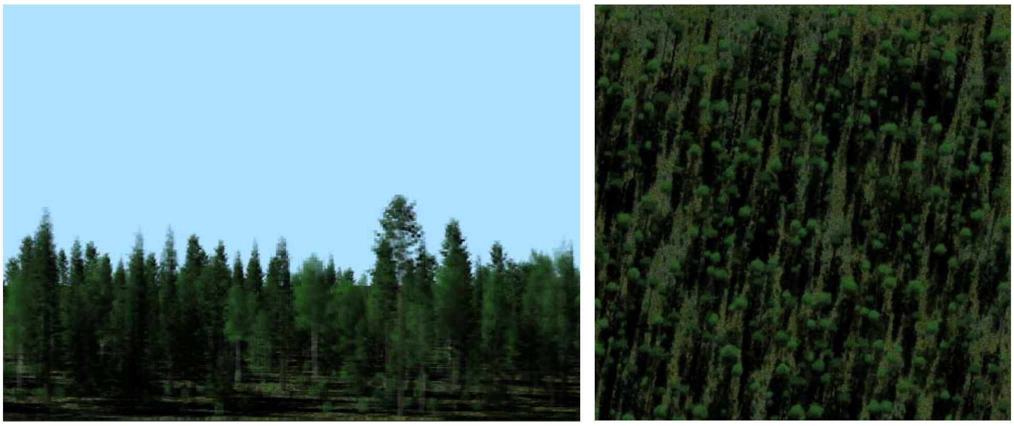

*Figure 1: Virtual images created by the geometric-optical forest model.*

### 2.4 Gaussian filters

A series of Gaussian filters, with the standard deviation of 1.67, were applied to the virtual image and the aerial image. The Gaussian surface, the first and second differentials of the Gaussian surface (in the x and y direction) and the cross differential of the Gaussian surface, was used giving six filter answers for each pixel in the aerial images.

### 2.5 Network configuration

A three layer back propagation neural network was trained with inputs from the Gaussian filter answers from the virtual image, figure 2. To give an equal amount of tree top positions, tree crown edge positions and positions in between the trees, a selection of positions in the image was chosen for the input when training the network. For each tree top position in the image two extra points were chosen with the radial distance of 3 pixels and 6.4 pixels from the tree top. The counter clockwise angle from the tree top was chosen randomly. The training was stopped after 500 epochs giving the network weights to be used on the aerial test image.

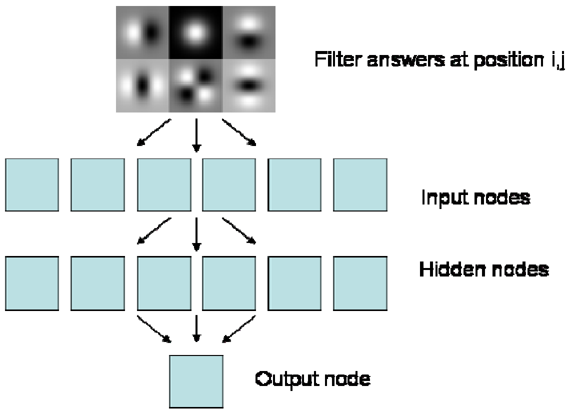


*Figure 2: The three layer back propagation neural network that was used in the study. At each position i,j in the image, six filter answers were used as input to the network, during training and testing.*

## 3 RESULTS

The results from the training of the neural network show that with this small setting only large and well defined tree canopies seem to be detected, figure 3.

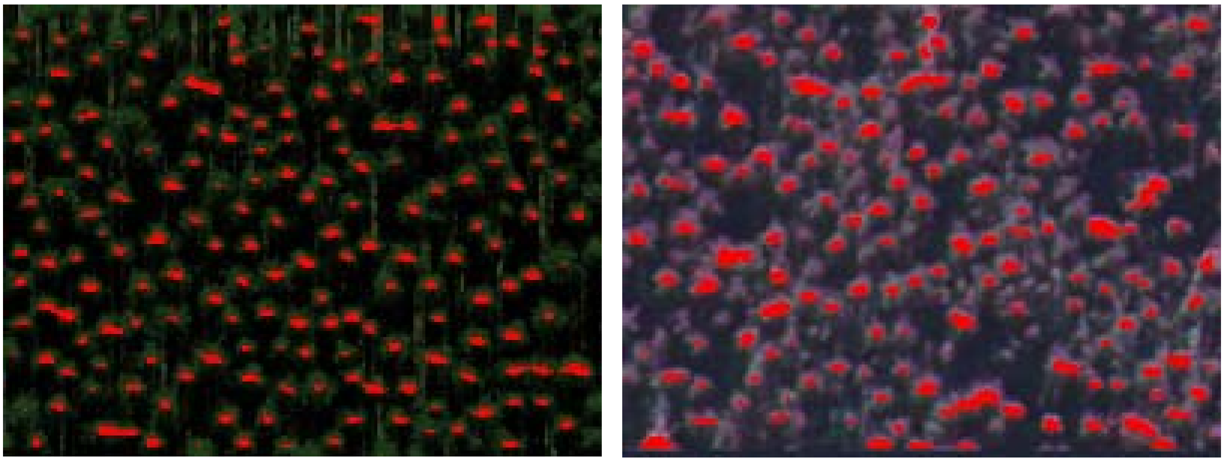

*Figure 3: A virtual aerial image to the left and a real aerial image to the right. The coloured areas in the images correspond to possible single tree canopies detected by the neural network. The figure to the left was used as input when training the neural network. The figure to the right was used as a testing data set where the weights from the previous training were used when propagating the network to detect trees.*

## 4 DISCUSSION

The canopies in the real aerial image that seem to be detected by this small network are well defined and large. Using more scale levels with smaller filters could increase the detection of small tree crowns. Also using filter answers from the neighbourhood should be tested since cast shadows from neighbouring trees can affect the appearance.

## 5 CONCLUSIONS

Using neural networks together with a geometric-optical model as a single tree detector is a possible technique even though much research remains. The forest model needs to be improved and a feedback loop in the network should also be tested. A large study on choosing filters for the input data is also necessary.

## ACKNOWLEDGEMENTS

This project is financed by the Swedish National Space Board.

## REFERENCES

Atzberger, C., 2001: Development of an invertible forest reflectance model: The INFOR-model. In: A Decade of Trans-European Remote Sensing Cooperation, Buchroithner (ed.) Balkema, Rotterdam, ISBN 90 5809

Brantberg, T., 1999: Automatic Individual Tree-Based Analysis of High Spatial Resolution Remotely Sensed Data. PhD Thesis, Centre for Image Analysis, Swedish University of Agricultural Sciences, Uppsala, Sweden.

Dralle, K., Rudemo, M., 1996: Stem number estimation by kernel smoothing of aerial photos. Can. J. For. Res. 26:1228-1236.

Franklin, S.E., Maudie, A.J., and Lavigne, M.B., 2001: Using Spatial Co-Occurrence Texture to Increase Forest Structure and Species Composition Classification Accuracy. Photogrammetic Engineering Vol. 67, No. 7, pp. 849-855.

Gougeon, F., 1995: A Crown-Following Approach to the Automatic Delineation of Individual Tree crowns in High Spatial Resolution Aerial Images. Can. J. of Remote Sensing. Vol. 21, No. 3, pp. 274-284.

Hagner, O., 1997: Textur i flygbilder för skattning av beståndsegenskaper. Department of Forest Resource Management and Geomatics, Swedish University of Agricultural Sciences. Arbetsrapport 29, ISSN 1401-1204, ISRN SLU-SRG-AR—29—SE.

Hagner, O., Olofsson, K. (2005). A high resolution geometric-optical forest model for development of single tree detection algorithms. In Proceedings. Remote Sensing and Geographical Information Systems for Environmental Studies. Applications in Forestry. Göttingen Germany. Schriften aus der Forstlichen Fakultät der Universität Göttingen und der Niedersächsischen Forstlichen Versuchsanstalt, band 138. pp. 43-52.

Holmgren, P., Thuresson, T., 1998: Satellite Remote Sensing for Forestry Planning – A Review. Scand. J. For. Res. 13: 90-110

Jensen, J.R., Fang, Qiu., Minhe, Ji., 1999: Predictive modelling of coniferous forest age using statistical and artificial neural network approaches applied to remote sensor data. International Journal of Remote Sensing, Vol. 20, No. 14, pp. 2805-2822.

Kimes, D.S., Nelson, R.F., Manry, M.T., Fung, A.K., 1998: Attributes of neural networks for extracting continuous vegetation variables from optical and radar measurements. International Journal of Remote Sensing, Vol. 19, No. 14, pp. 2639-2063.

Lang, M., Kuusk, A., Nilson, T., Lükk, T., Pehk, M., and Alm, G., 2002: Reflectance spectra of ground vegetation in sub-boreal forests. Web page. Available on-line [http://www.aai.ee/bgf/ger2600/] from Tartu Observatory, Estonia. Accessed May 2, 2002.

Li, X., Strahler, A.H., 1986: Geometric-Optical Bidirectional Reflectance Modeling of a Conifer Forest Canopy. IEEE transactions on geoscience and remote sensing vol. GE-24, No. 6, pp. 906–919.

Maltamo, M., Tokola, T., and Lehikoinen, M., 2001: Estimating Tree Stocks Using an Approach Combining Single Tree Recognition from Digital Video Image and a Diameter Distribution Model. In: Heikkinen et al (ed) Procedings of SNS Meeting in Solvalla, Finland April 17-19, 2001. Finnish Forest Research Institute Research papers 860, pp. 73-79

Nilson, T., Kuusk, A., Lang, M., and Lükk, T. 2003: Forest reflectance modeling: Theoretical aspects and applications. Ambio 32:535-541.

Olofsson, K., 2002: Detection of single trees in aerial images using template matching. ForestSat 2002, Operational Tools in Forestry using Remote Sensing Techniques. Proceedings CD-ROM, talk FI6.3, session Forest Inventory 6, Monitoring Forest Establishment and Development.

Pollock, R. J., 1996: The Automatic Recognition of Individual Trees in Aerial Images of Forests Based on a Synthetic Tree Crown Image Model, PhD Thesis, University of British Columbia, Vancouver, Canada.

Pierce, L.E., Sarabandi, K., and Ulaby, F.T., 1994: Application of an artificial Neural Network in Canopy Scattering Inversion, International Journal of Remote Sensing. Vol 15, No 16, pp. 3263-3270.

Pinz., 1989: Final results of the vision expert system VES: Finding trees in aerial photographs. In: Pinz, A. (ed.): Wissensbasierte Mustererkunnung (Knowledge-based pattern recognition), OCG-Schriftenreihe 49, Oldenbourg Verlag, pp. 90-111.

Pinz, A., Zaremba, M.B., Bischof, H., Gougeon, F.A., Locas, M., 1993: Neuromorphic methods for recognition of compact image objects, In: Machine GRAPHICS and VISION Vol. 2, No. 3, 1993, pp. 209-229.

Syrén, P., 1990: Reflektans för fysiska modeller av skogsbestånd som funktion av belysningsgeometri. Rapport, Naturgeografiska institiutionen, Stockholms universitet.

Udelhoven, T., Atzberger, C., and Hill, J., 2001: Retrieving structural and biochemical forest characteristics using artificial neural networks and physically based reflectance models. In: A Decade of Trans-European Remote Sensing Cooperation, Buchroithner (ed.) Balkema, Rotterdam, ISBN 90 580

Åkesson, H., 1999: Neurala modeller och simulering av klavräd i Riksskogstaxerigen. Report UMNAD 265.99, Department of computing science, Umeå University, Sweden

# TREE SPECIES DISCRIMINATION BY AID OF TEMPLATE MATCHING APPLIED TO DIGITAL AIR PHOTOS

*Jonas Bohlin, Håkan Olsson, Kenneth Olofsson and Jörgen Wallerman*

Swedish University of Agricultural Sciences, Department of Forest Resource Management and Geomatics, Umeå, Sweden; e-mail to corresponding author: hakan.olsson@resgeom.slu.se

## ABSTRACT

In 2004, the Swedish National Land Survey acquired a Z/I DMC digital mapping camera which registers four colours with more radiometric information per pixel than earlier scanned aerial photographs. The aim of this study is to investigate the accuracy with which tree species can be discriminated automatically using spectral information obtained with the Z/I DMC and extracted from automatically detected tree canopies. Single tree canopies are located with a modified version of the template matching method developed by Richard Pollock of Canada. This method is based on the use of 3D model trees which are rendered in 2D with the correct view angle and illumination for each tested position in the digital image. The template trees are then correlated with the digital image and tree positions are identified as locations with maximum local correlation. The matched templates are used for extracting pixel values for the sunlit part of the canopy. Two tests were carried out at the Remningstorp estate in southern Sweden (lat. 58°30' N, long. 13°40' E), using Z/I DMC imagery from October 14, 2003 (altitude 3000 m) and from June 28, 2005 (altitude 4800 m) respectively. In the October image, 89 % of the detected trees could be separated into the three classes Pine *(Pinus Sylvestris)*, Spruce *(Picea Abies)* and deciduous, using the spectral information only. In the June image, 88% of the detected trees could be correctly separated. These results indicate a considerable potential for automated tree species mapping using the new routinely available images.

**Keywords:** Tree species, Digital air photo, Template matching.

## 1 INTRODUCTION

In 2004, the Swedish National Land Survey acquired a Z/I DMC digital mapping camera. According to a new government policy, an area corresponding to one-third of Sweden will be photographed annually, which is a considerable increase in aerial photo acquisition. The altitude of photography will normally be 4800m, and in selected areas, 3000m. From the year 2007 only digital cameras will be used and the entire production line will be digital. The large amount of high quality, digital images that now are being made available motivates further studies about how the imagery could be interpreted using computer aided procedures. Sweden has 22.9 million ha of forest land that is used for production of timber and pulp wood. Of the growing stock, 44% is spruce *(Picea abies),* 40% is pine *(Pinus sylvestris* and less than then 1 % *Pinus Contorta*). The remaining 16% is a mix of deciduous species, mainly birch *(Betula spp).* Thus, it is of interest to investigate whether normal altitude Z/I DMC imagery could be used for automated species discrimination into these three groups.

In forestry remote sensing, different schemes for detection of single trees in digital imagery with pixel sizes on the order of 0.5 m have been developed. One of the first was developed at BOKU in Vienna by Pinz (1989). Pinz, as well as later authors (e.g., Dralle 1997) identified tree positions by detecting the bright sunlit part in the tree crowns that is visible from above. Another class of algorithms is based on segmentation of single tree crowns (Gougeon 1995; Erikson 2003a). In this paper, we identify single tree crowns with a third approach, which is based on correlating synthetic images of tree crowns with the image data. By use of templates which for each position in the image are appropriate 2D projections of 3D synthetic tree canopies, the variations in view angles and illuminations within an image can be handled. This template matching method was originally developed by Pollock (1996) and further developed by Larsen and Rudemo (1997), Larsen (1998), Olofsson (2002), and Korpela (2004). Once the positions for the trees that are visible from above are identified, this information could be used in a number of ways in forest inventory schemes, for example, in combination with field data for stem number accounting (Dralle 1997), and for segmentation of stand boundaries. In this article, we extract spectral information from the tree canopy for tree species identification on single tree level.

For a test site in northern Sweden, Brandtberg (2002) obtained 60% overall accuracy for a cross validated linear discriminant analysis of spruce, pine, birch, and aspen using colour and morphological information from the central part of scanned low altitude colour IR imagery with a pixel size of 3 cm. Erikson (2003b) used the same dataset as Brandtberg, but developed a new stepwise procedure for the species identification. Of the trees that were automatically detected he then obtained an overall accuracy for the species discrimination of 77%. Using another data set with 10 cm pixels Erikson (2003b) discriminated spruce, pine, birch, and aspen with 71 % overall accuracy. In the USA, Key *et al.* (2001) obtained an overall accuracy of 76 % for classification of four hardwood species at single tree level, using colour IR images scanned with a pixel size of 36 cm. For old growth forest in western Canada, Leckie et al. (2005) reported per species classification accuracies on the order of 40 – 80% for trees that had been automatically detected. Both Key *et al*. and Leckie *et al.* report about the considerable difficulties with single tree approaches in dense multi-story forests in North America, but still conclude that the approach is promising. Thus, it is even more motivated to evaluate it in the sparse, often even aged, coniferous dominated forests of Scandinavia.

The aim of this paper is to provide an early report about how well tree species can be separated automatically in typical Scandinavian production forest dominated by Scots Pine and Norway Spruce using template matching techniques adopted to Z/I DMC imagery from normal flying altitudes. Z/I DMC imagery from two different dates, October 13, 2003 and June 28, 2005 have been used. The results from the October 2003 image are also being published as a short communication (Olofsson *et al.*, 2006), whereas the results from the more realistic time of photography, June, have not been communicated elsewhere. The same test area and dates of photography but with photos from 1200 m has also been used in combination with laser scanner data (Persson *et al.*, 2004, 2006).

## 2 MATERIALS

The test area is located at the Remningstorp research estate in the south west of Sweden (lat. 58° 30' N, long. 13° 40' E). The estate is located in hemi-boreal forest and is dominated by spruce and pine which is grown for timber production.

### 2.1 Image data

Results from two different Z/I DMC (http://www.intergraph.com/dmc/) image acquisitions at the same test site are reported (Table 1). The bands used are green, 500 – 650 nm; red, 590 – 675 nm; NearIR, 675 – 850 nm; and panchromatic. The colour information had been pan-sharpened with 4*4 panchromatic pixels for each registered colour pixel. The images were ortho-rectified to the Swedish geodetic system RT90. The images were delivered as 12 bits per band, but converted to 8 bits per band covering the mean value of the DN values, +/- 3 standard deviations.

*Table 1: Dates and flying altitudes for the Z/I DMC images used.*

| | **Test A** | **Test B** |
|---|---|---|
| Date | October 13, 2003 | June 28, 2005 |
| Time (GMT -1) | 10:30 | 08:20 |
| Flying altitude . | 3000 m | 4800 m |
| Pixel size for pan sharpened image | 30 cm | 48 cm |

### 2.2 Field data

Four rectangular field plots (20×50 $m^2$) were inventoried in the year 2000 and re-surveyed 2005 after Hurricane Gudrun. The dominating tree species (greater than 80% of the stem volume) were Norway spruce (*Picea Abies)* for two of the plots and Scots pine *(Pinus Sylvestris)* for two plots. Additionally, one plot of 80×80 $m^2$ was inventoried in 2002, located within a birch *(Betula spp)* dominated forest stand. There were also a few trees belonging to other deciduous species, such as alder *(Alnus glutinosa)* and ash *(Fraxinus excelsior)* in this plot. The position of the tree stems was measured using kinematic GPS equipment, and stem diameters and tree species were recorded.

*Table 2: Inventory data for the used field plots*

| | Mean height (m) | No of stems/ha | Pine % | Spruce % | Deciduous % |
|---|---|---|---|---|---|
| Plot 1 | 30.7 | 280 | 100 | 0 | 0 |
| Plot 2 | 19.6 | 650 | 97 | 0 | 3 |
| Plot 3 | 24.3 | 480 | 0 | 100 | 0 |
| Plot 4 | 25.2 | 620 | 2 | 98 | 0 |
| Plot 5 | 18.0 | 625 | 0 | 3 | 97 |

## 3 METHODS

In the applied template matching technique, a library of 3D virtual model trees is cross-correlated against any potential tree position in the digital image (Pollock 1996; Olofsson 2002). The tree positions and tree templates with the highest correlations are considered as likely trees. The library trees are generated from generalized ellipsoids of revolution and it is possible to create trees with different crown shapes by changing the parameters of the surface. Three different templates were used. Fig. 1 shows grey-level templates projected for different view angles. To extract the spectral information from each detected tree, a mask consisting of the sunlit part of the generated template was created by setting all non-black pixels in the template to TRUE. When overlaying the mask upon the aerial image, the pixels within the mask are averaged and the resulting 3-band triplet for each template hit is saved.

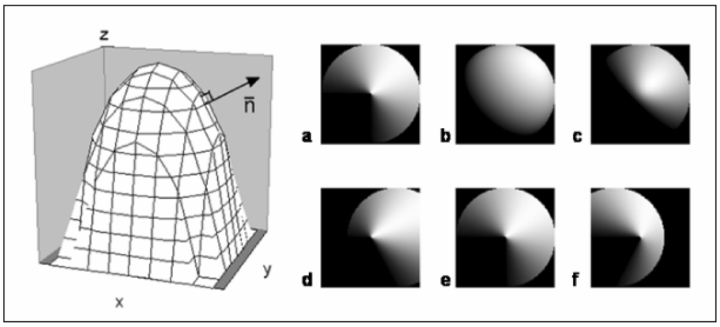


*Figure 1: examples of tree crown templates, a-c for three different crown shapes, d-f for 3 different view angles.*

For the validation, visible trees in the aerial images were linked to the positions of the field survey. The tree crowns of these trees were then manually digitized into polygons. Small hidden and shaded trees were not digitized. Then, template-matching-based tree detection was performed on the aerial images. The template sunlit area polygons were intersected by the evaluation tree polygons. The intersections with an area greater than 50% of the template area or the evaluation tree polygon area were considered to be a “hit”. If there was more than one template for each evaluation tree, the tree with the largest intersection area was chosen. For each true hit, the tree species from the field survey was connected to the corresponding mean value in the digital image, as defined by the template. Altogether, 256 trees were used for test A and 170 for test B. The possibility of separating the tree species based on the spectral mean values was tested by applying cross-validated discriminant analysis using equal prior probabilities for each class (function “lda” in the R statistical computing environment, R Development Core Team, 2004, http://www.R-project.org).

## 4 RESULTS

The results from cross-validated discriminant analysis are shown in Table 3 and the location of the tree canopies in the spectral space are shown in Figure 2.

*Table 3: Cross-validated classification accuracies using different band combinations.*

| Bands used | | | Overall accuracy % (and kappa value) | |
|---|---|---|---|---|
| Green | Red | NIR | October 2003<br>3000 m altitude | June 2005<br>4800 m altitude |
| X | X | X | 88.7 (0.82) | 87.6 (0.80) |
| X | X | | 83.6 (0.74) | 83.5 (0.74) |
| X | | X | 61.3 (0.43) | 85.9 (0.78) |
| | X | X | 83.6 (0.75) | 69.4 (0.52) |

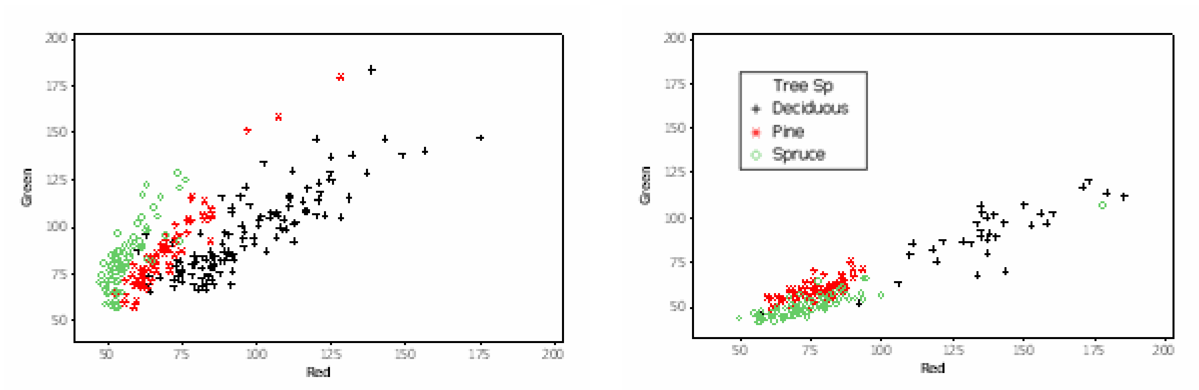


*Figure 2: Scatterogram for DN mean values per tree crown for the red (X-axis) and green (Y-axis) bands for tree canopies of spruce, pine and deciduous trees, measured October 13, 2003 (left) and June 28, 2005 (right).*

## 5 DISCUSSION

In spite of the large pixel size for the colour information in the DMC images, the possibility to discriminate around 88 % of the visible trees into spruce, pine or deciduous show a considerable potential for automated species discrimination into the three main groups of importance for Swedish forestry, using the digital camera and flying altitude that will be routinely used from 2006 and onwards. The National Land Survey is still working with modifications of exposure times and also with the algorithm used for pan-sharpening, in order to avoid saturation of the bands. Once the final routines for obtaining correct image radiometry are in place, there is a need to repeat this test with more images, trees, and test areas. Since a shift in the relation between the colour for pine and spruce can be seen between the October image and the June image, it is also important to repeat this test with images from several time points during the vegetation season.

The template matching routine in this test was only used for finding the tree canopies that were visible from above and extracting pixel values from them. Template matching also has the potential to detect different sizes and shapes of tree canopies and to contribute to stem volume estimates. Furthermore, the pattern of detected tree canopies in combination with spectrally based species information will probably be useful for automated stand delineation. This must however be verified, including the outcome for different view angles.

## ACKNOWLEDGEMENTS

This research was funded by the Carl Trygger foundation, the Kempe foundation and the Heureka research program. The Hildur and Sven Wingquist foundation contributed images and field data.

## REFERENCES


Brandtberg, T. (2002). Individual tree-based species classification in high spatial resolution aerial images of forests using fuzzy sets. Fuzzy sets and systems *132*:371-387.

Dralle K (1997) Locating Trees by Digital Image Processing of Aerial Photos. PhD thesis. Royal Veterinary and Agricultural University. Frederiksberg, Denmark.

Erikson, M. (2003a). Segmentation of individual tree crowns in colour aerial photographs using region growing supported by fuzzy rules. Canadian Journal of Forest Research *33*:1557-1563.

Erikson, M. (2003b). Species classification of individually segmented crowns in high resolution aerial images using radiometric and morphological image measures. Remote Sensing of Environment 9:469-477.

Gougeon, F. A. (1995). A crown-following approach to the automatic delineation of individual tree crowns in high spatial resolution aerial images. Canadian Journal of Forest Research *21*:274-284.

Key, T., Warner, T.A., McGRaw, J.B., Fajvan, M.A. (2001). A comparison of multispectral and multitemporal information in high spatial resolution imagery for classification of individual tree species in a temperate hardwood forest. *Remote Sensing of Environment 75*, 100-112.

Korpela, I. (2004). Individual Tree Measurements by Means of Digital Aerial Photogrammetry. PhD Thesis. The Finnish Society of Forest Science, The Finnish Forest Research Institute, SILVA FENNICA Monographs 3-2004

Larsen, M. (1998). Finding an optimal match window for spruce top detection based on an optical tree model, in proceedings of the International Forum on Automated Interpretation of High Spatial Resolution Digital Imagery for Forestry, 10-12 February 1998, Victoria, B. C., Natural Resources Canada, Canadian Forest Service, Victoria, B. C., pp. 55-66.

Larsen, M., and Rudemo, M. (1997). Using ray-traced templates to find individual trees in aerial photographs, in proceedings of the Scandinavian Conference on Image Analysis, 9-11 June, Lappenranta, Finland. Pattern Recognition Society of Finland, Jounsuu, Finland, pp. 1007-1014.

Leckie, D.G., Gougeon, F.A., Tinis, S., Nelson, T., Burnett, C.N., and Paradine, D. (2005). Automated tree recognition with high resolution digital imagery. Remote Sensing of Environment 94:311-326.

Olofsson, K. (2002). Detection of Single Trees in Aerial Images using Template Matching. In ForestSat 2002, Operational tools in forestry using remote sensing techniques. Proceedings CD-ROM, talk FI6.3, session Forest Inventory 6, Monitoring Forest Establishment and Development, Forest Research, Forestry Commission, Heriot Watt University, Edinburgh, Scotland, August 5th-9th, 2002.

Olofsson, K., Wallerman, J., Holmgren, J., and Olsson, H. (2006). Tree species discrimination using Z/I DMC imagery and template matching of single trees. Scandinavian Journal of Forest Research 21:106-110.

Persson, Å., Holmgren, J., Söderman, U., and Olsson, H. (2004). Tree species classification of individual trees in Sweden by combining high resolution laser data with high resolution near-infrared digital images. International Society of Photogrammetry and Remote Sensing, Proceedings of the ISPRS working group VIII/2, Laser-Scanners for Forest and Landscape Assessments, Freiburg, Germany, October 3 to 6, 2004.

Persson, Å., Holmgren, J., Söderman, U. (2006). Identification of tree species of individual trees by combining very high resolution laser data with multispectral images. In proceedings from EARSeL ISPRS Workshop on 3D Remote Sensing in Forestry, Vienna, February 2006.

Pinz, A. (1989). Final results of the vision expert system VES: finding trees in aerial photographs, in Wissensbasierte Masterkennung. (Knowledge-based pattern recognition.) OCG-Schriftenreiche 49, Oldensbourg Verlag. pp 90-111.

Pollock, R. J. (1996). The automatic recognition of individual trees in aerial images of forests based on a synthetic tree crown image model. Ph.D. thesis, The University of British Colombia, Vancouver, B. C.

# LASER SCANNERS WITH ECHO DIGITIZATION FOR FULL WAVEFORM ANALYSIS

*Peter Rieger, Andreas Ullrich and Rainer Reichert*

Riegl Research GmbH, 3580 Horn; prieger@riegl.co.at, aullrich@riegl.co.at, rreichert@riegl.co.at

## ABSTRACT

Scanning LIDARs for airborne applications based on echo digitization enable the user to gain access to the complete target information which is available by laser ranging. Information is extracted from acquired digitized echo signals by the so-called full waveform analysis, usually in off-line processing. The output of the analysis is provided in different formats for further data processing. We present the principle of echo digitization and full waveform analysis, the key features of the laser scanner RIEGL LMS-Q560, and some sample data in different representations. We discuss the potential of waveform digitizing scanning LIDARs for different surveying applications emphasizing applications in forestry. An outlook on further developments will be given.

**Keywords:** laser scanning, LIDAR, full waveform analysis, echo digitization

## 1 INTRODUCTION

Laser scanning devices used for airborne laser scanning (ALS) applications are usually based on laser range finding using the time-of-flight measurement principle. Short infrared high-peak-power pulses are emitted in highly collimated beams. The echo signals scattered back by the targets within the laser beam are detected and processed to retrieve the range to the target. When taking a look at airborne scanning LIDARs from a physical point of view the following question may occur: what are the physical parameters of the targets that can be estimated directly from the backscattered laser-echo signal? The first thing in mind is of course the range to the target giving subsequently, when combined with the actual scan angle, the three-dimensional coordinate of the surface location hit by the laser pulse. Furthermore the amplitude of the reflected laser signal is giving information about the reflectivity of the target, or to be more precise the laser radar cross section of the target, which includes the geometrical cross-section, the surface reflectivity at the laser wavelength, and the directivity of the backscattered radiation. Especially in ALS for forestry applications, a frequently observed case is that single laser pulse hits more than one target due to its spatial dilatation or beam spread, so the reflected laser beam is a superposition of many backscattered pulses with different amplitudes at different time of arrivals corresponding to the different ranges to the targets. Another case to be observed is that the laser beam hits a sloped surface giving rise to a backscattered pulse which is broadened in time. As already shown the method of analyzing the received waveform of the reflected laser beam influences the accuracy and information content of the measurement directly (Wagner et.al. 2004). A common method of conventional LIDAR imaging systems is to deliver two returns from multiple targets illuminated by a single laser pulse usually as first and last target with respect to range, some systems provide up to four returns depending on the complexity of the system's electronics. As these systems provide discrete ranges for every target but no information on the actual shape of the echo pulse these systems are addressed as discrete systems. For these systems the user has commonly no information on how the electronics of the LIDAR actually determine the range to the returns, nor on any change of the pulse echo's shape due to surface structures and / or due to nonlinearities of receiver electronics, as system manufacturers do not disclose the pulse detection methods employed. The conclusion is to give the user every information available from the received pulse echo's for further post processing, he has to have access to the complete digitized echo signal. While this approach has been already proposed nearly 30 years ago (Mamon et.al. 1978) only the advances in modern electronics of the last few years have made it possible to design LIDAR systems providing the capabilities necessary for high speed signal detection, data processing and storage. Also these modern systems combine reliability and ruggedness in a relatively small enclosure at moderate costs.

The commercially available waveform-digitizing scanning LIDAR system RIEGL LMS-Q560 (*RIEGL* 2006) gives the user complete access the waveform data. Thus, the user has the potential possibility to define the way target range is calculated in post-processing – and so making the range measurement process more transparent, potentially more robust by applying complex sophisticated algorithms and thus improving accuracy to the utmost. It also enables a much more detailed analysis of distributed targets with respect to ranging depth, which is of significant advantage for example in forest and vegetation areas. In contrast to the discrete laser rangefinder, the digitized echo waveform of the LMS-Q560 reveals all the information the laser pulse collected during its trip to the surface and back to the instrument, disclosing the detailed depth distribution of targets in the beam path and their laser radar cross-section. The advantageous use of echo digitization in forestry and agricultural applications is, e.g., discussed by (Wagner et.al. 2006) based on experimental results with the LIDAR mapping system LiteMapper-5600, being based on the RIEGL LMS-Q560.

The subsequent sections describe the principles of the echo digitization and full waveform analysis, provide a description of the LIDAR scanner system and present experimental results from airborne data acquisition.

## 2 METHODS

### 2.1 Echo Digitization and Full Waveform Analysis

Figure 1 visualizes different cases of possible target situations giving rise to echo signals of varying complexity. The difference between the discrete interpretation and the actual waveform of the backscattered echo is illustrated.

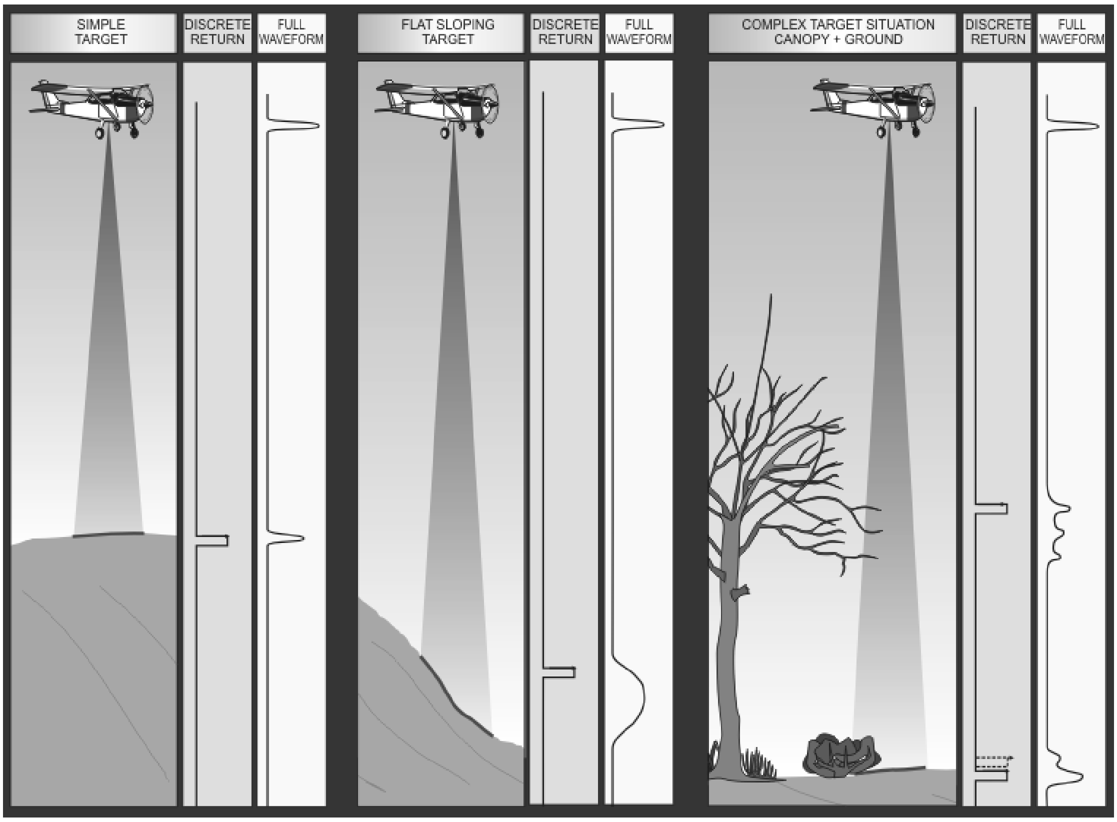


*Figure 1: Echo signals from different target situations. For every target type from left to right: sketch of target and laser beam, discrete return result, full waveform echo signal.*

In the first case (leftmost) the laser beam hits the almost horizontal smooth ground surface, leading to an echo signal with nearly the same pulse shape but much smaller signal strength than the transmitted pulse. Also with the conventional discrete system the target range and target reflectivity can be determined accurately.In case the laser beam hits a sloping surface, the echo signal may be considerably broadened with respect to the transmitted pulse due to the different ranges of the target object within the laser footprint. A digitizing system will preserve this information to be utilized in the subsequent full waveform analysis. In contrast, a discrete system provides again just a single range value. The range will depend on the type of detector used, for example, it may depend on the trigger threshold for stop pulse generation and the target range provides no information on the slope. Considering the laser beam footprint of about 25 cm – 50 cm at an altitude of 500 m above ground complex target situations like the one sketched on the right hand side of Figure 1 are to be observed. The laser beam hits partly the canopy first, then low vegetation, and finally the ground surface. A discrete return signal may provide a first and a last target, and may or may not give a third return with respect to the low vegetation strongly depending on signal strength and trigger threshold. By recording the digitized echo signal, the echo signal may be analyzed in detail in post processing by full waveform analysis revealing all the details on the different targets.

The process of echo signal digitization is illustrated in Figure 2. The top most line depicts the analog signal generated within the LIDAR’s receiver due to a backscattered echo signals as sketched in Figure 1: the first (left most) pulse relates to a fraction of the laser transmitter pulse, and the following pulses correspond to the reflections by objects within the laser beam. The temporal distance of each signal with respect to the transmitter pulse signal corresponds to the range. The last signal relates to the most distant target giving rise to a detectable echo signal. In the echo digitizing LIDAR system this analog signal is sampled at constant time intervals (middle line) and is subsequently analog-to-digital (AD) converted, resulting in a digital data stream (bottom line of the acquisition section). For surveying instruments in, e.g., airborne laser scanning applications, a single measurement is usually derived from a single laser pulse. Commonly the laser pulse repetition rate is chosen to match the range gate length, i.e., the maximum unambiguous detectable range. In this case, the data rate generated by echo digitization is huge, typically 2 Giga samples per second.

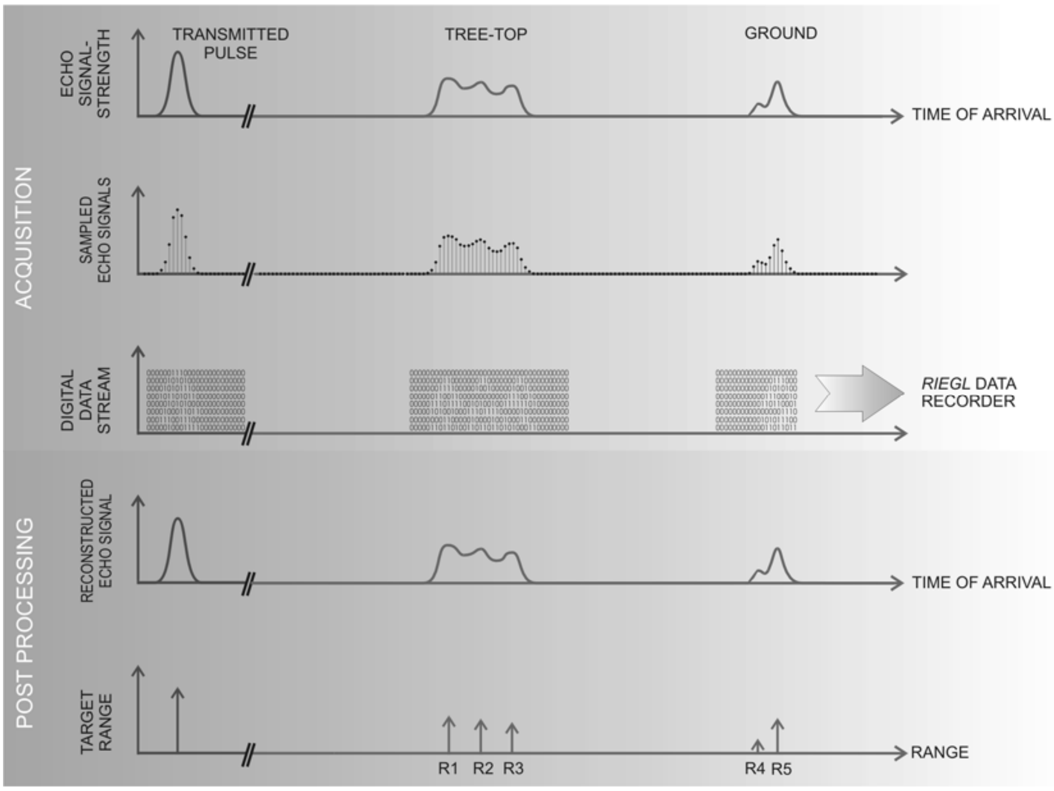


*Figure 2: Principle of echo digitization and full waveform analysis outlines as the process of sampling and digitizing the echo signal, data recording, echo reconstruction and echo analysis.*

In order to achieve reasonable data rates, the amount of data is reduced by means of thresholding. Thus only the sample data containing information on detectable targets is transmitted to a data recorder for further offline analysis, as depicted in Figure 2 for the airborne laser scanning system. The data are thus available for off-line post processing, as indicated in the post-processing section of Figure 2. The instrument is recording the full waveform information of the echo signal over a wide dynamic range. Thus, in post-processing the signal can be nearly perfectly reconstructed and analyzed in detail by applying appropriate algorithms, e.g., by calculating the center of gravity for every detected event or by fitting corresponding replica of the transmitted waveform to the echo signal, to name only a few possibilities. The selection of the algorithm to be applied has an impact on the computation time and the amount and accuracy of information extracted. The theoretical basis of modeling the waveform as a series of Gaussian pulses is shown by (Wagner et.al. 2006). The absolute target range is calculated by the temporal distance between the transmitted pulse and the center of the modeled waveform of the received pulse. Also the amplitude and the pulse width of the backscattered signal are available for further analysis. So conclusions about the target's laser radar cross section and, in case the target is large than the laser's footprint, the target reflectance are possible.

A broadening of the echo's pulse width may arise either from an inclination angle of the laser beam at the target, or from the surface roughness. A discrimination between the two mechanisms may be derived from neighboring measurements. Considering more or less homogenous targets with a reflection coefficient depending on penetration depth the broadened pulse width can deliver information about the volumetric depth of a target, e.g. a layer of fog or thin branches of trees.

Experimental data has demonstrated what is also expected from the summary above, that echo digitization and full waveform analysis gives access to an unlimited number of targets per laser measurement, an excellent multi-pulse resolution, and that it can provide information on surface roughness, and/or surface slope, and laser radar cross-section of the targets.

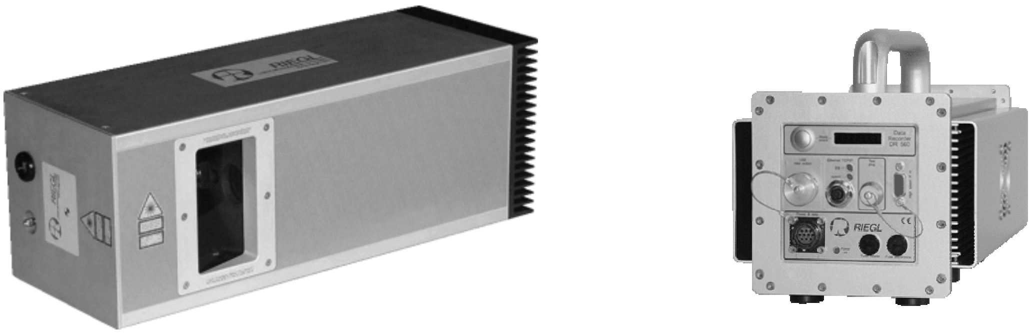

*Figure 3: RIEGL LMS-Q560 and RIEGL DR560*

*Table 1: Key specifications of RIEGL LMS-Q560*

| **Parameter** | **Value** |
|---|---|
| Measurement range | 30 m - 1500 m at target reflectivity of 80%<br>30 m - 850 m at target reflectivity of 20% |
| Ranging accuracy /<br>multi-target resolution | 20 mm / up to 0.5 m |
| Measurement rate | 100 000 measurements / sec (burst rate)<br>up to 66 000 measurements/ sec (average) |
| Scan range | 45°(up to 60°) |
| Scan speed | Up to 160 lines / sec |
| Synchronization | GPS PPS & serial IF |
| Time stamping | resolution 1 µsec, unambiguous range > 1 week |
| Size / weight | 560 x 200 x 217 mm /20 kg |
| Laser safety | Laser class 1 / wavelength near infrared |

## 2.2 Echo Digitizing Laser scanner RIEGL LMS-Q560

Figure 3 shows the RIEGL LMS-Q560 and the data recorder RIEGL DR560. The laser instrument is in principle a high-speed high-performance 2D laser scanner, 1 dimension arising from ranging, the second dimension provided by opto-mechanically scanning the laser signals. Combining the laser scanner with INS/GPS gives a state-of-the-art airborne LIDAR mapping system. The high measurement rate and the high line scan rate provide a superior density of measurements on ground with an even distribution of laser footprints. The operational parameters of the RIEGL LMS-Q560 can be configured to cover a wide field of applications. The instrument is extremely rugged, therefore ideally suited for the installation on aircraft. Also, it is compact and lightweight enough to be installed in small single-engine planes, helicopters or ultra-light planes. The instrument provides online monitoring range and angle data while logging the precisely time-stamped and digitized echo signal data to the rugged RIEGL Data Recorder DR560. Table 1 summarizes the key specification of the laser scanner.

# 3 RESULTS

## 3.1 Example data

Numerous airborne laser scanning systems incorporating the RIEGL LMS-Q560 are already in use. The data provided subsequently have been acquired by Milan Flug in April 2005 on the area of Schloss Schönbrunn, Vienna Austria. The leaves on the trees where still negligible at that time of the year, thus the data may be representative for ALS data taken during winter time. The system of Milan Flug makes use of an IMU/GPS measurement system provided by IGI. Post-processing of the flight data has been done by Milan Flug, post-processing of the laser scan data has been done by RIEGL making use of the tools RiANALYZE (for the full waveform analysis), RiWORLD (for transforming the scan data into WGS84), and by RiSCAN PRO and RiVIEW 560 for visualizing the data.

Figure 4 shows a view of the helicopter-borne ALS system as used by Milan Flug and a small fraction of the data set as a color-encoded point cloud showing an area around the Gloriette. The ponds south and north to the Gloriette give only very few returns and are thus shown as black faces.

*Figure 4 (a): Helicopter-borne ALS system as a payload beneath the cabin holding RIEGL LMS-Q560, DR560, together with IMU and Rollei camera.*

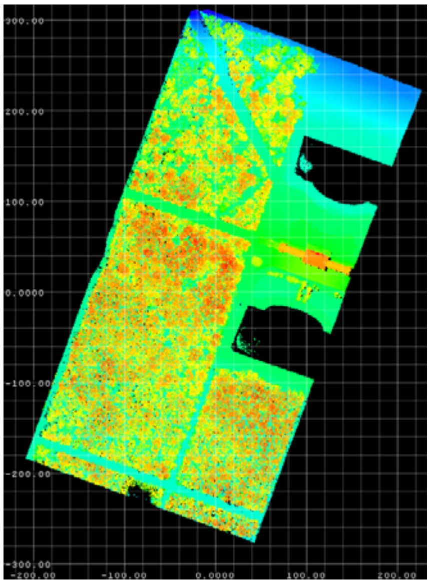

*Figure 4 (b): Small fraction of the data set a point cloud, color according to height.*

The full waveform data of a fraction of a single scan line take south to the Gloriette is visualized in Figure 5. The horizontal axis gives the coordinates across the flight path and thus along the scan line. The vertical axis represents the height above ground. All pixels not colored black indicate that waveform data have been stored during data acquisition. The signal strength of the echo signal is represented by the brightness of the pixels. As expected from a measurement at winter time, the ground penetration is excellent. Additionally, numerous target returns from the canopy can be identified.

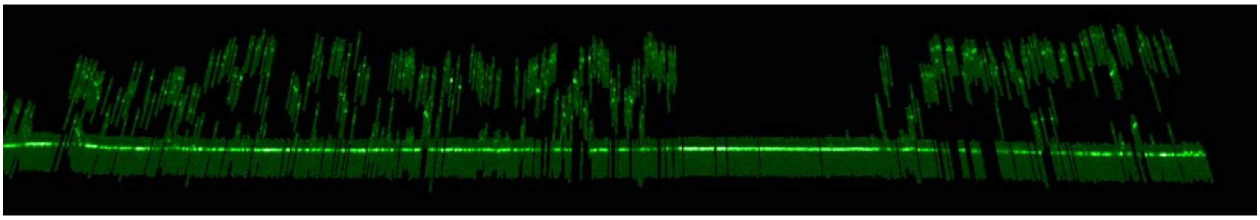

*Figure 5: Raw waveform data of a single scan line. Horizontal axis represents lengths along scan line, vertical axis gives height above ground, and pixel brightness gives signal strength of echo signal.*

Figure 6 depicts some of the waveforms acquired within the scan line shown in Fig. 5. The vertical axes give the range from the LIDAR instrument, the horizontal axes give the signal strength in units of the least significant bit of the digitized data. The examples from left to right show laser measurements to the ground alone, to the canopy alone, ground and canopy simultaneously, to two targets in the canopy and to the ground, and three targets in the canopy and to the ground. Note that in the leftmost diagram low vegetation can be recognized.

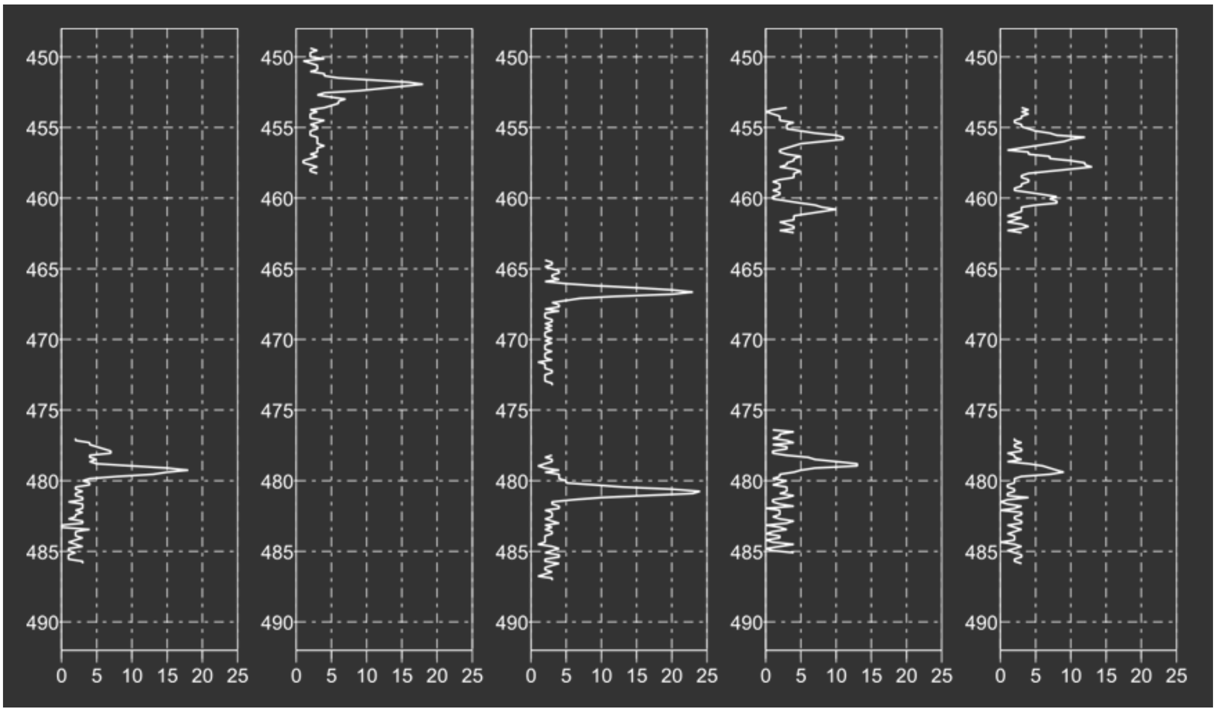


*Figure 6: Examples of the digitized echo signal from the scan line depicted in Figure 5.*

## 4 CONCLUSION

This paper discusses the principle of full waveform analysis in LIDAR applications. Technical information about the airborne LIDAR *RIEGL* LMS-Q560 is given and experimental full-waveform-data acquired with this instrument is presented. By analyzing the completely recorded digitized echo signal, additional valuable information on the target properties can be extracted. Especially in forestry applications, full waveform analysis is of significant advantage as it improves the ability to resolve multiple targets for a single laser pulse. With appropriate post processing of the digitized echo waveform, the analysis of vertical structure of vegetation, the discrimination of vegetation against ground, and subsequent volumetric estimations for forest inventory can be improved with respect to conventional systems.

## REFERENCES

Mamon, G., et al. (1978), Pulsed GaAs laser terrain profiler, Applied Optics, 17(6), pp. 868-877.

RIEGL Laser Measurement Systems GmbH (2006), technical specifications at www.riegl.com.

Wagner, W., et al. (2004), From Single-Pulse to Full-Waveform Airborne Laser Scanners: Potential and Practical Challenges. IAPRS, 35, Part B, pp. 201 ff.

Wagner W., et al. (2006), Gaussian Decomposition and Calibration of a Novel Small-Footprint Full-Waveform Digitising Airborne Laser Scanner. ISPRS Journal of Photogrammetry & Remote Sensing.

# 3D VEGETATION MAPPING AND CLASSIFICATION USING FULL-WAVEFORM LASER SCANNING

*Vesna Ducic[1], Markus Hollaus[1], Andreas Ullrich[2], Wolfgang Wagner[1] and Thomas Melzer[1]*

[1] Christian Doppler Laboratory for Spatial Data from Laser Scanning and Remote Sensing, Vienna University of Technology, Vienna, Austria; vd@ipf.tuwien.ac.at, mh@ipf.tuwien.ac.at, ww@ipf.tuwien.ac.at, tm@ipf.tuwien.ac.at

[2] Riegl Research GmbH, Horn, Austria; aullrich@riegl.co.at

## ABSTRACT

Classifying vegetation points from 3D airborne laser scanner (ALS) point clouds is a challenge and focus of current research. In particular, low vegetation points are very difficult to identify. The basic problem is that so far the majority of ALS systems have provided only the 3D coordinates of scattering objects and most of the criteria used in classifying points had to rely on simple geometric characteristics of a point relative to its neighbourhood. Methods for ALS data processing could be much improved if ALS systems measure, in addition to the range, further physical observables which can be used for vegetation classification. New ALS systems, which record the full echo-waveform, may provide crucial information for the classification of vegetation points. In this paper we show that the additional features derived from the full-waveform data – the amplitude, the pulse width and the number of pulses - can be used to discriminate between vegetation and non-vegetation points without using geometry information. Thus, a truly three dimensional representations of the classified ALS points can be obtained. The classification algorithm is based on a decision tree technique. The applicability of this method is demonstrated on data collected by the RIEGL LMS-Q560 sensor over the Schönbrunn area of Vienna. The performance of the classification algorithm was checked manually on 500 points randomly distributed and on several test zones selected over the study area. We found an overall accuracy of 88.6% with a kappa coefficient of 0.8.

**Keywords:** Laser scanning, classification, vegetation, forestry, full-waveform

## 1 INTRODUCTION

The RIEGL airborne laser scanner LMS-Q560 is one of the first commercial small-footprint full-waveform digitizing laser scanners with a data logger capability for recording the digitised waveforms of both the transmitted laser pulse and the backscattered signal (Riegl 2004). The digitization feature of the instrument enables the user to analyse the waveform off-line in post-processing and thus to use different detection methods for range determination or even a combination of methods in order to extract additional information from the data. Wagner et al. (2006) showed that small-footprint waveform data can be modelled as a series of Gaussian pulses. The decomposition of an observed laser waveform into Gaussian components not only improves the ranging accuracy of the laser measurement (Hofton et al. 2000) but also allows deriving further physical observables in addition to the range – the amplitude and the standard deviation of each pulse (namely pulse width). Figure 1 shows an example of a measured waveform from a forested area. These additional features constitute a valuable source of information for classification purposes.

In this paper we investigate the possibility of using the amplitude, the pulse width and the number of pulses derived from the full-waveform analysis to classify the vegetation points (trees and bushes) without including any geometric information. The first part of this paper describes the study area and the classification algorithm. In the second part, results are presented and discussed highlighting the advantages and the possibilities of the full-waveform observables in forestry applications.

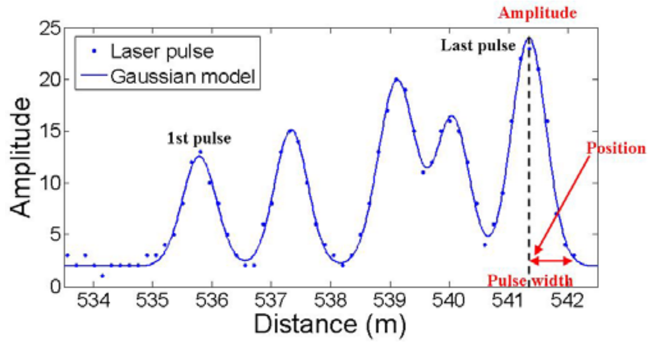


*Figure 1: Example of a measured versus a modeled waveform (Wagner et al., 2006).*

# 2 METHOD

## 2.1 LMS-Q560 data

The LMS-Q560 data used in this study were acquired on August 30, 2004 by Milan-Flug over the Schönbrunn area of Vienna. The instrument was installed on an airplane equipped with GPS and INS. The scanned area comprises natural forest and a large variety of land cover types, including the buildings and park of Schloß Schönbrunn, densely built up areas, residential areas and allotment of gardens. The flight altitude was about 500 m above ground, which resulted in a laser footprint size of 25 cm on ground. An area of about 2 km$^2$ was covered by eleven parallel flight tracks. The area analysed in this paper represents approximately 400x650 m$^2$. The scan rate was set to 66 kHz which resulted in a mean point density of four measurements per square meter. The maximum scan angle was 25°. More detailed information is given in Wagner et al. (2006).

## 2.2 Classification algorithm

To gain an understanding of the information provided by full-waveform data we chose to use a classification tree approach to extract the vegetation points. Decision tree theory for land cover classification has been applied previously to remotely sensed data (Michaelson et al. 1994, Hansen et al. 1996). The tree approach has a number of advantages over traditional classification methods (Hansen et al. 1996). It requires no assumptions regarding the distribution of input data, as in a maximum likelihood approach, and also provides an intuitive classification structure. Moreover, from a practical point of view, it is immediately apparent which variables contribute to the discrimination between classes (DeFries et al. 1998). This can be very useful for defining subsequent suitable inputs for vegetation point characterizations. In this study we built a decision tree classifier based on object signatures analysis.

# 3 RESULTS AND DICUSSION

## 3.1 Features derived from the full-waveform

The RIEGL LMS-Q560 system is able to record all returns per pulse. Figure 2a depicts a 3D point cloud of the study area. The colour shows the index of the corresponding scatterer. Up to 7 scatterers have been observed for a given waveform (from first to last pulse). The multiple echoes appear mainly in forested terrain (Figure 2b). The multiple returns can therefore be of importance in filtering and modelling algorithms related to vegetation and ground surface separation and for deriving forest parameters. Multiple echoes can also be found at the edges of buildings, thus indicating a very fast change in elevation.

Another estimate derived from the full-waveform analysis is the amplitude. The amplitude or power of the return signal depends on several factors: the total power of the transmitted pulse, the fraction of the laser pulse that is intercepted by a surface, the reflectance of the intercepted surface at the laser's wavelength, and the fraction of reflected illumination that travels in the direction of the sensor. Some authors have already used amplitude data successfully in classification algorithm, e.g. finding a specific geometric or statistic structure, such as buildings or vegetation (Rottensteiner et al. 2005) or discriminating between different types of vegetation cover (Schreirer et al. 1985).

In Figure 3a, a 3D point cloud of the area is shown, where the colour indicates the amplitude of the points. The red colour corresponds to low amplitude and the blue one to high amplitude measurements. The surface classes - forest, grass and buildings - can be distinctly identified in the amplitude image. However, the vegetation presents the same range of amplitude as asphalt streets (section 3.2). Therefore, the amplitude information is not recommended to be used alone for *a priori* classification of objects. The amplitude can be used for visualization of the scene but also to improve filtering/removal and classification/separation of objects in combination with the range and other information. The amplitude value can also be used for separating segments of artificial objects from vegetation (Hug&Wehr, 1997).

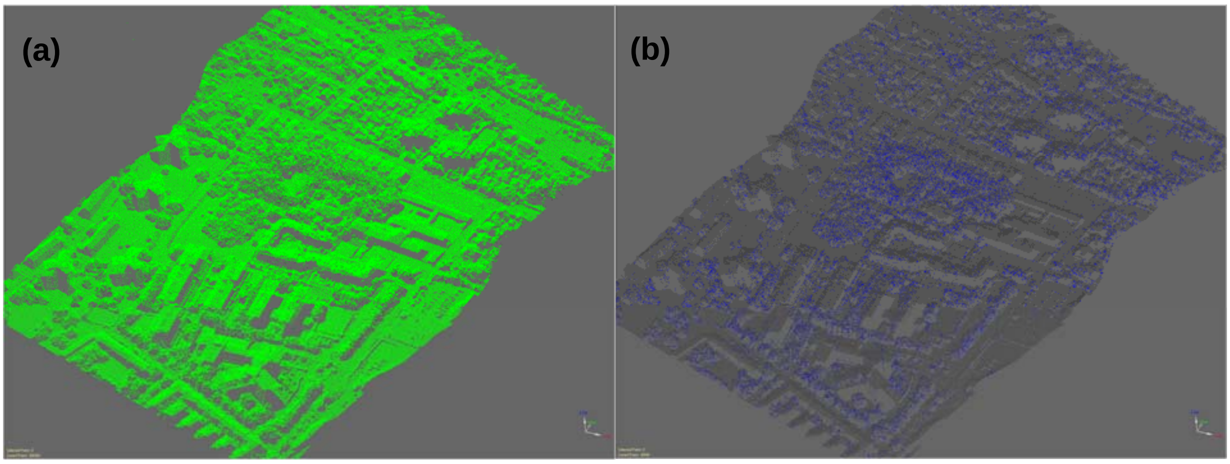


*Figure 2: 3D point cloud of the study area. The colour shows the index of the corresponding scatterer. (a) Points presenting only one echo pulse. (b) Points presenting two echoes and more.*

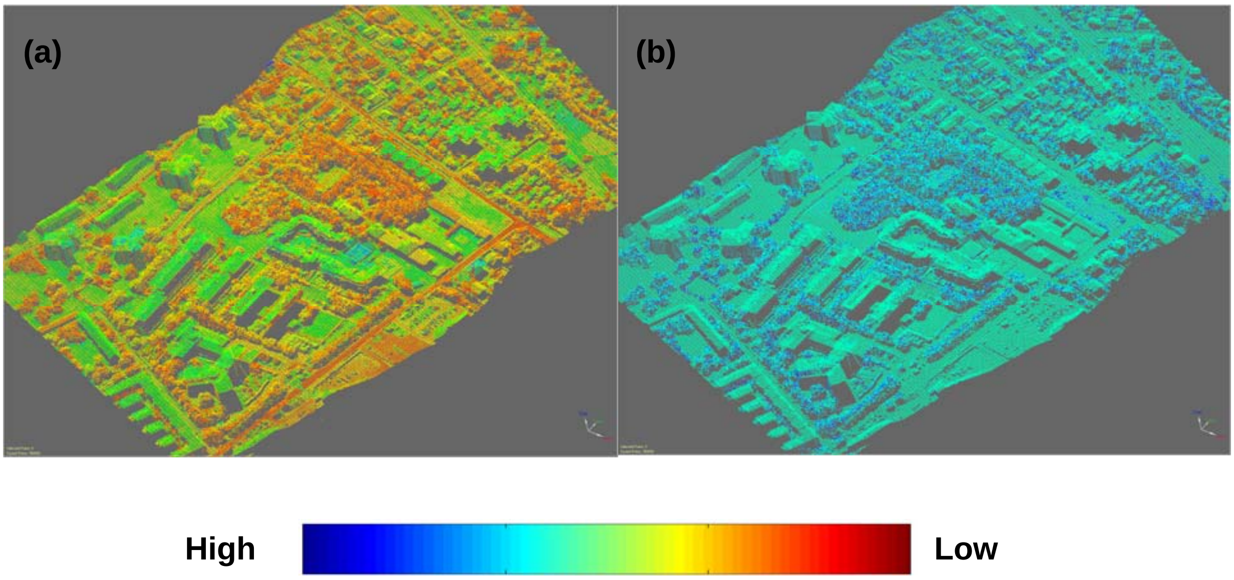


*Figure 3: (a) Amplitude image showing trees, vegetation, access roads and buildings. (b) Pulse width image.*

The full-waveform provides also an estimate of the standard deviation describing the width of each Gaussian component. In Figure 3b the pulse width is illustrated. The dark points correspond to wide echoes pulses, the light points correspond to narrow echo pulses (flat and no-tilted surfaces). For vegetation points, we observe systematically a broadening of the pulse width. The pulse width appears therefore to be a very useful parameter to discriminate between vegetation and non-vegetation points (Persson et al. 2005).

## 3.2 Object signatures

In order to determine the input variables and the corresponding thresholds to be used in the decision tree classifier, we selected manually 5000 training points and did the signature analysis for the classes: vegetation (trees and bushes), grass, asphalt road and various roofs (buildings and houses). In Figure 4 the histograms of the pulse width (a) and the amplitude (b) for these classes are shown. We observe that the multiple echoes correspond mainly to vegetation points. Points with amplitude higher than 75 amplitude units correspond mostly to roofs and grass and points presenting a pulse width wider than 1.9 ns are vegetation points.

We can see that substantial overlap exists in the amplitude-pulse width space for different classes. It is for example impossible for narrow pulse width points to separate vegetation from buildings or road based only on the pulse width. Also, laser points corresponding to grass present the same range of amplitude as building roofs. Given this overlap we merged the classes road, grass and roofs in one class “non-vegetation”. Now, the issue is how to define a decision tree algorithm such that the classes vegetation and non-vegetation can be accurately discriminated and mapped in an efficient and repeatable fashion. It is clear that only the combination of different features allows distinguishing between these two classes.

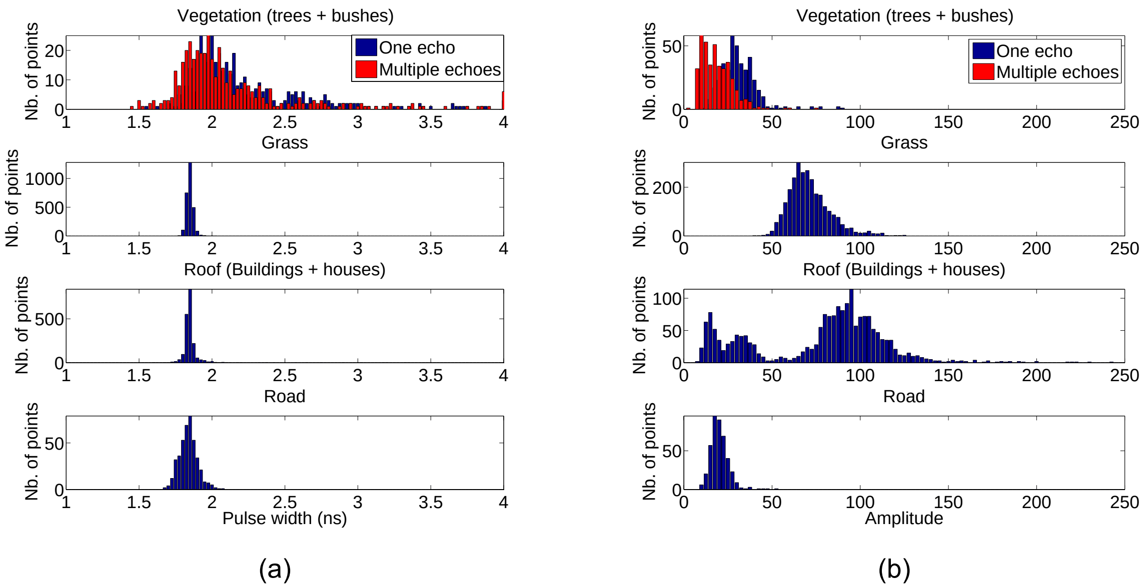


*Figure 4: (a) Histogram of the pulse width of points. (b) Histogram of the amplitude of points. The blue points correspond to one echo and the red ones to multiple echoes.*

## 3.3 Decision tree

To grow the tree we used the previous signatures. Figure 5 illustrates a portion of the hierarchical structure of the tree. The complete tree has six final nodes. The first split uses the number of scatterers per pulse to partition the data. Combining together the pulse width, the amplitude and the multiple returns provided simultaneously by the laser scanner, classification of vegetation points can be done automatically.

## 3.4 Evaluation of the results of classification

The results of classification are shown in Figure 6. The green points correspond to vegetation points and the red ones to non-vegetation points. In general the classification algorithm gives satisfying results. The vegetation areas are correctly identified; even low vegetations (bushes) are correctly mapped. Also, non-vegetation points corresponding to buildings, houses, grass and asphalt streets are precisely classified.

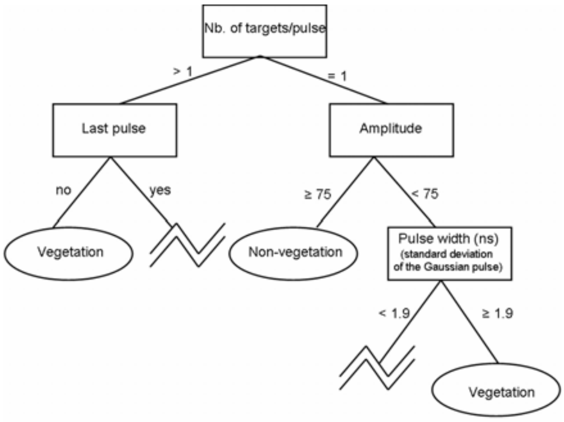


*Figure 5: Partial classification tree for the study area. Rectangles are non-terminal nodes, and circles are terminal nodes with class assignments within each node. The corresponding input parameter is shown within each rectangle. The associated thresholds are shown on diagonal edges.*

To provide a realistic estimate of the classifier performance for discriminating vegetation from non-vegetation points, we checked manually 500 points randomly distributed over the study area. Approximately half of these points were vegetation points. This showed that there were 17 vegetation points classified as non-vegetation and 40 non-vegetation points classified as vegetation, indicating that the decision tree classification algorithm works rather well. One reason for having more non-vegetation misclassified than vegetation points is the difficulty to correctly classify off-terrain points below trees canopy. Also some points belonging to building edges and facades are misclassified. They present a broadening of the pulse width comparable to vegetation points. Non-vegetation points corresponding to flat surfaces like building roofs, grass or asphalt road are very well classified.

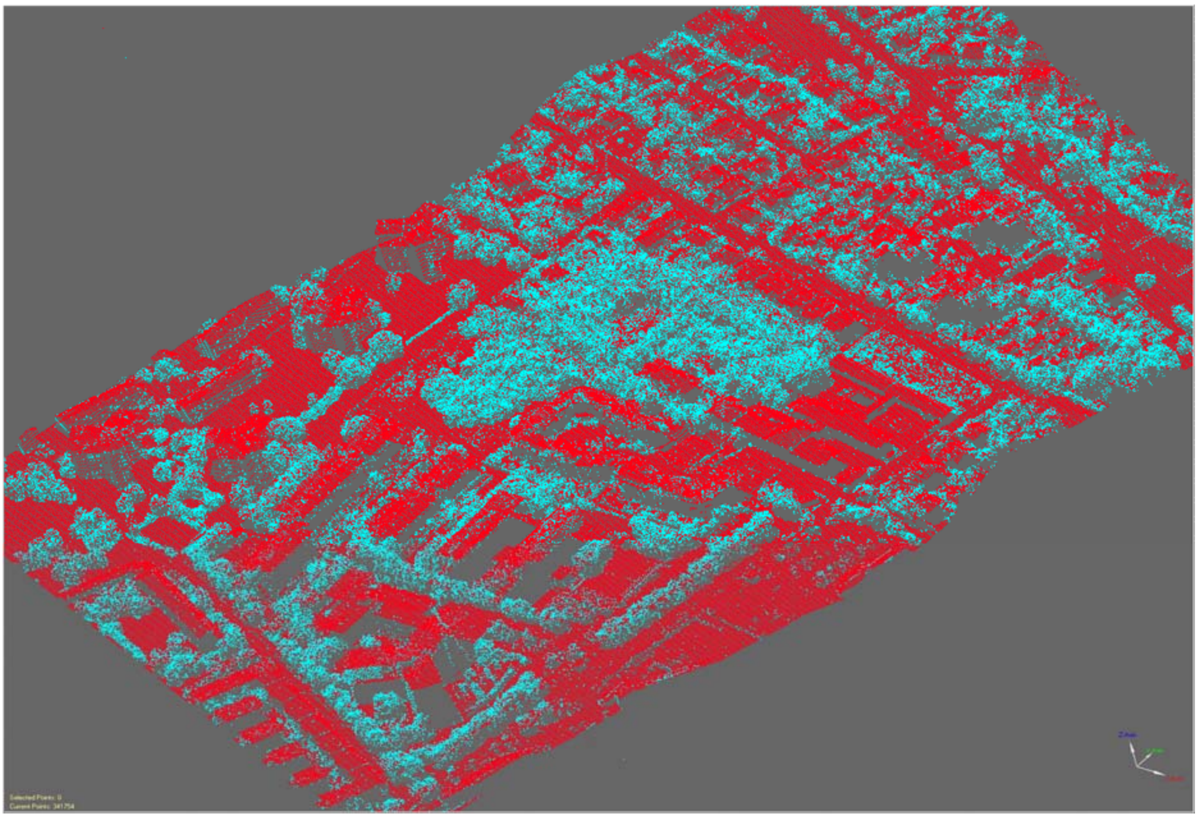

*Figure 6: Classification result obtained with the decision tree algorithm. The green points correspond to vegetation points and the red ones to non-vegetation points.*

For the final accuracy assessment we have analysed in addition several training areas corresponding to non-vegetation and vegetation regions (more than 10000 points). The overall accuracy of the classification is 88.6% with a kappa coefficient of 0.8. The advantage of this method is the possibility to assign a label to the laser point. As opposed to the existing 2.5D models derived form first/last-pulse laser scanner systems, a truly three dimensional representations of the vegetation has been obtained

# 4 CONCLUSIONS

So far, ALS systems have provided only 3D coordinates, compelling segmentation and classification approaches to rely on geometric information only. With a full-waveform laser scanner, by pulse-wise analysis of the backscattered signal, it is possible to determine quality parameters for a given range measurement as pulse amplitude or pulse width, which can be used as a direct input into further classification steps.

In this paper we investigated the potential of the additional observables derived from the RIEGL LMS-Q560 full-waveform to classify and to map the vegetation points without using the geometry information. A decision tree algorithm was implemented. The overall accuracy of the decision tree classifier is 88.6% with a kappa coefficient of 0.8. This suggests that incorporation of amplitude, pulse width measurements and number of pulses in classification schemes will result in significant progress towards detailed mapping of natural and man-made objects.

The classified vegetation points can be very useful as input parameters for existing filtering and classification algorithms, improving at the same time the resulting digital terrain model (DTM) and therefore the normalized digital surface model (nDSM) product. It can also help segmentation purposes and can be used for “internal” validation of classification. On the other hand, the direct retrieval of vegetation points can also facilitate analysis and extraction of vegetation parameters, which is particularly interesting for forestry applications. It would be thus possible to derive a truly three dimensional representations of the vegetation as opposed to the prevalent 2.5 models derived form first/last-pulse data.


# ACKNOWLEDGEMENTS

We would like to thank the Schloß Schönbrunn Kultur- und Betriebsges.m.b.H for their support of the data acquisition campaign. Also we would like to thank all colleagues from TU Wien and RIEGL who have been involved in carrying out the field campaign and processing of the data.


# REFERENCES


DeFries, R.S., Hansen, M., Townshend J.R.G. and Sohlberg R. (1998). Global land cover classification at 8 km spatial resolution: the use of training data derived from Landsat imagery in decision tree classifiers. Int. J. Remote Sens. Vol. 19, No. 16, 3141-3168.

Hansen, M., Dubayah, R. and DeFries, R. (1996). Classification trees: An alternative to traditional land cover classifiers. Int. J. Remote Sensing, Vol. 17, 1075-1081.

Hofton, M.A., Minster, J.B., Blair, J.B. (2000). Decomposition of laser altimeter waveforms. IEEE Trans. Geosc. Remote Sens. 38(4):1989-1996.

Hug, C. and Wehr A. (1997). Robust Detecting and identifying topographic objects in imaging laser altimeter data. International Archives of Photogrammetry and Remote Sensing, Vol. 32, Part3-4W2I, “3D Reconstruction and modelling of topographic objects”, Stuttgart, Germany, 17-19 September, pp. 19-26.

Maas, H.-G. (2001). The suitability of airborne laser scanner data for automatic 3D object reconstruction. “Third Int'l Workshop on Automatic Extraction of Man-Made Objects”, 10-15 June, Ascona, Switzerland.

Michaelson, J., Shmiel, D.S., Riedl, M.A., Davis, F.W. and Dubayah, R.O. (1994). Regression tree analysis of satellite and terrain data to guide vegetation sampling and surveys. Journal of vVegetation Science, 5, 673-686.

Persson, Å, Söderman, U., Töpel, J., Ahlberg, S. (2005). Visualization and analysis of full-wavefrom airborne laser scanner data. International Archives of Photogrammetry, Remote Sensing and Spatial Information Sciences 36 (Part 3/W19), 103-108.

Riegl Laser Measurement Systems (2004). Website: www.riegl.com

Rottensteiner, F., Trinder, J., Clode, S., Kubik, K. (2005). Using the Dempster Shafer method for the fusion of LIDAR data and multi-spectral images for building detection. Information Fusion 6(4), 283-300.

Schreier, H., Lougheed, J., Tucker, C., and Leckie, D. (1985). Automated measurement of terrain reflection and height variations using an airborne laser system. Int. J. Remote Sensing 6:101-113.

Wagner, W., Ullrich, A., Ducic, V., Melzer, T. and Studnicka, N. (2006). Gaussian Decomposition and Calibration of a Novel Small-Footprint Full-Waveform Digitising Airborne Laser Scanner. ISPRS Journal of Photogrammetry & Remote Sensing, in press.

# FULL-WAVEFORM ANALYSIS OF SMALL FOOTPRINT AIRBORNE LASER SCANNING DATA IN THE BAVARIAN FOREST NATIONAL PARK FOR TREE SPECIES CLASSIFICATION

*Josef Reitberger[1], Peter Krzystek[2] and Marco Heurich[3]*

[1] University of Applied Sciences, Department of Geoinformatics, Munich, Germany; jreitberger@web.de

[2] University of Applied Sciences, Department of Geoinformatics, Munich, Germany; krzystek@fhm.edu

[3] Bavarian Forest National Park, Grafenau; marco.heurich@npv-bw.bayern.de

## ABSTRACT

This paper reports on recent results of full waveform data analysis for forestry. The waveform data have been collected by the TopEye MK II system in the Bavarian Forest National Park. In the first part of the paper a special data structure for the efficient management of the huge data amount of a full waveform scanner is shortly described. The laser scanner data are set up in binary hierarchical data files covering the entire flown area in quadratic sub areas. The paper also discusses an approach for the decomposition of a waveform that fits a sum of Gaussian functions by least squares adjustment to the measured waveform. Due to the special waveform characteristics of the TopEye system special conditions must be embedded into the mathematical model of the decomposition to avoid erroneous 3D points. Point distributions are derived in sample tree areas and compared with the numbers from the standard point detection of the MK II system. Furthermore, special metrics based on the 3D points are generated showing clearly that characteristic features can be provided for tree species classification.

**Keywords:** LIDAR, full-waveform, decomposition, tree species classification

## 1 INTRODUCTION

### 1.1 Advances in LIDAR technology

Laser scanning has become the leading edge technology for the acquisition of topographic data and the mapping of the Earth's surface. So far, most of the conventional systems record two or at the most five single echo returns from multiple reflections of the laser beam. This technique does not only limit the number of recordable 3D points, but also appears as a black box to the user who has absolutely no insight how the recorded pulse is detected. Also, the inherent information about the reflecting object and its geometric and physical characteristics are totally neglected.

Recent technological improvements in electronic devices for fast digitizing and storing mass data have made it possible to push the commercial laser scanning technology one step further by digitally sampling the entire laser pulse echo as a function of time. This characteristic amplitude profile of the recorded reflections is usually referred to as the waveform. First pilot applications for topographic applications and vegetation analysis go back to the 1990s, which used experimental large footprint waveform systems both from satellite platforms (GLAS-instrument on ICESat) and airborne platforms (LVIS; SLICER) (Blair et al., 1999; Hardin et al., 2001).

Meanwhile, three commercial systems for airborne applications are available. Hug et al. (2004) announced the Litemapper-5600 full waveform LIDAR system and presented first preliminary results. This scanner is based on the Riegl LMS-Q560 scanner, like also the Harrier 56, which is flown by TopoSys. This scanner has interesting technical features. The length of the waveform is basically unlimited under normal conditions, since it automatically cancels the recording in case the incoming amplitude drops below the noise level. Also, the system provides an excellent optical dynamic range of about 480 DB. Thirdly, the transmitted pulse is recorded which makes a user-defined and precise decorrelation of the waveform feasible. A second full waveform scanner has also been introduced in

2004 by TopEye. This scanner – known as MK II – has a limited waveform length of about 19 m. Its radiometric resolution is 8 bit and the transmitted pulse is not recorded. The redesigned version provides also waveforms with unlimited length and a dynamic range of 16 bit. Very little is known about the Optech ALTM 1225 full waveform scanner. Gutierrez et al. (2005) report on first experiments and results with a system owned by the University of Texas at Austin.

Since the waveform is a function of the geometric and physical characteristic of the object, an analysis of the waveform data can take advantage of the inherent object information. Object detection, reconstruction and classification applied in normal topographic areas and – more specifically – in forestry will become more sophisticated and precise compared to methods using LIDAR data from conventional systems.

Our research work is focused on automated forest parameter extraction by laser remote sensing techniques. The overall goal is to replace time consuming and expensive methods of forest inventory by new techniques that use especially LIDAR data from new full waveform scanners. Typical forest parameters like mean tree height, mean diameter, stem number and timber volume should be automatically derived from the data. In the first step, we concentrate on tree species classification using certain metrics derived either directly from the 3D points or from the original waveform signal.

This paper reports on first results when analyzing and processing full waveform data collected in fall 2004 by the TopEye MK II system in the Bavarian Forest National Park. The first part shortly describes the special data structure we introduced to efficiently process the huge amount of waveform data. The second part describes an approach to decorrelate full waveform data based on a least squares adjustment. Numerical results are discussed when generating 3D points from the waveform at certain tree species. Finally, we report about preliminary results of a tree class classification using height and density dependent variables derived from the 3D points in tree segments.

### 1.2 Study area

The research was conducted in the Bavarian Forest National Park that is located in south-eastern Germany along the border to the Czech Republic (49° 3' 19" N, 13° 12' 9"E). Within the park three major forest types exist: There are sub alpine spruce forests with Norway spruce (Picea abies) and partly Mountain ash (Sorbus aucuparia) above 1100m. Mixed mountain forests with Norway spruce, White fir (Abies alba), European beech (Fagus sylvatica) and Sycamore maple (Acer pseudoplatanus) can be found on the slopes between 600 and 1100 m Finally, spruce forests with Norway spruce, Mountain ash and birches (Betula pendula, Betula pubescens) occur in valley bottoms with wet depressions often evidencing cold air ponds.

### 1.3 LIDAR Data

The waveform data have been collected by the TopEye MK II system that is a new full waveform system operating at a wavelength of 1550 nm and a PRF of 50 kHz. The scan angle varies within 14 and 20 degrees. The system was flown in late September 2004 at a flying height of 200 m resulting in a point density of approximately 25 points/m$^2$. Due to the fixed sampling length of 128 samples, the waveform was limited to about 19 m. The sampling rate for the waveform was 1 GHz providing a vertical resolution to 15 cm. The pulse length of 5 ns created a pulse width with a standard deviation of 25 cm. Finally, the footprint was 20 cm because of the beam divergence of 1 mrad.

## 2 EFFICIENT DATA STRUCTURE TO MANAGE WAVEFORM DATA

Fast and efficient processing of LIDAR data for large areas becomes really challenging when full waveform data must be handled. So far, only few approaches for LIDAR data collected by conventional systems have been presented. Peng et al. (2004) report on a data base solution from ESRI which stores the original information on points, lines and areas in tiles. For visualization purposes the data are setup in data pyramids. Also, the updating of the data is possible. Cothren (2005) presents an experimental data base solution with Oracle 10g, ArcGIS and GeoMedia. Nothing is known whether commercial solutions from Niirs10 or Terra Solid can cope with full waveform data.

Our solution is to subdivide the entire area (=block) into binary sub blocks of quadratic size (Hug et al., 2004; Unteregger at al., 2005). These sub blocks are also tiled in order to guarantee efficient data access. The sub blocks are hierarchically structured in several layers which may contain - for instance

- the original LIDAR data and all the levels of a data pyramid which represents the LIDAR data in different spatial resolutions. The individual layer are composed by sub layers containing all the possible attributes LIDAR points may have like intensity, track number, time stamp, status, RGB value etc. In case the LIDAR points have been recorded by a full waveform system the sub layers are containing the 3D starting point of the waveform, the direction vector and the binary waveform data with variable length. Once the waveform data have been decomposed the generated 3D points can be added to the sub block as an additional layer.

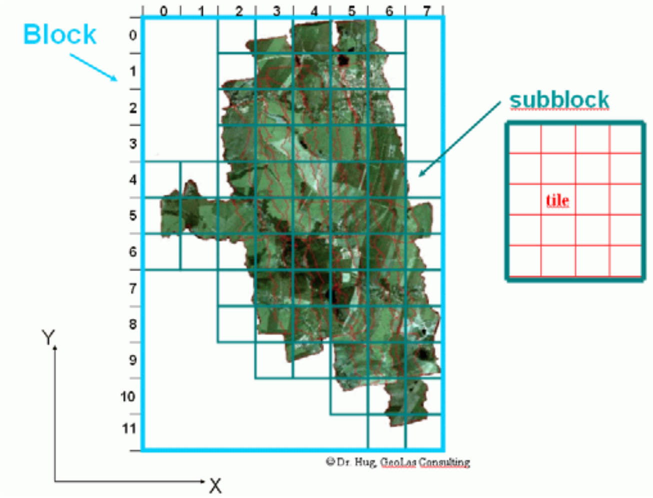


*Figure 1: Subdivision of a block into sub blocks*

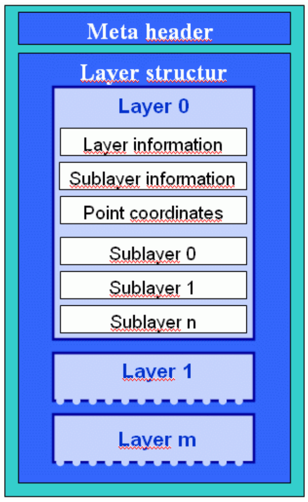


*Figure 2: Structure of a sub block*

## 3 DECOMPOSITION OF FULL WAVEFORM DATA

### 3.1 General remarks

The theoretical model of a waveform depends on parameters of the transmitted pulse, the atmosphere and the object. Wagner et al. (2004) present a theoretical model for the interaction of a single laser beam with topographic targets like leaves, power lines, roofs and trees. For simplification, it neglects the mitigation of the laser beam when travelling through a tree volume. Several theoretical waveform models exist for tree structures. Sun et al. (2000) present a waveform model that works on a hot spot condition and incorporates a bidirectional gap probability. Other approaches use optical and radiative transfer models (Ni-Meister, 2001) and stochastic radiative transfer models (Kotchenova et al., 2003). They have been primarily developed for large footprint waveform scanners like SLICER and LVIS. When analyzing forest structures on the tree level such comprehensive waveform models might be advantageous to estimate tree parameters from waveform data. In order to get an entire waveform for a tree, the single small footprint waveforms must be decomposed and analyzed.

Several approaches to decompose a single waveform have been published. Hofton et al. (2000) suggest to fit several Gaussian distribution functions in a nonlinear least squares adjustment to the waveform. The approach is applied to decorrelate the waveforms from the GLAS-instrument of the ICESat mission (Brenner et al., 2000). Likewise, Jutzi et al. (2005) model the waveform from an experimental system with Gaussians by a Gauss-Newton method. It is pointed out, that the neighbourhood relations of the waveform are essential for a correct interpretation of each pulse. Finally, Persson et al. (2005) introduced another method based on the Expectation Maximation algorithm. First results about the decomposition of waveforms collected by the MK II system from TopEye in forest areas are reported.

### 3.2 Approach

Our approach to decompose the full waveform data is based – similar to Hofton et al. (2000) - on the assumption, that the transmitted pulse is of Gaussian type and the registered waveform is composed from several single laser returns that are also of Gaussian type. Thus, we model the waveform w(t) with a sum of single Gaussian distribution functions (1).

$$w(t) = \varepsilon + \sum_{m=1}^{N_p} A_m \exp\left[ -\frac{(t-t_m)^2}{2\sigma_m^2} \right] \tag{1}$$

with

$N_p$ : Number of peaks in the waveform

$A_m$ : Amplitude of the m$^{th}$ peak

$\varepsilon$ : Bias (noise level) of the waveform

$t_m$ : Time position of the m$^{th}$ peak

$\sigma_m$ : half width of the m$^{th}$ peak at a height of $\frac{A_m}{\sqrt{e}}$ (standard deviation).

A least squares adjustment is used to estimate the model parameters ($\varepsilon$, $A_m$, $t_m$, $\sigma_m$) by fitting the theoretical model to the observed waveform. Since the adjustment is nonlinear initial values for the unknown parameters are necessary. The median of the waveform w(t) is used as starting value for $\varepsilon$. Initial values for the amplitude $A_m$ and the time position of the peak $t_m$ are found by smoothing the original signal by a 1x3 Gaussian filter and the first derivative of the smoothed curve, respectively. In order to distinguish between real peaks, that result from reflections of the laser beam, and noise, a threshold $C_{threshold}$ based on the median absolute deviation (MAD) of the waveform w(t) is calculated. The MAD is a measure of dispersion of a distribution about the median (Rousseeuw and Leroy, 1987)

$$\text{MAD} = \text{median}(|\text{waveform} - \text{median}(\text{waveform})|) \tag{2}$$

It is multiplied by a factor of 1.4826 to achieve consistency with the standard deviation for asymptotically normal distributions. The threshold $C_{threshold}$ is set to

$$C_{threshold} = median(w(t)) + 3*1.4826*MAD \tag{3}$$

We just select potential local maxima with amplitude larger than the threshold $C_{threshold}$. The starting values for $\sigma_m$ are set to 0.25 m which is equivalent to a standard deviation of the transmitting pulse (pulse length 5 ns) assuming that it is of Gaussian type. The initial value for each model parameter can be introduced as an additional constraint in the adjustment scheme.

Experiments showed that the standard least squares adjustment cannot clearly extract single returns from the registered waveform if return pulses are overlaying. Thus, we introduced a Levenberg-Marquardt (LM) (Levenberg, 1944; Marquardt, 1963) iteration scheme, which turned out to be more robust. The key idea of the LM iteration is to weight the diagonal elements of the normal equation by a damping factor (1+λ), where λ is initially set to $10^{-3}$. The damping factor λ is scaled down by the factor 10 as long as the solving the normal equations shows a good convergence. In case of a divergence the damping factor λ is multiplied by 10 and the normal equations are solved again. This process continues until the normal equation converges significantly. Typically there are 5 or 6 iterations necessary to achieve results as shown in figure 3.

There are interesting features of the adjustment approach worth to mention. Firstly, by using the LM iteration scheme we avoid the divergence of the adjustment in cases of incorrect initial values and overlaying single returns. Figure 4 shows, that three overlaying return pulses could be clearly separated. The corresponding peaks have a distance of 0.4 m and 0.7 m respectively, which is in the order of the nominal height discernability derived from the pulse length of 5 ns. It is important to mention, that conventional LIDAR systems can practically discern two return pulses with a distance of about 3 m.

Furthermore, the adjustment approach has the advantage that quality measures like standard deviations of the model parameters can be estimated by error propagation. For instance, we get for the 3D points extracted from all the waveforms of the test data set a mean standard deviation of 2 cm. This precision is equivalent to a height standard deviation because of the laser beam’s inclination angle and is roughly by the factor 7 better than the height resolution of 15 cm.

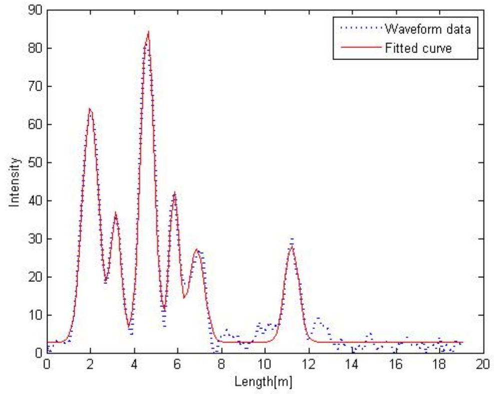


*Figure 3: Sample waveform with 6 single returns*

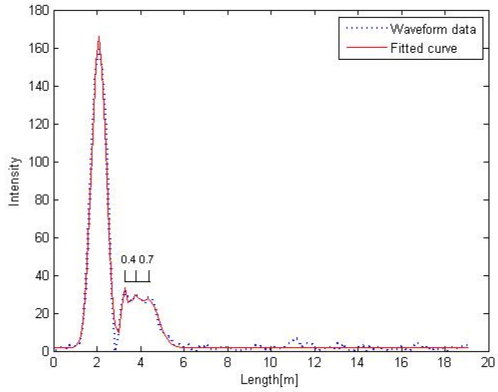


*Figure 4: Separated overlaying returns*

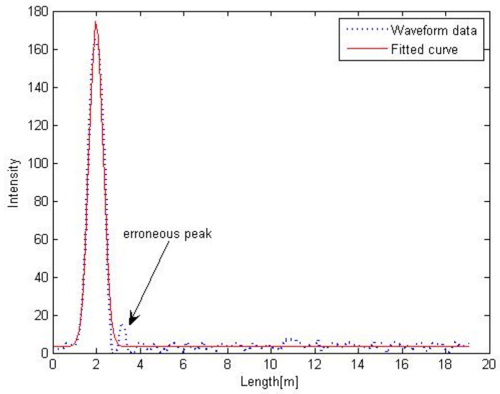


*Figure 5: Waveform from a roof with an erroneous peak and the fitted curve where this peak is ignored*

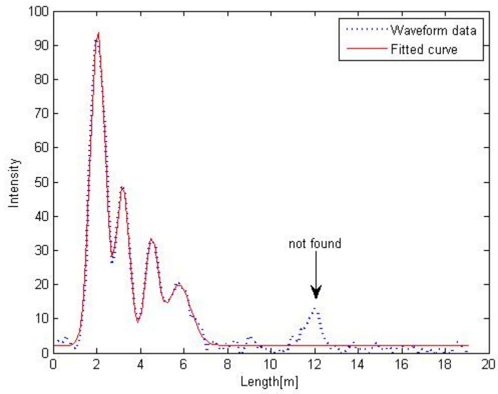


*Figure 6: Waveform and fitted curve where a peak is not found*

Due to electronic characteristics of the laser system smaller peaks occur right after big ones. This phenomenon is mainly caused by a typical effect of bandwidth limited receiver electronics called “ringing" and can be observed - most prominently - when the registered light intensity is high. In worst cases there might even occur 2 additional pseudo peaks after the dominant large peak that only results from a reflection of the laser beam. Figure 5 shows a typical example of a waveform resulting from a roof reflection. Two rules have been established to avoid the extraction of pseudo 3D points in that case. The second peak is ignored if it is closer than 1.5 m to the first peak and, secondly, if its amplitude is smaller than 1/5 of the amplitude of the first peak.

So far, the biggest difficulty in our approach is the clear distinction between noise and significant peaks when determining the initial values. The thresholding mentioned above works well in most of cases. However, in very few cases smaller peaks are not found, although they result from reflections of the laser beam (see figure 6). As long as the number of undetected returns is significantly small, the remaining large number of 3D points will strongly contribute to the intended tree species classification.

### 3.3 Extraction of 3D points

The estimated positions $t_m$ of the Gaussian functions are used along with the starting point of the waveform and its direction vector to generate 3D points. Also, these points get important additional attributes about the width $W_m$ of the response signal that is set to twice the estimated standard deviation $\sigma_m$ ($W_m = 2 * \sigma_m$), and the intensity $I_m$. The intensity $I_m$ is derived from the integral of the Gaussian function which can be approximated with $I_m = 2 * \sigma_m * A_m$. From the adjustment we also get values for the accuracy of the estimated parameters as a quality measure. For example, we exclude all points with a standard deviation for $t_m$ larger than 0.05 m from any further analysis.

### 3.4 Point distribution in trees

We applied the preliminary software to several tree species and a meadow area we found in the test area. Firstly, an area of interest was defined in digital orthophotos by manually digitizing a polygon. Secondly, 3D points were generated from all the waveforms intersecting the corresponding prismatic volume segment. The resulting 3D points were grouped into the 3 classes "First", "Last" and "Middle". The classes "First" and "Last" contain all the points derived from the first and last detected peak ($t_1$, $t_N$). All the other points referring to $t_m$ ($m = 2, N_p – 1$) were classified as "Middle". For comparison, we selected also the first and last pulse points the TopEye system created conventionally with a standard detection procedure. Figure 7 and table 1 illustrate graphically the area of interests and numerically the number of points extracted by the TopEye system and our waveform decomposition. Note that the single trees 1, 2 and 3 are free-standing. Tree 4 refers to a group of trees in closed forest.

Table 1 shows clearly, that the waveform decomposition provides significantly more points than the standard TopEye detection mode. The smallest improvement of about 25% can be observed at tree 1, which is a small deciduous tree in a leaf-on situation. In the area of tree 3, which is a coniferous tree, the waveform decomposition creates even more than 100% additional points. Two main reasons can be found for this. Firstly, the waveform decomposition decorrelates all the significant returns of the laser beam, especially the ones between the first and last echo. Sometimes, up to four or even more points can be found between the first and last peak of the waveform. Such points are totally ignored by a conventional system. The percentage of the "Middle" points to the total number of decorrelated points varies between 10% and 30%. Secondly, since the waveform decomposition can be flexibly controlled by tuning parameters it also decorrelates points with a low intensity. Again, most of such points are not registered by a conventional system due to the internal threshold for signal detection. In other words, the higher sensitivity of the waveform decomposition leads to much more points. This becomes especially apparent in area 5 (=meadow), where only first pulse points occur. Note that the high point distribution also unveils the tree structure. Even branches and the stem can be identified.

*Table 1: Comparison of points derived by the TopEye system and by the waveform decomposition*

| Area | Tree specie / object type | Size [m$^2$] | Points from TopEye | | | Points derived from waveforms | | | |
|---|---|---|---|---|---|---|---|---|---|
| | | | Total | First | Last | Total | First(%) | Last(%) | Middle(%) |
| 1 | deciduous (leaf- on) | 21.9 | 768 | 503 | 265 | 943 | 553(59) | 280(30) | 110(11) |
| 2 | deciduous (leaf- off) | 72.2 | 5594 | 4168 | 1426 | 7436 | 4648(62) | 1548(21) | 1240(27) |
| 3 | Coniferous | 22.2 | 1109 | 882 | 227 | 2555 | 1483(58) | 727(28) | 345(14) |
| 4 | deciduous (leaf- on) and coniferous | 86.7 | 1602 | 1191 | 411 | 3261 | 1678(51) | 969(30) | 614(19) |
| 5 | Meadow | 28.3 | 362 | 362 | 0 | 456 | 456(100) | 0(0) | 0(0) |

### 3.5 Metrics for tree species classification

Tree species classification with LIDAR data needs characteristic features representing the individual tree. If using waveform data they can be derived solely from the 3D points, from the 3D points and their attributes or directly from the waveform signal. Several metrics for tree characterization have been proposed and used - for instance - by Holmgren (2003) and Naesset (2004). We use the latter ones which are also referred to as height dependent and density dependent variables. The height dependent variables are the percentiles of the LIDAR point height distribution in a tree area. We define the density dependent variables as the proportion of LIDAR points in a given tree height segment to the total number of LIDAR points.

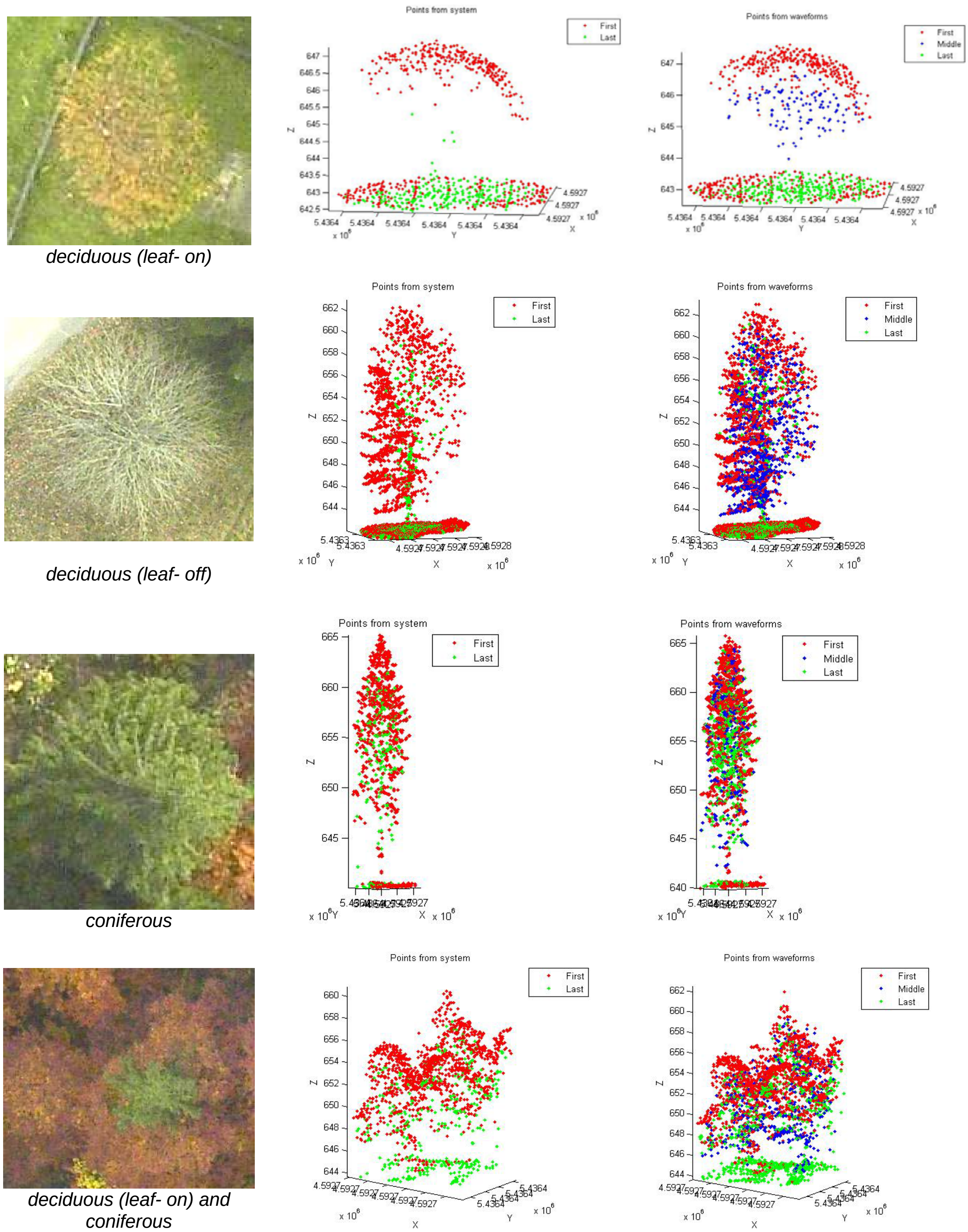


*Figure 7: Aerial images of areas 1 to 4 in column1; Points derived by the TopEye system in column2, grouped in "First" and "Last" pulse points; Points derived from the waveforms in column3, grouped in "First" and "Last" pulse points and points between "First" and "Last" pulse (labelled as "Middle" points)*

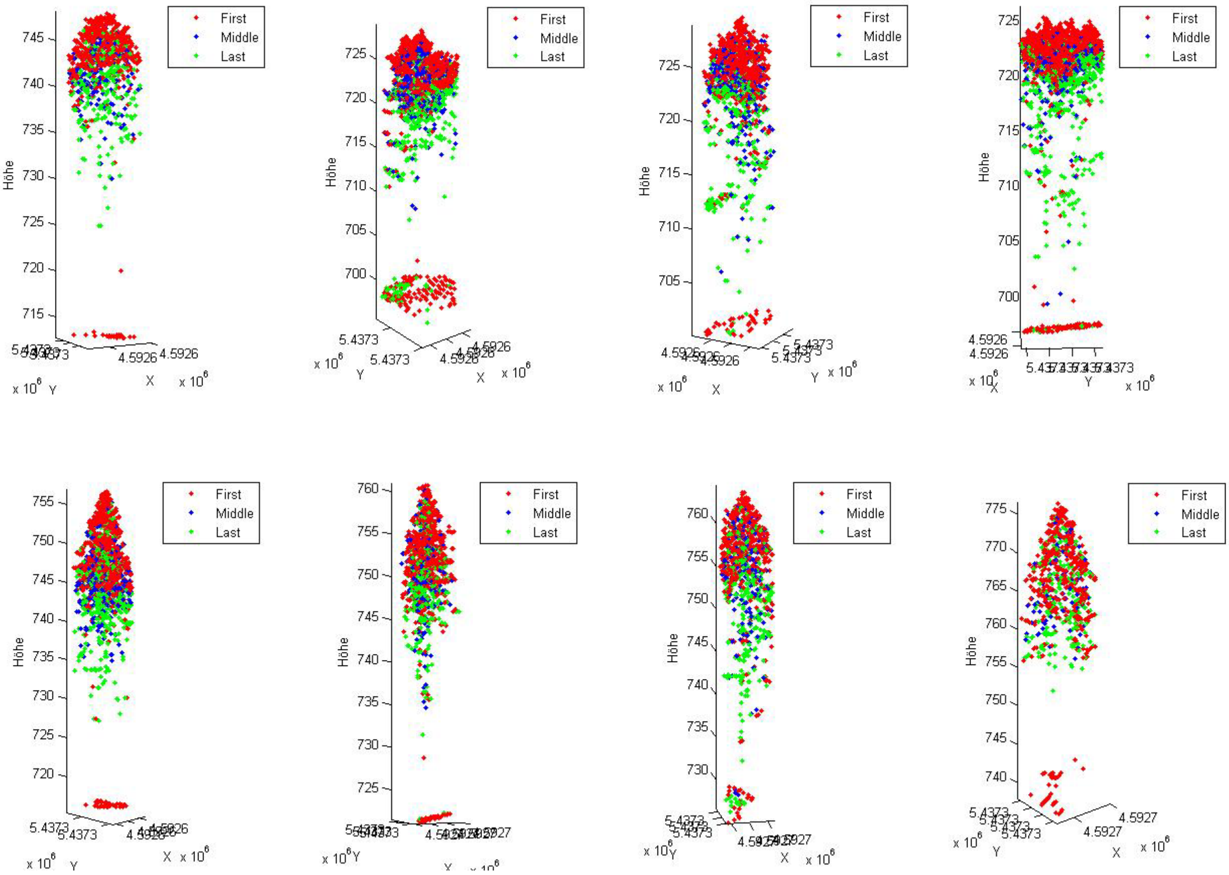


*Figure 8: Point distribution for tree species. First row shows European beech. Second row shows Norway spruce. Point colors are: Red (= First pulse), green(= Last pulse), blue = detected pulses between first & last pulse).*

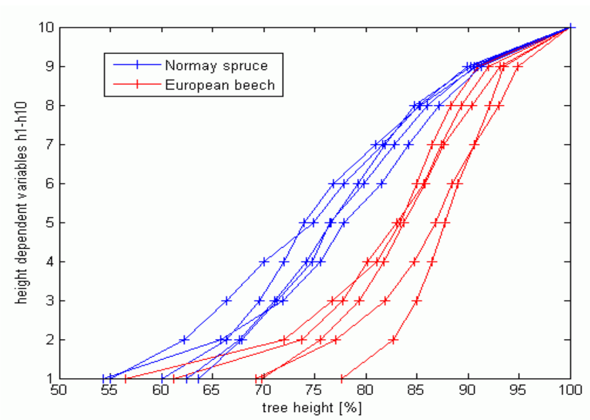


*Figure 9: Height dependent variables for tree species*

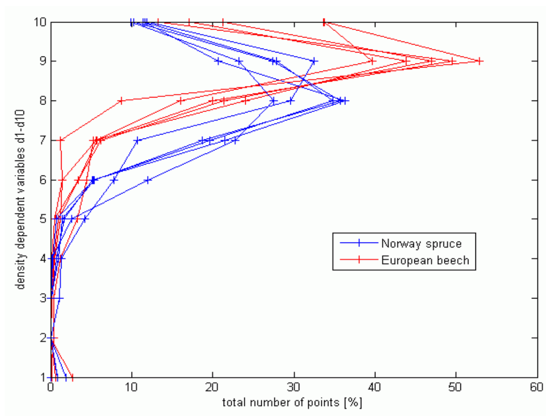


*Figure 10: Density dependent variables for tree species*

Firstly, we selected five sample trees for the two tree species European Beech and Norway Spruce each. The polygons delineating the trees resulted from a segmentation applied to a LIDAR DSM. Figure 8 shows the point distribution for four examples of the selected tree species. Because of the high point density the characteristic shape of the tree species is clearly visible. The crowns of the coniferous trees have a conic shape whereas the crowns of the deciduous trees appear more curved. Again, some points apparently result from hits of the laser beam with the stem.

In the next step, height and density dependent metrics were computed for all the trees. The interval was 10% for the height percentiles ($h_{10}$, $h_{20}$, …, $h_{100}$) and 1/10 of the tree height for the density dependent variables ($d_1$, $d_2$, …, $d_{10}$), respectively. Figure 9 and 10 show graphically the two metrics for the two tree species. The density dependent metric indicate that the deciduous trees contain more laser hits in the upper part of the tree crown. The number of laser hits reduces drastically at 50% of the tree height for both tree species. However, most important is that both metrics are clearly different for the two tree species. Thus, a tree species classification using the investigated metrics as a feature vector appears highly promising.

## 4 DISCUSSION

Research on the application of small footprint full waveform scanners in forestry has recently started with the availability of several commercial systems. Currently, most of the work is focussed on waveform decomposition and analysis of the waveform data and derived information.

Our presented approach for decorrelation of the waveforms works well in most circumstances. It creates significantly more points compared to conventional LIDAR systems, and even copes with the “ringing” effect. The algorithm based on least squares adjustment provides internal quality measures that can be used for quality control. In exceptional cases, return pulses are ignored if the threshold for detecting a peak is tuned too small. This might be overcome by comparing the sigma naught of the adjustment with an a-priori value for the signal noise. Once the adjustment indicates a significant deviation of the estimated noise from the expected noise, it introduces – if possible - a new possible peak and iterates again through the adjustment.

Since the waveform decomposition extracts all possible laser hits as 3D points the point density is extremely high. It reveals tree structures like branches and stems better than conventional system because of the higher sensitivity and the computation of points within the entire waveform. Our preliminary experiments with well-known tree metrics indicate that characteristic features can be derived for a subsequent tree species classification. Obviously, the number of extracted points drops down drastically at 50% (~ 20 m) of the tree height. Primarily, this is due to the limited length of the waveform of about 19 m. However, the inclination angle of the laser beams, which lies always between $14^o$ and $20^o$, plays also a role. Very likely, some of the laser beams do not only pass through the individual tree but also through the neighbouring trees. Thus, both reasons limit the number of laser hits per tree segment considerably. The derived metrics are therefore only statistically representative in the upper parts of the tree area. It is to be expected that a better penetration rate can be expected in the lower parts of the tree areas if another LIDAR system with an unlimited waveform length and a different scanning principle is used.

## 5 CONCLUSIONS

The presented study results show clearly the potential of full waveform data for the successful analysis of tree structures. By just using numerous points derived from the waveform detailed tree structures become visible and reliable metrics can be provided for tree species classification. One step further is to directly use the signal information of the waveform. A waveform for the complete tree - derived from the single waveforms – is a function of tree parameters like for instance the crown shape, the gap probability or foliage reflectance. Future research should evaluate (1) new metrics for tree species classification based on the waveform signal (2) derivation of tree waveform from waveform measurements (3) and adjustment of theoretical tree waveforms to measured waveforms.

## ACKNOWLEDGEMENTS

We would like to thank A. Persson for providing the segmentation of the tree crowns.

Also, we appreciate the allocation of the waveform data by TopEye and the National Park Bavarian Forest.

This research has been funded by the German Department of Education and Research (BMBF) under the contract number 17311B04. The authors are fully responsible for the content of the publication.

# REFERENCES


Blair, J.B., Rabine, D.L., Hofton, M.A. 1999. The Laser Vegetation Imaging Sensor: a medium-altitude, digitisation-only, airborne laser altimeter for mapping vegetation and topography. ISPRS Journal of Photogrammetry and Remote Sensing 54, 115 –122 pp.

Brenner, A.C., Zwally, H.J., Bentley, C.R., Csatho, B.M., Harding, D.J., Hofton, M.A., Minster, J., Roberts, L., Saba, J.L., Thomas, R.H., Yi, D. 2000. Derivation of range and range distributions from laser pulse waveform analysis for surface elevations, roughness, slope, and vegetation heights. Algorithm theoretical basis document. Version 3.0. Greenbelt, MD: Goddard Space Flight Center.

Cothren, J. 2005. Managing Very Large LIDAR Point Clouds in an Enterprise Database. GIS for Local Government Conference, Penn State University, October 19.

Gutierrez, R., Neuenschwander A., Crawford, M.M. 2005. Development of Laser Waveform Digitization for Airborne LIDAR Topographic Mapping Instrumentation. International Geoscience and Remote Sensing Symposium, Seoul, Korea, 25-29 July.

Harding, D.J., Lefsky, M.A, Parker, G.G., Blair, J.B. 2001. Laser Altimeter Canopy height Profiles – Methods and Vallidation for closed-canopy, broadleaf forsests. Remote Sensing of Envirornment (76), pp. 293 – 297.

Hofton, M., Minster, J., Blair. J.B. 2000. Decomposition of Laser Altimeter Waveforms. IEEE Transactions on Geoscience and Remote Sensing, 38:1989-1996.

Holmgren, J. 2003. Estimation of Forest Variables using Airborne Laser Scanning. Doctoral thesis, Swedish University of Agricultural Sciences, Umea.

Hug, Ch., Ullrich, A., Grimm, A. 2004. LITEMAPPER-5600 – A Waveform-Digizing Lidar Terrain and Vegetation Mapping System. In: THIES, M.; KOCH, B.; SPIECKER, H.; WEINACKER, H. (eds.): Laser-Scanners for Forest and Landscape Assessment. Proceedings of NATSCAN-Conference on Laser-Scanners for Forest- and Landscape Assessment. International Archives of Photogrammetry, Remote Sensing and Spatial Information Sciences Vol. XXXVI, Part 8/ W2: 66- 70. ISSN 1682-1750.

Hug, Ch., Krzystek, P., Fuchs, W. 2004: Advanced LIDAR data processing with LasTools. Int. Arch. Of Photogrammetry and Remote Sensing, Commision II, ISPRS 20th Congress, Istanbul, Turkey, 13th - 23rd July.

Jutzi B., Stilla U. 2005. Waveform processing of laser pulses for reconstruction of surfaces in urban areas. In: Moeller M, Wentz E (eds) 3th International Symposium: Remote sensing and data fusion on urban areas, URBAN 2005. International Archives of Photogrammetry and Remote Sensing. Vol 36, Part 8 W27.

Kotchenova, S.Y., Shabanov, N.V., Knyazikhin, Y., Davis, A.B., Dubayah, R., Myneni, R.B. 2003. Modelling lidar waveforms with time-dependet stochastic radiative transfer theory for remote estimations of forest structures. Journal of Geophysical Research, Vol. 108(D15), 4484, doi:10.1029/2002JD003288.

Levenberg, K. 1944. A method for the Solution of certain non-linear problems in least-squares. Quart. Appl. Math. 2, pp 164-168 .

Marquardt, D. W. 1963. An algorithm for least-squares estimation of nonlinear parameters. J. Soc. Indust. Appl. Math. 11, pp 413-441.

Naesset, E. 2004. Practical Large-scale Forest Stand Inventory Using a Small-footprint Airborne Scanning Laser. Scandinavian Journal of Forest Research 19, pp. 164 – 179.

Ni-Meister W., Jupp, D.L.B., Dubayah, R. 2001. Modeling Lidar Wavrforms in Heterogeneous and Discrete Canopies. IEEE Transactions on GeoSceience and Remote Sensing. Vol. 39, September.

Persson, Ǻ, Söderman, U., Töpel, J., Ahlberg, S. 2005. Visualization and analysis of full-waveform airborne laser scanner data. In The International Archives of the Photogrammetry, Remote Sensing and Spatial Information Sciences, Enschede, Netherlands, Vol. XXXVI, Part 3/W19, pp. 103-108.

Rousseeuw, P.J., Leroy, A.M. 1987. Robust Regression and Outlier Detection, Wiley-Interscience, New York (Series in Applied Probability and Statistics), 329 pages. ISBN 0-471-85233-3.

Sun, G., Ranson, K.J. 2000. Modeling Lidar Returns from Forest Canopies. IEEE Transactions on GeoSceience and Remote Sensing. Vol. 38, NO. 6, November.

Unteregger, G., Krzystek, P. 2005: Robuste Filterung von Laserscanning-Daten mit Hilfe von finiten Elemente. Oldenburger 3D-Tage, 2. - 3. Februar, Fachhochschule Oldenburg.

Wagner, W., Ullrich, A., Briese, C. 2003. Der Laserstrahl und seine Interaktion mit der Erdoberfläche. Österreichische Zeitschrift für Vermessung und Geoinformation (VGI), 91(4); 223 - 235.

# ANALYSIS OF REPEATED ICESAT FULL WAVEFORM DATA: METHODOLOGY AND LEAF-ON / LEAF-OFF COMPARISON

*Hieu Duong[1], Norbert Pfeifer[2] and Roderik Lindenbergh[1]*

[1] Delft University of Technology, Delft Institute of Earth Observation and Space systems, Delft, The Netherlands; (h.vanduong, r.c.lindenbergh)@lr.tudelft.nl

[2] University of Innsbruck, Institute of Geography, Austria; norbert.pfeifer@uibk.ac.at

## ABSTRACT

Analysis of the full waveform return pulse of laser altimeter systems is expected to increase the possibilities and accuracies in well-known applications of laser altimetry like forestry, digital terrain model generation, and earth surface analysis. In this study, at first, the ICESat full waveform data, which is acquired by NASA's ICESat Geoscience Laser Altimeter System (GLAS), is introduced and visualized. We analyze two epochs of data of the same groundtrack: the first epoch is recorded in the early winter season of 2003; the second contains data along the same track recorded at the end of the summer of the same year. First, the method of data analysis is discussed. The paper points out how to model the raw, noisy waveforms as a sum of Gaussian components obtained by a least square fit using suited parameters. The Gaussian components enable the decomposition of a full waveform into single constituent modes corresponding to certain reflecting objects within the laser footprint, for example tree canopy or ground surface. Moreover, normalization and shifting of the full waveform data is taken into account as well. This contribution contains the first investigation into the possibility of using repeated ICESat tracks to detect and describe changes in the forest area due to seasonal influences. Finally, results, possible error sources and future perspectives are discussed.

**Keywords:** ICESat, full waveform analysis, change detection, forestry

## 1 INTRODUCTION

ICESat stands for Ice, Cloud and land Elevation Satellite. ICESat was launched in January 2003 with the principal objectives to measure: polar ice-sheet elevation change; atmospheric profiles of cloud and aerosol properties; land topography profiles referenced to a global datum; and height of vegetation canopies. These objectives are accomplished using the Geoscience Laser Altimeter System (GLAS) combined with precise orbit determination. GLAS uses a laser altimeter to measure the range distance between the satellite and the earth surface. The instrument time stamps each laser pulse emission, and measures the echo pulse waveform from the surface. In fact, GLAS has 3 lasers on board, but laser 1 is not used anymore due to unexpected anomalies (NSIDC, 2005b). GLAS acquires elevation profiles of the entire earth consisting of 70m diameter footprints spaced every 175m along the profile. A waveform, recording laser back scatter energy as a function of time, is digitized for each footprint with a temporal resolution of 1ns.

As (Drake et al., 2002) put it: "[…] Forest canopy structure provides information about the primary surfaces of energy and matter exchange between the atmosphere and a major reserve of terrestrial aboveground carbon (Dixon et al., 1994). Knowledge of the total carbon content in […] vegetation provides a critical initial condition for studies […] which examine carbon flux caused by natural […] and anthropogenic […] processes. However, the accurate estimation of […] e.g., aboveground biomass […] of forest vegetation remains a major obstacle in conventional methods (Dubayah, 1997)."

The ICESat full waveform data gives new possibilities to extract more information about forest areas. The full waveform, digitized in 544 consecutive bins of 1ns over land (NSIDC, 2005a), corresponds to a vertical profile of energy returned from a reflecting area of 70m diameter. The land waveform 1ns sampling yields an 81.6m height range (544 waveform bins x 15cm/bin) of 15cm vertical resolution (Harding, 2005). Therefore, the waveform over forest area gives a multi-mode signal (Brenner et al., 2003), containing information about tree tops, crown thickness, canopy structure and ground surface.

Information on the forest structure can be extracted by means of a fitting algorithm which assumes that the waveform is a sum of Gaussian components. For ICESat the emitted waveform is a Gaussian and therefore the returning echo is a convolution of the vertically distributed scattering cross section with a Gaussian. For objects with homogeneous reflectivity this results in a Gaussian return if the scattering object is flat (horizontal or slanted) or has a Gaussian distribution of heights. Assuming this for the scatterers, as it is done in this paper, the Gaussian components of the echo bear information on the scatterers. Because no assumptions are made on the reflectivity or the size of the scatterers, only vertical characteristics can be inferred. The derived parameters of each Gaussian are used for extracting information on the forest structure. For example, the first Gaussian corresponds to a reflection from the tree canopy. A range from the first to the last Gaussain is a practical measure of tree height. The width of the first Gaussian is a measure of crown thickness. This is a justification for the decomposition. In addition, parameters derived from the Gaussian decomposition allow us to study deformation of the forest structure by considering changes in the parameter values.

In the next section we will first describe several processing steps that we used before we actually compare waveforms from different epochs. We explain how to standardize the waveforms via normalization and shift operations as well as how to fit the Gaussians to the waveforms. Then we introduce our comparison methods. In the results section we present our data set and give the results of the comparison between summer and winter waveforms. We finish with conclusions and remarks on further research. While the data used is from ICESat, the methods described below are more general.

## 2 METHODOLOGY

ICESat's data distribution consists of 15 data products called GLA01, GLA02, …, GLA15 (A. C. Brenner et al., 2003). In this study, we have investigated the products GLA01, which is the global full waveform data, and GLA14, the global land surface altimetry data. The GLA14 is a product obtained after precise geolocation, used here for visualizing the ICESat groundtracks, see Figure 4. The GLA01 is the product that contains the full captured waveform. This is the product that is used for our further waveform analysis. A GLA01 waveform is linked to a GLA14 location by index and shot number. The index and shot number are computed by relating the shooting time of an individual pulse to the starting time of the ICESat operation and the shooting frequency. ICESat full waveform data is distributed in binary format. We first converted it into ASCII format by an IDL program developed by the National Snow and Ice Data Center (the software/tools can be found at http://nsidc.org/data/icesat/tools.html, IDL_Readers). The waveform data that is originally in counts (from 0 to 255) is converted into voltage units for further analysis.

### 2.1 Waveform Normalization

The voltage waveform is then normalized. The purpose of the normalization is to enable comparison of waveforms, captured in different epochs. Due to e.g. different atmospheric conditions or changes in the behaviour of the laser device, the amount of energy in the laser return pulse may vary with time, even if the ground didn't change at all. These effects make it almost impossible to compare the absolute energy levels of particular constituents of different waveforms. The normalization step consist of dividing the received energy $V_i$ at moment i by the total energy $V_T$, defined by $V_T = \sum_{i=1}^{544} V_i$ . This implies that the area under any normalized waveform equals one. That is, the normalization is described as $V_N(i) = V_i / V_T$ .Two normalized full waveforms are shown in Figure 1.

### 2.2 Smoothing and initial parameter estimation

The voltage waveform is smoothed by a Gaussian filter. In this filter approach, weights for available observations are obtained by the relative height of a Gaussian shape at a observation location. The Gaussian shape is positioned such, that it maximum coincides with the filtering location. The width of the Gaussian shape is defined in terms of sigma. However, when the Gaussian is used for smoothing, it is usual to describe the width of the Gaussian with the Full Width at Half Maximum (FWHM). The FWHM is related to sigma by the formula:

FWHM = sigma * sqrt (8*log (2)).

We used a FWHM value of 3 for the smoothing step. The shape of the Gaussian is given by the normal distribution. After noise has been removed by the Gaussian filter, we can estimate the locations and amplitudes of the peaks in the smoothed waveform.

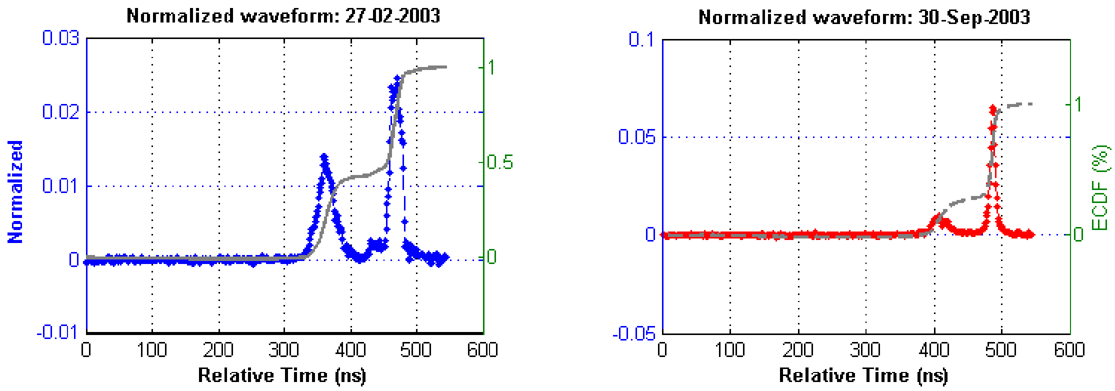


*Figure 1: Two normalized waveforms from February, 2003 (on the left, blue) and from September, 2003 (on the right, red), are displayed together with their cumulative distribution curve (in gray).*

Peak locations are estimated by a searching window 5 ns wide. The window moves from the beginning to the end of the waveform with an interval of 1ns. If the waveform value at the middle of the window is higher than at the four other window positions, and if moreover points on the left and the right are higher than the two outside points as well, the centre position is considered as the location of a peak. Then, the amplitude of the peak is extracted by the peak location in the voltage waveform. Finally, the width parameter or FWHM is calculated as a half distance between two neighbouring peaks. Moreover, the distance between neighbouring peaks is set to at least 5ns.

## 2.3 Fitting algorithm

In the fitting step, so-called Gaussian components are fitted to the normalized and smoothed waveform *w*(*t*). Every Gaussian component $W_m$ corresponds to one Gaussian bell curve. So, we assume that the smoothed waveform *w(t)* is a sum of Gaussian components $W_m$. That is, we write

$$w(t) = \sum_{m-1}^{N_p} W_m(t)\text{, with} \qquad W_m(t) = A_m e^{\frac{-(t-t_m)^2}{2\sigma_m^2}}$$

where *w(t)* is the amplitude of the waveform at time *t*, $W_m$ (t) is the contribution from the *m*-th Gaussian component, $N_p$ is the number of Gaussians found in the waveform, $A_m$ is the amplitude of the *m*-th Gaussian, $t_m$ its position and $\sigma_m$ its standard deviation.

The least squares approach is used to compute the model parameters, that is, the values for $A_m$, $t_m$, and $\sigma_m$ in the above equation are obtained by fitting the theoretical model to the observed waveform in such a way that the difference between model and observation is minimized in the least-squares sense. Two results of the fitting algorithm are shown in the Figure 4. The square sum of the residuals itself can be used to quantify the quality of the fit. And due to our normalization step this minimal sum and therefore the quality of the fit can be compared between the different waveforms.

In the following we will refer to the rightmost Gaussian component of the waveform decomposition as the *last mode,* as this mode corresponds to the energy reflected by the surface hit last. In forest applications, the last mode will in general correspond to the bare earth below the trees, as long as the earth surface is not completely hidden by vegetation. On the other hand, the leftmost Gaussian component is referred to as the first mode, as this component corresponds to the first feature in the laser footprint that is reflecting. Over forest area's, the first mode will mostly originate from reflection by the tree canopy.

Figure 2 shows the results of the fitting algorithm. On the left hand side the algorithm found four modes, on the right, in February, only two modes were found.

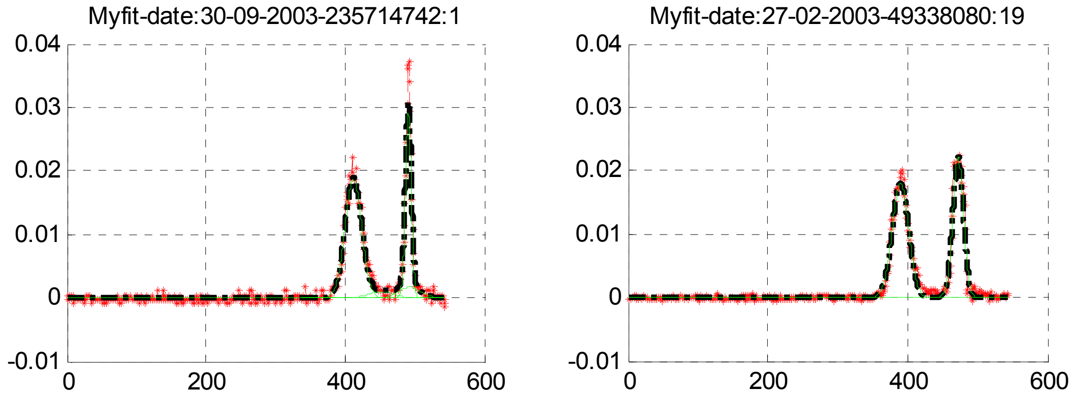


*Figure 2: Two fitted waveforms (dashed black) are displayed together with the raw waveform (red) and the Gaussian components (green) for February, 2003 (left) and September, 2003 (right).*

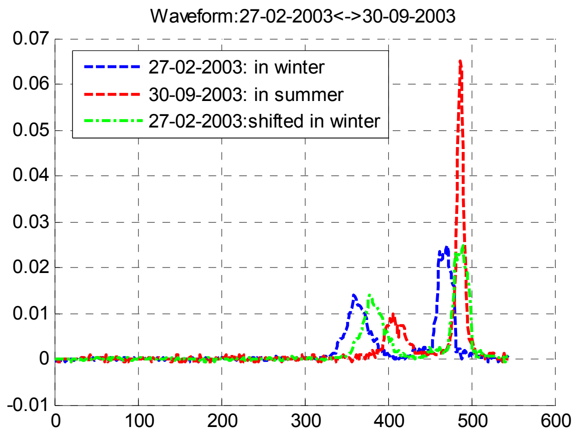


*Figure 3: An original waveform in winter season (blue) is shifted to right (green) displayed with an original waveform in summer (red)*

## 2.4 Shifting Computation

It appears that sometimes there occurs a shift error of the full waveform data between two epochs of data. The shift happens along the relative time axis, and could be caused by changes in the settings in the emitter/receiver unit of the GLAS instrument during the period in between the two epochs. Therefore, optimal shift parameters are computed in order to make the normalized waveforms better comparable along the y-axis. The shift computation is either applied on the complete waveform or on just the last mode of the waveform. The latter case is useful in case of rather different waveform shapes in the two epochs. In that case, the ground surface is still thought to be stable, which implies that the last modes of the two epochs should be matching.

The shift between two individual waveforms in two epochs is calculated by a cross correlation method. Due to the shift error, the waveform data of the second epoch is shifted to the left or the right in comparison to the first, or reference epoch. The shift error can be found by determining the cross-correlation $\hat{R}_{xy}(m)$ for time interval m, by

$$\hat{R}_{xy}(m) = \begin{cases} \sum_{n=0}^{N-m-1} x_{n+m} y_n^*, & m \geq 0 \\ \hat{R}_{yx}(-m), & m < 0 \end{cases}$$

This function returns the cross-correlation sequence as a length 2N-1 vector, where x and y are length N vectors (N>1). By determining that m that minimizes the length of the cross-correlation sequence $\left\|\hat{R}_{xy}(m)\right\|$, an optimal value for the shift is found. Note that in our case, N can be length of the entire waveform (N=544) or just the length of the last mode of the waveform (N≈100).

The shift operation is illustrated in Figure 3. The blue waveform is the one recorded in February; the red waveform is recorded at approximately the same location in September. It is clear that the two last modes don't match. As the terrain is very flat, this change cannot be caused by differences in the terrain height in the non-overlapping part of the respective footprints. Therefore a shift is determined with the cross-correlation method, which results in the, shifted, green February waveform. Now the last modes of the summer waveform and the shifted winter waveform do match.

## 2.5 Waveform deformation classes

After having applied the normalization and shifting operation, we are able to quantify the difference between a corresponding summer and winter waveform. Using these quantified differences, we divide the pairs of corresponding waveforms in four deformation classes.

The first class, class I, consists of pairs of waveforms that are very similar. Such correspondence occurs over flat areas with small or no vegetation and no buildings, like flat grass land or airports. Over such areas, the shift in the footprint location that we inevitable have, does not cause big changes in the waveform.

The last class, class IV, on the other end, contains pairs of waveforms that are incomparable, even if the footprints at least partially match. This happens over very inhomogeneous topography, like over cities, where a small change in the location of the 70m diameter footprint may exclude a part of a high building from being covered by the footprint in the second epoch.

The two remaining classes, classes II and III, are of more interest for forest applications. These two classes contain pairs of waveforms that are different, even after the normalization and shifting operation, but still somehow comparable. An example of such a pair was shown in Figure 3. Before distinguishing between classes II and III, two different notions of waveform distance are introduced first.

## 2.6 Waveform distances

Consider two corresponding waveforms, one waveform WF, from February and its corresponding waveform WS, from September, both normalized and, moreover, matched by the shift operation. For the comparison of WF and WS we introduce two notions: a feature based ratio and an intensity based distance. It should be noted however that the peak ratio is not a distance in the strict mathematical sense.

Above we have introduced the first mode and last mode of a waveform. Let LM denote the position of the peak of the last mode and FM the position of the peak of the first mode. The peak ratio RP compares the length between first and last mode in the two epochs, that is:

$$RP(W_F, W_S) = \begin{cases} \dfrac{LM_F - FM_F}{LM_S - FM_S} - 1, & LM_F - FM_F > LM_S - FM_S \\[2ex] \dfrac{LM_S - FM_S}{LM_F - FM_F} - 1, & LM_F - FM_F \le LM_S - FM_S \end{cases}$$

Note that this ratio is computed along the x-axis. Moreover it should be noted that the absolute location of the peaks of the nodes is not important here, just the location of the first peak relative to the location of the last peak.

The intensity distance on the other hand is determined along the y-axis and equals the mean squared distance between the relative intensities of the February waveform and the September waveform:

$$DI(W_F, W_S) = \sum_{i=1}^{544} \frac{(V_F(i) - V_S(i))^2}{544}$$

These two distances like notions are used to classify pairs of Summer/Winter waveforms into four deformation classes. For a leaf forest for example, the peak ratio distance between summer and winter maybe close to 0, but the intensity distance will significantly differ from 0, as the width of the first mode in September will be considerably wider. We define a distance as *small* if a distance is between the 25% shortest distances between pairs of waveforms. As we have two distances we obtain four different classes: Class *same:* both RP and DI are small, Class *not comparable:* both RP and DI are not small; Class *strong change:* RP small but DI not small*;* Class *slight change*: RP not small but DI small. The class names 'strong change' and 'slight change' do not necessarily resemble specific tree types, but is indicative of forest types found in this region. The interest lies in the automatic classification itself.

# 3 RESULTS AND DISCUSSION

## 3.1 Test forest data

The data we analysed belongs to a track covering part of The Netherlands, Belgium, Luxembourg and France. The ICESat data used in this area is from two epochs, one from 27-02-2003 (winter season, 1840 waveforms) and the other from 30-09-2003 (end of summer season, 2942 waveforms). The GLA14 is used to visualize the geolocation of the waveform data which appears as a straight red line in Figure 1. Actually, it consists of approximately circular footprints of 70m diameter with an inter-footprint spacing of 175m. The data of the two epochs are overlapped and displayed in one global view. Therefore, in the figure only one track is visuable, -but actually there are two tracks.

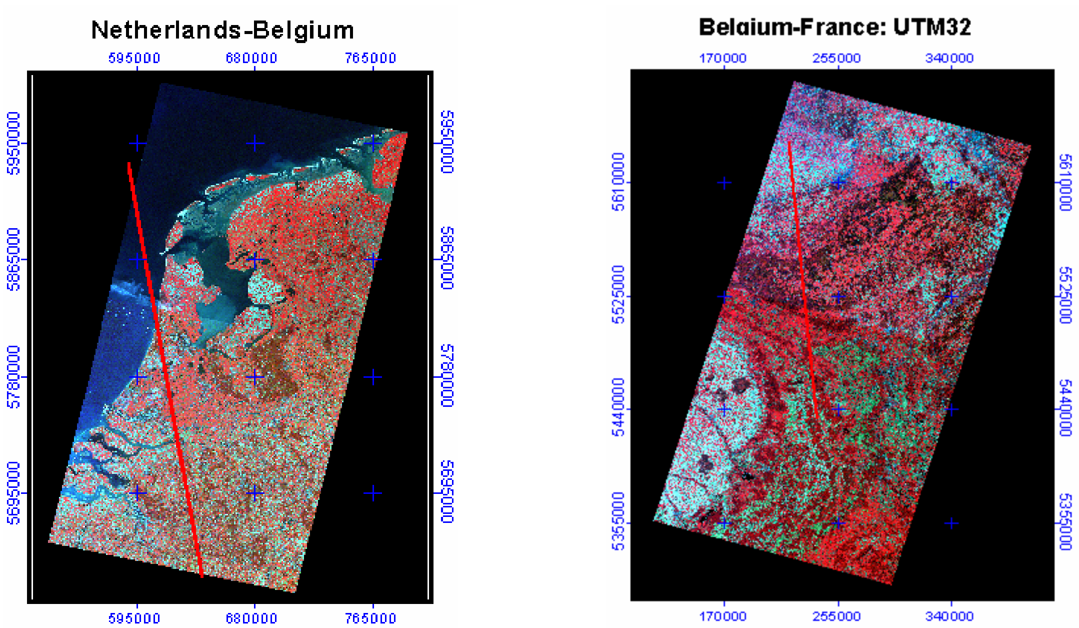


*Figure 4: ICESat groundtracks from February and September 2003 overlayed on LANDSAT false colour image. As both tracks almost coincide, they appear as one track in the image.*

The ICESat groundtracks are visualized together with 30m-LANDSAT images which are false colour composition. The LANDSAT images over the Netherlands, Belgium and the north of France were acquired in 2001 and 2000. The LANDSAT images were used to manually select waveform data from forest areas. Based on visual interpretation we selected 358 waveforms over forest. These data do not cover one big forest but rather several smaller patches of different kind of forest, including both pine and deciduous forest.

## 3.2 Footprint shifts

The repeated tracks do not overlap completely; the actual corresponding footprints of two epochs are shifted 73.8m in average. This causes inaccuracy in change detection in forest areas. However, if the area is a homogeneous forest, we may assume that similar waveforms are returned from all over the area, and moreover, we can detect seasonal changes in the forest structure by analyzing changes from even not fully overlapping footprints. In the above Figure, the red ellipse footprint is data tracked in September 2003, the green footprints are from February 2003.

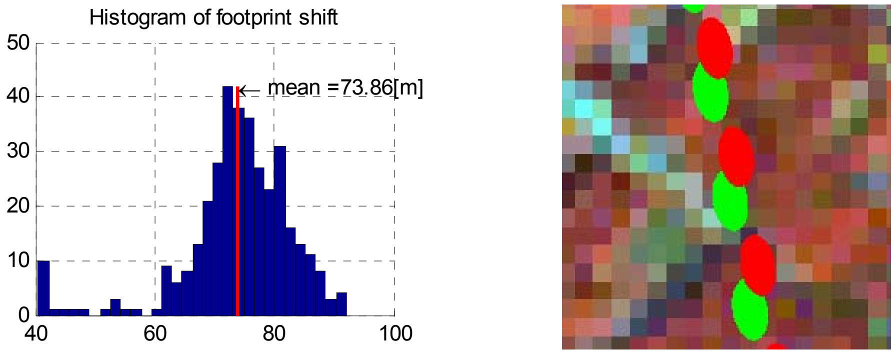


*Figure 5: Histogram of footprint shift and its mean (of left), visualization of footprint shift (on right) with 30m Landsat images. Footprint size of 53 x 97m (Abshire et al. 2005)*

## 3.3 Intensity comparison.

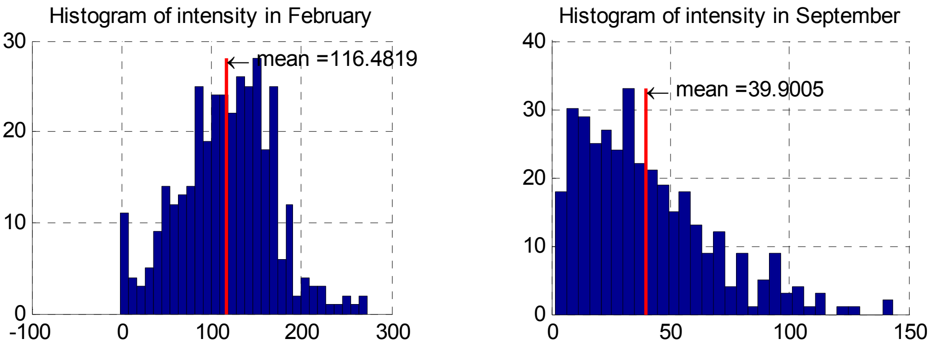


*Figure 6: Mean intensity for February and September Waveform on left and right, respectively*

The intensity or the full returned energy of waveform data in February is much larger than in September. This is illustrated in Figure 6, where histograms of the intensities in February and in September are given. The mean intensity differs by almost a factor 3. One of the reasons for this difference is the change of GLAS sensor L1 to sensor L2 aboard of the ICESat satellite. This implies that we cannot directly compare waveforms from the two different seasons. Therefore, relative intensities only should be considered in the further classifications steps.

## 3.4 Peak location, peak amplitude and shift distance

The first-last peak distance in winter and summer are comparable. In February the average distance equals 20.41 [m], in September it is 19.18 [m]. This difference could be explained by changes in the width of the modes between the seasons.

Above, we have introduced two methods for matching corresponding waveforms. The first method takes the full waveforms into account and with this method we find a mean shift of 4.26[m] downwards for the February waveform to match it optimally with the September waveform. If we match using the last mode only, we find a mean downwards shift of 4.84 [m]. These two shift values are comparable in size, but still they differ more then half a meter. Moreover, the size of the shifts found, shows that such a shift operator is really necessary. Again the reason for this big shift may be found in the change of sensor used aboard of the ICESat satellite.

The amplitude of the first mode in February is considerably lower than in September, see Figure 7. The mean first mode amplitude in winter equals 0.00418, in summer we found a value of 0.0056. This is probably caused by the more dense crowns of the trees in summer. The amplitudes of the last mode in summer and winter turn out to be quite similar, 0.0083 in winter versus 0.0088 in summer. This means that the ground surface is not changed much.

Except for the amplitudes, we also considered the width of the first and last modes. Again the differences for the last mode are small, but for the first mode we found a mean sigma of 4.28 [m] in winter and a mean sigma of 3.74[m] in summer. We do not have a good explanation for this difference, but it may be possible that in summer the first mode is often more restricted to the tree crowns, while in winter the first mode widens, and incorporates larger parts of the trees.

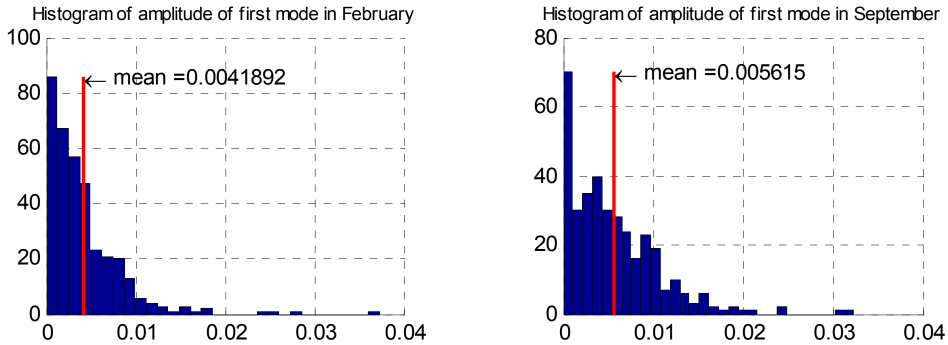


*Figure 7: Average amplitude last/first mode February and September*

### 3.4.1 Waveform distances

For about 358 pairs of summer-winter waveforms we determined both the Intensity Distance *DI* and the Peak Ratio *RP*. Based on the distances found we choose two critical threshold values *C_DI* and *C_RP*. These are both defined as the 0.25 quantile of the distances found. This procedure gives us for *C_DI* a value of 2.18e-6 and for *C_RP* a value of 0.12.

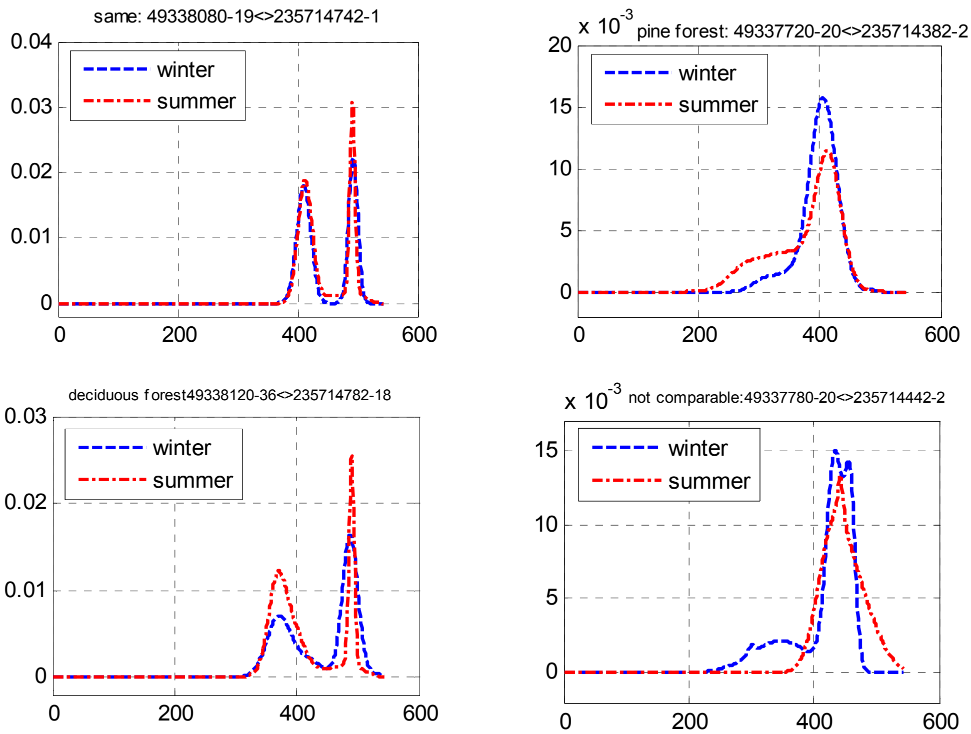


*Figure 8: Four representative pairs of waveforms in four different classes: same (top left), slight change (maybe pine forest, top right), strong change (maybe deciduous forest, bottom left), and not comparable (bottom right)*

If an intensity distance *DI* is smaller then *C_DI*, it is defined to be *small*, and similarly for *C_RP*. These two critical values allow us to divide the 358 pairs in the four deformation classes as introduced above. For each of the four classes representatives are shown in Figure 8.

There are 20 pairs of waveform in the class of *same*, 69 pairs in the class of *slight change*, 70 pairs in the class of *strong change* and 199 pairs in the class of *not comparable*.

The class of *slight change* contains pairs of waveform with *RP small* and *DI not small*, implying a change in waveform along the laser ray. Such changes could be caused by tree crowns that are getting larger in diameter; this class is useful for extracting and monitoring the canopy structure.

The class of *strong change* contains pairs with *DI small* and *RP not small*, implying a change in the height of the forest. This class is useful for monitoring or measuring the growth patch of trees in the forest.

The class of *same* contains pairs of similar waveforms. Here the forest is neither changing much in height (from February to September of the same year 2003) nor in foliage

The class of *not comparable* contains pairs of waveforms that are quite different. One of the reasons for such differences may be the appearance of new artificial objects like buildings within the footprints.

## 4 CONCLUSIONS AND FURTHER RESEARCH

The dataset we considered was far from ideal: the forest is not homogeneous, while the instruments used for the data acquisition differed between the two epochs. Still we were able to find considerable differences between the summer and winter data.

It seems like there are big differences in the intensities returned from forest and non-forest areas. In general, the intensities from forest areas are much lower. It would be interesting to quantify these differences and to investigate whether it is possible to use the results for enhancing classification or deformation detection and analysis methods.

In this paper we first identified some parameters that can be extracted from waveform data. In the next step we started to analyze changes in the parameter values. Further research could focus on identifying those parameters that are most significant for certain forest properties, like relative intensity of the returned signal, or ratio between the relative intensities of the first and the last mode. After identification of these parameters, a more sophisticated ‘waveform distance’ could be defined.

## ACKNOWLEDGEMENTS

We would like to thank the National Snow and Ice Data Center for their data distribution. This project is funded by the Delft Research Centre ‘Earth’.

## REFERENCES

Abshire, J. (2005). Geoscience Laser Altimeter System (GLAS) on the ICESat Mission: On-orbit measurement performance, Geophys. Res. Lett., doi:10.1029/2005GL024028, in press.

Brenner, A. C. (2003). Geoscience Laser Altimeter System Algorithm Theoretical Basis Document: Derivation of Range and Range Distributions from Laser Pulse Waveform Analysis, 92 pp. available at http://www.csr.utexas.edu/glas/atbd.html last visited on February 22, 2006

Dixon, R. K., Brown, S., Houghton, R. A., Solomon, A. M., Trexler, M. C., and & Wisniewski, J. (1994). Carbon Pools and Flux of Global Forest Ecosystems. Science, 263: 185-190.

Drake, J. B, et al (2002). Estimation of tropical forest structural characteristics using large-footprint lidar. Remote Sensing of Environment 79: 305– 319.

Dubayah, R., Blair, J. B., Bufton, J. L., Clark, D. B., JaJa, J., Knox, R. G., Luthcke, S. B., Prince, S., & Weishampel, J. F. (1997). The Vegetation Canopy Lidar mission. Land Satellite Information in the Next Decade II: Sources and Applications. American Society for Photogrammetry and Remote Sensing, Bethesda, MD, pp 100-112.

Harding, D. J. (2005). ICESat waveform measurements of within-footprint topographic relief and vegetation vertical structure. Geophysical Research Letters, 32, L21S10, doi:10.1029/2005GL023471.

National Snow and Ice Data Center (2005a). Frequently Asked Question, http://nsidc.org/data/icesat/faq.html, last visited on February 22, 2006.

National Snow and Ice Data Center (2005b). ICESat mission status. News, http://nsidc.org/data/icesat/news.html, last visited on February 22, 2006.

# ASSESSING PROTECTION FOREST STRUCTURE WITH AIRBORNE LASER SCANNING IN STEEP MOUNTAINOUS TERRAIN

*Luuk Dorren[1], Bernhard Maier[2] and Frédéric Berger[1]*

[1] Cemagref, Mountain Ecosystems Research, St. Martin d'Hères, France; luuk.dorren@cemagref.fr
[2] Stand Montafon - Forstfonds, Schruns, Austria; bernhard.maier@stand-montafon.at

## ABSTRACT

Protection forest management requires reliable data on the structural characteristics of forest stands with high spatial resolution, which could be delivered by airborne laser scanning. We subtracted a digital surface model (DSM), derived from the last LiDAR pulses, from a digital terrain model (DTM), derived from the first LiDAR pulses, to obtain a "normalized crown model" (nCM). The resolution of the rasters was 1 m × 1 m. With two methods that are based on local maxima identifiers individual tree tops were detected with a mean error of 33% when comparing the number of detected trees with the measured number of trees present in the validation plot. When only taking into account the dominant and co-dominant trees, this error decreased to approx. 10%. Position errors of the trees that were automatically identified in the nCM were between 0.5 and 3.5 m, when comparing to on-site GPS measured positions. Field investigations on the causes of errors in the number of detected trees showed that they are mainly caused by trees growing in collectives. Errors in tree positions are related to tilted trees and 'missed' tree tops during scanning, as well as the cumulative errors between GPS measured positions of the base of trees and the LiDAR position. In conclusion, we are of the opinion that airborne laser scanning provides excellent data for protection forest management. It provides reliable information on the positions of individual, dominating and co-dominating trees and on the position of collectives and the tree heights. In addition, it provides excellent input data for 3D natural hazard simulation models, even in steep terrain.

**Keywords:** Protection forest, local maxima, tree top identification, LiDAR

## 1 INTRODUCTION

Many forests in the Alps cover steep to very steep slopes (gradients of 35 - 70 degrees) and have an important protective function against natural hazards, such as rockfall and snow avalanches. In order to sustain the protective effect of these forests, they have to be managed. This requires reliable forest data with high spatial resolution, which could be delivered by LiDAR (Lim et al. 2003). The aim was to retrieve information on the structural characteristics of a protection forest stand, especially, the tree positions and the tree height using airborne LiDAR (Light Detection And Ranging, also called laser scanning), which has been shown to be feasible in less steep terrain by Popescu et al. (2002) and Zimble et al. (2002). We specifically investigated whether reliable information of trees growing on steep slopes can easily be obtained. As most foresters use raster data in standard Geographical Information Systems (GIS) instead of 3D point clouds, we tested two methods that are based on the identification of local maxima on raster data in this study.

## 2 METHODS

### 2.1 LiDAR data

The test site for this study is the 'Schmalzberg' forest, located in the Montafon region in the western part of Austria. The forest, which is dominated by Picea abies, covers a steep slope (up to 40º) and protects residential area downslope against rockfall and snow avalanches. This site has been scanned on the 10th of December 2002. The used laser scanner was a first/last pulse Airborne Laser Terrain Mapper (ALTM 1225) made by Optech Inc. (Canada). The pulse rate of the ALTM is 25 kHz, which resulted in a point density of 0.9 points m-2 at an average fly altitude of 1000 m above ground level. With a laser beam divergence of 0.3 mrad, the average footprint on the ground was about 0.30 m. The average ground swath width was about 725 m, the maximum scanning angle 20º (Wever 2002).

The data obtained by the ALTM have been filtered and interpolated by the TU Vienna to create a digital terrain model (DTM) and a digital surface model (DSM), both with a resolution of 1 m × 1 m and a size of 500 × 500 cells. Since most users of LiDAR data would obtain similar data, we used these two rasters as the basis data for our study. By subtracting the DTM from the DSM we obtained a "normalized crown model" (nCM), which gives an estimate of the height of vegetation or similar obstacles.

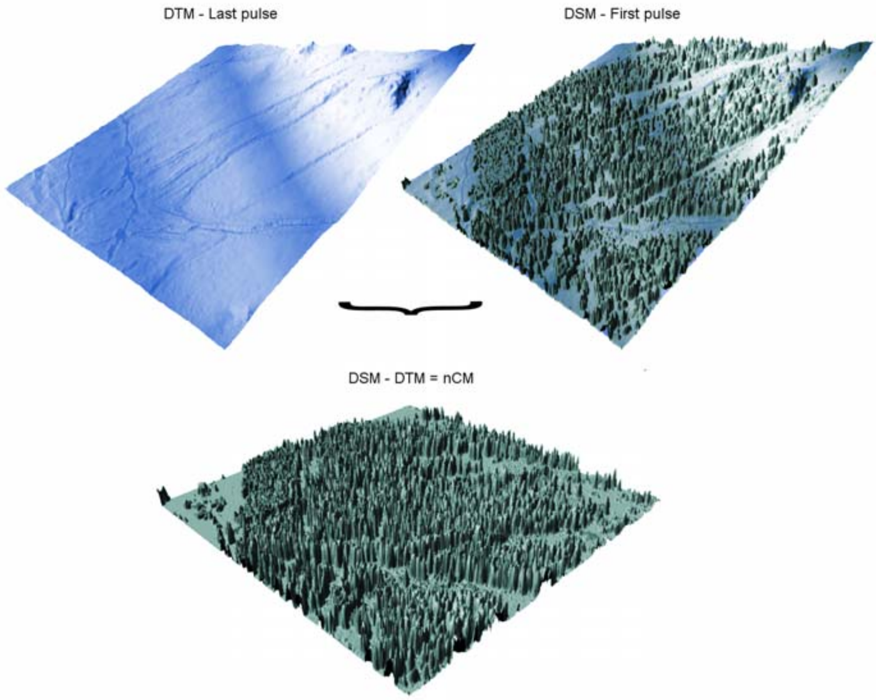


*Figure 1: The 500 $\times$ 500 rasters of the study area and the creation of the normalised crown model (nCM).*

## 2.2 Validation data

A detailed inventory within a sample plot with a 20 m radius has been carried out. Here, we measured the diameter at breast height (DBH), the tree height and the exact position of 30 trees with DBH>10 cm using a compass and an ultrasonic vertex from the sample plot centre. The position of the centre has been measured with a differential GPS. Position errors were estimated to be 0.43 m and tree height measurement errors between 0.5 and 1 m, due to the steep terrain (Maier 2005).

## 2.3 Tree heights and positions

To extract tree heights and positions from the nCM, we tested two methods that are based on the identification of local maxima, where those maxima are regarded as tree tops. The first method uses a variable window size (VWS) that is determined by the tree height, similar to Popescu et al. (2002). The VWS method is supported by an empirical relationship between the crown size and the tree height that is similar to Hasenauer (1997), but which is based on 500 measured tree crowns and heights in a similar forest in the area (Dünser 2002). For trees with a height up to 20 m a 1-cell window radius was used, for 20 – 30 m a 2-cell radius and for larger trees a 3-cell radius. The VWS method can be performed in a standard GIS. The second method, called Tree-top Window Analysis (TWA), is programmed in Matlab and evaluates for each cell in the nCM, which has a value larger than the defined minimum tree height, whether it is a local maximum. Each cell is evaluated with a 3×3 window. If the evaluated cell is a local maximum, the window diameter is enlarged with two cells. Then, the evaluation is repeated. As such the method assesses the dominance of the cell over all surrounding cells. The TWA method also provides information on 'sub-maxima'. This is a cell that adjoins the local maximum with a height gradient less then 45º between the two. Condition for a sub-maximum is that all cells in the window have a lower value except for the local maximum. Such a sub-maximum could represent a tree that grows in or near a tree collective.

# 3 RESULTS

Figure 2 shows the sample plot with the 30 measured and all the detected tree tops. The bigger the blue in this figure dots, the larger the probability of detecting a real treetop, as calculated by the TWA method. The plot also shows the positions errors between the measured tree positions (at breast height) and the detected tree tops. Nevertheless, the heights of the detected tree tops can be used to relate them to the measured ones. The result of this comparison is given in Table 1. This shows that the TWA method detected 25 trees in the sample plot of which 21 were correct. The VWS method detected 20 trees of which 19 were correct. Position errors between the measured tree bases and the detected tree tops ranged from 0.4 – 3.5 m. The error of identifying tree tops is 33% for the TWA and 36.7% for the VWS method, when comparing with all the trees present in our validation plots. When only the dominant and co-dominant trees (non hidden trees in collectives) are taken into account, the mean error decreases to approximately 10%.

*Table 1: Results of the comparison between measured trees and detected trees using the TWA method, the VWS method and two local maxima filters, one with a 2-cell radius and one with a 3-cell radius.*

| | | | Detected Height (m) | | | | |
|---|---|---|---|---|---|---|---|
| Tree nr | Species | Measured height (m) | TWA | 2-cell window radius (fixed) | 3-cell window radius (fixed) | VWS | dH |
| 1 | Picea abies | 29,0 | | | | | - |
| 2 | Picea abies | 35,0 | 35,6 | 35,6 | 35,6 | 35,6 | -0,6 |
| 3 | Picea abies | 35,5 | 40,3 | 40,3 | 40,3 | 40,3 | -4,8 |
| 4 | Picea abies | 21,0 | 18,7 | 18,7 | 18,7 | 18,7 | 2,3 |
| 5 | Picea abies | 32,0 | 33,2 | 33,2 | 33,2 | 33,2 | -1,2 |
| 6 | Picea abies | 37,0 | 40,1 | 40,1 | 40,1 | 40,1 | -3,1 |
| 7 | Picea abies | 15,0 | | | | | - |
| 8 | Picea abies | 22,5 | | | | | - |
| 9 | Picea abies | 36,5 | 31,3 | | | | 5,2 |
| 10 | Picea abies | 32,5 | 33,2 | | | | -0,7 |
| 11 | Picea abies | 34,0 | 36,0 | 36,0 | 36,0 | 36,0 | -2,0 |
| 12 | Snag | 22,5 | 35,0 | 35,0 | | 35,0 | -12,5 |
| 13 | Snag | 34,0 | 35,6 | 35,6 | 35,6 | 35,6 | -1,6 |
| 14 | Picea abies | 30,5 | 34,7 | 34,7 | 34,7 | 34,7 | -4,2 |
| 15 | Picea abies | 34,0 | 33,1 | 33,1 | 33,1 | 33,1 | 0,9 |
| 16 | Snag | 34,0 | 30,4 | 30,0 | 30,0 | 30,0 | 3,6 |
| 17 | Picea abies | 39,0 | 39,6 | 39,6 | 39,6 | 39,6 | -0,6 |
| 18 | Picea abies | 32,5 | 34,5 | 34,5 | | | -2,0 |
| 19 | Picea abies | 25,0 | | | | | - |
| 20 | Picea abies | 34,0 | 35,0 | 35,0 | 35,0 | 35,0 | -1,0 |
| 21 | Snag | 34,0 | 35,9 | 35,8 | 35,8 | 35,8 | -1,9 |
| 22 | Picea abies | 26,0 | | | | | - |
| 23 | Picea abies | 31,0 | 32,4 | 32,4 | 32,4 | 32,4 | -1,4 |
| 24 | Picea abies | 39,5 | 35,7 | 35,7 | 35,7 | 35,7 | 3,8 |
| 25 | Picea abies | 26,0 | 25,0 | 25,0 | 25,0 | 25,0 | 1,0 |
| 26 | Picea abies | 15,0 | | | | | - |
| 27 | Picea abies | 34,0 | 33,2 | 33,2 | 33,2 | 33,2 | 0,8 |
| 28 | Picea abies | 8,0 | | | | | - |
| 29 | Picea abies | 13,5 | | | | | - |
| 30 | Picea abies | 27,0 | | | | | - |
| Correctly detected | | | 21/30 | 19/30 | 17/30 | 18/30 | |
| Total trees detected (wrong ones) | | | 25(4) | 20(1) | 18(1) | 20(2) | |

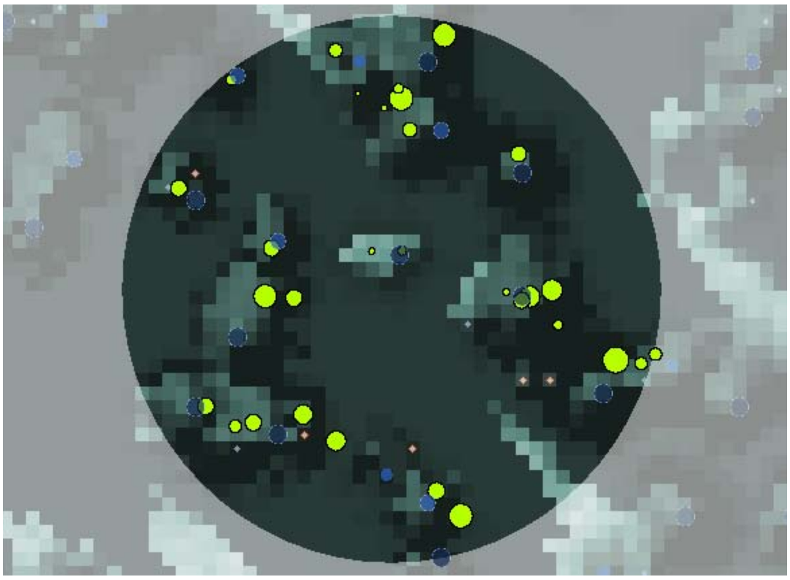

*Figure 2: The sample plot with the measured trees depicted as yellow circles. The trees detected by the TWA and the VWS method are depicted as blue and small grey dots. The small white dots with the red outline were only detected by the TWA method.*

## 4 DISCUSSION

The photos in Figure 3 illustrate examples of sources of error in LiDAR based tree detection. The detection of tree collectives (in German Rotten, see left photo) posed problems for all the methods used in this study. In collectives, trees are growing so close to each other that individual tree crowns cannot be detected, which results in one large collective tree crown after crown delineation. All the trees that were not detected by the LiDAR are growing in or near such collectives. The middle photo shows a dead standing tree (snag). Unexpectedly, all snags were detected in our sample plot, but their crowns were absent as almost no light beam is reflected by their branches. The right photo shows a tilted tree. Errors in tree positions are probably related to such tilted trees and 'missed' tree tops during scanning, as well as the cumulative errors between GPS measured positions of the base of trees and the error in the LiDAR detected tree top.

*Figure 3: Examples of sources of errors in a LiDAR derived nCM (see text for explanation).*

## 5 CONCLUSIONS

Methods based on the identification of local maxima work well for identifying the position of individual trees, as well as for determining their tree height, also in steep terrain. However, collectives consisting of multiple trees growing close to each other are detected as single tree crowns. Therefore the number of trees as detected by LiDAR in our test site is systematically underestimated. The size of the collective tree crown could probably be used as an indicator for the number of tree stems that constitute the collective in reality. Our final aim is to describe the structural characteristics of protection forest stands using LiDAR for (a) management planning, but also for (b) integrating stand characteristics (tree positions, tree heights and their DBH) in snow avalanche and rockfall simulation models (e.g., Dorren et al. 2004). Regarding tree collectives, which occur frequently in protection forests in the Alps, the problems encountered when using LiDAR can probably be solved satisfactorily by using spatial statistics and probabilistic approaches. Future research would have to focus on developing a generic and persistent method for estimating the number of trees that constitute a collective. Other solutions might be to use the raw 3D LiDAR data in combination with methods described by Zimble et al. (2003) and Maltamo et al. (2005) or the use of the full waveform LiDAR.

The DTM of steep mountainous terrain provided by LiDAR and the positions and heights of individual trees derived from the DSM have an enormous added value for natural hazard simulation models in comparison with traditional DEMs obtained from photogrammetry and tree positions derived from orthophotos. In the future we will focus on adding criteria in the TWA method to improve the estimation of the probability that a detected local maximum or sub-maximum is a real tree top. Then, the improved method should be tested and validated on a larger scale and in other types of forest than pure *Picea abies* stands, such as mixed montane forests and pole forests.

## ACKNOWLEDGEMENTS

Markus Hollaus at the TU Vienna is acknowledged for creating the DSM and the DTM from the raw LiDAR data.

## REFERENCES

Dorren, L.K.A., Maier, B, Putters, U.S. and Seijmonsbergen, A.C. (2004). Combining field and modelling techniques to assess rockfall dynamics on a protection forest hillslope in the European Alps. Geomorphology 57(3): 151-167.

Dünser, S. (2002). Ableitung von Auszeigekriterien für die Holzernte im Seilgelände auf Basis des Schutzwaldkonzepts Rellstal/Montafon (Vorarlberg). Diplomarbeit am Institut für Waldbau an der Univ. f. Bodenkultur, Wien.

Hasenauer, H. (1997). Dimensional relationships of open-grown trees in Austria. For. Ecol. Man. 96:197-206.

Lim, K., Treitz, P., Wulder, M., St-Onge, B. and Flood, M. (2003). LiDAR remote sensing of forest structure. Prog. Phys. Geog. 27:88-106.

Maier, B. (2005). Analyse von LiDAR-Baumkronen-Modellen mit Filtertechniken. SE Arbeit für Räumliche Modelle und Simulation SS 2, Institut für Geographie und Angewandte Geoinformatik, Univ. Salzburg: 20 p.

Maltamo, M., Packalén, P., Yu, X., Eerikäinen, K., Hyyppä, J. and Pitkänen, J. (2005). Identifying and quantifying structural characteristics of heterogeneous boreal forests using laser scanner data. For. Ecol. Man. 216(1-3): 41-50.

Popescu, S.C., Wynne, R.H. and Nelson, R.F. (2002). Estimating plot-level tree heights with lidar: local filtering with a canopy-height based variable window size. Comp. Elec. Agric. 37:71-95.

Wever, CH. (2002). Airborne Laser Scanning. Verfahren und Genauigkeiten. Vortrag im Rahmen des Fachforums VOGIS in Feldkirch. http://www.vorarlberg.at/pdf/vortrag_wever_23_09.pdf (27. Juli 2005).

Zimble, D.A., Evans, D.L., Carlson, G.C., Parker, R.C., Grado, S.C. and Gerard, P.D. (2003). Characterizing vertical forest structure using small-footprint airborne LiDAR. Rem. Sens. Env. 87:171-182.

# STANDWISE DELINEATION BASED ON 3-D INFORMATION FROM LIDAR

*Christoph Straub, Holger Weinacker, Oliver Diedershagen, Barbara Koch*

Universität Freiburg, Abteilung Fernerkundung und Landschaftsinformationssysteme (FELIS), Freiburg, Germany, ferninfo@felis.uni-freiburg.de

## ABSTRACT

Airborne Laser Scanning (ALS), also referred to as LIDAR, is an up-to-date, largely automated method for mapping, GIS data acquisition and topographic feature extraction, which can be used to derive forest inventory variables. Several studies have already shown the capability to accurately estimate important inventory parameters (Weinacker et al. 2004, Heurich et al. 2004, Diedershagen et al. 2004). The technology is used in Scandinavia to measure canopy heights. In this paper largely automated methods are described for the delineation and characterization of forest stand units based on 3-D information from ALS. All undertaken procedures during this study were based on digital image processing algorithms applied to digital terrain models (DTMs), digital surface models (DSMs) and normalized digital surface models (nDSMs) in two different study areas. A digital forest stand map provided by the Department of Forestry of the federal state of Baden-Württemberg was used as reference material. A visual comparison of the laser scanner models with the reference data showed that 85% of the stand boundaries could theoretically be identified in the elevation models. It was possible to delineate 50% of the forest stand boundaries using automated methods. Input from a human operator was required in order to achieve a complete and accurate delineation of forest stands. Finally an interactive graphical processing tool was developed combining several delineation methods in a single processing chain. Based on the stand boundaries important stand characteristics such as the average stand height and canopy closure were derived. High-quality maps were generated and imported into a Geographical Information System.

**Keywords:** Airborne Laser Scanning, Inventory, Forest Stands, Digital Terrain Model, Digital Surface Model, Digital Image Processing

## 1 INTRODUCTION

There is a long tradition of using remotely sensed data (particularly aerial photography) in forest inventories. In Germany these inventories are carried out every ten years. The data collections have been based on terrestrial measurements undertaken by field crews and the interpretation of aerial photographs. The results are extrapolated to forest stands, which are the smallest forest units. The forest stand boundaries are momentary extracted manually from analogue maps and/or aerial photographs. The results are verified by field surveys. Finally the boundaries are digitized. This approach is labour and time intensive. To reduce the costs of this task an automated and thus cost-efficient method is needed.

In recent years ALS has been investigated as an alternative technique to derive forest inventory variables and to analyze forest structures. The result of the measurements is a point cloud which provides complete 3D forest information both for the derivation of a digital terrain model, which represents the forest floor and a digital surface model which represents the top of the vegetation. The extraction of 3D objects out of point clouds and digital elevation models is still researched. In recent years most studies were concentrated on single tree delineation in forested areas. The investigations of this study evaluated ALS data for an automatic delineation of forest stands (communities of trees).

## 2 METHODS

### 2.1 Study Areas

Two different study areas were used for the investigations: “Mooswald” and “Günterstal”. Both study areas are located close to the city of Freiburg – Breisgau (Germany) and represent a typical mixture of tree species, forest stands and age class distributions for this region. The first site „Mooswald“ is a basically flat area in the Rhine Valley. The second area "Günterstal" is located in the mountainous regions of the Black Forest.

| Study area "Mooswald" (north-west of Freiburg) | Study area "Günterstal" (south-east of Freiburg) |
|---|---|
| Flat terrain | Mountainous terrain |
| Forested area | Forested area |
| Size: 20ha | Size: 70ha |
| About 250m above sea level. | 500 to 800m above sea level |
| Tree species: English oak and hornbeam, ash, red oak, Norway maple, one stand of Douglas fir | Tree species: mixed mountain forest, mostly beech (60%), fir (25 %) and spruce (10 %). |
| Rich in structure: canopy gaps, different age classes, double layered, very dense parts | Most stands are of uneven age, many stands have got an understory. |

## 2.2 Data Sets

The datasets for the study areas "Mooswald" and "Günterstal" were recorded by TopoSys with "FALCON" remote sensing system during winter and summer conditions. The "FALCON" LIDAR sensor consists of 127 fan-formed fibreglass cells at both the input and output sides of the device. An extra cell is used for calibration. In addition to the laser scanner a digital line scanner records intensity data in the visible and near infrared region of the electromagnetic spectrum. As a result a corresponding RGB/CIR dataset is available for each flight strip.

## 2.3 Reference Data

A digital forest stand map provided by the Department of Forestry of the federal state of Baden-Württemberg was used as reference material. Forest stands are integrated as polygon features. The forest stand boundaries were originally drawn manually from analogue maps and/or aerial photographs. After digitizing the polygon features were linked to a database with related information from field surveys (Diedershagen 2004).

## 2.4 Methodology

Several fully automated methods for the delineation of forest stand boundaries were developed and tested in both study areas. All methods were based on digital image processing algorithms, which were applied to DTMs, DSMs and nDSMs (nDSM = [DSM-DTM]).

### 2.4.1 Extraction of Forest Roads

In many cases stand boundaries are following the forest roads in the study areas. Therefore a method was developed to extract forest roads automatically from the DTM. The procedure is mainly applicable in mountainous and thus steep terrain, because the roads will have lower slope values compared to the surrounding terrain.

The method is based on a "gradient image" derived from the DTM. Gradient operators are generally used to extract edges - rapid changes (discontinuities) in the values within a small area of an image. To detect the borderlines on both sides of the roads a standard deviation operator was applied to the gradient image. This result was used as input into "Region Growing" to segment the image. Good results were achieved in study area "Günterstal" (mountainous terrain). In study area "Mooswald" (flat terrain) a draining channel alongside a road was extracted and was used for segmentation.

### 2.4.2 Segmentation with predefined Height Classes

Young forest stands can be divided into different height classes, which correspond to developmental stages (table 1). These height classes were used as parameters in a threshold operation for a segmentation of the canopy height model.

*Table 1: Height classes to differentiate young forest stands (according to Ebert 2003, slightly modified)*

| | |
|---|---|
| "juvenile": | < 2m |
| "sapling": | 2-10m |
| "pole": | 10-15m |
| "mature": | > 15m |

The result was improved by iteratively reducing the domain of the canopy height model in a loop, where the output of each preceding segmentation result (e.g. regions from segmentation with forest roads) was taken as the input of the next succeeding one. The new domain was calculated as the intersection of the old domain with the region. Thus, the new domain can be seen a subset of the region.

### 2.4.3 Delineation of Coniferous Forest Stands

ALS data obtained during conditions without foliage (winter) showed different penetration rates in coniferous and deciduous stands and was used as the basis for a differentiation of both stand types. A visual comparison of the three datasets: nDSM_[le_w] (**n**ormalized **D**igital **S**urface **M**odel (**L**ast **E**cho) from **w**inter ), CIR-images and existing stand maps revealed an isolation of the coniferous trees (clearly visible) in the nDSM_[le_w], while the deciduous trees having been largely eliminated. The nDSM_[le_w] was used as input in an automatic threshold operation to extract the coniferous trees (parameters for the threshold operation were determined automatically from the histogram).

### 2.4.4 Delineation of forest stands based on single tree segmentation

Another fully automated method was based on the comparison of a single tree with its neighbours. A forest stand is defined as a community of trees which is similar in height, canopy structure and tree species as to be distinguishable from adjoining areas. The method is based on single tree delineation as a first step. A single tree is taken and will be compared with its neighbours. If the neighbouring trees are similar in height or crown diameter they will be appended to the stand. Then the next neighbours of the created region are examined. This "growing process" is repeated until no trees remain which fulfil the conditions.

### 2.4.5 Semi-Automatic Classification of Forest Stands

A semi-automatic method was developed based on 3 different laser scanner models calculated from winter data and combined in a three-channel-image: 1. nDSM_[le_w] (**n**ormalized **D**igital **S**urface **M**odel (**L**ast **E**cho) from **w**inter, 2. nDSM_[fe_w] (**n**ormalized **D**igital **S**urface **M**odel (**F**irst **E**cho) from **w**inter, 3. (nDSM_[fe_w] – nDSM_[le_w]). Based on the three-channel image coniferous and deciduous trees can be classified based on their heights. The input of a human operator is restricted to the selection of training areas (supervised classification):

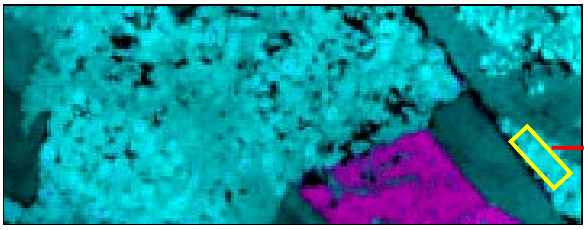

Three-channel-image: Deciduous trees are shown in blue colour whereas conifers are shown in violet. Bright colour will indicate high vegetation and darker values are nearer to the ground. This eases the selection of training areas. A training area (yellow rectangle) was digitized in a mature, deciduous forest stand.

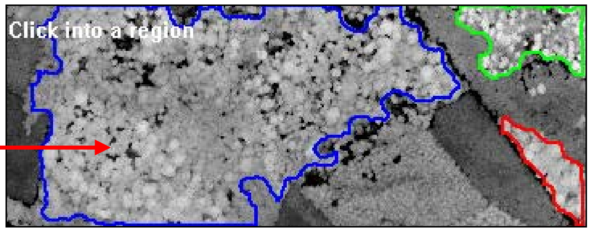


The margin of classified regions is shown in different colours. Only mature and deciduous trees were classified. Holes within the classified regions were removed and the boundaries were slightly smoothed with morphological operators. Appropriate regions can be selected by mouse click and the selection of a training area can be repeated.

*Figure 1 and 2: Supervised Classification based on laser scanner models for forest stand delineation*

# 3 RESULTS

An interactive graphical processing chain was developed. All segmentation methods were combined in a series of modules. After each segmentation step (module), the user has the option to select regions by mouse click, which will be stored. After the last segmentation step additional regions can be digitized on screen either with the help of a “canopy height model” or a “gradient image” as background information. This allows adding further regions which were not detected with one of the fully- automatic or semi-automatic methods. Finally all regions will be intersected and the boundaries will be smoothed and adapted automatically. The following images show a comparison of the delineation results with the reference data in study area “Mooswald” with different levels of interaction:

1. Fully-automatic delineation (without user interaction)

2. Fully-automatic delineation + supervised classification + on screen digitizing (Additional forest stands were digitized on screen, based on visible features in the DTM and DSM, which were not found with one of the automatic methods and/or supervised classification)

The following results can be summarized:

- With fully-automatic methods about 50% of the forest stands were delineated in both study areas.
- In both study areas around 85% of the forest stand boundaries were confirmed based on detectable and obvious features in the Laser Scanner- DTM and DSM (canopy structure, forest roads and ridgelines).

| | Results of the processing chain (Mooswald): | Reference data (Department of Forestry): |
|---|---|---|
| 1. | 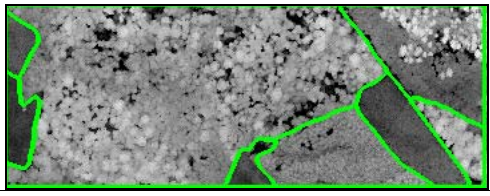 | 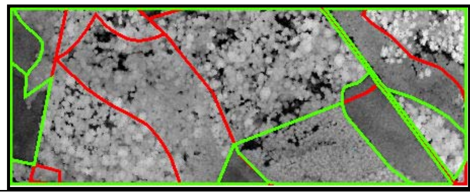 |
| | The image shows the delineation result after combining all fully-automatic segmentation methods without user interaction. 8 regions from 15 expected regions were delineated correctly. (Success rate: 53%) (Processing time: 1 min.) | The same regions can be found in the reference data (green lines). The red lines were not delineated automatically. |
| 2. | 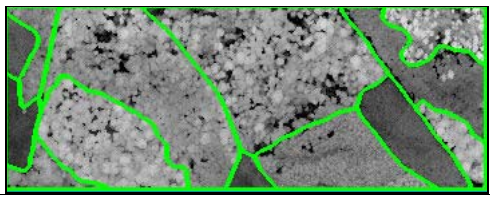 | 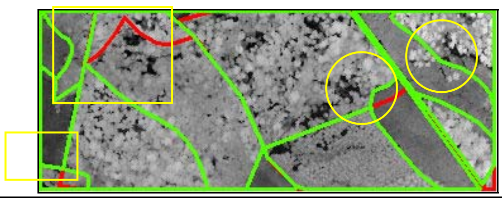 |
| | 3 additional regions were delineated with supervised classification and 2 regions were digitized manually (based on visible features in the DTM and nDSM), which were not found with automatic methods and/or supervised classification, now 13 forest stands were delineated. (Success rate:86%) (Processing time: 5 - 6 minutes) | Only 5 lines remain in the reference data (red colour) which were not delineated. Two expected forest stands (marked with a blue rectangle) were not detected in the laser scanner models. The boundaries inside the white circles could be interpreted as inaccuracies in the reference data. |

*Figure 3 to 6: Comparison of fully automatic delineation with the reference data and comparison of the results of the interactive processing with the reference data*

# 4 DISCUSSION

In contrast to artificial surfaces (buildings and other artificial features that have been crafted by human hand), natural surfaces (tree canopies) are more complex, a mixture of many different structures. A significant level of testing and experimentation was necessary to arrive at a solution which was transferable to both test sites. The success of an automatic procedure for the delineation of forest stand boundaries based on DTMs or DSMs will depend on the following main factors:

- Structure of the forest (good results will be achieved if the canopy structure is largely homogeneous)
- Raw Data (point density, season (the differentiation of deciduous and coniferous stand types is more reliable during winter (leaf-off) conditions due to different penetration rates in both stand types))
- Filtering / Interpolation Algorithm (the smoothness or roughness of a model will influence the possibilities for feature extraction and classification – the computation method has to be adapted to specific objectives)
- Image Processing Method (robustness of the algorithm)

# 5 CONCLUSIONS

The methods presented in this article showed good results for automatic stand delineation in the study areas. In some cases the stand boundaries delineated with the interactive processing chain, based on laser scanner models, were closer to reality and thus even more accurate as the reference data. This is due to the fact that the boundaries of the reference data are generally identified by visual interpretation of analogue maps and aerial photographs. Compared to conventional methods the processing time could be reduced considerably. Input from a human operator was required in order to achieve a complete and accurate delineation of forest stands. With the help of the interactive processing tool high-quality stand maps were generated and imported into a Geographical Information System.

## REFERENCES

Weinacker, H.; Koch, B.; Heyder, U.; Weinacker, R. (2004): Development of filtering, segmentation and modelling modules for LIDAR and multispectral data as a fundamental of an automatic forest inventory system In: Laser-Scanners for Forest and Landscape Assessment, International Archives of Photogrammetry, Remote Sensing and Spatial Information Sciences, Vol. XXXVI, 8/W2, Freiburg

Diedershagen, O.; Koch, B.; Weinacker, H. (2004): Automatic segmentation and characterisation of forest stand parameters using Airborne LiDAR data multispectral and FOGIS data, In: Laser-Scanners for Forest and Landscape Assessment, International Archives of Photogrammetry, Remote Sensing and Spatial Information Sciences, Vol. XXXVI, 8/W2, Freiburg

Ebert (2003): Waldbauliche Grundbegriffe, Vorlesungsskript im Studiengang Forstwirtschaft, Hochschule für Forstwirtschaft, Rottenburg

Heurich, M.; Günther, S.; Schröder, S.; Kennel, E. (2004): Baumhöhenmessung mit flugzeuggetragenen Laserscannern. In: AFZ - Der Wald 17, 945-947

# LAI DETERMINATION IN FORESTRY ECOSYSTEM BY LIDAR DATA ANALYSIS

*Andrea Barilotti[1], Sheera Turco[2], Giorgio Alberti[2]*

[1] University of Udine, Department of Geo-resources & Territory, Udine, Italy;
andrea.barilotti@uniud.it

[2] University of Udine, Department of Agricultural and Environmental Sciences, Udine, Italy;
turco@uniud.it – giorgio.alberti@uniud.it

## ABSTRACT

The assessment of the forest biomass is a fundamental cognitive process for the characterization of forest ecosystems and for a rational management of wood resources. Forest monitoring represents a important subject today in the context of greenhouse gas control because of trees capacity to turn atmospheric carbon into organic matter and bioenergy. This paper proposes a new method based on Airborne Laser Scanning (ALS) data for the automatic estimation of the Leaf Area Index (LAI) over vast forest areas. The study site is located in two mountain areas (37 $km^2$) of Friuli Venezia Giulia (NE-Italy), characterized by mixed spruce forests and by beech forests respectively. Laser data (density: 2 points $m^{-2}$) relative to the ground and to the vegetation were processed and a statistical index of the laser penetration through the leaf canopy (LPI) describing the three-dimensional structure of the forest, was computed. A number of plots were fixed through a stratified sampling; on-site measurements of the leaf area index were carried out on them using the *LAI-2000 Plant Canopy Analyser*. The correlation between LAI field data and LPI laser scanning data shows a high degree of significance ($P<0.001$). This correlation is highly significant even if a re-sampled low-density data is used (up to 25% of original points) with an evident advantage in terms of survey costs and computational time. The results show that the LPI can be used to estimate LAI on a broader scale.

**Keywords:** Forestry, Laser scanning, LAI, Vegetation indices

## 1 INTRODUCTION

The use of remote sensing to describe forest structures is becoming very important in recent years. This is particularly true in the case of biodiversity monitoring and of $CO_2$ forest uptake. As far as this last aspect is concerned, the third IPCC Report confirmed how land use changes and forests management can offer a significant contribution in the reduction of atmospheric $CO_2$ (Niles et al., 2004). In fact, the Kyoto Protocol underlines the need for an accurate estimation of afforestation, reforestation and deforestation undertaken since 1990 to quantify as precisely as possible forest carbon sinks (Patenaude, 2005).

Leaf Area Index (LAI), defined as the sum of the projected leaf surface per soil area (Schulze et al., 2005), is a widely used index to describe the active vegetation photosynthetic surface and, consequently, to model carbon cycle in forests. In fact, rapid, reliable and objective estimations of this index are essential for numerous studies of atmosphere–vegetation interaction, as LAI is very often a critical parameter in process-based models of vegetation canopy response to global environmental change. LAI changes depend on forest composition, density, structure and forest management (Scurloch, 2001). There are two main categories of procedures to estimate LAI: direct or indirect methods (Norman and Campbell, 1989). The former methods are based on measuring leaf area in a direct way while the latter group is based on easily (in terms of time, workload, technology) measurable variables correlated to light interception by forest canopy. These measures can be performed in the field using portable instruments (i.e. LiCor 2000) or can be done using remote sensing data (i.e. NDVI, EVI and so on). The use of the latter technique is generally faster, can be used on a broad scale and can be repeated in time but requires a ground validation (Gower et al, 1999).

It is possible to distinguish a lot of different remote sensing approaches to estimate LAI (Morsdorf et al., 2003), but the laser scanning technique (LiDAR) is one of the most useful because it is able to describe the forest structure in a three dimensional way (Lefsky et al., 2005).

A LiDAR survey represents the elements on the ground are as a clouds of georeferenced points. In particular, the forest and the single trees are surveyed by the discrete sampling of the forest crown. The high density of points for surface unit determines an almost homogeneus covering of the area (Barilotti et al.). Some authors have proposed differents methods to estimate the LAI value starting from LiDAR data (Riaño et al., 2004; Hyyppä et al., 2005; Morsdorf et al., 2005).

This paper presents a new index estimated using LiDAR data to describe LAI in two different forest types (a broad leaves mixed forest and a coniferous forest). On the base of medium-density LiDAR survey (2 point/$m^2$), the index applicability using lower points density was computer simulated.

# 2 MATERIALS AND METHODS

The study area is located in two mountain regions of Friuli Venezia Giulia (NE-Italy). Two different forest types can be distinguished:

- a coniferous forest (Rio Moscardo catchment basin, lat. 46°30' - long. 12°55') with an elevation range between 564 m and 2093 m a.s.l. and a total area of 21 $km^2$;
- a mixed beech forest (Taipana, Udine, lat. 46°15' - long. 13°05') with an elevation range between 435 m and 1140 m a.s.l. and a total area of 16 $km^2$.

## 2.1 LiDAR data and field survey

The LiDAR survey was performed as part of the Interreg IIIA Italy-Slovenja project in two different periods: September 2003 (Rio Moscardo) and July 2004 (Taipana). An Optech ALTM 3033 installed on an helicopter was used. The average fly height was 1000 m above the ground, the scanning angle was 18° and the light beam divergence was 2 mrad. For each emitted pulse by the instrument, the geographic position and reflection intensity of the first and last pulse were recorded. The survey density was about 2 points/$m^2$ for both the study areas.

During summer 2005, a field survey was performed using 20 forest plots (14 plots in the coniferous forest, 6 plots in the broad leaved forest). The plot areas range between 400 $m^2$ and 10,000 $m^2$. Each plot was georeferenced using a topographic total station and a Global Positioning System (GPS). Position of each tree was labelled and diameter at breast height (d.b.h., 1.30 m), total height, crown inserption height and crown projected area were measured. LAI was recorded using LiCor 2000 Plant Canopy Analyzer. The number of LAI measures taken and used for computation depends on total plot area.

## 2.2 LiDAR Penetration Index

LiDAR data were processed using Terrascan™ software ©Terrasolid, Finland. Ground points were filtered following an automatic procedure. The results of this filtering process were in general good, but, in the case of complex ground morphology, the algorithm parameters were manually setted and optimized (Axelsson, 2000). Vegetation points were divided in two classes: low vegetation (h ≤ 1 above the ground); high vegetation (h > 1 above the ground). Indirect LAI measurements are based on solar light transmission or reflectance through vegetation and this can be assumed similar to the transmission of the laser beams through the canopy. On the basis of this assumption, a Laser Penetration Index (LPI) was defined as follow:

$$LPI_{ij} = g_{ij} / (g_{ij} + v_{ij}) \qquad [1]$$

where $g_{ij}$ is the ground points density and $v_{ij}$ is the high vegetation points density.

$g_{ij}$ in the denominator allows to normalize local variations of sampling density due to LiDAR strips overlapping and variations of the helicopter speed. LPI was calculated using a cell raster resolution of 1 x 1 m. Because of the non-homogenous distribution of LiDAR sampling points in the studied areas, $g_{ij}$ and $v_{ij}$ were assigned to each cell on the base of a neighbour statistical analysis using a radius of 5 m that was considered appropriate to the initial sampling density. LPI values close to 0 describe a dense vegetation while values close to 1 are characteristic of an open stand or clear ground.

## 3 RESULTS AND DISCUSSION

An example of LiDAR data elaboration is given in figure 1: soil density points and vegetation density points are reported in figure 1.a and 1.b, respectively. LPI ranges between 0 (white) and 1 (black) as expected (figure 1.c).

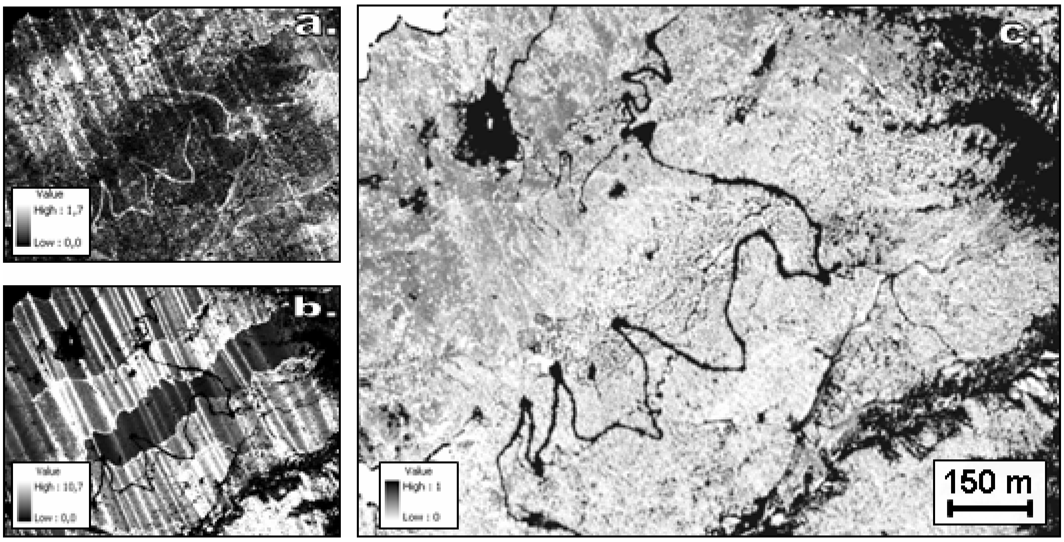


*Figure 1: Penetration index (LPI) elaboration with a cell resolution of 1 x 1 m in the coniferous forest of Pramosio with a laser point density of 2 pts/m$^2$. a) ground points densit; b) vegetation points density; c) Laser penetration Index.*

In table 1, results of the field survey and average LPI values for each plot are reported. The LAI values in the 400 m$^2$ plots is the average of five measuring points while in the 1 ha plots it is the average of 10 measures. LAI values are higher in the broadleaved plots than in the coniferous stands while LPI is lower in the forest type (one way ANOVA: $P < 0.001$). The measured LAI for the different forest types is close to that reported by Kimmins (1997) for similar forest stands.

The significant linear correlation between field LAI values and LPI ($R^2$=0.89, P<0.001, n=20) underlines the ability of the proposed index to estimate leaf area index using LiDAR data.

*Table 1 – Field survey results for each transect and mean calculated LPI in Spruce forest, spruce-fir forest, beech forest, ash mixed forest*

| area (m$^2$) | forest_cat | LAI | average ø (m) | average high (m) | average crown depth (m) |
|---|---|---|---|---|---|
| 400 | spruce | 3.73 | 41 | 35 | 16 |
| 400 | spruce | 3.8 | 36 | 28 | 17 |
| 400 | spruce | 3.83 | 35 | 30 | 14 |
| 400 | spruce-fir | 4.6 | 40 | 32 | 16 |
| 400 | spruce-fir | 4.56 | 43 | 34 | 15 |
| 400 | spruce-fir | 4.41 | 35 | 32 | 12 |
| 400 | spruce-fir | 4.27 | 34 | 26 | 11 |
| 400 | spruce-fir | 4.71 | 34 | 27 | 9 |
| 400 | spruce-fir | 4.13 | 33 | 25 | 10 |
| 400 | spruce | 4.18 | 33 | 26 | 8 |
| 400 | spruce | 3.54 | 31 | 27 | 9 |
| 400 | spruce | 3.64 | 27 | 26 | 10 |
| 10.000 | spruce-fir | 4.3 | na | na | na |
| 10.000 | spruce | 3.21 | na | na | na |
| 1.000 | beech | 5.78 | 22 | 14 | 7 |
| 1.000 | ash-mixed | 5 | 15 | 15 | 11 |
| 400 | ash-mixed | 5.42 | 15 | 16 | 11 |
| 400 | beech | 5.69 | 18 | 17 | 8 |
| 400 | beech | 5.42 | 26 | 28 | 22 |
| 10.000 | beech | 5.49 | na | na | na |

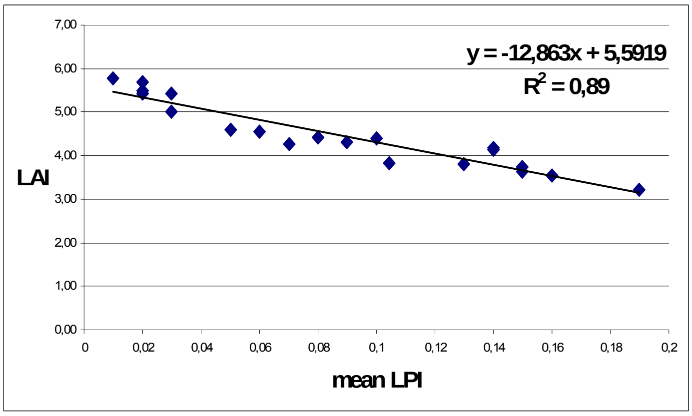


*Figure 2: Correlation between mean LPI and LAI with a laser points density of 2 p/m2. Points are field survey plots. LAI = -12.863 LPI + 5.5919 (n=20, R2=0.89, P<0.001)*

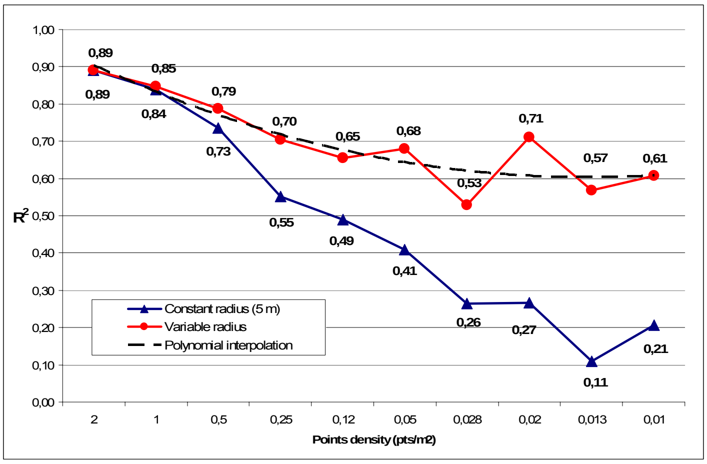


*Figure 3 – Variations of R2 as function of the radius of neighbour analysis. In blue, the results for a fixed radius (5 m) are reported; in red the results for a radius depending on simulated laser points density (5-70 m; see eq. 2).*

A random re-sampling procedure of LiDAR data to estimate different laser points densities was performed (from a density of 2 pts/m$^2$ to 1 pt/100 m$^2$). Figure 3 shows the variation of correlation coefficient ($R^2$) for the correlation between LPI and LAI at different points densities.

In blue is reported the pattern of correlation coefficient ($R^2$) between measured LAI and LPI calculated on the base of neighbour analysis performed using a 5 meters radius, as reported in par. 2. In this case, $R^2$ decreases very fast by reducing laser points density.

To have a constant number of sampling points, a variable radius for each re-sampling was used applying the equation:

$$r = (150 / \pi\rho)^{½} \qquad [2]$$

where "r" is in meters, "ρ" is the points density (pts/m$^2$) and 150 is the number of points with a radius of 5 m and a points density of 2 points m$^{-2}$. Following this approach, the decrease of $R^2$ is slower (red line in figure 3) and the correlation between LPI and LAI is still statistically significant for the lower points density of 1 pt/100 m$^2$ ($R^2$ = 0.61, P < 0.001).

## 4 CONCLUSIONS

The present research has investigated the relationships between LiDAR data and some forest ecosystems characteristics. In particular, a methodology to process raw data and to estimate a penetration index through forest canopy for laser signals (LPI) was tested. The proposed index depends on forest type and stand structure (i.e. stem density, height, crown depth). It allows to easily quantify the leaf area index, leaf biomass and forest biomass due to the correlation between LAI and biomass reported in literature but not investigated in this research. The analysis showed as the correlation between LPI and LAI is still statistically significant when very low laser points densities are considered (1 pts/100 $m^2$). This fact underlines the economic advantages of the proposed method to estimate forest biomass not only in comparison to field surveys but also in terms of LiDAR data collection and processing. Our results also show the possibility of using the proposed index to estimate carbon stocks and forest productivity on a broad scale.

## ACKNOWLEDGEMENTS

This work was carried out within the research activities supported by the INTERREG IIIA Italy-Slovenia 2003-2006 project "Cadastral map updating and regional technical map integration for the Geographical Information Systems of the regional agencies by testing advanced and innovative survey techniques". We thank also Enrico Bressan and Rossella Napoletano for the help during the field campaign.

## REFERENCES

Axelsson, P. (2000). DEM Generation from Laser Scanner Data Using Adaptive TIN Models. ISPRS, Vol.XXXIII, Amsterdam.

Barilotti, A., Turco, S., Ciampalini, R. (2005). Misurazione automatica dei singoli alberi attraverso analisi morfologiche su dati laser scanning. Atti 9° Conferenza Nazionale ASITA, Catania.

Gower, S.T., Kucharik, C.J., Norman, J.M., (1999). Direct and indirect estimation o Leaf Area Index, f(APAR), and net primary production of terrestrial ecosystem. Remote Sensing of Environment, 70, 29-51.

Hyyppä, J., Hyyppä, H., Litkey, P., Yu, X., Haggrén, H., Rönnholm, P., Pyysalo, U., Pitkänen, J., Maltamo, M. (2005). Algorithms and methods of airborne laser scanning for forest measurements. International Archives of Photogrammetry, Remote Sensing and Spatial Information Sciences, Vol. XXXVI – 8/W2.

Kimmins, J.P. (1997). Forest ecology. A foundation for sustainable management. 2nd edition. Prentice Hall, Upper Saddle River, NJ, 596.

Lefsky, M.A., Hudak, A.T., Cohen, W.B., Acker, S.A. (2005). Geographic variability in lidar prediction of forest stand structure in the Pacific Northwest. Remote Sensing of Environment, 95, 532-548.

Morsdorf, F., Meier, E., Koetz, B., Nüesch, D., Itten, K., Allgöwer, B. (2003). The potential of high resolution airborne laser scanning for deriving geometric properties of single trees. In EGS - AGU - EUG Joint Assembly, Nice, France., 2003.

Morsdorf, F., Koetz, B., Meier, E., Itten, K.I., Allgöwer, B. (2005). The potential of discrete return, small footprint airborne laser scanning data for vegetation density estimation. ISPRS WG/3, III/4, V/3 Workshop “Laser scanning 2005”, Enschede, the Netherlands, September 12-14, 2005.

Niles, J.O., Brown, S., Pretty, J., Ball, A.S., Fay, J. (2002). Mitigazione del carbonio e paesi in via di sviluppo, in CO2 e biodiversità – Un approccio integrato a favore del clima e del patrimonio naturale. Edizioni Ambiente, Milano, 2004, 77-94.

Norman, J.M., Campbell, J.S. (1989). Canopy structure in Plant Physiological Ecology, field methods and instrumentation. Chapman et Hall, London, 301-325.

Patenaude, G., Milne, R., Dawson, T.P. (2005). Syntesis of remote sensing approaches for forest carbon estimation: reporting to the Kyoto Protocol. Environmental Science & Policy, 8 (2005), 161-178.

Riaño, D., Valladares, F., Condés, S., Chuvieco,. E. (2004). Estimation of leaf area index and covered ground from airborne laser scanner (Lidar) in two contrasting forests. Agricultural and Forest Meteorology, 124, 269-275.

Schulze, E.D., Beck, E., Müller-Hohenstein, K., Lawlor, D. (2005). Plant ecology, Springer eds., Berlin

Scurloch, J.M.O., Asner, G.P., Gower, S.T. (2001). Wordwide historical estimates of Leaf Area Index 1932-2000. ORNL/TM, 2001, 268.

# ESTIMATING STRUCTURAL FOREST ATTRIBUTES USING HIGH RESOLUTION, AIRBORNE HYPERSPECTRAL AND LIDAR IMAGERY

*Henning Buddenbaum and Stephan Seeling*

University of Trier, Remote Sensing Department, Trier, Germany;
buddenbaum@uni-trier.de; seelings@uni-trier.de

## ABSTRACT

Methods for estimating structural forest attributes using HyMap, LIDAR, Quickbird, and RADAR data of the same forest in south-western Germany have been explored. Algorithms for tree height measurement from LIDAR data and for tree counting in Quickbird data are presented. Hyperspectral Two-Band Vegetation Indexes are used to estimate forest variables from the HyMap data. Only first results can be presented for the Radar data yet.

**Keywords:** Hyperspectral, LIDAR, Tree Height, Stem Density.

## 1 INTRODUCTION

This ongoing study evaluated several remote sensors and several methods regarding their ability to measure structural forest attributes. In recent years, advanced sensor systems have increasingly been used to map variables relevant to forest inventories and ecosystem modelling. For instance, laser scanning data provide accurate measurements of tree or canopy height (e.g. Næsset & Gobakken 2005); high spatial resolution images allow detailed insight into the stand structure; hyperspectral images proofed to be capable of estimating leaf area index (e.g. Lee et al. 2004; Schlerf et al. 2005), chlorophyll content (e.g. Zarco-Tejada et al. 2004) and other biochemical values. Additionally a new generation of radar sensors, providing different incident angels and polarisations even on the L-band domain (ASAR, PALSAR), are expected to complement the endeavours to obtain structural information (Mougin et al. 1998).

## 2 MATERIAL

### 2.1 Area of study

The area of study (49°40'N, 7°10'E) is the Idarwald forest in south-western Germany on the north-western slope of the Hunsrück mountain ridge. The dominant tree species are Norway spruce (*Picea abies*), beech (*Fagus sylvatica*), oak (*Quercus petraea*) and Douglas fir (*Pseudotsuga menziesii*). Active forestry practices in this area include selective cutting, plantation establishment and thinning.

### 2.2 Field data

A field campaign was carried out in September 2005. 15 stands of Norway spruce and 13 stands of beech were sampled in 30 m x 30 m plots (smaller plots when the stand was very dense). Values gathered include tree height, crown height, crown radius in four directions, stem diameter at breast height, LAI (measured by a Li-Cor LAI 2000 Plant Canopy Analyzer), number of trees and canopy closure. Hemispherical digital photos have been taken using a fish-eye lens.

### 2.3 HyMap data

A hyperspectral HyMap data set of the study area was acquired on July 14, 2003 by DLR. The data consists of 126 spectral channels with a pixel size of 5 m x 5 m. The data was parametrically geocoded using the software Parge (Schläpfer et al. 1998) to subpixel accuracy. An across-track illumination correction has been applied to the data to eliminate view angle effects, but no radiometric correction.

### 2.4 LIDAR data

A LIDAR altimetry data set was recorded on September 2005 by a LiteMapper 5600 laser scanner flown in a helicopter by Hansa Luftbild Geoinformationssysteme GmbH, Münster, Germany. The average pulse density was about 2.6 $m^{-2}$. First, last and only pulses were recorded. The data was then re-sampled into a 1 m by 1 m raster. A canopy height model was produced by subtracting the combined last and only pulses data set from the combined first and only pulses dataset. As the provider's preprocessing steps are not yet finished only a preliminary data set consisting of the first strip was used. This data set encompasses the south-eastern part of the Idarwald forest. Ten of the 28 field sites are included in the data.

### 2.5 Quickbird data

The Quickbird image was acquired on August 24, 2003 with a geometric resolution of 61 cm (panchromatic) and 244 cm (multispectral). The data was geometrically corrected with standard methods. Then a pan-sharpened and an illumination corrected image of the multispectral data was generated.

### 2.6 RADAR data

For retrieving biophysical properties of native forests in the Idarwald region the following sensors and types of image are under investigation: ERS2 (C-band, VV polarisation, 23° inclination), ENVISAT ASAR (C-band, VV and cross polarisation, gentle inclination), JERS (L-band, VV polarisation, coherent images), and PALSAR (L-band, VV and cross polarisation, different inclinations (requested). For the Test region, a set of three ASAR and four ERS-2 scenes is actual available. All images have been geometrically corrected and co-referenced. The refining of two corresponding scenes of the L-band sensor on board the Japanese satellite JERS, flown between 1992 and 1998, is still in progress.

## 3 METHODS AND RESULTS

### 3.1 HyMap: Hyperspectral Two-Band Vegetation Indexes

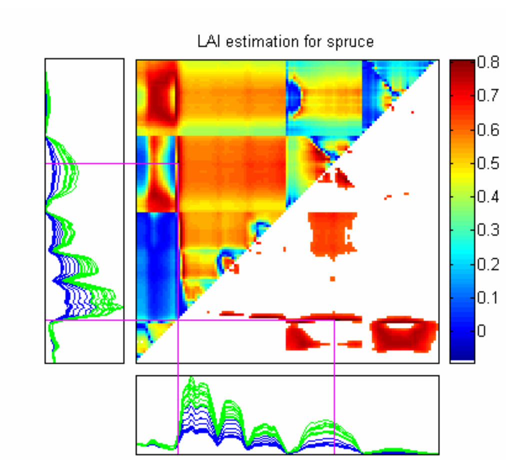


*Figure 1: 2-dimensional plot of correlation between LAI and all possible Simple Ratios from HyMap data. Areas of high correlation are red. For more details see text.*

Indexes like NDVI, Simple Ratio, or PVI, have been calculated from different input channels (see also Schlerf et al. 2005). Every possible combination of two input channels in the hyperspectral data set has been tested in order to find the optimal band combination to estimate vegetation structural parameters. Correlation ($R^2$) between each index value and the structural variable has been calculated to select the best wavelenghths for each variable. The differences between the tested indexes were small; only the results for the Simple Ratio calculations are shown.

The 2-dimensional correlation plot (Figure 1) shows all $R^2$-values in the upper left region. The best correlations are shown again in the lower right region. The selected bands are marked in the reflectance plots at the left hand side and the bottom of the figure. These plots show the atmospherically uncorrected spectra of Norway spruce (blue) and beech (green) in the 28 stands. A similar plot has been created for each structural variable. Table 1 shows the found best correlations, the correlations after cross-validation and the two wavelengths used.

*Table 1: Results of hyperspectral two-band vegetation index forest parameter estimations.*

| Parameter | Species | $R^2$ | $R^2$ cross-validated | Wavelength 1 [nm] | Wavelength 2 [nm] |
|---|---|---|---|---|---|
| Crown Closure | Spruce | 0.74760 | 0.69423 | 1052.7 | 1037.2 |
| | Beech | 0.76273 | 0.71254 | 1783.4 | 450 |
| | All | 0.34768 | 0.26806 | 600.2 | 585.2 |
| Mean Tree Height | Spruce | 0.58143 | 0.4702 | 1052.7 | 1021.7 |
| | Beech | 0.63298 | 0.36513 | 974.6 | 874.3 |
| | All | 0.38051 | 0.29727 | 1037.2 | 895.4 |
| Mean Circumference at breast height | Spruce | 0.49601 | 0.33846 | 2258 | 2240.8 |
| | Beech | 0.77528 | 0.65323 | 1112.9 | 1098 |
| | All | 0.30902 | 0.19059 | 911.1 | 895.4 |
| Crown length | Spruce | 0.71562 | 0.61991 | 2258 | 2240.8 |
| | Beech | 0.52254 | 0.28093 | 2357.4 | 2082.1 |
| | All | 0.38688 | 0.28718 | 926.9 | 895.4 |
| Age | Spruce | 0.6054 | 0.51772 | 828.5 | 813.4 |
| | Beech | 0.80244 | 0.69257 | 1006.4 | 974.6 |
| | All | 0.41108 | 0.32319 | 959.1 | 895.4 |
| Number of Trees | Spruce | 0.69294 | 0.24161 | 508.5 | 450 |
| | Beech | 0.90365 | 0.88037 | 1271.6 | 1200.4 |
| | All | 0.36016 | 0.15054 | 2170.8 | 1489 |
| LAI | Spruce | 0.81664 | 0.7591 | 1673.2 | 707.5 |
| | Beech | 0.77322 | 0.70396 | 1673.2 | 462.4 |
| | All | 0.53175 | 0.46604 | 1685.7 | 1647.8 |

## 3.2 LIDAR tree height measurements

Tree heights derived from LIDAR are suspected for systematic under-estimation, as the tips of the trees are usually missed (Yu et al. 2004). To account for this, a statistical method to find the real heights was used: a Gaussian normal distribution was fitted to the upper half of a histogram of the LIDAR-measured tree heights in the environment of the field sites. The height of the dominant tree layer was estimated as $Height_{LIDAR} = Mean + 2.5 \cdot StdDeviation$ .

A very good agreement ($R^2$ = 0.9279) between the field measured tree heights and the calculated LIDAR heights was observed (see Figure 2). The agreement was best for spruce stands; the height variation of beech stands in the data set was very low, so no definite conclusion can be made for beeches.

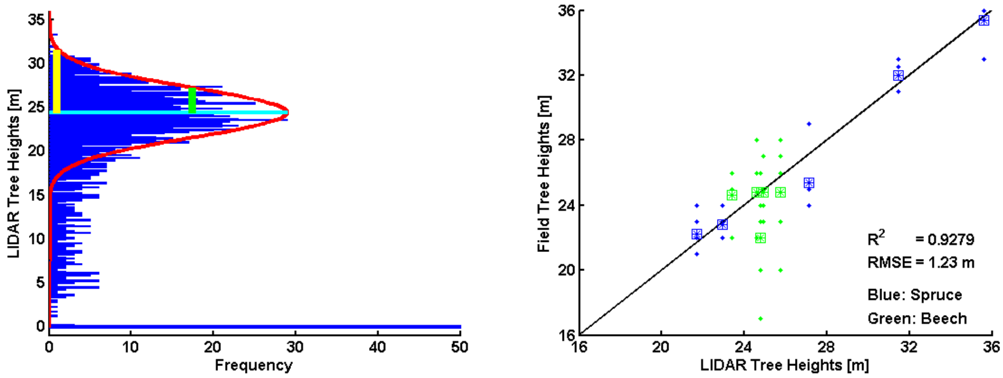


*Figure 2: Left: Gaussian normal distribution (red) fitted to histogram (blue) of LIDAR-measured tree heights in one stand; the mean is marked in cyan, the standard deviation in green and 2.5 standard deviations in yellow. Right: Agreement between field measured and LIDAR-measured tree heights. The dots show the single tree heights measured in the field, the boxes show the mean stand heights. The black line is the 1:1-line.*

## 3.3 Quickbird tree counting algorithm

The spatial high resolution data from the Quickbird satellite was used to test methods to estimate the stem density. The first step in the simple tree counting algorithm discussed here was the extraction of near infrared (Quickbird channel 4) subsets of the surroundings of the ground measurement sites. A moving window function was applied to the subsets. The maximum reflectance value inside the window was intentified. If the reflectance was larger than a threshold value the pixel was nominated a tree tip. The number of found tree tips was translated to stem density per hectare. This simple algorithm led to good results for spruce stands (see Figure 3) when one stand with very young and dense trees was omitted where single trees were indistinguishable even in this high-resolution data set. In beech stands the tree tops are too uniformly illuminated to be distinguished.

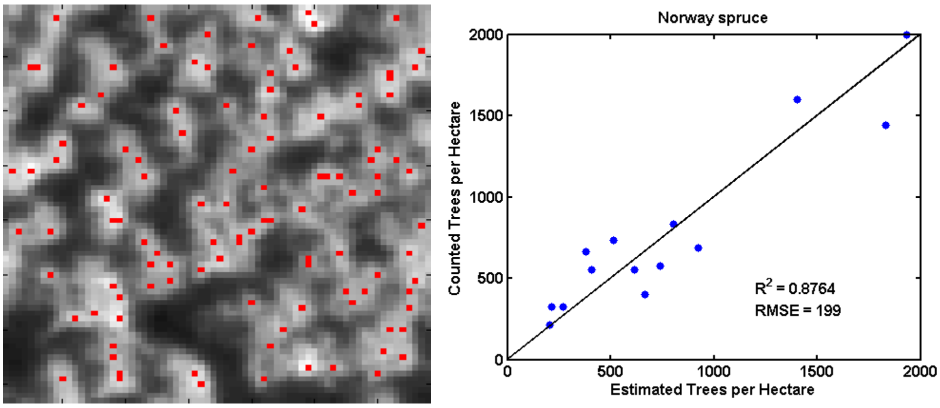


*Figure 3: Tree counting algorithm. Left: The local window maximum search retrieves the tree tops (red dots). Right: There is a good agreement between the stem densities measured in the field and in the image.*

## 3.4 RADAR multitemporal analysis

For the discrimination of different forest types a combination of SAR scenes (ENVISAT, ASAR swath I2, descending) from January 6th, February 10th and April 21st 2005 of the Idarwald region was arranged (Figure 4). Based on the leaf development of deciduous trees within this period the differentiation was put into action. Further investigations are aimed at the utilisation of homogeneously structured regions for more sophisticated classifications and at the correlation between L-band backscatter and spruce density (Mette et al. 2004).

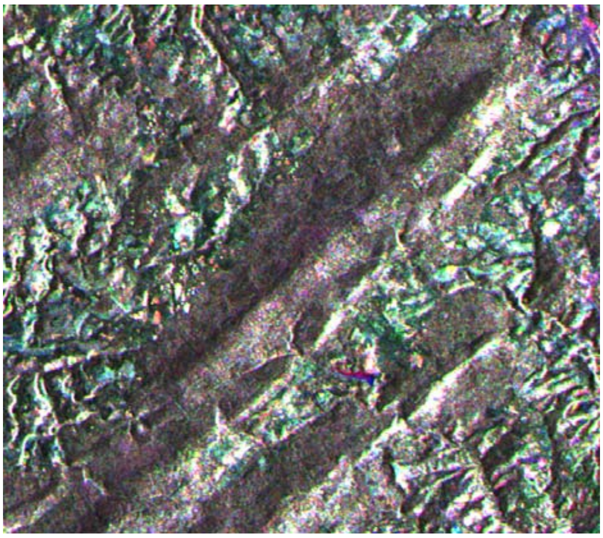

*Figure 4: Combination of SAR scenes of January 6th, February 10th and April 21st 2005 from the Idarwald region (ENVISAT, ASAR swath I2, descending)*

## 4 DISCUSSION

The discussed methods show promising first results. The HyMap data is able to deliver fair estimations of many structural attributes. As expected, the LIDAR is very well suited for tree height estimation. The algorithm presented is an alternative to the established algorithm by Næsset & Bjerknes (2001), but it still has to be tested on a larger number of stands. The Quickbird tree counting algorithm that was utilized cannot be transferred to deciduous stands, so other methods will have to be tested in the future. Further progress is expected of the incorporation of radar data in the L-band domain.

## REFERENCES

Lee, K.-S., Cohen, W. B., Kennedy, R. E., Maiersperger, T. K. and Gower, T. (2004): Hyperspectral versus multispectral data for estimating leaf area index in four different biomes. Remote Sens. Environ., 91: 508-520.

Mette, T., Papathanassiou, K., Hajnsek, I., Zimmermann, R. (2004): Forest biomass estimation using polarimetric SAR interferometry. Proceedings IGARSS 2004, IGARSS 2004, Anchorage.

Mougin, E., Proisy, A., Lopes, A., Ducrot, D., Rivalland, V., Marty, G., Dufrêne, E., Le Dantec, V., Souyris, J.C., Adragna, F., Horn, R. (1998): Radar Remote Sensing of a Mixed Deciduous Temperate Forest: Results and Perspectives. Papers to ESTEC workshop Retrieval of Bio- and Geo-Physical Parameters from SAR Data for Land Applications.

Næsset, E. and Bjerknes, K-O. (2001): Estimating tree heights and number of stems in young forest stands using airborne laser scanner data. Remote Sens. Environ. 78:328-340.

Næsset, E. and Gobakken, T. (2005): Estimating forest growth using canopy metrics derived from airborne laser scanner data. Remote Sens. Environ. 96: 453-465.

Schläpfer, D., Schaepmann, M. and Itten, K. (1998): PARGE: Parametric geocoding based on GCP-calibrated auxiliary data. SPIE International Sympo sium on Optical Sciences, Engineering, and Instrumentation, San Diego (CA), 334-444.

Schlerf, M., Atzberger, C. and Hill, J. (2005): Remote Sensing of forest biophysical variables using HyMap imaging spectrometer data. Remote Sens. Environ. 95: 177-194.

Yu, X., Hyyppä, J., Kaartinen, H. and Maltamo, M. (2004): Automatic detection of harvested trees and determination of forest growth using airborne laser scanning. Remote Sens. Environ. 90: 451-462.

Zarco-Tejada, P. J., Miller, J. R., Morales, A., Berjón, A. and Agüera, J. (2004): Hyperspectral indices and model simulation for chlorophyll estimation in open-canopy tree crops. Remote Sens. Environ., 90: 463-476.

# INDREXII – INDONESIAN ARIBORNE RADAR EXPERIMENT CAMPAIGN OVER TROPICAL FOREST IN L- AND P-BAND POLARIMETRIC INTERFEROMETRIC SAR

*Florian Kugler[1], Irena Hajnsek[1], Konstantinos Papathanassiou[1], and Dirk Hoekman[2]*

[1] German Aerospace Center, Microwave and Radar Institute, PO BOX 1116, 82243, Germany;
Tel / Fax: +49-(0)8153-28-3507/1449 E-mail: florian.kugler@dlr.de

[2] Wageningen University, Department of environmental sciences, Wageningen, Netherlands;

## ABSTRACT

Tropical forests are complex, heterogeneous, dense, remote and changing forest ecosystems and represent therefore a big challenge for radar remote sensing. Low frequency synthetic aperture radar (SAR) techniques allow monitoring and potentially estimation of key forest parameters such as vertical structure (height) and biomass. However, a suitable radar data base over tropical forests necessary to support the development and assessment of mapping and inversion techniques is missing. In order to close this gap, the European Space Agency (ESA) conducted - in the framework of its Earth Observation Envelope Programme – INDREXII, an experimental airborne radar campaign in Indonesia, in November 2004. In the frame of INDREX II single- (@ X-band), dual- (@ C-band), and quad-pol (@ L-, and P-band) SAR data acquired in a single (@ X-band) or repeat-pass (@ L-, and P-band) mode supplemented by a set of extensive (in the tropical context) ground measurements.

One of the most important - for a wide range of applications - forest parameter is biomass. Biomass appears to be more or less directly related to forest height, which can be estimated from model based inversion of polarimetric-interferometric SAR (Pol-InSAR) data. Indeed, successful height inversion has been demonstrated in several airborne experiments over temperate and boreal forests. In this paper results of model-based L- and P-Band Pol-InSAR data inversion are shown, including validation against the ground measurements. The potential and limitations are discussed.

**Keywords:** Tropical forest mapping, Synthetic aperture radar (SAR), Interferometric SAR (InSAR), Polarimetric SAR Interferometry (Pol-InSAR), Forest height and biomass.

## 1 INTRODUCTION

Polarimetric interferometric SAR is a technique that allows the estimation of forest heights by means of SAR technology. In this sense, INDREX-II was designed to provide answers about the feasibility of low frequency (L- and P-band) Pol-InSAR techniques to estimate forest height in tropical environments. In order to support this, ground measurements have been performed in different tropical forest types and repeat pass fully-polarimetric interferometric L- and P-band data have been acquired with the Experimental Synthetic Aperture Radar (E-SAR) of the German Aerospace Centre (DLR) [4]. In the following first inversion results of the INDREX-II campaign are presented and discussed.

## 2 THE CAMPAIGN

### 2.1 Ground Campaign

Two main test regions have been selected for INDREX-II in Indonesia on the Kalimantan island. The first area is the Mawas conservation area located in the province of Central Kalimantan in the vicinity of its capital city Palangkaraya. The second area is located in the Province East Kalimantan close to the province's largest city Balikpapan. These two areas comprise samples of all main broad forest types: lowland dipterocarp forest and peat swamp forest (see *Table 1*). A 15.4 ha large forest block transect was established in the Sungai Wain dipterocarp forest, 540 m in length and 286 m wide. Within this block 26 sub-blocks (in total 2.1 ha) are being measured. In *Table 1* the parameter dbh and total tree height for the two test sites are listed. Eight transects in the Mawas peat swamp forests have been established. Within these transects similar observations have been made.

*Table 1: Characteristics of the test sites*

| Test Site | Forest Type | Forest height [m] | Forest Biomass [t/ha] |
|---|---|---|---|
| Mawas | Peat | 10 – 30 | 20 – 250 |
| Sungai Wain | Lowland Dipterocarp | 10 – 60 | 100 – 400 |

### 2.2 Flight Campaign

The flight measurements campaign for INDREX-II has been executed with DLR's experimental airborne SAR system (E-SAR) with the following configuration displayed in *Table 2*.

*Table 2: E-SAR flight modes for each test site*

| Mode | Frequency | Baselines (nominal) |
|---|---|---|
| Pol-InSAR: Quad-pol, Repeat-pass | L-Band | 5m,10m,15m |
| Pol-InSAR: Quad-pol, Repeat-pass | P-Band | 15m, 30m, 60m |

## 3 EXPERIMENTAL DATA

In a first processing step the interferometric coherences at L- and P-band for the available baselines have been calculated. The variation of the interferometric coherence with the spatial baseline depends on the vertical structure of the scatterers within the scene. Volume scatterers (e.g. forests) are characterised by decreasing coherence values with increasing spatial baseline; an effect known as volume decorrelation. In contrast to volume scatterers, the interferometric coherence of surface scatterers (e.g. bare terrain) is - after range spectral filtering - independent from the spatial baseline and in the absence of other decorrelation sources equal to one. In addition, as the effective vertical structure of the scatterers varies with polarisation, the interferometric coherence becomes a function of polarisation too.

*Figure 1* shows on the right hand side (top row) an HH polarised amplitude image of the Mawas test site at L-band. In the upper part a river (low backscatter) meanders through the scene, while a peat swamp appears darker (surface scatterer). The rest of the image is covered with forest. The corresponding interferometric phase and vertical wave-number (kz) images for the 5m spatial baseline are shown on the bottom row. The small and smooth phase variations indicate the flatness of the terrain; the phase difference in the transition from peat swamp to forested areas (known as vegetation bias) is also visible. The vertical wave-number image expresses the 2-D baseline variation: In the airborne case, from near to far range due to the incidence angle variation, and along azimuth due to the movement of the platform. The strong variations along azimuth are typical for an airborne system at L-band. The interferometric coherence images in the HH, HV, and VV polarisations - scaled from 0 to 1 - are shown on the left hand side (top row). In accordance with the considerations above, the peat swamp area has a high coherence (close to 1), the river decorrelates completely (coherence of 0) as a result of temporal decorrelation and low SNR, while the forest is characterised by volume decorrelation that varies with baseline from near to far range (as indicated by the vertical wave-number image). Note that in contrast to the amplitude images forest structures become visible in the coherence images (as for example logging trails) due to the sensitivity of the coherence to structure. On the bottom of *Figure 1* the three optimum coherence images are shown, indicating the range of coherence variation with polarisation. This variance is a direct indication for the presence of a ground scattering contribution under the forest layer [1]. Next to the optimised coherences is the interferometric phase image that already indicates how flat the Mawas test site is. In *Figure 2* the corresponding images for the 10m baseline are shown. With increasing baseline the volume decorrelation over the forested areas increases. The coherence decreases drastically in near range because of the larger effective baseline. In contrast to the forest, the coherence over the surface scatterers remains the same. In the phase image now, the vegetation bias becomes more evident due to the larger baseline. A smaller relative variation of the vertical wave-number along azimuth can be observed.

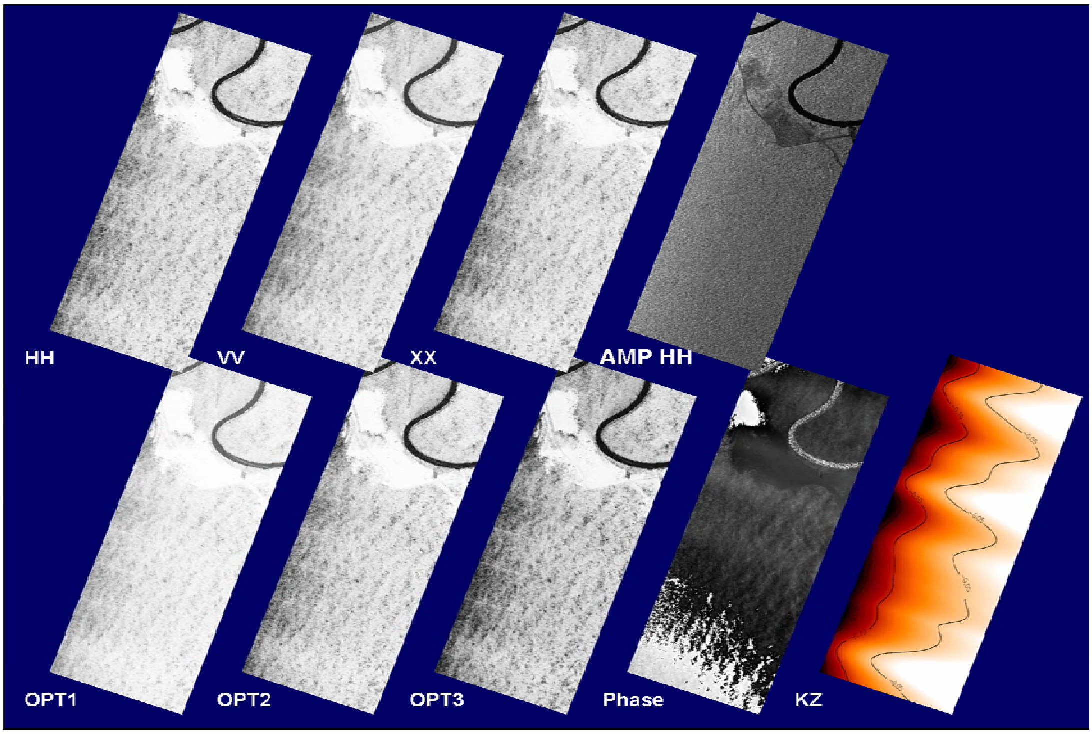


*Figure 1: Test Site Mawas; Interferometric coherence for a 5m spatial baseline; from left to right upper part: coherence in HH, VV, and XX polarisation, amplitude image of HH polarisation; from left to right lower part: optimized coherence 1 to 3, interferometric phase of the HH polarisation, vertical wavenumber (kz).*

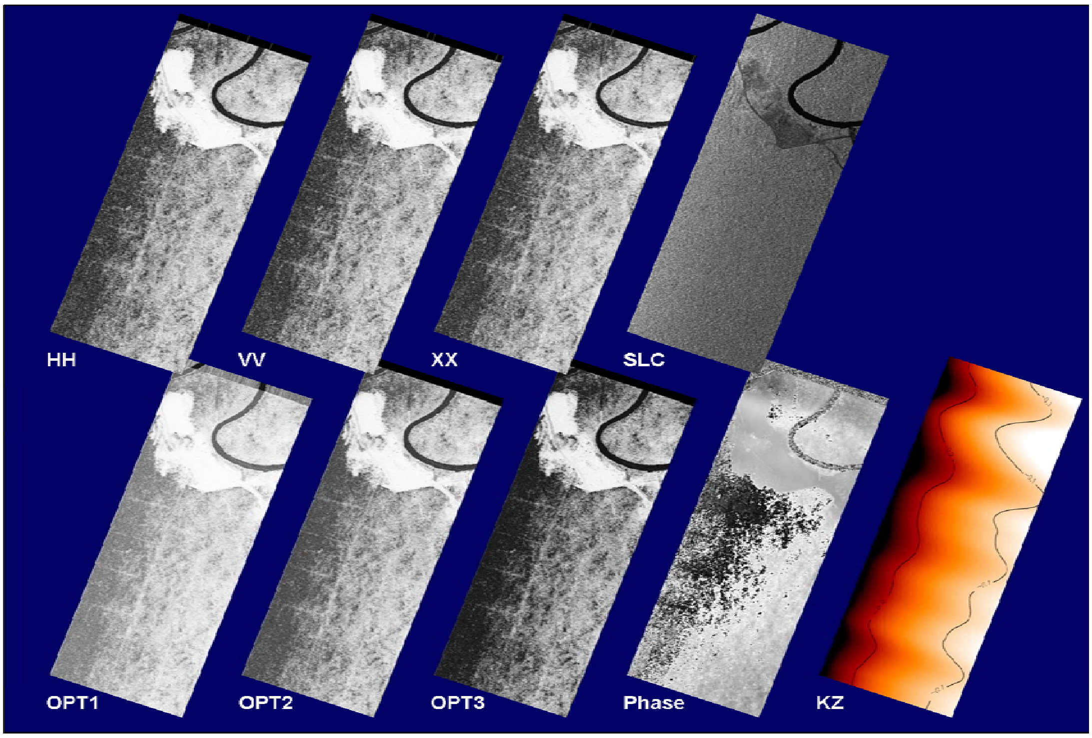


*Figure 2: Test Site Mawas; Interferometric coherence for a 10m spatial baseline; from left to right upper part: coherence in HH, VV, and XX polarisation, amplitude image of HH polarisation; from left to right lower part: optimized coherence 1 to 3, interferometric phase of the HH polarisation, vertical wavenumber (kz).*

# 4 FOREST HEIGHT

## 4.1 Quantitative Results

For the Sungai Wain test site, forest height has been estimated by inverting single-baseline fully-polarimetric InSAR data using the Random-Volume-over-Ground model (RVoGm) [1]. The inversion has been applied at each frequency individually: at L-band using the 10m spatial baseline and at P-band using the (equivalent in terms of wavelength scaling) 30m spatial baseline. From the inversion process areas affected by geometrical and coherence constrains - that make a meaningful inversion impossible - have been excluded. Three kinds of masks were applied:

1. Coherence mask: Low coherences are affected by large phase variance [2] making accurate inversion at high spatial resolution not-possible. Therefore areas with coherences lower than 0.4 have been excluded. This mask acts across the whole image.

2. Mask for high kz values: At large effective baselines (i.e. large kz values) the sensitivity of the coherence to forest height may saturate at heights lower than the forest heights in the scene. Such areas are masked out. The mask acts primarily in near range (threshold: kz < 0.15).

3. Mask for small kz values: At small effective baselines (i.e small kz values) the unfavourable coherence to height scaling leads to high height errors for small residual (un-calibrated) decorrelations. Such areas are also masked out. This mask acts primarily in far range (threshold: kz > 0.05).

After height inversion and masking out of non valid points, the obtained forest height maps at P-band and L-band are shown in *Figure 3*. The height maps are scaled from 0-60m (left image shows the inversion results at L-band, right image the estimates at P-band). Comparing the results at both frequencies, no significant differences appear. Both images cover the same height range and reflect a similar forest height structure. The L-band height variance is higher than in P-band because of the lower coherence level of the L-band data.

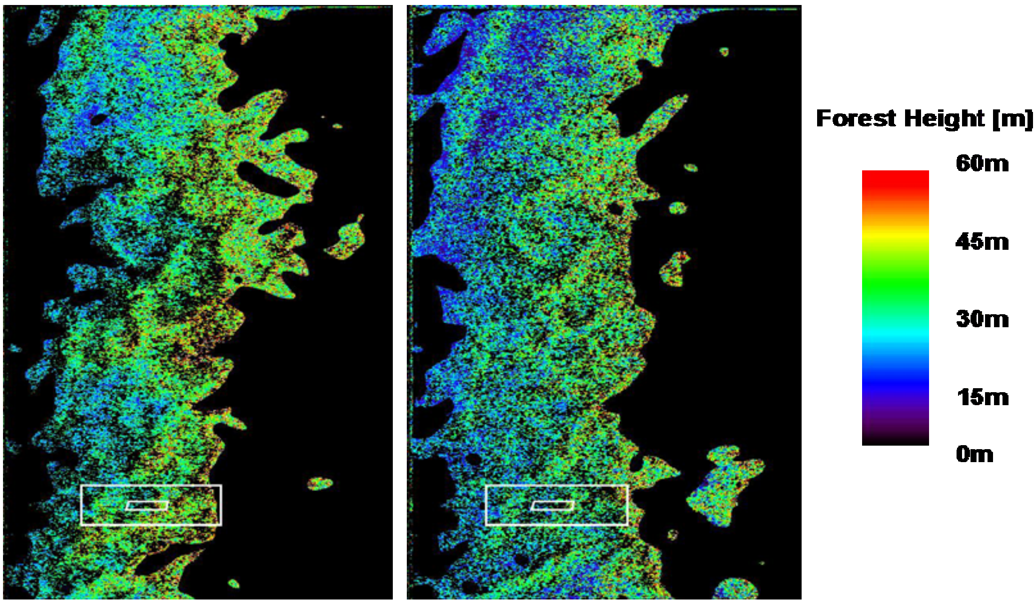


*Figure 3: Height map for the Sungai Wain forest: left: L-band 10m baseline, right: P-band 30m baseline. Black are the masked areas; the white rectangle indicates the position of the ground measurements plot.*

## 4.2 Comparison with Ground Measurements

The white rectangle in the height map (*Figure 3)* represents the location of the ground measurement plot. The forest height varies mainly between 15m and 40m. The ground measurements are represented in three graphs in *Figure 4*: the plot on the right represents the structure and height of the

Sungai Wain forest, the upper left plot the height distribution of all measured trees and the lower left plot the diameter at breast height against (DBH) the forest height. At the upper left the plot shows that most of the heights are between 10m and 20m, much lower than the estimated forest heights. However, looking on the other two plots it becomes obvious that the estimated radar heights do not depend on every single tree. They are more related to the higher trees which form the upper canopy layer. For temperate forests the so called h100 [3] was used as a reference height which seems to be useful for even aged single species forests, in tropical forests a reference height needs still to be defined. Assuming that the diameter in breast height (DBH) reflects the dominance of a tree within a forest, one can conclude that the canopy of an uneven aged forest is formed by a small number of trees, as indicated by the red circle in the upper left plot of *Figure 4*. The height of these trees fits to the estimated height from the radar data.

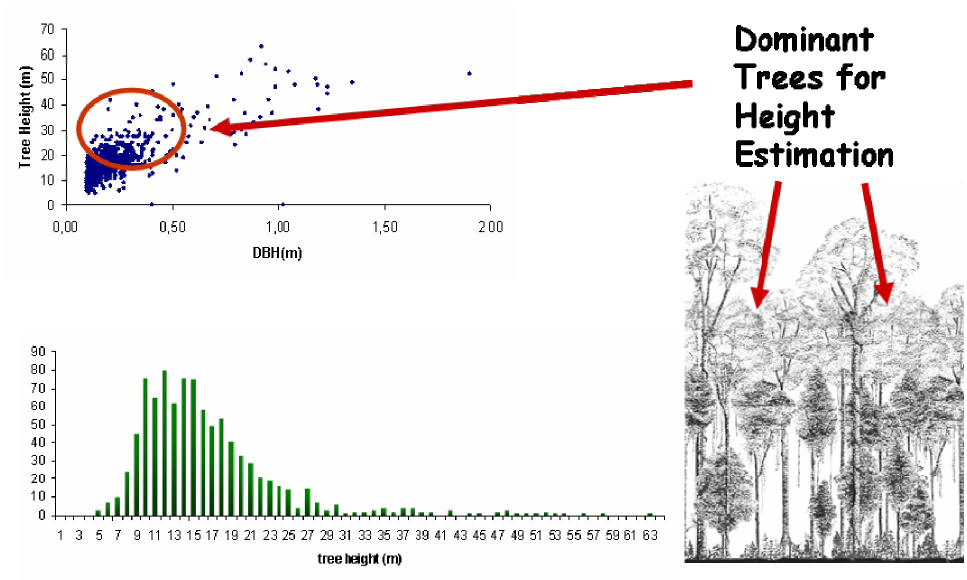


*Figure 4: Ground measurements of Sungai Wain plot; upper left: DBH (diameter in breast height) – height distribution; lower left: stem number – tree height distribution; lower right: structural sketch of lowland dipterocarp forest; the red circle in the upper left shows the dominant trees which represent the height of the of the forest*

## 5 SUMMARY AND CONCLUSIONS

In this work the interferometric coherences at different baselines, polarisations and frequencies have been analysed and forest height estimation from the inversion of single-baseline fully-polarimetric InSAR data using the Random-Volume-over-Ground model has been applied at two frequencies. The results demonstrate the potential of Pol-InSAR techniques at longer radar wavelengths (L- and P-band) to provide accurate forest height estimates. For accurate inversion the calibration of system, processing and temporal decorrelation processes that superimpose the volume decorrelation contribution is essential.

## ACKNOWLEDGEMENTS

We like to express our gratitude to the Indonesian Ministry of Forest for their invaluable help throughout the campaign. This project was executed under the ESA contract 18602/04/NLCB.

## REFERENCES

[1] Papathanassiou, K.,& Cloude, S.;Single Baseline Polarimetric SAR Interferometry; Transactions on Geosccience and Remote Sensing, 2001, vol. 39, no. 11, pp. 2352-2363

[2] Bamler,R., Hartl, P., 'Synthetic aperture radar interferometry', Inverse Problems 14 R1 – R54 (1998)

[3] Mette, T., Papathanassiou, K & Hajnsek, I., 'Biomass estimation form polarimetric SAR interferometry over heterogenous forest terrain', Proc. IGARSS04, 20.-24. Sept. 2004, Anchorage, vol. I ,pp. 511-514

[4] Hajnsek, I., Kugler, F., Papathanassiou, K., Scheiber, R., Horn, R. Moreira, A., Hoekman, D., Davidson, M., INDREX – Indonesian Airborne Radar Experiment Campaign over tropical forest in L- and P-band, Workshop PolinSAR, ESA, ESRIN, Italy, January 2005, http://earth.esa.int/cgi-bin/confpol.pl?abstract=193

# USING REDUNDANCY IN AERIAL LIDAR POINT CLOUD TO GENERATE DTM IN STEEP FORESTED RELIEF

*Andrej Kobler[1], Norbert Pfeifer[2], Peter Ogrinc[3], Ljupčo Todorovski[4], Krištof Oštir[5], Sašo Džeroski[6]*

[1] Andrej Kobler, Slovenian Forestry Institute, Ljubljana, Slovenia; andrej.kobler@gozdis.si
[2] Norber Pfeifer, Technical University Delft, Delft, The Netherlands, n.pfeifer@lr.tudelft.nl
[3] Peter Ogrinc, Slovenian Forestry Institute, Ljubljana, Slovenia; peter.ogrinc@gozdis.si
[4] Ljupčo Todorovski, Jozef Stefan Institute, Ljubljana, Slovenia; ljupco.todorovski@ijs.si
[5] Krištof Oštir, Scientific Research Centre of the Slovenian Academy of Sciences and Arts, Ljubljana; [1] Slovenia, kristof@zrc-sazu.si
[6] Sašo Džeroski, Jozef Stefan Institute, Ljubljana, Slovenia; saso.dzeroski@ijs.si

## ABSTRACT

In order to perform detailed forestry related analyses of aerial lidar point-clouds, the relative heights of vegetation points above the bare ground can be computed using a lidar-based DTM. We propose a novel method for removing the off-ground points and for generating a DTM, intended specifically for very steep and forested areas with dense to sparse canopy cover. First an initial filtering of the point-cloud is applied, which involves removal of all negative outliers, and removal of most, but not necessarily all, off-ground points by some existing filtering algorithm. Subsequently, we remove the residual off-ground points by making use of the redundancy in the initially filtered point-cloud. Multiple independent samples are taken from the initially filtered point-cloud. From each sample, ground elevation estimates are interpolated at individual DTM locations. Because the lower bounds of the distributions of the elevation estimates at each DTM location are almost insensitive to positive outliers, the true ground elevations can be approximated by adding the global mean offset to the lower bounds of distributions. The random sampling makes the proposed method unique among the methods of filtering airborne laser data. Other filters behave deterministically, always generating a filter error in special situations. In the proposed method, because of its random aspects, these errors do not occur in each sample taken, and typically cancel out in the final step of computing final elevations at the DTM locations.

**Keywords:** Lidar, airborne laser scanning, digital terrain modeling, forest

## 1 INTRODUCTION

Because of its immediate generation of 3D data, high spatial resolution and accuracy, airborne laser scanning (ALS) data is becoming popular for the reconstruction of digital terrain models (DTM, Sithole and Vosselman 2004). Since lidar signal has the ability to penetrate vegetation and reflect from different parts of trees it is also used for measuring tree height and estimating other forest stand parameters (Hyyppä et al. 2004).

The ALS provides points measured on objects between the sensor and the ground surface, depending on where the laser beam is reflected. As it can be reflected by power lines, vegetation leaves, house roofs, etc., many points do not lie on the ground surface. Due to multi-path reflection points which apparently lie below the Earth's surface can also be obtained. Classification of all these points into ground and off-terrain points is called filtering. This is an essential step necessary for digital terrain model (DTM) generation.

As the filtering methods work purely in an automated mode, i.e., with one set of parameters for the entire area (typically several km$^2$ to several hundreds of km$^2$) the resulting DTMs are not optimal in all parts of the area. Steep wooded terrain is especially considered as a problem in filtering. Therefore, there is a tangible need for precise terrain information in difficult relief. Within this paper we present a new filtering algorithm for steep relief under dense forest cover, where other filtering algorithms typically have problems distinguishing between ground returns and points reflected in the vegetation. It is able to deal with sparse ground returns under dense forest canopy on one hand, but also with highly redundant ground returns in forest openings on the other hand. The problem of negative outliers, originating from multi path reflections, is also addressed by this new algorithm.

The motivation for our work is to get high quality terrain elevations as basis for further forestry related analysis of lidar data. The specific contribution of this work is that it results in a method that provides a precise and reliable DTM even if the laser scanner ground hits very irregularly distributed. Variation in the number of ground hits may vary on all scales as it is affected by vegetation type, terrain characteristics, and scanner characteristics. The portion of points on the grounds is affected by the vegetation, where different tree species lead to different penetration rates, and by the sampling pattern of the laser sensor, which does not necessarily lead to equal point postings on the ground. This results in higher and lower point densities, respectively, within one swath.

## 2 METHODS

We propose a two-stage method to generate a DTM in steep relief covered by dense heterogeneous forests (implying a high variation in the number of ground returns), where the existing filtering algorithms are less efficient. In the first stage, called initial filtering stage, the negative outliers and most, but not necessarily all, off-ground returns (positive outliers) are removed. To achieve the latter we use existing filtering techniques, for instance morphological filtering (Vosselman 2000). In the second stage, called filtering and DTM generation stage, the DTM is produced from the initially filtered point-cloud. For this task, we propose a new algorithm which is able to deal with a partially filtered point-cloud in steep relief. It makes use of multiple ground elevation estimates at individual DTM points in a grid or a TIN (Triangulated Irregular Network), interpolated from surrounding ground returns. These elevation estimates are generated from multiple independent samples taken from the initially filtered point-cloud. TINs are used for computing the elevation of the DTM points. Instead of TINs however, any suitable spatial interpolation method could be used for computing elevations at DTM points.

It is important that during the initial filtering stage all the negative outliers are removed from the point-cloud. This is achieved as follows. For each point in the point-cloud, we compute its vertical displacement $D$ to the average elevation of its $k$ neighboring points (neighborhood being considered in the X-Y plane). We then rank all the points according to $D$ and discard $P$ percent of points having the largest negative $D$ values. $P$ should be small, but at the same time it must be large enough to ensure no significant negative outliers are retained, even at the cost of removing some non-outliers.

The input into the final filtering and DTM generation stage is thus a filtered point-cloud containing mostly ground points scattered within the error band, some positive outliers, and no negative outliers. The error band is the buffer zone along the surface of the true bare ground. It is caused by the lidar point scattering due to the lidar range measurement errors, microrelief, grass and low herbal vegetation. Because the steep relief imposes a high slope threshold used in the morphological filter, among the initially filtered lidar points (FLP) there usually remain some positive outliers, i.e., vegetation points. These outliers would introduce errors into the DTM, if it were generated directly from FLP. Instead of this, a DTM is fitted to the ground points within the error band, as follows.

The true elevations at those locations in the X-Y plane, that we want to include into the DTM (termed DTM locations), can be approximated from repeated independent estimates of relief, based on the point-cloud of the initially filtered ground points (Figure 1). Each estimate is based on an independent random unbiased sample (termed FLPs) taken from the FLP. During each iteration the points of each FLPs are used as nodes to build a triangulated irregular network (TIN). Elevations at DTM locations are interpolated from each triangulated irregular network (Figure 2). After repeating the interpolation a number of times we get a distribution of elevation estimates at each DTM location. The true elevations can be estimated from those distributions, based on two observations.

The first observation: while the lower bounds of the distributions are almost insensitive to positive outliers, the negative outliers have also no effect, assuming they were removed previously. This means that, within comparable forest and relief circumstances, the lower bounds have a more or less constant vertical offset to the true bare-ground surface (Figure 2, Figure 3). The second observation: the majority of the distribution bounds are closely related to the error band, assuming (a) the sampling rates to collect FLPs were not too low and (b) relatively few positive outliers remained in the FLP. The assumption (a) implies that only rarely elevation interpolations would smooth out the relief curvature between sampled points. The assumption (b) implies that only a few distributions have anomalous upper bounds (Figure 3). Further assuming that the width of the error band is constant within comparable forest and relief circumstances, we are able to estimate the global mean offset between the lower distribution bounds and the true relief elevations (*gmo*). The *gmo* equals the average of differences $d_{ij} = z_{ij} - z_{j,min}$ over all DTM locations, where $z_{ij}$ is the *i*-th elevation estimate at the *j*-th DTM location and $z_{j,min}$ is the lowest elevation estimate at the *j*-th DTM location. After computing *gmo* and all the $z_{j,min}$, we can estimate the true elevation $z_j$ at the *j*-th DTM location as $z_j = z_{j,min} + gmo$.

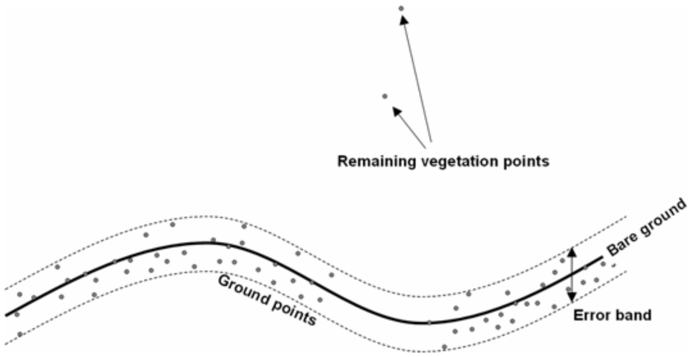


*Figure 1: The result of the initial filtering stage (using, e.g., morphological filter) are ground points with few remaining unfiltered vegetation points and no negative outliers. Note the redundancy of ground points within the error band. The scattering within the error band is caused by measurement errors, microrelief, grass and low herbal vegetation.*

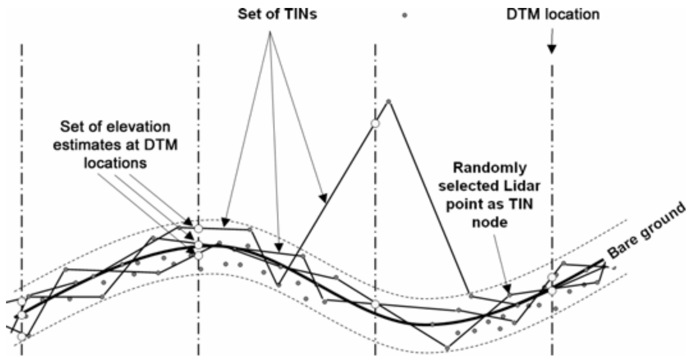


*Figure 2: Repeated random selections of lidar points are used to build a set of TINs, out of which sets of elevation estimates are interpolated at the locations of DTM pixels. Note that also the remaining unfiltered vegetation points may become TIN nodes.*

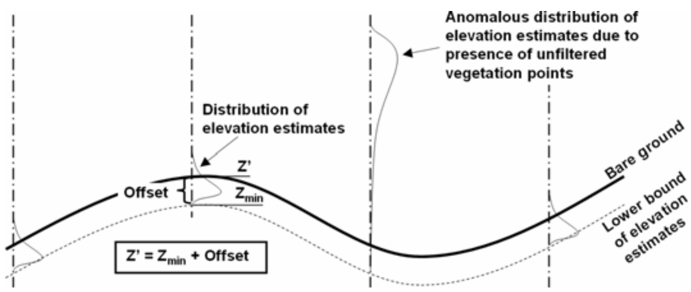


*Figure 3: DTM elevations are approximated by adding global mean offset to the lower bounds of elevation distributions, which are unaffected by the unfiltered vegetation points.*

Note that simply drawing a random sample out of the available ground points during each iteration would yield TINs that are overly detailed in areas of high point density and too generalized in areas of low point density. Such irregularities are caused by variable penetration rates in a heterogeneous forest and by irregularly spaced scan-lines. It is therefore important that each sample of points used as TIN nodes should be geographically as unbiased as possible. This is ensured by a selection procedure, where a set of random locations in X-Y plane is generated within the bounds of the filtered point-cloud and then the nearest point found for each random location is chosen. Thus the sparse lidar ground returns under very dense forest canopy can be given higher weight than the more frequent ground returns in less dense forest stands, enabling more consistent results irrespective of canopy cover.

We tested the performance of the new method in a test area encompassing 200 m by 400 m of steep forested relief in central Slovenia (Figure 4). The test area was scanned on April 30, 2003, when the vegetation was almost fully developed. The data acquisition was done in the first-last mode with an Optech ALTM model 1020 lidar, mounted onto a helicopter. The flying height was 260 – 300 m above the ground, the ground speed was 25 – 50 km/h, and the beam divergence was 0.3 mrad. The obtained point cloud density was 6.4 $m^{-2}$ and 8.5 $m^{-2}$ for first and last returns, respectively. Only the last returns were used to generate the DTM. The average terrain slope of the test area is around 30°, while the slopes along the forest road embankment and in the erosion dykes reach up to 70°. The test area is covered with a mixed *Pinus sylvestris* and *Castanea sativa* forest with 18 m average tree height, estimated from a normalized digital surface model. The average forest canopy cover is 0.67 with extreme values up to 0.86. Canopy cover was estimated for circular plots (r = 5 m) centered at reference ground points as the proportion of first and last lidar returns higher than 1 m above ground versus all first and last lidar returns. The reference ground points (N = 2029) for estimation of DTM quality were visually identified (in Y-Z plane) from among last returns within 5 transects oriented in North-South direction, each 0.5 m wide and 200 m long.

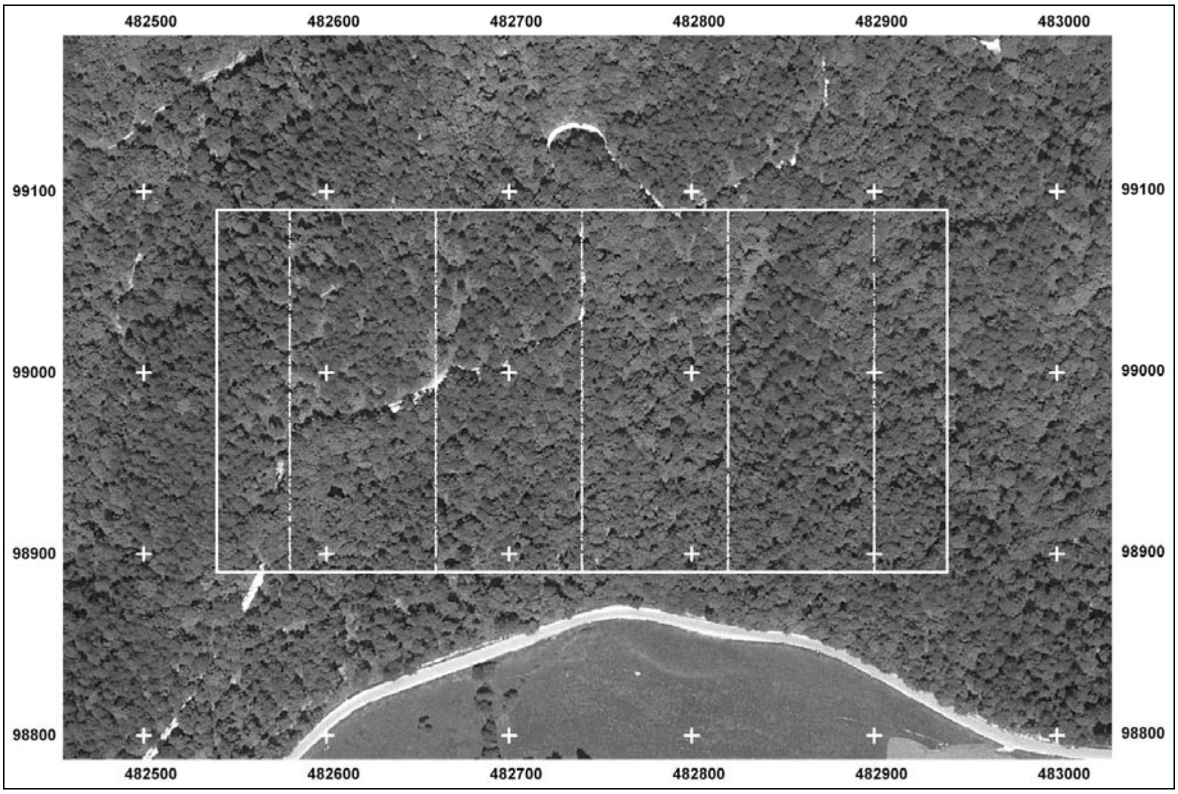


*Figure 4: The aerial photograph of the test area. The test area covers 200 m by 400 m (white rectangle) of Pinus sylvestris and Castanea sativa mixed forest on steep terrain in central Slovenia. The white dots in 5 vertical rows within the test area indicate the 0.5 m wide transects containing 2.029 reference ground points.*

## 3 RESULTS

The DTM grid generated in the study area has a horizontal resolution of 1 m by 1 m. The optimal *k* and *P* values for removing negative outliers were determined experimentally and finally set to 10 and 0.2%, respectively. The slope threshold for the morphological filter was set to 70°, which is the steepest slope observed in the test area. The point density of last returns thus decreased from 8.5 $m^{-2}$ for all last returns to 4.3 $m^{-2}$ in the initially filtered point set. By using 5 iterations and a point-cloud sampling rate of 23 % (i.e. a sample size of 10000 points per ha) a RMS elevation error of 0.15 m was achieved in the final DTM of the test area (Figure 5).

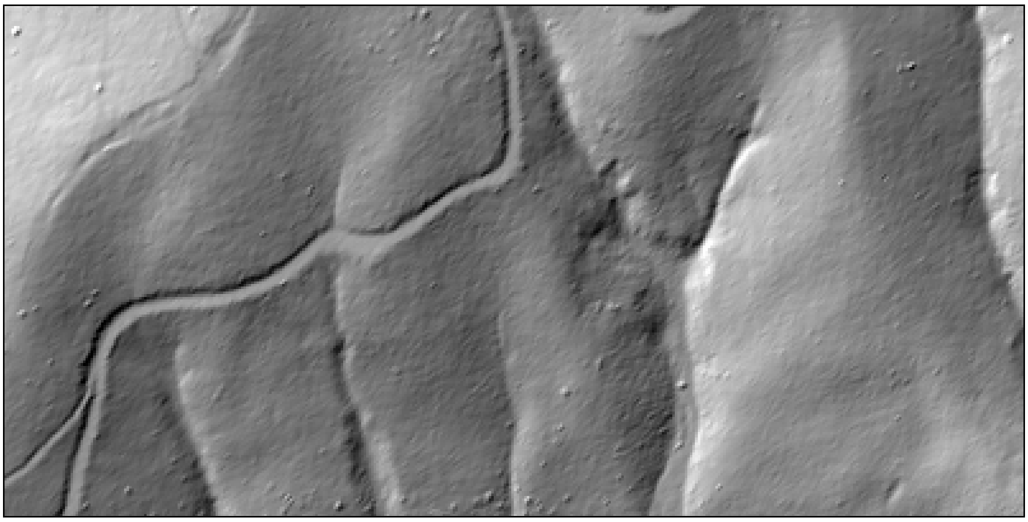

*Figure 5: The shaded relief image of the generated DTM with a horizontal resolution of 1 m by 1 m.*

## 4 DISCUSSION AND CONCLUSIONS

We presented a new method for DTM computation from the raw airborne laser scanning point-cloud. It is especially applicable in steep, forested areas where other filtering algorithms typically have problems distinguishing between ground returns and off-ground points reflected in the vegetation.

The core idea is to make use of the redundancy in the initially filtered point-cloud FLP in order to mitigate the effect of the residual off-ground points. Multiple independent samples are taken from the FLP, while each part of the area of interest gets equal probability of being sampled, irrespective of the local ground return density. Based on each sample, ground elevation estimates are computed at individual DTM locations, using some spatial interpolation method, for instance TIN based interpolation. Because the lower bounds of the distributions of the elevation estimates at each DTM location are almost insensitive to positive outliers, the true ground elevations can be approximated by adding the global mean offset to the lower bounds of distributions. Assuming that relatively few off-ground points remained in the FLP, the global mean offset can be estimated over all DTM locations by averaging offsets of all elevation estimates to the lower bounds of their respective elevation distributions.

While random sampling is used to select lidar points in each iteration, it is also ensured that each part of the area of interest gets equal probability of being sampled, irrespective of the local ground return density. These properties enable us to deal with sparse ground returns under dense forest canopy on one hand, but also with highly redundant ground returns in forest openings on the other hand. This results in a homogeneous DTM even under inhomogeneous data input conditions. The problem of negative outliers, originating from multi path reflections, is also addressed. The random sampling makes the proposed method unique among the methods of filtering airborne laser data. Other filters behave deterministically, always generating a filter error in special situations. Because of its random aspects, these errors do not occur in each sample and typically cancel out in the final step of computing final elevations at the DTM points.

The proposed method does not impose a certain DTM data structure. It can accomodate either DTM as a regular grid or as a TIN. Furthermore, it operates by interpolating DTMs from several independent samples of lidar points. This enables a straightforward parallelization, potentially leading to a considerable reduction of processing time.

In further work a validation with ground reference points is planned and the influence of different parameterisations (number of iterations and point-cloud sampling rate) on the DTM accuracy will be analyzed. Also further tests are needed to get a better assessment of performance in different forest types and under various scanning conditions.

## ACKNOWLEDGEMENTS

The authors would like to thank Polona Kalan, Slovenian Forestry Institute, and George Sithole, TU Delft, for fruitful discussions of the algorithm. We owe special thanks to ELES company, Slovenia, for kindly giving us the lidar data of the test area. The study was funded by the Slovenian Research Agency and by the Slovenian Ministry of Agriculture, Forestry, and Food within the research project “Processing of Lidar Data” (contract 3311-04-8226575), and by the Slovenian Ministry of Defense and by the Slovenian Research Agency within the research project “Forecasting GIS Model of Fire Danger in Natural Environment” (contract 3311-04-828032).

## REFERENCES

Hyyppä, J., Hyyppä, H., Litkey, P., Yu, X., Haggrén, H., Rönnholm, P., Pyysalo, U., Juho Pitkänen, J., Maltamo, M. (2004). Algorithms and Methods of Airborne Laser-Scanning for Forest Measurements. International Archives of Photogrammetry and Remote Sensing, Vol XXXVI, 8/W2, Freiburg, Germany.

Sithole, G., Vosselman, G. (2004). Experimental comparison of filter algorithms for bare-Earth extraction from airborne laser scanning point clouds. ISPRS Journal of Photogrammetry & Remote Sensing 59 1-2 (August 2004), ISSN 0924-2716, pp. 85 –101.

Vosselman, G. (2000). Slope Based Filtering of Laser Altimetry Data. In: Proceedings of the XIXth congress of ISPRS, Amsterdam, 17-7-2000,"International Archives of Photogrammetry and Remote Sensing", vol XXXIII, part B3/2, commission III, ISSN 0256-1840, pp. 935- 942.

# AIRBORNE LASER SCANNING TO GENERATE 3D MODELS OF MICRORELIEF FEATURES FOR THE PURPOSES OF FOREST ECOLOGICAL AND ARCHAEOLOGICAL SURVEYS

*Benoît Sittler[1], Sabine Schellberg[1], Daniel Siepmann-Schinker[1], Holger Weinacker[2]*

[1] University of Freiburg, Institute of Landscape Management (Ger) benoit.sittler@landespflege.uni-freiburg.de, sabine.schellberg@landespflege.uni-freiburg.de, daniel.siepmann-schinker@landespflege.uni-freiburg.de

[2] University of Freiburg, Department of Remote Sensing and Landscape Information Systems (Ger) holger.weinacker@felis.uni-freiburg.de

## ABSTRACT

Documenting micro-topography features is a special component of disciplines related to landscape ecology and the evolution of the cultural landscape. On sites where such features are covered by woodlands, their assessment is often difficult due to methodological constraints imposed by the obscuring vegetation, which prevents systematic observation.

Airborne laser altimetry was tested as a means of obtaining high resolution measurements of the surface elevations of various objects, such as the remains of past cultural landscapes (ridge and furrow, irrigation fields, etc.), as well as of forests functioning as floodwater overflows in south western Germany. The purpose was both to detect and to map at a high resolution the microtopography in order to generate 3D models of the surface features. In addition to revealing structures that had previously escaped observation, such contour maps were also designed to differentiate ecological conditions arising from topographic differences (such as in the case of submersion).

Data for this pilot study were obtained from flight missions carried out by the state survey agency of Baden-Württemberg, who commissioned the collection of data for the purposes of upgrading the state's altimetric database. The filtering and processing of the raw data and the subsequent use of GIS facilitated the generation of realistic 3D terrain models representing the earth's surface void of any forest or vegetation cover.

The resolution of this data, which produces true-to-life renderings, compares favourably with terrestrial mapping procedures, allowing large areas of landscape to be captured as three dimensional surface data. This technology promises to open up the landscape topography generally and previously hidden historic structures in particular to more visually detailed, accurate and efficient examination.

**Keywords:** Lidar, cultural heritage, terrain model, retention basins, ancient field irrigation systems

## 1 INTRODUCTION

In many earth science and environment related disciplines, elevation data and landform information are of paramount importance in the assessment of surface patterns and the identification of the processes at work. However, such information is not readily available at the desired levels of accuracy and quality. Currently the occurrence and distribution of surface features are often modelled at best at a one metre contour interval and generalised at greater scales. On the one hand, ground surveys, i.e. geodetic levelling (geodetic measurements), to collect fine scale resolution data are too labour intensive to be conducted across larger areas. At the same time, conventional remote sensing imagery obtained for the purposes of estimating surface topography is usually constrained by the lack of a third vertical dimension and is limited to the horizontal resolution of the imaging sensor.

Capable of achieving decimetre-level accuracy, laser altimeters represent a promising alternative for the generation of high resolution topographic maps. However, the profiling of topography beneath vegetation remains a particular challenge. When one considers the fact that woodlands make up in excess of half of the landscape of certain European countries (e.g. Finland), the need for insights into the applicability of this technique in such situations becomes apparent.

Presented here are examples drawn from landscape management projects incorporating this technique. In addition to illustrating the range of potential applications, the examples also convey details of the benefits and limitations.

# 2 METHODS

## 2.1 Rationale – Research questions

Airborne lidar - the principle behind which does not need to be detailed here - is a relatively new remote sensing approach (Ackermann 1999) with few applications in the field of landscape management to date. Recent preliminary applications of this new technique have shown it to be a promising means of digital terrain modelling in wooded areas (Pfeiffer et al. 1999; Hyyppä et al. 2000). However, from these studies it remains questionable whether finer microtopography characteristics such as those displayed by geomorphological or archaeological features on the forest floor can be detected and quantified to produce fine scale terrain models.

Driven by the need for high fidelity digital topography data, various projects currently running at the Institute of Landscape Management of the University of Freiburg recently opted to apply this technique. These included:

- The documentation of the patterns of a medieval ridge and furrow field system fossilised under forests.
- The mapping of the remains of ancient irrigation systems.
- The generation of DEM of forested water retention basins in order to assess sedimentation and the responses of vegetation communities.

The purpose here is to present to the reader the laser-based DEM generated for each of these study sites and to analyse whether their accuracy meets the specific project requirements.

## 2.2 The study sites

### 2.2.1 The medieval ridge and furrow field system at Rastatt

Ridge and furrow are corrugated fields dating back to the Middle Ages. They generally display height differences of 30 to 50 cm, their width ranging between 5 and 20 metres and their lengths often in excess of 200 metres. When fossilised under forests, these relicts of past arable cultivation are often barely visible from the ground due to the presence of obscuring vegetation. One such site is located near Rastatt, some 30 km south of Karlsruhe in the upper Rhine Valley. These relicts are covered by various stands of older mixed forests (beech, pine and Norway spruce), as well as areas with more densely stocked young stands.

### 2.2.2 The ancient field irrigation systems of the Freiburg valley

Like ridge and furrow, historical irrigation systems are relicts of ancient cultural landscapes characterized by man-made microrelief features that deserve mapping and assessment. This is the purpose of a study devoted to an ancient irrigation complex along the Dreisam River in the Freiburg valley near the Kaiserstuhl region. Designed to irrigate meadows, it dates back to the 19th century. Different techniques were applied depending on the local conditions (especially the gradient of the plots) and the pursued aims of meadow irrigation. The chosen example of the research area used artificial structures to disperse the water to the meadow (see figure 1). Elevation differences generated by this system were of the order of a few decimeters, but ditches depended on the category depths exceeding one meter. While no longer in use since more than 40 years, many of these structures were levelled off because of the current use as acre and are often no longer visible due to minor elevation differences. Therefore this project involves testing whether laser altimetry can be used to detect the historical landscape structures, to reconstruct the current ditch network and the terrain form (may be represented as 3D models) in order to complement the historical analysis of landscapes characterised by irrigated meadows.

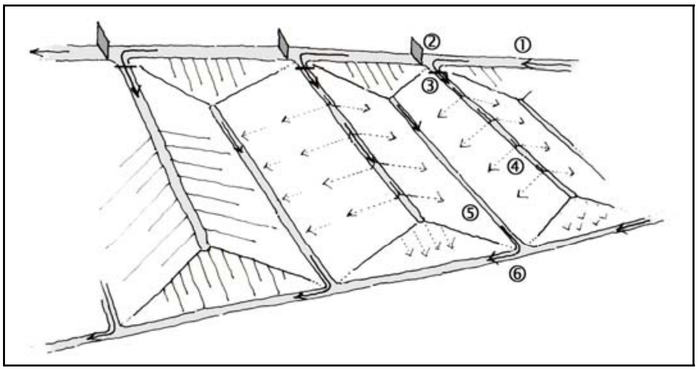


*Figure 1: Simplified model of surface topography of one form of the overland flow method according Schewior 1941 (Schellberg, 2005); ① head main, ② sluice, ③ hatch, ④ main, ⑤ drain, ⑥ head drain*

## 2.3 Forested retention basins

Floodplain management and flood prevention are major environmental issues in the upper Rhine Valley. Therefore, there is a growing need for fine scale resolution data in relation to channel morphology, width, fluvial patterns, slope and other physical attributes. This applies also to projects aimed at assessing the impact of flooding on forest stands in retention basins in Baden-Württemberg. In order to gain greater insights into how flood events disperse water and sediment, and affect vegetation exposed to flooding, a characterisation of topography and surface gradients was tested for several forested basins using laser altimetry. Highlighted here are the results of the investigation into the use of this approach as a means to generate 3D models of the Freiburg-Nord retention basin.

## 2.4 The Baden Württemberg laser scanning DEM project

The Baden-Wurttemberg state surveying agency has adopted the airborne laser scanning technique for the purposes of constructing an accurate DEM for the entire state (Hoss, 1997; Gültlinger et al., 2001). The aim of the project was to provide comprehensive altimetry data at a resolution of around one meter mesh width in space and less than 50 cm in height. The demand for such high accuracy was mainly from flood protection agencies, but additional interest was also shown by a wide range of other potential users. The company Topscan was commissioned to carry out the flight campaigns and deliver the data sets. The project started in 2000 and was due to be completed by the end of 2006. Technical details of the flight missions are listed in the table below.

The Rhine Valley, including the ridge and furrow site at Rastatt, the irrigation systems and part of the retention basins, was surveyed during the initial stage of the project and raw data were made available to test its usefulness.

*Table 1: Topscan laser scanner performance parameters*

| Altitude | Scan frequency | Scan angle | Wavelength | Strip width | Pulse repetition | Point spacing | Flight velocity |
|---|---|---|---|---|---|---|---|
| 1000 m | 25 Hz | +/- 20° | 1.55 µm | 400 m | 25.000 Hz | 1.5 m | 80 m/s |

## 2.5 Data processing

The dataset provided by Topscan was first pre-processed by the state surveying agency. This step included the filtering of ground and height points, and the georeferencing of the data according to the Gauss Krüger coordinate system. The files were available in ASCII format. By interpolating the data in Erdas Imagine, a DSM was created from the height points, while the corresponding DTM was obtained from the ground points.

# 3 RESULTS

## 3.1 The detection of ridge and furrow topography

While the first pulse imagery (figure 2a) does not reveal the ridge and furrow microrelief, the DTM (figure 2b) clearly shows the typical corrugated surface topography. This is especially evident when viewing the images in 3D with different viewing directions (figure XXX, below). These figures clearly portray the pattern of the earlier medieval landscapes, consisting of strips and furlongs. Additional structures that may be detected at a first glance include tumuli or earthen mounds, as can be seen in the upper right part of figure 2b. By contrast, in the open landscape ridge and furrow structures may no longer be detected as they have been levelled off, which is often the case on arable land. In some of these modern fields, the ancient patterns have been revealed in aerial photographs as crop marks appearing in the refilled furrows (Braasch, unpubl.).

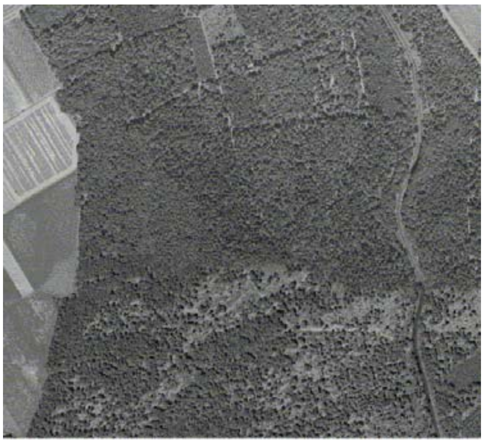
(a)

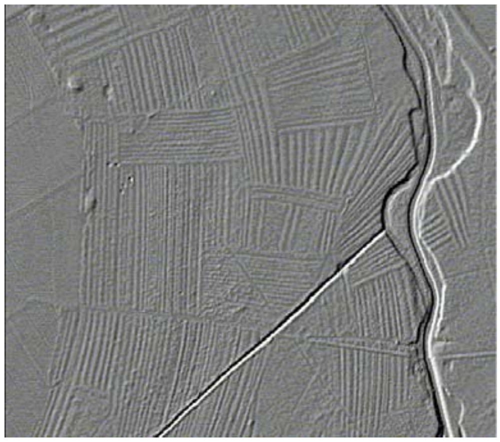
(b)

*Figures 2a and b: Surface model generated by first pulse data (left) and digital elevation model derived from last pulse data (right).*

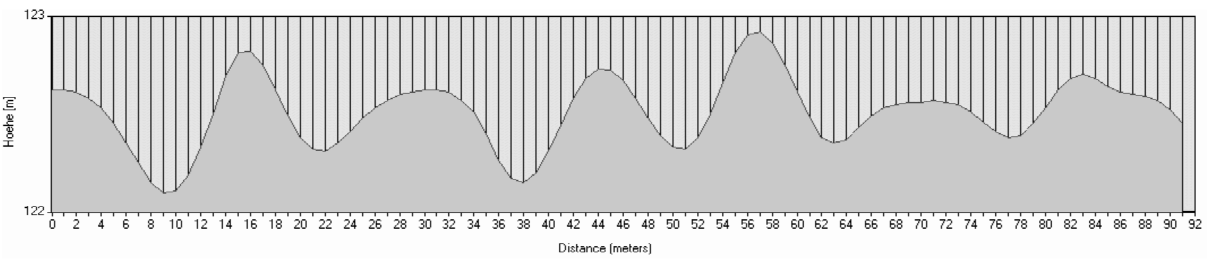


*Figure 3: Exaggerated profile of a ridge and furrow*

The determination of height proceeded with the establishment of spatial profiles of the ridges using the 3D analyst extension of Arc View 3.2. The spatial profiles were subsequently depicted in the form of graphs from which height values could easily be read. As can be seen from figure X, the distance was plotted on the horizontal axis and the elevation on the vertical axis.

## 3.2 The ancient field irrigation system

The relicts of the irrigation construction near Nimburg are obtained because the area is still used as pasture today. The artificial irrigation structures in the landscape become clearly illustrated in the last pulse sceneries obtained from the Laser Scanning flight missions. While the system of the major drains still displaying elevations differences of more than 50 cm is well presentable, also the still more slight elevations differences in the range of a few decimeters between the median part of the fields and the borders do not escape visualisation, this 3D giving shape to nearly all features of the former irrigation systems. As part of the mapping of the irrigation structures and ditches, the latter were grouped according to size classes and cross sections were measured amongst others for comparison with laser scanning data. The evaluation is not yet complete, but the comparisons made thus far are indeed promising.

### 3.3 The 3D assessment of the forested retention basin

In order to illustrate the accuracy of laser scanning height data derived from 3D models, a graphic comparison between a geodetically levelled transect and the profile of the same transect generated from a 3D model was generated (see figure 4). With the exception of extremely low or high objects like drains (37 and 326 m) and the exposed root plates of windthrown trees (100 m), in this case laser scanning data provided heights lying in a range of accuracy of between 5-20 cm.

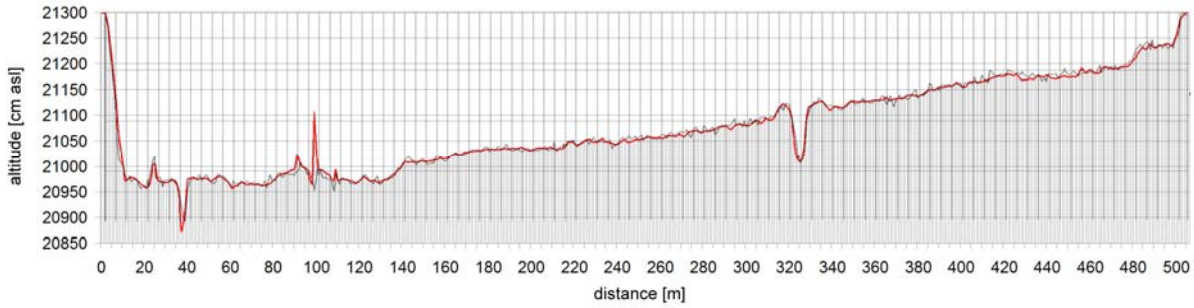


*Figure 4: Graphic comparison of the Freiburg-Nord retention basin in profile as assessed by geodetic levelling (red line) and from 3D laser scan models (black line) illustrated in a 3D model.*

## 4 DISCUSSION

The approaches adopted proved quite an efficient means of recognising structures, as was well illustrated in the case of the ridge and furrow relicts, where the primary purpose was to assess the extent and the pattern of this field system dating back to the Middle Ages. Given that the forest cover was quite uneven in terms of density, composition and height, there is evidence that even dense vegetation cover does not fully prevent laser rays reaching the soil surface, making possible 3D recognition of corrugated structures. Compared to the terrestrial mapping (Hauger et. al, 2001), this image unveils many details and structures overlooked during the ground surveys. In addition, the position of other structures included in this landscape as revealed by the laser data is quite instructive. For example, the River Sandbach is shown to intersect the ancient pattern of ridge and furrow, indicating that it is of anthropic origin. The same applies of course to the very straight ditch crossing the area. In this case, as there are written archives suggesting that it was built during the 15th century, evidence is provided revealing that the ridge and furrows were generated at an earlier date.

The fossilised overland flow system was clearly depicted in the last pulse images, showing that in the absence of tree cover, altimetric differences of the order of 10 to 20 cm can be traced easily. Therefore, the technique can be recommended for the purposes of identifying linear structures of this kind.

The depiction of the Freiburg-Nord retention basin, which has a flat topography with a slight slope of only 0.56 %, and the representation of the differences in contour lines by decimetres also shows how powerful this technique is, as the terrestrial profile generated using geodetic levelling devices departed only slightly from the profile obtained by laser scanning. For the assessment of the ecological site conditions (duration of submersion events) induced by this topographic gradient, the precision of the decimetre range may be considered acceptable, especially when compared to the poor resolution of other altimetric databases pertaining to forested areas.

The accuracy of the measurements still remains to be tested by making comparisons against ground measurements.

As costs are generally a major constraint associated with this technique, it seemed appropriate to address the financial aspect here. The minimum price for smaller projects in Germany ranges from less than € 7000 to upwards of € 20000, depending upon the data provider. Of course, for projects of the order of only tens of acres, the per acre cost becomes significantly higher due to the fixed costs of mobilising the lidar sensor. In the case of Baden-Württemberg, for which comprehensive coverage of almost the entire area of the federal state (35000 km²) is now available, data may be made available through the surveying agency (LVA) at a cost of € 15/km² for untreated data and € 60/km² for end-products usable for DEM generation.

## 5 CONCLUSIONS

As a whole, for landscape ecologists as well as for archaeologists, these examples stress how microrelief structures and archaeological sites can be subjected to more visually detailed and efficient examination. The technique can, therefore, be regarded as a very useful complement to aerial photographs, especially when forest canopies prevent the visual identification of hidden patterns. The resolution of this data and the relative ease of capture compares favourably with existing data sources. Large areas of landscape can be captured as three dimensional surface data facilitating a scientific, analytical approach to the landscape. Algorithms may be developed (De Boer, 2005) to search data sets for certain types of structures, enabling large scale prospecting of hidden archaeological remnants.

## ACKNOWLEDGEMENTS

Our deepest gratitude goes out to Mr. Hauger (Rastatt) who initiated and supported this ongoing programme in many ways. Many other participants and institutions are also involved in the project, including the Landratsamt Rastatt, the Landesdenkmalamt Baden-Württemberg as well as the Landesvermessungsamt Baden-Württemberg. Their efforts are much appreciated.

## REFERENCES

Ackermann F., 1999, Airborne laser scanning – present status and future expectations. ISPRS Journal of Photogrammetry and Remote sensing 54, 64-67.

Beresford M., Saint Joseph J., 1979, Medieval England – an aerial survey. 2nd edition. Cambridge University Press.

De Boer, A. (2005) Using pattern recognition to search LIDAR data for archeological sites. In: The World is in your eyes, CAA, Book of abstracts Tomar, 95-96.

Gültlinger M., Schleyer A., Spohrer M., 2001, Flächendeckendes, hochgenaues DGM von Baden-Württemberg. Mitteilungen des Vereins für Vermessungswesen, 48-2. 63-77.

Hauger K., Riedinger R., Sittler B., 2000. Wölbäcker bei Rastatt – eine Dokumentation zur Analyse und Erhaltung überkommener Altackerkomplexe. Kulturlandschaft – Zeitschrift für Angewandte Historische Geographie. Jg. 10 (2) 113-118.

Hoss H., 1997, Einsatz des Laserscanner-Verfahren beim Aufbau des digitalen Geländehöhenmodells (DGM) von Baden-Württemberg. DVW Mitteilungen, 44-1. 5-26

Hyyppä J, Pyysalo U., Hyyppä H , Samberg A., 2001, Elevation accuracy of laser scanning-derived digital terrain and target models in forest environment. 20 th EARSel Symposium and Workshops, Dresden, Germany, 14-17 June 2000.

Pfeiffer N., Kraus K., Köstli A., 1999, Restitution of airborne laser scanner data in wooded areas. GIS, 2, 18-21.

Schellberg S., 2005, Meadow irrigation in the federal state Baden-Württemberg, Portrayal of a nearly forgotten land use system. In: Schriften der Deutschen Wasserhistorischen Gesellschaft, Sonderband 2: 123-131.

Schewior G., 1941, Wiesenbau und Bewässerung, Leipzig.

# DISCRIMINATION OF TREE SPECIES IN AUSTRALIAN WOODLANDS USING HYPERSPECTRAL CASI DATA

*Peter Bunting[1], Michelle Paterson[2] and Richard Lucas[1]*

[1] Institute of Geography and Earth Sciences, The University of Wales Aberystwyth, Aberystwyth, Ceredigion, SY23 2EJ, UK; {pjb00|rml}@aber.ac.uk

[2] School of Biological, Earth and Environmental Sciences, The University of New South Wales, High Street, Kensington, New South Wales, 2052 Australia. m.paterson@unsw.edu.au

## ABSTRACT

Approaches to the discrimination of Australian tree species using hyperspectral Compact Airborne Spectrographic Imager (CASI) data were evaluated. Specifically, reflectance spectra were extracted from the sunlit (meanlit) area and maximum (bright) point of 343 crowns delineated using an approach developed within eCognition Expert, with these locations defined using a range of reflectance bands, band ratios and colour indices. Using the $\rho_{741}/\rho_{714}$.band ratio to identify the meanlit area of the crown, over 87 % and 76 % of crowns reserved for training and testing purposes respectively were classified correctly using Multiple (Stepwise) Discriminant Analysis (MDA); an increase of > ~ 10 % compared to when other data were used. Data extracted from the maximum points within crowns, regardless of the datasets used, provided least separation. Prior delineation of crowns, extraction of the meanlit area using the $\rho_{741}/\rho_{714}$ ratio, and classification using MDA is therefore recommended as an approach to species mapping using CASI data in this forest environment.

**Keywords:** Forests, species, hyperspectral, discriminant analysis, Australia

## 1 INTRODUCTION

Within fine (~ 1 m) spatial resolution hyperspectral remote sensing data, individuals or clusters of crowns can generally be discerned but the discrimination of tree species is often difficult as contributions to reflectance from tree components, the understorey, and the ground surface leading to variations in overall reflectance, both within and between crowns (Lucas *et al*., 2004). However, several studies (e.g., Leckie *et al*., 2005) have indicated previously that by taking spectra from certain areas of the crown, better discrimination of species can be achieved. Using Compact Airborne Spectrographic Imager (CASI) data acquired over Australian mixed species forests, this study aimed to establish the areas of the crown from which extracted spectra would provide best discrimination and also the optimal bands or derived measures for identifying these areas.

## 2 STUDY AREA

The study focused on a 40 x 60 km area of mixed species forests (Latitude –25° 32'; Longitude 147° 32') located within the Southern Brigalow Belt, a biogeographic region of southeast central Queensland, Australia (Figure 1). Common tree species include Brigalow (*Acacia harpophylla*), Poplar Box (*E. populnea*), White Cypress Pine (*Callitris glaucophylla)* and Silver-leaved Ironbark (*E. melanaphloia*). Here, forest communities exist in varying states of degradation and regeneration as a result of prior disturbance (e.g., broad scale clearing, altered fire regimes and spread of exotic species) and are structurally similar to over 80 % of those occurring in Australia.

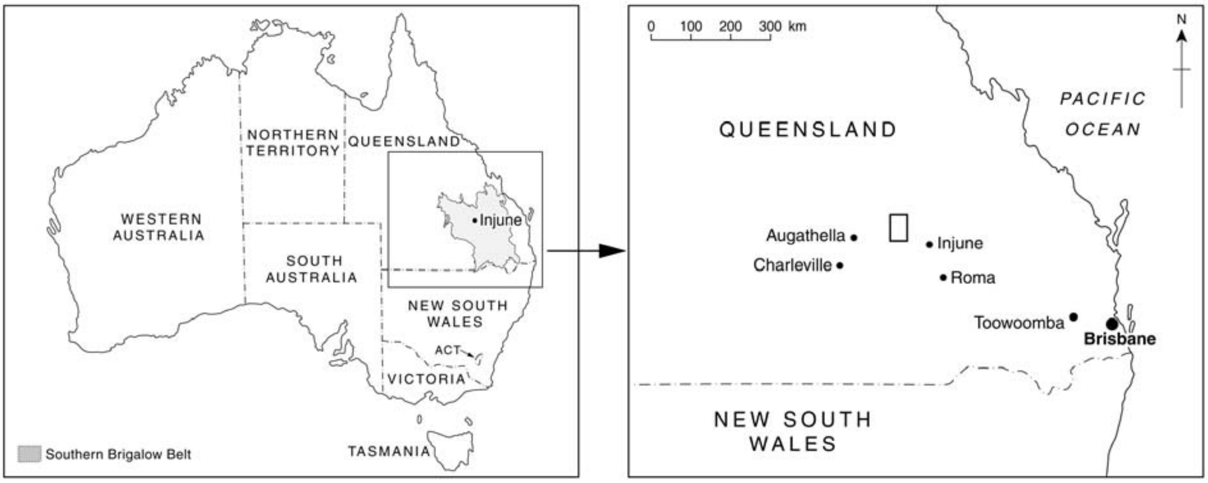


*Figure 1. The study area located near Injune, southeast central Queensland, Australia*

## 3 DATASETS

CASI data (nominally 1 m spatial resolution) were acquired over each of 150 500 x 150 m Primary Sampling Units (PSUs) on either August 29th or September 1st 2000. The data were acquired at a flying height of approximately 500 m and in fourteen wavelength regions (12 bit) covering the visible to near infrared regions of the electromagnetic spectrum, including several along the red edge. Following acquisition, the CASI data were converted to surface reflectance (percent) using the ENVI empirical line calibration (Research Systems Inc., 2003) method and reflectance spectra collected from ground calibration targets at the time of the overflights.

## 4 TREE CROWN DELINEATION

To delineate crowns within the CASI data, an algorithm developed within eCognition Expert (Bunting and Lucas, 2006) was used. The algorithm has six components: 1) differentiation of forest, non-forest and understorey using a Forest Discrimination Index that combines the near infra-red, red edge and blue reflectance channels; 2) initial segmentation of the forest areas and allocation of segments (objects) to larger objects associated with several distinct forest spectral types; 3) identification of object maxima within these larger objects and their expansion to create initial crowns and clusters; 4) subsequent classification-based separation of these objects into crown and cluster classes, based mainly on shape (e.g., roundness) and spectral indices; 5) further iterative splitting combined with classification of clusters using stricter rules to delineate more crowns; and 6) identification and subsequent merging of oversplit objects into crowns or clusters based on the relative position of the crown (object) maxima in relation to the crown boundary. With reference to field data, the delineation process provided accuracies averaging ~ 70 % (range 48 % – 88 %) for individuals or clusters of trees of the same species with diameter at breast height (DBH) exceeding 10 cm (senescent and dead trees excluded). The lower accuracies were associated with dense stands containing several canopy layers.

## 5 SPECIES MAPPING

Once delineated, single spectra were extracted from the brightest point within the crown and also the sunlit area of crowns, with the latter defined by taking the average spectra from pixels that were above the average for the crown as a whole (termed here the meanlit spectra). In both cases, the maximum bright point and meanlit spectra were defined using a single band; either one of the 14 reflectance bands, a band ratio or a colour index (e.g., hue, saturation and intensity).

Multiple (Stepwise) Discriminant Analysis (MDA) was used to then classify the crowns to species based on spectra extracted using the various bands or derived measures. MDA presented several advantages for classification in that a) the optimal band set for maximising discrimination of tree species could be identified, thereby reducing redundancy in the hyperspectral bands, and b) unknown crowns could be classified using the discriminant functions generated from MDA, with these functions tailored to focus on those species known to be present within the area imaged.

The MDA was trained using half of 343 delineated crowns that were isolated from others and could be associated with species of the genera Eucalyptus, Angophora, Acacia, Callitris and Eremophila, either using field data or with reference to Large Scale (1:4000) aerial photography. Classification was undertaken successively for each dataset (e.g., reflectance band) used for spectral extraction. Once generated, the discriminant functions were used to classify remaining crowns, including the 50 % of identified crowns which were reserved for validation, based on spectra extracted from different points or areas in the crown. An example of the classification output for a 500 x 150 m area is shown in Figure 2.

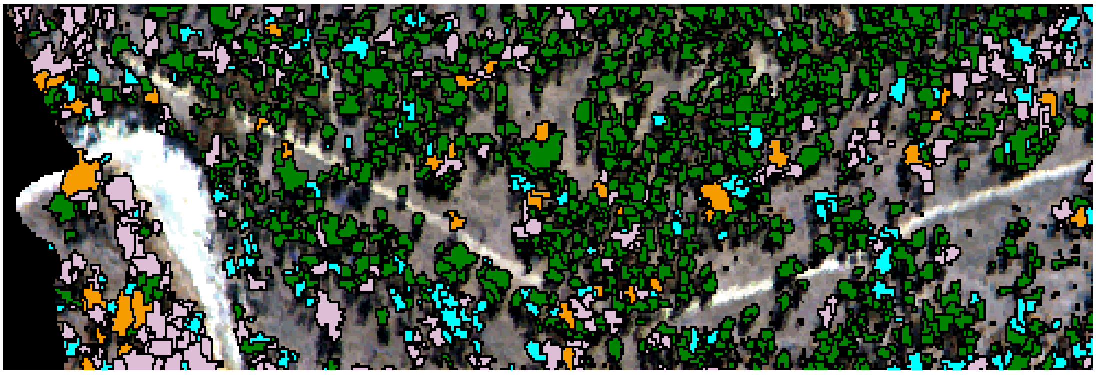

*Figure 2. The distribution of Eucalyptus melanphloia (cyan), E. populnea (orange), E. chlorochlada (pink) and Callitris glaucophylla (dark green) mapped from the CASI data for one PSU.*

## 6 ACCURACY OF TREE SPECIES CLASSIFICATION

As expected, crowns associated with the training dataset were classified to higher levels of accuracy compared to those used for validation (Table 1).

*Table 1. Accuracy of discrimination of tree species based on spectra extracted from areas (mean-lit) or points (maximum) of crowns, as determined using reflectance bands or indices.*

| | Mean Lit | | | | | Maximum | | | | | |
|---|---|---|---|---|---|---|---|---|---|---|---|
| % Correct | $\rho_{741}/\rho_{714}$ | Saturation | NIR | Green | Intensity | $\rho_{680}/\rho_{714}$ | NIR | Intensity | $\rho_{741}/\rho_{714}$ | Green | Saturation |
| Training | 87 | 84 | 83 | 81 | 81 | 72 | 70 | 66 | 65 | 61 | 55 |
| Validation | 77 | 76 | 75 | 71 | 71 | 69 | 66 | 63 | 60 | 53 | 47 |

When mean-lit rather than maximum spectra were used for classification, increases in accuracy of > 10 % were achieved. This was attributed to a wider range of spectra for each species being considered within the training datasets compared to when spectra were extracted from single pixels (associated with local maxima of reflectance data or indices). Meanlit spectra extracted using the $\rho_{741}/\rho_{714}$ band ratio gave the greater accuracies (> 81 % for all species), as this band ratio identified only those areas where a red edge slope was evident within the extracted spectra and therefore more likely to be sunlit. However, for crowns used for validation, accuracies of classification were lower (by ~ 10 %). The accuracy of classification of individual species varied for the validation dataset, with between 64 % - 71 % of *A. aneura*, *C. glaucophylla*, *E. chloroclada* and *E. mitchelli* crowns but only 40 % of *A. harpophylla* crowns being correctly identified. The crowns of the remaining *Eucalyptus* and *Angophora* species were classified with accuracies exceeding ~ 83 %.

## 7 CONCLUSIONS

In the forests studied, the delineation of tree crowns prior to classification to species was fundamental to the subsequent discrimination and mapping of species. The delineation algorithm developed within eCognition was advantageous as it allowed the extraction of spectra from different points or areas within the crown based on different reflectance bands or derived indices.

The study supports previous research (e.g., Leckie *et al*., 2005) that spectra extracted from the meanlit area of crowns rather than single pixels of maximum 'brightness' allow better discrimination of species. However, it extends this work by demonstrating that meanlit spectra extracted using the $\rho_{741}/\rho_{714}$ ratio image provide better discrimination (> 80 % and > 70 % for the training and validation set respectively) compared to those extracted using simple reflectance bands, other ratios or colour indices.

The classification does assume some *a priori* knowledge of the species composition of stands and errors increase as the diversity of species increases. However, the approach is considered the best available for automated species mapping in these Australian forests, particularly as only a few genera typically dominate and many exhibit distinct spectral characteristics.

## ACKNOWLEDGEMENTS

The authors would like to thank the Australian Research Council, Queensland Department of Natural Resources and Mines (QDNR&M), Queensland Herbarium, Bureau of Rural Sciences (BRS), Australian Greenhouse Office, CRC for Carbon Accounting and Queensland Department of Primary Industries (QDPI) Tropical Beef Centre. Ursula Benz and Definiens are especially thanked for providing the facilities and software for Peter Bunting, who was funded by an EU AMPER Training Network Scholarship and by the Institute of Geography and Earth Sciences and Computing Science Department, University of Wales Aberystwyth. Ball Aims are thanked for acquiring the CASI data.

## REFERENCES

Bunting, P. and Lucas, R.M. (2006). The delineation of tree crowns within CASI data of Australian mixed species woodlands. Remote Sensing of Environment (in press; March)

Leckie, D.G., Gougeon, F.A., Tinis, S., Nelson, T., Burnett, C.N., & Paradine, D. (2005). Automated tree recognition in old growth conifer stands with high resolution digital imagery. Remote Sensing of Environment, 94, 311-326.

Lucas, R.M., Rowlands, A.R., Niemann, O., & Merton, R. (2004a). Hyperspectral Sensors: Past, Present and Future: In P. K. Varshney and M. K. Arora (Eds.) Advanced Image Processing Techniques for Remotely Sensed Hyperspectral Data, Chapter 2, 11-49.

Research Systems Inc. (RSI) 2003, ENVI user guide.

# IN SITU LAI DETERMINATION IN FOREST STANDS: FROM 2-D TO 3-D

*Inge Jonckheere, Dimitry Vanderzande and Pol Coppin*

Katholieke Universiteit Leuven, Biosystems Department, Geomatics Engineering Group, Leuven, Belgium; Inge.Jonckheere@biw.kuleuven.be

## ABSTRACT

Hemispherical canopy photography as a close-range remote sensing technique studies plant canopies via photographs acquired through a hemispherical lens from beneath the canopy and provides a permanent record and valuable information for position, size and distribution of canopy gaps. However, the photographs are only a 2-D projection of the canopy, so data about the vertical leaf distribution is missing. In this study, therefore the commercially available SICK Laser-Measurement-System-200 (LMS200, SICK AG) was used to obtain three-dimensional structural datasets with high resolution. An artificial tree was constructed in an experimental setup, thereby creating the possibility to arrange the structural key elements (leaves and branches) according to predetermined patterns. The multidirectional accuracy and quality of the laser measurement setups (lateral sideway, lateral bottom up, hemispherical bottom up) subsequently were compared based on the development of a mathematical description of each case. Vertical plant profiles were computed for the different experimental setups showing the direct influence of the vertical distribution pattern of the laser beams on the estimation of plant material in a certain height bin.

**Keywords:** LAI, hemispherical canopy photography, laser system, forest stands

## 1 INTRODUCTION

Leaf Area Index (LAI), defined as one half the total intercepting area of foliage per unit ground area (Chen and Black, 1992), is the most common and, arguably, most useful comparative measure of vegetation structure in forest canopies. Accurate measurements of forest vertical LAI profiles are of fundamental importance as a basis for estimating the exchange of carbon, water, nutrients, and light at the stand, landscape and ecosystem scale. LAI is thus a critical parameter in physiology-based models of forest responses to global environmental change. There are several procedures to estimate LAI, both directly and indirectly (see reviews of both methods in Jonckheere et al., 2004). Examples of well-documented indirect optical instruments are the LAI-2000, DEMON, Sunfleck Ceptometer, and hemispherical cameras.

### 1.1 Hemispherical canopy photography

A hemispherical photograph provides a permanent record and is therefore a valuable information source for position, size and distribution of canopy gaps. LAI estimations from hemispherical images are based on the inversion of gap fraction data, in other words the precise measurement of geometric distribution of canopy openings. This is accomplished by quantifying the percentage of radiation transmitted through the canopy. In essence hemispherical photographs produce a 2-D projection of a hemisphere of directions on a plane (Rich, 1990). The exact nature of the projection varies according to the lens that is used. The simplest and most common hemispherical lens geometry is the polar or equiangular projection (Fig. 1) (Frazer et al., 1997).

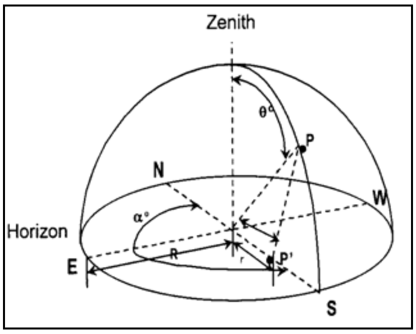


*Fig. 1. The polar hemispherical projection. Points within the sky hemisphere (P) will be projected (P') onto a circular image according to the geometry of the projection transformation (After Rich, 1990).*

*Fig. 2. Hemispherical image*

A polar projection assumes that the zenith angle of an object in the sky is directly proportional to the distance along a radial axis within the image plane. The direction to all objects relative to a fixed point on the ground surface can be uniquely defined within a hemispherical object region. In a perfect equiangular projection of a 180° field of view, the resulting circular image shows a complete view of all sky directions, with the zenith in the centre of the image and the horizons at the edges (Fig. 2).

LAI as measure to describe forest canopy structure (e.g. Welles and Norman, 1991) can be calculated indirectly using a mathematical inversion of gap fraction (GF) (Chen et al., 1997). Gap fraction, or the percentage of gaps in the canopy as a function of the solar zenith angle, can be determined after situating the exact position of the gaps in the canopy on hemispherical photographs. The inversion techniques are based on relationships between gap fraction and canopy geometry. These relationships are derived from theoretical models, which link LAI and canopy architecture with the penetration of solar radiation into the canopy. The models describe the probability of interception of radiation within canopy layers.

### 1.2 Laser technology

Laser technology provides a rising tool creating the possibility to generate a unique and comprehensive mathematical description of tree structure. A laser system emits a light pulse and determines the distance to the object (e.g., leave, branch) in the path of the light pulse. This is possible by measuring the time interval between the emitting and returning of a light pulse after it has reflected on an object, which is defined as the 'time of flight' (Sick AG, 2003). By emitting light pulses in a 3-D pattern, the total environment of a laser system can be scanned. By performing a 3D-scan of the object of interest, a laser system is able to create three-dimensional structural high-resolution datasets to extract structural parameters in a computer environment. Several studies about measuring the structure of forest canopies with laser technology were published in literature, going from beneath the canopy with terrestrial systems, to airborne systems looking downwards and potentially even with space-born sensors (among which e.g. Thies and Spiecker, 2004). These systems provide several structural tree and forest stand parameters with great prospects of applicability. Examples of these forest structural parameters are tree height, stem number, wood volume, crown diameter, biomass profiles, tree architecture, just to name a few. Laser technology offers by far more options to model canopy structure, and these need to be more investigated up to nowadays. By application of the laser technology, the question rises if the difference in geometric measurement patterns influences the accuracy of the extracted structural parameters, since these parameters are measured with a wide range of different laser devices, mounted on different types of platforms (airborne versus terrestrial).

## 2 METHODS

The terrestrial laser device and measurement system used in this study consisted of a commercially available SICK Laser Measurement System 200 (LMS200, Sick AG, Germany), mounted on a dynamic measurement platform, enabling measurements in a lateral or hemispherical pattern. The LMS200 device is a non-contact optical active sensor which scans its surroundings two-dimensionally.

The scanning system does not require special target-object reflectivity, and as a consequence no reflectors or position marks are needed. The LMS operates by measuring the time of flight of laser light pulses: a pulsed laser beam is emitted and reflected when it meets an object. The pulsed laser beam is deflected by an internal rotating mirror so that a 2D fan-shaped scan is made of the surrounding area (Sick Ag., 2003). In this manner an individual tree or forest canopy is measured in a 2-D polar plane over a range of 180° (or 100°) with an angular resolution of 0.5° (or 0.25°).The third dimension can be obtained by moving the LMS200 in the direction perpendicular to the polar plane (lateral measurement pattern), or by rotating the laser system 180° around its central axis (hemispherical measurement pattern).


*Fig. 3. LMS200, SIC*

The lateral platform consisted of an aluminum frame allowing the LMS200 to be moved a predetermined distance, 1cm by default, after a scan has been performed (Fig. 3). The hemispherical measurement platform was developed to ensure fully automated laser measurements from a tree or canopy. The LMS200 was mounted on a rotating table, turned by a step motor (Fig. 3). In this way, the LMS200 could be rotated 180° around its central axis with intervals of 0.15° between every two scans measuring in a upwards manner.

## 3 RESULTS

Vertical plant profiles were extracted from the preprocessed data, firstly by using the direct vertical distribution of the laser hits i.e. voxel counting method, and secondly by introducing a statistical approach i.e. gap probability method. The results of these two algorithms were compared and studied to understand the influence of the geometric measurement pattern and the shadowing, which caused a variation in the 3-D resolution of the laser data, and consequently on the quality of the data sets to extract this type of structural information.

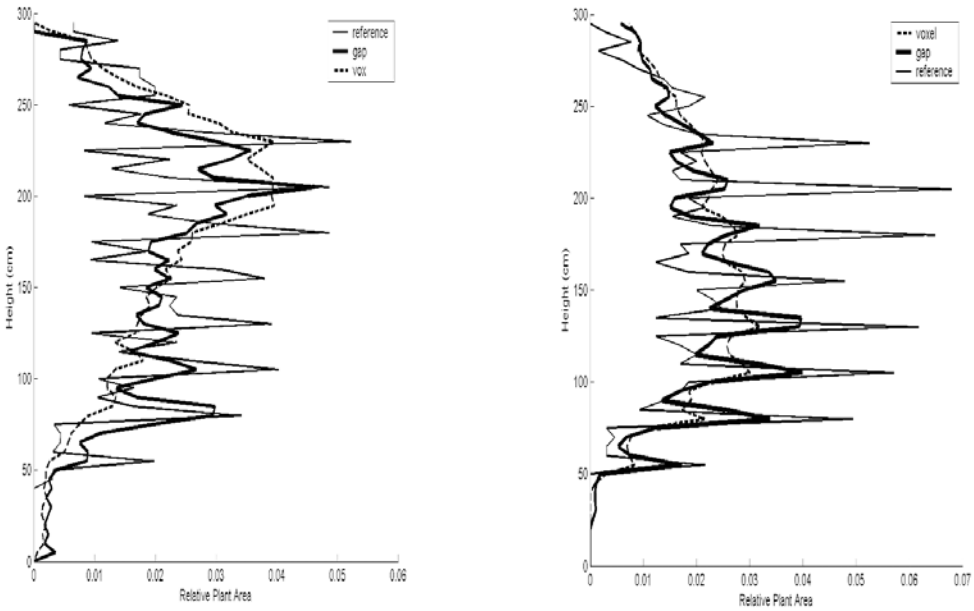


*Fig. 4. Comparison between the plant profiles calculated from the voxel counting method (---) and the corrected version extracted using the gap probability method ( ▬ ) with the reference profile (--- ) as a standard. This comparison was made for the lateral top down measurement set-up (left graph) as well as for the hemispherical bottom up set-up (right graph).*

## 4 DISCUSSION

Considering the error assessments, the gap probability based profile extracted from the bottom up data sets did not show any significant improvements compared to the voxel based plant profile. An average error of 10% which is actually an increase of 3% was obtained, but considering the actual profiles the gap probability method produced a qualitatively more correct plant profile. These results indicate the capacity of the statistical approach to compensate for estimation errors for the vertical plant profile caused by the variable 3-D resolution in these specific cases.

If the laser pulses distribution is quasi-equally divided for the entire measured object, the variability in the resolution is minimal such as the case with the lateral sideway measurement pattern and no statistical correction is needed to obtain acceptable results. After statistical correction, the average error amounted up to 12% which was an increase of 8% compared to the results of the voxel counting method, and thus showing the strength of this simple algorithm in optimal conditions. This experiment proves that a measuremental set-up which was optimized to extract a particular structural parameter obtains the best results, even without statistical post-processing.

## 5 CONCLUSIONS

Each of the three laser measurements patterns, lateral sideway, lateral top down and hemispherical bottom up were compared in their capacity to accurately measure the artificial tree where the extracted vertical plant profile was used as an objective measure. As expected, the sideway lateral measurement pattern was found the most appropriate to describe the structural aspects of the artificial tree. This can be explained by the optimization of the 3D resolution: a quasi-equally dense laser pulse coverage was obtained in the different height bins by minimizing the shadowing.

## ACKNOWLEDGEMENTS

Funding for this research has been provided by KULeuven (PDM grant 3E050788), and FWO (Project nr. G.0407.05), Flandres.

## REFERENCES

Chen, J.M. and Black, T.A., 1992. Defining Leaf-Area Index for Non-Flat Leaves. Plant Cell. Environ., 15, 421-429

Chen, J.M., Rich, P.M., Gower, S.T., Norman, J.M. and Plummer, S., 1997. Leaf Area Index of Boreal Forests: Theory, Techniques, and Measurements. J. Geophys. Res.–Atmos., 102: 29429-29443.

Frazer, G. W., J. A. Trofymow, and Lertzman , 1997. A method for estimating canopy openness, effective leaf area index, and photosynthetically active photon flux density using hemispherical photography and computerized image analysis techniques. K.P. Natural Resources Canada, Canadian Forest Service, Pacific Forestry Centre, Victoria, BC. Information Report BC-X-373, 73 p.

Jonckheere, I., S. Fleck, K. Nackaerts, B. Muys, P. Coppin, M. Weiss, and F. Baret. 2004. Review of Methods for in-situ LAI Determination, Part I: Theories, sensors and hemispherical photography. Agr. For. Meteorol., Vol. 121 (1-2): 19-35.

Rich, P. M., 1990. Characterizing Plant canopies with hemispherical photographs, Rem. Sens. Rev., 5, 13-29.

Sick AG., “Technical description LMS200.” http://www.sick.de, 2003.

Thies, M., Spiecker,H., “Evaluation and future prospects of terrestrial laser scanning for standardized forest inventories.” Proceedings of Natscan Conference: Laser-Scanners for Forest and Landscape Assessement - Instruments, Processing Methods and Applications. 3-6 October, Freiburg im Breisgau, Germany. 192–197, 2004.

Welles, J. M. and J. M. Norman, 1991. Instrument for Indirect Measurement of Canopy Architecture, Agronom. J., 83, 818-825.

# BIOPHYSICAL PARAMETER RETRIEVAL FOR GLOBAL MODELLING FROM SATELLITE LASER ALTIMETRY

*Jacqueline Rosette[1], Peter North[2] and Juan Suárez[3]*

[1] Swansea University, Department of Geography, Swansea, U.K.; ggrosette@swansea.ac.uk
[2] Swansea University, Department of Geography, Swansea, U.K.; p.r.j.north@swansea.ac.uk
[3] Forest Research, The Agency of the Forestry Commission, Midlothian, U.K.; juan.suarez@forestry.gsi.gov.uk

## ABSTRACT

Data from the Geoscience Laser Altimeter System (GLAS) aboard the Ice Cloud and land Elevation Satellite (ICESat) offer an unprecedented opportunity for large scale canopy height retrieval. However, complications associated with large footprint LiDAR have been recently documented and these are examined with reference to the Forest of Dean, UK. The effect of LAI, canopy height and fractional cover on LiDAR waveforms are demonstrated through radiative transfer simulations. The majority of GLAS footprints located on vegetated sites were found to produce bimodal waveforms irrespective of underlying surface relief. Single peak waveforms corresponded well with Open or newly planted (2004) land, although waveforms of adjacent footprints often appeared to retain characteristics associated with a lack or absence of vegetation. Pulse broadening is considered and a slight positive relationship is seen between the width of the returned waveform and within footprint surface variation. However, data are greatly dispersed with $R^2$ of 0.05, 0.05 and 0.07 for 3x3, 5x5 and 9x9 DTM pixel matrices (10m resolution). In almost all cases, ground returns beneath vegetation canopies were successfully obtained with detail such as discrete ground elevations being discerned. The ability of satellite LiDAR to retrieve data for such a complex and diverse area further indicates the potential of this technique.

**Keywords:** Radiative Transfer, Satellite LiDAR, ICESat, Canopy height

## 1 INTRODUCTION

This research aims to evaluate the potential of satellite light detection and ranging (LiDAR) for the retrieval of land surface biophysical parameters, in particular over forest biomes. The data source is the Geoscience Laser Altimeter System (GLAS) aboard the Ice Cloud and land Elevation Satellite (ICESat). This new instrumentation has the potential to directly estimate key land surface parameters such as canopy height, currently difficult to obtain by other means. In addition, data from airborne LiDAR experiments have been shown to offer information on the vertical distribution of leaf area index (LAI), and, by correlation, biomass. The research is undertaken using field data supplied by the Forestry Commission GB (FC). The FC plans a change in management practice, retaining a number of mature trees when an area is cleared allowing a more natural process of regeneration. Parameters such as canopy cover would be considered important indicators of regeneration success whilst biomass calculations provide measurements of stand productivity (G. Patenaude pers. comms.)

This research aims to combine field measurements and a modelling approach to explore which parameters may be retrieved from satellite LiDAR data and evaluate use in support of land surface and climate modelling.

### 1.1 Ice Cloud and Land Elevation Satellite

ICESat was launched in 2003 and aims to have a 5 year lifespan with subsequent missions extending data acquisition to around 15 years. Repeat ground tracks or cross-over points of tracks potentially allow changes over time to be detected. The nature of data acquisition (sequential sampling along-track 172m apart) and broad footprint size (approximately 60m diameter) offer challenges for the interpretation of GLAS waveforms as ground and vegetation elevations can be combined within the waveform. Data obtained in conjunction with existing projects covering a range of locations and vegetation types are being explored to evaluate the utility of satellite retrieval in support of land surface modelling.

### 1.2 Study Site – Forest of Dean

The first of these areas is the Forest of Dean, Gloucestershire, UK, which consists of heterogeneous woodland spanning an area of approximately 11,000 hectares. It was designated a National Forest Park in 1938 and is one of England's few remaining ancient forests (Forestry 2006). Together with its undulating landscape, these factors combine to create a challenging study area for the application of satellite LiDAR.

The influence of topography on waveform interpretation is considered and comparison made between parameter estimates inferred from waveforms and field data kindly provided by the Forestry Commission.

## 2 METHODS

This study has used the following products from GLAS release V022: level 1A GLA01 (Global Altimetry data) and level 1B GLA05 (Global Waveform-based Range Corrections data) captured on 4th October 2004 (Zwally et al. 2005a and 2005b). V022 Level 2 products (GLA06, Global Elevation data and GLA14 Global Land Surface Altimetry data) providing respectively an algorithm pick of the ground surface as well as more precise footprint locations and model fit to the waveform, are due for future release (dates yet to be announced); this study therefore utilises only the raw returned waveform. The GLAS Visualizer Tool (November 29th 2005 version) was used to explore the waveform, as well as to identify and extract parameters of interest.

The raw waveform in the form of return time (ns) from the spacecraft to the intercepted surfaces was converted to one way distance in metres so relative distances between features could be calculated. Following Harding and Carabajal (2005), the alternate 'signal begin' and 'signal end', determined by exceeding a background noise threshold, were taken as estimates of the highest and lowest intercepted surfaces within a footprint. Remaining consistent with the terminology of Lefsky (2005), this distance is referred to as Waveform Extent. Where relief is small, vegetated surfaces typically produce a bimodal LiDAR waveform with a narrow abrupt peak indicating the ground return and a relatively broader, more complex return from the canopy. Thus, in keeping with Harding and Carabajal (2005), the distance between 'signal begin' and the location on the waveform of the ground peak (determined by manual inspection) is assumed to be indicative of maximum canopy height.

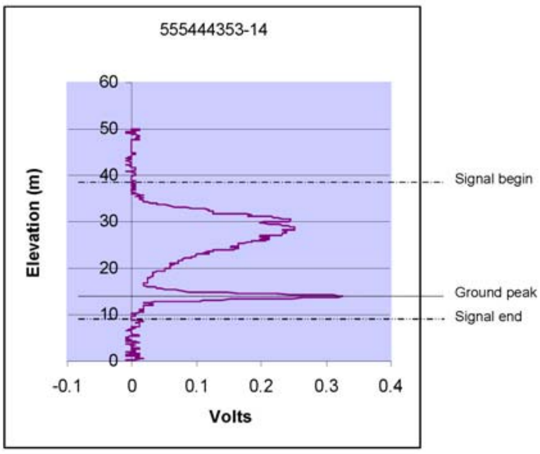


*Figure 1: Footprint classed as Norway Spruce, planted 1967 at 1.7m spacing. Illustration of Waveform Extent (signal begin – signal end) and Maximum Canopy Height (signal begin – ground peak) measurements.*

Radiative transfer modelling was additionally used to explore the influence of leaf area index (LAI), canopy height and fractional cover on waveform characteristics.

To assess the contribution of topographic relief on waveform interpretation, terrain indices for each footprint location were calculated. This was formed by the difference in metres between the highest and lowest elevations contained within a square DTM grid (OS 2006) with centre closest to the footprint location. Lefsky (2005) had found the terrain index from a 3x3 matrix of elevations to provide the most appropriate estimation of height difference irrespective of DTM resolution. In keeping with this principle, terrain indices were calculated for 30x30m (3x3 matrix, representing the centre of the footprint as laser energy diminishes towards the footprint margins), 50x50m (5x5 matrix, the closest to the average footprint size of 47x61m produced by Laser 3 operation (Abshire 2005)) and 90x90m (9x9 matrix, corresponding to the 3x3 SRTM data matrix at 30m resolution used by Lefsky (2005) at their North American study sites and encompassing surrounding topography thus allowing for error in footprint location).

# 3 RESULTS AND DISCUSSION

## 3.1 Waveform Interpretation

Preliminary results indicate a potential for deriving valid parameters from ICESat/GLAS data. The majority of footprints produced bimodal waveforms regardless of underlying surface relief. Indeed somewhat unexpectedly, and in contradiction to the findings of Harding and Carabajal (2005), the waveform with highest Terrain Indices (14m, 23.9m and 36.9m for 30, 50 and 90m matrices respectively) also demonstrated the bimodal form.

Waveform characteristics demonstrated in Figure 2 are interpreted by Harding and Carabajal (2005) to be those of a location with significant relief, dense vegetation cover and little laser penetration to the ground. However, Terrain Indices at this location are unremarkable at 2.7m, 5.2m and 9.9m for each DTM matrix. Comparison with the Forestry Commission subcompartmental database classifies the vegetation as Scots Pine (planting year 1992). Two further locations are classed as Scots Pine, one of which (planted 1932) suggests dense vegetation canopy although does succeed in obtaining a ground return. This suggests the waveform shown in Figure 2 may represent high attenuation through the canopy preventing or greatly reducing penetration to the ground.

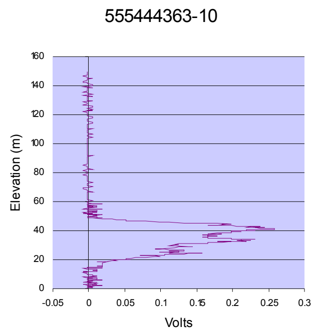


*Figure 2: Interpretation of an atypical waveform showing Scots Pine (Pinus sylvestris)*

ICESat/GLAS successfully returned single peak waveforms for seven of the nine footprint locations classified by the Forestry Commission as Open land or newly planted (2004). On two occasions, footprints adjacent to non-vegetated subcompartments also produced waveforms with single peaks or bimodal forms indicating scarce vegetation. Additionally one location returned a single peak with sparse vegetation adjacent to this within subcompartments which are classed as vegetated. These errors require further analysis to determine whether they are an artefact of footprint location error or misclassification.

Clearly further investigation of waveform characteristics is necessary to fully understand the ways in which surface features are represented, although it is acknowledged that this form of detailed analysis would be unfeasible if the technique is to be applied for large scale parameter retrieval.

## 3.2 Topography

ICESat/ GLAS waveforms appear to have captured surface relief beneath canopies reasonably well including the two discrete surfaces suggested in Figure 3.

As mentioned above, on this occasion, surface relief does not appear to have prevented the identification of vegetated footprints through the presence of bimodal waveforms. Initial consideration of the effect of Terrain Index on Waveform Extent may indicate a slight positive relationship explaining 5%, 5% and 7% of the variance for the 30 x 30m, 50 x 50m and 90 x 90m DTM matrices respectively. Further work is required concerning the question of topographic influence on waveforms.

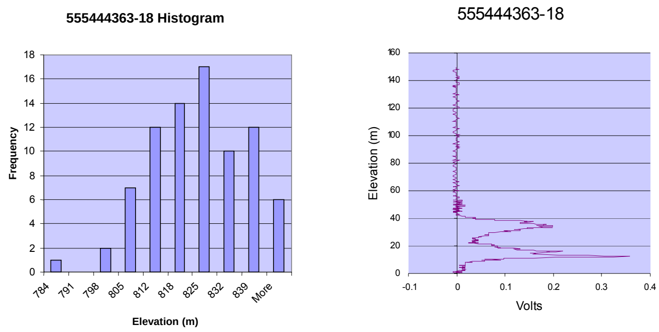


*Figure 3: Representation of two discrete ground elevations within a footprint.*

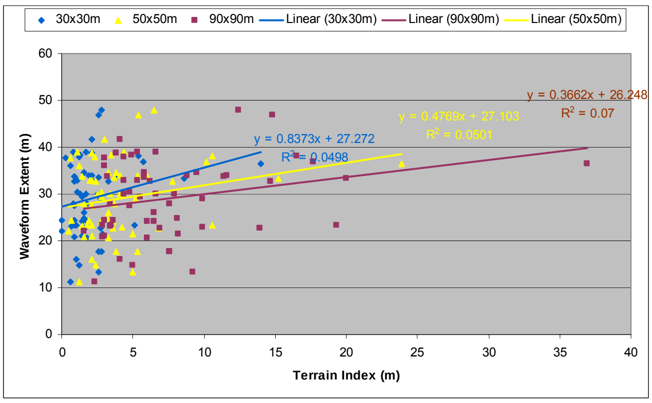


*Figure 4: Relationship between surface relief and breadth of Forest of Dean waveforms.*

The importance of DTM resolution for Terrain Index was investigated and, in agreement with the findings of Lefsky et al., a linear relationship was found with $R^2$ = 0.87 between the 30x30m and 90x90m DTM terrain indices.

## 3.3 Radiative Transfer simulation

The FLIGHT model is based on Monte Carlo simulation of photon transport (North (1996); Disney et al. (2000); Barton and North (2002)), and has been developed to simulate the observed reflectance and LiDAR response of three-dimensional vegetation canopies. Evaluation of bidirectional reflectance is achieved by simulation of the photon free-path within a canopy representation, and simulation of the chain of scattering events incurred by a photon in its path from the source to the receiver or to its absorption. Multiple scattering between different foliage elements and with the ground is thus modelled. LiDAR waveform response is simulated by including a time variable in the calculation. Foliage is approximated by structural parameters of area density, angular distribution, and size, and optical properties of reflectance and transmittance. Leaves are approximated as bi-Lambertian scatters, and the angular distribution of incident diffuse light may be modelled explicitly. The method is efficient for simulation of LiDAR and high spectral resolution data, as the time limiting step is the sampling of photon free-path, which need only be performed once. Initial results (Figure 5) suggest retrieval of further parameters, e.g. LAI, may be possible from ICESat. Work is in progress to develop a model inversion scheme for this retrieval.

## 4 CONCLUSIONS

Initial results suggest great potential for the relevance of ICESat/GLAS for extracting forest parameters. Discrepancies have been identified and will be subject to further investigation.

Future work will compare maximum canopy height obtained from ICESat waveforms with ‘top height’ estimates (average height of trees with maximum diameter at breast height within the area of interest) from Forestry Commission yield models (following Patenaude et al. 2004). The relationship between the top height measurements and Waveform Extent and Terrain Index will be assessed using regression analysis as applied by Lefsky et al. (2005). The ability of maximum canopy height derived from ICESat to estimate above ground biomass using allometric equations will also be assessed and compared with Forestry Commission stemwood volume predictions. The ratio of area under the ground peak to area under the full waveform will also be explored as a potential indicator of canopy cover.

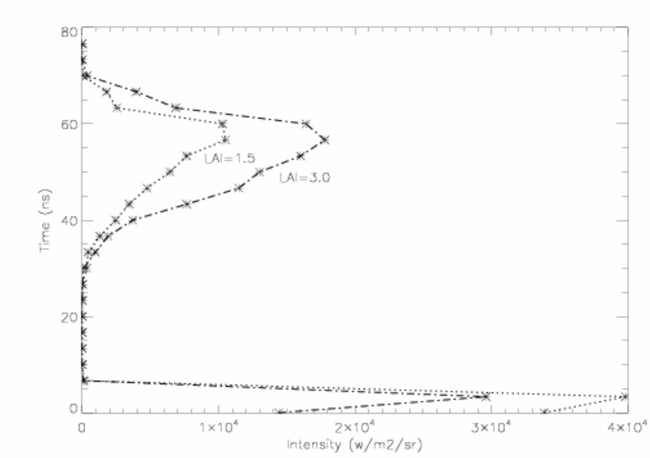


*Figure 5: Simulated waveform response for a dense (LAI=3.0) and sparse (LAI=1.5) forest canopy using the FLIGHT 3D radiative transfer model. Canopy height = 11m, fractional cover = 60%.*

## ACKNOWLEDGEMENTS

This project is based at the Department of Geography within the School of Environment and Society, University of Wales Swansea, Singleton Park, Swansea SA2 8PP, UK. The PhD is funded by the Natural Environment Research Council and forms part of the objectives of the Climate and Land Surface Systems Interaction Centre (CLASSIC).

Recognition is also extended to the Forestry Commission GB for their assistance with this work; in particular to Genevieve Patenaude (g.patenaude@staffmail.ed.ac.uk) for her explanation of FC practices, advice and efforts to create links with existing FC field data, and to Juan Suárez for providing access to FC yield models and data within the subcompartmental database for the Forest of Dean as well as his guidance for the use of these.

## REFERENCES

Abshire J. et al. (2005) Geoscience Laser Altimeter System (GLAS) on the ICESat Mission: On-orbit measurement performance. Geophysical Research Letters 32: L21S02

Barton, C.V.M. and North, P.R.J., 2001, Remote sensing of canopy light use efficiency using the photochemical reflectance index: model and sensitivity analysis, Remote Sensing of Environment, 78, 164-273.

Brenner et al. (2003) Derivation of Range and Range Distributions From Laser Pulse Waveform Analysis for Surface Elevations, Roughness, Slope, and Vegetation Heights. Algorithm Theoretical Basis Document V4.1. http://www.csr.utexas.edu/glas/pdf/Atbd_20031224.pdf (accessed March 2004)

Disney, M., Lewis, P. and North, P. (2000) Monte Carlo ray tracing in optical canopy reflectance modelling. Remote Sensing Reviews, Vol 18, No. 2-4, 197-226.

Forestry (2006) Royal Forest of Dean; History. http://www.visitforestofdean.co.uk/history.htm (accessed 6th February 2006)

Harding, D. and Carabajal, C. (2005) ICESat waveform measurements of within-footprint topographic relief and vegetation vertical structure. Geophysical Research Letters 32: L21S10

Lefsky, M. et al. (2005) Estimates of forest canopy height and aboveground biomass using ICESat. Geophysical Research Letters 32: L22S02

North, P. R. J., 1996, Three-dimensional forest light interaction model using a Monte Carlo method, IEEE Trans. Geosci. Rem. Sens., 34(4):946-956.

OS (2006) OS Land-Form PROFILE DTM, 1:10000 ©Crown Copyright/database right 20(yy). An Ordnance Survey/EDINA supplied service

Patenaude, G. et al. (2004) Quantifying forest above ground carbon content using LiDAR remote sensing. Remote Sensing of Environment 93:368-380

Schutz B. et al. (2005) Overview of the ICESat Mission. Geophysical Research Letters 32: L21S01

Zwally, H.J., R. Schutz, C. Bentley, J. Bufton, T. Herring, J. Minster, J. Spinhirne, and R. Thomas. (2005a) updated current year. GLAS/ICESat L1A Global Altimetry Data V022, 15 October to 18 November 2003. Boulder, CO: National Snow and Ice Data Center. Digital media.

Zwally, H.J., R. Schutz, C. Bentley, J. Bufton, T. Herring, J. Minster, J. Spinhirne, and R. Thomas. (2005b) GLAS/ICESat L1B Global Waveform-based Range Corrections Data V022, 15 October to 18 November 2003. Boulder, CO: National Snow and Ice Data Center. Digital media.

# IKONOS IMAGERY SEGMENTATION TRIALS FOR EUCALYPTUS STANDS MAPPING IN A FRAGMENTED LANDSCAPE IN NW SPAIN

*María Flor Álvarez[1], Henrique Lorenzo[2], Juan Picos[3] and Michael A. Wulder[4]*

[1] University of León, E.S.T. Ingeniería de Minas, Ponferrada (León), Spain; flor.alvarez@unileon.es
[2] University of Vigo, Department of Natural Resources, Pontevedra, Spain; hlorenzo@uvigo.es
[3] University of Vigo, Department of Natural Resources, Pontevedra, Spain; jpicos@uvigo.es
[4] Canadian Forest Service, Pacific Forestry Centre, Victoria (British Columbia), Canada; mwulder@nrcan.gc.ca

## ABSTRACT

National Forest Inventories are carried out in Spain each 10 years, involving a lack of updating in areas where fast-growth plantations are the prevailing land use. The main objective was mapping *Eucalyptus globulus* stands by means of high resolution satellite imagery, in order to achieve update cartography. Therefore, an object-oriented land cover classification was performed for *Eucalyptus* stands mapping in NW Spain. One IKONOS image was segmented at four different levels (scale parameters of 10, 30, 50 and 100) to find the most suitable one in a very fragmented and heterogeneous landscape. A total of 1 121 training areas were defined for twelve land cover classes and an independent sample of 163 areas was used for validation. IKONOS object-oriented classifications achieved overall accuracies between 67% and 77%. Accuracy was different depending on segmentation level, and the highest accuracy (76.69%) was achieved using a scale parameter of 30. For larger segment sizes, accuracy was below 70%. The number of pixels classified as eucalypt stands was compared using the scale parameters of 10 or 30 in the classification; the increase of 25% was achieved mainly by means of decreasing the pine plantations area and broadleaved forest areas. Segmentations using scale parameters greater than 70 were not recommended for IKONOS classification in this area, due to the high degree of fragmentation of this landscape. Compared to pixel-based classifications in the same area, mapping accuracy for eucalypt stands was greater using the segment based approach, although omission error was also significantly higher.

**Keywords:** *Eucalyptus globulus*, IKONOS, object-oriented, mapping, segmentation

## 1 INTRODUCTION

Forest economic planning is the basis for decisions of the forest industry, the official forest policy and forest owners, and requires information about forest resources in order to manage them in an optimal and sustainable way. Forest inventory data have been collected primarily by means of field surveys, which is both expensive and time-consuming. National Forest Inventories are carried out in Spain each 10 years, involving a lack of updating in areas where fast-growth plantations (e.g. *Eucalyptus globulus)* are the prevailing land use. Successful forest management and strategic planning in these areas depends on the existence of a reliable and updated inventory. Important variables for forested landscapes, such as general vegetation types or forest composition (e.g. *Eucalyptus* versus *Quercus*) can be discriminated by means of remotely sensed data (Franklin et al. 2003). Many procedures commonly applied to the classification of remote sensing images are based on the radiometric information contained in the image bands. The utility of per-pixel classification of spectral reflectance for identifying land use cover is limited, as a result of various sources of error or uncertainty that are present in areas of significant landscape heterogeneity (e.g. rural–urban fringe, forest silvicultural thinning). Improvements in traditional per-pixel classifications have been developed over the last decade and include image segmentation and object-oriented classification (Treitz and Rogan 2004). Moreover, previous studies on high-resolution data (Gougeon 1995) proved that traditional spectral-based methods result in rather poor or incorrect classification.

The objective of this research was mapping *Eucalyptus globulus* stands by means of satellite imagery, in order to get and updated cartography. It was aimed to (i) test the suitability of object-oriented image analysis using high spatial resolution imagery (IKONOS), (ii) determine the importance of image segmentation in object-oriented image analysis to map *Eucalyptus globulus* stands in a fragmented landscape, and (iii) compare the results of object-oriented image analysis to those achieved in a previous pixel-based classification in the same target area.

## 2 STUDY AREA

The study area comprises 221 km$^2$ on the coastal area in the West of Pontevedra (Galicia, NW Spain). It is centered at 42º 23' 4.54'' N, 8º 35' 30.80'' W (Reference system: European Datum 1950). Slope ranges from 0º to 82º (mean value of 6.39º), with higher slopes in the highest areas. Mean elevation for the mainland area is 169.3 m, ranging from 0 to 747 m. Landscape is very fragmented (agricultural lands smaller than 0.5 ha) and there are not many large and homogeneous areas regarding land cover, as it is characteristic in Galicia. There is an extensive road-network which involves highways, national roads and a large amount of no-asphalt roads through the forest and rural areas. Several infrastructures such as mining areas are located out of the main settlements. The main area is occupied by forests (mainly plantations) and agricultural lands (vineyards, grasslands, market gardens, orchards). Most common tree species are *Eucalyptus globulus,* maritime pine *(Pinus pinaster)* and oak *(Quercus robur)* (IFN3 2001). Native broadleaved forests are common along the rivers, being alder (*Alnus glutinosa*) the dominant species. Radiata pine *(Pinus radiata)* plantations also appear in the area. The rainy and warm weather involves a continuous growth of understory the whole year.

## 3 IMAGERY AND ANCILLARY DATA

A 12.3 km × 17.3 km Geo 4 multispectral IKONOS image was acquired on 4th July 2003, originally centered at 29T5535044692416 (UTM Zone 52 / WGS84). The IKONOS image was already pre-processed: standard geometrically corrected, georectified to an inflated ellipsoid, North-oriented and corrected for systematic distortions due to the sensor, the platform and the Earth rotation and curvature (EUspaceimaging, 2005). However, the nominal 15 m georeferencing accuracy was verified to be higher (more than 1 000 m), so the IKONOS image was converted to reference system European Datum 1950 (ED50), projected to UTM Zone 29T and geometrically corrected by means of 251 GCPs, identified at the image and at the 1: 5 000 topographic maps (ED 50), using a 2D polynomial affine function. The result was a RMS error of 50 m. Despite of the high number of GCPs it was not feasible to achieve a smaller error. A nearest neighbour algorithm was used to resample the image with an output 4 m grid. In order to minimize changes in DN and simplify the process, the image was not orthorectified. Additional radiometric corrections were not performed because theoretical analysis and empirical results indicate that only when training data from one time or place are applied in another time or place is atmospheric correction for image classification needed (Song et al. 2001).

Orthophotographs from a photogrammetric flight on scale 1: 20 000 gathered in 2001-2002, and vector data from the Third National Forest Inventory (IFN3), which consisted of provincial polygon maps delimited on scale 1: 50 000 in 1998, were used in the training areas location and for the accuracy assessment. These data were checked by field work in July-August 2004.

## 4 METHODS

An object-oriented supervised classification was performed, therefore as first step a legend with 12 classes was defined (Table 1): agricultural lands (AG), water (W), infrastructures (I), shrub rangeland (H), areas with low cover (LC), *Quercus* spp. forest land (OA), *Alnus glutinosa* forest land (AL), conifer forest land (*Pinus pinaster, Pinus radiata*) (PI), *Acacia dealbata* forest land (AC), clouds (feature) (CF), clouds (shadow) (CS), and *Eucalyptus globulus* stands (EU). These classes were defined taking into account the IFN3 data.

The second step consisted on segmenting the image using the software eCognition™, which involved the definition of two parameters: the heterogeneity criterion and the scale parameter. The image was segmented in four levels using spectral information of the 4 bands, scale parameters of 10 (Level 1), 30 (Level 2), 50 (Level 3) and 100 (Level 4) (increasing size of segments). The homogeneity criterion was defined by a value of 0.8 for Colour and 0.2 for Shape, because the shape criterion works at cost of spectral homogeneity and it can therefore reduce the quality of segmentation results (Bentz et al. 2004). Smoothness and compactness were equally assigned (0.5), due to the existence of different nature features (natural and man-made) and because higher smoothness values imply spectral differences are not very much taken into account (Baatz et al. 2004).

Training segments were selected on the Level 1 segmented image, by displaying RGB 321 and 432 band combinations and verifying land cover by 1: 5 000 scale orthophotographs from the SIXPAC. Forest cover maps and plot location from the IFN3 were also considered to assess land cover, but the not very successful overlapping between the image and cartography and the coarse scale of the IFN3 data, suggested to use them only as ancillary information. RGB 543 and 453 Landsat-5 TM band combinations of an image of the same area were also displayed and considered to differentiate doubtful areas. Table 1 shows the number of training areas and the corresponding number of pixels for each class. Sites were dispersed throughout the scene to increase the chance that the training data were representative of all the variations in the cover types present in the scene (Lillesand and Kiefer, 2001).

*Table 1. Training areas for IKONOS image: number of samples for each class (n) and corresponding number of pixels (np). Validation points for IKONOS image: number of points for each class (npv).*

| ID | Class name | Training | | Validation |
|---|---|---|---|---|
| | | n | np | npv |
| W | Water | 140 | 6185 | 16 |
| I | Infrastructures (urban areas, roads) | 254 | 2549 | 16 |
| LC | Low cover (newly afforested areas, unproductive areas) | 83 | 583 | 14 |
| AG | Agricultural land (grasslands, vineyards, farming areas) | 155 | 1437 | 9 |
| SH | Shrub rangeland | 82 | 1179 | 8 |
| PI | Pine forest land | 104 | 2402 | 22 |
| OA | Oak forest land | 56 | 844 | 20 |
| AL | *Alnus glutinosa* forest land | 55 | 759 | 9 |
| AC | *Acacia dealbata* forest land | - | - | 2 |
| EU | *Eucalyptus globulus* stands | 67 | 799 | 28 |
| CS | Cloud (Shadow) | 33 | 605 | 6 |
| CF | Cloud (Feature) | 92 | 665 | 13 |

Each one of the four images resulting of segmenting the IKONOS image was classified applying the nearest neighbour classifier to a feature space defined by the mean values of IKONOS band 1, 2, 3 and 4, and the ratio of bands 1 and 4. Classification required defining the function slope, with values ranging between 0 and 1; a higher function slope value will result in more classified image objects with less separability (Baatz et al. 2004). IKONOS image classifications were performed using a membership value at standard deviation of 0.2 because, although low function slope values produce more unclassified image objects, they also result in a better classification stability.

The sequence for conducting the supervised classification concluded by evaluating the classification performance (Campbell 2002). An independent sample of 163 areas was used for validation. Ground truth areas were delineated on the image by displaying RGB 321 and 432 band combinations, verifying land cover by using 1:5 000 scale orthophotographs and data from the IFN3. Each area was converted into a point (X,Y) corresponding to the polygon centroid, defined as the geometric centre of the feature (Esri 2004). The land cover class attribute of the polygon was assigned to the centroid. This validation was performed using ERDAS software, because using eCognition™ it is not possible to import points as validation data set. Table 1 shows the number of validation pixels for each land cover class. These validation data were used for calculating the error matrix for each classification and the accuracy assessment statistics. The overall accuracy of each classification, and user's and producer's accuracy for each land cover class were calculated, not only the values, but also the adjusted Wald confidence intervals at 95% confidence level (Sauro and Lewis 2005). It was computed the KHAT statistic (an estimate of Kappa), based on the difference between the actual agreement in the error matrix and the chance agreement (Congalton 1991).

## 5 RESULTS AND DISCUSSION

IKONOS object-oriented classifications achieved overall accuracies between 67% and 77% for 12 target classes (Table 2). Overall accuracy was different depending on segmentation, and the highest accuracy (76.69%) was achieved using a scale parameter of 30. For larger segment sizes, accuracy decreased below 70%. Results using scale parameters of 10 and 30 were similar for the eucalypt class, attaining user's and producer's accuracy ca. 67%. Mapping accuracy was highest using a scale parameter of 100 (75%), but the Kappa analysis (KHAT = 0.41) showed that accuracies were worse than the accuracies that would result from a random assignment, as for the classification using scale parameter of 70. Therefore, segmentations using scale parameters greater than 70 were not recommended for IKONOS classification in this area. These results can be due to the high degree of fragmentation in this landscape. Differences between using a scale parameter of 10 or 30 were very slight, for user's and producer's accuracy considering the eucalypt class.

*Table 2. Comparison of object-oriented IKONOS classifications regarding user's (UA) and producer's (PA) accuracies and KHAT value for eucalypt class and overall values. In brackets: 95% Wald confidence intervals.*

| Scale parameter | *Eucalyptus* stands class (EU) | | | Overall | |
|---|---|---|---|---|---|
| | UA (%) | PA (%) | KHAT | OA (%) | KHAT |
| 10 | 67.86 (49-82) | 67.86 (49-82) | 0.61 | 74.85 (74-87) | 0.72 |
| 30 | 65.52 (47-80) | 67.86 (49-82) | 0.58 | 76.69 (70-84) | 0.74 |
| 70 | 47.22 (32-63) | 60.71 (43-77) | 0.36 | 68.71 (62-76) | 0.65 |
| 100 | 51.22 (36-65) | 75.00 (56-88) | 0.41 | 66.87 (60-75) | 0.63 |

The results agreed with those obtained by Cho (2002), who achieved an overall accuracy of 81.9% (KHAT = 0.8) in an IKONOS image classification using a scale parameter of 25 and a maximum likelihood classifier. Producers' accuracy for forest types ranged from 100.0% to 57.7% and commission error were below 20% for all classes but mixed forests and *Pinus densiflora* (30% and 50%, respectively). The results are better than those achieved by Gomes and Marçal (2003), who revised the 1995 land cover dataset for the Vale do Sousa region (Northwest Portugal) by supervised classification of a multi-spectral image from the ASTER sensor. The landcover classes considered were: urban, water, burned areas, eucalypt forests, mixed forests, hardwood forests, pine forests, uncultivated, and agricultural areas. The segmented image was classified using an algorithm based on fuzzy logic. The average accuracy was 46.3% for the image segmented at Level 1 (smallest objects), 42.2% for Level 2, and 42.9% for Level 3 (largest objects); for eucalypt stands the validation results showed accuracies of 37.0% (segmentation Level 1), 38.9% (segmentation Level 2), 33.3% (segmentation Level 3). The difficulty in discriminating between the four forest land cover classes was mainly due to their spectral similarity. The authors pointed out that the classification of a multi-spectral image segmented into objects should provided more realistic results than treating pixels as individual observations, independently from their neighbourhood, because the pixel was in many cases a too small unit, and its fixed size was also a limitation.

Regarding the number pixels classified for each use, the increase (25%) showed in the number of pixels classified as eucalypt stands (EU) comparing the classifications with scale parameters of 10 and 30 was achieved mainly by means of decreasing the pine plantations area (PI) and broadleaved forest areas (alder (AL) and oak (OA) forest lands). These latter land covers are characterized by their high fragmentation and small size, so when segment size increases, more frequent and more extent uses are favoured (e.g. eucalypt stands). The classifications with scale parameters of 10 and 30 obtained feasible results, such as alder (*Alnus glutinosa*) stands locations near rivers and streams.

Figure 1 compares visually the results of using a scale parameter of 10 and 100 for multi-resolution segmentation; the latter did not gather information with enough accuracy and missed too many details. Thus, this scale parameter is not recommended after the visual analysis, either.

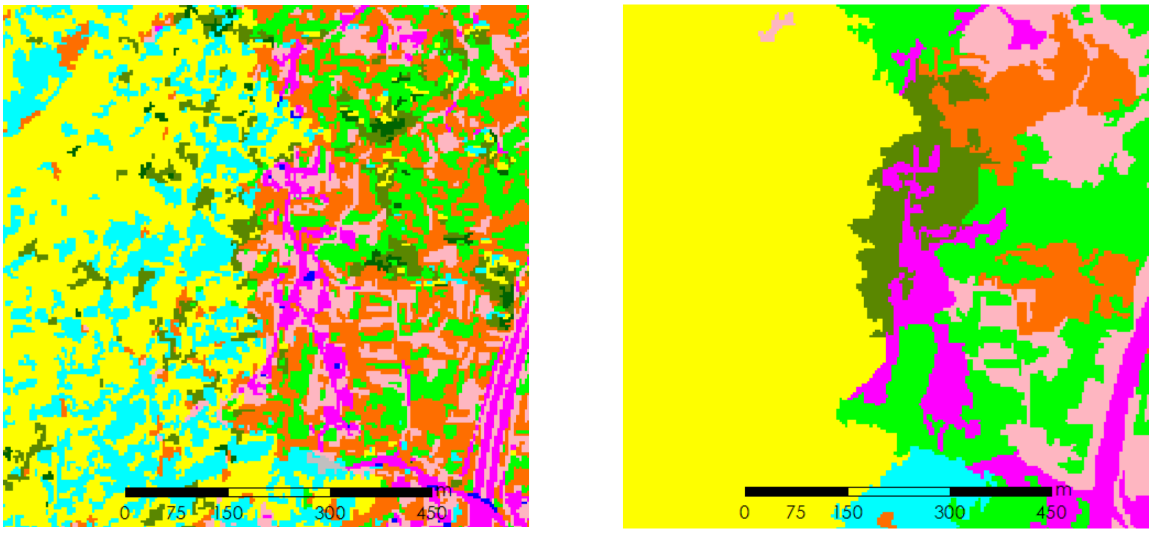


*Figure 1. IKONOS classification output using a scale parameter of 10 (left) and 100 (right) for segmentation.*

The results were compared to those achieved by a pixel-based classification of the same image using the maximum likelihood algorithm in a fuzzy approach (3 x 3 window) (Álvarez 2006). Using the same validation data, it was showed that greater overall accuracy values were achieved by the pixel-based approach. Commission error was significantly lower for pixel-based classification (5.56% vs. 39.29%) for the eucalypt class, while mapping accuracy was higher for the object-oriented approach (67.86% vs. 60.71%). Thus, the object-oriented classification was recommended if it was aimed to minimize omission error. For both methods, commission errors were due to confusion with other forest land uses, mainly broadleaved forests (oak and alder stands); therefore the low separability between these classes had a stronger effect on accuracy than the classification approach. The main reason for the better performance of the per-pixel approach in the target area can be the small size of the parcels and the so fragmented landscape, so that very large objects could not be generated if accurate results wanted to be achieved, because they will not be homogeneous segments. It agrees with Giakoumakis (2002), who found that IKONOS spectral information was sufficient to distinguish some basic land cover classes (water vs. land, vegetation vs. bare land) by means of object-oriented classification, but after a certain stage, spectral identification in these four bands appeared to be the same for particular classes, such as broadleaved trees and grasses, making it difficult to distinguish among them.

## 6 CONCLUSION

It is possible to map accurately and in a timely manner *Eucalyptus globulus* stands in Galicia using IKONOS imagery through object-oriented classification. The accuracy was found to be dependent on the segmentation scale parameter, which is affected by the landscape fragmentation in the target area. According to accuracy reports and map appearance, a scale parameter of 30 is recommended for 4-meter IKONOS imagery in the target area. To improve classification accuracy it is suggested to consider shape and texture characteristics.

## ACKNOWLEDGEMENTS

This research is partially supported by the Research Project PGIDIT03RFO37101PR “I+D da Aplicación de Teledetección e SIX para a caracterización do estado sanitario das masas de *Eucalyptus globulus* en Galicia, con particular aplicación á avaliación dos danos por *Gonipterus scutellatus*” 2003-2005 (Xunta de Galicia).

## REFERENCES

Álvarez, M.F. (2006). Remote sensing and Geoinformation Systems applied to the forest management of *Eucalyptus globulus* stands affected by *Gonipterus scutellatus* in Galicia. PhD Thesis. University of Vigo (Spain). (unpublished)

Baatz, M., Benz, U., Dehghani, S., Heynen, M., Höltje, A., Hofmann, P., Lingenfelder, I., Mimler, M., Sohlbach, M., Weber, M. and Willhauck, G. (2004). User guide 4. eCognition Professional 4.0. Definiens imaging. Munich, Germany.

Bentz, U. C., Hofmann, P., Willhauck, G., Lingenfelder, I. and Heynen, M. (2004). Multi-resolution, object-oriented fuzzy analysis of remote sensing data for GIS-ready information. ISPRS Journal of Photogrammetry and Remote Sensing, 58: 239–258

Campbell, J. B. (2002). Introduction to remote sensing. 3rd Ed. The Guilford Press, New York, USA.

Cho, H. (2002). Untersuchungen über die Erfassung von Walflächen und deren Veränderungen mit Hilfe der Satellitenfernerkundung und segmentbasierter Klassification, Dissertation. Fakultät für Fortwissenschaften und Waldökologie. Georg-August-Universität Göttingen. Germany. pp. 137 (in German).

Congalton, R. G. (1991). A review of assessing the accuracy of classifications of remotely sensed data. Remote Sensing of Environment, 37: 35-46.

Esri (2004). ESRI Software Documentation Library CD, ArcGis. Copyright © 2004 ESRI.

EUspaceimaging (2005). European Space Imaging, Available online at: www.euspaceimaging.com (accessed 30 October 2005).

Franklin, J., Phinn, S., Woodcock, C. L. and Rogan, R. (2003). Rationale and conceptual framework for classification approaches to assess forest resources and properties. In Remote sensing of forest environments: concepts and case studies, M. Wulder and S. Franklin (Eds.), pp. 519, Kluver Academic Publishers, London, UK.

Giakoumakis, M. N., Gitas, I. Z. and San-Miguel, J. (2002). Object-oriented classification modelling for fuel type mapping in the Mediterranean, using LANDSAT TM and IKONOS imagery preliminary results. In Forest Fire Research & Wildland Fire Safety, Viegas (ed.), Millpress, Rotterdam, The Netherlands.

Gomes, A. and Marçal, A. (2003). Land cover revision through object based supervised classification of ASTER data. In Proceedings of the ASPRS 2003 Annual Conference, Anchorage, Alaska, USA.

Gougeon, F. A. (1995). Comparison of possible classification schemes for tree crowns individually delineated on high spatial resolution aerial images. Canadian journal of remote sensing, 21: 1–9.

IFN3 (2001). Tercer Inventario Forestal Nacional, Visor del IFN 3, Versión 1.2.0. Ministerio de Medio Ambiente, Dirección General de Conservación de la Naturaleza, Subdirección General de Montes (CD-ROM). (In Spanish)

Lillesand, T. M. and Kiefer, R. W. (2001). Remote sensing and image interpretation. 4th, Ed. John Wiley & Sons, Inc., New York, USA.

Sauro, J. and Lewis, J. R. (2005). Estimating completion rates from small samples using binomial confidence intervals: comparisons and recommendations. In Proceedings of the Human Factors and Ergonomics Society Annual Meeting (HFES 2005), Orlando, FL, USA.

Song, C., Woodcock, C. E., Seto, K. C., Lenney, M. P. and Macomber, S. A. (2001). Classification and change detection using Landsat TM data: When and how to correct atmospheric effects? Remote Sensing of Environment, 75: 230-244.

Treitz, P., and Rogan, J. (2004). Remote sensing for mapping and monitoring land-cover and land-use change-an introduction. Progress in Plannig, 61: 269-279.

# MAPPING FIRE DEVELOPMENT POTENTIAL USING LANDSAT SATELLITE IMAGERY

*Bahar DINC DURMAZ[1], Ali İhsan KADIOGULLARI[1], Ertuğrul BILGILI[1], Emin Zeki BASKENT[1] and Bülent SAGLAM[2]*

[1] Karadeniz Technical University, Faculty of Forestry, Trabzon, Turkey; b.dinc@ktu.edu.tr, alikadi@ktu.edu.tr, bilgili@ktu.edu.tr, baskent@ktu.edu.tr

[2] Kafkas University, Faculty of Forestry, Artvin, Turkey, bsaglam@ktu.edu.tr

## ABSTRACT

To minimize the threat of loss from wildfires, fire managers must be able to plan protection strategies appropriate for local areas. A prerequisite for this planning is the ability to assess and map, for broad areas, the local potential for a major fire to occur. Using such geospatial information, managers can establish priorities for prevention activities to reduce the risk of wildfire spread and for allocating suppression forces to improve the probability of quickly controlling fires in areas of high concern. The launch of satellite sensors with increased spatial resolution may improve the accuracy and reduce the cost of fire development potential and fuel mapping.

In this study, an attempt was made to develop a Fire Development Potential Index based on cover type, composition, stand closure, stand age, the stage of stand development, slope data and insolation. The required properties are derived from the Normalized Difference Vegetation Index and supervised classification from the Landsat imagery. The Fire Potential Index model is developed to incorporate both satellite and stand type maps produced from interpreted aerial photographs and ground measurements made in 1972, 1987, 1993 and 2001. The index correlates well with fire occurrence and can be used to map fire potential from national to local scales. Application of the fire potential index will be tested in a Mediterranean ecosystem in Turkey. The results of the study will prove useful and serve overall fire management purposes.

**Keywords:** Fire Development Potential, Fire Danger, Fuels, Satellite imagery, GIS, Turkey

## 1 INTRODUCTION

Fuel and fire potential maps are very important tools that land managers use to develop fire management plans (Mutch et. al. 1993; Covington et. al. 1994; Ferry et. al. 1995, Burgan et. al., 1998). These plans identify where fuels and terrain features pose the greatest fire danger, where fires should be allowed to burn, and where they can mostly safely be stopped. Better methods are needed to assess fire potential and risk to more effectively manage natural resources (Hernandez-Leal, P.A., 2005). In this regard, some approaches with a potential embrace the integration of remote sensing and geographic information system's (Keane, et. al. 2001; Falkowski, et. al. 2005, Fassnacht, K., et. al., 2005). Such analyses may have the potential to provide consistent maps of fire development potentials across a diversity of stands developments, silvicultural treatments and topographic features, and a means to update such maps at regular intervals.

Some of the most important factors influencing fire potential and fire behaviour are the type, composition, and distribution of fuels that humans can control (Chuvieco and Congalton, 1989, Bilgili and Saglam, 2003). Other important factors are slope, aspect or insolation of terrain, which modify fire propagation patterns that humans can not interfere. Thus, information about vegetation patterns, change in fire potential over time, and susceptibility to crown fire is highly useful for designing management strategies and fire suppression tactics (Flannigan et. al., 2000). Any mapping of fire danger and fire development potential should be driven by the intended use of data – from broad planning purposes to detailed fire behaviour (Keane et. al., 2003) and portray fire effects posed by a probable fire occurrence across both large geographic areas and for local areas (Burgan et. al., 1998). Methods to assess fire development potential both strategically and tactically must also evolve.

Assessment of fire potential at any scale requires basically the same information about the fuels, topography, and weather conditions that combine to produce the potential fire environment. The objective of this paper is to evaluate the accuracy and utility of LANDSAT imagery coupled with ancillary data for mapping fire development potential. This paper describes and evaluates the method used to spatially predict fire development potential based on inputs depicting stand characteristics (tree species, composition, stage of stand development and crown closure) and topographic features (slope, aspect or insolation). Geographic Information Systems (GIS) was used for greatly improving the capability to assess fire potential at much finer spatial and temporal resolution.

### 1.1 Fuel model maps

Wildland fuels are typically divided into three strata: ground fuels, surface fuels, and crown fuels (Pyne et al., 1996). Most wildland fires start in, and are carried by, surface fuels. Since fuel stratum relationships are extremely complex, fire managers often describe fuels by grouping vegetation communities, However, since the distribution and accumulation of fuels is highly variable (Brown and Bevins, 1986) and highly dependent upon vegetation type, stand history, and disturbance regime (Keane et al., 2001; Brandis and Jacobson, 2003), fuel quantity and distribution are not often directly related to vegetation types (Pyne et al., 1996). Because it is difficult to describe all physical characteristics for all fuels in an area, a generalized description of fuel properties, called a fuel model (Riano et al., 2004; Anderson, 1982), based on similar potential fire behaviour, is often created. Fuel maps are essential to fire management at many spatial and temporal scales. Fuel maps can be generally discriminate four groups: (1) course scale fuel maps, (2) broad area fuel maps, (3) mid-scale or regional-level fuel maps, (4) fine scale or landscape-level fuel maps (Keane et al., 2001). Fine scale or landscape-level fuel maps are essential for local fire management because they also describe fire potential for planning and prioritizing specific burn projects (Chuvieco and Congalton 1989; Pala et al. 1990; Maselli et al. 1996; Keane et al., 2001). More importantly, such maps can be used as inputs to spatially explicit fire growth models to simulate planned and unplanned fires to more effectively manage or fight them (Stow et al. 1993; Hardwick et al. 1996; Gouma and Chronopoulou-Sereli 1998; Grupe 1998; Keane et al. 1998)

### 1.2 Remote sensing of fuel mapping

The inability of optical sensors such as Landsat TM and multi-spectral scanner (MSS) to penetrate the forest canopy (Miller et al., 2003, Crouse, J.E.,and Fulé, P.Z., 2003, Andersen, H.E., et. al. 2005) limits their utility for mapping surface fuels where tree canopies are present (Keane et al., 2000). As a result, most studies using remote sensing to characterize surface fuels first classify an image into vegetation categories, then assign fuel types or fuel models to each category (Keane et al., 2001, Hernandez-Leal, P.A., 2005). Chuvieco and Salas (1996) characterized fuel types through the classification of Landsat TM data. Chuvieco and Congalton (1989) and Castro and Chuvieco (1998) used similar methods to map fuel types in Spain and Chile, respectively. Wilson et al. (1994) applied maximum likelihood decision rules to a Landsat MSS image to directly classify fuel types across Wood Buffalo National Park, Canada. Riano et al. (2002) improved a fuel type classification by incorporating two seasonal Landsat TM images into a classification algorithm to account for phenological differences in vegetation. Remotely sensed hyperspectral data have also been used to map fuel types and vegetation moisture content for a chaparral community in Southern California (Roberts et al., 1998; Roberts et al., 2003,).

Convolved surface and crown spectra are difficult to decouple. Also, it is difficult to train spectral classifications to discriminate between surface and crown fuel types in forests because the sensor cannot see the forest floor (Belward et al. 1994). As a result, image classifications often differentiate vegetation characteristics rather than fuel attributes. Another disadvantage is that few fuel classifications integrate all fuel components into one model. Robust fuel models and classifications that will be useful to many mapping efforts are badly needed for comprehensive fuel mapping activities.

## 2 DATA AND METHODOLOGY

The map of FDP is a digital cartography of fire danger based on stand and topographic features in a specific region. FDP Index model was developed to incorporate both satellite and surface observations in an index that correlates welt with fire occurrence and that can be used to map fire potential from national to local scales through the use of a GIS.

The variables that have been considered in the generation of fire development potential index are: stand composition, stand crown closure, the stage of stand development, slope, insolation. Using specific modules like the gradient operator, maps of slope and insolation can be defined. The higher the values adopted by the variables, the higher the danger of fire. So, for humidity and temperature values, upper altitude regions have a higher danger than lower ones. On the other side, the areas with a high slope do not have intrinsically a higher risk of fire but in case of an ignition event, flames can quickly spread, representing an additional factor of danger. As for the insolation, the areas facing south suffer a greater water stress than the rest, and as a consequence it results in an increase in the probability of a fire occurrence and fire spread.

*Table 1: Weights and ratings assigned to variables and classes for forest fire development potential modelling*

| Serial No | Variables | Classes | | Value Assigned | Fire Potential |
|---|---|---|---|---|---|
| 1 | Stand composition | (1) Calabrian pine + black pine | | 10 | Very High |
| | (weight = 10) | (2) Scots pine | | 7 | High |
| | | (3) Beech+Fir | | 4 | Moderate |
| | | (4) Oak + Coppice | | 6 | Moderate |
| | | (5) Agriculture | | 2 | Low |
| | | (6) Settlement | | 1 | Low |
| 2 | Stand crown closure | (7) Bare Land | | 1 | Low |
| | (weight = 9) | (8) % 11- % 40 | | 5 | Moderate |
| | | (9) % 41- % 70 | | 8 | High |
| | | (10) % 71> | | 10 | Very High |
| 3 | The stage of stand development (weight = 10) | (11) (a) regenerated -average dbh: < 8 cm | | 10 | Very High |
| | | (12) (a) regenerated and (b) young - average dbh: < 0 – 8 and 8 – 19,9 cm | | 10 | Very High |
| | | (13) (b) young - average dbh: 8 – 19,9 cm | | 9 | High |
| | | (14) (b) young and (c) mature - average dbh: 8 – 19,9 cm and 20 – 35,9 cm | | 7 | Moderate |
| | | (15) (c) mature - average dbh: 20 – 35,9 cm | | 6 | Moderate |
| | | (16) (c) mature and (d) overmature - 20 – 35,9 cm >36 cm | | 4 | Low |
| | | (17) (d) overmature - average dbh: >36 cm | | 3 | Low |
| 4 | Slope | (18) 0 – 3 % | | 2 | Low |
| | (weight = 5) | (19) 3 – 5 % | | 3 | Moderate |
| | | (20) 5 – 10 % | | 4 | Moderate |
| | | (21) 10 – 15 % | | 5 | High |
| | | (22) 15 – 35 % | | 6 | Very High |
| | | (23) > 35 % | | 10 | Very High |
| 5 | Insolation | (24) 0- 23 | N | 1 | Low |
| | (weight = 3) | (25) 23- 68 | NE | 2 | Moderate |
| | 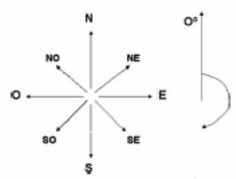  | (26) 68 -113 | E | 3 | Moderate |
| | | (27) 113 – 158 | SE | 4 | High |
| | | (28) 158 – 203 | S | 8 | Very High |
| | | (29) 203 – 248 | SW | 4 | High |
| | | (30) 248 – 293 | W | 3 | Moderate |
| | | (31) 293 – 338 | NW | 2 | Moderate |
| | | (32) 338 – 360 | N | 1 | Low |

*Table 2: Criterion-based analysis for forest fire development potential zoning*

| Stand composition weighting Category (SC) | Stand crown closure weighting Category (C) | Stage of stand development weighting Category (SD) | Slope weighting category (*S*) | Insolation weighting category (IS) | Forest fire development potential category | Fire Development Potential index * |
|---|---|---|---|---|---|---|
| $V_{10}$ | $V_{10}$ | $V_{10}$ | $V_{10}$ | $V_8$ | Very High | 364 |
| $V_7$ | $V_8$ | $V_9$ | $V_6$ | $V_4$ | Very High | >274 |
| $V_6$ | $V_5$ | $V_7$ | $V_5$ | $V_3$ | High | >209 |
| $V_4$ | $V_1$ | $V_4$ | $V_4$ | $V_3$ | Moderate | >118 |
| $V_2$ | $V_1$ | $V_3$ | $V_2$ | $V_1$ | Low | <=118 |

Subscript: SC: Stand composition, C: Stand crown closure, SD: the development stage of stand, S: slope factor, IS: Insolation factor. Letter: V: very high, H: high, M: moderate, L: low.
*$10SC_i$=1–6+9$C_j$=1–4 + 10S$D_k$=1–7 + 5$S$=1–6 + 3ISm=1-9

On the other hand, structure and fuel loading can dramatically change fire danger and potential. The accumulation of crown and surface fuel increases depending on stand age and development. (Chao Li vd., 1996; Boychuk vd., 1997, Bilgili, E., 2003). The increasing fuel accumulation and stand crown closure in relation to stand development determine fire spread and intensity. The differences in stand structure and ignition probability of a stand produce different fire behaviour (Van Wilgen, 1990, Bilgili ve Sağlam, 2003, Bilgili, E., 2003) and, thus, differences in the probability of fire hazard and fire spread. Based on stand fuel characteristics, factors affecting the FDP in an area were analyzed. Having determined the influence of each factor on forest FDP, the different classes of each factor were given suitable ratings. A higher rating indicates that the factor has a high degree of influence on the FDP in an area. The considered factors were then integrated for calculating the forest FDP index (Table 1). The different classes in the thematic maps were labelled separately based on their sensitivity to forest fire as very high, high, moderate or low. Then suitable weights were assigned (Table 1).

The equation used in a GIS for the fire development potential modeling and for mapping the fire development potential areas is: FDP =$10SC_i$=1–6+9$C_j$=1–4 + 10S$D_k$=1–7 + 5$S_n$=1–6 + 3I$S_m$=1-9 where FDP is the numerical rating of fire development potential, SC Stand composition (with 1–6 classes), C stand crown closure (1–4 classes), SD the stage of stand development (1–7 classes), S slope factor (1–6 classes) and, IS insolation factors (1–9 classes). The subscripts i, j, k, m, n indicate subclasses based on a relative importance in determining fire potential. Finally, criterion-based analysis (Table 2) was carried out to create the fire development potential zone map showing different categories (Figure 2).

## 2.1 Study area

Inegöl is in a sub-temperate forest land covering an area of 175,000 ha along the coast of Sea of Marmara (692848–742684 E, 4415460-4473973 N, UTM ED50 datum Zone 35N) (Figure 1). The altitude varies between 100 and 2500 m above sea level with an average slope of 17%. The vegetation is composed of tree species of Pinus brutia, Pinus silvestris, Pinus nigra, Fagus orientalis, Quercus and an orchard species of Peach.

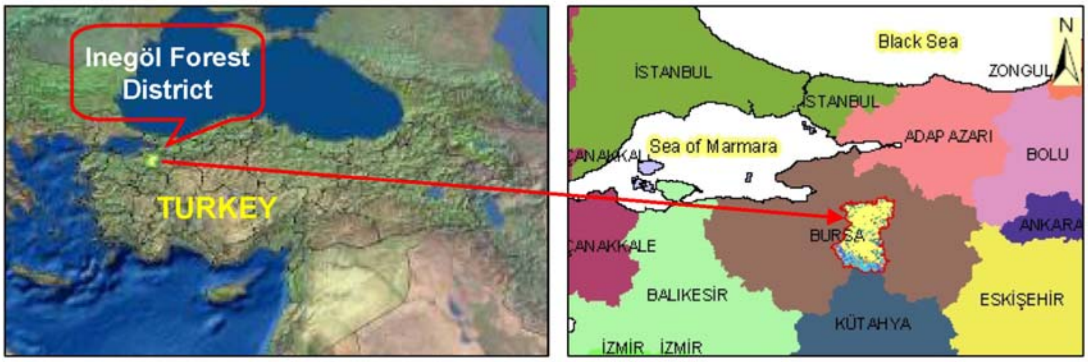


*Figure 1. The geographic location of the study area surrounded with solid red lines.*

### 2.2 Geometric Correction of Landsat Images and Digitizing Stand Type Maps

Subsets of satellite images were rectified using 1:25,000 scale Topographical Maps with UTM projection (ED 50 datum) using first order nearest neighbor rules. A total of 27 ground points were used to register the ETM image subset with the rectification error of less than 1 pixel. The TM images, however, were registered to the already registered ETM images through image-to-image registration technique with rectification errors of less than 0.5 pixels.

### 2.3 Data analysis

To determine the change spatially of fire development potential, we used stand type maps for the years 1972 and 1993 and Landsat images for the years 1987 and 2001. Stand crown closure and the stage of stand development were obtained from stand type maps for all years, in that discrimination of stand crown closure and the stage of stand development could not be measured from the images available at the level of acceptable accuracy.

## 3 RESULT AND DISCUSSION

Most fire danger rating systems use the input data - fuel maps, terrain, and weather data. Using the Inegöl Forest District, Bursa, Southwestern Turkey as an example, the study discusses how fire development potential maps can be created using cover type, composition, tree crown closure, the stage of stand development, slope data, and insolation focusing specifically on estimated fire spread rate and intensity.

Fire development potential (FDP) maps are shown in Figure 2. The maps were generated for the years 1972, 1987, 1993 and 2001 in Inegöl Forest District. These maps reflect fire danger potential and the estimation of total area that could possibly be affected by fires. Table 3 lists fire development potential areas in each fire potential category for the years 1987 and 2001 using Landsat images and for the years 1972 and 1993 using stand type maps.

According to forest management plan maps, change between 1972 and 1993 favored forest areas too with a net increase of 3.3% of landscape. Similarly, land cover type change between 1987 and 2001 favored the forested areas about 7% of landscape. When the forest dynamics area evaluated in terms of crown closure, between 1972 and 1993 years, sparsely covered areas increased 1118 ha and medium coverage areas increased 6288 ha while fully covered areas decreased 1526 ha. Additionally, increased afforestation, open areas decreased and residential areas increased because of demographic change. This Land cover change show that fire potential of İnegöl landscape increased between 1972 and 2001 years (Table 3).

Fuel maps are difficult to create because of the obstruction of the forest canopy, limitations of remote sensing products, high variability of fuels, and of the difficulty of the construction of fuel models. Four approaches were used to map fuels but none appear highly accurate or consistent. A possible strategy for mapping fuels with current technology involves assigning fuel models to combinations of three classifications that describe species composition, and stand structure. Future technologies for mapping fuels need to meld all approaches to create the most useful maps, but other remote sensing technologies are still needed. Sensor technology that penetrates the forest canopy and senses ground complexity is needed for accurate mapping of crown and surface fuels. Ecosystem simulation modeling will play an important role in quantifying those gradients responsible for fuel distributions to aid in image classification, ecological understanding, and fuels map revision and refinement.

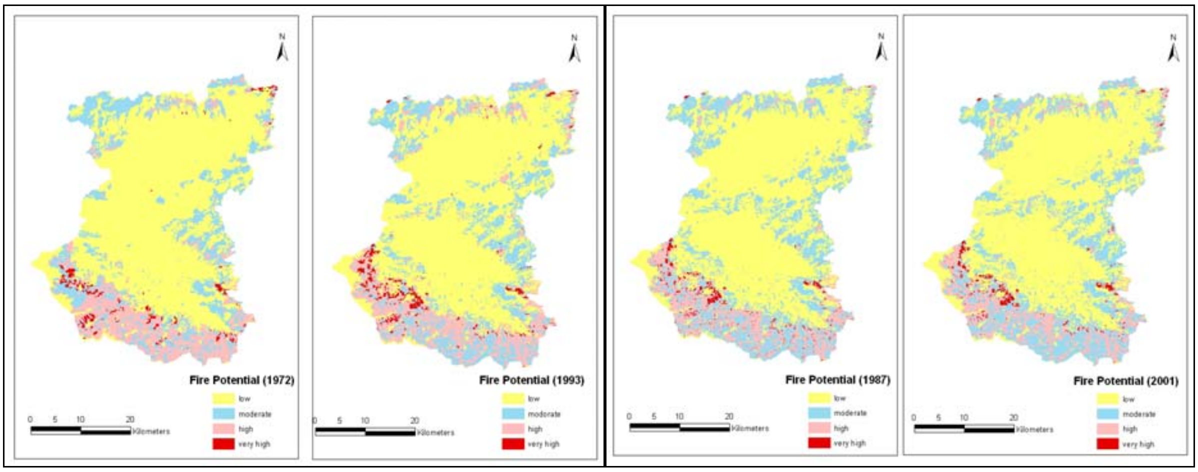


(a) (b) (c) (d)

*Figure 2: Fire development potential maps for Inegöl Forest District (a) during 1972 using stand type maps, (b) during 1993 using stand type maps, (c) during 1987 using Landsat imaging, (d) during 2001 using Landsat imaging*

*Table 3: Total areas of forest fire development potential in each fire potential category in the study area using Landsat image (1987 and 2001) and stand type maps (1972 and 1993)*

| Fire development potential | The stand type map in 1972 (ha) | The stand type map in 1993 (ha) | Landsat Image in 1987 (ha) | Landsat Image in 2001 (ha) |
|---|---|---|---|---|
| Low | 117882 | 112006 | 111032 | 108453 |
| moderate | 32981 | 35713 | 43448 | 45595 |
| High | 24468 | 26856 | 20962 | 21497 |
| Very high | 2503 | 3221 | 2355 | 2252 |

## 4 CONCLUSION

A model for a FDP Index has been proposed as a tool for effective fire management planning. Maps depicting fuel characteristics are essential to fire and land management at many scales because they can be used to compute fire hazard, risk, behavior, and effects for planning and real time applications. Collectively, these analyses are designed to provide information for managers that will help them in developing their Fire Management Plan. The resulting maps provide fine-grained, broad-scale information to spatially assess fire hazards and wildland fire potential when making decisions about how best to protect forests of Mediterranean ecosystems in Turkey.

## REFERENCES


Andersen, H.E., McGaughey, R.J., Reutebuch, S.E. 2005, Estimating forest canopy fuel parameters using LIDAR data, Remote Sensing of Environment 94 (2005) 441–449

Anderson, H.E., 1982. Aids to determining fuel models for estimating fire behavior. US Department of Agriculture Forest Service, Intermountain Research Station, Ogden, UT. General Technical Report, INT-122, pp. 1–22.

Bilgili, E., 2003. Stand Development and Fire Behavior, Forest Ecology and Management 179, 333-339.

Bilgili, E. ve Sağlam, B., 2003. Fire Behavior in Maquis in Turkey, Forest Ecology and Management 184, 201-207.

Chuvieco E, Congalton RG (1989) Application of remote sensing and geographic information systems to forest fire hazard mapping. Remote Sensing of the Environment 29, 147–159.

Covington WW, Everett RL, Steele R, Irwin LL, Daer TA, Auclair AND (1994) Historical and anticipated changes in forest ecosystems of the Inland West of the United Stages. Journal of Sustainable Forestry 2(1/2), 13–63.

Crouse, J.E., Fulé, P.Z., 2003. Species and canopy cover map development using Landsat 7 Enhanced Thematic Mapper Imagery for Grand Canyon National Park. In: Proceedings of the Ninth Forest Service Remote Sensing Applications Conference. USDA Forest Service/American Society for Photogrammetry and Remote Sensing (electronic publication).

Falkowski, M. J.; Gessler, P. E.; Morgan, P.; Hudak, A.T.; Smith, A.M.S. (2005) Characterizing and mapping forest fire fuels using ASTER imagery and gradient modeling, Forest Ecology and Management xxx (2005) xxx–xxx, FORECO-9377; No of Pages 18

Ferry GW, Clark RG, Montgomery RE, Mutch RW, Leenhouts WP, Zimmerman GT (1995) Altered fire regimes within fire-adapted ecosystems. 'Our Living Resources: a report to the nation on the distribution, abundance, and health of U.S. plants animals, and ecosystems.' pp. 222–224. (USDI National Biological Survey: Washington, D.C.)

Flannigan, M.D., Stocks, B.J., Wotton, B.M., 2000. Climate change and forest fires. Sci. Total Environ. 262, 221–229.

Fassnacht, K.S., Cohen, W.B., Spies, T.A., 2005, Key issues in making and using satellite-based maps in ecology: A primer, Forest Ecology and Management xxx (2005) xxx–xxx, FORECO-9509; No of Pages 15

Gouma V, Chronopoulou-Sereli A (1998) Wildland fire danger zoning—a methodology. International Journal of Wildland Fire 8(1), 37–43. Grossman DH, F

Grupe MA (1998) Assessing the applicability of the Terrestrial Ecosystem Survey for FARSITE. Master's Thesis, University of New Mexico, Albuquerque, New Mexico, 95 pp.

Hardwick PE, Lachowski H, Forbes J, Olson R, Roby K, Fites J (1996) Fuel loading and risk assessment for Lassen National Forest. In 'Proceedings of the seventh Forest Service remote sensing applications conference. Nassau Bay, Texas, 6–10 April 1998'. (Ed. JD Greer) pp. 328–339. (American Society for Photogrammetry and Remote Sensing: Bethesda, MD)

Hernandez-Leal, P.A., M. Arbelo, M., Gonzalez-Calvo, A., 2005, Fire risk assessment using satellite data, Advances in Space Research xxx (2005) xx

Keane, R. E., Burgan, R. and Wagtendonk J.V., (2001) Mapping wildland fuels for fire management across multiple scales: Integrating remote sensing, GIS, and biophysical modeling, International Journal of Wildland Fire, 2001, 10, 301–319

Keane RE, Long DG, Schmidt KM, Mincemoyer S, Garner JL (1998) Mapping fuels for spatial fire simulations using remote sensing and biophysical modeling. In 'Proceedings of the seventh Forest Service remote sensing applications conference. Nassau Bay, Texas, 6–10 April 1998'. (Ed. JD Greer) pp. 301–316. (American Society for Photogrammetry and Remote Sensing: Bethesda, MD)

Keane, R.E., Finney, M.A., 2003. The simulation of landscape fire, climate, and ecosystem dynamics. In: Veblen, T.T., Baker, W.L., Montenegro, G., Swetnam, T.W. (Eds.), Fire and Climatic Change in Temperate Ecosystems of the Western Americas. Springer, New York, pp. 32–68.

Maselli F, Rodolfi A, Bottai L, Conese C (1996) Evaluation of forest fire risk by the analysis of environmental data and TM images. International Journal of Remote Sensing 17(7), 1417– 1423

Mutch RW, Arno SF, Brown JK, Carlson CE, Ottmar RD, Peterson JL (1993) Forest health in the Blue Mountains: A management trategy for fire-adapted ecosystems. USDA Forest Service General Technical Report PNW-GTR-310. 14 pp.

Pala S, Taylor D, Holder G (1990) Integrating satellite-derived forest fuel data into fire management decision support models. Proceedings, 2nd National GIS conference, Ottawa, 5–8 March 1990.

Pyne, S.J., Andrews, P.L., Laven, R.D., 1996. Introduction to Wildland Fire. John Wiley & Sons Inc., New York, pp. 1– 769.

Riano, D., Chuvieco, E., Condes, S., Gonzalex-Matesanz, J., Ustin, S., 2004. Generation of crown bulk density for Pinus sylvestris L. from lidar. Rem. Sens. Environ. 92, 345–352.

Stow D, Hope A, McKinsey D, Pray H (1993) Deriving dynamic information on fire fuel distributions in southern Californian chaparral from remotely sensed data. Landscape and Urban Planning 24, 113–127.

Van Wilgen, B.W., Higgins, K.B. ve Bellstedt D.U., 1990, The Role of Vegetation Structure and Fuel Chemistry in Excluding Fire from Forest Patches in the Fire-Prone Fynbos Shrublands of South Africa, Journal of Ecology, 78, 210-222.

# EVALUATING MODIS SATELLITE VERSUS TERRESTRIAL DATA DRIVEN NPP-ESTIMATES IN AUSTRIA

*Richard Petritsch[1], Céline Boisvenue[2], Hubert Hasenauer[3] and Steve Running[4]*

[1] University of Natural Resources and Applied Life Sciences, Department of Forest- and Soil Sciences, Vienna, Austria; richard.petritsch@boku.ac.at

[2] University of Montana, Numerical Terradynamic Simulation Group, Missoula, US; celine@boisvenue.com.

[3] University of Natural Resources and Applied Life Sciences, Department of Forest- and Soil Sciences, Vienna, Austria; hubert.hasenauer@boku.ac.at.

[4] University of Montana, Numerical Terradynamic Simulation Group, Missoula, US; swr@ntsg.umt.edu.

## ABSTRACT

Sensors, such as the Moderate Resolution Imaging Spectroradiometer (MODIS) on NASA's Terra satellite, are developed for monitoring global and/or regional NPP. Although these systems should allow us to assess carbon sequestration issues, forest management impacts, etc., relatively little is known about the consistency and accuracy in the resulting satellite driven estimates versus production estimates driven from ground data. In this study we compare the following NPP estimation methods: (i) NPP estimates as driven from the MODIS satellite and available on the internet; (ii) estimates resulting from the off-line version of the MODIS algorithm and DAO meteorological data; (iii) estimates using regional meteorological data within the offline algorithm; and (iv) NPP estimates from a species specific biogeochemical ecosystem model adopted for Alpine conditions. All these results are compared with 624 forested sites across Austria during 2000 to 2003. 144 of the 624 locations were previously used in a validating effort to produce species-specific parameter estimates of the ecosystem model. The remaining 480 sites are from the Austrian National Forest Soil Survey and include soils, humus as well as forest growth information. Georeferences for each site in latitude and longitude were used to calculate the three satellite-based NPP estimates prior to the calculation of the two ground-based estimates, ensuring the independence of the satellite-driven NPP estimates from the ground-based predictions. All five estimates are compared in pairs and the linear association between each of them is evaluated by correlation analysis.

**Keywords:** Forest production, NPP, ecosystem modeling, MODIS

## 1 INTRODUCTION

Global monitoring of net primary production (NPP) is needed for the purposes of evaluating trends in biospheric behaviour (Nemani et al., 2003), understanding the role of the biosphere in the global carbon cycle, and investigating large-scale patterns in food and fiber production (Running et al., 2004). Sensors, such as the Moderate Resolution Imaging Spectroradiometer (MODIS) on NASA's Terra satellite, are being used for monitoring global NPP. Forests play a large role in the global carbon cycle, and they are already responding to global climate and atmospheric changes (Boisvenue & Running, 2006). Forest NPP, however, cannot be directly measured, it must be inferred even for on-site estimates. Reliable and globally available estimates of NPP at a site level would be a large contributor to decisions leading to sustainable forest management and would support monitoring of carbon sequestration amid forest management practices. Comparisons of satellite-based estimates of biosphere production from the MODIS sensor, which are globally available, to ground-based estimates have already taken place (e.g, Heinsch et al., 2006). Most of these evaluations, however, are for global or regional application. In this study we introduce the concept for comparing five forest NPP estimation methods on 624 sites across Austria over four years (2000 to 2003) and assess the site applicability of MODIS estimates.

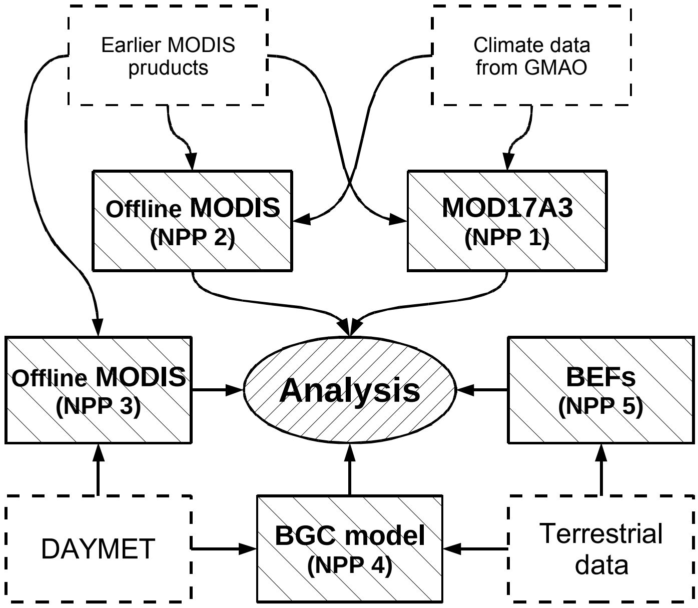


*Figure 1: Overview of the proposed analysis.*

# 2 METHODS

## 2.1 Satellite estimates

The MODIS NPP algorithm developed by NTSG at the University of Montana derives annual NPP from GPP estimates. The GPP algorithm in MODIS is based on Monteith (1977) relating gross photosynthesis to the amount of photosynthetically active radiation (PAR) absorbed by biomass. GPP estimates require meteorological data which, for the MODIS products available on the web, are retrieved from NASA's Global Modeling and Assimilation Office (GMAO). Daily GPP, and subsequently annual NPP, are then calculated for a 1km X 1km pixel (see Heinsch et al., 2003, for details). An in-house off-line version of the MODIS (GPP & NPP) algorithm uses a slightly different compilation algorithm than the on-line one but permits the use of local meteorological data.

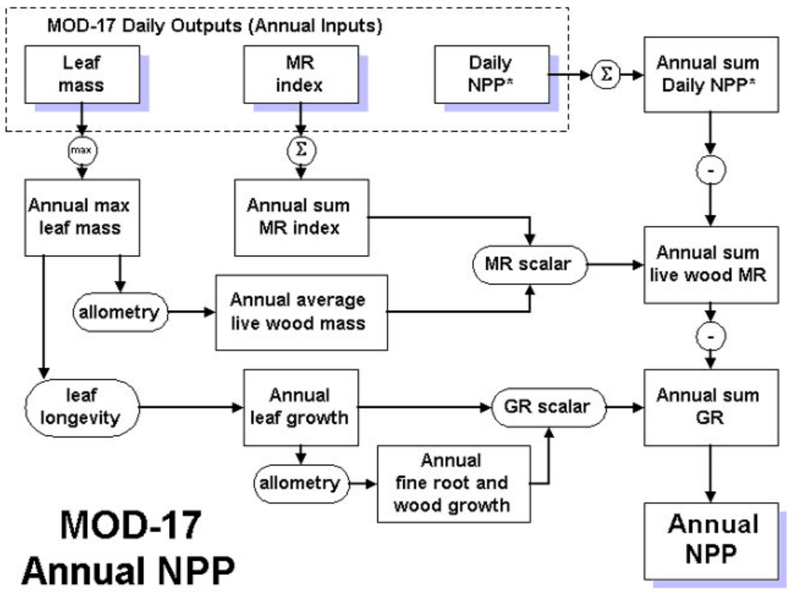


*Figure 2: Overview of the performed tasks within the MOD17A3 algorithm.*

- **NPP 1:** Our first NPP estimate is from MODIS available on the web. It is based on Collection 4.5 MODIS NPP (MOD17A3) data available from the NTSG anonymous ftp site (ftp.ntsg.edu/pub/MODIS) and caculated on average per hectare value.
- **NPP 2:** Our second estimate results from the off-line algorithm together with GMAO meteorological data.
- **NPP 3:** The third estimate uses the off-line algorithm and climate data estimated by the Austrian version of DAYMET (Hasenauer et al., 2003).

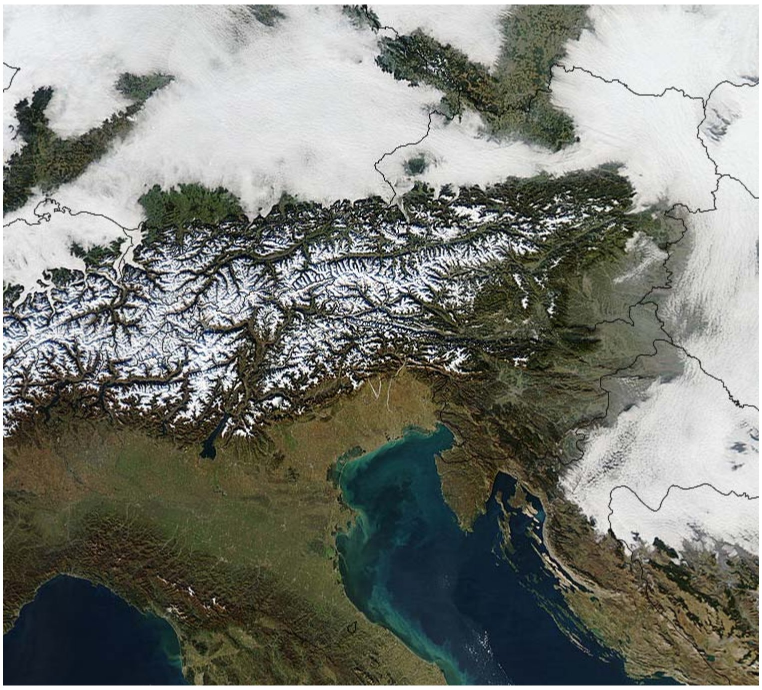

*Figure 3: MODIS snapshot showing the Eastern Alps (Austria together with Switzerland and Northern Italy).*

## 2.2 Terrestrial estimates

Daily climate data essential for the application of the BGC model were interpolated using the Austrian version of DAYMET (Hasenauer et al., 2003) based on climate stations provided by ZAMG. Values for nitrogen deposition are taken from literature (see Schneider, 1998 for current and Holland et al. 1999 for pre-industrial values respectively).

Forest soil and stand data come from the Austrian National Forest Soil Survey (WBZI). Appropriate biomass function can be found in the literature (e.g. Zianis et al., 2005) which relate total biomass to tree-level measurements common in forest inventories. They will be tested for their suitability as part of the analysis. If necessary growth and yield models (see Hasenauer, 2005 for an overview) can be used to extrapolate tree-level measurements for the period 2000 to 2003.

- **NPP 4:** Biome-BGC Version 4.1.1 (Thornton et al., 2002) with extensions (Pietsch et al., 2003), species-specific parameters (Pietsch et al., 2005) and daily climate data from DAYMET.
- **NPP 5:** allometric equations and single tree data from WBZI for biomass estimation and subsequent conversion of biomass to carbon (NPP) for each site.

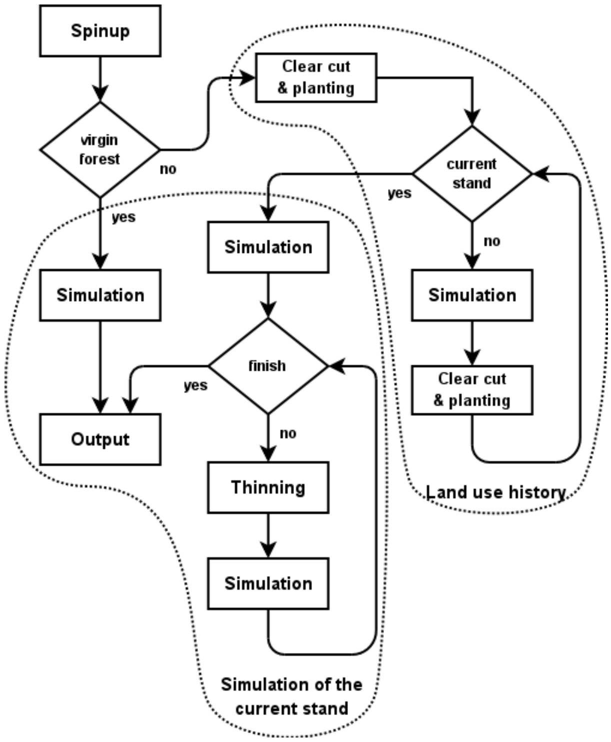


*Figure 4: Flow diagram of a typical simulation run with the BGC model.*

### 2.3 Climate data

Daily surface global climatology on a 6-hour timestep is provided by the NASA's GMAO. This data is derived using a glocal circulation model (GCM) based on both satellite and terrestrial observations. It is distributed at a coarse resolution (1° by 1.25°) but assumed to be constant within a pixel, so that it can easily be scaled to the 1km by 1km resolution used by MODIS.

DAYMET on the other hand interpolates climate variables based on terrestrial measurements. It was applied globally (see Thornton et al., 1997) but also validated for Austrian purposes (Hasenauer et al., 2003). It uses a least squares regression technique based on a 3D Gaussian filter to interpolate surface minimum and maximum temperature as well as precipitation. Incident solar radiation together with vapor pressure is derived from temperatures and precipitation using the algorithm described in Thornton et al. (2000).

## 3 ANALYSIS

Once all necessary calculations are completed, pair-wise correlation analyses will be used to evaluate the linear association among our five estimates. Individual years will also be analysed separately to assess the effects of inter-annual climate variations on NPP estimates. Of interest is the contribution of each of these estimates to the underlying site NPP (actual NPP). A site's actual NPP can be seen as a latent variable - a variable that cannot be directly measured. An analysis of the multivariate covariance character of the data (such as a confirmatory factor analysis) can tell us how much each of our five surrogate measures contributes to the variation they have in common, which is assumed to be a part of the actual underlying NPP. A confirmatory factor analysis will be completed to evaluate the contribution of each of our estimates to their common data structure.

## 4 DISCUSSION

It is important to notice that NPP1,2 are purely satellite derived estimates, while NPP 3 comes from satellite data supported by terrestrial measurements. The difference between NPP 1 and 2 represents the improvements due to the off-line algorithm. NPP 3 differs from NPP 2 in using climate data from surrounding stations. Thus an analysis of two common MODIS improvements can also be obtained within this concept.

NPP 4 uses a process model based on generally available site data and NPP 5 is a completely statistical approach using site data. These terrestrial approaches do not rely on any satellite-based measurements.

## REFERENCES

Hasenauer, H. 2005: (ed.) Sustainable Forest Management: Growth models for Europe. Springer, Berlin, 398p.

Hasenauer, H., Merganičová, K., Petritsch, R., Pietsch, S.A. and Thornton, P.E. (2003): Validating daily climate interpolations over complex terrain in Austria. Agric. & For. Met. 119: 87-107.

Heinsch, F. A., Zhao, M., Running, S. W, Kimball, J. S., Nemani, R. R. and Davis, K. J. (2005): Evaluation of remote sensing based terrestrial productivity from MODIS using tower eddy flux network observations. IEEE Transactions on Geoscience and Remote Sensing, (in press).

Holland, E.A., Dentener, F.J., Braswell, B.H. and Sulzman, J.M. (1999): Contemporary and pre-industrial global reactive nitrogen budgets. Biogeochemistry 46: 7-43.

Nemani, R.R., Keeling, C.D., Hashimoto, H., Jolly, W.M., Piper, S.C., Tucker, C.J., Myneni, R.B. and Running, S.W. (2003): Climate-Driven Increases in Global Terrestrial Net Primary Production from 1982 to 1999. Science 300: 1560-1563.

Monteith, J. L. (1977): Climate and efficiency of crop production in Britain. Philosophical Transactions of the Royal Society of London. B 281, 277– 294.

Pietsch, S.A., Hasenauer, H., Kučera, J. and Čermák, J. (2003): Modeling effects of hydrological changes on the carbon and nitrogen balance of oak in floodplains. Tree Physiology 23: 735-746.

Pietsch, S.A., Hasenauer, H. and Thornton, P.E. (2005): BGC-model parameters for tree species growing in central European forests. Forest Ecology and Management 211: 264-295.

Running, S.W., Nemani, R.R., Heinsch, F.A., Zhao, M., Reeves, M. and Hashimoto, H. (2004): A Continuous Satellite-Derived Measure of Global Terrestrial Primary Production. BioScience 54(6): 547-560.

Schneider, J. (1998): Kartierung der nassen Deposition in Österreich. Umweltbundesamt Wien, 24p.

Thornton, P.E., Running, S.W. and White, M.A. (1997): Generating surfaces of daily meteorological variables over large regions of complex terrain. Journal of Hydrology 190: 214-251.

Thornton, P.E., Hasenauer, H. and White, M.A. (2000): Simultanous estimation of daily solar radiation and humidity from observed temperature and precipitation: an application over complex terrain in Austria. Agricultural and Forest Meteorology 104: 255-271.

Thornton, P.E., Law, B.E. and Ellsworth, D.A. (2002): Modeling and measuring the effects of disturbance history and climate on carbon and water budgets in evergreen needleleaf forests. Agricultural and Forest Meteorology 113: 185–222.

Zianis, D., Muukkonen, P., Mäkipää, R. and Mencuccini, M. (2005): Biomass and stem volume equations for tree species in Europe. Silva Fennica Monographs 4, 63 p.

# REMOTE SENSING OF FOREST PARAMETERS DESCRIBING THE PROTECTION EFFICIENCY OF FORESTS IN ALPINE AREAS

*Alfred Pitterle[1], Helmut Fuchs[2], Tatjana Koukal[2] and Werner Schneider[2]*

[1] forCERT – Forest Certification GmbH, Mauerbach, Austria; alfred.pitterle@for-cert.com

[2] University of Natural Resources and Applied Life Sciences (BOKU), Department of Landscape, Spatial and Infrastructure Sciences, Institute of Surveying, Remote Sensing and Land Information, Vienna, Austria; helmut.fuchs@boku.ac.at, tatjana.koukal@boku.ac.at, werner.schneider@boku.ac.at

## ABSTRACT

Forests perform various functions and provide various products and services. This paper concentrates on the protective function of forests. Some different scientific, technical, organisational, administrative and legal theories, methods and tools are available for dealing with protective functions of forests. These theories, methods and tools include expert knowledge on the mechanisms of hazards, terrestrial inventories and remote sensing, GIS analysis and spatial modelling, certification methods, hazard zoning and others.

In this paper, remote sensing is considered as the main data source for identifying and quantifying the protective functions of forests within a forest certification system. FOMUMIIS® (Forest Multiple Use Measurable Indicator Identification System) is a scientific method and a software- and GIS-based tool to process the information necessary for certification of forest products and services. It has been developed to meet requirements of international forest policy and is suitable for application to all forest types and products/services at all scales from the local to the global level.

The protection efficiency of forests depends on the type of hazard, on site conditions such as slope angle and length, soil type and depth, a.o. and on the properties/qualities of the forest, which can be described by a number of parameters. These parameters can partly be summarised and integrated to the categorical parameter "forest development phase". So the protection efficiency of forests differs from phase to phase. Beside site information, a series of remote sensing techniques are available for collecting information on forest parameters relevant for protection efficiency. These techniques are listed here and ranked according to their significance for describing the various forest parameters and according to their costs.

## 1 INTRODUCTION: INFORMATION REQUIREMENTS

Forestry provides not only timber and wood products: Forests perform various functions and provide various services and products including also non-wood products. The list of important forest functions and services comprises, amongst others, the provision of wildlife habitats for maintaining biodiversity, the allocation of areas important for recreation and tourism, contributions to carbon sequestration, to water conservation and soil conservation, and, last but not least, various protective functions such as rockfall protection, landslide protection, avalanche protection and erosion control.

While this is generally recognised since a long time, it is only in recent years that these functions and services are seen in the context of a market-based economic system. In such a system, where the goods and services have to be distinctly identified and quantified for a transparent allocation of costs, one needs reproducible, traceable, confirmable information on the individual forest functions and on the expenses to maintain them. This information is needed in a spatially explicit form.

This paper concentrates on the protective function of forests. Various scientific, technical, organisational, administrative and legal theories, methods and tools are available for dealing with protective functions of forests. These theories, methods and tools include expert knowledge on the mechanisms of hazards, terrestrial inventories and remote sensing, GIS analysis and spatial modelling, certification methods, hazard zoning etc. In the following, remote sensing is considered as the main data source for identifying and quantifying the protective functions of forests within a forest certification system.

## 2 FOREST CERTIFICATION

Certification of a product or a service denotes the documentation of evidence that the product or service is suitable for a specified purpose according to recognised standards. It may include the proof that the processes of production and service comply with given environmental and social standards. Certificates are based on criteria (specifying the purposes of the products and services as well as the recognised standards for the assessment) and on measurable indicators (representing the reproducible assessment results).

Forest Certification usually puts emphasis on ensuring the sustainability of the supply of wood products, but it is not restricted to this.

FOMUMIIS® (Forest Multiple Use Measurable Indicator Identification System) is a scientific method and a software- and GIS-based tool to process the information necessary for certification of forest products and services. It has been developed to meet requirements of international forest policy and is suitable for application to all forest types and products/services at all scales from the local to the global level (Pitterle and Perzl, 1998).

Applying FOMUMIIS® to protection forests, four components have to be considered:

- the type of hazard and the mechanisms of interaction between the hazard event and the forest
- the territory of human interest to be protected – this can include settlements, areas for infrastructure, economy, tourism, recreation, natural resources etc.
- the characteristics of the site of release and of extension of the hazards, including site conditions of the forests, characterised by climate, topography, geology, soil, hydrogeology etc., which determines the potential natural forest type and the local forest protection potential, and
- the actual forest condition, determining the actual forest protection efficiency.

From the analysis of the protection process under the special requirements defined by the human interests and the natural site conditions, and taking into account the actual forest conditions, proper methods and priorities of forest treatment and management are deduced (Fig. 1).

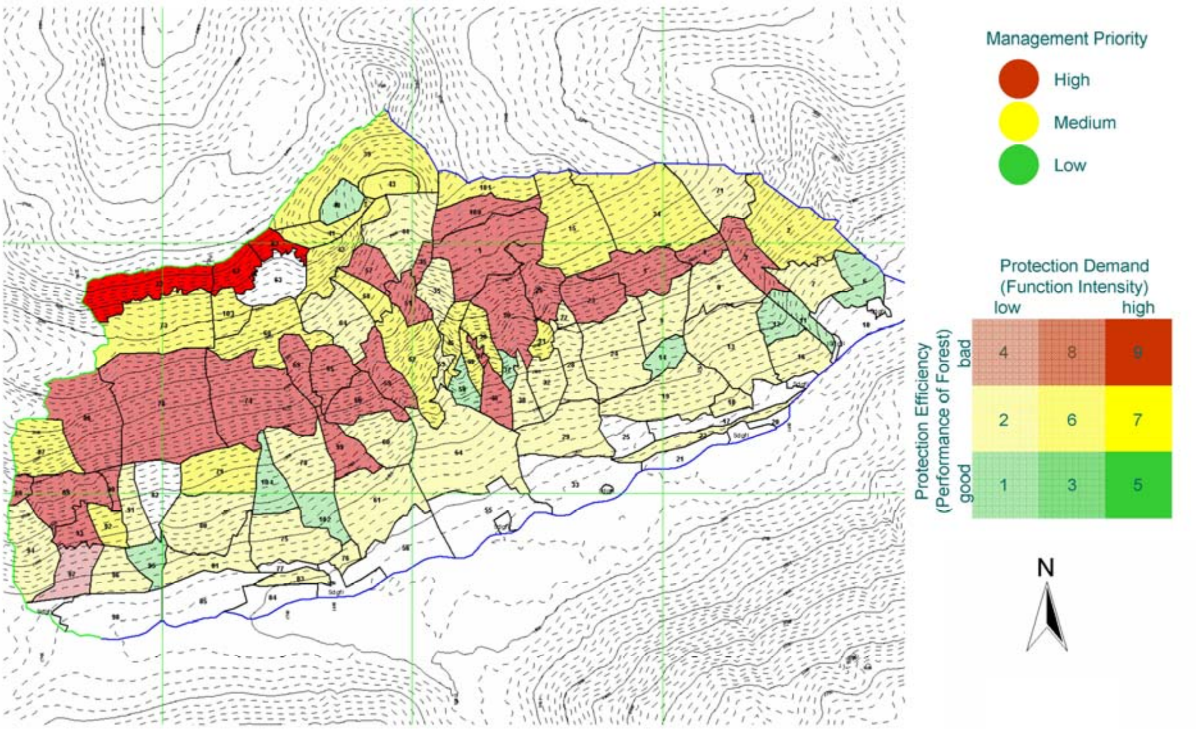


*Figure 1: Priorities of forest management measures for preventing avalanche release (output of the FOMUMIIS® certification process)*

# 3 FOREST PARAMETERS RELEVANT FOR PROTECTION EFFICIENCY

The protection efficiency of forests depends on the type of hazard, on site conditions such as slope angle and length, soil type and depth, a.o. and on the properties/qualities of the forest. The latter can be described by the following parameters: tree species, trees height, dbh (diameter at breast height), crown diameter, crown number per unit area, crown closure, crown condition, horizontal structure, vertical structure and the properties of the ground layer (debris, herb layer, stools, deadwood etc.).

While the definitions of some of these forest parameters are obvious, others need further specifications. The concepts of crown condition, horizontal structure and vertical structure are particularly vague, but they can be and need to be exactly defined. E.g., crown condition can be specified in terms of density of green biomass, leaf area index, or, on a stand basis, in terms of percentage of dead trees. Horizontal structure may need a number of parameters for a proper description, e.g. distribution of trees in the categories even – irregular – highly irregular (defined in terms of the relative or the absolute variation of gap size), with further subdivisions according to gap shape and gap orientation. The gap size in downhill direction is of particular importance. Vertical structure has to be defined in terms of relative or absolute tree height variation.

The above mentioned parameters can partly be summarised and integrated to the categorical parameter “forest development phase”. The concept of forest development phases is applied to uneven-aged natural forests, because age classes are not suitable to characterise the stage of such forests. It describes the natural dynamics of forests. Usually the following phases are distinguished (Leibundgut, 1986; Mayer and Ott, 1991):

- Optimum phase: This phase is characterised by closed, one-storey stands. The number of trees is high and the individuals are very viable.
- Terminal phase: The majority of individuals loose vitality, some of them die, and gaps emerge. The number of mature trees per unit area is much lower than in the optimum phase, but the average diameter is bigger. Partly, the gaps get filled by self-seeding seedlings and the understorey gets denser.
- Disintegration phase: In this phase, tree vitality declines significantly, and there is a rapid dying of old individuals. The remnants of the old stand are surrounded by seedlings from self-seeding or, if regeneration is delayed, treeless areas are covered by dense forbs and shrubs.
- Regeneration phase: This phase follows when moderate rate of dying among old trees is accompanied by speedy self-seeding from trees which are still viable. The number of old trees is low, whereas the number of trees in the undergrowth rises rapidly by natural regeneration. The young generation of trees appears in clumps of various age. In this phase, the stand shows the highest level of differentiation into storeys.
- Juvenile phase: The juvenile phase follows the disintegration phase when regeneration in the disintegration phase is delayed. Self-seeding (mostly from nearby stands) begins after some years, forming clumps of trees of various age. Moreover, there are still some gaps.
- Initial phase: There are groups of trees of various age, and there may also be some old trees (the youngest and most viable ones of the previous generation). In this phase, the stands are differentiated into storeys. Selection processes proceed, where the weakest trees in the understorey die.

The protection efficiency of forests differs from phase to phase. Therefore, it is changing over the time for a particular site, and management measures may be required. As a pre-requisite, it is necessary to be able to derive the future pattern of development phases from the present pattern on the basis of expert knowledge on the dynamics of forest development phases. However, parameters of this dynamics are also largely unknown.

The interaction processes between hazard events and the forests are usually well-established (Fig. 2), although the concrete parameter values describing these processes are rather tentative. E.g, for snow avalanches, there is agreement that the main contribution of forest to the protection against avalanches is its ability to prevent the release of avalanches, whereas avalanches that are released high above the forest line cannot be stopped by the forest. (Imbeck, 1987; Margreth, 2004)

It is known that the forest stabilises the snow cover. The snow cover within the forest is more structured and less massive compared to the open land. The climate within the forest is rather balanced. Therefore, the genesis of various layers, which often leads to the release of avalanches, is not promoted. Moreover, snowdrift is reduced, and the stems pin down the snow cover if they stick out of it. The required number of stems per hectare depends on slope and snow height.

Although the general mechanisms are known and many rules of thumb are applied to assess the efficiency of forests in the protection against avalanches, the scope of application of these rules is uncertain, and there is still a shortage of well-described avalanches. In particular, extreme (and seldom) weather conditions and their influence on the system need further investigations.

Both parameters of dynamics of forest development and parameters of hazard-forest-interaction processes can be deduced from large-area-assessment of forest parameters as it is possible with remote sensing methods.

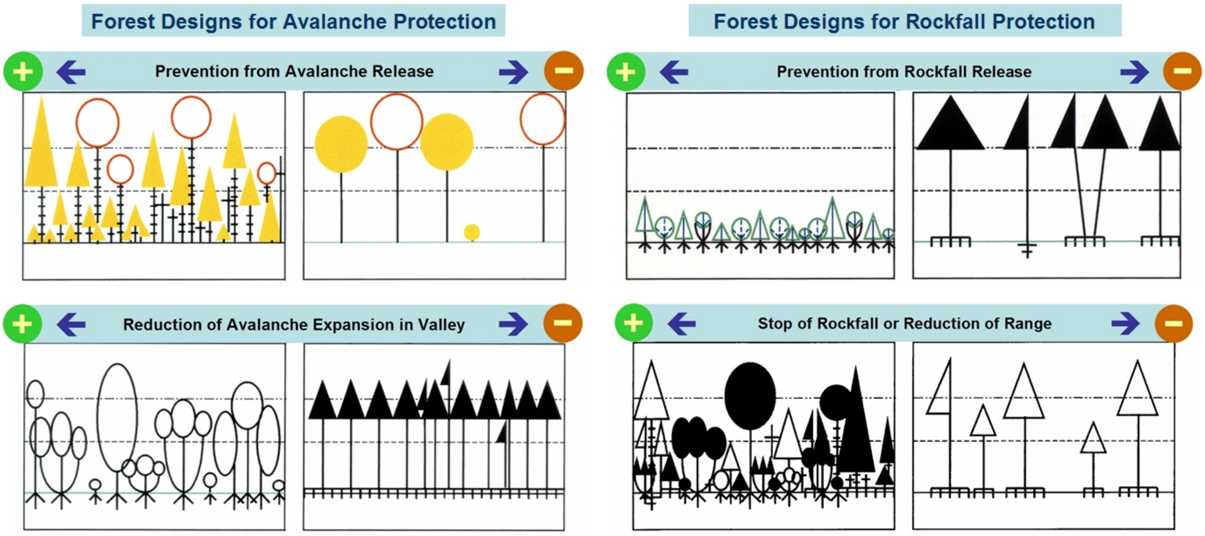


*Figure 2: Forest designs with low (-) and high (+) protection efficiency for different hazard types*

## 4 INFORMATION FROM REMOTE SENSING

Remote sensing is an appropriate method for obtaining essential information on three of the four above-mentioned components relevant for managing forests with special emphasis on their protective function: These three components are the area to be protected, the site of release and of extension of the hazards, including site conditions of the forests on these sites determining the protection potential, and the actual forest characteristics.

Information from remote sensing on the area to be protected and on the site of hazards mainly concerns location, extent and topographic characteristics (altitude, slope etc.). Standard methods of remote sensing for mapping and acquisition of digital elevation models are to be used here.

This paragraph concentrates on remote sensing of forest parameters relevant for the protective function. A series of remote sensing techniques are available for this purpose. These techniques are listed here and ranked according to their significance for describing the various forest parameters and according to their costs (Fig. 3). Given concrete circumstances, the method most appropriate can be selected from this list.

SAR and INSAR (IFSAR) techniques are not considered here, as they do not yet seem sufficiently developed for operational application.

Aerial photos in analogue form (recorded on film) are used since many decades for obtaining information on forests. For image scales of 1:10.000 and above, single-tree assessment is feasible. Forest parameters based purely on geometry and structure can be derived from panchromatic images with good reliability. Using colour-infrared film, tree species and crown condition can also be obtained. Vertical structure is a weak point, as lower forest layers may be not visible. dbh is not directly accessible, but may be deduced from other parameters (e.g. from tree height and crown diameter) by regression analysis. Kusche et al. (1994) gives an overview of mapping of protection forest formation phases from analogue aerial photos.

Aerial photos in digital form, as they become available now to an increasing degree, have some advantages due to their superior spectral and radiometric quality: The spectral bands show less overlap than those in film systems, so that species and crown conditions can be identified more reliably. The dynamic range is clearly improved, so that sunlit and shadowed image details can be interpreted and analysed at the same time. As high longitudinal overlap can be realized in digital aerial photography without additional costs, it is quite common to acquire digital aerial photos with 90 % overlap. These aspects in combination lead to better conditions for assessment of vertical structure.

Satellite images of high spatial resolution of the type Ikonos may replace aerial photos to a certain extent. However, their spatial resolution is still inferior to that of aerial photos, and it is not yet common practice (albeit possible in principle) to acquire and to work with stereo pairs of high-resolution satellite images. As a consequence, these images are less suited to derive tree height, crown diameter and vertical structure.

Landsat-type satellite images of medium spatial resolution offer a cost-effective method for acquiring forest information on large areas. Single-tree assessment is of course not possible. Most forest parameters can only be derived by indirect means, either using statistical methods or knowledge-based models. The main field of application for these medium-resolution satellite images therefore is screening to narrow down the area for subsequent more detailed analysis.

Airborne Laser Scanning provides true 3D information on forests. Tree height, crown diameter, crown number as well as horizontal and vertical structure can be determined with a quality and reliability satisfying all needs of protection efficiency assessment. Problems may arise from mission planning in mountainous areas, which may lead to higher costs. The information on tree species and crown condition may have to be augmented with optical reflectance data from aerial photos or from high resolution satellite images.

Terrestrial laser scanning may supplement field work for assessing forest parameters. In particular, this technique may quantify and objectify the terrestrial appraisal.

| | Costs | **Forest Parameters Relevant for Protection Efficiency** | | | | | | | |
|---|---|---|---|---|---|---|---|---|---|
| | Costs *) | Tree Height | Crown Diam. | Crown Number | Crown Condition | Tree Species | Horizontal Structure | Vertical Structure | dbh |
| Analogue Aerial Photos (Scale 1:10.000) | **2** | **2** | **2** | **2** | **2** | **2** | **2** | **1** | **1** |
| Digital Aerial Photos (Pixel Size 15 cm) | **2** | **2** | **2** | **2** | **3** | **3** | **2** | **2** | **1** |
| Ikonos-Type Satellite Image | **2** | **1** | **1** | **2** | **2** | **2** | **2** | **1** | **1** |
| Landsat-Type Satellite Image | **3** | **0** | **0** | **0** | **1** | **1** | **1** | **0** | **0** |
| Airborne Laser Scanner Data | **1** | **3** | **3** | **3** | **1** | **1** | **3** | **3** | **1** |
| Terrestrial Laser Scanner Data | **0** | **1** | **1** | **2** | **1** | **0** | **2** | **1** | **3** |

*) per unit area

| | **For Costs** | **For Parameters** |
|---|---|---|
| **0** | very high | unsuitable |
| **1** | high | moderate |
| **2** | moderate | good |
| **3** | low | very good |

*Figure 3: Ranking of different remote sensing methods for the acquisition of forest parameters relevant for protection efficiency*

# 5 CONCLUSIONS

The basis for the sustainable management of protection forests with optimised efficiency and transparent allocation of costs is given by

- the FOMUMIIS® certification tool for the processing of the spatial information on locations of human interests, hazard sites, forest conditions on these sites, and hazard-forest-interactions, as well as
- remote sensing tools for the acquisition of spatial input information on locations of human interests, hazard sites and forest conditions on these sites.

The detailed parameters of the spatial models of

- forest development phase dynamics and of
- the interaction mechanisms between hazard events and forests (describing forest protection efficiency in given situations)

are not yet known with sufficient reliability and for all scenarios of interest.

As a consequence, work that remains to be done involves the parameterisation of these models and the insertion of remote sensing methods into the FOMUMIIS® certification tool. Further projects and investigations are in progress at the Institute of Silviculture and the Institute of Surveying, Remote Sensing and Land Information (BOKU, Vienna) in cooperation with for-CERT GmbH.

## REFERENCES


Fuchs, H., Pitterle, A. (1999): GIS als Werkzeug im Risikomanagement alpiner Bereiche 1999.–Österreichische Zeitschrift für Vermessung & Geoinformation, 87, 2+3, 76-84.

Imbeck, H. (1987): Die Lawinenschutzwirkungen des Waldes. Internationales Symposion über die Bildung, Bewegung und Wirkung von Lawinen. Mitteilungen des Eidgenössischen Institutes für Schnee- und Lawinenforschung Davos 43.

Kusché, W., Schneider, W., Mansberger, R. (1994): Schutzwaldphasenkartierung aus Luftbildern. Centralblatt für das gesamte Forstwesen 111, 1, 23-55.

Leibundgut, H. (1986): Unsere Gebirgswälder: Natur – Zustand – Bewirtschaftung. Bern, Stuttgart: Haupt.

Margreth, S. (2004): Die Wirkung des Waldes bei Lawinen. Forum für Wissen 2004: 21-26.

Mayer, H., Ott, E. (1991): Gebirgswaldbau – Schutzwaldpflege: ein waldbaulicher Beitrag zur Landschaftsökologie und zum Umweltschutz. Stuttgart: G. Fischer.

Pitterle, A. (2006): Because of approval as patent 2006 no publications on FOMUMIIS® are available yet. Details will be published soon.

Pitterle, A., Perzl, F. (1998): Waldleistungspotentiale von Schutz- und Wohlfahrtsfunktion sowie deren Bewertung. Unveröffentlichter Projektbericht. Waldbau-Institut, Abteilung Gebirgswaldbau, BOKU-Wien.

# ORTHORECTIFICATION OF HIGH RESOLUTION IKONOS SATELLITE IMAGES WITH DIGITAL ELEVATION MODEL: A CASE STUDY BULANIKDERE, CAMILI, ARTVIN IN TURKEY

*Günay CAKIR[1], Emin Zeki BASKENT[2], Selahattin KÖSE[3]*

[1] Karadeniz Technical University, Faculty of Forestry, Department of Forest Resources, Trabzon, Turkey, Dr., gcakir@ktu.edu.tr

[2] Karadeniz Technical University, Faculty of Forestry, Department of Forest Resources, Trabzon, Turkey, Prof., baskent@ktu.edu.tr

[3] Karadeniz Technical University, Faculty of Forestry, Department of Forest Resources, Trabzon, Turkey, Prof., skose@ktu.edu.tr

## ABSTRACT

The paper addresses the assessment of final accuracy during the orthorectification of high-resolution satellite images processed with Digital Elevation Models (DEM). The IKONOS PAN high resolution images cover a portion of the three-test areas; Artvin Forest Planning Unit, Camili Forest Planning Unit, and Bulanikdere Forest Planning Unit in Turkey. Igneada is generally flat area with an average slope of 12%. Artvin and Camili Forest Planning Units are steep areas with and average slope of 61%. After the accuracy assessment of the digital terrain model, trough the comparison with external DEM, a broad range of orthorectification procedure with high resolution satellite images is conducted. The DEM is generated from the 1/25000 scale topographic maps with 10 meter-counter lines by ERDAS software with a 3x3 pixel size. The accuracy in final positioning provided by the orthorectification of IKONOS imagery with derived elevation dataset was evaluated using an evenly spaced set of Ground Control Points obtained from GPS and DEM survey. The achieved accuracy could meet the requirements according to technical cartography specifications (up to 1:10000), update of well recognizable features or entities and generic mapping procedures. The results indicated that slope is an important parameter for orthorectification of high resolution satellite images. The RMS errors were found to be ± <1.5 m in flat areas area and ± <3.5 m in steep areas. DEM accuracy with fine grid spacing is required in addition to the well-defined GCPs.

**Keywords:** Remote Sensing, Orthorectification, IKONOS, DEM/DSM, High Resolution Image, Accuracy, GPS, GIS

## 1 INTRODUCTION

Over the last couple of decades, satellite images with varying resolutions have been used in detecting natural resources. Due to low spatial resolution and infrequent coverage's of a given area, new era satellite images with high resolution and more frequent visit were introduced and used in particularly evaluating forest resources. IKONOS-2, the commercial satellite with the highest publicly available resolution, was successfully launched in 1999. The satellite's sensor can generate 1-m panchromatic and 4 m multiband images with off-nadir viewing up to 600 in any azimuth for a better revisit rate and stereo capabilities. These capabilities enable along and across track stereoscopic images to be acquired for Digital Elevation Model (DEM) generation (Cheng and Tountin, 2001). The introduction of high resolution satellite images has made it necessary to revise the geometric correction techniques that are used in this field. There has been a transition, on the basis of evaluations aimed at the definition of map scale for which they can reasonably be defined polynomial models derived from IKONOS photogrammetry. When the investigated zone is a forest area or when the territory is characterized by discontinuities, a classical type of orthoprojection could be insufficient for mapping purposes and might need to be substituted with a more rigorous approach. The orthoprojection of satellite images is a procedure that is used to correctly represent orthogonal projection, on a prefixed plane, of the area framed by the sensor during the acquisition. This product is obtained through the orthogonal projection of each pixel of the image of the territory onto a cartographic plane, in such a way that the original perspective representation (a deformed cylindrical perspective in the case of push broom acquisition) is transformed into an equivalent metrically correct image. It is in fact possible to measure angles and distances on the orthophoto, but also to read the cartographic coordinates of significant points exactly like on a map (Barbarella et al., 2003 a). This study aims to address both the process of orthorectification of high resolution satellite images and the assessment of the final accuracy achieved when Digital Elevation Models (DEM) is generated with topographic maps

## 2 MATERIALS AND METHODS

Hereafter 1/25000 scale topographic maps for DEM generation, the high resolution IKONOS satellite data and ground GPS survey methodologies will be briefly discussed after a description of the study area. Topographic maps that using 85% of Remotely Sensed data produced by General Command of Mapping in Turkey. It contains counter by 10 meters, roads, river, lake, city, villages etc. When the maps colour is green, it has been forest, scups, and nuts. The other map colour is white such as rangeland, city or village. IKONOS, the first commercial satellite with highest publicly available resolution, which was successfully launched September 24 1999, can fill these requirements. The satellite's sensor generates 1 m panchromatic (pan) and 4 m multiband (XS) images with off-nadir viewing up-to-600 in any azimuth (Space Imaging 2004). In order to the appropriate use of this new source of data, different research studies have addressed the potential of high-resolution imagery for mapping. GCPs are less than 5-m accurate, over the full image is a good compromise to obtain 3-4 m accuracy in the bundle adjustment. When they are better than 1-m, 25 GCPs are then enough to increase 2-3 m accuracy with either pan or multiband images. Since GCP residual reflect the input data errors (map or GPS) these errors didn't propagate through the modelling. Quantitative and qualitative evaluations of ortho-images were performed with either independent checkpoints or digital vector files overlaid. Generally, the measured errors confirm the predicted errors or even were slightly better, and 2-4 meter positioning accuracy is achieved for the ortho-images depending of the elevation accuracy (DEM).

### 2.1 Site location

In this paper the use of high resolution optical satellite data for both DEM generation and subsequently image orthorectification have been addressed in three test area in Turkey (Figure 1). The geographic coordinates of the study area are provided in Table 1.

*Table 1. Geographic coordinates of the test areas*

| Test Areas UTM Zone | X min Coordinate | Y min Coordinate | X max Coordinate | Y max Coordinate |
|---|---|---|---|---|
| **Bulanikdere FPU 35. Zone** | $27^0$50'30''E | $41^0$47'00''N | $28^0$04'23''E | $42^0$00'01''N |
| **Artvin FPU 37. Zone** | $41^0$45'57''E | $41^0$07'29''N | $41^0$53'57''E | $41^0$15'00''N |
| **Camili FPU 37-38. Zone** | $41^0$49'55''E | $41^0$20'33''N | $42^0$03'55''E | $41^0$31'36''N |

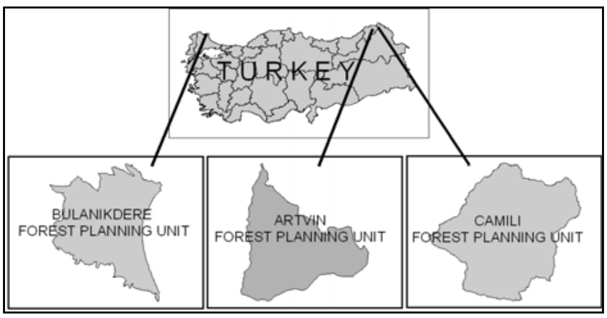


*Figure1. Test areas*

The IKONOS PAN high resolution images cover a portion of the three-test areas; Artvin Forest Planning Unit, Camili Forest Planning Unit, and Bulanikdere Forest Planning Unit in Turkey. The Bulanikdere Forest Planning Unit (FPU) surrounds Igneada and is characterized by a flat terrain with an average slope of %12.0 and an altitude from 0 to 400 m above seal level. The Artvin FPU area surrounds the city of Artvin and characterized by a predominantly steep and rough terrain with an average slope of %62.0 and an altitude from 200 to 2000 m above sea level. Camili FPU is characterized by a steep topography with an average slope of %60.5 and altitude from 400 to 3200 m above sea level. The Artvin FPU and Camili FPU extend entirely in the steep portion of the whole area (Table 2).

*Table 2. Test areas Slope class*

| SLOPE CLASS | Bulanikdere FPU | | Camili FPU | | Artvin FPU | |
|---|---|---|---|---|---|---|
| | Area ha | Range % | Area ha | Range % | Area ha | Range % |
| **Flat area %0-3.0** | 3207.58 | 37.71 | 720.94 | 2.83 | 519.90 | 9.94 |
| **Few slope %3.1-9.0** | 2036.19 | 23.94 | 20.16 | 0.08 | 4.63 | 0.08 |
| **Medium slope %9.1-17.0** | 1549.73 | 18.22 | 185.18 | 0.72 | 46.33 | 0.88 |
| **High Slope %17.1-36.0** | 1317.34 | 15.49 | 2081.86 | 8.21 | 589.07 | 11.26 |
| **Steep %36.1-58.0** | 320.26 | 3.77 | 7156.35 | 28.18 | 1572.11 | 30.06 |
| **Scarp %58.1-100.0** | 72.20 | 0.85 | 12766.38 | 50.28 | 2203.41 | 42.14 |
| **Very steep >%100.1** | 2.89 | 0.03 | 2464.71 | 9.70 | 294.52 | 5.64 |
| **Total area** | 8506.19 | 100.00 | 25395.61 | 100.00 | 5230.00 | 100.00 |
| **Average slope** | **% 12.00** | | **% 60.50** | | **% 62.00** | |

## 2.2 DEM Editing and Extraction

For both processes of DEM extraction and IKONOS image orthorectification ERDAS Imagine Orthobase software has been used. It implements a rigorous model for IKONOS images and a Rational Function Model for orthorectification of these images. We imported images as generic files with average parameters derived from metadata. Once edited the DEM, its accuracy has been evaluated by comparing elevation with an available and accurate DEM derived from the digitalization of 1:25000 scale topographic maps with a gridding space equal to 10 meters. There is some reason to use DEM. For this reason, the extracted DEM has been interpolated with a rigging algorithm and resampled to the lower spacing. Its worth to notice that while DEM represents the real morphology of the terrain, the satellite derived DEM represents the surfaces of features in the scene, as the bare soil in non-vegetated areas, the tree canopies in wooden areas and the building obstructions in urban environment. Using the new photogrammetric processing utilities available in ERDAS Imagine, a 3x3 pixel post spacing Digital Surface Model, was generated from topographic maps. Table 3 is show number of GCPs (collected from 1:25000 maps and GPS) for every image has been used IKONOS-2 geometric correction.

# 3 ORTHOIMAGE GENERATION

The orthorectification of the IKONOS image, based upon the discussed DEM, has been performed using ERDAS Imagine 8.6 software. The software adopts different geometric correction models, among them the parametric rigorous model and the rational polynomial model are the most accurate. The rigorous model can be applied through the knowledge of a certain number (around 25) of ground control points well and evenly distributed over the whole scene. The Rational Polynomial Model can be theoretically applied without knowing ground control points, but just using the coefficients (RPC, Rational Polynomial Coefficient) delivered with metadata (ERDAS, 2002).

In this work the geographic transformation between UTM datum ED50, that is the reference system in which RPC are computed, to the National grid system, that is the final required system, has been applied using a set of GCP in the latter system. A large set of points have been surveyed through a differential DEM survey. A subset of the whole dataset will be used for geocoding the IKONOS image (Ground Control Points), the remaining for validating the final accuracy achieved (Independent Check

Points). For the DEM extraction from control points for geocoding image has been derived from 1:25000 maps.

The orthorectification of the IKONOS image, based upon the discussed DEM, has been performed using ERDAS Imagine software. The software adopts different geometric correction models, among them the parametric rigorous model and the rational polynomial model are the most accurate ones. The rigorous model can be applied through the knowledge of a certain number (around 20) of ground control points well and evenly distributed over the whole scene. The Rational Polynomial Model can be theoretically applied without knowing ground control points, but just using the coefficients (RPC, Rational Polynomial Coefficient) delivered with metadata (ERDAS, 2002).

In this work the transformation between UTM ED50 -which topographic maps have an UTM ED50 coordinate system- the reference system in which RPC are computed, and the National grid system. Figure 2a shows a perspective view of the area with the high-resolution multispectral IKONOS image draped over the terrain model. Figure 2 b, IKONOS image illustrating with the DEM and stand type map, in the Artvin FPU. They are evenly distributed over the scene and cover all of the elevation range of the relieves. The percentage of the correlation successfully performed was around the 99%. The grid spacing of the extracted DEM has been selected to 3x3 pixels, corresponding for DEM processed, to approximately 5.0 m. The resulting file is composed of more than 10 million of points with an elevation ranging between 200 and 2000 m a.s.l.

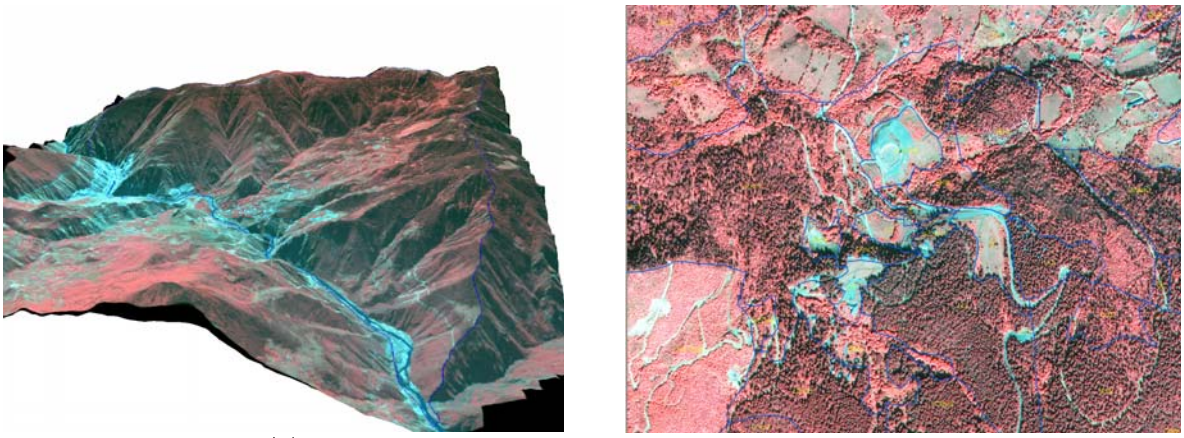

(a) (b)

*Figure 2. a. DEM and IKONOS images Artvin Forest Planning Unit and b. Overlay of portion of the raster orthoimage and the stand map layer.*

### 3.1 Orthoimage accuracy assessment

Results of the orthorectification tests are generally expressed in terms of Root Mean Square Error (RMSE) along the East and North grid axis computed using a series of known and independent checkpoints which are clearly recognizable on the orthoimage (Barbarella et al., 2003 b). On the other hand, it is well known from literature that the accuracy achieved in the orthorectification may be fixed in 1 or 2 pixels. The overall quality of the final orthoimage map could be also checked by the comparison with cartography at the higher scale than possible.

## 4 CONCLUSIONS

The generation of Digital Elevation Models from satellite high-resolution images and its use in the ortho-reprojection of external high-resolution satellite, images (we discussed the case of an IKONOS image) should be considered, as a productive methodology when the accuracy requested in map production has to meet the requirements of cartography at scale as large as 1:5000.

In particular, within the spatial methodology for terrain modelling, the use of 4 band panchromatic images acquired by the IKONOS constellation may be considered one the possible choice. Problems may arise in the correlation procedure (low data quality, cloud coverage, atmospheric effects or shadowing in densely urbanized area, and very sloppy area), producing lack of data in the DEM or erroneous elevations.

GCP points should be very precisely selected, measured and interpreted in the process of ortho-adjustment. For IKONOS data non-parametric (RPC) approach has better stability and needs less GCPs points for orthorectification. The input values of Z in the process of ortho-adjustment on the basis of used points GCP “read only ” from DTM or GPS survey, it gives almost the same accuracy for ortho -rectification process. For flat areas it is enough to apply DEM of accuracy in range 2< meters for IKONOS imaging with minimum number of 25 GCP, achieving accuracy of average 1.5 meter. Sloppy areas is enough to DEM of accuracy in range 4< meters for IKONOS imaging with minimum number of 25 GCP, achieving accuracy from 2.0 to 4.0 meters.

*Table 3. IKONOS-2 geometric correction values*

| Test area and Image Name | Number of DGPs | RMS pixel X | RMS pixel Y | Total RMS pixel |
|---|---|---|---|---|
| IKONOS ARTVIN FPU 15600_bgrir_0000001 | 32 | 1.44 | 2.05 | 2.50 |
| IKONOS CAMILI 13399_bgrir_0000000 | 36 | 2.12 | 2.18 | 3.04 |
| IKONOS CAMILI 13399_bgrir_0000001 | 47 | 2.19 | 2.47 | 3.30 |
| IKONOS CAMILI 13399_bgrir_0000002 | 56 | 1.54 | 1.56 | 2.20 |
| IKONOS CAMILI 13399_bgrir_0000003 | 37 | 1.36 | 1.87 | 2.31 |
| IKONOS CAMILI 13399_bgrir_0010000 | 25 | 2.13 | 1.98 | 2.90 |
| IKONOS CAMILI 13399_bgrir_0010001 | 49 | 2.34 | 2.28 | 3.27 |
| IKONOS CAMILI 13399_bgrir_0010002 | 57 | 2.49 | 2.14 | 3.29 |
| IKONOS CAMILI 13399_bgrir_0010003 | 58 | 2.02 | 1.99 | 2.84 |
| IKONOS BULANIKDERE 9118_bgrir_0000001 | 39 | 1.22 | 1.33 | 1.80 |
| IKONOS BULANIKDERE 9118_bgrir_0000002 | 91 | 1.20 | 1.21 | 1.71 |
| IKONOS BULANIKDERE 9118_bgrir_0000003 | 36 | 1.11 | 1.24 | 1.66 |
| IKONOS BULANIKDERE 9118_bgrir_0010001 | 46 | 1.01 | 0.94 | 1.38 |
| IKONOS BULANIKDERE 9118_bgrir_0010002 | 25 | 0.77 | 1.26 | 1.48 |

1 pixel equal to 1 meter

## ACKNOWLEDGMENTS

We thank the General Directory of Forest in Turkey for providing satellite images (INTA SPACETURK) and the DTM data, Karadeniz Technical University Forest Faculty of Forest Engineering staff.

## REFERENCES

Barbarella, M., Mancini, F., & Zanni, M., 2003 a. Rectification of high resolution satellite data: evaluating accuracy for map updating. Proceedings of the ASPRS/MAPPS conference “Terrain data: application and visualization, making the connection”, Charleston, SC, USA.

Barbarella, M., Mancini, F., & Zanni, M., 2003 b. Processing of high resolution satellite data for map updating, Proceedings of 30th International Symposium on Remote Sensing of Environment, Honolulu, Hawaii, USA.

Cheng P., Tountin T., 2001, Orthorectificaiton and DEM Generating from High Resolution Satellite Data, 22nd Asian Conference on Remote Sensing, 5-9 Nov., Singapure.

Çakır, G., 2006. Establishing Spatial Data Base for Forest Management Planning

Using Remote Sensing and Geographic Information Systems, Phd Thesis, Karadeniz Technical University, Graduate School Natural and Applied Science, 127 pp.

ERDAS, 1982-2004, ERDAS Field Guide. 6th Edition. Atlanta, Georgia.

Space Imaging, 2005, http://www.spaceimaging.com

# USING THE IKONOS 2 IMAGERY IN FOREST MANAGEMENT PLANNING ACTIVITY. AN EXPERIMENT

*Vladimir Gancz[1], Marius Petrila[2]*

[1] Forest Research and Management Institute, Sos. Stefanesti 128, 077190 Voluntari, Romania, tel:+4021-350 3243, fax: +4021-350 3245, e-mail: vladgancz@icas.ro

[2] Forest Research and Management Institute, Sos. Stefanesti 128, 077190 Voluntari, Romania, tel:+4021-350 3243, fax: +4021-350 3245, e-mail: ariuspetrilam@icas.ro

## ABSTRACT

Topographic maps, classic source of geographic information, could be many times, especially in Romania, without necessary accuracy, mainly because are not up-dated and the reality has been changed meanwhile. Exclusive terrestrial surveying is expensive and time-consuming task. An alternative is use of very high spatial resolution satellite imagery (VHSRSI) occurred on civilian users market as soon as the Ikonos satellite was launched in 1999, September 24. First experiment was done in Romanian forestry upon a test area within "Săcele" Experimental Forest District. One of the most important topic was the image georeference with necessary accuracy required by 1:5,000 maps, used in forest management planning works. Accuracy assessment was performed by picking-up check points, using GPS devices, from the terrain. Resulting RMS of GPS survey was 3.6 meters. Minimal number of necessary checkpoints analyse was performed and accuracy of the RMS was evaluated. Displaying limits of the planning elementary units on top of the image reveal a lot of wrong placed and missing limits. Orthophotomas were built according with topographic map standards in respect with Gauss frames. These mapsheets were delivered to forest management planning team and used within forest management planning work, performed during 2003. This team use the maps to correct and add missing limits and, consequently, the vectorial database was up-dated. Also, field check up of several limits was performed using GPSs.

**Keywords**: VHSRSI, image processing, orthorectification, accuracy assessment, orthophoto maps, forest management planning

## 1 INTRODUCTION

The forest management planning activity in Romania was completed first time in 1956. Management planning activity is done every 10 year on the same area. This activity is organizing forest districts and their areas vary between 5,000 and 15,000 ha. Each ten years interval an inventory is done, in a detailed way, from elementary units (sub-parcels), defined and delimited as homogenous from biometrical point of view. Its minimum size is 0.5 ha. There are over 1,000,000 elementary units within Romanian forest found. The changed/new elementary units borders are surveyed with classical topographic methods and are drown down, according with forest management planning rules, onto topographic maps at 1:5,000 scale (or 1:10,000, where maps at 1:5.000 scale are not available). This maps are, majority of them, obsolete, because were not up-date from, at least, 15 years. Many of them are 30, or more, years old.

Beside this, these maps have no details within forest cover. The limits of forest management planning elementary units surveyed could be accurate, or not. To check the accuracy of these limits means to be surveyed again. This is not an acceptable method because of supplementary costs in terms of time and money.

Starting with new very high spatial resolution satellite imagery (VHSRSI) occurrence on public market, a new tool is at our disposal. Our remote sensing and GIS team has began to study the possibilities of using VHSRI in forestry, especially in forest management planning in 2001. After several years of work on this topic we can consider these imagery extremely useful in forestry, in general, and especially in forest management planning.

# 2 TEST AREA. MATERIALS, EQUIPMENT AND METHODS

## 2.1 Test area

The test area was within Experimental Forest District "Sacele" (named within this paper Sacele) on a mountain region laying on Eastern part of the Central Carpathians (known also as Transylvanian Alps) on the North side (general aspect is Northward). The lowest altitude is around 700 m and the highest is around 1700 m and there is a various relief.

The forest cover is situated mainly between 1000 and 1200 m (56%) and the highest belt is between 1200 and 1475 m (30%). The lowest belt is situated between 770 and 1000 m (14%).

Forest formations are: spruce (*Picea abies*) -fir *(Abies alba)* mixture 1%, pure fir 4%, fir-mountain beech (*Fagus sylvatica)* mixture 36%, pure mountain beech 57% and other broad-leaved 2% from total forest found area of 4710 ha. (Taras, 1994)

This area is partially covered (23,800 ha) by an Ikonos 2 image (acquisition date 2001-09-23).

## 2.2 Materials and Equipment

- Geographic digital databases. There are 75 topographic mapsheets (1:5,000 scale) covering Sacele test area used to build geodatabase. The projection of these maps is *Stereografic 1970*. This projection system (stereographic, secant plane, Krasowsky ellipsoid, Dealu-Piscului datum) is specific for Romania and it is used for maps at scales larger than 1:10,000. The Geographic database structure is presented within table 1.
- Digital Terrain Models (DTM) were built based on contour lines (5 meters interval) for both areas.
- Satellite imagery: Ikonos 2 (acquisition date 2001-09-23), MS-PAN orthoready bundle.
- Software systems used were: ArcInfo (ArcGIS 8) and ArcView 3.2 for GIS purposes and ERDAS Imagine 8.6 for image processing purposes, digital elevation model and 3D building, both on PC Windows 2000 platform.
- Field data collection equipment: GPS Trimble ProXRS - for ground checkpoints co-ordinates collection.

*Table 1. Geographic database structure*

| Layer | Type | Attribute |
|---|---|---|
| watershed network | line | permanent/temporary |
| contour lines | line | altitude |
| roads | line | road type |
| forestry limits | line | limit type |
| Planning elementary units (PU) | polygon | planning inventory data |
| forestry benchmarks | point | benchmarks ID |

## 2.3 Methods

### 2.3.1 Image georeferencing

Before image georeferencing, the images coming from the four channels, delivered as GeoTIFF format, were imported into ERDAS format (.img) and stacked in one multispectral file (band 1 - blue, band 2 - green, band 3 - red, band 4 - IR and band 5 - PAN. This stack aloud georeference of all bands at once, taking the advantage of the best spatial resolution of PAN (one meter).

This task was done using RPC coefficients, DTM, and 6 GCPs collected from vectorial map. Consequently the projection system of the image has been changed to *Stereografic 1970* (original image was delivered in UTM/WGS84 system).

### 2.3.2 Accuracy assessment

To have a more accurate assessment of the real accuracy, in terms of RMS, checkpoints were collected from the ground, picking-up the most visible and sharp feature within imagery that could be clearly recognized within terrain.

During two campaigns (2002 and 2003) 64 checkpoints were measured, from which the most confident 28 were used.

The coordinates from the image were carefully collected using ERDAS Imagine "Inquire Cursor" and copying (copy-paste) the co-ordinates into MS Excel spreadsheet. The GPS measured co-ordinates were collected from the exported shapefile (as decimal degree), transformed into *Stereographic 1970* co-ordinates and introduced, also, into the same MS Excel spreadsheet. The RMS was calculated for all 28 coordinates pairs (image-field checkpoints) but also for each set of values, adding one by one, starting from the first pair, adding the second, the third, and so on, up to the 29th. In this way it was revealed variation of the RMS value with the each new CGP added. A graph was build based on these values (RMS versus number of GCPs).

### 2.3.3 Image enhancement

Images fusion between MS and Pan were done using PCA method.

The images were enhanced for a better visual interpretation. Contrast adjustments were carefully performed for an optimal forest vegetation visual discrimination. False color composition of color infrared (IR band - red, red band - green, green band -blue) was displayed.

### 2.3.4 Orthophotomaps building

For the covered area were built map sheets according with topographic map standards in respect with Gauss frames. Within map area were laid following strata: the image (fusion), IR false colour as raster stratum, contour lines, roads, watershed network and forest management planning limits as vector layers. Were add also main geographical feature names (valleys, edges, picks, etc) and forest management planning elementary units ID. Out of map frame were added standard information such as map code (Gauss frames system), co-ordinates grid, scale, information concerning image and vectors, etc. Also was added a legend for non-standard features (i.e. forest management planning limits).

### 2.3.5 Use of orthophoto maps in forest management planning

For covered area the orthophoto maps were plotted out on paper support and delivered to planning teams. Planning field activities were done during 2003 year.

Visual checking of these maps revealed that many of the planning limits of the elementary units were wrong. Also there were obvious limits between stands missing on the maps. All wrong and not existing limits revealed on the images were checked-out on the field and were corrected and added, respectively. Also some limits were checked-out and measured with the GPS device.

## 3 RESULTS

Two details of the georeference image are shown in figure 1. Limits of planning elementary units are displayed as yellow/black lines. GPS check-up lines (kinematic method) are displayed in blue and check-up points (static method) in red.

Accuracy assessment show the calculated RMS is 3.6 ± 0.1 m. The North direction RMS ($RMS_x$) is 3.0 m and the East direction RMS ($RMS_y$) is 1.9 m. Within figure 2 is displayed the graph of the RMS variation depending on number of check points.

Figure 3 shows an orthophoto map from Sacele area based on Ikonos 2 imagery. Based on the corrected limits on the orthophoto maps the digital geodatabase was corrected.

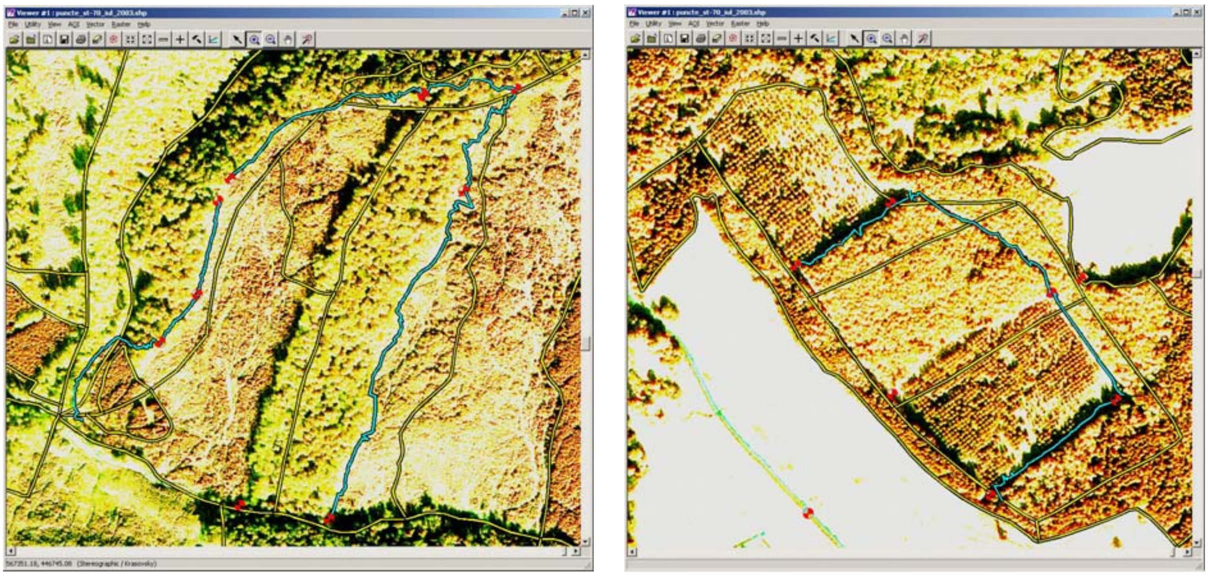

*Figure 1: Forest management planning limits on top of Ikonos 2 fusion image (false color infrared). Limits of planning elementary units are displayed as yellow/black lines. GPS check-up lines (kinematic) are displayed in blue and check-up points (static) in red.*

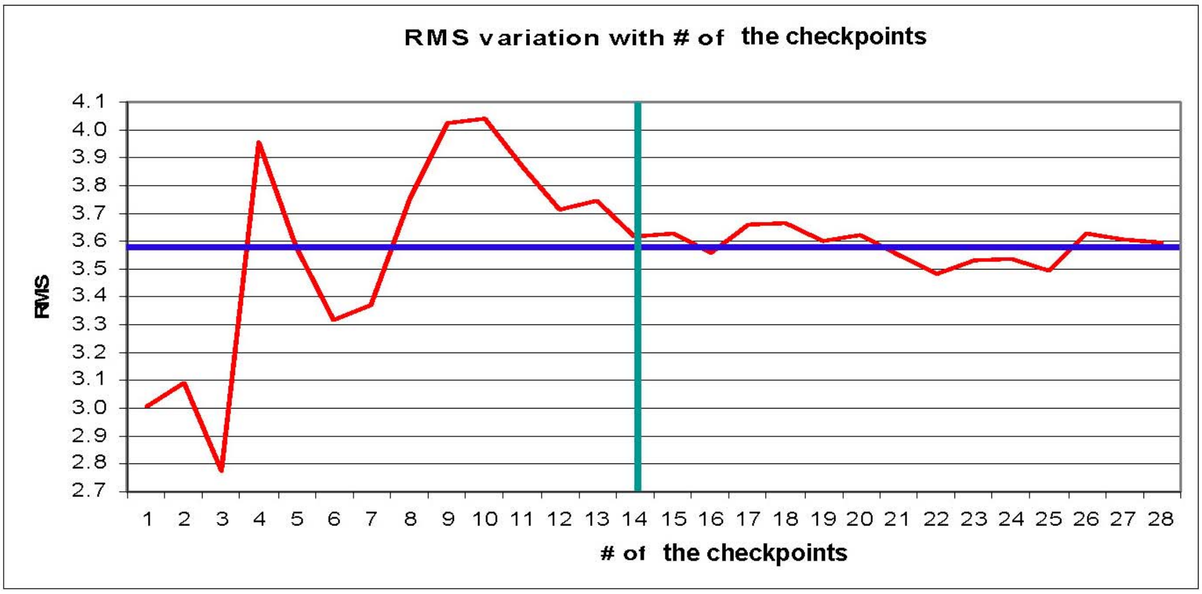


*Figure 2: The graph of the checkpoints variation against number of GCPs*

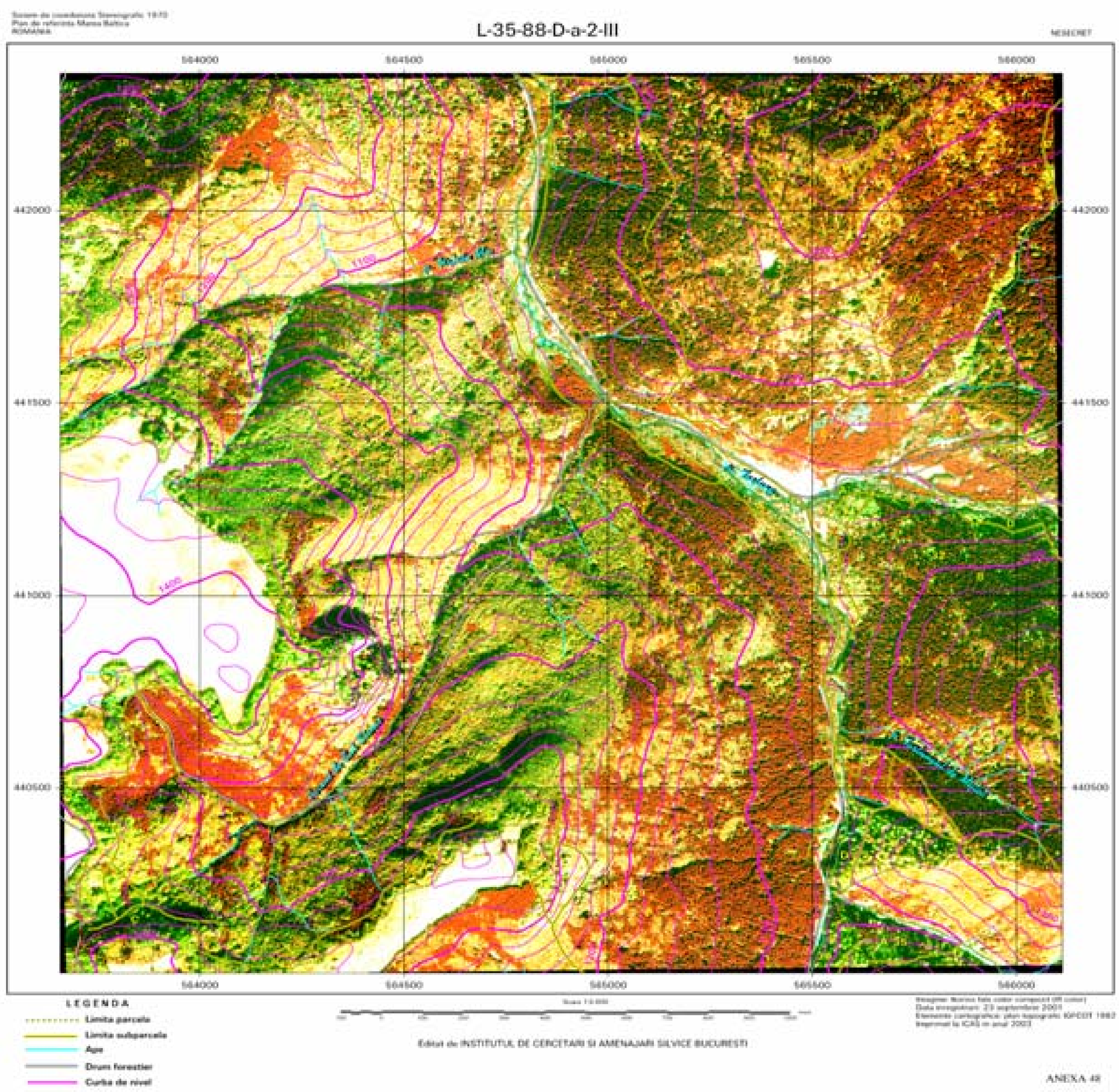


*Figure 3: An orthophoto map sheet*

## 4 DISCUSSIONS

As it can be seen within figure 1 some forest management planning limits are obviously wrong mapped out with classical surveying method. This method uses surveyor's compass and a rapid survey technique. Results are graphically transferred on the topographic maps (1:5,000 or 1:10,000 scale). Even theoretically the method is enough accurate for these scales, in reality many measurements are affected by the human mistakes, especial within difficult areas. It is almost impossible to check-out if this surveyed limits are correct or not and mistakes could not be put into evidence onto topographic maps. Using VHSRSI checking become relatively easy.

Geometric correction accuracy assessment, using GCP collected with GPS devices, shows a RMS of 3.6 m, enough good for 1:5,000 scale. It has to be mentioned that the errors include image orthorectification errors, targeting errors of the GCP on the image and GPS errors. Taking into account that the sensor elevation angle is 74,65 degrees, and "higher elevation angles tend to result in lower RMS" and "satellite elevation angle above 75 degrees tend to maximize geometric accuracy…" (D. Helder et al., 2003) we consider this result rather good.

To answer to the question: there were enough checkpoints for accurate calculation of RMS? it was used a graphical method. Within figure 2 the graph of RMS variation against the checkpoints collected shows that after 13 points, variation of RMS become insignificant: ± 0.1 meter. This means also that RMS calculated value could be trust within ±0.1 m range that it is very good, taking into consideration that pixel size is 10 times bigger (1m). Also we may conclude that a number of 15-20 points could be enough for such area and such relief conditions. Of course, this could not be automatically extrapolated for any other area, but calculating the RMS after each CGP collection (using a field computer) the collection effort could be optimized.

After the accuracy assessment the imagery was considered suitable for cartographic purpose and orthophoto maps, 1:5,000 scale, were build (43 map sheets). These maps were used during 2003 field campaign by the forest management planning team in charge with planning revision of Sacele Experimental Forest District. After one day training on false infrared colour image interpretation, the team members were able to use it in a proper manner. Many wrong limits of the elementary units were re-shaped and several new elementary units occurred or disappeared. According with the team members, these maps were extremely useful in terms of decreasing fieldwork effort, due to possibility to detect the errors previously and just checking-up it in the field.

Some GPS checking-up of some limits, together with the planning team, increase the confidence in accuracy of these maps (see figure 1). Consequently, the digital geodatabase was up-dated.

# 5 CONCLUSIONS

The results of these studies show the possibility to use VHSRSI in forest management planning activity as superior alternative to classical topographic maps. This approach could increase accuracy and decrease the efforts in terms of time and costs.

High geometrical accuracy of image georeferencing allows Ikonos image, at least within Sacele area, to be used as topographic base up to 1:5,000 scale. It has to mentioned that other authors consider Ikonos imagery suitable up to 1:10,000 scale (Kayitakire et al, 2002)

Also the results are very encouraging in use this imagery for planned forest maintenance work and logging monitoring at a very accurate scale.

It is also promising the possibilities to map out different details such as exploitation roads and gathering places, deforestation areas and erosion effects, constructions, etc. The relatively low costs of the imagery and fast image processing and exploitation are strong arguments to use it as a common instrument in forestry for very various purposes.

Also it shows an important potential for forest ecosystems studies: canopy horizontal structure, stands discrimination, detailed upper individual trees crown study and measurement.

# ACKNOWLEDGMENTS

Ikonos 2 imagery used within Sacele experiment was purchased in the framework of TAFIMRO (Technical Assistance in Forest Management in Romania) project, a collaboration between GIS Support Center of the Flemish Land Agency, Flemish Region, Belgium and Forest Research and Management Institute, Romania. Flemish Region Government financed, mainly, this project. A part of the studies presented within this paper were done in the framework of this project.

# REFERENCES

Helder, Dennis, Coan, M., Patrick, K., Gaska, P. (2003). Ikonos geometric characterisation. Remote Sensing of Environment 88, p.69–79, Elsevier

Kayitakire, F., Farcy, Cristine, Defourny, P. (2002). Ikonos-2 Imagery Potential For Forest Stand Mapping. ForestSAT Symposium 5th-9th August 2002, Heriot Watt University, Edinburgh, Scotland

Taras, D. (1994). Amenajamentul Ocolului Silvic Experimental Săcele [*Experimental Forest District Sacele Management Planning Work-out*]. Forest Research and Management Institute archive

# OBJECT-ORIENTED CLASSIFICATION OF QUICKBIRD DATA FOR IDENTIFICATION AND MAPPING OF FOREST HABITATS

*Fabio Giannetti[1], Alessandro Canavesio[1]*

IPLA S.p.A., C.so Casale 476, 10132, Torino, Italy, giannetti@ipla.org

## ABSTRACT

Habitat mapping is an important task in the framework of the requirements that follow from the European Union Directive on Habitat conservation. In this context, it is also relevant the implementation of automated procedures to develop replicable methods useful for periodic monitoring of the habitat status. Very high resolution satellite images have a high potential for extracting habitat information but traditional semi-automatic classifications based on spectral comparisons of pixels seem inapplicable due to the high within-class spectral variability. Regional approaches that cluster pixels basing on homogeneity criteria and classify the resulting objects appear more promising. In this work the image analysis software eCognition (Definiens Imaging), integrating complex object description and object-based classification algorithms, was used to classify forest habitats in a Nature Reserve that is part of the Natura 2000 network. After orthorectification and pansharpening, a Quickbird image was segmented using adequate scale parameters. Nearest-neighbour classification algorithm was then applied using spectral and textural information together with extra knowledge, such as shape and context. Classification accuracy was then assessed with reference to an independent set of ground surveyed points. The results confirm that object-oriented approach is a promising tool for forest mapping based on high-resolution satellite images. Further research needs to be done for developing more flexible tools capable of meeting specific requirements associated to forest areas characterized by low spectral differentiation and complex edges.

**Keywords:** Object-oriented classification, Quickbird, Habitat mapping, Segmentation

## 1 INTRODUCTION

The implementation of the European Union Directive on the conservation of natural habitats (92/43/EEC – Flora-Fauna-Habitat) involved standardised scientific studies and monitoring on the resulting Natura 2000 network. In this context, habitat mapping of the pSCIs (Proposed sites of community importance) is required in order to provide a better understanding of the distribution and extent of main habitats. This knowledge is essential to establishing sensible approaches to the conservation needs of each habitat and facilitating territory management through a correct evaluation of the impact of human activities. It's also worth considering that the Habitat Directive prescribes regular updating of the data, which is more easily achievable through the application of semi-automatic procedures based on Earth Observation data. (Langanke et al. 2004).

In order to fulfil these requirements, habitat types (following the Corine Biotopes classification scheme) (Devillers et al. 1991) were mapped in some Italian Nature Reserves during the EU-funded project "Flora and habitats in the South-western Alps" (Interreg IIIA Alcotra). Six "Natura 2000" sites in the Piemonte region (North-western Italy) were mapped at 1:10.000 scale using remotely-sensed data and image interpretation. We delineated the main physiognomic units by manually classifying Quickbird satellite images and using ground-surveys to label the habitats recognized on the satellite image. This traditional approach is labour-intensive and depends on the personal experience and skill of image interpreters and thematic experts. The development of a more objective and replicable methodology was considered a value-added result of the project, which will be particularly important for meeting European requirements in geo-information production.

This paper deals with an experimental approach carried out in a study area where we aimed to test an object- based classification of Quickbird satellite images for identification and mapping of forest habitats. Very high-resolution satellite sensors (e.g. Ikonos, QuickBird) can be considered an important tool in forest applications even though the automated classification of such data is problematic due to greater within-class spectral variation that prevents an effective application of the standard pixel-based classification algorithms. A good deal of information is actually contained in the spatial relationships of the pixels (Haralick and Shapiro 1992) and some studies already showed that object-oriented approach is promising when classifying VHR data (Leckie et al. 2003). This approach, implemented in the image analysis software eCognition (Definiens Imaging) was adopted in forest habitat classification.

## 2 STUDY AREA

The study area is included in the Vauda Nature Reserve, which is characterized by an ancient plateau scattered with ponds and small lakes. Wetlands and moors are mainly covered by a steppe-like vegetation made up of heathers and grasses while forest is dominant in deep linear depressions induced by river erosion. The dominant forest species are chestnut (*Castanea sativa*), black locust (*Robinia pseudoacacia*), oaks (*Quercus robur*, *Quercus petraea*), ash (*Fraxinus excelsior*), and alder (*Alnus glutinosa*) in the riverine forest. On the plateau, invasion woodland dominated by poplar (*Populus tremula*) and birch (*Betula pendula*) became widespread in recent years as a consequence of the reduction of traditional pastoral activities and wildfires. Black locust is also an invasive and presently occurs in many former agricultural areas, in disturbed areas and in transitional zones. The main forest areas of the Reserve, both in the erosion valleys and on the undulated plateau, were taken into account for the object-oriented classification procedure.

## 3 METHODS

A Quickbird image of the study area was acquired on 26th September 2004 with a view angle of 14.9 degrees. The image was orthorectified through a generic model based on rational polynomial coefficients with less than 2 m RMSE on independent check points. A pan-sharpening procedure was then applied to the original bands and non-forested areas were then masked out.

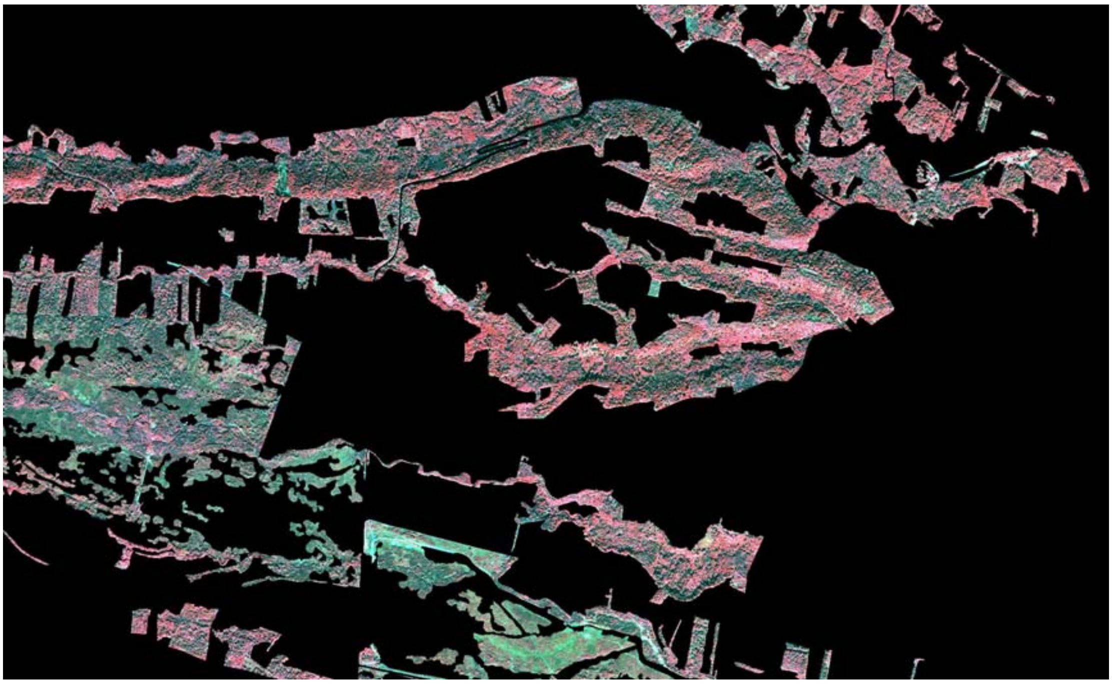

*Figure 1: Quickbird image of the study area in RGB composition of bands 4, 3 and 2. Non-forested areas were masked out*

Further additional channels were processed applying a texture filter with a 5x5 kernel size. The occurrence mean, calculated for the green, red and near infrared bands, was then selected for the classification after testing the contribution to class separability of different texture measures.

A hill shade image derived from a DEM was also added to the layers set because the spatial distribution of some forest classes is influenced by topographic elements such as slope and aspect.

After choosing the image layers to be used for the classification, we carried out a preliminary segmentation of the Quickbird image. The segments were then classified using several spectral, textural and relational features. Finally, classification accuracy was assessed by means of an error matrix built using an independent set of ground-survey points as reference data.

## 3.1 Segmentation

Image segmentation is a commonly applied technique that allows the grouping of neighbouring pixels into regions (or segments) on the basis of similarity criteria (digital number, texture).The delineation of homogeneous image objects in remotely-sensed images enormously reduced the number of elements to be considered in the following classification. Segmentation methods can be divided into point-based (e.g. grey-level thresholding), edge-based (e.g. edge detection techniques) and region-based (e.g. split and merge) methods (Pal and Pal 1993). The bottom-up region merging technique, implemented in eCognition (Baatz and Schäpe, 2000), starts from individual pixels and progressively merges pairs of objects to form larger segments on the basis of local homogeneity criteria, describing the similarity between adjacent image objects. The process stops when the smallest increase of homogeneity exceeds a user-defined threshold (the so-called scale parameter). Segmentation can further be constrained by weighting image layers differently according to their importance to the subject being analysed. In our case, we set weight 2 for the near infrared band, considering its relevance for differentiating forest types, and 1 for the other bands. The homogeneity threshold is composed of criteria such as pixel values (colour) and polygon shape properties (eCognition, 2002). The latter can further be broken into segment border smoothness and segment compactness. It is up to the user to find the optimal scale factor and homogeneity criterion for the best object delineation and feature extraction. For this application the best segmentation resulted applying a scale factor 70 and a colour factor of 0.7. Furthermore in the shape factor segment compactness versus smoothness was weighted 0.8-0.2.

## 3.2 Classification

The training set for the classification was built starting from the habitat map produced by the manual interpretation of the satellite image and the ground survey. Some habitats of the Corine classification scheme had to be grouped in order to define classes that were based on dominant species easily discernible through spectral and textural characters (Table 1).

*Table 1: Correspondence between the Corine Biotopes classification (Devillers et al. 1991) and the classes used for the development of this work.*

| Corine Biotopes class | Class used in this work | Dominant species |
|---|---|---|
| 41.5, 44.44, 41.24 | Oak | Quercus robur, Quercus petraea, Carpinus betulus |
| 83.324 | Black locust | Robinia pseudoacacia |
| 41.9 | Chestnut | Castanea sativa |
| 41.b14, 41.d2 | Birch - poplar woodland | Populus tremula, Betula pendula |
| 44.3, 41.3 | Riverine ash - alder woodland | Fraxinus excelsior, Alnus glutinosa |

Sample objects for each class were then characterized by calculating spectral, shape and textural features. The selected spectral features were channel means, standard deviations and brightness integrated by shape (Object Length/Width proportion and a Shape Index) and texture features.

The Nearest neighbour classification was applied to the whole image data set composed of 3 raw bands (green, red, NIR), texture mean calculated on the same bands and hill shade image of the study area.

Classification accuracy was assessed with reference to an independent test set composed of 120 points surveyed in 2004 on the study area. For each point a buffer of 1.5 metres was created in order to take into account the positional error in the GPS logging.

# 4 RESULTS

The analysis of the error matrix (Table 2) showed that birch-poplar, ash-alder and oak stands were classified with a relatively good accuracy (over 50%), while the most problematic class was chestnut with less than 40% of accuracy. With reference to this class the main ambiguities are with oak and black locust stands. Chestnut and oak have similar spectral and textural characteristics and very often the two species are mixed in coppice stands with oaks forming the dominant layer and chestnut as the most frequent tree in the understorey. The presence of mixed stands increased in the last years with the abandonment of cultivated chestnut orchards. Misclassification rate was also high between birch - poplar and black locust. These species often share the same ecological niches as they dominate early forest regeneration stages and are pioneers on disturbed soils and burnt sites.

*Table 2: Error matrix of classification accuracy assessment. The overall accuracy is 0,6 with the Kappa index of agreement (KIA) equal to 0.45.*

| **User \ Reference** | **Riverine ash - alder** | **Black locust** | **Oak** | **Chestnut** | **Birch - poplar** | **Sum** |
|---|---|---|---|---|---|---|
| Riverine ash - alder | 58 | 0 | 0 | 8 | 56 | 122 |
| Black locust | 13 | 187 | 89 | 33 | 78 | 400 |
| Oak | 14 | 15 | 136 | 67 | 52 | 284 |
| Chestnut | 0 | 47 | 1 | 63 | 14 | 125 |
| Birch - poplar | 16 | 109 | 14 | 0 | 504 | 643 |
| Sum | 101 | 358 | 240 | 171 | 704 | |
| Producer | 0.574 | 0.522 | 0.567 | 0.368 | 0.716 | |
| User | 0.475 | 0.468 | 0.479 | 0.504 | 0.784 | |
| KIA Per Class | 0.538 | 0.360 | 0.471 | 0.314 | 0.520 | |

# 5 DISCUSSION AND CONCLUSIONS

The reported results, although encouraging, showed that more research is still required on classification of forest cover type through very high resolution satellite data.

Several factors may account for the relatively low accuracies obtained for some classes. Among them should be cited challenges in extracting the training areas, spectral limitations of the Quickbird data and the characteristics of the reference data. The problematic classes are composed by broadleaved tree species that are similar in their spectral response and therefore difficult to separate using remote sensing data (Lennartz and Congalton 2004). Multispectral scanners with bands analogous to Quickbird have serious limitations from this point of view, while the addition of middle infrared bands could improve classification separability between forest species. Moreover the analysed forest stands are composed of a mixture of species so that the identification of a forest cover type as training area for image classification includes sampling multiple trees. It's important to remark that even if the sample areas were selected among polygons (Minimal Mapping Units, MMU, 2,000 square metres) assigned to a defined habitat, these areas, according to the definition of the Corine Habitat manual, can account for a significant presence of other tree species. On the contrary the accuracy was calculated with reference to a set of surveyed points and the MMU were dissimilar between the classified and the reference data set (Plourde and Congalton 2004).

Future research should be done collecting spatially precise training areas in order to extract spectral information regarding the canopy of only a few trees. This will minimize variability and ensure that a single species of tree is taken into account. Alternative classification algorithms should be experimented to more closely match the procedures for identifying forest cover types applied on the ground. Finally, current reference data should be collected at a scale matching that of the Quickbird classified image so emphasizing a more rigorous accuracy assessment.

## ACKNOWLEDGEMENTS

The authors would like to acknowledge funding for this research from Piemonte Region and European Commission in the framework of the INTERREG III A ALCOTRA project “Conservation and management of flora and habitat in south-western Alps”. In particular the authors wish to thank Antonio Aschieri of the “Ente di Gestione dei Parchi e delle Riserve Naturali del Canavese” for the cooperation in habitat mapping and ground survey and Luca Borghesio for the kind revision of the manuscript.

## REFERENCES

Baatz, M. and Schäpe, A. (2000). Multiresolution segmentation - an optimization approach for high quality multi-scale image segmentation. In Angewandte Geographische Informationsverarbeitung. Wichmann-Verlag, Heidelberg, pp.12-23.

Devillers, P., Devillers-Terschuren J. and Ledant J. P. (ed.), (1991) - CORINE biotopes manual. Habitats of European Community. Commission of the European Communities, DG Environment, EUR 12587/3; 300 pp.

eCognition (2002). User Guide. Definiens Imaging GmbH, Munich, 65 pp. Website: www.definiens-imaging.com , accessed January 2006.

Haralick, R. and Shapiro, L. (1992). Computer and Robot Vision vol. I. Chap. 9. Texture. Addison-Wesley, Reading, USA, pp. 453-494

Langanke, T., Blaschke, T. Lang, S. (2004) An object-based GIS/remote sensing approach supporting monitoring tasks in European-wide nature conservation, First Mediterranean Conference on Earth Observation (Remote Sensing), April 21-23, 2004, Belgrade, pp. 245-252.

Leckie, D.G., Gougeon, F.A., Walsworth, N., Paradine, D. (2003). Stand delineation and composition estimation using semi-automated individual tree crown analysis. Remote Sensing of Environment 85: 355–369

Lennartz, S. P. and Congalton, R. G. (2004). Classifying and mapping forest cover types using Ikonos imagery in the northeastern united states, ASPRS Annual Conference Proceedings May 2004, Denver, Colorado.

Pal, N. R. and Pal, S. K., (1993) A review on image segmentation techniques. Pattern Recognition, 26 : 1277-1294.

Plourde, L. and R. Congalton, R. G. (2003). Sampling method and sample placement: How do they affect the accuracy of remotely sensed maps? Photogrammetric Engineering and Remote Sensing. Vol. 69(3): 289-297.

# DETERMINING THE APPROPRIATE GEOGRAPHIC DISTRIBUTION OF SAMPLE POINTS FOR FOREST INVENTORY WITH HIGH RESOLUTION 3D IMAGES AND GIS A CASE STUDY OF YALNIZÇAM AND CAMILI FOREST PLANNING UNITS IN TURKEY

*Ali İhsan Kadıoğulları, Günay Çakır, Emin Zeki Başkent*

Karadeniz Technical University, Faculty of Forestry, Trabzon/TURKEY;
alikadi@ktu.edu.tr, gcakir@ktu.edu.tr, baskent@ktu.edu.tr

## ABSTRACT

Forest inventory relating forest values such as timber, water, biodiversity provides necessary data about forest management decisions. The quality and the speed of data collecting process depend highly on the inventory method and the information technology used. The accuracy assessment relates to the best representation of whole area with the appropriate number of sample points distributed over forest area. We used a probability systematic sampling approach (300x300m) to determine the geographic location of sample plots based on old stand type maps and high resolution satellite imagery (İKONOS 1m) with 3D modelling in GIS. The geographic locations of the sample points are generated with GIS functions and those intersected with non-forest areas were eliminated. The appropriateness of actual ground location of sample plots was compared with old maps and satellite images in both Camili and Yalnızçam Forest Planning Units. Camili (25428.60 ha) has high slope value (62%) and mix stand type (Chestnut, Beech, Fir, Spruce, Alder). Yalnızçam (44664,59 ha) has pure Scotch pine stand and high elevation areas (1900-2600 m).

Out of total 2285 sampling points covering the whole area of Camili, only 929 sample plots were found to cover the productive forest areas based on old stand type map (1360 sample plots eliminated). However, only 755 sample plots were found to cover the productive forest areas based on the high resolution IKONOS images (1530 eliminated). However, in Yalnızçam out of total 4955 sampling points, only 620 sample plots were found to cover the productive forest areas based on old map (4335 eliminated). However, only 535 sample plots were found to cover the productive forest areas based on the IKONOS images (4420 sample plots eliminated). In Camili, nearly 174 sample points were successfully saved with %19 success rate, while 85 sample points with %14 success rate in Yalnızçam due mainly to better characterization of forest areas with satellite imagery. However, based on the actual terrain conditions 400 out of 755 were actually measured in Camili saving further 355 sample plots (%47) and 520 out of 535 in Yalnızçam with only 15 saved plots (%2). In conclusion, satellite imagery allowed us to better represent the productive forest areas and to save sample plots. Yet, when both case study areas are compared, the success rate was much higher in Camili then Yalnızçam due mainly to terrain conditions. Satellite imagery is found an important vehicle just in simple determination of sample plots in forest inventory and should be used effectively in natural resource management.

**Keywords**: Remote Sensing, IKONOS, Sample Plots, High Resolution Images, GIS, Forest Inventory

## 1 INTRODUCTION

Over the last couple of decades, satellite images with varying resolutions have been used in detecting natural resources. Due to low spatial resolution and infrequent coverage's of a given area, new era satellite images with high resolution and more frequent visit were introduced and used in particularly evaluating forest resources (Cheng and Tountin, 2001). The IKONOS satellite (Space Imaging, Thornton, CO, USA) was launched into low Earth orbit in September 1999. IKONOS provides the first operational meter-scale resolution satellite observations of Earth for use by the civilian sector. The instrument has a panchromatic band (0.45–0.90 Am) with a 1-m spatial resolution, as well as four multispectral bands, each with 4 m spatial resolution. The panchromatic data provide an opportunity to observe plant canopies at spatial scales approaching the size of individual crowns and vegetation clusters (Asner et al., 2002; Franklin, Wulder, & Gerylo, 2001).

In this paper, we demonstrated the capability of eliminating sample plots in non-forest and degraded forest areas in two case study areas by comparing the stand type map drafted from Ikonos image with the old stand type created from photo interpretation process.

## 2 SITE LOCATION

Camili Forest Planning Unit (25428.60 ha) has high slope value (62%) and mix stand type (Chestnut, Beech, Fir, Spruce, Alder). Yalnızçam FPU (44664,59 ha) has pure Scotch pine stands located generally over high elevation areas (1900-2600 m). Both case areas are situated along the Eastern part of Turkey. Camili FPU is within the 37-38 zone of ED 50 Datum and 735500- 758330 north, 4581210- 4601870 east coordinates. Yalnızçam FPU is within the 38. zone of ED 50 datum and 267795- 299573 north, 4539570- 4566220 east coordinates (Figure 1).

Yalnızçam FPU has 5483 ha productive forest area, 632 ha degraded forest areas and 38548 ha non-forest areas (agriculture, residence, range, treeless areas). Camili FPU has 8607 ha productive forest areas, 7480 ha degraded forest areas and 8980 ha non-forest areas (Table 1).

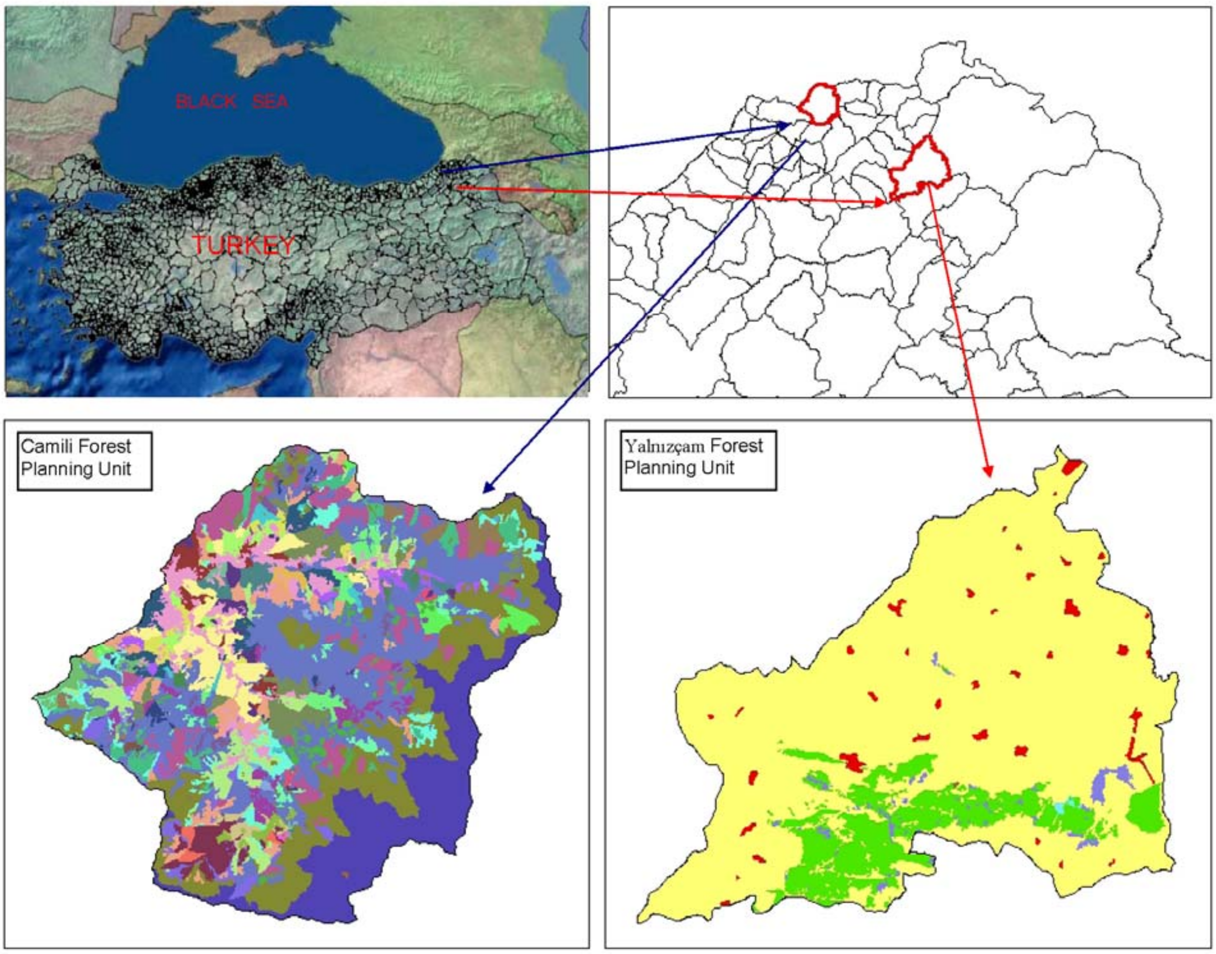


*Figure 1. The geographic location of Yalnızçam and Camili Forest Planning Units*

*Table 1. Land Use Types of Yalnızçam and Camili FPU determined from old stand type map*

| Land Use Type | Yalnızçam 1999 year (ha) | Camili 1985 year (ha) |
|---|---|---|
| Productive Forest | 5483,39 | 8607,09 |
| Degraded forest | 632,29 | 7480,77 |
| Non-forest areas | 38548,91 | 8980,75 |
| Total (hectare) | 44664,59 | 25428,60 |

## 3 MATERIALS AND METHODS

The data used in this research are old stand type maps with 1/25,000 scale in 1985 for Camili Forest Planning Unit (FPU) and 1999 for Yalnızçam FPU. Ikonos image of Camili was gathered in 2004 and Ikonos image of Yalnızçam gathered 2005. The old stand types, used as ground truthing, were originally generated from both the stereo interpretation of black and white aerial photos with an average 1/25000 scale and ground measurements with 300x300 sampling points. The Ikonos images were registered and interpreted with ERDAS image analysis programme.

Hereafter the 1/25000-scale topographic maps for Digital Elevation Model (DEM) with UTM projection (ED 50 datum) system and the high resolution IKONOS satellite data are registered with Topographic maps for 4 meter positioning accuracy. The topographic maps with 85% of RS are produced by General Command of Mapping in Turkey. It contains 10 meter-counter lines, roads, rivers, lakes, cities, villages etc.

### 3.1 Digitizing Old Stand Type Maps and Draft Stand Type Map with Ikonos Images

The old stand type maps used in this research were, first of all, scanned, saved in tiff format and then registered to the digital topographic maps in the same manner as to the Ikonos images. Rectified forest stand type maps were digitized with a 1/3000 to 1/5000 screen view scale with Arc/Info 9.0TM GIS. The draft stand type maps produced from Ikonos Images were digitized with 1/2500 screen view scale with Arc/Info 9.0TM program. This allowed direct comparison of maps produced from Ikonos images and old stand type map with vector format.

### 3.2 Generating and Eliminating Sample Plots

Sample plots were generated with *Generate & Fishnet* command of Arc/Info 9.0™ program. This plots actually have been located on a 300X300m intervals and eliminated with Draft stand type map and old stand type map. Some sample plots of Camili FPU were eliminated within the old stand type map of 1985 year with Arc/Info 9.0 program. Out of 2285 sample plots 929 of total plots were found to cover productive forest areas. Only were 1356 sample plots eliminated. Some sample plots of Camili FPU were eliminated within the draft stand type map. Out of 2285 sample plots 755 of total plots were found to cover productive forest areas. Only were 1530 sample plots eliminated. In Camili, 174 sample plots were successfully saved with use of draft stand type maps.

Some sample plots in Yalnızçam were eliminated with old stand type map of 1999 year with Arc/Info 9.0 program. Approximately620 of total 4955 sample plots were found to cover productive forest areas and 4335 sample plots were eliminated (Figure 3). Yalnızçam sample plots are eliminated based on draft stand type map. Nearly 535 out of 4955 sample plots were found to cover productive forest and 4420 sample plots were eliminated. In Yalnızçam, 85 sample plots were successfully saved with use of draft stand type maps (figure 2).

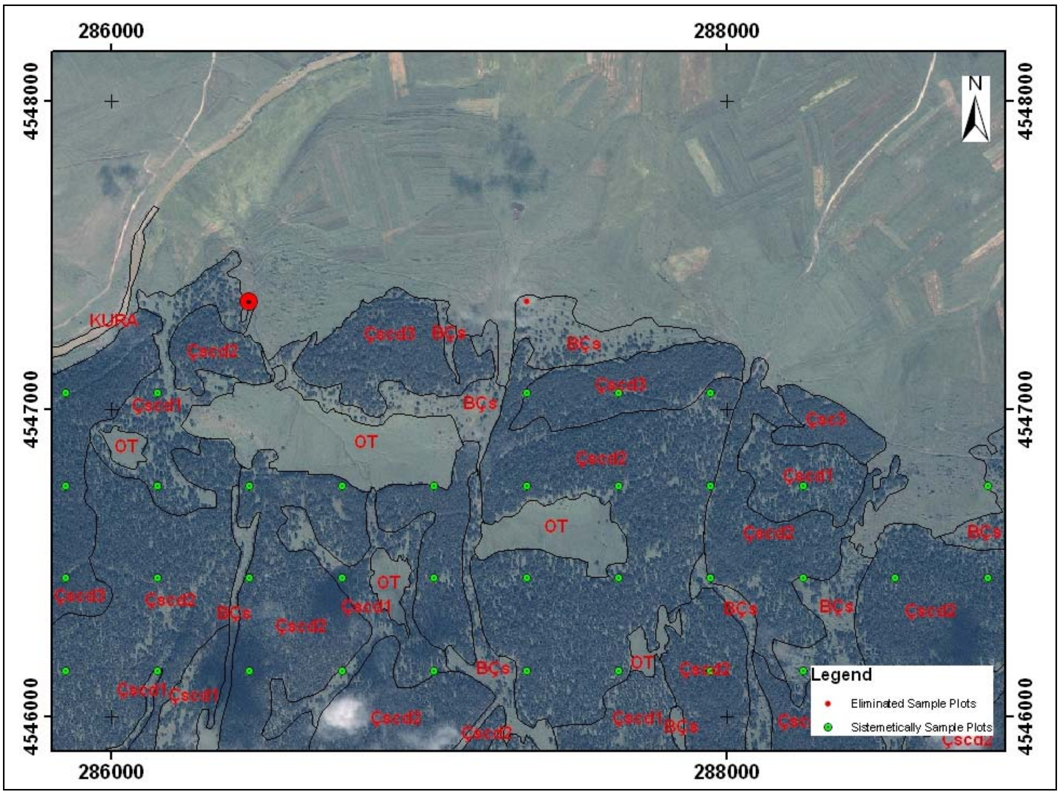


*Figure 2. Spatial distribution of some sample plots based on draft stand type map of Ikonos Image in Yalnızçam. Red ones are eliminated.*

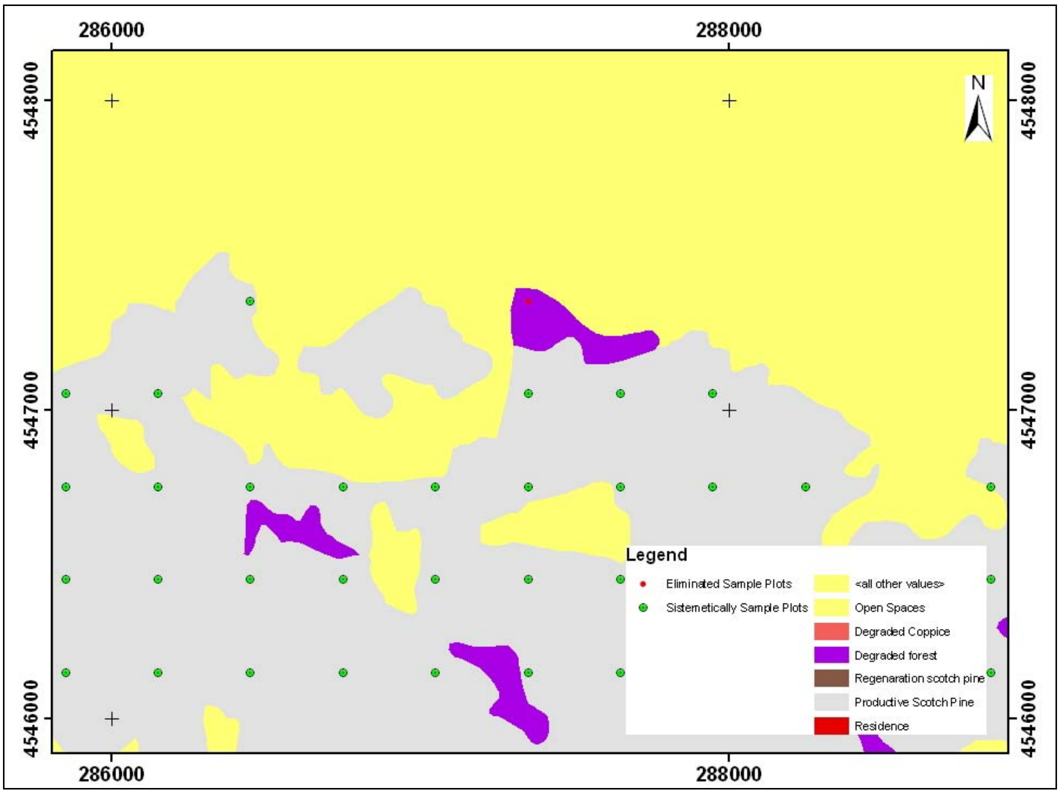


*Figure 3. Spatial distribution of some sample plots based on old stand type map in Yalnızçam. Red one is eliminated*

## 4 CONCLUSIONS

In conclusion, satellite imagery allowed us to better represent the productive forest areas and to save sample plots. Forest management team consist of one forest engineering and two forest workmen and almost measurement 7 sample plots daily. If we use satellite imagery to eliminate sample plots, we save 174 sample plots in Camili and 25 workdays for a forest management team. In Yalnızçam, 85 sample plots saved and 12 workdays for a forest management team.

Yet, when both case study areas are compared, the success rate was much higher in Camili than that in Yalnızçam due mainly to mountainous terrain conditions. Satellite imagery is found an important vehicle in simple determination of sample plots in forest inventory and should be used effectively in natural resource management.

## ACKNOWLEDGMENTS

We thank the General Directorate of Forestry in Turkey for providing satellite Images and the DTM data. Financial support for this research was provided by the Research Fund of Karadeniz Technical University, Turkey.

## REFERENCES

Asner, G.P., Palace, M., Keller, M. , Pareira, R. Jr., Silva, J.N.M., & Zweede, J.C. (2002). Estimating canopy structure in an Amazon forest from laser rangefinder and IKONOS satelite observations. Biotropica, 24, 483–492.

Cheng P., Tountin T., 2001, Orthorectificaiton and DEM Generating from High Resolution Satellite Data, 22nd Asian Conference on Remote Sensing, 5-9 Nov., Singapure.

Çakır, G., 2006. Establishing Spatial Data Base for Forest Management Planning Using Remote Sensing and Geographic Information Systems, Phd Thesis, Karadeniz Technical University, Graduate School Natural And Applied Science, 127 pp.

ERDAS, 1982-2004, ERDAS Field Guide. 6th Edition. Atlanta, Georgia.

Franklin, S. E., Wulder, M. A., & Gerylo, G. R. (2001). Texture analysis of IKONOS panchromatic data for Douglas-fir forest age class separability in British Columbia. International Journal of Remote Sensing, 22, 2627– 2632.

Space Imaging, 2005, http://www.spaceimaging.com

# APPLICATION OF STEREO AERIAL PHOTOGRAPHS TO STUDY NATURAL GAP DYNAMICS IN A BEECH FOREST

*Kata Kenderes[1], Tibor Standovár[1], Gábor Timár[2], Gábor Molnár[2] and Zsolt Pataki[3]*

[1] Eötvös University, Department of Plant Taxonomy and Ecology, Budapest, Hungary, kinderes@ludens.elte.hu

[2] Eötvös University, Institute of Geography and Earth Sciences, Space Research Laboratory, Budapest, Hungary

[3] Tájinformatika Bt., Vác, Hungary

## ABSTRACT

We used remote sensing methods to reconstruct natural stand dynamics of a semi-natural beech forest (Őserdő Forest Reserve, Bükk Mountains, Northern Hungary). We mapped canopy gaps using aerial photographs taken in 1975, 1980, 1993 and 2000, then we built a GIS database containing the geocoded photographs, the digitised gap contours for each time step, and digital elevation model. The purposes of our analyses were *i)* to test the applicability of this method; *ii)* to define descriptive gap characteristics; *iii)* to analyse gap dynamics of 25 years by following the fate of individual gaps.

Our results show that remote sensing is an important tool for studying the above phenomena. The observed canopy gaps covered 2.3–4.2% of the total area in the different years. Gap creation did not show any preference for special altitude, aspect, or slope steepness within this small study area. Average gap size increased from 39.4 $m^2$ to 61.3 $m^2$ during the 25 years study period. The number of gaps varied between 125 and 151. On average, slightly more new gaps were created than old ones closed each year (1.75–9.3%, and 3.21–7.89% of original number, respectively). The annual change of gap-area was 0.14–0.53%.

In addition to the information we gained from the stand dynamics of our study site, we also concluded, that the applicability of time series of aerial photographs (limited by differences in tilt and shadow in each photograph) could be greatly enhanced by applying 3D stereo images for delineating gaps.

**Keywords:** aerial photograph, GIS, beech, semi-natural, gap dynamics

## 1 INTRODUCTION

Gap formation – driven by the death of one or a few old trees – has an important role in the natural stand dynamics of temperate deciduous forests (Runkle 1985, White & Pickett 1985, Peterken 1996). In moist humid temperate regions this dynamics results in forests characterized by fine-scale mosaic of patches in different phase of forest development, by heterogeneous stand structure and by high diversity of habitats suitable for specialized forest-dwelling species (Standovár & Kenderes 2003). A clear understanding of natural stand dynamics is a prerequisite of developing nature-based management techniques for such forests.

Remote sensing techniques can help us understanding this process as these methods extend our observation both in space and back in time. With the ever increasing resolution of available techniques, nowadays remote sensing can be used in forest studies both at the landscape and the stand scales.

The purposes of our analyses were *i)* to test the applicability aerial photographs in retrospective analysis of stand dynamics; *ii)* to define descriptive gap characteristics (size, number, area, and spatial distribution among patches with different topographic characteristics, such as altitude, aspect, slope steepness) at each time step; *iii)* to analyze gap dynamics of 25 years by following the fate of individual gaps, i.e., to quantify the speed and importance of creation of new gaps, closure of gaps by lateral expansion versus by infilling of young undergrowth.

## 2 METHODS

The study area (Őserdő Forest Reserve) is a small (25 ha) beech-dominated stand situated on the plateau of the Bükk Mountains (48° 03'N, 20° 27'E), in Northern Hungary. Elevation ranges from 830 to 900 m. Mean annual temperature is 6.1 °C (January: -4.1 °C, July: 15.5 °C), the annual precipitation is 896 mm. The age of dominant beech trees varies between 150-200 years. It was managed and cut in the past, but it has been developed freely during the last 60 years. Stand structure is heterogeneous with trees of different sizes, canopy gaps and regeneration patches.

We used aerial photographs of two origin: *i*) Hungarian State Forest Service takes photos every ten years for forest management planning; *ii*) Photos have been taken for military and general land survey purposes by responsible institutes. We could use only those photos that were taken during the growing season. Most photos are black and white and we used the scanned images of the films. Canopy gaps were mapped using photographs taken in 1975, 1980, 1993 and 2000. First, we built a GIS database that contains the geocoded photographs, and the digital elevation model of the area. Then we digitised the contour lines of the gaps for each study year using two different working environments. For each time step we drew the contour lines into a polygon layer of our GIS database in ArcView 3.3 environment. To resolve ambiguities and uncertainties caused by differences in shade and tilt in each photograph, we also used 3D images generated from pairs of photographs by using the stereo analyst module of ERDAS IMAGINE.

An ArcView extension (Patch Structure) was developed, which not only calculates gap characteristics for each time step, but also follows the fate of individual gaps. This provided us with data to quantify the speed and importance of certain dynamical processes: creation of new gaps, closure, dissection of gaps, merger of neighbouring gaps.

## 3 RESULTS

Figure 1 contains the four maps showing the distribution of canopy gaps in the four study years.

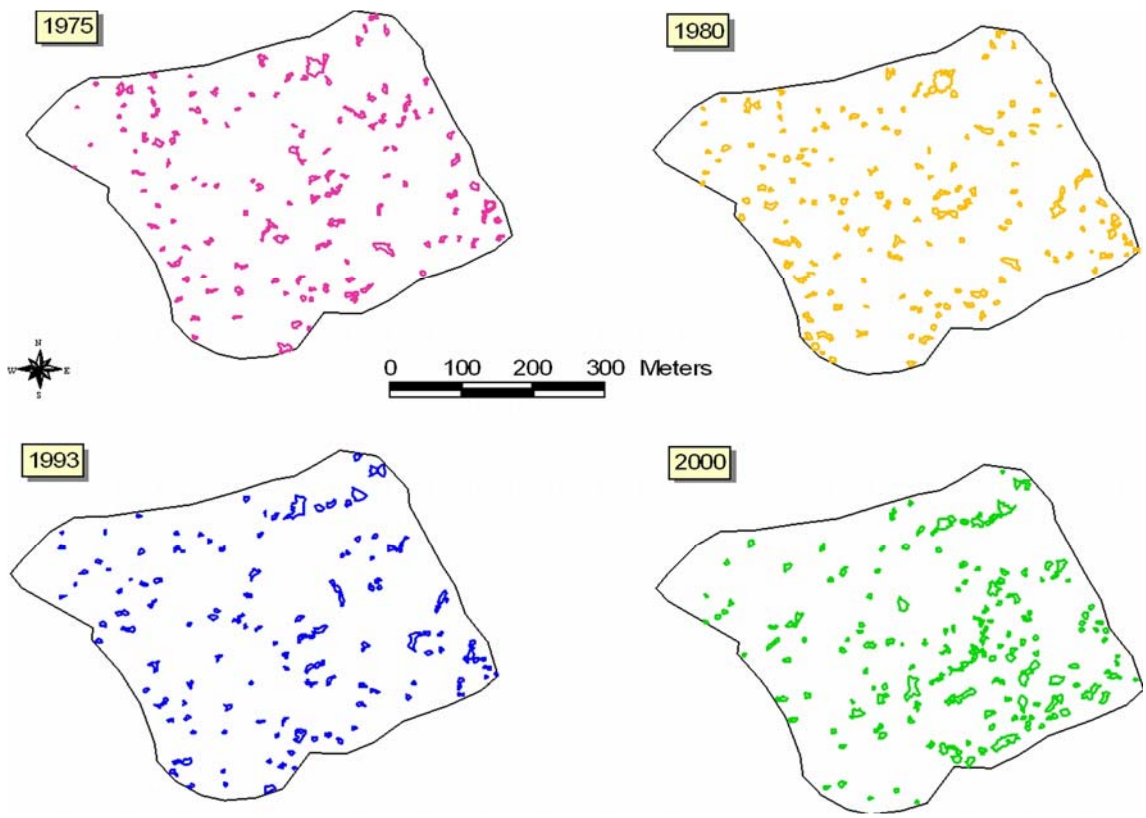


*Figure 1: Distribution of canopy gaps in the Őserdő Forest Reserve in 1975, 1980, 1993 and in 2000 as they were delineated using aerial photographs taken in respective years.*

Table 1 shows descriptive statistics of canopy gaps in the four study years. The number of gaps varied between 125 and 151 in the different years. The observed canopy gaps covered 2.3–4.2% of the total area. Both mean gap size and total gap area increased during the 25 years study period (from 39.4 m² to 61.3 m² and from 4928.22 m² to 8954.55 m², respectively). The most significant change took place between 1993 and 2000, especially in the south-eastern part of the area (cf. Fig. 1).

*Table 1: Descriptive statistics of canopy gaps in the four study years.*

| | 1975 | 1980 | 1993 | 2000 |
|---|---|---|---|---|
| Number of gaps | 125 | 151 | 114 | 146 |
| Total gap area (m²) | 4928.22 | 6592.12 | 5223.82 | 8954.55 |
| Percent of total area covered by gaps (%) | 2.31 | 3.09 | 2.45 | 4.20 |
| Mean gap size (m²) | 39.43 | 43.66 | 45.82 | 61.33 |
| Standard deviation of gap size | 52.76 | 67.34 | 58.24 | 71.02 |
| Maximum gap size (m²) | 487.36 | 731.05 | 454.55 | 377.61 |
| Minimum gap size (m²) | 3.25 | 5.60 | 4.08 | 4.36 |

Maximum gap size decreased during the study period. Determination of minimum gap size is a matter of a rather subjective decision that – among others – depends on the aim of the study. However, it is not reasonable the distinguish gaps smaller than 3 m² in size. Gaps occupied similar topographic positions at each occasion, i.e., gap creation did not show any preference for special altitude, aspect, or slope steepness within the study area.

As Tab. 2 shows, except for the period from 1980 to 1993, slightly more new gaps were created than old ones closed each year. The annual change of gap-area was 0.14–0.53%.

Figure 2 shows examples of all possible events: There are gaps that were closed during the study period (e.g., gaps No. 1, 2 or 10 in the line of the year 1975); there are newly created gaps (e.g., gaps 1, 2 and 3 in the line of the year 1980), there are about the same number of gaps that were merged (gaps No. 11 and 12), as gaps (e.g., No. 6, 7, 14, 16) that were dissected by infilling trees into several sister gaps.

*Table 2: Characteristics describing different aspects of gap dynamics occurred during the three periods covered by our study.*

| | 1975-1980 | 1980-1993 | 1993-2000 |
|---|---|---|---|
| Number of new gaps | 44 | 26 | 95 |
| Proportion of new gaps (%) | 29.14 | 22.81 | 65.07 |
| Proportion of gaps opened annually (%) | 5.83 | 1.75 | 9.30 |
| Area of newly created gaps (m²) | 1549.06 | 1294.95 | 4941.09 |
| Percent of total area covered by new gaps (%) | 0.73 | 0.61 | 2.31 |
| Number of closed gaps | 23 | 63 | 63 |
| Proportion of closed gaps (%) | 18.40 | 41.72 | 55.26 |
| Proportion of gaps closed annually (%) | *3.68* | *3.21* | *7.89* |
| Area of closed gaps (m²) | 565.58 | 1795.78 | 2067.51 |
| Percent of total area covered by closed gaps (%) | 0.00 | 0.01 | 0.01 |
| Change of gaps surviving the period (m²) | 680.42 | -867.47 | 857.15 |
| Change of total gap area (m²) | 1663.90 | -1368.30 | 3730.73 |
| Change of total gap area (%) | 0.78 | -0.64 | 1.75 |
| Annual change of gap area (%) | 0.16 | -0.05 | 0.25 |
| Area where gap creation or closure occurred (m²) | 2795.06 | 3958.20 | 7865.75 |
| Proportion of area where gap creation or closure occurred (%) | 1.31 | 1.85 | 3.69 |
| Annual proportion of area where gap creation or closure occurred (%) | 0.26 | 0.14 | 0.53 |

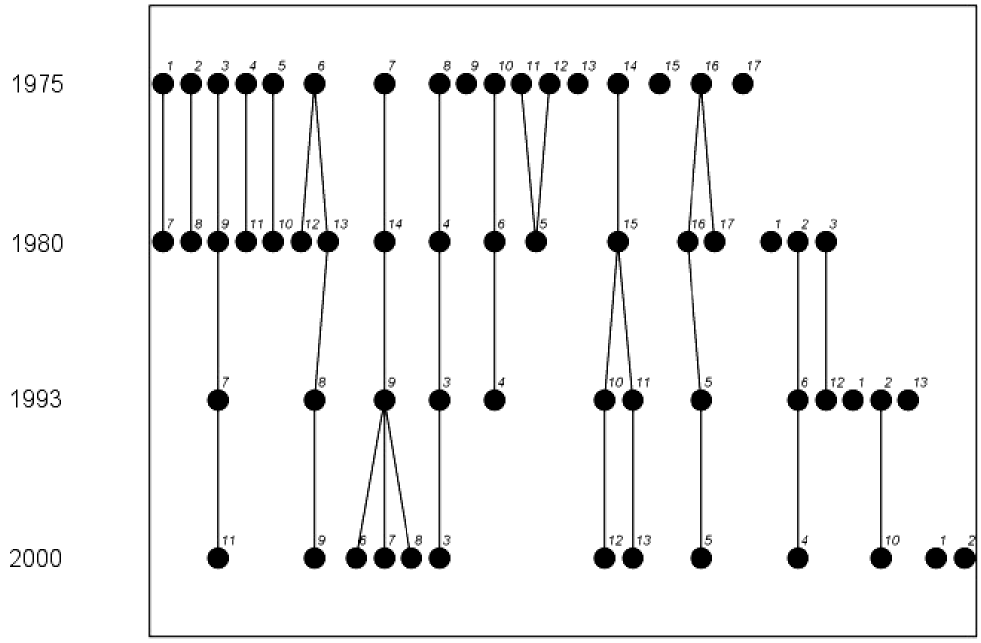


*Figure 2: A small part of the large figure showing the fate of each gap: closure, creation, dissection and merger of neighbouring gaps. Numbers at the beginning of each line indicate the study year. Black dots indicate individual gaps, connecting lines indicate relationships (e.g., gap 7 in 1980 overlaps with gap 1 in 1975). Gaps can be traced back in the map by their identification numbers.*

## 4 DISCUSSION

In answering our first question, we can state that our results show that application of aerial photographs is an important tool in studying gap dynamics. When applying this simple method – airborne photography –, the photos themselves set the limit of applicability. For our purposes the two major weaknesses of the photos we used were: *i)* the position of our stand in the photo was different in each time step; *ii)* the spatial resolution of the photos. The effects and limits set by the resolution are straightforward. However, the fact that our forest stand was viewed from different angles in the different photos, caused several difficulties. Not only the position of gaps "moved around" in time, but also the size and shape of gaps changed. The first problem was treated by the ArcView extension we developed while digitising the gap polygons. The effects of different viewing angles could be moderated by the stereo analysis, however not properly. In the photographs taken in 1993 our study site has extremely marginal position, for this reason, data collected from these images should be treated with caution. We assume that several small gaps could not be recognized, and also data on gap area might be underestimated. In addition to real dynamical processes, these effects might play a role in breaking the trend of increasing total gap area from 1975 to 2000 (cf. data in Tabs. 1 and 2).

We aimed at defining descriptive gap statistics of this semi-natural beech stand for several reasons. It has both theoretical and practical implications. Our results show that both total gap area, and average gap size in the Őserdő Forest Reserve are similar to those found in different temperate and tropical forests (Runkle 1982, Lorimer 1989). From a practical viewpoint we think our results have importance in demonstrating that natural processes usually create rather small gaps for regeneration, which is not in harmony with contemporary forestry practices. We did not find evidence of preferential gap formation at certain altitudes, slope steepness or aspects. However, as Figure 1 shows, by 2000 relatively large new gaps had been created in the south-eastern part of the reserve. This part is characterized by the best site conditions. The deep soil has always enabled large annual increment for the trees that had been freed up by regular tending cuts before the reserve was designated. As a result, the beech trees in this part of the reserve are spaced quite far from each other, could develop large canopies, and were not suppressed during their life. Consequently these large, old individuals are rather susceptible to different disturbance agents (e.g., fungi, wind). Even the death of single trees creates relatively large gaps.

With the help of the ArcView extension we could follow the fate of individual gaps throughout the 25 year study period. The average percentage of canopy that was converted to gaps in the Őserdő Forest Reserve is in harmony with literature data (e.g. Sousa 1984). We showed that in each period two to four times larger area was affected by dynamical processes than simple change of total gap area would indicate (cf. Tab. 2). This means that intensive gap creation and closure took place simultaneously. We have to emphasize that our estimates on gap number, gap size and on the importance of different dynamical processes (creation closure, merger, dissection) depend on the conventions we applied in drawing the gaps.

Finally, we want to stress, that the size of the study area in itself set limits to drawing general conclusions about the dynamics of this beech forest, since it was definitely smaller than the minimum dynamic area (sensu White and Pickett 1985). However, we – as many other colleagues in Europe – had to live together with constraints set by the long and intensive land use history of our forest that has left very little near natural forests for such studies.

## ACKNOWLEDGEMENTS

The research was financed by the NAT-MAN Project, nature-based management of beech in Europe, for the European Community fifth Framework Programme (Grant No. QLKS-CT-1999-01349) and by the Hungarian Science Foundation (OTKA T043452).

## REFERENCES

Lorimer, C. G. (1989). Relative effects of small and large disturbances on temperate hardwood forest structure. Ecology 70: 565-567.

Peterken, G. F. (1996). Natural Woodland – Ecology and conservation in northern temperate regions. Cambridge University Press, Cambridge, pp. 91-95.

Runkle, J. R. (1982). Patterns of disturbance in some old-growth mesic forests of eastern North America. Ecology 63: 1533-1546.

Runkle, J. R. (1985). Disturbance Regimes in Temperate Forests. In Pickett, S. T. A. and White, P. S. (eds) The Ecology of Natural disturbance and Patch Dynamics. Academic Press, Orlando, pp. 17-33.

Sousa, W. P. (1984). The role of disturbance in natural communities. Ann. Rev. Ecol. Syst. 15: 353-391.

Standovár, T. and Kenderes, K. (2003). A review on natural stand dynamics in beechwoods of East Central Europe. Appl. Ecol. and Env. Res. 1 (1–2): 19–46.

White, P. S. and Pickett, S. T. A. (1985). Natural disturbance and Patch Dynamics. In Pickett, S. T. A. and White, P. S. (eds) The Ecology of Natural disturbance and Patch Dynamics. Academic Press, Orlando, pp. 3-13.

# 3D STEREO MAPPING BY MEANS OF ULTRACAMD DATA

*Martin Ofner[1], Manuela Hirschmugl[1], Hannes Raggam[2] and Mathias Schardt[1&2]*

[1] Technical University of Graz, Institute of Remote Sensing and Photogrammetry, Graz, Austria, martino@sbox.tugraz.at, manuela.hirschmugl@joanneum.at

[2] Joanneum Research, Institute of Digital Image Processing, Graz, Austria, (hannes.raggam, mathias.schardt)@joanneum.at

## ABSTRACT

The integration of the 3D component in the extraction of forest information from optical stereo data is a very recent research topic. Investigations carried out in the past have shown that it was already possible to derive information like mean stand height by mean of photogrammetric methods. However, it was found out that the possibilities of the derivation of very high resolution and highly detailed digital surface models (DSMs) from classical stereo data are limited when it comes to the modelling of detailed crown surface, single trees or small gaps in the forest. One alternative system is LiDAR, able to deliver highly detailed DSMs, but at quite high costs. Series of multi-overlapping, digital and very high resolution images can be seen as a high-qualitative as well as cost-effective alternative so far. In this study, images of UltracamD large format digital camera with an along-track overlap of 90% were used for the generation of such a detailed DSM. Due to the large overlap, new methods concerning stereo analysis are to be developed as the same object is visible from different viewing angles in several images. Based on the different viewing angles, valid results can be derived also for the problematic areas mentioned above. A “feature vector” matching method was used for image matching (Caballo-Perucha, 2003). Due to the multiple images involved, more than one matching result is obtained. For each point, the results with the highest quality are then used for the DSM generation. The so-generated DSM is compared to a standard DSM (60 % overlap, only two images) as well as to a LiDAR DSM. The quality of the DSMs was assessed using in situ measured tree heights. It is shown, that the improvements of using more than two images are significant and the quality of the resulting DSM is almost comparable to the quality of the Lidar DSM.

**Keywords:** UltracamD, DSM generation, high resolution image data, digital airborne camera

## 1 INTRODUCTION

For the extraction of detailed forest inventory parameters (tree height, stocking density, timber volume or crown area), several sensor types like very high resolution satellites, analogue as well as digital airborne cameras are used. Aside from the spectral information, there has recently been a growing demand for area-wide 3D information. This information can precisely be obtained by means of Laserscanning (LiDAR, Hyyppä et al, 2003), but at quite high costs. Stereoscopically generated high resolution DSMs based on automatic image matching would be an economic alternative. The generation of these models becomes more and more important in silviculture. The requirements for such a model would be an accurate representation of forest borders and small forest gaps as well as an approximate tree crown surface reconstruction. Since digital camera technique finds its way into remote sensing new possibilities in stereo analysis arise. With the large format digital array cameras like the UltracamD from Vexcel (http://www.vexcel.co.at/), it is now possible to record panchromatic and multispectral information with one single flight. Another benefit of the UltracamD is to get an image series with a forward overlap up to 90% with no higher data costs. With this series of multiple overlapping images (see Figure 1 for a sample acquisition scenario) it is now possible to generate DSMs with a higher quality even for heterogeneous stand structures. Against this background the question to be answered by this investigation is: Are digital aerial cameras like the UltracamD able to derive high quality 3D information fulfilling the requirements mentioned above of forested areas?

## 2 ULTRACAMD CAMERA DESCRIPTION

The UltracamD is designed as a so called multi-head sensor, which concept is to combine single images of several CCD arrays to one big image that satisfies central perspective. The camera is equipped with four cones (9 CCD arrays) for the panchromatic data and four cones (4 CCD arrays) for the multispectral (RGB and NIR) data (see Table 1 and for further details Leberl et al, 2003 and Kremer et.al, 2004). Figure 1 shows an exemplified UltracamD image acquisition scenario. The horizontal projection shows only subsets of the entire image. In this case all five images depicting the same point on the ground can be combined in the stereo extraction process. Combining only image 1 and 5, the scenario corresponds to the photogrammetric standard case with two images having 60% forward overlap.

*Table 1: UltracamD technical specification (based on Vexcel Imaging Austria, www.vexcel.co.at)*

| **Digital Camera Sensor Unit (SU)** | **panchromatic** | **multispectral** |
|---|---|---|
| Panchromatic image size | 11500 * 7500 pixels | 4008 * 2672 pixels |
| Panchromatic physical pixel size | 9 µm | 9 µm |
| Panchromatic lens focal distance | 100 mm | 28 mm |
| Lens aperture | f= 1/5.6 | f=1/4.0 |
| Field-of-view, cross-track (along-track) | 55° (37°) | 65° (46°) |
| Physical format of the focal plane | 103.5 mm * 67.5 mm | |
| Shutter speed options | 1/500 to 1/60 second | |
| Forward-motion compensation (FMC) | TDI-controlled | |
| Maximum FMC capability | 50 pixels | |
| Smallest pixels on the ground at flying height of 500 m (300 m) | 5 cm (3 cm) | |
| Radiometric resolution | > 12 bit | |

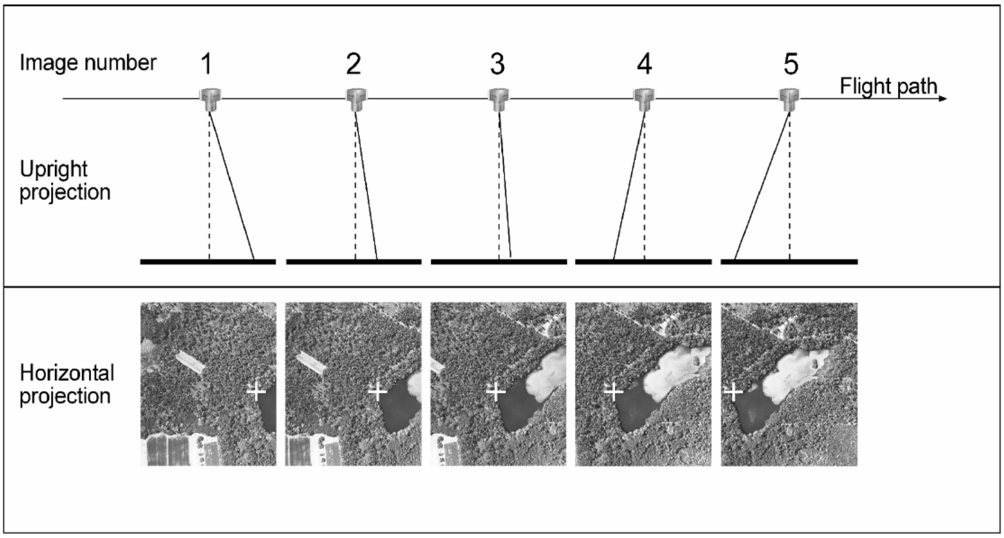


*Figure 1: UltracamD image acquisition scenario*

## 3 DATA AND TEST SITE

The testsite Burgau is located in south-east Austria with an average height of 300m above sea level. The leading tree types in this region are spruce, pine and oak trees. A single strip of UltracamD images with a forward overlap of 90% were obtained for the test site. With a chosen flying height of about 1800m above ground, the images offer a geometric resolution of 15 cm for the panchromatic data and approximately 55cm for the multi-spectral data. The selected resolution of 15cm shows a good compromise between costs, coverage and spatial detail. For the present study panchromatic and multi-spectral bands were fused to high resolution colour infrared (CIR) images using IHS transformation (Perko, 2004).

# 4 3D DATA EXTRACTION

The following chapter gives a short introduction to the DSM generation process with the Remote Sensing Software Graz (RSG) developed at Joanneum Research, Graz (JOANNEUM RESEARCH, 2003). For geometric modelling of the available UltracamD data, the required ground control points were measured using a Differential Global Positioning System (DGPS). Additionally homologous points were measured in the respective images to connect them. In order to guarantee the consistency of geometric properties (orientation, pixel resolution) for the stereo partners, an epipolar resampling (relative registration) has to be done in order to keep the search window for the following image matching small. During the matching process homologous points have to be found automatically in the reference image as well as in the search image (see Figure 2(a)). In RSG different matching procedures are available. For this investigation the feature-vector-matching method has proven to be the best matching approach (Caballo-Perucha, 2003). A so called “feature-vector” contains derivatives of the original images to be matched. Features like the crosscorrelation coefficient, edge filters, variance or convolution filters were used. This feature-vector method is not limited to one or two properties of an image like other matching techniques but offers endless options for combining several features depending on the used image data.

In order to make a confident quality assessment for the matching results the so called back-matching distance is used. The back-matching distance is defined as the spatial distance between the predefined pixel location $P_r$ and the backward matching result $P'_r$ (see Figure 2(b)). This distance gives a confidence measure for the matching result which is only acceptable in cases where it doesn’t exceed a predefined threshold, i. e. a specified number of pixels. To determine 3D coordinates in East, North and Height for the output of the image correlation a point intersection progress following a least squares adjustment has to be done.

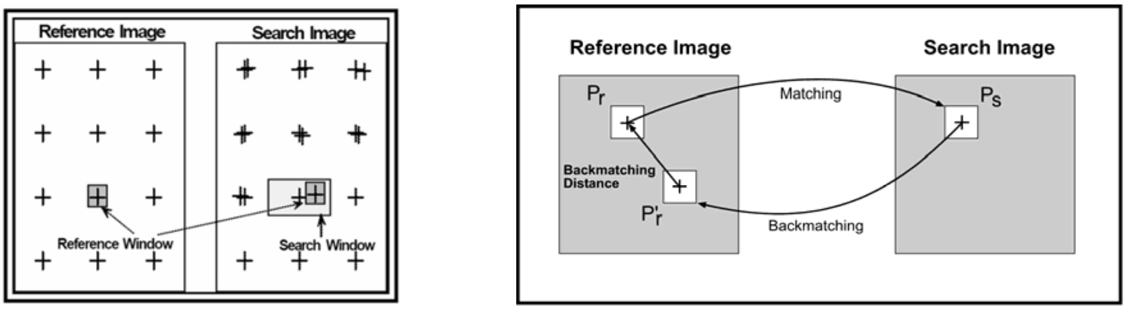


(a) image correlation (b ) backmatching

*Figure 2: Illustration of two main steps of the DSM generation process*

## 4.1 Block based approach

For gathering the best 3D information from the UltracamD images, another technique opposite to the conventional stereo processing is needed. A block based approach recently developed at JOANNEUM RESEARCH and integrated in RSG, has been used (Joanneum Research, 2003). This approach involves multiple adjacent images (in this study five) instead of two and is therefore expected to return higher quality results. The central image, (image 3 in Figure 1) is subsequently matched with all other images. This leads to multiple matching results for each pixel in the reference image. In this study, the ideal case would return four valid matching results. Especially in wooded areas with their rough crown surface, the standard case (two images, 60% overlap) is often unable to produce valid result during the image matching process (the dashed lines in Figure 3 show the standard stereo configuration). If the surface has a strong vertical structure, the matching might often produce invalid results. The reason for this effect is simple: If it is not possible to see the same point in both images of a stereo pair the matching process is unable to find corresponding pixels (see Figure 3). The advantage of multiple viewing angles is shown in Figure 3. Especially in areas with a heterogeneous vertical structure like small forest clearings, along forest borders or for the reconstruction of crown shapes, matching is only possible with a stereo intersection angle small enough to show the same pixel in at least two images. On the one hand the smaller base-to-height-ratio provides a less robust intersection but on the other hand a valid matching and furthermore a valid point intersection is at least possible. The multiple projection rays lead to multiple matching results. A least squares algorithm is applied in order to find the best fitting target point coordinates. In this algorithm, the squared sum of the spatial difference of the resulting ground location with respect to the projection rays is minimized. Erroneous and unreliable results can be found and discarded. As long as two projection rays (i.e. one valid matching result) are available, point intersection can be performed.

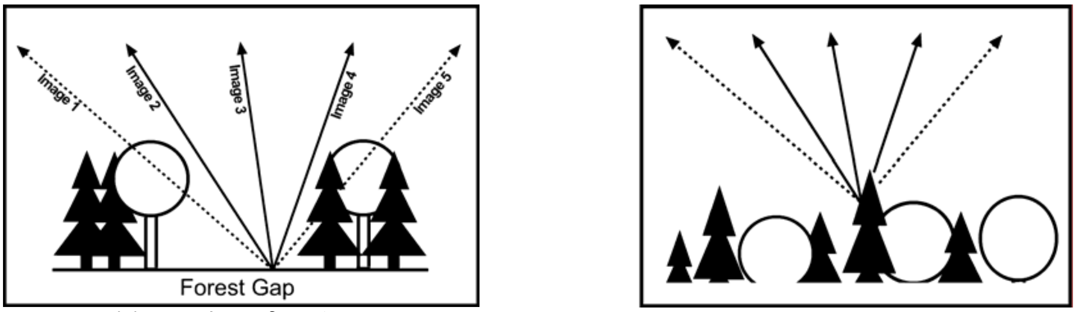


*(a) mapping a forest gap* *(b) detailed view on a treetop*

*Figure 3: Multiple projection rays*

Typical situations are shown in figure 3: The projection rays displayed with the dashed lines represents the conventional stereo scenario with two pictures with 60% overlap. The same pixel is not visible from these two projection rays, and thus, no valid matching result can be derived. For the block based approach there are still three combinations of projection rays possible (2 with 3, 3 with 4, 2 with 4).

# 5 ACCURACY ANALYSIS

Accuracy analysis consists of two parts. The first part (chapter 5.1) is a quantitative analysis comparing the generated DSMs (both with block based and standard approach) and an available LiDARDSM with terrestrially measured tree heights in order to assess their absolute height accuracy. Vegetation height models (VHMs) had to be generated by subtracting a digital terrain model (obtained by LiDAR) from the three DSMs. The resulting VHMs (BLOCKVHM, STANDARDVHM and LiDARVHM) are then used for comparison. The purpose of the second analysis part (chapter 5.2) is to assess the accuracy of the surface structure. To do so, the LiDARVHM is used as reference.

## 5.1 Verification Tree Heights

For the verification of the tree heights, both the position and important forest attributes of 549 trees organized in 10 representative well distributed sample plots were measured. The sample plots were selected in order to be representative in regard to tree types, age classes and densities, whereas the plot size depends on the average DBH of the trees. The location of each tree stem was measured at breast height (1.3 m above ground) using differential GPS and a tachymeter. For each tree, its diameter at breast height (DBH), tree type and height were recorded. The DBH was measured with a slide calliper and the tree heights with a VERTEX III hypsometer (Haglöf, Sweden). According to Barron (2001), the height accuracy of measurements with this instrument is about one meter (tested with different operators). For this accuracy analysis, only trees of the upper layer, which are trees higher than two thirds of the maximum height of each plot, were used (356 trees), as it is not possible to measure the height of suppressed trees from above.

Nevertheless, the location of the stem at breast height and the location of the highest point of a tree do not necessarily match. The social position of a tree and the constant competition for light (phototrophism) are factors that might force trees to grow bent resulting in the fact that the highest point of the tree crown might easily be a few meters off the stem location at breast height. In order take this circumstances into consideration two procedures are conceivable:

1. automated assignment of terrestrially measured stem position to tree tops derived from photogrammetry based on a buffer around the measured stem location larger than the possible offset which easily can amount up to 3m (Fuchs, 2003) or

2. shifting manually the point of the measured stem location to the tree top visible in the DSM.

The first procedure mentioned above is difficult to handle, because a buffer of e. g. 6 meters (corresponding to 3 meters offset in each direction) would particularly in dense forests lead to overlapping buffers and multiple "correct" results. Therefore the second possibility was chosen. Three sources of information were used to support the visual allocation of the points: the LiDARDSM from 2005, as it shows a good geometric correspondence with the photogrammetrically derived DSMs, the UltracamD true ortho images (rectified using the DSM) and the UltracamD DSM itself.

Table 2 shows a comparison of the 356 in situ measured tree heights with the VHMs. The statistical parameters in the table demonstrate the advantage of the block based approach compared to the standard stereo approach. The mean difference and the standard deviation of BLOCKVHM and LiDARVHM are about the same.

*Table 2: Statistic parameters for tree height accuracy based on 356 terrestrially measured tree heights*

| n = 356 | **STANDARDVHM** | **BLOCKVHM** | **LiDARVHM** |
|---|---|---|---|
| Mean | 1,34 m | 0,77 m | -0,62 m |
| Standard deviation | 4,52 m | 2,39 m | 2,00 m |

## 5.2 Verification of the surface structure

This chapter shows some visual comparisons between the VHMs to point out how detailed the surface could be reconstructed. To accomplish fair conditions the invalid pixels in all three DSMs have been filtered with a 3x3 maximum filter by only affecting invalid pixel values. The first comparison (Figure 4 (a - d)) shows, how a gap is mapped by the three VHMs and how it appears in the UltracamD ortho image. Due to orthophoto geometry (based on the DTM) there is a slight shift between the gap location appearing in the VHMs and the orthophoto. The red line marks the forest gap as visible in the LiDARVHM. The dark single pixels visible in the LiDARVHM show, where the LiDAR pulse penetrated the crown surface and returned from the ground. Single black pixels in the other two models are invalid pixels resulting from poor matching, which were not filled by the maximum filter. As seen in Figure 4 the gap is clearly visible in the LiDARVHM and in the BLOCKVHM but nearly invisible in the STANDARDVHM. Additionally, it can be seen, that single tree crowns within the forest can be distinguished much clearer in the BLOCKVHM compared to the STANDARDVHM.

Another comparison is shown in Figure 5. The Figures show two free-standing trees to visualize the quality of the BLOCKVHM. When comparing Figure 5 (c) and (d), the benefits of the block based approach are evident. The free-standing single trees reconstructed within the BLOCKVHM show a good correspondence to the LiDARVHM, whereas both trees are hardly visible in the STANDARDVHM.

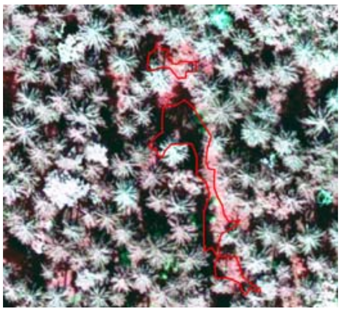

*(a) ortho image*

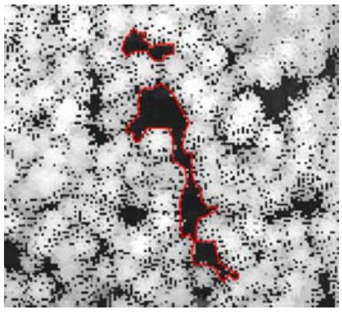

*(b) LiDARVHM*

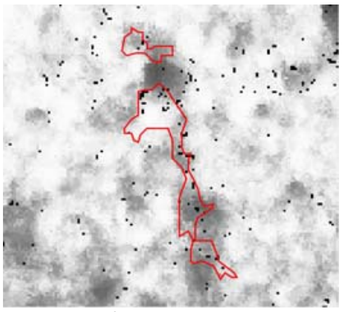

*(c) VHM from standard stereo*

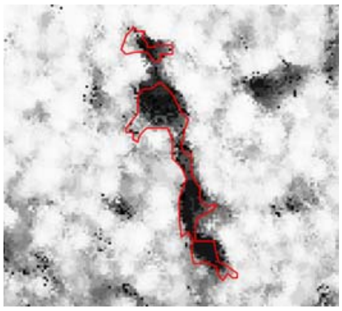

*(d) VHM from block based approach*

*Figure 4: Mapping of a forest gap: orthophoto and results in different VHMs*

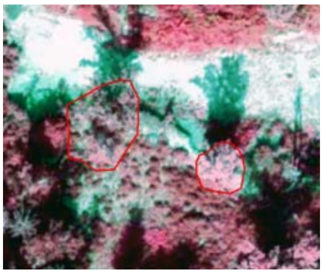

*(a) single trees in the ortho image*

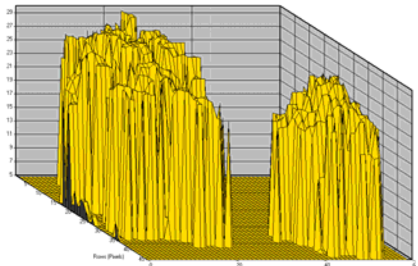

*(b) 3D tree surface from LiDARVHM*

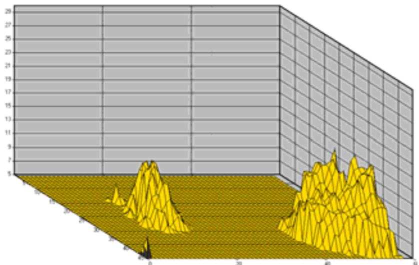

*(c) 3D tree surface from STANDARDVHM*

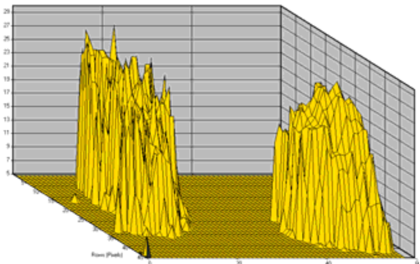

*(d) 3D tree surface from BLOCKVHM*

*Figure 5: 3D surface from free standing single trees*

## 6 DISCUSSION

Digital airborne cameras like the UltracamD offer new opportunities for the photogrammetric 3D data extraction. Especially the use of multiple projection rays can be seen as one important achievement. This study shows potential of this new method for difficult forested areas. Compared to terrestrially measured tree heights, the BLOCKVHM shows a mean difference of 0.77 m (standard deviation 2.39

m) compared to the STANDARDVHM with a mean of 1.34 m (4.52 m). The figures clearly show the superiority of the block based approach. Regarding the surface structure, the comparison also gives encouraging results.

## 7 CONCLUSIONS

The high quality of the BLOCKDSM allows it to be used for a variety of different applications so far only possible with LiDAR data. Examples are single tree segmentation, mapping of 3D changes like damages and small clear cuts, mapping of forest roads or forest stand segmentation. From optical very high resolution data only, such elements are difficult to detect, as they are often not clear in the sense of spectral reflectance differences. The integration of 3D- and spectral data in terms of geometric adjustment as well as thematic combination are still questions to be answered. Segmentation and classification algorithms have to be adjusted to handle the complementary information to exploit its full potential for practical forestry. Furthermore, research is necessary to investigate the use of more than one strip of images with an additional side overlap. It has to be investigated, if the integration of projection rays across the flight line can further improve the results.

## REFERENCES

Barron, R. J. (2001). Precision of three tree height measuring devices in forest conditions. In: Research Note 1/2001, Forest Research Branch, Department of Agriculture and Rural Development, Government of Northern Ireland. http://www.forestserviceni.gov.uk/publications/research_notes/research_note_no_1_2001.pdf

Caballo-Perucha, M. (2003). Development and analysis of algorithms for the optimisation of automatic image correlation. Master thesis, Post-graduate University Course Space Science, Karl-Franzens-University Graz, December 2003.

Fuchs, H.-J. (2003). Methodische Ansätze zur Erfassung von Waldbäumen mittels digitaler Luftbildauswertung. PhD thesis, Georg August University Göttingen, 138p.

Hyyppä, J., Hyyppä, H., Maltamo, M., Yu, X. W., Ahokas, E. and Pyysalo, U. (2003). Laser Scanning of Forest Ressources – Some of the Finnish Experience. ScandLaser Scientific Workshop on Airborne Laser Scanning of Forests, Umea, Sweden, pp. 53 – 59.

JOANNEUM RESEARCH, (2003). RSG in Erdas Imagine. Software Documentation, Version 2.1, RSG-Release 4.60.

Kremer, J. and Gruber, M. (2004). Operation of the UltraCamD together with CCNSa/Aerocontrol – first Experiences and Results. International Archives of Photogrammetry and Remote Sensing, XXth ISPRS congress, Istanbul, 12 – 23 July 2004, published on DVD, 6 pages.

Leberl, F., Gruber, M., Ponticelli, M., Bernögger, S. and Perko, R. 2003. The UltraCam Large Format Aerial Digital Camera System Proceedings Of The American Society For Photogrammetry & Remote Sensing, Anchorage, Alaska, 5-9 May, 2003; http://www.vexcel.co.at/products/photogram/ultracam/downloads.php.

Perko, R. 2004. Computer Vision for Large Format Digital Aerial Cameras. PhD thesis, Graz University of Technology - Institute for Computer Graphics and Vision. Graz, October 2004, 158 p.

# SPECTRAL VARIABILITY OF AERIAL IMAGERY TEMPORAL SERIES AS FACTOR IN FOREST HEALTH STATUS CLASSIFICATION

*Rastislav Raši*

National Forest Centre, Forest Research Institute, Department of Ecology and Biodiversity of Forest Ecosystems, Zvolen, Slovak Republic, rastislav.rasi@fris.sk

## ABSTRACT

The study was oriented to discover relations between field observed characteristics of trees health status (colour changes, tree crown foliage density) and characteristics derived from colour infrared photos (image density of image components, derived spectral indices and principal components). 3D models derived from aerial photos were used to generate DTM for image orthorectification and to improve identification of individual trees. The time series of stereo pairs of large scale (approx. 1 : 3 000) aerial photos were processed in this study. The colour infrared film Kodak 2443 was used. The field coordinates of individual trees on monitoring plots were measured by theodolite in local coordinate system, tree crown projections were measured in four horizontal directions. The colour changes of leaves and foliage density of individual tree crowns were evaluated during field observation. Individual tree crowns were delineated for image parameters extraction. The correlation analysis was performed to analyse relations between field observed and image derived characteristics. The correlation of individual image components with field observed foliage colour changes and crown foliage density showed expected tendency, but correlation coefficients did not have satisfactory values. Better results were obtained for component indices of which index representing NDVI components combination (NIR – R / NIR + R) showed the best correlation with both field observed characteristics. The conclusion of this study is that all image components should be involved in regression model, but better choice should be derived characteristic selection for forest health status evaluation.

**Keywords:** colour infrared photos, defoliation, discoloration, spectral indices

## 1 INTRODUCTION

Forest health condition and its changes are good markers of environment status and its changes. From forestry point of view, changes of forest health status are influencing factor of economic activity and wood production as well. Consequently, respective attention is devoted to this topic and forest health status is evaluated yearly. Field investigations with applied sampling designs are used for detailed data collection due to the extent of woodland area. Large areas should be evaluated by means of progressive satellite remote sensing methods. The aerial photos are traditional source of information in forestry, and are important in forest health status evaluation as well. The advantage of this material is the possibility of film material selection and photo scale determination with regard to intended aims and details importance. The other advantage is possibility of archiving, comparison and interpretation of data series. The most frequently used material for forest health condition evaluation is reversal color infrared (CIR) film and products of Kodak company are preferred. Films compose of Estar base layer and three sensitive layers. The "false color" picture is result of chemical processing of film, blue response is produced by green light, green response by red light and red response after near infra-red (NIR) irradiation. To produce final image principle of subtraction is applied. Detailed description of CIR material should be found in Lillesand, Kiefer (1994). The sensibility of film to the NIR part of spectra is useful for cellular structural change and biomass amount detection. Healthy vegetation reflects NIR radiance intensively than damaged. Kodak 2443 material was tested for detection of forest damage interpretation and manual for visual interpretation on the base of color and crown structure characterization was compiled by experts (CEC 1991). The problem of automated detailed forest health status classification using this material arises from different light conditions influenced by terrain, forest stand structure and sun geometry. Different light conditions of two missions complicate direct comparison of spectral parameters when time series are compared. The influence of spectral variability of time series CIR photos on foliage damage is analyzed.

## 2 METHODS

The input data were collected in homogenous deciduous forests at permanent monitoring plots (PMP) of intensive level of forest health status monitoring (Bucha et al. 2002). The percentage of foliage loss and foliage discoloration of each tree is visually (using binocular) evaluated each year in the same period of the year. These data were used as ground truth and were compared with spectral characteristics of individual trees at CIR aerial photos. The aerial photos were taken in the same period as terrestrial evaluation was performed. The shape of plots is square, the length of each side is 50 meters and each tree is permanently marked with specific number. The local coordinates of trees were measured in preparation stage and horizontal tree crown projections were measured in four perpendicular directions from which one was oriented to the north. These data were necessary for identification of individual trees on aerial photos. The experiment was realized at two pure oak monitoring plots, one covered by pedunculate oak (PMP Gabčíkovo) and second covered by Turkey oak (PMP Čifáre). The foliage loss and discoloration of trees were determined using harmonised methods of ICP Forests programme and percentage values were assigned to individual trees in the range from 0 to 100%, five percent step was applied. The characteristics of field investigation are summarized in Table 1. Detailed information on monitoring plots is in Bucha et al. 2000.

*Table 1: The summary of terrestrial investigation of foliage loss and discoloration on selected permanent monitoring plots (PMP).*

| Year | PMP | Foliage loss [%] | | | | Discoloration [%] | | | | Number of evaluated trees [n] |
|---|---|---|---|---|---|---|---|---|---|---|
| | | min. | max | mean | RMS | min. | max. | mean | RMS | |
| 1999 | Gabčíkovo | 0 | 70 | 36,313 | 12,747 | 0 | 40 | 10,500 | 9,400 | 80 |
| 2000 | Gabčíkovo | 0 | 85 | 31,688 | 11,582 | 0 | 0 | 0 | 0 | 80 |
| 2001 | Gabčíkovo | 0 | 45 | 28,797 | 6,366 | 0 | 70 | 14,114 | 12,879 | 79 |
| 2000 | Čifáre | 10 | 40 | 22,877 | 5,247 | 0 | 50 | 4,456 | 8,583 | 146 |
| 2001 | Čifáre | 15 | 60 | 26,096 | 6,526 | 0 | 0 | 0 | 0 | 146 |

The photos were taken on PMP Gabčíkovo in 22.8.1999, 24.8.2000, 6.8.2001 and on PMP Čifáre in 24.8.2000 and 6.8.2001. The semi-metric camera Hasselblad MK 70 was used to obtain stereo pairs of photos. The transparencies were scanned and digital outputs were files containing three spectral components: red (R), green (G) and blue (B). Digital photos were processed in photogrammetric software, digital model of forest canopy relief (DMR) was derived for overlapping areas. The model was involved in orthorectification process of photos. This process was realized for better identification of individual trees and correct joining of photos with measurements from the field. The polynomial transformation was used for precise adjustment of time series of photos. GIS platform was used to overlap digital photos with thematic layer containing tree positions and horizontal crown projections. 3D observation was used for individual trees identification as well. The polygons of crown projections from field measurement were not ideally corresponding to those visible on photos, so identified individual crowns were manually delineated for spectral analysis (see Figure 1.). Selected were only trees, which were well identified with regard to field measurements. The spectral characteristics derived from digital images were determined for each polygon delineating crown of tree. The following characteristics were determined for each polygon area:

- mean of each image component R,G, B,
- indices i.e. ratios of components R/G, R/B, G/B,
- normalized indices i.e. ratios NRG = (R-G)/(R+G), NRB = (R-B)/(R+B),
- mean values PC1, PC2, PC3 representing each polygon, derived from output components of principal component analysis derived for area of whole PMP from R, G, B channels and
- mean values PCN1, PCN2, PCN3 representing each polygon, derived from output components of principal component analysis of R, G, B channels in area of all selected polygons.

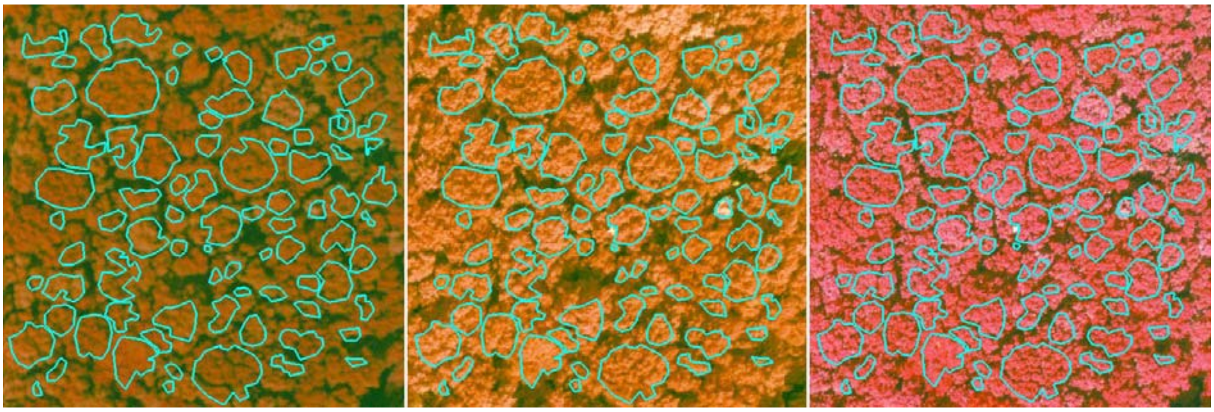

*Figure 1: Time series of color infrared photos (Kodak 2443) of permanent monitoring plot Gabčíkovo. The images differ spectrally due to different light conditions during photographing. (photographed in 22.8.1999, 24.8.2000, 6.8.2001).*

Correlation analysis of these characteristics and results of field observation, i.e. values of visually determined foliage loss and discoloration was performed. The correlation coefficients are given in tables 2 and 3. Multiple-regression models for each year and monitoring plot were analyzed for foliage loss and discoloration determination (independent variables) where R, G, B components were used as dependent variables. The parameters of regression models are given in tables 4 and 5.

## 3 RESULTS

The correlation coefficients are measures of relations between foliage loss and discoloration determined in field investigation and characteristics derived from digital images. Variables mentioned in previous chapter did not correlate very strongly with variables from field observation. This is mainly due to fact, that the range of values of defoliation and discoloration was very narrow and values were concentrated around their mean. The variability of estimation in field should be considered as well. The values of correlation coefficients of dependence between foliage loss of individual trees and characteristics derived from aerial images are in Table 2. The values of correlation coefficients of dependence between discoloration of individual trees and characteristics derived from aerial images are in Table 3.

*Table 2: The values of correlation coefficients of dependence between foliage loss of individual trees and characteristics derived from aerial images for these trees.*

| Year | PMP | Values of image components and derived characteristics | | | | | | | | | | | | | | n |
|---|---|---|---|---|---|---|---|---|---|---|---|---|---|---|---|---|
| | | R | G | B | R/G | R/B | G/B | NRG | NRB | PC1 | PC2 | PC3 | PCN1 | PCN2 | PCN3 | |
| 1999 | Gabčíkovo | -0,132 | 0,246 | 0,258 | -0,059 | -0,251 | -0,220 | -0,219 | -0,257 | -0,110 | 0,282 | 0,279 | -0,107 | 0,290 | 0,245 | 80 |
| 2000 | Gabčíkovo | -0,086 | 0,116 | 0,109 | 0,333 | -0,069 | -0,055 | -0,287 | -0,162 | 0,203 | -0,195 | 0,277 | 0,207 | -0,102 | 0,282 | 80 |
| 2001 | Gabčíkovo | -0,107 | 0,116 | 0,042 | -0,167 | -0,030 | 0,003 | -0,172 | -0,053 | 0,005 | -0,133 | 0,192 | 0,020 | -0,158 | 0,178 | 79 |
| 2000 | Čifáre | 0,071 | 0,207 | 0,164 | -0,261 | -0,156 | -0,145 | -0,258 | -0,164 | 0,146 | -0,173 | 0,285 | 0,165 | -0,145 | 0,268 | 146 |
| 2001 | Čifáre | -0,132 | 0,025 | -0,078 | -0,160 | -0,015 | 0,115 | -0,137 | 0,066 | -0,114 | 0,069 | 0,150 | -0,095 | -0,081 | 0,240 | 146 |

critical values: $r_{0,05;80}$=0,22; $r_{0,05;146}$=0,162; n – number of trees

Results should be interpreted that health status of tree foliage is coded to third component of principal component analysis, next appropriate characteristics are NRG (representing normalized vegetation index), R/B (representing ratio of reflectance of near infra-red and red part of spectra) and image component B (representing reflectance of red part of spectra). The positive values of correlation coefficients for specific variable derived from digital image are markers, that this marker is growing with independent variable (defoliation/discoloration) and negative values of correlation coefficients show that specific variable is decreasing when independent variable is growing. The most stable coefficients were identified for derived variables PCN3, PC3, NRG, R/B and component B.

*Table 3: The values of correlation coefficients of dependence between discoloration of individual trees and characteristics derived from aerial images for these trees.*

| Year | PMP | Values of image components and derived characteristics | | | | | | | | | | | | | | n |
|---|---|---|---|---|---|---|---|---|---|---|---|---|---|---|---|---|
| | | R | G | B | R/G | R/B | G/B | NRG | NRB | PC1 | PC2 | PC3 | PCN1 | PCN2 | PCN3 | |
| 1999 | Gabčíkovo | -0,031 | 0,256 | 0,317 | -0,147 | -0,221 | -0,218 | -0,142 | -0,286 | -0,034 | 0,290 | 0,233 | -0,030 | 0,293 | 0,198 | 80 |
| 2000 | Gabčíkovo | 0,000 | 0,000 | 0,000 | 0,000 | 0,000 | 0,000 | 0,000 | 0,000 | 0,000 | 0,000 | 0,000 | 0,000 | 0,000 | 0,000 | 80 |
| 2001 | Gabčíkovo | -0,166 | 0,233 | 0,128 | -0,314 | -0,074 | -0,001 | -0,316 | -0,150 | 0,056 | -0,277 | 0,299 | 0,083 | -0,311 | 0,262 | 79 |
| 2000 | Čifáre | -0,034 | 0,073 | 0,064 | -0,138 | -0,084 | -0,077 | -0,139 | -0,068 | 0,026 | -0,075 | 0,166 | 0,054 | -0,151 | 0,140 | 146 |
| 2001 | Čifáre | 0,000 | 0,000 | 0,000 | 0,000 | 0,000 | 0,000 | 0,000 | 0,000 | 0,000 | 0,000 | 0,000 | 0,000 | 0,000 | 0,000 | 146 |

critical values: $r_{0,05;80}$=0,22; $r_{0,05;146}$=0,162

Note: At PMP Gabčíkovo in the year 2000 and at PMP Čifáre in the year 2001 no discoloration was recorded during field observation

For practical purposes, the multiple regression analysis was performed, where individual channels R, G, B were involved as dependent variables and foliage loss from field observation was representing independent variable. The parameters of this analysis are in Table 4.

*Table 4: The parameters of multiple regression models of individual trees foliage loss dependence on corresponding mean values of CIR aerial image components R, G, B.*

| Year | PMP | Parameters of multiple regression models | | | | | | Number of trees [n] |
|---|---|---|---|---|---|---|---|---|
| | | Regression coefficient | | | Intercept | Correlation coefficient of multiple regres. | RMS | |
| | | R | G | B | | | | |
| 1999 | Gabčíkovo | -0.244 | 1.232 | -0.244 | -47.467 | 0.324 | 12.295 | 80 |
| 2000 | Gabčíkovo | -0.505 | 0.838 | -0.171 | 40.487 | 0.298 | 11.272 | 80 |
| 2001 | Gabčíkovo | -0.051 | 0.357 | -0.144 | 16.728 | 0.214 | 6.341 | 79 |
| 2000 | Čifáre | -0.165 | 0.520 | -0.180 | -3.710 | 0.298 | 5.061 | 146 |
| 2001 | Čifáre | -0.005 | 0.854 | -0.261 | -36.332 | 0.251 | 6.383 | 146 |

The foliage loss of individual trees between two periods is usually strongly correlated. The status of damaged trees is not improved in the next season rapidly and healthy trees are usually not heavily damaged in the next season as well. So correlation of individual trees between two seasons is very strong usually. It was also found for the majority of CIR image components and derived characteristics (see Table 5.).

*Table 5: Correlation coefficients of the dependence of values between years for foliage loss, CIR image components R, G, B and derived characteristics.*

| Years | PMP | Correlation coefficients for image components and derived characteristics and foliage loss | | | | | | | | | | | | | | | n |
|---|---|---|---|---|---|---|---|---|---|---|---|---|---|---|---|---|---|
| | | R | G | B | R/G | R/B | G/B | NRG | NRB | PC1 | PC2 | PC3 | PCN1 | PCN2 | PCN3 | Foliage loss | |
| 1999-2000 | Gabčíkovo | 0,16 | 0,52 | 0,64 | 0,42 | 0,41 | 0,47 | 0,20 | 0,54 | 0,19 | -0,69 | 0,35 | 0,18 | -0,55 | 0,39 | 0,37 | 80 |
| 2000-2001 | Gabčíkovo | 0,37 | 0,58 | 0,50 | 0,12 | 0,24 | 0,21 | 0,80 | 0,46 | 0,16 | 0,71 | 0,26 | 0,22 | 0,54 | 0,17 | 0,53 | 79 |
| 1999-2001 | Gabčíkovo | 0,16 | 0,62 | 0,54 | 0,09 | 0,25 | 0,19 | 0,27 | 0,50 | 0,13 | -0,81 | 0,31 | 0,14 | -0,72 | 0,19 | 0,38 | 79 |
| 2000-2001 | Čifáre | 0,53 | 0,68 | 0,67 | 0,23 | 0,37 | 0,49 | 0,51 | 0,65 | 0,56 | 0,68 | 0,67 | 0,63 | 0,62 | 0,56 | 0,32 | 146 |

The changes of foliage loss should be interpreted by variable which reflects changes of defoliation between seasons. The correlation between annual changes of foliage loss and differences of image components/derived characteristics was analyzed. Correlation coefficients are in Table 6.

*Table 6: Correlation coefficients of the dependence between component/derived variable annual changes and annual changes of individual trees foliage loss.*

| Years | PMP | Image component/derived characteristic | | | | | | | | | | | | | | n |
|---|---|---|---|---|---|---|---|---|---|---|---|---|---|---|---|---|
| | | R | G | B | R/G | R/B | G/B | NRG | NRB | PC1 | PC2 | PC3 | PCN1 | PCN2 | PCN3 | |
| 1999-2000 | Gabčíkovo | -0,17 | 0,09 | 0,09 | -0,36 | -0,39 | -0,33 | -0,31 | -0,27 | -0,08 | 0,14 | 0,26 | -0,09 | 0,27 | 0,12 | 80 |
| 2000-2001 | Gabčíkovo | 0,03 | 0,16 | 0,07 | -0,20 | 0,05 | 0,07 | -0,20 | -0,06 | 0,09 | -0,08 | 0,25 | 0,08 | -0,08 | 0,17 | 79 |
| 1999-2001 | Gabčíkovo | -0,09 | -0,08 | -0,04 | 0,06 | -0,20 | -0,16 | -0,08 | -0,07 | -0,14 | 0,18 | 0,05 | -0,15 | 0,20 | 0,03 | 79 |
| 2000-2001 | Čifáre | -0,20 | 0,10 | -0,22 | -0,14 | 0,13 | 0,21 | -0,10 | 0,22 | -0,16 | 0,21 | 0,07 | -0,19 | 0,04 | 0,19 | 146 |

The results in Table 6 supported expectation, that change of derived characteristic NRG (representing normalized vegetation index should be used for foliage loss changes evaluation. The stability of this indicator is given by remaining trend (negative correlation with foliage change in all periods). Change of third principal component is stable as well, but absolute values of correlation coefficients of this variable are smaller.

## 4 DISCUSSION

Results supported the assumption, that field assessment of foliage loss and discoloration are probably more subjective than measurement of spectral characteristics of CIR images and correlation between these two data types should be weak, mainly if the range of foliage loss is narrow. The derived characteristics NRG (representing normalized vegetation index) and third component of principal component analysis should be used to interpret foliage loss of trees from digital color infrared photos.

## 5 CONCLUSIONS

Results of analyses supported known fact, that with increasing damage of tree foliage, the reflectance in infrared part of reflected spectra is decreasing and red part is increasing. Combination of reflectance in these two spectral regions into one variable – normalised difference vegetation index should be appropriate for forest health status classification from aerial color infrared photos. The next appropriate variable is third component of principal component analysis.

## ACKNOWLEDGEMENTS

This task was accomplished under grant of Slovak Ministry of Agriculture No. 2729.

## REFERENCES

Bucha T. et al. (2000): Forest health status in Slovakia. Report from monitoring 2000. Forest research institute Zvolen, Slovakia

CEC (1991): Remote sensing Applications for forest health status assessment. Manual. Commission of European Communities, Walphot S.A., Belgium

Lillesand T., M. and Kiefer R., W. (1994): Remote Sensing and Image Interpretation. John Willey and Sons, Inc., Canada

# MULTISCALE IMAGE TEXTURE ANALYSIS FOR MAPPING FOREST STAND STRUCTURE

*Björn Reu[1], Sebastian Schmidtlein[2]*

[1] University of Bayreuth, Biogeography, 95440 Bayreuth, Germany; b.reu@gmx.de

[2] University of Bayreuth, Biogeography, 95440 Bayreuth, Germany; sschmidtlein@gmx.de

## ABSTRACT

Aim of the present study is to provide maps of forest stand structure for forest management and conservation in Southern Kyrgyzstan. Due to the remoteness of the investigated areas, ground inventories are not a promising choice for this task. Hence, forests are mapped by relating ground plot data to high resolution satellite data (Quickbird). The analysis is based on multiple texture layers derived from the Quickbird panchromatic band. Six different kernel-sizes ranging from 45 m to 120 m and eight textural descriptors are applied. The resulting 48 texture layers are candidate predictors in partial least squares regression analysis. The approach requires no *a priori* definition of the appropriate scale level for texture analysis but relies on the presence of good predictors in a multi-scale layer set. Model errors are assessed by full leave-one-out cross-validations. The coefficients of determination for the regression-models ranged from $r^2$=0.44 to $r^2$=0.66 in cross-validation, depending on the type of parameter under study. Limitations lay mainly in topographic illumination effects that could not be entirely removed due to a misfit between the spatial resolutions of DEM and Quickbird imagery. However, the simultaneous consideration of numerous textural predictors allowed for efficiently mapping the parameters of interest.

**Keywords:** remote sensing, forest inventory, co-occurrence matrix, GLCM, Kyrgyzstan, walnut-fruit forests

## 1 INTRODUCTION

Forest stand structure is an important parameter for forest inventories, which serve as a source of information for decision making in management and conservation (Shiver & Borders 1996a, Pretzsch 1997, Bebi 2001). Stand structures are the result of dynamic processes including human impact, competition for light, water and nutrients (Wulder 1998b); hence, patterns in forest stand structure are also relevant for ecological investigations.

Mapping forest structure by ground inventories demand extensive time and man-power, particularly in remote areas and with rough terrain. For management and conservation of Kyrgyz mountain forests, stand level forest structure maps are required. In order to compile them in an efficient manner, structural parameters such as basal area and stem-density are mapped by means of high resolution imagery. Since physiognomic structures of forest stands emerge significantly in image texture, a textural approach is considered as appropriate (St-Onge & Cavayas 1997, St-Onge et al. 1998b).

For the investigation of Kyrgyz mountain forests, we introduce a new approach that quantifies stand parameters deductively by using multiple-scale co-occurrence measurements (Haralick et al. 1973) with large kernels (45 – 120 meters). Recent studies stress the significance of the scale issue for textural remote sensing approaches (Marceau et al. 1990, Franklin et al. 1996, Hay et al. 1997, Marceau & Hay 1999). In the current study we use multiple co-occurrence measurements simultaneously, including different scale levels by varying kernel-sizes. In consequence, the present approach requires no *a priori* definition of the appropriate scale for texture analysis but relies on the presence of good predictors in a multi-scale set of layers.

## 2 AREA OF INVESTIGATION

The study area is situated at 41.5°N latitude and 73°E longitude at the south slopes of the Fergana range (Kyrgyzstan). The investigated walnut-fruit forests can be found on an altitudinal belt between

1100 and 2100 meter above sea level (Kolov 1998b) and cover about 75 km². Most of the forests occur on mountain slopes and provide a soil and water protective function (Musuraliev 1998b). In addition, they serve as a natural resource for the subsistent livelihood strategies of the local population (Schmidt 2005). After 1991, political and socio-economic transformation processes caused management conflicts that endanger the worlds' unique walnut-fruit forests.

A variable and fine grained topography causes many sources of heterogeneity in growth conditions, such as water supply, solar radiation and disturbances. This led to the development of a structural diverse mosaic of forest stands. The vegetation of the area hosts 16 endemic species. Beside the dominant walnut (*Juglans regia*), 183 species of trees and shrubs occur within these forests (Kolov 1998b). On north-facing slopes, walnut (*Juglans regia)* is associated with maple (*Acer turkestanicum*), plum trees (*Prunus sogdiana*) and varieties of apple trees (*Malus siversii*). In contrast, on south facing slopes occurs a mosaic of open grassland and shrubby vegetation rich in species (Epple 2001).

## 3 METHODS

The approach combines semi-automated interpretation of high spatial resolution digital imagery and field methods of vegetation ecology. Texture analysis of panchromatic Quickbird satellite data was used for the extrapolation of ground plot data. The plot data determines structural attributes of Kyrgyz walnut-fruit forests. The spatial extrapolation of the plot data was implemented using a partial least squares regression (PLSR) analysis.

### 3.1 Image data & texture analysis

Quickbird panchromatic imagery with a ground resolution of 0.6 m was acquired on 12 June 2004 at 11:33 local time. Georeferencing and orthorectification were based on a digital elevation model (DEM) and on 12 ground control points measured by GPS during fieldwork. The DEM was derived from Soviet topographic maps (1:25 000). For adjusting effects of topographic illumination a *Minnaert* correction (McDonald 2000) was applied to the imagery.

For texture analysis co-occurrence measurements based on the grey-level co-occurrence matrix (GLCM) were used. A set of texture layers was derived from the Quickbird panchromatic band applying six different kernel sizes ranging from 75 to 199 pixels and eight textural descriptors as proposed by Haralick et al. (1973). Thus, 48 texture layers were implemented into the predictor matrix that consists of all possible combinations of kernel sizes and texture algorithms (Tab.1).

*Table 1: Eight texture algorithms are applied to six kernel sizes*

| A) texture algorithm | B) kernel size |
|---|---|
| 1. sum average | 1. 75 by 75 pixels |
| 2. sum of squares | 2. 99 by 99 pixels |
| 3. inverse difference moment | 3. 125 by 125 pixels |
| 4. angular second moment | 4. 149 by 149 pixels |
| 5. dissimilarity | 5. 175 by 175 pixels |
| 6. entropy | 6. 199 by 199 pixels |
| 7. correlation | |
| 8. contrast | |

Co-occurrence measures use grey-tone spatial dependence matrices to calculate texture values. These matrices contain the relative frequencies *p*, with which grey tones co-occur in neighbouring pixels, separated by distance *d* with angle *a.* These dependence matrices are computed for various angular relationships between neighbouring pixels (*a*= 0°, 45°, 90°, 135°). The averaged set of these probabilities is stored in the grey-level co-occurrence matrix (GLCM). An image of 8 bit results in a GLCM with dimensions of 256 rows and 256 columns. Haralick et al. (1973) proposed a quantitative analysis of the GLCM through 14 textural descriptors calculated from *p* by stepping through the entire matrix; eight of them are realized in the current study. Marceau et al. (1990) point out, that decisions concerning the GLCM are required, including interpixel distance *d* and the angular relationship *a*; in the present case *d* was set 1 and only horizontal and vertical angular relationships were calculated.

### 3.2 Ground truth data

Rough terrain exerts its negative effect on data pre-processing as well as on allocation and number of field plots. Compromises had to be made between standards in accuracy, statistical rigor and sampling intensity. Structural characteristics of forest stands within the Kyrgyz mountain forests were examined on 60 sample sites in August 2004. A preferential sampling design with stratified attributes (Shiver & Borders 1996) according to the Russian forest typology (B. Venglovski, *pers. communication*) was used to assure the acquisition of full structural variation within the forests. In order to assess structural heterogeneity within a sample, a subplot design was applied. Three circular subplots with 30 m in diameter were arranged triangularly. In each quantitative structure measurements were made on stem-density and basal area, based on the Point-Centered Quarter Method (PCQM, Cottam & Curtis 1956, Mitchell 2001). For regression analysis the data of the three subplots were averaged and combined to one whole-plot.

### 3.3 Regression analysis – The PLSR model

Partial least squares regression (PLSR) analysis is a technique that generalizes and combines features from principle component analysis and multiple linear regression (Wold 1966b, Martens & Martens 2000, Wold et al. 2001). It is specifically useful when predicting one or a set of dependent variables from a very large set of independent variables (Davies 2001). In our case it is of particular interest because it can deal with strongly collinear (correlated) and noisy data.

PLSR searches for a set of latent variables similar to principle components that perform a simultaneous decomposition of independent and dependent variables with the constraint to explain as much as possible of the covariance. In the following regression step the decomposition of the predictor matrix is used to predict the variable of interest. The problem of multi-colinearity is eliminated by the orthogonality of the latent vectors (Abdi 2003).

For the regression step the grey-values of all texture layers at ground plot locations are stored in the predictor matrix. A proper selection of significant predictors is conducted making use of Martens' uncertainty test (Martens & Martens 2000) and considering the weighted regression coefficients. Model errors are assessed by full leave-one-out cross-validation and expressed in coefficients of determination and root mean square errors.

## 4 RESULTS

Graphical results are consistent with our observations made during fieldwork and with results from earlier studies (Kolov 1998b, Epple 2001, Gottschling et al. 2005). E.g., on north slopes with closed forest dominated by walnut, basal area is significantly higher than on south slopes consisting of shrubby vegetation (Fig.1). Model qualities ranged from $r^2$= 0.44 for stem-density to $r^2$= 0.66 for basal area in cross-validation. A comparison of model results (Tab. 2) agrees with statements made by St-Onge et al. (1998b) who found that parameters causally linked to image texture (e.g. basal area) show better accuracies in classification success than indirectly linked parameters, like stem-density. The analysis did not reveal a specific scale level as being more indicative for predictions than others. But, the more predictors were considered the better the chance to include significant ones (and the better the models).

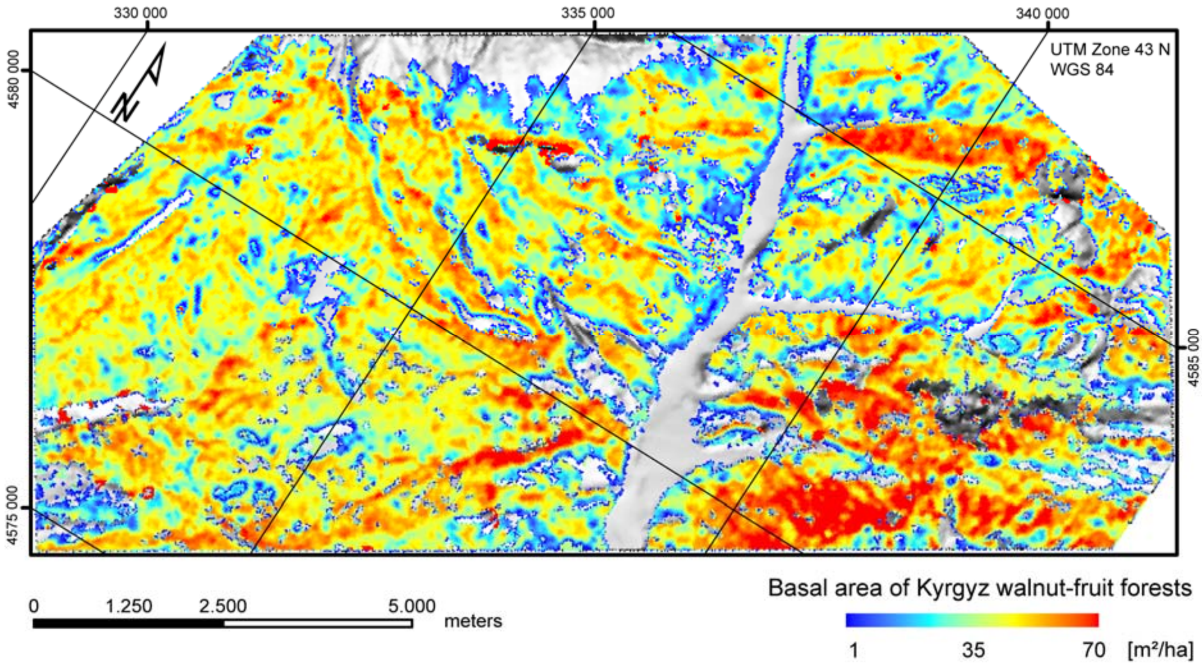


*Figure 1: Predicted basal area derived from 23 texture layers.*

*Table 2: Model parameters for three important structural stand attributes*

| Texture-model | Basal area [m² / ha] | Stem-density [stems / ha] | Proportion of stems with DBH*> 24cm [%] |
|---|---|---|---|
| Nr. of texture input layer | 23 | 13 | 10 |
| RMSE [%] in cross-validation | 12.6 | 14.4 | 20.7 |
| $R^2$ in cross-validation | 0.66 | 0.44 | 0.60 |

* DBH: diameter at breast height

## 5 DISCUSSION

Approaches to forest stand structure can be inductive or deductive. An inductive method is the individual tree crown approach (ITC) frequently used for the delineation and identification of single tree crowns (Gougeon 1998b, Leckie et al. 2003). It proofed to work well in homogenous and coniferous stands (Wang et al. 2004). In deciduous stands the problem emerges that tree crowns consist of clusters of branches, which complicate the segmentation process (Warner et al. 1998b). In very complex situations like in the Kyrgyz walnut-fruit forests with a mixture of shrubs and deciduous trees, a tree-crown approach is hardly applicable.

Apart from the GLCM method there are alternative deductive approaches that can be used in the PLSR framework. One possibility is directional semivariogram estimates, used by St-Onge & Cavayas (1997) to map forest structure from high resolution imagery. However, this technique is originally designed for one dimension. The interpretation becomes difficult when a multi-scale structure in the data is encountered and when the data is of non-stationary character (Burrough 1995b). Another option is the measurement of the distribution of gap sizes that has been termed lacunarity by Mandelbrot (1983a). The gliding-box algorithm introduced by Allain & Cloitre (1991) and further developed by Plotnick et al. (1993 & 1996) for the analysis of spatial pattern can also be used as a top-down approach to quantify texture and its heterogeneity. It can be seen as a measure of the "gappiness" or "hole-iness" of a geometric structure (Plotnick et al. 1993). For structural stand characteristics, such as canopy cover and gap volume it has been used by Frazer et al. (2005).

Probably the most important consideration in texture analysis is the question of scale over which texture is measured (Marceau et al. 1990, Franklin et al. 1996, Hay et al. 1997, Marceau & Hay 1999). For that reason we introduce multi-layer co-occurrence measurements in order to facilitate the inclusion of various scales. A problem that arises is that texture measures from different scales (based on varying kernel-size) result in highly correlated predictors. Thus, methods primarily known from imaging spectroscopy can be considered as good candidates for appropriate data treatment. An example is the PLSR approach that was previously applied in hyperspectral imaging (e.g. Smith et al. 2002, Schmidtlein 2005) and takes full account of the colinearity between predictor layers. In order to produce a stable texture measure at the stand level, large kernels were needed (75-199 pixels). Large kernels produce large edge effects. Consequently, borderlines within the image data, such as transition from forested to non-forested area create considerable artefacts. In order to avoid these, non-forested areas were masked out and buffers of 30m were implemented. As a result model success is overestimated due to a slight reduction of forested area. Topographic illumination effects on grey-values were adjusted by means of a *Minnaert* correction (McDonald 2000). Due to the misfit of spatial resolution of DEM (15m) and Quickbird data (0.6m) overcorrection artefacts were created. Four plots, situated in affected regions had to be excluded from regression analysis. In consequence, the already small number of sampling sites was further reduced.

Further efforts should be made to cope with the “elusive notion of texture” (Mandelbrot 1983a), focusing on multiple scales. A combination of techniques, such as wavelet-decomposition, lacunarity analysis, semivariogram estimates and co-occurrence measurements is conceivable with PLSR analysis as a linking tool.

## 6 CONCLUSIONS

We present a method of image texture analysis that provides a maximum flexibility in the inclusion of scale levels. In the unfavourable conditions of southern Kyrgyzstan, with very complex stand structures and continuous transitions in stand properties, this flexibility proofed to be advantageous since no *a priori* selection of scale had to be made. The logic is simple: The more predictors at multiple scale-levels were included in the models, the better the probability to hit independent variables with high predictive power. There is no theoretical limitation to the addition of other relevant predictors from multiple scales and sources, allowing for a further increase of model quality.

## ACKNOWLEDGEMENTS

We would like to thank the DAAD (Deutscher Akademischer Austausch Dienst) and the Volkswagenstiftung for the financial support to carry out fieldwork in Kyrgyzstan. Thanks to the people from the Dep. of Biogeography, University of Bayreuth, to the HIRSE team and to H. Pretzsch. Special thanks to B. John for her kind support in technical questions.

## REFERENCES

Abdi, H. (2003b): Partial least squares (PLS) regression. In: Lewis-Beck, M., Bryman, A. & Futing, T. (Eds.): Encyclopedia for research methods for the social sciences. Thousand Oaks (CA), Sage, USA, pp. 792-795.

Allain, C. & Cloitre, M. (1991): Characterizing the lacunarity of random and deterministic fractal sets. Phys. Rev. A 44: 3552-3558.

Bebi, P., Kienast, F. & Schonenberger, W. (2001): Assessing structures in mountain forests as a basis for investigating the forests’ dynamics and protective function. For. Ecol. Manage. 145: 3-14.

Burrough, P.A. (1995b): Spatial aspects of ecological data. In: Jongman, R.H.G., TerBraak, C. J. F., van Tongeren, O.F.R. (Eds.): Data analysis in community and landscape ecology. University Press, Cambridge, UK, pp. 213-251.

Cottam, G. & Curtis, J.T. (1956): The use of distance measures in phytosociological sampling. Ecology 37: 451-460.

Davies, H.C. (2001): Uncertainty testing in PLS regression. Spectroscopy Europe 13: 16-19.

Epple, C. (2001): A vegetation study in the walnut and fruit-tree forests of Southern Kyrgyzstan. Phytocoenologia 31: 571-604.

Ferro, C.J.S. & Warner, T.A. (2002): Scale and texture in digital image classification. Photogramm. Eng. Remote Sens. 68: 51-63.

Franklin, S.E., Wulder, M.A. & Lavigne, M.B. (1996): Automated derivation of geographic window sizes for use in remote sensing digital image texture analysis. Comput. Geosci. 22: 665-673.

Frazer, G.W., Wulder, M.A. & Niemann, K.O. (2005): Simulation and quantification of the fine-scale spatial pattern and heterogeneity of forest canopy structure: A lacunarity-based method designed for analysis of continuous canopy heights. For. Ecol. Manage. 214: 65-90.

Gottschling, H., Amatov, I. & Lazkov, G. (2005): Zur Ökologie und Flora der Walnuß-Wildobst-Wälder in Süd-Kirgisistan. Archiv für Naturschutz und Landschaftsforschung 44: 85-132.

Gougeon, F.A. (1998b): Automatic individual tree crown delineation using a valley-following algorithm and a rule-based system. In: Hill, D.A. & Leckie, D. G. (Eds.): Automated interpretation of high spatial resolution imagery for forestry. Canadian Forest Service, Victoria, Canada, pp. 11-24.

Haralick, R.M., Shanmuga, K. & Dinstein, I. (1973): Textural features for image classification. IEEE Trans. Syst. Man Cybern. SMC3: 610-621.

Hay, G.J., Niernann, K.O. & Goodenough, D.G. (1997): Spatial thresholds, image-objects, and upscaling: A multiscale evaluation. Remote Sens. Environ. 62: 1-19.

Kolov, O. (1998b): Ecological characteristics of the walnut-fruit forests of southern Kyrgyzstan. In: Blaser, J., Carter, J. & Gilmour, D. (Eds.): Biodiversity and sustainable use of Kyrgyzstan´s walnut-fruit forests. IUCN - The World Conservation Union, Cambridge, UK, pp. 59-61.

Leckie, D.G., Gougeon, F.A., Walsworth, N. & Paradine, D. (2003): Stand delineation and composition estimation using semi-automated individual tree crown analysis. Remote Sens. Environ. 85: 355-369.

Mandelbrot, B.B. (1983a): The fractal geometry of nature. W.H. Freeman and Company, New York, USA, pp. 469.

Marceau, D.J. & Hay, G.J. (1999): Remote sensing contributions to the scale issue. Can. J. Remote Sens. 25: 357-366.

Marceau, D.J., Howarth, P.J., Dubois, J.M.M. & Gratton, D.J. (1990): Evaluation of the gray-level cooccurrence matrix-method for land-cover classification using spot imagery. IEEE Trans. Geosci. Remote Sensing 28: 513-519.

Martens, H. & Martens, M. (2000): Modified Jack-knife estimation of parameter uncertainty in bilinear modelling by partial least squares regression (PLSR). Food Quality and Preferences 11: 5-16.

McDonald, E.R., Wu, X., Cacetta, P. & Campell, N. (2000): Illumination correction of Landsat TM data in South East NSW. Proceedings of the 10th Australasian Remote Sensing & Photogrammetry Conference, Adelaide, Australia, Vol. 1, pp. 1375, http://www1.cmis.csiro.au/RSM/research/pdf/McDonalde_illumcorweb2000.pdf (accessed 26.04.05).

Mitchell, K. (2001): Quantitative analysis by the point-centered quarter method. Department of Mathematics and Computer Sciences, Geneva, NY, http://people.hws.edu/mitchell/PCQM.pdf (accessed 11.11.04).

Musuraliev, T.M. (1998b): Forest management and policy for the walnut-fruit forests of the Kyrgyz Republic. In: Blaser, J.,Carter, J. & Gilmour, D. (Eds.): Biodiversity and sustainable use of Kyrgyzstan´s walnut-fruit forests. IUCN - The World Conservation Union, Cambridge, UK, pp. 3-18.

Plotnick, R.E., Gardner, R.H., Hargrove, W.W., Prestegaard, K. & Perlmutter, M. (1996): Lacunarity analysis: A general technique for the analysis of spatial patterns. Phys. Rev. E 53: 5461-5468.

Plotnick, R.E., Gardner, R.H. & Oneill, R.V. (1993): Lacunarity indexes as measures of landscape texture. Landsc. Ecol. 8: 201-211.

Pretzsch, H. (1997): Analysis and modeling of spatial stand structures. Methodological considerations based on mixed beech-larch stands in Lower Saxony. For. Ecol. Manage. 97: 237-253.

Sandmann, H. & Lertzman, K.P. (2003): Combining high-resolution aerial photography with gradient-directed transects to guide field sampling and forest mapping in mountainous terrain. For. Sci. 49: 429-443.

Schmidt, M. (2005): Utilisation and management changes in South Kyrgyzstan's mountain forests. J. Mount. Sci. 2: 91-104.

Schmidtlein, S. (2005): Imaging spectroscopy as a tool for mapping Ellenberg indicator values. J Appl Ecol 42: 966-974.

Shiver, B.D. & Borders, B.E. (1996a): Sampling techniques for forest resource inventory. John Wiley & Sons Inc., New York, USA, 356 pp.

Smith, M.-L., Ollinger, S.V., Martin, M.E., Aber, J.D., Hallett, R.A., & Goodale, C.L. (2002): Direct estimation of aboveground forest productivity through hyperspectral remote sensing of canopy nitrogen. Ecol Appl 12: 1286–1302.

St-Onge, B.A. & Cavayas, F. (1997): Automated forest structure mapping from high resolution imagery based on directional semivariogram estimates. Remote Sens. Environ. 61: 82-95.

St-Onge, B.A., Couture, M. & Lodin, M. (1998b): Forest stand structure mapping using a species-controlled textural approach. In: Hill, D.A. & Leckie, D. G. (Eds.): Automated interpretation of high spatial resolution imagery for forestry. Canadian Forest Service, Victoria, Canada, pp. 321-331.

Wang, L., Gong, P. & Biging, G.S. (2004): Individual tree-crown delineation and treetop detection high-spatial-resolution aerial imagery. Photogramm. Eng. Remote Sens. 70: 351-357.

Warner, T.A., Lee, J.Y. & McGraw, J.B. (1998b): Delineation and identification of individual trees in the eastern deciduous forests. In: Hill, D.A. & Leckie, D. G. (Eds.): Automated interpretation of high spatial resolution imagery for forestry. Canadian Forest Service, Victoria, Canada, pp. 81-91.

Wold, H. (1966b): Estimation of principle components and related models by iterative least squares. In: Krishnaiah, P.R. (Eds.): Multivariate analysis. Academic Press, New York, USA, pp. 391-420.

Wold, S., Sjöström, M. & Eriksson, L. (2001): PLS-regression: a basic tool of chemometrics. Chemometrics Intell. Lab. Syst. 58: 109-130.

Wulder, M. (1998b): Image spectral and spatial information in the assessment of forest structural and biophysical data. In: Hill, D.A. & Leckie, D. G. (Eds.): Automated interpretation of high spatial resolution imagery for forestry. Canadian Forest Service, Victoria, Canada, pp. 267-282.

# ASSESSING FOREST STAND DENSITY USING HIGH-RESOLUTION MULTI-SPECTRAL REMOTE SENSING IMAGERY

*Michael Sprintsin[1], Samuel Sprintsin[2], Pedro Berliner[1], Shabtai Cohen[3] and Arnon Karnieli[1]*

[1] Jacob Blaustein Institute for Desert research, Ben Gurion University of the Negev, Sde Boker Campus 84990, Israel, sprintsi@bgu.ac.il

[2] Land Development Authority, Forest Department, Southern Region, Jewish National Found, Israel

[3] Institute of Soil, Water and Environmental Sciences, A.R.O. Volcani Centre, Bet Dagan, Israel

## ABSTRACT

The current study demonstrates the ability to assess stand density of a dryland planted forest by high spatial resolution imagery. The study was conducted in the mono-culture (dominated by Pinus halepensis), even-aged Yatir forest locating in the transition zone between arid and semi-arid climatic zones (a long-term aridity factor (precipitation/potential evapotranspiration) equals to 0.17). A 4-m spatial resolution multi-spectral IKONOS image was acquired under clear sky conditions on March 25, 2004. The forest fractional vegetation cover (FVC), i.e., canopy cover (CC), was computed by applying the Normalized Differences Vegetation Index (NDVI) and a linear mixture model. Ground observations include 646 standing trees sited at 72 circular plots (200 $m^2$). Allometric relationships between basic biometrics for tree and for stand level were determined during a field campaign. Stand density was expressed by absolute (a number of trees per hectare; TPH) as well as by relative (crown competition factor; CCF) measures. The latter was highly and significantly correlated with both FVC ($r^2$=0.50; p<0.05) and TPH ($r^2$=0.72; p<0.05) allowing a two-step procedure for mapping the forest stand density. The relationships between stand density, clumping index and leaf area index (LAI) were used to evaluate the validity of an approach. LAI was calculated using a non-linear relationship to FVC and then compared with ground truth measurements performed by the Tracing Radiation and Architecture of Canopies (TRAC) canopy analyzer. Results show a high level of correlation ($r^2$=0.79, p<0.01) but underestimation relative to 1:1 line. This underestimation was overcome by correcting the predicted values for forest clumpiness determined through the empirical relationships between TPH, crown width, and stand area. The results were much closer to 1:1 with improved level of correlation ($r^2$=0.81; p<0.01). In summary, it is shown that a combination between conventional forest inventory and remote sensing methods can increase the accuracy of quantifying stand density in a dryland planted forest.

**Keywords:** Stand density, Dryland forest, IKONOS, Clumpiness, Leaf Area Index

## 1 INTRODUCTION

The relationship between satellite spectral reflectance and wood parameters was presented by many studies at spatial and spectral levels for monitoring forest variables such as basal area, height, volume, etc. A common approach is to combine between remote sensing observations and the data collected in-situ from training plots for estimating forest variables for each pixel of the image and averaging the pixel estimation within a stand (Tokola et al., 1996; Makela and Pekkarinen 2004), which description involves manipulation of factors that are assumed to control eco-physiological mechanisms determining forest growth and function. One of those factors is forest stand density, which is the major parameter that can be manipulated by foresters during stand development (Zeide 2005). This leads to ability to influence species establishment, stem quality and diameter, forest productivity and clumpiness. The latter affecting radiation regime within the canopy, rainfall interception, evapotranspiration, photosynthesis, respiration and litterfall, and related to leaf area index (LAI).

Despite the importance of such information applying a remote sensing approach to stand density parameterization has rarely been reported. This lack of treatment may be explained by the limitations of most commercially available spaceborn sensors to observe only the fraction of the surface covered by the summation of the trees crowns instead of the single tree. Unfortunately, this vegetation fraction is not always linearly correlated with the actual number of standing individuals, especially in hardly vegetated areas. It follows that the chances of identifying individual elements increases with decreasing density. Consequently, implement remote sensing methods in dryland forestry, which is usually planted and much sparser than other ecological regions, may be an appropriate tool for obtaining basic stand parameters and quantitative stand description. Accordingly, the objective of this study was to show the ability of combination of direct (*in-situ*) and indirect (remote sensing) methods to quantify stand density in dry-land planted forest.

# 2 METHODS

## 2.1 Study area

The study was conducted in Yatir forest located in the transition between arid and semi-arid climatic zones (Figure 1). The mean annual precipitation, 275 mm, is characterized by high annual fluctuations. The average total annual potential evapotranspiration is 1600 mm year$^{-1}$. The average maximum (July) and minimum (January) annual temperatures are 32.3˚C and 6.9˚C, respectively. The forest is entirely planted, its mature and largest part is almost even-aged (planted during the late 1960's – early 1970's) and is close to a monoculture dominated by *Pinus halepensis*. The trees grow mostly on shallow Rendsina soil and lithosols (0.2 – 1 m deep) overlay chalks and limestone (Grunzweig et al. 2003) and there is little understory vegetation cover.

## 2.2 Sampling design

72 circular plots of 200 m$^2$ each were selected within the most mature section of the forest. For each tree within selected plots the (a) *diameter at breast height* (DBH; 1.37 m above the ground) using a calliper, (b) *crown width* (CW) using a metric tape, and (c) *tree height* (H) using a clinometer were measured. Tree canopy was assumed to be circular, thus CW that represents an equivalent canopy diameter was used to compute the crown area (CA). At plot level, *canopy cover* (CC) was calculated as a ratio of the sum crown area of all trees within a plot and plot area itself.

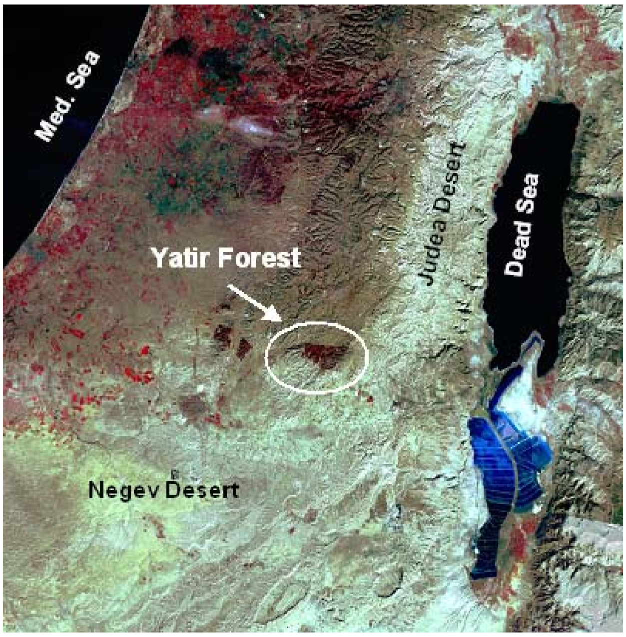


*Figure 1: Landsat-TM of Central Israel. Note the location of the Yatir forest on the desert fringe, visible as the sharp contrast between bright tones (semi-arid zone) and dark tones (sub-humid zone).*

## 2.3 Stand density definition

Stand density firstly was expressed by a number of trees per hectare (TPH). However, downward looking sensors are able to detect only the proportion of the forest floor covered by the vertical projection of the trees, referred to as canopy cover. The relationship between the latter and the number of individual trees within a stocked area is not straightforward and requires additional information about plants ages and sizes. Such information is included into relative measures of the density that are directly related to the products of the number of individuals and their sizes.

The Crown Competition Factor (CCF) reflects the area available to the average tree in the stand in relation to the maximum area it could use if it were open-grown Krajcek et al., (1961). If every tree in a stand had its full crown development and if all ground space were occupied, the CCF would be 100. Consequently CCF exceeding 100 indicates crown recession or even suppression mortality while for open-grown trees CCF would be less than 100.

Since the CW-DBH relationship for open-growth trees is not influenced by competition, this relationship was established as a first step of CCF computation and then, Maximum Crown Area (MCA), i.e. the maximum area that can be occupied by the crown of a tree of specific DBH, was calculated. Finally, to express the area occupied by both a single tree and a sum of trees, CCF was computed by summing the MCA values for all trees in the stand and dividing by the stand area:

$$CCF = \frac{1}{area} \cdot \left( a \cdot \Sigma n_i + b \cdot \Sigma DBH_i n_i + c \cdot \Sigma DBH_i^2 n_i \right) \qquad (1)$$

where $n_i$ is the number of trees in *i*th DBH class, $DBH_i$ is a midpoint of *i*th DBH class (cm) and *area* is in hectare and *a*, *b* and *c* are empirical constants.

### 2.4 Image data retrieval and processing

A 4-m spatial resolution multispectral IKONOS image was acquired on March 25, 2004. The image was radiometrically and atmospherically corrected and geo-rectified to the UTM grid. A Linear Mixture Model (LMM) was implemented for calculating the total surface reflectance measured by the satellite sensor in a specific pixel. The LMM weights the surface reflectances of end-members (e.g., vegetation and soil) by their relative ground cover. Consequently, the *fractional vegetation cover* ($f_c$) was calculated from the minimum and maximum Normalized Difference Vegetation Index ($NDVI_{min}$ and $NDVI_{max}$, respectively) values (Goel 1989):

$$fc = \frac{NDVI - NDVI_{\min}}{NDVI_{\max} - NDVI_{\min}} \qquad (2)$$

The $NDVI_{min}$ (soil reflectance) value was calculated over a background reflectance (primary needle dry litter) measured *in-situ* using the LICOR LI-1800 field spectroradiometer, while a canopy reflectance was calculated from red and near-infrared reflectances of a specific 100% covered area (2 by 2 pixels).

## 3 RESULTS AND DISCUSSION

### 3.1 Allometric relationships in tree and plot levels

As expected, the relationships between basic trees biometrics - as it was defined for 646 measured trees - show high and significant correlations ($R^2$ = 0.96; p <0.01 for H and $R^2$ = 0.95; p <0.01 for CA; Figure 2). Figure 3 depicts behaviour of CA, DBH and H as functions of stand density (TPH) and shows that as average individual tree size increases, so does competition for resources and therefore tree density decrease. This decrease can result from natural tree die-back and/or from managerial thinning of the stand as it grows. These results indicate that the ability to predict the number of trees per unit area will lead to an ability to assess standing tree parameters.

### 3.2 Fractional Vegetation Cover

FVC was calculated according to Eq. 2 using 0.13 and 0.75 values as $NDVI_{min}$ and $NDVI_{max}$ respectively. FVC ranged from 0.4 to 0.7 with an average of 0.48±0.07 (± standard deviation). These values correspond to an average canopy cover calculated according to *in-situ* measured crown width of 48±9%.

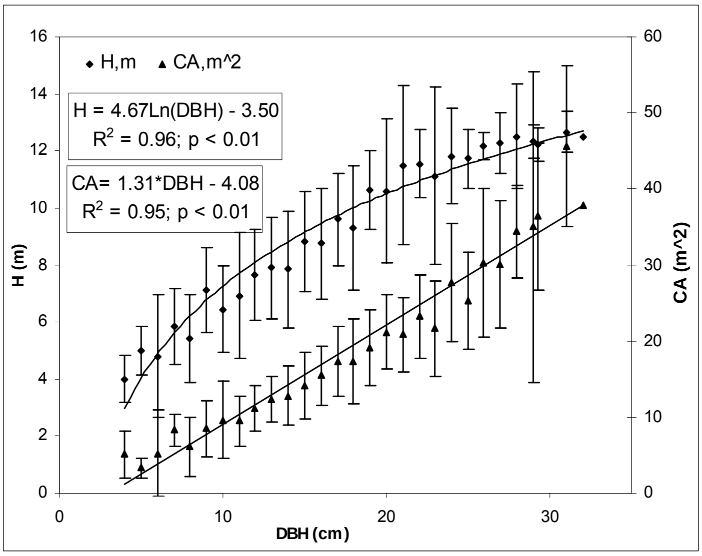


*Figure 2: Allometric relationships for height (H) and crown area (CA) vs. diameter at breast height (DBH). Vertical bars represent standard deviation.*

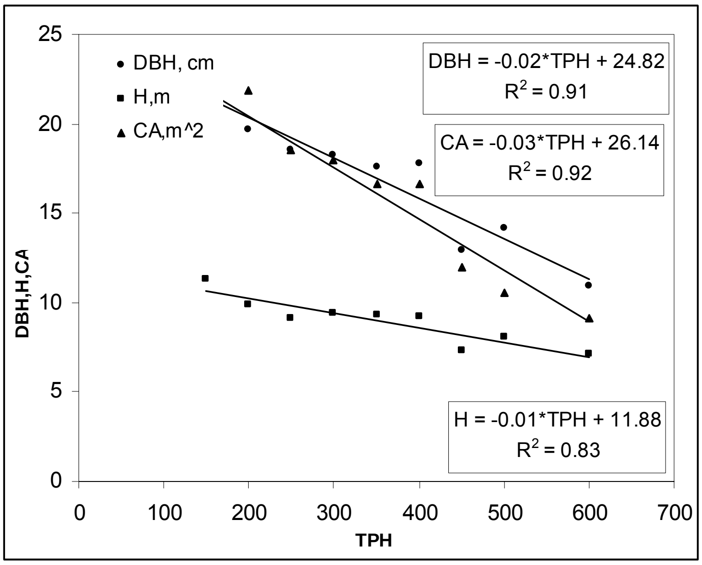


*Figure 3: The relationship between average diameter at breast height (DBH), height (H), crown area (CA) and number of trees per hectare (TPH) averaged on a plot basis, grouped into TPH classes.*

## 3.3 Stand density

FVC as a proxy for CC is a necessary variable that combines surface reflectance, measured by remote sensor, with standing trees and stand characteristics, defined by inventory activity. However, a large value of CC can result not only from a large number of trees, but also from a small number of large individuals; therefore the relationship of FVC to TPH is not expected to be unique. Moreover, the inversion in this relationship could appear as result of: (1) an upper limit of the number of individuals that the site can bear; or/and of (2) a saturation threshold for the remote sensor, indicating its inability to detect higher stand density. Theoretically, beyond this CC decreases, and soil fraction observed by the satellite increases. This situation is indicates a decrease in near–infra red surface reflectance measured by the sensor and a decrease in calculated VI values, which limits our ability to relate VI to a real number of individuals per unit area. The inversion point should be considered when evaluating optimal stand density. Moreover, it should be remembered that density, expressed as the number of plants per unit area, does not tells how crowded the area is, because in fact density is a function of two variables: plant number and their size (Zeide, 2005). Accordingly, we assume that a relative density measure seems more applicable, since it gives an idea about the interaction between the target tree and its neighbours.

55 open-grown trees were chosen within the forest. CW-DBH relationship was determined and CCF was computed for each training plot. The relationship between CCF and FVC (Figure 4) could be highlighted by three points:

- As expected, the relationship is more monotonous and useful than that for FVC vs. TPH.
- A non-linear relationship can lead to a threshold occurring at high levels of canopy cover. The approximation of this threshold could be done empirically and for the Yatir forest was found to be at $FVC \approx 0.75 - 0.8\,(CCF \approx 103 - 105)$.
- The average CCF for 72 training plots is equal to 84 (FVC=0.52). This value is well compatible with forest CC, which varied from 0.48 to 0.53. Over the whole studied area of the Yatir forest, CCF value decreased to 75, corresponding to a decrease in average FVC (0.43).

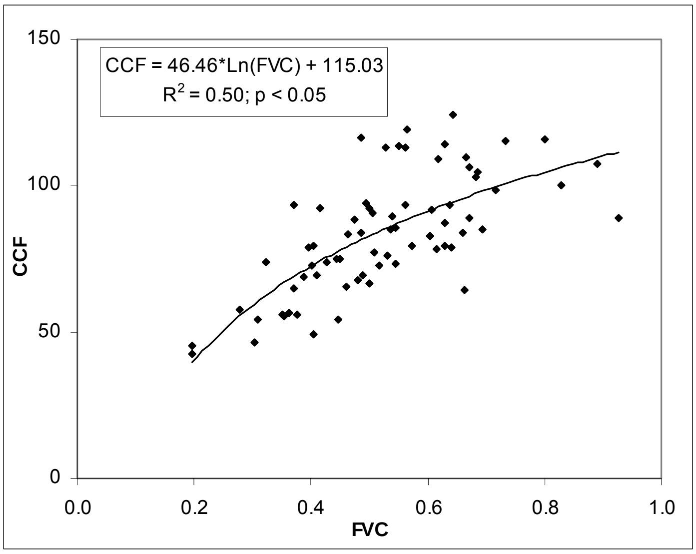


*Figure 4: Relationship between Crown Competition Factor (CCF) and Fractional Vegetation Cover (FVC) for the Yatir forest.*

As the next step, the relationship of TPH to CCF was established and a high correlation was obtained ($r^2 = 0.72$, $p<0.05$). This relationship was then used to produce a map of stand density in the forest (Figure 5), which provides a view of the TPH spatial distribution gives some insight into forest structure and can be used for further monitoring.

The spatial organization of a conifer forest is highly variable with such structures as shoots, branches, crowns, and tree groups. This result in non-random distribution of canopy elements and a clumping index has been utilized to characterize the non-randomness of the canopy with respect to interception of radiation (Chen, et al., 2005). At the stand level, clumping (groups of trees) affects the gap fraction, which is mostly influenced by crown dimensions and stand density. Therefore the relationships between clumping index, stand density and LAI were used to evaluate the validity and accuracy of a model.

LAI was calculated after Norman et al. (1995) as:

$$LAI_t = \frac{-\ln(1-f_c)\,/\,k}{\Omega(\theta)} \tag{3}$$

where LAIt is the true leaf area index of randomly distributed leaves, $f_c$ is the FVC, k is the extinction coefficient for the canopy (the ration of foliage projection coefficient (taken as 0.5) and cosine of solar zenith angle) and $\Omega(\theta)$ is the clumping index which is a function of solar zenith and was expressed after Kucharik et al., (1999) as:

$$\Omega(\theta) = \left[ \frac{\left( N \cdot CW / \sqrt{A} \right)^{0.7}}{1 + b \cdot \exp(2.38 \cdot \theta^{1.72})} \right] \Big/ 1.7 \tag{4}$$

where the numerator quantifies the effect of foliage clumping at scales larger than shoot with *N* as the number of trees and *CW* as the crown width (m) within a pixel of area *A*, and *b* that can be found by solving Eq.5 for one measurement of clumping index. The denominator represents the effect of foliage clumping within a shoot (*needle-to-shoot area*).

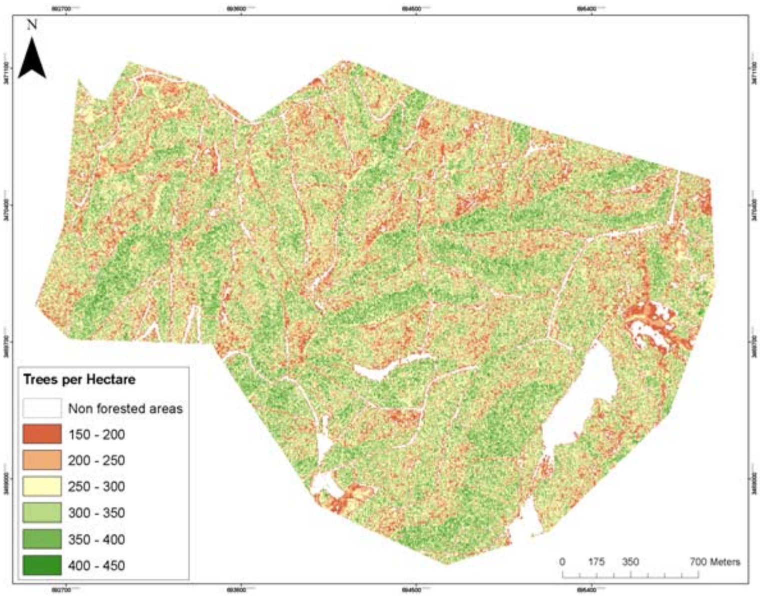


*Figure 5: Map of number of Trees per Hectare over the studied area in the Yatir forest.*

Ground truth LAI data was collected over ten plots, of 1000 $m^2$ (approximately 32 x 32 m) each, using the Tracing Radiation and Architecture of Canopies (TRAC; Chen and Cihlar, 1995) as a series of seven 32 m long transects, three times a day for different zenith angles. Figure 6-a compares between TRAC and remote sensing measured LAI showing high correlation with a small underestimation especially for high LAI, which presumably results from canopy clumping nature of studied forest.

Figure 6 shows the results corrected for clumping based on stand density using Eq. 5, and compares between TRAC measured and remote sensing estimated and corrected LAI. High correlation ($R^2$ = 0.81) and proximity to the 1:1 line indicates that (1) using the relationship between forest structure and clumping improves accuracy of LAI assessment and (2) the forest parameters applied were sufficiently accurate.

## 4 CONCLUSIONS

The current study shows the ability of remote sensing to estimate forest stand density needed to assess the success of forest regeneration or as an input for indirect measurements. Density, defined here as number of trees per unit area, may also be compared with a management target, e.g. to determine if the stand is over - or under-stocked. The proposed approach to forest inventory inspection fills a gap between detailed observations of small parts of forest area and reliable techniques to extrapolate from these limited observations to the whole area of interest. Moreover, real time estimates of stand density obtained from a spectral vegetation index can be valuable for forest surveys. The study shows that a combination between conventional inventory methods and remote sensing techniques can be simple, accurate, and useful in man-planted relatively homogeneous forests, being a possible way for forest managers to evaluate their management approach, making it thrifty and efficient.

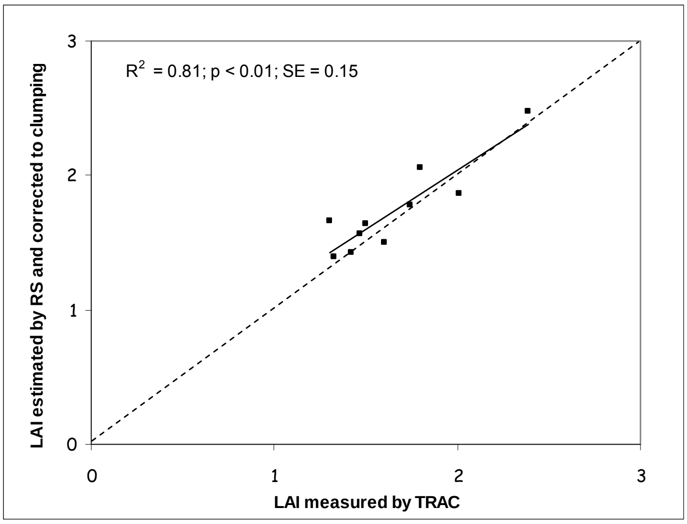


*Figure 6: A comparison between TRAC and remote sensing measured LAI corrected for clumpiness.*

## ACKNOWLEDGEMENTS

Thanks to Mr. A. Goldberg and the GIS team of Israeli Forest Service for help with the field campaigns during this study, and to Prof. Dan Yakir and Dr. Eyal Rotenberg of the Department of Environmental Sciences and Energy Research at the Weizmann Institute of Science (Rehovot, Israel), for use of the TRAC instrument.

## REFERENCES

Chen, L.M., Menges, C.H. and Leblanc, S.G. (2005). Global mapping of foliage clumping index using multi-angular satellite data. Remote Sens. Env. 97: 447-457.

Goel, N. S., (1989), Inversion of canopy reflectance models for estimation of biophysical parameters from reflectance data. In G. Asrar (Ed), Theory and Application of Optical Remote Sensing. John Wiley & Sons. pp. 205-251.

Grunzweig, J.M., Lin, T., Schwartz, A. and Yakir, D. (2003). Carbon sequestration in arid-land forest. Glob. Ch. Biol. 9 (5): 791-799.

Krajicek, L.E., Brinkman, K.A. and Gingrich, S.F. (1961). Crown competition – A measure of density, For. Sc. 7: 35-42.

Kucharik, C. J., J. M. Norman, & Gower, S. T. (1999). Characterization of radiation regimes in nonrandom forest canopies: theory, measurements, and a simplified modeling approach. Tree Phys. 19: 695-706.

Makela, H. and Pekkarinen, A. (2004). Estimation of timber volume at the sample plot level by means of image segmentation and Landsat TM imagery. Remote Sens. Env. 77: 716-723.

Norman, J.M., Kustas, W.P. and Humes, K.S. (1995). Source approach for estimating soil and vegetation energy flaxes in observations of directional radiometric surface temperature. Agr. Forest Meteo. 77: 263-293.

Tokola, T., Pitkanen, J., Partinen, S and Muinonen, E. (1996). Point accuracy of a non-parametric method in estimation of forest characteristics with different satellite materials. Int. J. Remote Sens. 17(12): 2333-235.

Zeide, B. (2005). How to measure stand density. Trees, 19: 1-14.

# INDIVIDUAL TREE CROWNS IDENTIFICATION FROM COLOR INFRARED AERIAL IMAGES USING GIS TOOLS

*Jan Tuček[1], Andrea Majlingova[2]*

[1] Technical University in Zvolen, Department of Forest Management, Zvolen, Slovakia; e-mail: tucek@vsld.tuzvo.sk

[2] Technical University in Zvolen, Department of Fire Protection, Zvolen, Slovakia; e-mail: amajling@vsld.tuzvo.sk

## ABSTRACT

Nowadays, there is always higher accent given to environmental field, which has also impact on management in forests. New and stricter legislative norms increase the ambitiousness of forest management. Present tools for information contraction do not fulfill these higher requirements, therefore there is need to develop modern implements for their obtaining and processing. As one of the implements for information management and storage there are marked geographical information systems. Collection of space data about landscape, which are inputs for creation of geoinformatics systems, belongs between tasks that can be realized by different methods like geodetic, photogrammetric, remote sensing, GPS or aerial altimetry methods. Generally, one of the focus problems of GIS applications in forestry practice is question of data resources and technologies input into digital database systems. In this article, there is introduced methodology of individual tree crown identification from color infrared aerial images using focal functions and cost distance analysis that offers GIS environment. Focal functions were used mainly for individual tree crowns tops identification and detection of individual crowns boundaries. Cost distance analysis were used for determination of individual pixels membership to individual tree crown (region growing principle) using before found local maxima and focal maxima imagery. After segmentation of images into regions containing individual tree crowns, there was made tree species classification on raster representation of obtained tree crowns using tools of the eCognition software environment. Preliminary results show that this is one of possible ways to obtain detailed data about forests more quickly and effectively.

**Keywords:** *Color infrared aerial image, distance operators, friction surface, GIS*

## 1 INTRODUCTION

### 1.1 High spatial resolution materials

In present, there is a big accent given to more effective methods of earth surface data collection. Also forest monitoring sphere progresses from ground methods of forest parameters and forest constitution information acquisition towards automatic data collection based on aerial or satellite images evaluation. In fact, it is necessary to remark that we can not depend only on results of automatic processing and evaluation yet. Still, there is need to combine both methods – aerial or satellite images data survey approximation and its next comparison with ground truth.

The market supply quantity of data resources with information about land cover (aerial images, satellite images). Special part is represented with high spatial resolution data enabling very detail information acquisition. Following data are characterized with high user interpretation, rich information content, image sharpness, precision, high resolution and integrity of image.

High spatial resolution images enables to deduce more precise information about stem number, stem density, crown closure, forest stock, forest area, forest species composition, forest constitution and structure in comparison with lower spatial resolution images.

In the group of data with high spatial resolution belong aerial images with spatial resolution from few meters up 10 – 100 cm/pixel. Very significant is classification by Gougeon (1998) who separate image materials by image spatial resolution to materials with low spatial resolution with image feature extent of 10 – 100 m, medium spatial resolution 1 – 10 m and high spatial resolution 0.1 – 1 m.

## 1.2 Individual tree crowns identification

In the world, there are more experts dealing with problem of individual tree crowns identification from high resolution images and there also exist more approaches to tackle this problem.

One of the approaches is individual tree crowns identification based on their separation from shadow and from other vegetation background (Gougeon 1998 a), (Gougeon a Leckie 1999 b). To reach this goal, there is used so called ITC (individual tree crown) approach at work. Usually the first step of this approach is individual tree crowns extraction (individual tree crowns isolation) produced by automatic processing. The next step is individual tree crown species recognization and their next grouping into the forest stand. This approach can lead to very detailed forest inventory, especially in case we consider that the groupings can be organized in way to survey criteria not included in present inventories yet.

The important image characteristic, that allows photo interpretator to identify individual tree crowns in conifer forest stands (crown separation of broadleaves species is less precise) from aerial or other types of images, is existence of shadow thin zones separating crowns.

According to this knowledge there was used automated isolation tree crowns procedure („valley following" algorithm) based on shadow valleys monitoring, in view of grey color intensity.

In opened, less compact areas the „valley following" technique has to bank on preprocessing techniques. The preprocessing procedure can eliminate (using mask) not shadowed material from background or separate forest areas from non forest. This process is followed by rule based process that is based on tree crowns boundary line following and their next enclosing. Result of this processing is bitmap with tree crowns that can be used in next analysis.

Next approach presented here, it is methodology for local maxima image spectral values identification (tree crown tops identification). This problem is more described in work of Larsen (Larsen 1997 a), (Larsen 1998 b), (Larsen 1999 c). There was used circle form mask, derived from optical model of tree crown and geometry of image acquisition, to estimate positions of individual trees from aerial images with high spatial resolution. The process consists from local maxima correlation function finding according to successful moving masks over the image. At work there are described 3 procedures to improve this methodology. The first procedure is correlation image filtering using Gaussian filter with standard deviation $\rho = 1$ and then the local maxima of correlation selection from filtered image. In the second procedure is correlation image also filtered using Gaussian filter, but with standard deviation growing up until the image consists only given number of local maxima points (depends on tree number at test area). The third procedure is selection of candidates in given ranges, leading from the highest to the lowest correlation and elimination of all candidates inside given radius of each selected candidate. For evaluation of described procedure were used data from thinning experiment in Norway spruce stand. The whole approach results to images where the trees are lighted by Sun from the back. It is situation that can bring approximately the most precise estimates of tree crown tops for spruce and other species with similar morphology (fir).

Next there is described approach that offer eCognition system environment. eCognition follows a new, object oriented approach towards image analysis. eCognition allows homogeneous image object extraction in any desired resolution. This entails the simultaneous representation of image information on different scales. The segmentation procedure detects local contrasts and was especially developed to work even on highly textured data, such as VHR or radar imagery. Based on image objects, the problem of multi source data fusion is tackled by enabling parallel evaluation of image information of arbitrary source. eCognition features a set of interfaces which make information about image objects, features and classification transparent and accessible. The classification process is based on fuzzy logic, to allow the integration of a broad spectrum of different object features such as spectral values, shape, or texture for classification. Utilizing not only image object attributes, but also the relationship between networked image objects, it results in sophisticated classification incorporating local context.

Other approach is presented in work of Šumbera. This work is oriented to the use and application of digital image processing methods with multispectral images with high spatial resolution. These images processing there were tree tops and outlines detection methods proposed. Majority of these methods were built in Kernel Processor system. Problem of tree crowns identification is separated to 2 partial procedures. The first is tree tops and then tree outlines finding. Identification of tree tops is based on filtration with rotated window selecting pixel with the highest reflectance, located in his centre. On the rotated window size depends smaller or bigger tree crowns identification. To identify tree outlines he used different methodologies – methodology based on histogram equalization, methodology of differential histogram, outlines detection using Laplace`s operator, detection of tree outlines using accumulative surface and outlines detection by frequency minima calculation. The accuracy of automated detection depend on canopy cover, image filtration rate, rotated image size and tree species composition.

In this article described methodology arises is estimation of methodology published in Tuček, Schmidt 2002 a, and Tuček 2003 b.

## 2 METHODS

The color infrared aerial images (ortho photos) with 0.4 m, 0.8 m, 1.6 m and 3.2 m spatial resolution from 1999 were used to identify individual tree crowns in area of the University Forest Enterprise – Kovacova. According to problem complicity, preliminary checking of methodology described here, there was used only sub-plot image produced from color infrared aerial image. At image acquisition the trees were 80 years old. The average tree height was 22.8 m, the average width was 29.2 m, canopy closure 0.5. Species composition of this area is created from species like fir, spruce, beech, hornbeam and oak. There were 929 trees visible and manually digitized using stereo model in Image Station software environment. This layer was used to verify the results of tree crowns automated identification in Idrisi 32 software environment.

The preprocessing was the first step of experiment. From original color infrared aerial image (1200 dpi) was produced its ortho rectification in Image Station environment. The result of this process was ortho photo used in next analysis (Fig.1a).

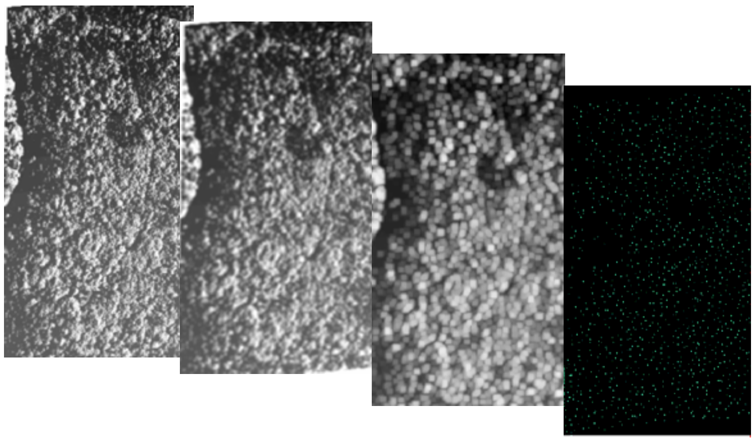

*Figure 1: The example of individual procedures results on subplot of color infrared aerial image with 1.6 m spatial resolution:*
*a. Original color infrared aerial image with 1.6 m spatial resolution*
*b. Filtered image*
*c. Focal maxima image*
*d. Local maxima image – identification of tree tops*

From the reason to compare the possibilities for individual tree crowns identification from images with different pixel size (0.4 m, 0.8 m, 1.6 m and 3.2 m), the original image (1200 dpi with 0.4m pixel size) was resampled to spatial resolution 600 dpi with 0.8 m pixel size, 300 dpi with 1.6 m pixel size and 150 dpi with 3.2 m pixel size next. By this way, there were produced 5 images to compare. Each of them was processed by methodology described here. In process of individual tree crown identification we came out of sooner published methodology TUČEK (2003).

Automated individual tree crowns identification was produced in Idrisi 32 software environment. The input data for processing were focal maxima image (Fig.1c) and filtered image (Fig.1b) of the sub-plot original aerial image (input for focal maxima image production), both produced in Arc Info software environment.

To identify individual tree crowns, there was used focal maxima image. The tree crown tops (local maxima of sub-plot image) were determined by subtraction (map algebra tools) focal maxima image from filtered image of sub-plot aerial image and its next reclassification (RECLASS module). Resultant tree crown tops (Fig.1d) were obtained by multiplying reclassified image of tree crown tops with image of shadow. This process led to distinguishing between forest area from shadow area and also to elimination of undesirable crown tops located in shadow area.

To identify probable tree crowns there were applied distance operators – cost functions (COST, COSTPUSH module) to create friction distance surface image. The focal maxima image and the local maxima image were the inputs to the friction surface image production. Final tree crowns were identified using flow functions – module for pixels allocation (ALLOCATE module). So, the origin feature identifier was assigned to each pixel, which the distance was calculated from.

By the conversion of polygon features from raster/grid format to vector format (POLYVEC module), the vector layer of individual tree crowns was obtained. There was compared the vector layer of tree crowns identified by described methodology to tree crowns vector layer produced from stereo model in Image Station photogrammetric software environment.

## 3 RESULTS AND DISCUSSION

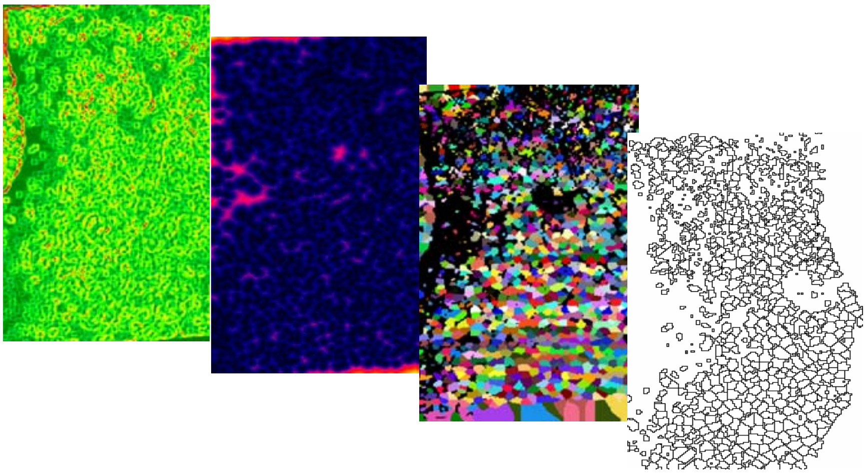

*Figure 2: Partial results of described procedure:*
*a. Inversion of input filtered image*
*b. Focal function – cost distance surface image*
*c. Flow function – pixels allocation image*
*d. Vector layer of individual tree crowns*

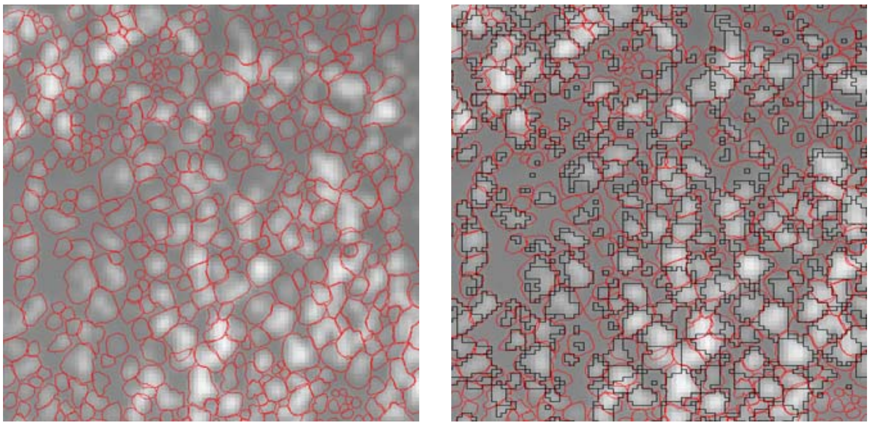

*Figure 3: Vector layer of identified tree crowns used in results comparison and evaluation*
*a. Tree crowns vector layer produced from stereo model in Image Station*
*b. Comparison of both vector layers – one as product of Idrisi environment analysis, other as product of Image Station environment.*

Partial results of procedure were also inputs into next analysis. Some of them are presented in Fig.2. Individual images were processed by methodology presented in the section Material and methodology. In the experiment there were compared 4 images. One of 0.4 m spatial resolution and next with 0.8 m, 1.6 m and 3.2 m spatial resolution. Obtained vector layers of identified tree crowns were compared to the tree crowns vector layer produced from stereo model in Image Station. In Fig. 3b there is presented result of comparison tree crown vector layers produced on image with 1.6 m spatial resolution. giving the best results according to visual evaluation and also number identified trees in test area (Table 1).

*Table 1: Results of tree crowns number identification from GIS environment in comparison to visual assessment from stereo model in Image Station environment (marked as ground true)*

| Spatial resolution of image | Number of identified crowns | Difference against Image Station vector layer (929 crowns) |
|---|---|---|
| 0.4 m | 4166 | +3237 |
| 0.8 m | 1723 | +794 |
| 1.6 m | 939 | +10 |
| 3.2 m | 464 | -465 |

Owing to results showed in Table 1, it is required to note that with higher spatial resolution of input image increases number of inaccurate identified tree tops \ crowns (overestimation errors) . Using image with 0.4 m spatial resolution we got very low accuracy of number of tree crowns identification. Results of analysis with 0.8 m spatial resolution image are also not satisfying. In case of image with 3.2 spatial resolution there appeared omit errors (49.95 %). The best results we have reached with analyzing 1.6 m spatial resolution image (1.08 % overestimation error).

Also the problem of threshold determination for separation vegetation areas from background and shadow area has been shown as the most important for final tree tops and crowns identification. This problem is going to be tackled in future works.

## 4 CONCLUSIONS

In the article introduced methodology is useful for color infrared aerial images. In the analysis we used image only from infrared band. In the world, there exists more approaches to tree crowns identification, some of them were described in Introduction section. In opposite to methodology presented here, they require high-powered software environments and huge amount of computer programmer effort. Methodology described here we consider to simply because it uses only standard GIS analysis – filtering, focal maxima identification, focal and flow functions.

Owing to results, the input image spatial resolution influence has been proved. Relationship between image element size (pixel size) and identified objects size (tree crowns size) has been showed as very important. Results of this approach can be applied in various forest applications e.g. stem diameter assessment, stem volume assessment and also volume stock assessment.

In the future, we would like to orient our work to: other high spatial resolution materials application, transformation and threshold image procedures use for separation shadows areas and background from vegetation, identification of terrain topography and radial distorts of image and verifying methodology in pure coniferous stands color infrared aerial images.

## ACKNOWLEDGEMENTS

This article has special assistance to APVT – 51-037902 and VEGA – 1/0630/03 research grant projects.

## REFERENCES

Gougeon, F.A., (1998). Automatic Individual Tree Crown Delineation Using a Valley-Following Algorithm and Rule-Based System. In: Automated Interpretation of High Resolution Digital Imagery for Forest, Natural Resource Canada, Victoria, British Columbia., pp. 11-23.

Gougeon, F.A., Leckie, D.G. (1999). Automated Interpretation of High resolution Digital Imagery for Forest, Natural Resource Canada, Victoria, British Columbia, Canada, pp. 141-152.

Larsen, M., Rudemo, M. (1997). Using Ray-Traced templates to Find Individual Trees in Aerial Photos. In: Frydrych, M., Parkkinen, J., Visa, A. editors, Proceedings of the 10th Scandinavian Conference on Image Analysis, vol. 2, Lappeenranta, Finland, p. 1007-1014.

Larsen, M., Rudemo, M. (1998). Optimizing templates for finding trees in aerial photographs. In: Pattern Recognition Letters, vol. 19, no.12, p.1153-1162.

Larsen, M. (1999). Jittered Match Windows Voting for Tree Top Positions in Aerial Photographs. In: Ersbøll B. K., Johansen, P.editors, Proceedings of the 11th Scandinavian Conference on Image Analysis, vol. 2., p. 889-894, Kangerlussuaq, Greenland, June 7-11, DSAGM / Lyngby, Denmark.

Šumbera, S. (2001). Digitální klasifikace druhové a prostorové skladby lesních porostů z materiálů DPZ. Dizertačná práca, Mendelova zemědělská a lesnická univerzita v Brne, str.137.

Tuček, J., Schmidt, M. (2000). Digitálna klasifikácia drevinového zloženia z materiálov CIR s využitím DTM vo vysokohorských podmienkach. III. Medzinárodné sympózium Aplikácia Diaľkového prieskumu Zeme v lesníctve, Zborník referátov, str.133-142.

Tuček, J. (2003). Špecifické metódy digitálneho spracovania materiálov DPZ s vysokou priestorovou rozlišovacou schopnosťou pre lesnícke účely. 15. kartografická konferencia s medzinárodnou účasťou Geoinformatizácia v kartografii, Zborník referátov, str. 280-293.

eCognition Application Notes (2001): Counting trees from VHR hyperspectral data. Vol. 2, No 1, March 2001.

# COMBINED USE OF SATELLITE IMAGERY AND LASERSCANNER DATA FOR THE ASSESSMENT OF FOREST STAND PARAMETERS

*Roland Wack*

Joanneum Research, Institute of Digital Image Processing, Graz, Austria; roland.wack@joanneum.at

## ABSTRACT

Since an increasing amount of provinces in Europe are covered by high resolution laser scanner data, an investigation was carried out to what extent this data can be used for the extraction of forest parameters like tree number, basal area and timber volume. The developed approach was tested at two test sites. Test site Burgau with 500ha, dominated by spruce (picea abies), pine (pinus silvestris) and oak(quercus sp.), was located in the eastern part of Austria whereas a second test site was located in the northern part of Austria, dominated by spruce fir and beech (fagus sylvatica). Ground truth data was provided by the local forest management and additional field measurements. This information served as a reference for the estimation of the forest parameters timber volume, tree number, basal area and biomass on stand level based on the vertical forest structure provided by LIDAR data. Results show that at least a separation of coniferous and deciduous forest is required as an additional information for each forest stand to achieve good results. Therefore the usage of high resolution multi-spectral satellite imagery is suggested which will allow a separation of coniferous and deciduous forest.

**Keywords:** forest stand parameters, data fusion, laser scanning, forest attributes

## 1 INTRODUCTION

For the determination of forest parameters for large areas like countries or provinces cost intensive sampling methods are used to provide ground truth data for statistical methods. By this way accurate estimations of forest parameters can be generated which provide information on the entire area as such. Nevertheless information on the spatial distribution of timber volume or biomass is not available. To provide such information data sets are required which cover large areas, e.g. satellite imagery. The potential of satellite remote sensing for the classification of forests has been demonstrated by many projects (Schardt et al., 2000). But optical sensors are not able to provide reliable information on the vertical forest structure. Also the structure below the vegetation top layer, vertical forest structure and tree heights can hardly be assessed. The classification of different development stages of alpine forests is only possible with an unsatisfactory accuracy. This is particularly true in inhomogeneous forests which are typical for the Alps. Also forest openings are frequently classified as deciduous forest when dense vegetation predominates in the undergrowth.

More suitable information for the vegetation structure can be provided by laser scanner data. Due to the fact that laser pulses are capable to penetrate the tree crown or vegetation layer, information on the vertical forest structure can be derived. Many large areas of several 10.000 km² are already covered with LIDAR data in Europe. Therefore an assessment of forest parameters using LIDAR data was investigated.

Based on high density airborne LIDAR data the modelling of individual forest trees is possible at a high success rate (Persson 2003). Especially coniferous trees require a high laser point density (> 1 pt/m²) since the small tree tops need to be hit by the laser pulse to achieve good results for the tree heights. If the forest has been captured with lower point densities such as one point per m² and less, the modelling of individual trees becomes rather uncertain. Almost all areas in Europe that are covered with LIDAR data have point densities below 1 pt/m² for cost reasons. Therefore the forest parameters are estimated at stand level as suggested by Naesset (Naesset, 2002).

# 2 EXTRACTION OF FOREST STAND PARAMETERS

## 2.1 Study Areas

The test site Burgau is located near Burgau in the eastern part of Austria and covers an area of 500 ha. The terrain is undulating at 300m above sea level and covered with a mixed forest. The dominant species are spruce (picea abies), pine (pinus silvestris) and oak (quercus sp.), but about 6 additional species need to be considered. For this site LIDAR data, captured by Toposys at flying heights of 800m above ground, as well as a multi-spectral IKONOS scene were available. The local forest management provided GIS data for 212 stands containing information on the species mixture and the timber volume of each stand. In addition basal area, dominant height and stem number were measured of 10 reference plots.

The second test site, Kobernausser forest, is located in upper Austria, 40 km northeast of Salzburg city. The major forest types are spruce (picea abies), pine (pinus silvestris) and beech (fagus sylvatica). The required LIDAR data was captured by Toposys at flying heights of 800m above ground. In addition a multi-spectral IKONOS satellite image was used with a panchromatic resolution of 1m and multi-spectral resolution of 4m. During a field campaign forest parameters within 43 sample plots (20m*20m) were measured.

## 2.2 Vertical Vegetation Structure Analysis

In a preprocessing step the IKONOS satellite images were geo-referenced and ortho-rectified. The LIDAR preprocessing required the calculation of a digital terrain model (DTM) from the LIDAR last pulse data using the methods described by Wack (Wack, 2002). By subtraction of the DTM from the digital surface model (DSM) of first pulse laser points, a normalized DSM (nDSM) was generated. This nDSM contained the heights above ground for the 3D point cloud of the vegetation. To extract information on the vegetation structure for each forest stand, the nDSM was segmented based on the GIS data of the stand boundaries used by the forest management. At the Kobernausser forest no such GIS data was available. Therefore a segmentation for the generation of forest stands was carried out manually based on LIDAR data. The average segment size was 0,25 ha. After this segmentation 43 field plots were measured within selected segments to consider different age classes, forest mixtures and crown closures. The selection was based on LIDAR data and IKONOS satellite imagery.

To create a waveform like height distribution that shows the different stand characteristics, all laser points of a stand were accumulated according to their height above ground. Furthermore each data set was scaled by the stand area, thus making it possible to directly compare the waveform like distribution (see figure 1).

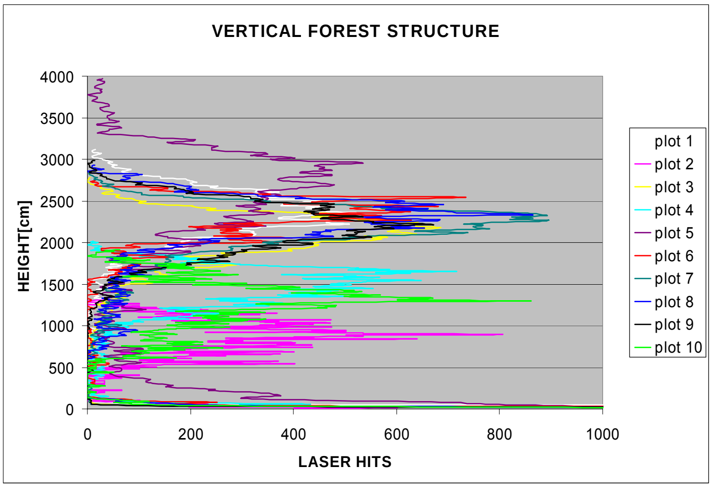


*Figure 1: Vertical vegetation structure from LIDAR data - the different profiles show the distribution of LIDAR hits for each sample plot. The variations between the vertical forest structures are caused by different age classes, species and growing conditions at each site.*

Research on small footprint LIDAR data summarized to a waveform like data distribution of a forest stand has shown that such profiles contain enough information to extract parameters like timber volume, basal area and dominant height (Naesset et al, 2004). To access the information of the waveform like profiles a set of parameters need to be defined which help to characterise the shape. Based on these parameters different predictive models can be set up and tested with regression analysis using ground truth data. To characterise the shapes of the LIDAR profiles of the stands and plots Means et al (1999) suggested the following parameters for full waveform scanner data:

- mh - mean canopy height
- qmh – quadratic mean canopy height
- refl – canopy reflectance

In addition the parameter *$hdom^L$ – height at 95% of all laser hits* - were used together with the first significant maxima from top described by its magnitude and height (*max_a – maximum amplitude; max_a_h – vegetation height at maximum amplitude)*. These parameters were used before for the estimation of forest parameters of eucalyptus plantations with good results (Wack, 2004). First, all forest stands (212) of the test site Burgau were used in a regression analysis to estimate timber volume. In case of good results it would be possible to estimate forest parameters regardless of the species composition of the forest stands. But the correlation coefficient was 0.89 with a rmse value of 59 (32%). In relationship to the average stem volume a rather pure result. In a next step the 10 sample plots in Burgau were used for a regression analysis. Besides timber volume also the extraction of dominant height, basal area and tree number for each stand was investigated. The results are shown in table 1.

*Table 1: Results of a regression analysis for 10 mixed plots; mh = mean canopy height; refl = canopy reflectance; hdom = dominant height (95%); r² = correlation coefficient; max_a = number of hits at first significant maxima from top; max_h = height at first significant maxima from top*

| **Reference parameter** | **Parameters from LIDAR data used for regression analysis** | **r²** | **Rmse** |
|---|---|---|---|
| timber volume | $hdom^L$, max_ a_h,refl, mh | 0.94 | 53.1 (15%) |
| dom. height | $hdom^L$, refl, mh | 0.94 | 1.5 (8%) |
| basal area | $hdom^L$, max_a, max_ a_h,refl, mh | 0.85 | 5.7 (19%) |
| stem nr. | $hdom^L$,max_a, max_a_ h_refl | 0.90 | 274.4 (22%) |

The results of the regression analysis for the 10 plots with mixed forest in Burgau are better. This may be caused by the small number of plots and accurate field measurements. Concerning the 212 forest stands, the species dependent tree shapes affect the shape of the profiles. To investigate the influence of the species on the result of the regression analysis, the forest stands were separated into 4 stratums. Stratum I consisted of all stands with a share of over 30% on deciduous trees. Stratum II covers all stands with 100% spruce. Stratum III contains all coniferous stands and stratum IV consists of all coniferous stands where the content of spruce was lower than 50%. The results of the regression analysis are shown in table 2.

*Table 2: Results of a regression analysis for the estimation of tree volume using 4 stratums in Burgau*

| **Stratum** | **Parameters from LIDAR data used for regression analysis – timber volume** | **r²** | **Rmse** |
|---|---|---|---|
| I (24stands) | $hdom^L$, max_a, max_ a_h,refl, mh | 0.96 | 10.5(8%) |
| II (16 stands) | $hdom^L$, max_a, max_ a_h,refl, mh | 0.89 | 17.3(10%) |
| III (134 stands) | $hdom^L$, max_a, max_ a_h,refl, mh | 0.95 | 24.7(18%) |
| IV (25 stands) | $hdom^L$, max_a, max_ a_h,refl, mh | 0,95 | 22,9(12%) |

In contrast to the results achieved by a regression analysis using all forest stands with an rmse of 59 (32%), an improvement could be achieved by separating the stands according to the tree species. The most significant distinction to be made is the one between coniferous and deciduous trees. A separation of spruce and pine will yield to a further improved of the results. For the test site Kobernausser forest GIS data from the forest management was not available. Therefore the forest stands were segmented manually, creating segments with homogenous vertical LIDAR data structures. The average size the segments was 0,25 ha. In addition to the forest stand structures from

LIDAR data, IKONOS multi-spectral imagery was used to add information on the species mixture to each segment. For the a regression analysis was the same stratums as in Burgau were created and also the same equations. The regression analysis only introduced new coefficients to the equations (table 3).

*Table 3: Results of a regression analysis for the estimation of timber volume using 3 stratums in Kobernausser forest using the same equations as at the Burgau test site with different coefficients*

| **Stratum** | **Parameters from LIDAR data used for regression analysis – timber volume** | **$r^2$** | **Rmse** |
|---|---|---|---|
| I (9stands) | $hdom^L$, max_a, max_ a_h,refl, mh | 0.99 | 41(5%) |
| II (14 stands) | $hdom^L$, max_a, max_ a_h,refl, mh | 0.98 | 118(12%) |
| III (33 stands) | $hdom^L$, max_a, max_ a_h,refl, mh | 0.97 | 126(16%) |

The regression analysis for the estimation of the timber volume showed, that the equations used in Burgau yielded to good results also in Kobernausser forest, even though the two test sites differ in their productivity per hectare at a scale of about 3. A 100 year old stand of spruce contains at Burgau about 350 m³ of timber per hectare whereas in Kobernausser forest it contains over 1000 m³. Nevertheless only the coefficients of the equation had to be adapted.

In addition also the estimation of the forest parameters tree number, basal area and biomass were investigated (see table 4).

*Table 4: Results of a regression analysis for the estimation of timber volume, tree number, basal area and biomass using 3 stratums in Kobernausser forest: all plots, only coniferous plots(stratum IV) and plots with over 50% deciduous trees(stratum V)*

| | **All plots (43) [$r^2$ / rmse / rmse%]** | **Coniferous only(33) [$r^2$ / rmse / rmse%]** | **Over 50% deciduous (9) [$r^2$ / rmse / rmse%]** |
|---|---|---|---|
| timber volume/ha | 0,88 / 212 / 24 % | 0,97 / 126 / 16 % | 0,99 / 41 / 5 % |
| tree number/ha | 0,93 / 340 / 21 % | 0,96 / 251 / 15 % | 0,93 / 335 / 30 % |
| basal area/ha | 0,93 / 7,6 / 15 % | 0,96 / 6,7 / 13 % | 0,98 / 1,9 / 4 % |
| biomass/ha | 0,96 / 51 / 14% | 0,96 / 50 / 14% | 0,99 / 18 / 4 % |

Again a regression analysis was applied using all plots of Kobernausser forest regardless of the species mixture. But again the definition of different stratums like all stands with coniferous trees or stands with over 50 % deciduous trees improved again the results.

## 3 CONCLUSIONS AND OUTLOOK

For the test sites Burgau and Kobernausser forest a stand wise estimation of forest parameters based on LIDAR data was carried out, to investigate the suitability of such an approach within a mixed forest. The results achieved by regression analysis showed, that a subdivision of the forest stands according to the tree species mixture or at least the mixture of coniferous and deciduous trees is necessary to improve the results. A significant improvement was achieved by separating coniferous and deciduous forest. A classification of additional tree species can again improve the result. Therefore a combination of LIDAR and a classified high resolution satellite multispectral imagery is suggested for the extraction of forest stands based on 3D structure and tree species. Such an approach will be tested at the test site Burgau and Kobernausser forest using IKONOS data for the determination of the species mixture with forest stands delineated based LIDAR data. Another test site will be the province of South Tyrol (7500 km²), which will soon be covered with LIDAR data and a SPOT V scene. This will help to investigate the suggested approach on a larger scale.

## ACKNOWLEDGEMENT

This investigation on the extraction of forest stand parameters was partly financed by the EU within the project CarboInvent (Contract number: EVK2-2002-00157).

## REFERENCES

Means J, Axcker St., Harding D., Blair B, Lefsky M, Cohen W., Harmon M, McKee W, 1999. *Use of Large Footprint Scanning Airborne Lidar To Estimate Forest Stand Characteristics in the Western Cascades of Oregon*, Remote Sensing of Environment 67, pp. 298-308.

Naesset E, Bollandas O.M., Gobakken T.(2005) Comparing regression methods in estimation of biophysical properties of forest stands from two different inventories using laser scanner data. Remote Sensing of Environment 94, pp. 541-553

Naesset E, (2002). Predicting forest stand characteristics with airborne scanning laser using a practical two-stage procedure and field data.Remote Sensing of Environment 80, pp. 88-99

Harding D., Lefsky M, G. Parker, Blair B (2001). *Laser altimeter canopy height profiles Methods and validation for closed-caopy, broadleaf forests*, Remote Sensing of Environment 67, pp. 298-308.

Hochbichler E., Bellos P., Lick E., (2005): Biomass functions and expansion factors for spruce, pine, beech and oak in Austria. Austrian Journal of Forest Science, Special Issue on Austrian Biomassfunctions, in preparation.

Persson A., Holmgren J., Söderman U., (2003). Detection, *Measurement and species Classification of Individual trees for Forest Inventory and Visualization*. Proceedings Scandlaser Scientific Workshop Umea Schweden, pp223-234

SCHARDT, M.; Schmitt, U.; Granica, K. & GALLAUN, H. (2000): Satellite Remote Sensing for Risk Assessment in the Alps. Tagungsband „Workshop on Advanced Techniques for the Assessment of Natural Hazard in Mountain Areas, 5 – 7 June 2000, Innsbruck-Igls, Austria.

Wack R.,Oliveira T.,(2005) Analysis of vertical vegetation structures for fire management by means of airborne laser scanning. *Application in forestery- University of Göttingen*. pp 127-135

Wack, R. & Wimmer, A. ( 2002): Digital Terrain Models from Airborne Laserscanner Data – a Grid based approach Proceedings of the ISPRS Commission III Symposium Graz, pp. 293-296.

Ziegler, M., Granica, K., Schmitt U., Wimmer A., Gallaun H., Schardt M. (2002): Satellite Remote Sensing and Laserscanning - Forest Inventory and Monitoring in the Alps, Geoinformatics, Vol. 5, July/August 2002, pp. 28.31.

# PROCESS DEVELOPMENT AND SEQUENTIAL IMAGE CLASSIFICATION FOR AUTOMATIC MAPPING USING CASE STUDIES IN FOESTRY

*Roeland de Kok[1], Piotr Wezyk[2]*

[1] landConsult.de

[2] Lab. Of GIS & RS, Faculty of Forestry, Agricultural University of Cracow

**Keywords**: anchor objects, automatic calibration, automatic image classification

## 1 INTRODUCTION

Traditional remote sensing algorithms for classification are centred around a mean and standard deviation per class. These algorithms favour classes with a normal gaussian distribution in feature space. New developments in sequential and hierarchical classification processes allow tailor-made solutions for classifying different classes in the same scene according to different classification rules. Adaptation to each of these classes allows the integration of the spatial features, which are more stable and thus transferable over various image scenes. Together with an auto calibration procedure, by measuring the selected population of automatically derived samples, the classification rules can be fine tuned for each image without the need of operator sampling. This opens the way for full automatic image classification.

## 2 AUTOMATIC SAMPLING

An essential part of image classification is the selection of samples. Selected samples are defining the spectral mean and standard deviation for the complete class population.

The spectral conditions for imagery from land observation systems are not constant. Therefore the mean and standard deviation per class have to be re-established before each image classification. For full automatic image classification it is necessary to apply a procedure of full automatic sampling where an auto calibration procedure redefines spectral mean and standard deviation before image classification takes place.

The selection of test and training areas is an operator dependent procedure. The selection is based upon existing knowledge of the scene. Operator knowledge of the scene is normally extensive. Full automatic systems must therefore incorporate initial knowledge of the scene. The geo-coordinates of the scene incorporate already an enormous potential for delivering existing information over the areas under investigation, for example, if boreal forest can be expected.

An initial sample sets can be relatively small in comparison with the total population of class members. Due to the dependency of spectral mean and standard deviation, a sample population however must have a minimum number.

In object-oriented analysis, the *spatial* characteristics of objects have an ever-increasing role in defining the classification. Considering the conditions of an object in relationship with its sub objects, the spatial relationships for some object classes can be defined as unique.

In theory, a sample based upon *spatial* characteristics is not essential for defining a mean and standard deviation of a class, but the sample gives a unique description of a *spatial combination* for each class members. Therefore even a single object is sufficient to represent the complete class. Knowing the *exact spatial* relationships for image object inside a class makes even the sampling procedure superfluous. Under such conditions, the classification remains consistent, transferable and fit for full automatic processing.

Due to the limited knowledge, at present, on unique spatial relationships, compromises on sampling for spectral characteristics and spatial relationships have to be made.

## 3 A CLARIFYING EXAMPLE

In the pre-processing phase, sharp edge detection allows for edge preservation as image objects in the segmentation phase (Wezyk, de Kok 2005).

The construction of an ‘edge’ as an image object from ‘edge pixels’ is by definition spectrally heterogeneous. The image object ‘edge’ is in itself a spatial construction and very much depending on its defining neighbours. A sharp contrasting edge in an image is most likely an edge from the population of the class buildings or infrastructure. If a satellite image such as Quickbird or IKONOS or a digital aerial imagery contains buildings or infrastructure, then most contrasting edges must belong to this population.

The generalized class ‘artificial area’ must contain contrasting edges. The population of contrasting edges can be found without sampling. The exact value separating ‘most contrasting edges’ and ‘all contrasting edges’ is more difficult to define.

The population of most contrasting edges also have spectral properties. When the most contrasting edges belong to artificial areas, the NDVI mean and standard deviation can be measured from this population of contrasting edges. This NDVI mean and standard deviation value is representative for a large part of the non-vegetative areas. The mean and standard deviation of the NDVI changes per scene and acquisition date. Contrary to the spectral values, the spatial characteristics do not change per scene. Artificial areas are obliged to contain contrasting edges. These contrasting edges therefore can be considered as samples for the class ‘artificial areas’. They can be found full automatically and serve to redefine the spectral mean and standard deviation of the class characteristics per scene or mosaic part within the cut lines.

In the example, we can now define these contrasting edges as ‘anchor objects’. They serve as an initial start population to measure a spectral mean and standard deviation only valid for this scene or part of the mosaic. The spectral values from the anchor objects can be stored in process variables. They change in value per scene but their sequential use in the classification process remains fixed. The overall architecture of sequential and hierarchical classification remains intact. The changes are linked to value changes of the process variables.

When a class can be found by predefining its anchor objects and their spatial characteristics, full automatic object recognition is feasible. At the moment the spatial characteristics of ‘trees with orthotropic monopodial trunks’ (after Halle, Oldeman, 1978) can be described according to their unique neighbourhood in a dark forest environment. In any scene from VHR image data with resolutions higher than 60 Centimetre, the unique spatial characteristics for trees with orthotropic monopodial trunks' are stable and transferable. This makes automatic tree counting possible for a limited number of tree species. The knowledge on spatial conditions of other trees with different architecture or outside dark forests has to be developed further.

## 4 ALTERATIONS OF THE WORKFLOW

Image classification has a traditional workflow where an operator selects samples and chooses the classification algorithm; it is maximum likelihood, nearest neighbour etc. The influence of the operator is large during sample selection but rather limited after the classification algorithm has been selected. Due to the scene specific conditions of the samples and the subjectivity of its selection there is little use in discussing the quality of the selection with peer-experts. The need to avoid large spectral overlap or spectral confusion remains a rule of thumb during the sample selection. However if spatial explicit differences per class allow good separation, spectral confusion problems will be resolved. The manipulation possibilities of the sample selection and its effect on the resulting classification are huge. It induces a workflow that supports an increasing amount of time investment for an increasing improvement in the final results. As the timeframe between academic output and practical commercial output is generally considerable different, academic output with an ‘time-overkill’ spend on sampling allows a flattered demonstration of the practical potential in a commercial environment. This remains a hindrance in remote sensing applications.

Full automatic sample selection will not be effected by an increment in the timeframe of the sample selection by the operator. This allows academic timeframes becoming more and realistically closer to practical commercial applications. This would serve the remote sensing community as a whole.

Basically the whole procedure of operator based sample selection is a solitary job without the evaluation of expertise from a colleague group.

The new workflow for sequential object classification as shown in figure 1 (produced with eCognition 5.0.4) allows for extensive evaluation and development by peers. Each step in the workflow can be evaluated under scrutiny of fellow experts. This allows the whole process to become mature and stabilizes during the development period. In the end, best practise would lead to initial standards for basic classification per sensor type.

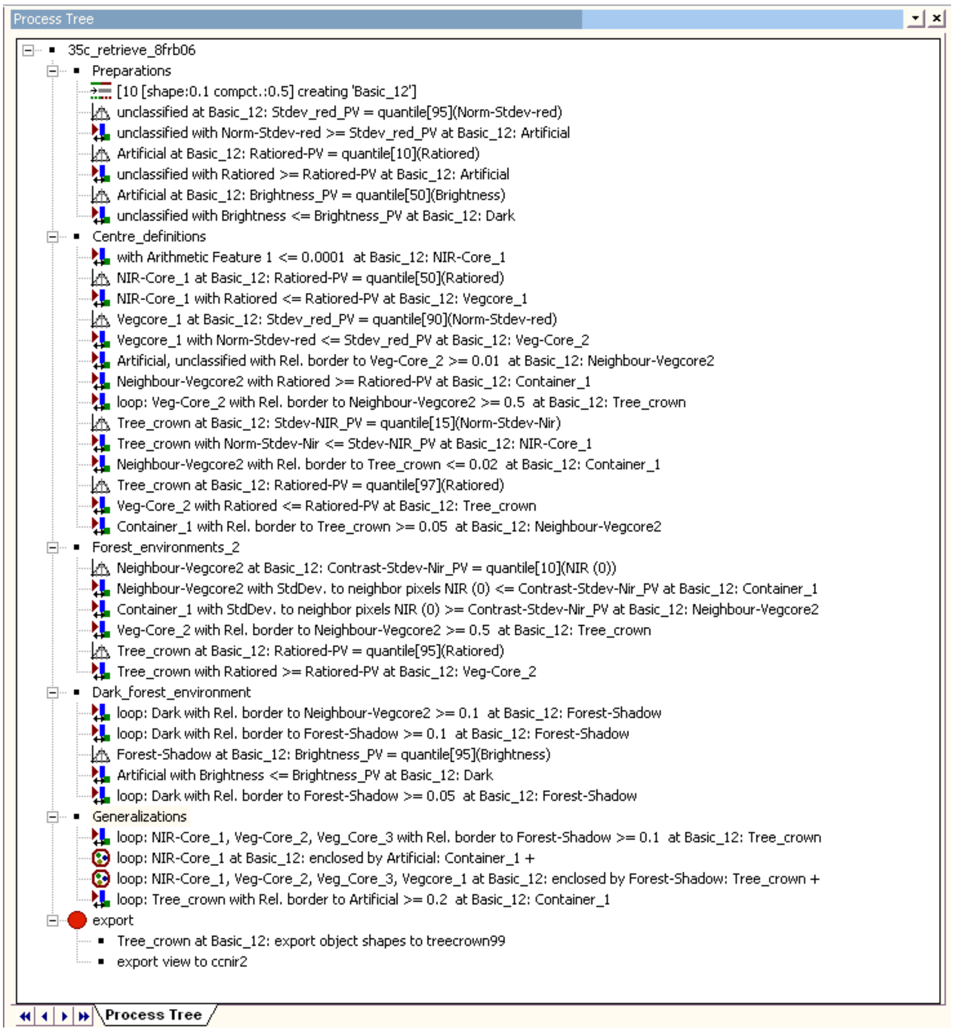


*Figure 1: A process flow from the eCognition 5 version under construction. The 45 Lines are sufficient for automatic tree detection in Ultracam imagery such as in figure 2.*

The Process in figure 1 shows a hierarchy with various sub processes as can be programmed in the latest eCognition version 5.0.4. Processes described here as ‘Preparations’ and ‘Centre_definitions’ consist of a sequential list of sub-processes. It is now possible to task sharing and expert evaluation. Various experts can concentrate on improving sub-processing parts and fuse them together in an overall classification. After ‘Preparations’ (Line 2 to 9 in figure 1) it is possible to integrate for example a ‘Cloud detection’ process with subroutines developed by a team who concentrates on atmospheric conditions and after standardization shares this process-part with environmental or forest application teams.

The process in figure 1 also demonstrates the need to classify forest environment. In case forest stand polygons exist in the forest GIS, the whole workflow simplifies considerably. The quality of the final results would also receive a considerable boost. In the case of evaluation of the process potential it would be fair to allow the role of synergy of existing GIS information to be included.

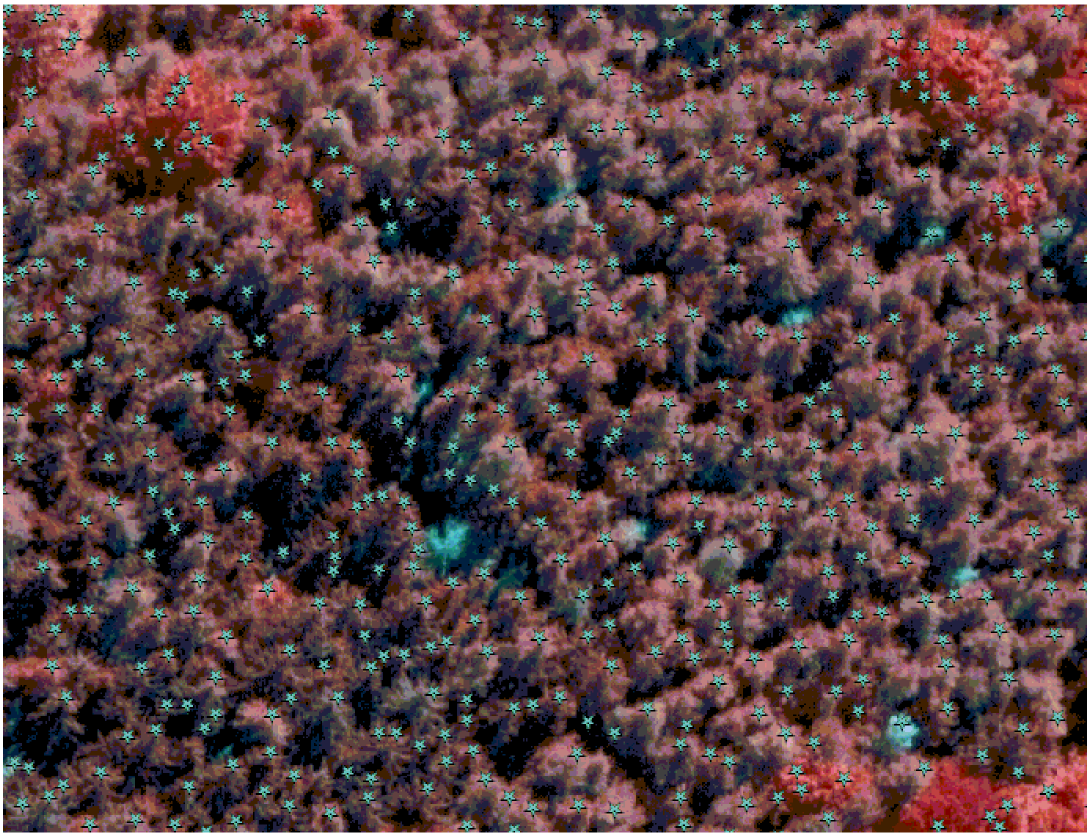

*Figure 2: A snapshot over coniferous forest from a Vexel-Ultracam image (courtesy of BoKu Vienna). Each blue star should point out a single crown.*

## 5 AUTOMATIC TREE COUNTING

The process flow from figure 1 incorporates the spatial rules for detecting trees with monopodial orthotropic architecture such as *picea* and *abies*. When crowns of various broadleaved species do not form complete canopy closure under conditions existing in Scandinavia the algorithm functions as well. The process allows for testing on digital aerial imagery, such as Vexel-Ultracam data applied in the EuroSDR test of Commission II ed; Test of ISPRS commission III/3 as well as Ultracam data from the BoKu test forests.

The first important evaluation is that complete automatic procedure functions and returns centre of trees on every image. Regardless of the 'best results' possible. Even with 60 to 70 % correct tree counting, the system demonstrates its independency of operator influences. In time due, correct classification up to 90% for plantation forest especially with coniferous dominance, become within reach. For all data types, even Quickbird satellite imagery, the spatial characteristics of tree crowns for monopodial orthotropic trunks seem to hold. Experiments in polish forests are ongoing with restrictions on the publication right for imagery. For the process however, the only condition is that the image is taken during the growth season. Therefore details on exact acquisition date are less relevant and not given in figure 2. At this stage of development, the process just demonstrates potentials and not full possibilities. The workflow in itself, according to hierarchical sequential processes, however remains the 'best practise' and will form the basis for further improvements on full automatic classification.

## 6 CONCLUDING REMARKS

At this stage, the new workflow of object classification and it's function as automatic classifier with minimal user input has priority over the demonstration of 'best results possible' including a detailed accuracy analysis. It is enough now to remark the absence of a drift in the output, it means the process always returns crown-centres for all processed images and does not shift considerably to failures of commisssion into other class domains.

The automatic detection of anchor objects and the auto calibration of the classification rules by measuring features and assigning features to process variables are a major step in full automatic image analysis. The flexibility to evaluate image objects with different tailor made classification procedures not per scene but per class opens up a new chapter in remote sensing applications.

Full automatic tree counting over larger sets of very high-resolution imagery can now be demonstrated on screen. The need for quality improvement is obvious with details such as species detection and crown diameter measurement being still on the list of most wanted features. The strength of the procedures for image object analysis however is promising. The task sharing and expert review of standarized procedures will lead to a process library for standard land cover classes per sensortype. For a variety of CORINE type Landcover classes, such procedures already exist and landcover classes for large scale (1:10.000) mapping are showing huge progess (artificial areas, forest types, parcel detection etc.) Their impact on the remote sensing community will be noticed.

## REFERENCES

Hallé F., Oldeman R.A.A., Tomlinson P.B., Tropical trees and forests. An architectural analysis, Berlin, Germany.Springer Verlag, 1978.

Wezyk, P. , de Kok, R. , 2005; Automatic mapping of the dynamics of forest succession on abandoned parcels in south Poland. Angewandte Geoinformatik 2005, Beiträge zum 17 AGIT Symposium (Strobel et al. Hrsg.), Salzburg, pp. 774-779 Wichmann Verlag Heidelberg.